Department of Chemistry
Adran Chemeg

CARDIFF UNIVERSITY
PRIFYSGOL CAERDYDD

The catalytic reaction of CO and alcohols over supported gold catalysts

Thesis submitted to Cardiff University for the Degree of Doctor of Philosophy in Chemistry

By

Abdullahi Nuhu

2008

ProQuest LLC
789 East Eisenhower Parkway
P.O. Box 1346
Ann Arbor, MI 48106-1346

Declarations

This work has not been previously accepted in substance for any other degree and is not being concurrently submitted for any degree.

Sign..... (Candidate)

Date.....7/11/08....

STATEMENT 1

This thesis is being submitted in partial fulfilment of the requirements for the degree of PhD.

Signed..... (Candidate)

Date.....7/4/08...

STATEMENT 2

This thesis is the result of my own investigations, except where otherwise stated.
Other sources are acknowledged and explicit references are cited where appropriate.

Signed..... (Candidate)

Date.....7/11/08..

STATEMENT 3

I hereby give consent for my thesis, if accepted, to be available for photocopying and for inter-library loans.

Signed..... (Candidate)

Date.....7/11/08.

TABLE OF CONTENTS

Chapter 1- Introduction

Chapter 2- Experimental

Chapter 3- Gold catalyst for CO oxidation

Chapter 4- Gold catalysts for Methanol oxidation

Chapter 5- Higher alcohol oxidation over Au/TiO_2 catalysts

Chapter 6 –Conclusions and future work

ACKNOWLEDGEMENT

This work would only been accomplished due to advice, help and support of many people.

I would first like to thank God for all His blessings over the years.

My appreciation and gratitude must go to my supervisor and co- supervisor namely; Prof, Michael Bowker and Dr Albert Carley for offering me the opportunity to study in Cardiff University and for their assistance and guidance during the three years of my project.

I must also thank my mentor Dr Stuart Taylor, whose knowledge has been extremely important and for his help and advice especially for his advise during my the course of my PhD.

Many thanks to Professor Kingsley Cavell, for his cordial relation and monitoring in ensuring all necessary facilities and equipments are provided for this project. My appreciation must also be expressed to all members of the staff of Physical Science Group, most notably, Professor Kenneth Harris, Professor Graham Hutchings, Professor Gary Attard and the staff of Catalysis and surface science unit for their constructive criticism and advice especially during six monthly viva and student presentation sessions.

Thanks must be given to the Vice Chancellor of Kano State University of Science and Technology, Wudil, Professor Ibrahim Shehu Diso for his endless help and encouragement and sourcing funds for us despite all the difficulties through out the time of this project. I would also like to show my appreciation to the management, all those at Kano University of Science and Technology, Wudil and Kano State Government of Nigeria especially those who have provided input throughout the three years of my course.

I would also like to express my gratitude and appreciation to the past and present fellow group members and technical staff who have provided support and help with work. I am particularly, thankful to Dr Thomas Davies, Dr David Morgan, Dr Matts House, Dr Andrew Watts, Layla Al-Mazroai, Polina Yeseneva, Alun Davies and Gerald Crocker, for their help, assistance and provided serene atmosphere which I very much enjoyed during the initial and final stage of this project.

This project, will not be accomplished, with out expressing my appreciation and gratitude to my family especially to my wife Mrs. Saddiqa Abdullahi and my son Musa (Muhsin) Abdullahi and daughter, Fatima Abdullahi for their patient, love, support, understanding and encouragement through out the three years of this project.
I must also thankful to my colleagues Aminu Ahmed, Yusuf Daraja, Ado Mukhtari Bichi, Abdullahi Mustapha, Ibrahim Abdullahi, Abdulhadi Aminu, Bello Makama, my friends here in UK in general for their encouragement and support through out my PhD project. I am particularly thankful to Dr Shehu Yakasai, Dr Usman Gambo Abdullahi, Abdulkadir, Maikudi Dala, Dr Edwin Njantua, Raja Alqutabi, Ahmed Yakasai, Haruna Musa, and Mukhtari Atiku for making my stay in Cardiff and UK so enjoyable.

LIST OF ABBREVIATIONS

Å	Angstrom
A	Pre-exponential factor or frequency factor
AAS	Atomic absorption spectroscopy
AMU	Atomic Mass Units
BET	Brunauer- Emmet- Teller
cc	Cubic cent- metre
DME	Dimethyl Ether
DRIFTS	Diffuse Reflectance Infrared Spectroscopy
E_a	Activation energy
EDAX	Energy- dispersive X-ray analysis
FTIR	Fourier Transform Infrared
FWHM	
g	Gram
G	Gibb's free energy
h	Hour
H	Enthalpy or heat
H_l	Heat of condensation
IR	Infrared
k	rate constant
K	equilibrium constant
K_a	Rate constants for adsorption
K_d	Rate constant for desorption
keV	Kilo electron volt
KIE	Kinetic Isotope Effect
kV	kilo volt
λ	Wavelength
min	Minute
ml	milli liter
mol	Mole
Δ	Change
ΔH	Enthalpy or heat change
nm	Nano meter
°	Degree
°C	Degree Celsius
P	Equilibrium pressure
PFR	Pulsed Flow Reactor/Reaction
P_o	Saturated vapour pressure of gas at temperature of experiment
θ	Fraction of surface covererage
R	Gas constant
s	Second
S	Entropy
SEM	Scanning electron microscopy
STP	Standard condition of temperature and pressure
T	Temperature
TCD	Thermal Conductivity Detector
TOF	Turn Over Frequency
TPD	temperature programmed desorption
TPPFR	temperature programmed pulse flow reaction

TWV	Two way valve
μ	Micro
UHV	Ultra High Vacuum
V	Amount of gas adsorbed or volume
V_m	Monolayer coverage or volume of monolayer
WGC	World Gold Council
wt	Weight
XAFS	X-Ray Absorption Fine Structure
XPS	X-ray photoelectron spectroscopy
XRD	Powder X- ray diffraction

ABSTRACT

Studies of CO, methanol and some higher alcohol oxidations over gold supported on TiO_2 (Degussa), γ-Al_2O_3 and SiO_2 were investigated. The methods of preparation of catalysts used are deposition precipitation and incipient wetness impregnation.

Several parameters have been investigated for CO oxidation over Au/TiO_2 prepared by deposition precipitation, such as temperature programmed pulse flow reaction, isothermal and continuous flow CO oxidation, anaerobic CO reaction, calcination temperature, effect of moisture (in the presence of water, and methanol), kinetics and CO oxidation in the presence of hydrogen etc. The catalysts are demonstrated to have high activity even at room temperature. Gold supported on TiO_2 (Degussa) was characterized by BET surface area method, powder X-ray diffraction, SEM, EDAX, XPS, and Raman spectroscopy.

The CO oxidation reaction studied on Au/γ-Al_2O_3 and Au/SiO_2 catalysts prepared by deposition precipitation (DP) and incipient wetness impregnation (IW) methods showed that the Au/γ-Al_2O_3 catalyst prepared by DP method is much more active than Au/γ-Al_2O_3 and Au/SiO_2 prepared by the incipient wetness impregnation method. Presumably, the low performances of the IW catalysts are ascribed due to presence of chloride which leads to gold sintering in the catalyst. However, the performance of these catalysts with respect to CO oxidation was less than the Au/TiO_2 catalyst prepared by DP method. The characterization of the catalyst shows the BET surface area of Au/γ-Al_2O_3 and Au/SiO_2 catalysts to be 128 and 320m^2/g respectively. The XRD of the Au/γ-Al_2O_3 shows mainly the support, which indicated high dispersion of gold on the catalyst. Nevertheless, XPS, SEM, Raman Spectroscopy and EDAX were used for characterisation of the Au/γ-Al_2O_3 and Au/SiO_2 catalysts. The CO oxidation reaction studied show that the activity of the catalyst decreases in the following order: $Au/TiO_2 > Au/\gamma$-$Al_2O_3 > Au/SiO_2$.

The adsorption and reaction of methanol with Au/TiO_2, Au/γ-Al_2O_3 and Au/SiO_2 catalyts using temperature pulse programmed reaction over the reactor, TPD, SEM, EDAX, XPS and DRIFTS were investigated. Several factors were investigated such as pH, calcination, comparison with the reference WGC catalyst, kinetic isotope effect etc. The TiO_2 (P25), γ-Al_2O_3 and SiO_2 surface adsorbed about a half monolayer of methanol, much of it in a dissociative manner forming methoxy groups associated

with the cation sites and hydroxyl groups at anions. For, TiO_2, the methoxy is relatively stable until about 250°C, at which point decomposition occurs, producing mainly dimethyl ether by bimolecular surface reaction. As the concentration of methoxy on the surface diminishes, so the mechanism reverts to a de- oxygenation pathway, producing mainly methane and water (at ~ 330°C in TPD), but also with some coincident CO and hydrogen. In contrast, in the case of γ-Al_2O_3 and SiO_2, dimethyl ether (DME) was observed as the main product. The effect of gold catalysts prepared by DP and IW on the reactivity is marked. The pathway which gives methane, which is characteristic of TiO_2 (P25) for Au/TiO_2 catalysts, remains the same but a new feature of the reaction is the evolution of CO_2 and H_2 at lower temperature, and the elimination of the DME- producing state. Clearly, this is associated with the presence of gold and appears to be due to the high amount of formate species on the catalyst surface. The formate species involved in the reaction of methanol over TiO_2 and Au/TiO_2 catalysts results in a combustion pathway being followed, with complete conversion occurring by ~130°C. Similarly, the main methanol oxidation reaction observed on Au/γ-Al_2O_3 and Au/SiO_2 are dehydration products, mainly, DME, with CO and hydrogen as the main products.

The oxidation reaction of higher alcohol (ethanol, propan-1-ol, and propan-2ol) has been studied over Au/TiO_2 catalyst prepared by deposition precipitation (DP) method using Temperature Programmed Pulsed Flow Reaction, TPD, and DRIFTS. TiO_2 (P25) adsorbed about half monolayer of ethanol, propan-1ol and propan-2ol. The presence of the gold (as in the case of Au/TiO_2 catalysts) eliminates most of the dehydration products and increases the production of formate species, which results in a combustion pathway being followed, with complete conversion of ethanol, propan-1-ol and propan-2-ol. The results are mainly dehydrogenation, dehydration, de-oxygenation and decomposition products but, in each case, the reaction is a complete oxidation reaction.

Chapter 1- Introduction

1.1 Introduction

In this chapter, the general aspects of catalysis and chemistry of gold will be reviewed. Generally, gold catalyst will be considered with emphasis more towards CO and Alcohol oxidation and other related reactions. However, preparation methods, activation, deactivation, and chemistry of compounds involved in the catalyst preparation will also be discussed.

1.2 Catalysis

Baron Jöns. Jakob, Berzelius a Swedish scientist was first to bring out the idea of catalysis to the field of chemistry knowledge in 1836. The word catalysis came from a Greek words meaning breaking down and was used during the ancient Greet for the collapse of moral and ethical constraint, in Berzelius employed the word and used it because of the removal of normal barrier of the chemical reaction. Several other scientists were linked with early catalysis, in 1831; Alexander Mitscherlich was referred to Contact Process and John Wolfgang Döbereiner who spoke of contact action in 1820. Humphrey Davy discovered the use of platinum in catalysis while in 1880s; Wilhelm Ostwald determined the acids and bases strength and awarded a Noble Prize in Chemistry in 1909.[1]

Based on the contribution of these scientists, a catalysis can be define as a way, method or path of accelerating or speeding of up of chemical reaction by means of contacting or mixing of the reactants with other substances called catalyst, with out (the catalyst) being involve or consumed in the overall reaction. A catalyst provides an alternative route to products by lowering the activation energy than in uncatalised reaction. The catalyst came from a Greek word meaning to annul or unite or to pick up.

In general, there are two types of catalysis; homogeneous catalysis when the catalysts are in the same phase with the reactants and heterogeneous catalysis when the catalysts are in different phases with the reactants. In homogeneous catalysis, the catalyst acts as a molecule, which facilitates the reaction. It initiates the reaction with one or more of the reactants to form an intermediate, which subsequently leads to the formation of the products and the regeneration of the catalyst. While in the case of heterogeneous catalysis, the catalyst is providing the surface on the reactants, which begins with adsorption of the reacting gases on the surface, and the intermolecular bonds are broken or weakened sufficiently for new bond to be created. Since the

bonds between the products and the catalyst are weaker, the adsorbed species on the surface finally desorbed to form products from the surface in to the gas phase, thereby generating the active sites on the surface. Several possible reaction mechanisms for the surface reaction are known, depending on the how the adsorption takes place. Some of the examples of heterogeneous catalysts are iron in Haber process and vanadium oxide in the contact process.

A catalyst's activity refers to its ability to convert reactant to products while its selectivity is the ability to convert reactant to a particular product. The international system derived for measuring the catalytic activity of the catalyst is katal, (moles/s). The degree of activity of a catalyst can also be described by the turn over number (TON), and the turn over frequency (TOF). The lifetime of a catalyst refers to how long it can maintain its activity while deactivation is a term use to express the drop in a catalyst's activity, selectivity or both over time.

Similarly, for a catalyst to be successful in its performance, it should be active, have optimum selectivity and an economic lifetime (low deactivation tendency). Catalyst's light off temperature is the temperature at which conversion or yield changes from a very low value to a high value. The lower the light –off temperature and the temperature of maximum yield of product, the higher the selectivity of the catalyst

1.3 Back ground

The concept and theory of catalytic reactions have been fully discussed and studied in many publications.[7] This section gives a brief summary of these concepts and the theory governing catalysis.

1.3.1 Catalytic activity, Conversion, Selectivity and yield

For a catalytic reaction, the performance of the catalyst is measured by its activity and selectivity. The rate at which the reactants are consumed or decreased in its initial amount to form product is known as the catalyst activity. Similarly, the Conversion can be defined as the fraction of the reactants converted in to both product; and selectivity as the fraction of products, which the substance represents or is the fraction of the product that it constitutes of the total products while its yield is the conversion multiplied by its selectivity. The majority of the catalysts investigated in this thesis (chapter 3-5) are metal supported catalysts (i.e. made up of gold supported on other

material- mostly metal oxides). The activity and selectivity of such catalyst are often provided by three components; active component, support and promoter (modifier).

1.3.2 Active phases or components

Active components are mostly metals, oxides/sulphide or aluminosilicates. In this thesis, Au is used as active components for metal- supported catalysts for CO and alcohol oxidation. The main role of the active component is to speed up the rate at which a desired chemical reaction approaches equilibrium by providing an easier selective path for the reaction to follow.

1.3.3 Supports

Supports are mainly metal oxides used as support for metal supported catalysts. In this thesis TiO_2, Al_2O_3, and SiO_2 have been employed as supports for gold. The support provides particle size shape, strength and thermal stability. It also provides high internal surface area, optimum pore shape, size, and disperse active component. The area of the support affects the dispersion of the active component, which then also tends to have a low surface area if the support is of low area.

1.3.4 Promoters or Modifiers

Promoters or Modifiers are substances, which are not catalytically active by themselves but allow or modify the active component or the support to be active to its maximum. In this thesis no promoter or modifier is used for both CO and alcohol oxidation. The promoter increase the rate at which the reaction proceeds by modifying the properties of the active component or support. Modifiers also help in providing alternative easier routes for the catalytic process.

1.3.5 Thermodynamics of catalysed reactions

The word thermo- is a Greek word means heat, while dynamic means- power, the thermodynamic of the systems describes the system respond to the surrounding. In general, the thermodynamic of catalysed reaction deals with whether or not a reaction will proceed. Thermodynamic of a system is indicative of the maximum yield of product than can be attained under some specified conditions. Irrespective how fast a reaction might proceed, if the yield is low (small equilibrium constant),

the entire process is still not viable. On the other hand, it is absolutely of no use to have a large equilibrium constant (high yield), provided the equilibrium is reached only extremely slowly. Process economics therefore requires both high yield and speed of production.

Catalysts cannot make energetically unfavourable reactions possible- they have no effect on the chemical equilibrium of a reaction because the rate of both the forward and the reverse reaction are equally affected. The net free energy of a reaction is the same whether a catalyst is used or not; the catalyst just makes it easier to activate.

There are number of parameters which most be considered when dealing with thermodynamic of catalysed reaction. For a chemical reaction to be feasible, the Gibbs free energy, G of that reaction must be negative. While a positive value of G signifies a backward reaction, a zero value represents an equilibrium condition. The change in Gibbs free energy (ΔG) for any system is given by equation 1

$$\Delta G = \Delta H - T\Delta S \quad \text{.....1}$$

Where:

ΔH= enthalpy change, ΔS = entropy change and T = temperature

ΔG, ΔH and ΔS are called state functions because they are independent of the path of a reaction and only depend on the initial and final state of the system. Thus, ΔG, ΔH, and ΔS for the oxidation of CO and alcohols (and all other reactions) must be the same for both catalysed and uncatalised reactions.

1.3.6 Kinetics of catalysed reactions

Thermodynamics and kinetics constitutes the most essential considerations in the design and monitoring of a chemical process. Kinetics deals with how fast the reaction will proceed. The thermodynamic and kinetic parameters of the catalysed reaction is essential, as both concepts are inseparable and must be put together in order to achieve

the best possible outcome. Example, determination of kinetic parameters such as order of a catalysed reaction is essential. Knowledge of the orders of reaction with respect to reactants and products, are important in understanding the catalysed reaction mechanism, in the best design of the catalytic reactor, including the size and shape of the catalyst bed and in understanding the nature of the slowest step in the total catalysed reaction process.

As mentioned earlier, a catalyst is any substance that will alter the rate of a reaction without itself undergoing any change. The primary effect of a catalyst on a chemical reaction is thus to increase its rate. However, prolonged usage and temperature treatment often leads to loss in activity and or selectivity. The primary effect of most catalysts is to speed up the rate of a chemical reaction (increase the rate coefficient of the reaction). The rate coefficient for a reaction is related to the temperature at which the reaction occurs given by the Arrhenius equation, (2)

$$k = e^{-Ea/RT} \quad \ldots\ldots\ldots\ldots\ldots 2$$

Taking ln on both sides of equation 2 gives:

$$\ln k = \ln A - \frac{E_a}{RT} \quad \ldots\ldots\ldots 3$$

Where k= rate constant

A= pre- exponential factor or frequency factor

Ea= activation energy

R= gas constant

T= temperature in Kelvin

Ea can be obtained from a plot of lnk against 1/T. the gradient of the line increases with increase in the value of Ea, signifying a stronger temperature dependence of the rate constant. A zero value of Ea means that k is independent of T. The use of a catalyst provides an alternative path with lower activation energy and as such ensures

that a reaction that will normally occur at very high temperatures can actually proceed at relatively lower temperatures.

1.3.7 Sequences in a heterogeneous catalysed reaction

The oxidation of CO and alcohols in the presence of a catalyst is similar to all other catalytic reactions. It involves the transfer of reactants in the gas phase to surface of the catalyst, adsorption of the reacting gases on the surface of the catalyst, where intermolecular bonds are broken or weakened. Next, the adsorbed species react on the surface, some times, in several consecutive steps. Finally, the products adsorb from the surface in to the gas phase, thereby regenerating the active site on the surface for catalytic cycle. Figure 1-1 shows the schematic representation of the steps involved for catalytic CO oxidation.

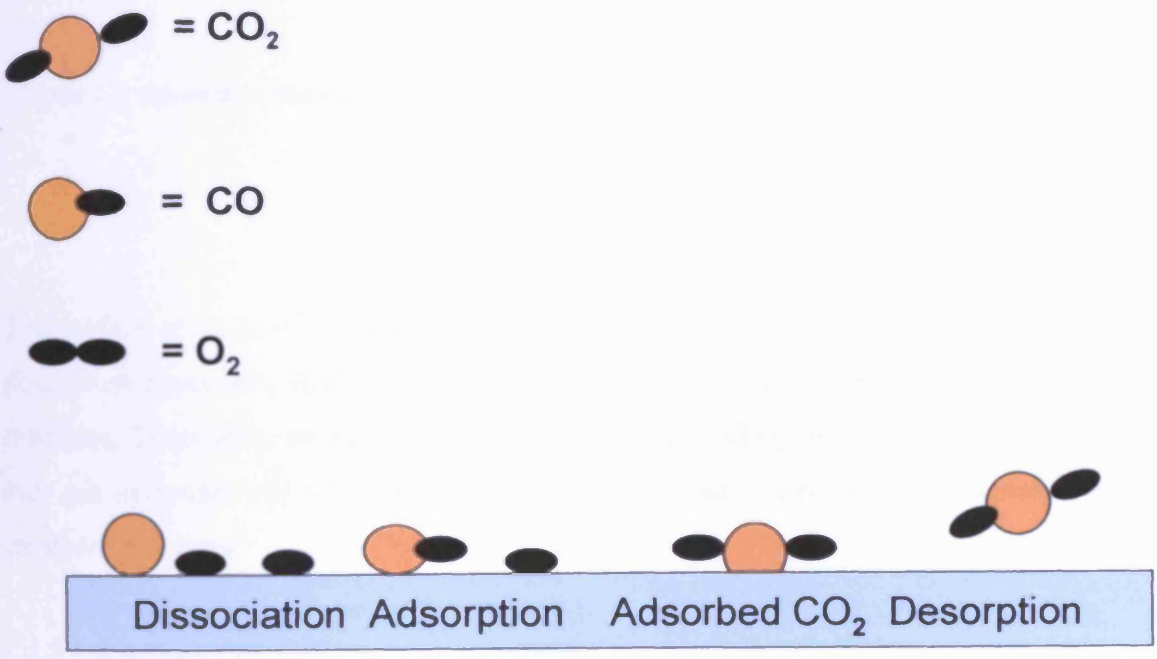

Figure 1.1: schematic representation of a CO catalysed oxidation reaction processes

However, the adsorption of the free molecules on the surface of the catalyst can be either associative or dissociative adsorption. Figure 1-2, shows the possible associative and dissociative adsorption for CO oxidation reaction as depicted in figure 1.1.

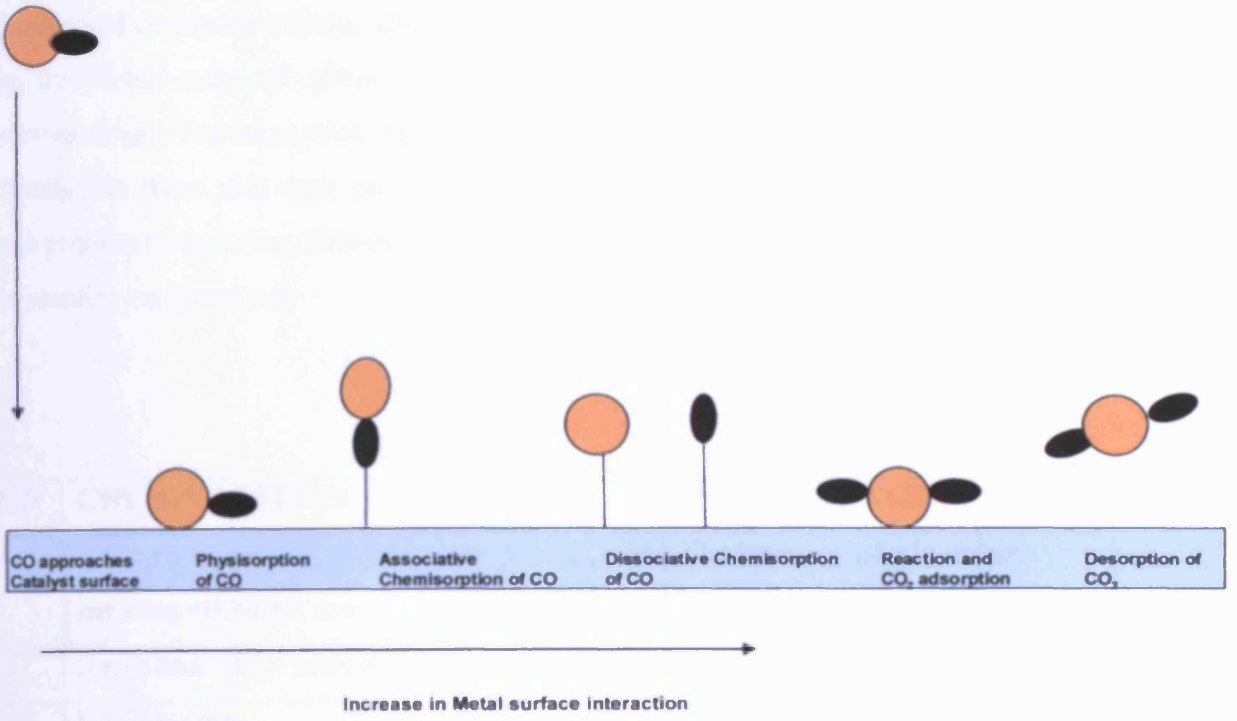

Figure 1.2: schematic representation of possible CO adsorption surface for CO catalysed oxidation reaction on the catalyst

The surface reaction of the catalytic reactions depends solely on the adsorption and desorption processes. Both process are important and control the rate of catalytic reactions. There fore, we need to have sound understanding of these processes since they are important and form the basis for the quantitative measure of the kinetics of catalysed reactions.

1.3.7.1 Adsorption and desorption process

There are many forms of adsorption, which are recognised to occur at the surface of the solid (catalyst). One form of adsorption, which occurs because of a molecule's interaction with free valencies, is known as chemisorption or some time called chemical adsorption. Chemisorption has been regarded as a chemical reaction because there is a rearrangement, sometimes drastic, of electrons within the molecule. The other form of adsorption, which occurs at the solid surface (catalyst), known as physisorption or physical adsorption. The physical adsorption occurs as result of van

der Waal forces, which exist between molecules themselves in the liquid state. When these forces are exerted between an atom or molecules (adsorbate) and a surface, there is physical attraction without alteration of the molecules. Similarly, desorption refers to the detachment of already adsorbed adsorbate from the surface in to the surroundings. The adsorption (chemisorption and physisorption) are often difficult to distinguish them, but each process has a unique characteristics, which differentiate one process to the other. However, table 1.1 shows some parameters, which often used to identify each process:

S/N	CHEMISORPTION	PHYSISORPTION
1	The enthalpy of adsorption $-\Delta H_{ads}$ is between 40-800kJ mol^{-1}	The enthalpy of adsorption $-\Delta H_{ads}$ is between 8-20kJ mol^{-1}
2	Small amount of activation energy needed	No activation energy needed
3	It is selective	It is unselective
4	Bond in adsorbed molecules can be changed in strength (associative) or broken (dissociative chemisorption)	No breakage of molecular bonds and negligible changes in bond energies
5	Occurs at low temperature, which depends on activation energy.	Occurs at low temperatures which depend on boiling point
6	Occurs at low temperatures which depend on boiling point	Occurs at low temperature which depends on E
7	Involved covalent interactions	Weak Van der- Waal forces involved
8	Number of layers adsorbed is not more than one layer(monolayer adsorption involved)	Number of layers adsorbed is more than one layer(multilayer adsorption involved)

Table 1.1: showing characteristics features for distinguishing between chemisorption and physiorsorption

1.3.7.2 The Langmuir adsorption isotherm

The Langmuir adsorption isotherm gives the relationship of the variation of surface coverage at a given temperature with pressure, for a free and adsorbed gas molecule at equilibrium. The Langmuir isotherm forms the basis for quantitative analysis of the catalytic reaction by providing a good basis of quantitative description of the degree and strength of adsorption of different molecules at the surface. It also use for measuring the surface area of the catalyst, as we shall see in chapter 2. The Langmuir isotherm is based on the following three assumptions:

1. the adsorption is confined to only monolayer
2. the surface of the catalyst is assumed to be uniform and equivalent for all sites
3. for adsorption of a molecule at a given site is independent of the occupation of neighbouring sites.

The dynamic equilibrium that exists between the free molecules and adsorbed molecules as shown in equation 4

$$M_{(g)} + S_{(surface)} \underset{k_a}{\overset{k_d}{\rightleftharpoons}} MS \quad \text{.....} 4$$

With equilibrium constant given by:

$$K = \frac{k_a}{k_d} \quad \text{.....} 5$$

Where:

k_a and k_d being the rate constant for adsorption and desorption respectively. However, the rate of change of surface coverage due to adsorption is proportional to the partial

pressure P of M molecule and the number of the vacant site N(1- θ), where N is the total number of sites.

$$\frac{d\theta}{dt} = k_a PN\,(1-\theta) \quad \text{.....6}$$

Similarly, the rate of change of θ due to desorption is proportional to the number of adsorbed species (Nθ) as shown in equation

$$\frac{d\theta}{dt} = -k_d(N\,\theta) \quad \text{.....7}$$

However, the total change of surface coverage at equilibrium is zero; therefore, the sum of k_a and k_d is zero and solving for θ, gives the Langmuir Isotherm.
The surface coverage θ for associative adsorption is given by:

$$\theta = \frac{KP}{(1+KP)} \quad \text{.....8}$$

And for dissociative adsorption,

$$\theta = \frac{(KP)^{0.5}}{(1+KP)^{0.5}} \quad \text{.....9}$$

1.4 Brief General History of Gold

Gold as first discovered in its natural state, in streams all over the world as shining, yellow nuggets (figure 1-3), it depends on where you find it. Gold in ancient times was made into shrines and idols (known as the Golden Calf), plates, cups, vases and

vessels of all kinds, and of course, jewellery for personal adornment. Gold, beauty, and power have always gone together. Gold has become a part of every human culture, it brilliance, natural beauty, and lustre, and its great malleability and resistance to tarnish made it very enjoyable to work and play with.

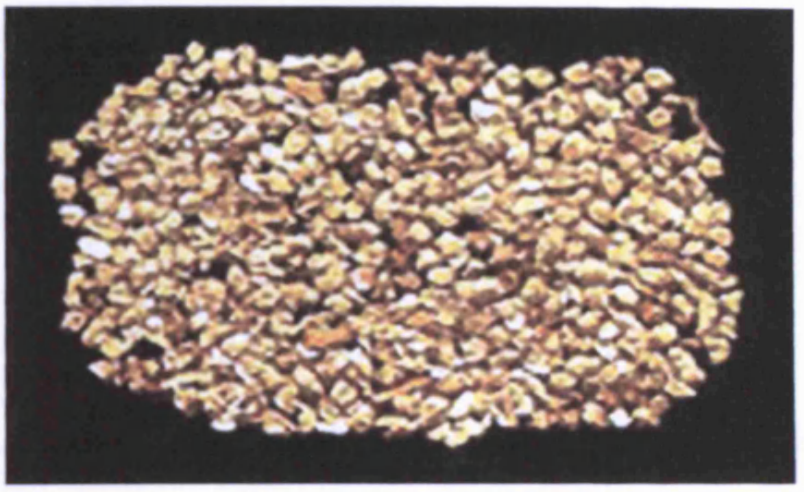

Figure 1-3: Gold

Gold has a long and complex history, from the first gold discovery; it was symbolized with wealth and guaranteed power. It causes obsession in men and nations, destroyed some cultures and gave power to others. According to archaeologist, gold use began in the Middle East where the first known civilization began. The oldest piece of gold jewellery was found in Egypt in the tomb of Queen Zer and that of queen Pu-abi of Ur in Samaria. After the third millennium BC, most of Egyptian tombs were raided, but the tomb of Tutankhamen was discovered undisturbed and was found large collection of gold and jewellery. The Persian Empire, (Iran now), have frequently use gold in artwork as part of their religion of Zoroastrianism

The recent study of the world gold production (figure 1-4) shows China as the main producer of gold with 11.3, followed by South Africa, USA and Australia with 11.1%, 10.4% and 10.3% respectively. While 7.0%, 6.9%, 6.2% and 3.8% as the world gold production due to Indonesia, Peru, Russia and Canada respectively. However, 32.9% was observed as the gold production due to other rest of the world.

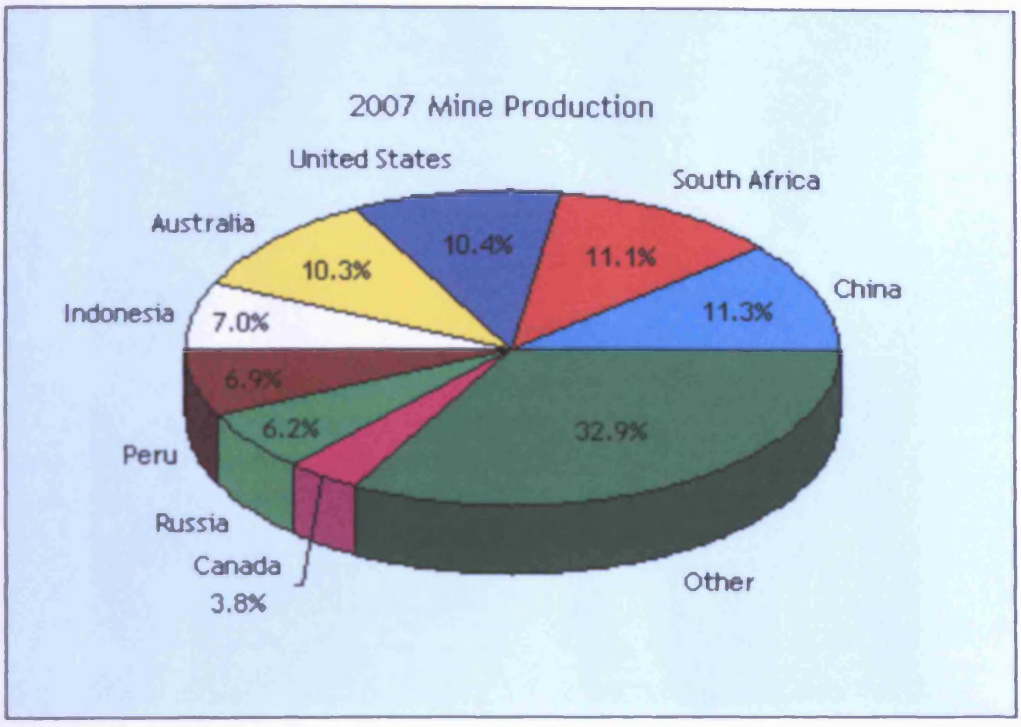

Figure 1-4: World Gold Production[8]

1.5 Gold occurrence and extraction

The occurrence and distribution of gold through out the world have been extensively studied and it was found that gold occurred widely, normally in very low concentration. It has been observed that gold has a great affinity to some elements; several compounds of gold found in nature are the telluride, typically calaverite ($AuTe_2$), petzite ($(AuAg)_2Te$), sylvanite ($(AuAg)Te_2$) among others. Gold is found in native form in both lode and alluvial deposits formed because of several influences such as the cracks of rocks due to variation of temperature or concentration's of the planet surface. In the largest world gold reefs such as china and South Africa, gold is found to be present as veins and stringers in a quartz matrix (figure 1-5), sometimes accompanied with pyrite and quartz sand. Many pyrite and pyrhotite minerals contain gold from which the metal is recovered during the extraction of copper, silver, lead, zinc and nickel. Although in low concentration, gold is found to present in the seawater. It has been estimated that the ocean contain 70 million tons of gold solution.

Figure 1-5: quartz containing gold sand[9]

The extraction and isolation of gold now a days, involved crushing to powder of the gold ores (depending on the type of mixtures) so as to expose the small gold particles. These are dissolved by treatment of the fine mixture of the ore with cyanide solution in air. Zinc powder was then added to the resultant mixture solution of gold cyanide complex in order to precipitate out gold.

$$4Au + 8NaCN + O_2 + 2H_2O \rightarrow 4Na[Au(CN)_2] + 4NaOH$$

$$2Na[Au(CN)_2] + Zn \rightarrow 2NaCN + Zn(CN)_2 + Au\ (s)$$

1.6 General Gold uses

Gold has been considered as one of the most useful mineral mined from earth. The gold usefulness was as results of its diverse special properties. Gold conducts electricity and does not tarnish and it is easy to work and can be drawn into wire, can be hammered in to sheets, alloys with many other metals, can also be melted and cast in to highly detailed shapes.

The gold standard was once used by many nations but it eventually became too cumbersome and is no longer used by any nation. Today, the use of gold as a financial backing for currency was most often held in the form of gold bars, also

known as gold "bullion". Many governments, individuals and institution hold investment of gold in the convenient form of bullion

One of the most recent industrial uses of gold was in the manufacture of electronics. It has been observed that solid-state electronics uses low voltage and current, which are usually interrupted by corrosion or tarnish at junction. However, being gold as a good conductor and can carry this low voltage and free from corrosion, makes it possible to be used in electronic devices. Hence, small amounts of gold is used in many electronic such computer, cell phone, calculators and some television sets

The uses of gold cannot be accomplished without mentioning its uses in modern and traditional medicine. Gold is known to have been used in dentistry as early as 700 B.C. its chemical inertness, nonallergenic and easy to work, makes it possible by the dentists to be used dental fillings because of its superior performance and aesthetic. However, other uses of gold in the modern medicine include treatment of a number of medical conditions such as in treatment of rheumatoid arthritis by injecting a weak solution of sodium aurothiomalate. It has also been reported to use in treatment of cancer by using a radioactive gold isotope, which are implanted in tissues, which serve as a radiation source. Similarly, gold is used in remedy a condition in eye patient with lagophthalmos (inability of a person to close eye completely) by injecting small amount of gold in the upper eyelid, which helps the patient to close the eye completely. Many surgical, electronic and life-support devices are made using small amount of gold because it is non-reactive in the instrument and is highly reliable in the instrument. Small amount of gold colloid solution is used to track as a beta emitter as it passes through the body.

Other uses of gold include use as satellite components and because of high esteem, status, and it is associated with positive qualities, it used in making crown for kings. Gold has also been used in given an award to the first winner because of its status and value, example in Olympic Games, gold is used to be given to the first winner, and in academic award, Music's Grammy Awards and important achievement. Gold has also been used in Glass making, by using it as pigments for reflecting solar radiation outward, helping the building stay cool in the summer and reflect internal heat inward, helping them stay warm in winter.

1.7 Brief Gold chemistry

Gold, silver and copper constitutes Group 11 metals. They are found together at the foot of the reactivity series, which means the metals are not easily oxidised to form positive ions. The attack resistance of these metals by acid or oxygen is increases from copper through silver to gold. Their resistance to chemical attack by water, some atmospheric components and oxygen make them uncreative and have therefore been used for making coins and medals. They are some times called "coinage metals" due to their ability to form many alloys with many other metals. Chemist called them noble metals due to their inertness.

	Cu	Ag	Au
Electronic Configuration	$[Ar]3d^{10}4s^{1}$	$[Kr]4d^{10}5s^{1}$	$[Xe]4f^{14}5d^{10}6s^{1}$
Atomic number	29	47	79
Atomic weight	63.546	107.8682	196.9665
Structure	fcc	fcc	fcc
MP/°C	1083	961	1064
BP/°C	2570	2155	2808
Density (20 °C) gcm^{-3}	8.95	10.49	19.32
Electrical resistivity (20 °C)μohm-cm	1.673	1.59	2.35
Electro negativity	1.9	1.9	2.4
Electron affinity /$KJmol^{-1}$	87	97	193
ΔH (monoatomic gas) $KJmol^{-1}$	337	284	379
Metal radius in (12-coordination)/pm	128	144	144
Number of natural isotopes	2	2	1

Table 1-1: Comparison of some properties of group 11 elements

The special properties exhibited by gold when compared with other elements of group 11, make it special and unique. The high density, high boiling point and melting points coupled with high electro negativity and electron affinity make it stable and interest for research. Generally, metals exhibit their characteristic shininess, as the delocalised electron sea in the metallic bonds is able to absorb and re-emit photons over a wide range of frequencies. Thus, the reflectance spectra of most metals appear flat and they appear silver in colour. The unique yellow colour exhibited by gold is due to absorption of light in the near ultraviolet and blue region of the spectrum, which corresponds to an excitation of an electron from the filled d band to the conduction s-p band.

Although gold has been considered as a noble metal. It inertness because of half-filled s orbital makes it stable. However, it forms many and diverse compounds. The oxidation state of gold in its compound ranges from -1 to +5 but Au(I) and Au(III) dominate. Gold (I), referred to as the aurous ion, is the most common oxidation state with "soft" ligands such as thioethers, thiolates and tertiary phosphine. Au(I) compounds are generally linear. Example $Au(CN)_2$, which is encountered in mining as a soluble form of gold. Most drugs based on gold are Au(I) derivatives. However, gold (III) (known as auric) is a common oxidation state and is illustrated by gold (III) chloride, $AuCl_3$. It is derivative is chloroauric acid, HAuCl4, which form when gold dissolves in aqua regia. Au(III) complexes, like other d8 compounds, are typically square planner.

Less common oxidation states of gold are Au(-1), Au(II), and Au(V).Compounds containing Au- anion are called aurides. Considerable interest has been shown in the Au^{-1} oxidation state.[10] Gold dissolves in solution of the heavier alkali metals in liquid ammonia[11].Caesium aurides, CsAu that crystallizes in the caesium chloride motif. Gold (II) compounds are usually diamagnetic with Au-Au bonds such as $[Au(CH_2)_2P(C_6H_5)_2]_2Cl_2$. A noteworthy, legitimate Au(II) complex contains xenon as a ligand, $[AuXe](Sb_2F_{11})_2$.[11]. Gold pentaflouride is the sole example of Au(V), the highest verified oxidation state [12].

1.8 Gold Catalysis

Gold was generally considered to be non-reactive and to be least useful of the noble metals for catalytic purposes. Bulk gold surfaces do not chemisorb many molecules easily. The catalysis by gold has become the most rapid hot topic in chemistry, a

number of publications and patents' related in this area has never ceased to increase, with new discovery being made almost every week.

The low chemical activity of gold is due to the filled 5d shell and the relatively high value of its first ionisation potential, with the result that gold films hardly chemisorbs any gas. Due to its nobleness, it has always been regarded as unsuitable for heterogeneous catalysis, apart from a few isolated reports. [13, 14] However, the advent of nanoparticles gold, gold on high surface area oxide supports has demonstrated its high catalytic activity in many chemical reactions. Gold is active as heterogeneous catalyst in both gas and liquid phase, and complexes catalyse reaction homogeneously in solution. Gold catalysts have been found to be suitable for low temperature application, [14] with many reactions studied leading to many new application areas in pollution control, chemical processing, sensors and fuel cell technology. One of the most promissory catalytic application of gold which received more attention in the literature, Haruta Masatake was the first to report CO oxidation at ambient temperatures (-70°C).

The mixed oxides of Mn and Cu has been used for CO oxidation for long but are found to be less active than gold catalyst because of they are inactive at low temperature, not water tolerant and are prone to deactivation [15]. However, it has been accepted that any practical application of a catalyst will require a reliable method of manufacture, long-term stability, good response to operating conditions and more information on the kinetics and mechanism of the reaction.

It was demonstrated that gold is better than conventional Pd and Pt Catalysts and that the way gold acts catalytically is substantially different from the Pt group. It is now known that gold may catalyse a wide variety of reactions under comparatively mild conditions. Nowadays gold catalysis has been receiving increasing attention from many research groups around the world and Thompson and Bond [13, 16] have recently reviewed the subject. This relatively new field of gold catalysis has very promising applications.

Gold catalysts are more active than the platinum catalysts in terms of CO removal for fuel cell application, because of their ability to oxidize CO selectivity at high rates at temperatures corresponding to the operating temperature of the hydrogen fuel cell, without loss of large quantities of hydrogen.

There are a number of literatures on gold catalysed oxidation of CO. [17-24] The main applications of gold catalysts for low temperature CO oxidation are; in fuel cell

(selective CO oxidation in H_2 stream), in which CO content are being remove from the H_2 feed which otherwise will poison the Pt catalyst downstream.[25] Other include Car exhaust gas purification systems, [26] as air purification systems such as in the domestic application as currently used in Japanese toilets for odour reduction.[27]. It also used for on long space travels and as petroleum heaters; it has demonstrated industrial potential as well as for mining and coal industries as being used as a mask for CO, and used as in whether monitoring as a CO_2 laser whereby the CO produced as a by products decrease the efficiency of the CO_2 laser.

Other reactions catalysed by gold apart from CO oxidation include:

(i) Reactions of environmental importance, these comprised catalytic treatment of vehicle exhaust ,[28-30] such as reducing the problem of nitrogen oxides,[31, 32] selective reduction of nitrogen oxides with propene,[33-37] reduction of nitrogen oxides with carbon monoxide,[33, 38-41] reduction of nitrogen oxides by hydrogen,[41,42] removal of nitrous oxide,[42] others are: photocatalytic H_2 production, [43, 44] photocatalytic wastewater treatment, [45,46] decomposition of halogen compound, [47] Ozone and CO simultaneous elimination, [48] and Dioxin decomposition .[49]

(ii) Major chemical industry include water gas shift reaction ($CO + H_2O \rightarrow H_2 + H_2O$).[50,51] Propene epoxidation with H_2 and O_2, [52] CO hydrogenation, [53] hydrochlorination ethyne to vinyl chloride, alcohols conversion to aldehydes and ketones,[54] ethylene glycol oxidation to glycolic acid,[55] n-hexane isomerisation, [56] Methyl cylopentane reaction, [57] photocatalytic oxidation of sulphur, [58] Methanol synthesis from CO_2 and H_2, [59] Methane oxidation, [60] stream reforming. [61]

(iii) Commercial applications which include chemical processing such as vinyl acetate synthesis and vinyl chloride, production of Nylon precursors, methyl glycolate, selective oxidation of sugars, propene oxide, hydrogen peroxide, hydrotreating distillers, selective hydrogenation etc. others are pollution and emission control technologies such as air cleaning, Autocatalysts, catalytic wet air oxidation etc.

(iv) Homogeneous catalysis; this include chlorination of naphthalene to octachloronaphthalene, [62,63] oxidative carbonylation of amines to formamide, [62] others are oxidation of liquid phase, [64, 65] hydration of

phenylaceylene, [53] synthesis of biphenyls and furfuryl-substituted arenes, [66] and carbonylation of olefins. [62]

1.9 Preparation of gold catalysts

There are many different methods of preparation of gold catalyst. In each method, it has been found that the activity of the gold depend s on the small sizes of gold (2-5nm in diameter size) and interaction between the gold and metal support. The activity of the gold catalyst has been depends on the method of the preparation and the choice of the supports. It was found that it is difficult to deposit nanogold on metal oxides supports by impregnation methods due to low melting point and low affinity to metal oxides than Pt and Pd. Another reason is that during calcinations of crystallites, which are dispersed on the support surfaces, the chloride ion markedly enhances the coagulation of gold particles. Thus, methods of preparation of gold catalyst play a role on the activity of highly dispersed gold catalyst. However, from the literature, several methods of preparation of gold over supported oxides have been mentioned such as impregnation (IM), deposition precipitation (DP), coprecipitation (CP), colloidal method (CL), and vapour deposition (VD) which proved to deposit nanogold on metal oxide supports effectively. However, in this work, IM and DP were used.

1.9.1 Impregnation Method (IM)

This method is the first supported gold catalyst prepared. [67, 68] It is the simplest and less cost method that can be used with any support. In this method, a metal oxides support is impregnated with an aqueous solution of gold precursor and dried at a certain temperature. The method is said to be 'incipient wetness' (IW) if the volume of solution of gold precursor is enough to fill the pores. Chloroauric acid, [68-71] gold chloride [72] and sometimes ethylenediamine complex, [71, 73] has been used as a gold precursor. Several metal oxide supports have been used as a precursor, the first metal oxides supports used are silica, alumina and magnesia but of recent, other supports used are TiO_2 and ferric oxide.

One of the disadvantage of this method, it leads to the large gold particles (10-35nm) even for low gold loading (1-2wt %), and to catalyst sometimes with poor activity. Other disadvantages are low interaction between metal and support [74] and presence of chlorine, which was considered as poison and promotes mobility and

agglomeration of gold species during thermal treatment[75], [76, 77]. The chlorine remained in the catalyst even if after calcination to 873K[78]. However, reduction in hydrogen was found to remove it as HCl.[75]

1.9.2 Deposition-precipitation Method (DP)

This has been widely used for preparing gold supported catalyst having small sizes. It is commonly called DP because the metal oxides are precipitated as metal hydroxide [47, 79]. In this method, metal oxide support is dispersed in the aqueous solution of the gold precursor. The pH of the suspension is raised to a fixed value, usually 7, or 8, by adding Na_2CO_3 or NaOH solution in order for gold to be precipitated on to the support. The suspension and the precipitated solution is however, supposed to be heated at 343 or 353K with constant stirring for 1-2 hours, but due to little modification in this work, the suspension was not heated. It is however difficult to precipitate all gold from the solution and it is likely some gold is lost. After thorough washing with water to remove the sodium and chlorine as possible, the catalyst (product) is dried at 100-120°Cand some may require calcination in air at higher temperature.

The advantage of this method, it has numerous variations such pH, temperature of preparation and washing etc etc, [80, 81] others are uses of other bases such as ammonia etc.[82] Higher loading of gold has been reported by employing urea as a precipitating agent. This modification leads to 100% deposition of gold in solution. [83]

The deposition precipitation works well with supports having an isoelectric point greater than 5, such as magnesia, titania, alumina, zirconia and ceria. [75, 82]. The method is not suitable for silica, silica-alumina. tungsta, with isoelectric point of 2, 1, 1 respectively.[75]

1.9.3 Other conventional preparation methods

(i) Co-precipitation methods (CP)

This is another way in which small gold particles are dispersed over various metal oxides. The first co-precipitation method catalysts were obtained since 1987.[84, 85] This method involved addition of sodium carbonate to aqueous solution of the precursor and nitrate of the metal that will lead to the support. Example, preparation of

Au/Fe_2O_3 by co-precipitation (involved addition of Na_2CO_3 to aqueous solution of $HAuCl_4$ and $Fe(NO_3)_2$). The co- precipitates were washed, dried and calcined in air; the method is easy to carry out, but can cause some gold particles to be buried in the bulk of the support.[87] The characteristic of the catalysts prepared by this method have been reported[86]. However, the method is reported to work for certain metal oxides.

(ii) Chemical vapour deposition (CVD)

This method involve the use of volatile organic gold compound which reacts with the surface of a support, on which it decomposes to zero- valent particles of gold. Dimethylgold acetylacetonate ($Me_2Au(acac)$) was found suitable for this purpose. The catalyst prepared is then calcined and gave small particles of gold and the organic compound was removed on calcination. However, the chlorine contamination was avoided. [88,89]

(iii) Colloidal gold method (CL)

This method involved the use of gold colloids and metal oxide supports. It involved dipping of the metal oxide supports in the suspension of gold colloid, followed by washing and drying. The catalyst prepared in this method depends on the nature and concentration of the stabilizer, the stabilizer/ gold ratio and the nature of the support. It was found that polyvinyl alcohol is a good stabilizer for depositing gold on carbon and not suitable for silica or alumina. [90] The catalysts prepared by this method have found to have an average size (diameter 2nm).[91] Hayashi used this method and prepared Au/TiO_2 and Au/ZrO_2 catalysts. [92]

(iii) Cation exchange and adsorption method (CE)

This method has been used to prepare gold catalysts by cation exchange of zeolites or cation adsorption on metal oxide supports. It is easy to synthesised complex of chloride counter ions using this method[93]. This method is the most efficient way of introducing highly dispersed metal particles on zeloites. A good zeloites gold containing catalyst has been prepared with gold particles within 1-4nm in size. [94,95] The method has been used to deposit gold onto oxides supports, example Au/TiO_2 catalyst has been prepared with particle size 2.5nm after calcination at 573K.[96] The catalyst prepared by this method must be performed at room temperature as the cation decomposes above 333K.

1.9.4 Other less conventional preparation methods

There are number of methods which are less conventional and include the followings: Photochemical deposition; [97-100] Spray technique; [101] Sol gel;[102, 103, 89] sonochemical technique; [104] Low energy cluster or atom beam deposition; [105] solvent metal atom dispersion or impregnation (SMAD or SMAI); [106] pulse laser deposition [107]; dip-coating or liquid- phase grafting [59]; Co-sputtering [108]. Solution combustion method [109]; Arc-Melting [110]etc etc.

1.9.5 Promoters and poisons

(i) promoters and additives

Promoters are substances which, when added to a catalyst as minor component, improve one or more properties of the material with respect to product formation. The promoters in most cases are alkali metal and most often K^+. Several authors have extensively studied the role of the promoters in the gold catalyst preparation for CO oxidation. Zhang et al shows the role of Na^+ in preventing carbonates build-up and sintering, [111] while Wan and Kang[112] indicates the used of Fe as a gold promoter. Others include Iwasawa et al.[113] show the presence of Na^+ helps in catalyst activity (as a promoter). Several metal oxides have also been used as additives such as MgO, which used as additive to improve the preparation of gold particle on Au/Al_2O_3, the selectivity and the activity improvement have also been observed on gold catalysts by adding MnO_x and FeO_x. The activity of the catalysts for CO oxidation decreased in the order: $Au/FeO_x/Al_2O_3$ > $Au/MnO_x/Al_2O_3$ > $Au/CoO_x/Al_2O_3$ > $Au/CuO_x/Al_2O_3$ > $Au/NiO_x/Al_2O_3$.[114] Addition of Mg citrate in gold catalyst preparation has also been reported. It acts a sticking agent for gold nanoparticles on the metal oxides supports and prevents it from coagulation and suppress the transition of amorphous TiO_2 to anatase above 460°C and the so- called 'earthquake effect'. However, no additives or promoters used in this work.

(ii) poisoning

Poisons are substances when added or present in the catalyst reduces the performance of the catalysts by reducing one or properties of the materials with respect to products formation. Poisons can be electronegative elements such as Cl, S, P and C. They tend to block the active site on the catalyst surface, thereby reducing the total number of centres of activity. It has been shown by researchers that Chlorine is poison. [113] Number of publications have proved that gold catalysts prepared by IM method are prone to chlorine poisoning.[115] Others have reported how and the level of chlorine present may affect the deactivation of the catalyst.[116] According to Haruta *et al*[49]. suggested that the presence of chlorides in the catalyst promotes coagulation of gold particles and the contamination of Cl^- and Na^+ depends on gold loadings. Bond *et al.*[117]; suggest that the presence of Cl^- from AuC_{l4} which adsorbs on basic sites, upon decomposition, $AuCl_4^-$ yield $4Cl^-$, which will poison four Lewis acid sites. However, Kung et al.[118] suggested that the presence of chlorides displaces the OH group and hence facilitate the agglomeration of the Au particles.[119] There are number of speculations, suggestion, but the presence of chlorine in any case in the catalyst preparation should be avoided, and as such, several methods of chorine removal have been developed.[51, 120, 121]

1.9.6 Activation and deactivation of gold catalyst

The activation and deactivation of the gold catalyst have relied solely on a number of factors and has been the subject of controversy and debate. Pre-treatment of the prepared catalyst under different condition is one of the main factors surrounding this controversy and have been extensively studied by numerous researchers. Many authors reported that oxidative- pre-treatment of the gold catalyst before testing at high temperature leads to the good activity, [49, 121] others reported that increase in the calcination temperature of gold catalyst changes the morphology of the gold from spherical to hemispherical,[88] which leads to high activity than former. Baiker et al.[91] also suggested that the catalyst is active when prepared by CL method and dried in air. However, according to Uematsu *et al.*[122] claimed that if the calcination temperature is high, it leads to high activity and dispersion of gold. They also claimed that increase in the temperature of calcination decrease of the size of gold particles due to interaction of gold/support.

Several others claimed that pre-treatment of the catalyst at middle range temperature is also beneficial for high activity of gold. Haruta suggested that, high performance of the Au/TiO_2 catalyst was observed when pre-treated the catalyst at intermediate temperature of 473K. [123] A mild calcination temperature was considered best (100-200°C) for an optimum Au^0/Au^{n+} ratio and suggested that dried sample was rather inactive. [119] According Zhang *et al.* [111] suggested that the stability of the Au/ZnO catalyst prepared by CP increase in the order: 240 °C > 300 °C > 180 °C > 140 °C >> 50 °C. However, Wang et al suggested that optimum calcination temperature for a Au/ZnO catalyst is 300°C. [124] Others claimed that high activity was observed when calcined the catalyst at 200°C.[125]

The last but not the least, suggested that pre-treatment of the prepared gold catalyst under low temperature resulted on high activity gold catalyst.[91,116, 126] Bond et al.[86], suggested that calcination at high or moderate temperature of the reactant mixtures leads to the following reduction with CO: $Au^{n+} \rightarrow Au^{+} \rightarrow Au^{0}$. Studies of the Au/TiO_2 catalyst with XRD and TEM show that gold particles size increase with the temperature and decrease of the gold particles size was observed at low temperature. Calcination and the performance of the catalyst was also found to be the best.[127] At low temperature, the melting point of gold (1063°C) is lowered to about 300°C for gold particles with a diameter of 2nm due to the lowering of the coordination number of metal atoms.[128.]

Studies have also shown that pre-treatment of the catalyst in low temperature reduction followed by calcination resulted in significant activity of the gold catalyst.[129]. The idea of using hydrogen reduction is often to remove Chloride.[116] The pre-treatment in hydrogen or CO/O_2 mixture at 200°C is better than pre-oxidation due to reduction of Aun+ to $Au^{0.}$ [130.] Similarly, Au/Al_2O_3 sample was found to be deactivated when treated with oxygen, but the activity is recovered upon treatment in hydrogen to 573K.[131.]

In general, calcination may be beneficial and some time harmful or May leads to similar results. The pre-treatment of the catalyst has not much effect but depends heavily on the catalyst method of preparation. However, a lot has to be investigated on how the gold catalyst is activated or deactivated. In this work, high (400°C), and low (120°C) for pre-treatment will be studied for CO and alcohols.

1.10 Research objectives

This work will investigate the effect of catalyst preparation on CO oxidation and seek to understand the mechanism for the oxidation of methanol and higher alcohols over highly dispersed Au/TiO_2 catalysts prepared by deposition precipitation methods or incipient wetness impregnation. The results will be compared with other catalyst prepared over different metal oxide supports.

Chapter 1 deals with the general background of catalysis, some properties and uses of gold in catalysis and other reactions. Some methods for the preparation of gold supported catalysts will be discussed. Chapter 2 will include general methods for the experimental techniques involved. In chapter 3, a review of CO oxidation will be discussed and some parameters or factors affecting the CO oxidation over gold supported catalyst will be explored such as the kinetics, effect of moisture, presence of hydrogen and mechanistic investigation. The fourth chapter concerns with the oxidation of methanol over Au/ TiO_2 catalysts and other supported gold catalysts; similarly, some parameters such as pH, calcination effects, weight loadings gold etc will also be explored.

The fifth chapter investigates ethanol, propan-1-ol, and propan-2-ol oxidation over titania supported gold catalysts. The understanding and knowledge of the reactions involved will be used to propose mechanistic reactions in each case. Lastly, the sixth chapter will summarise the data and compare the objectives of the research.

1.11 References

1. M.Berzelius, Ann. Chim. Phys. (Paris), 61, 146 (1836).
2. Atkins and J. Paula, *Physical Chemistry,* seventh edition, 977-1003 (2002)
3. M.Bowker; *The Basis and Applications of Heterogeneous Catalysis*, oxford, (1998)
4. G. C Bond, *Hetrogeneous catalysis: Principles and Applications*, second edition, Clarendon Press- Oxford, pp 1-18
5. R. K.Grasselli and A. W.Sleight (Editors), *Structural Activity and Selectivity Relationships in Catalysis,* Royal Society of Chemistry and Contributors, (1982)
6. J. M. Thomas and W. J. Thomas, *Principles and Practice of Heterogeneous Catalysis,* VCH, Weinheim, (1997)

7. A. Clark, *The Theory of Adsorption and Catalysis*, Academic Press, New York, (1970)
8. Picture taken from website : http://www.goldsheetlinks.com/production.htmand http://www.marketwatch.com/news/story/story.aspx?guid=%7B8C528CE8%2D0262%2D485D%2DACEB%2D2247D18282CB%7D&siteid=rss
9. Picture taken from website : http://www.azmineral.com/minerals/gold_g104.shtml
10. Dan Plazak, *A Hole in the Ground with a Liar at the Top.* (salt Lake: Univ. of Utah Press, 2006)
11. S. Seidel, K. Seppelt, "*Xenon as a Complex Ligand*": The Tetra Xenono Gold (II) Cation in $AuXe_4^{2+}(Sb_2F_{11}^-)_2$". Science **290** (5489), 117-118 (2000)
12. S. Riedel, M. Kaupp, Revising the Highest Oxidation State of the 5d Elements: The case of Iridium (+VII)". *Angewandte Chemie* International Edition **45** (22), 3708- 3711 (2006)
13. D. W. Goodman, M. Valden, S. Pak and X. Lai, *Catalysis letters* **56,** 7 (1998)
14. M. Haruta, A. Ueda, S. Tsubota and R. M. Torres Sanchez, *Catalysis Today* **29,** 443 ((1996)
15. M. Haruta, T. Kobayshi, H. Sano and Y. N. *Chemistry Letters*, **405** (1987)43
16. M. Haruta, *Catal. Today,* **36,** 153 (1997)
17. D. L. Trimm, Appl. *Catal. A: Gen.* **296,** 1 (2005)
18. D. C ameron, R. Holliday and D. Thompson, *J. Power Sources* **118,** 298 (2003)
19. P. Landon, J. Ferguson, B. E. Solsona, S. Garcia, S. Al. Sayari, A. F. Carley, A. A. Herzing, C. J. Kiely, M. Makee, J. A. Moulijin, A. Overweg, S. E. Golunski and G. J. Hutchings, *J. Meter. Chem.* **15,** 1 (2005)
20. V. Plazak, J. Grache and R. J. Behm, Eur, *Fuel Cell News* **10 (2),** 8 (2003)
21. M. M. Schubert, A. Venugopal, M. J. Kahlich, V. Plazak and R. J. Behm, *J. Catal.*, **222,** 32 (2004)
22. A. W. Bone and R. V. Wheeler, Phil. *Trans.* **206A,** 1 (1906)
23. A. F. Benton and S. G. Podkozin, *J. Phys. Chem.* B **109,** 2262 (2005)
24. S. Naito and M. Tanimoto, J. Chem. Soc. *Chem.Commun.* 832 (1988)
25. CatGold New **6** (2004)

26. J. H. Marsh, A. N. Plazov, B. S. Grigorova, J. F. Greyling, K. Reddy and M. P. Letsoalo, *Catalyis Today*, **72,** 145 (2002)

27. M. Haruta, *Cattech*, **6,** 102 (2002)

28. G. C. Bond, Hetrogeneous Catalysis: *Principles and Applications,* 2nd edn. Oxford University Press, Oxford, p. 160, (1987)

29. J. M.Thomas and W. J. Thomas, *Principles and Practice of Hetrogeneous Catalysis,* VCH, Weinheim, p. 577 (1997)

30. E. S J. Lox and B. H. Engler in *Handbook of Hetrogeneous Catalysis*, G. Ertl, H. Knozinger and J. Weitkamp, (eds), VCH, Weinheim, **4,** 1559 (1997)

31. M. Bowker and R. W. Joyner, in Insights into *Speciality Inorganic Chemicals* D. T. Thompson, (ed.), Royal Society of Chemistry, Cambridge, UK, (1985)

32. P. Forzatti, *Appl. Catal. A*: Gen. **222,** 221 (2001)

33. A. Ueda and M. Haruta, *Gold Bull*, **32,** 3 (1999)

34. B. E. Nieuwenhuys, *Adv. Catal.* **44,** 259 (1999)

35. C. Mihut, C. Descorme, D. Dupez and M. D. Amiridis, *J. Catal.* **212,** 125 (2002)

36. E. Seker and E. Gulari, J. Cavataio, P. Lorpongpaiboon and S. Osuwan, *Appl. Catal.* A: Gen. **183,** 121 (1999)

37. A. Ueda, T. Oshima and M. Haruta, *Appl. Catal.* B: Env. **12,** 81 (1997)

38. N. W. Cant and P. W. Frederickson, *J. Catal.* **37,** 53 (1975)

39. T. P. Kobylinsky and B. W. Taylor, J.Catal. **33,** 376 (1974)

40. H. Murakami and Y. Fujitani, *Ind. Eng. Chem.* Prod. Res. Dev. **25,** 414 (1986)

41. J. M.Shwartz and L. D. Schmidt, *J. Catal.* **148,** 22 (1994)

42. S. A. C. Carabineiro, *PhD Thesis*, New University of Lisbon, (2000)

43. M. Haruta, *Catal. Survey of Japan,* **1,** 61 (1997)

44. K. Sayama and H. *Arakawa, Chemistry Letters* 253 (1992)

45. X. Z.Li and F. B. Li, *Appl. Catalysis* A: General, **228,** 15 (2002)

46. W. F. Maier, C. Lettmann and H. Hinrichs, *Angew. Chem. Int.* Ed. **40,**(17) 3160 (2001)

47. M. Haruta, *Catalysis Today,* **36,** 153 (1997)

48. Y. Liang, Z.-p. Hao, D. Cheng and Y. Guo, *Appl. Catalysis* B: Environmental , **33** (3) 217 (1997)

49. M. Haruta, *CatTech,* **6** (3) 102 (2002)

50. D. Andreeva, *Gold Bulletin*, **35**(3) 82 (2002)

51. M. Haruta, H. Sakurai, A. Ueda and T. Kobayashi, *Chem Commun.* 271 (1997)

52. M. Haruta, S. Tsubota, M. Okumura and B. S. Uphade, *Appl., Catalysis* A: General **190,** 43 (200)

53. H. Kimura. M. Shibata, N. Kawata and T. Masumoto, *Chemistry Letters,* 1605 (1985)

54. M. Rossi and S. Biella, *Chem. Commun.* 378 (2003)

55. H. Brendt, I. Pitish, S. Evert, K. Struve, M-M. Pohl, J. Radnik and A. Martin (2002)

56. A. Gomez-Cortes, A. Vazquez- Zavala and J. Garcia- Gomez, *Applied Surface Science,* **167,** 177 (2000)

57. J. Fraissard, G, Riahi, D. Guillemot, M. Polisset- Thfoin and A. A. Khodadadi, *Catal. Today,* **72,** 115 (2002)

58. E-I, Sato, Y. Matsumoto and Y. Ymaguchi, Bull. *Chem. Soc. Japan* , **58,** 1255 (1985)

59. M. Haruta and H. Sakurai, *Catalysis Today*, **29,** 361 (1996)

60. G. J. Hutchings, K. Blick, T. D. Mitrelias, J. S.J. Hargreaves, R. W. Joyner, C. J. Kiely and F. E. Wagner, *Catalysis Letters,* **50,** 211 (1998)

61. J. K. Norskov, I. Stensgaard, F. Besenbacher, I. Chorkendoff., B. S. Clausen, B. Hammer and A. M. *Molenbroek, Science*, **279,**1913 (1998)

62. Y. Souma, M. Fujiwara, Y. Imamura and Q. Xu, *J. Org. Chem.* **67,** 1594 (1997)

63. R. V. Parish, *Gold Bull.* **31,** 14 (1998)

64. M. Rossi, S. Biella, G. L. Castaglioni, C. Fumagalli, L. Prati and M. Rossi, *Catalysis Today,* **72,** 43 (2002)

65. F. Porta, L. Prati, M. Rossi and G. Scari, *J. Catalysis,* **211,** 464 (1989)

66. A. Stephen, K. Hashimi, T. M. Frost and J. W. Bats, *Catalysis Today,* **72,** 1 (2002)

67. G. C Bond and D. T. Thompson, *Catal Rev.-Sci. Eng.* **41,** 101 (2000)

68. P, A Sermon, G. C. Bond and P. B. Wells, *J. Chem. Soc, Faraday Trans,* I **75,** 385 (1979)

69. K. Blick, T. D. Miltrelias, J. S. J. Hargreaves, G. J. Hutchings, R. W. Joyner, C. J. Kiely and F. E. Wagner, *Catal. Lett.,* **75,** 385 (1998)

70. N. W. Cant and W. K. Hall, *J. Phys. Chem.,* **75,** 2914 (1971)

71. S. Galvagno and G. Parravano, *J. Catal.* **55,** 178 (1971)

72. S. D. Lin, M. Bollinger and M. A. Vannice, *Catal. Lett.* **17,** 245 (1993)

73. J. Y.Lee and J. Schwank, *J. Catal.* **102,** 207 (1986)

74. M. Che and C. O Bennett, *Advances in Catalysis* , **36,** 55 (1989)

75. M. Haruta, *Cattech.* **6,** 102 (2002)

76. H. H. Kung, M. C. Kung and C. K. Costello, *J. Catal.* **216,** 425 (2003)

77. H. S. Oh, J. H. Yang, C. K Costello, Y. M. Wang, S. R. Bare, H. H. Kung and M. C. Kung, *J. Catal.* **210,** 375 (2002)

78. Report of the Osaka National Research Institute, **393** (2003)

79. S. Tsubota, D. A. H. Cunningham, Y. Band o and M. Haruta, *Stud. Surf. Sci. Catal.*, **72,** 227 (1995)

80. S. –J. Lee and A. Gavriilidis, *J. Catal.* **306,** 305 (2002)

81. F. Mareau and G. C. Bond, *Appl. Catal.* A: Gen. **226,** 1 (2002)

82. A. Wolf and F. Schuth, M. Makkee and J. A. Moulijin, *Catal. Today* **72,** 59 (2002)

83. C. Loius, R. Zanella, S. Giogio, C. –H. Shin and C. R. Henry, *J. Catalysis,* **222,** 357 (2004)

84. M. Haruta, H. Kageyama, N. Kamijo, T. Kobayashi and F. Delannay, *Stud. Surf. Sci. Catal.* **44,** 33 (1988)

85. M. Haruta, T. Kobayashi, H. Sano and N. Yamada, *Chem., Lett.* **2,** 405 (1987)

86. R. D. Walters, J. J. Weimer and J. E. Smith, *Catal. Lett.*, **30,** 181 (1995)

87. R. M. Finch, N. A Hodge, G. J. Hutchings, A. Meagher, Q. A. Pankhurst, M. R. H. Siddiqui, F. E. Wagner and R. Whyman, *Phys. Chem. Chem. Phys.* **1,** 485 (1999)

88. M. Haruta et al., *Report of the research achievements of interdisciplinary basic research section (ONRI)- "The abilities and potential of God as a Ctalyst"* (1999)

89. P. Claus, S. Schimpf, M. Lucas, C. Mohr, U. Rodemerck, A. Bruckner, J. Bruckner and H. Hofmeiseter, *Catalysis Today,* **72,** 63 (2002)

90. F. Porta, L. Prati, M. Rossi, S. Coluccia and G. M atra, *Catal. Today,* **61,** 165 (2000)

91. A. Baiker, J. –D. Gruwaldt, C. Kiener and C. Wogerbauer, *J. Catalysis,* **181,** 223 (1999)

92. S. Hayashi, S. Deki and K. Sayo, *J. Colloid and Interface Chemistry,* **212** 597 (1999)

93. B. P. Block and J. J.C. Bailar, *J. Am. Chem. Soc.*, **73,** 4722 (1951)

94. D. Guillemot, V. Y. Boroskov, V. B. Kazansky, M. Polisset- Thofion and J. Fraissard, *J. Chem. Soc. Faraday Trans.* **93,** 3587 (1997)

95. D. Guillemot, M. Polisset- Thfoin and J. Fraissard, *Catal., Lett.,* **41,** 143 (1996)

96. R. Zanella, L. Delannoy and C. Loius, *Appl. Catal.* A: Gen. **291,** 62 (2005)

97. X. Z. Li nd F. B. Li, *Appl. Catalysis* A: General, **228,** 15 (2002)

98. M. Haruta, G.R. Bamwenda, S. Tsubota and T. Nakamura, J. *PhotoChem. Photobiol.* A: Chem. **89,** 177 (1995)

99. D. Li, J. T. McCann, M. Gratt and Y. Xia, *Chem. Phys. Lett.* **394,** 387 (2004)

100. S. C. Chan and M. A. Barteau, *Langmuir* **21,** 5588 (2005).

101. L. Fan, N. Ichikuni, S. Shimazu and T. Uematsu, *Appl. Catal.* A: Gen., **246,** 87 (2003)

102. Seker and E. Gulari, *Appl. Catal.*, A: Gen. **232,** 203 (2002)

103. J. Pietron, R. M. Stroud and D. R. Rollison, *Nano Lett*, **2,** 203 (2002)

104. A. Fasi, I. Palinko, J. W. Seo, Z. Konya, K. Hernadi and I. Klricsi, *Chem. Phys. Lett.* **372,** 848 (2003)

105.S. Arii, F. Mortin, A. J. Renouprez and J. L. Rousset, *J. Am. Chem. Soc.* **126,** 1199 (2004)

106. S,-H. Wu, X,-C. Zheng, S. –R. Wang, D. –Z. Han, W.-P. Huang and S.-M. Zhang, *Catal. Lett.* **96,** 49 (2004)

107. L. Guczi, D. Horvath, Z. Paszti and G. Peto, *Catalysis Today*, **72,** 101 (2002)

108. M. Haruta, *Catal. Surveys of Japan* **1,** 61 (1997)

109.M. S Hedge and P. Bera, *Catalysis Letters*, **79,** 75 (2002)

110. H. Kimura, M. Shibata, N. Kawata and T. Masumoto, *Chemistry Letters,* 1605 (985)

111. W. X. Zhang, T. H. Wu, G. Y. Wang, H. L. Lian and D. Z. Jiang, *Appl. Catalysis* A: General **239,** 1 (2003)

112.B. –Z. Wan and Y. –M. Kang, *Catalysis Today,* **26,** 59 (1995)

113.Y. I wasawa, Y. Yuan, A. P. Kozlova, K. Asakura, H. Wan and K. Tsai, *J. Catalysis,* **170,** 191 (1997)

114.Z. Hao, D. Wang, D. Cheng, X. Shi and C. Hu, *Journal of Molecular Catalysis* A: Chemical, **200,** 229 (2003)

115. B. –Z. Wan, and J. –N. Lin, *Appl. Catalysis B.* Environmental **41,** 83 (2003)

116.S. Authors in EuroCat- Symposium 19- *"Catalysis by Silver and Gold"*. Limerick, (2001)

117.G. C. Bond, P. A. Sermon and P. B Wells, *J. Chem. Soc.* Faraday Trans. I, **74,** 385 (1978)

118.J. H Marsh, A. N. Palazov, B. S. Grigorova, J. F. Greyling, K. Reddy and M. P. Letsoalo, *Catalysis Today*, **72,** 145 (2002)

119.H. H. Kung, C. K. Costello, M. C. Kung, H. –S. oh and Y. Wang, *Appl. Catalysis* A: General, **232,** 159 (2002)

120. M. Flytzani- Stephanopoulos, Q. Fu and H. Saltsburg, *Science,* **301,** 935 (2003)

121. A. K. Triphati and N. M. Gupta, *Gold Bulletin,* **34** (4), 120 (2001)

122. T. Uematsu, L. Fan, N. I chkuni and S. Shimazu, *Appl. Catalysis* A: General, **246,** 8 (2003)

123. M. Haruta, F. Boccuzzi, M. Date, Y. Ichihashi, T. Yamashita and A. Chiorino, *Catalysis Today,* **72,** 89 (2002)

124. X. Wang, J. Zhang, Y. Wang, B. Chen, C. Li and D. Wu, *Energy Conversion and Management*, **44,** 1805 (2003)

125.F. Schuth and A. Wolf, *Appl. Catalysis A*: General, **226,** 1-13 (2003)

126.S. D. Lim, M. –Y. Lee and Y. –S. Su, *Catalysis Letters*, **57,** 49 (1999)

127.S. –H. Wu, X. –C. Zheng, S. –R. Wang, D. –Z. Han, W.-P. Huang and S, -M. Zhang, *Catalysis Letters,* **96,(1-2)** 49 (2004)

128.J. –P. Borel and P. Buffat, *Physical Review* A, **13**(6) 2287 (1976)

129.D. W. Goodman, T. V. Choudhary, C. Sivadinarayana, C. C. Chusuei, A. K. Datye and J. P. Fackler Jr., *J. Catalysis,* **207,** 247 (2002)

130.B. E. Nieuwenhuys, M. J. Lippits and M. A. P. Dekkers, *Catalysis Letters,* **56,** 195 (1998)

131.K. Domen, K. Tamaru, J. Jia and J. N. Kondo, *J. Phys. Chem.* B, **105,** 3017 (2001)

Chapter 2- Experimental

2.1 Introduction

In this chapter, the experimental methods and techniques used for the preparation, characterization and testing of the catalysts are described in detail. The first section of this chapter deals with the preparation of the catalytic materials that were used for activity and selectivity in the pulsed flow reactor. Characterisation of the materials was performed by X-Ray diffraction (XRD), Raman spectroscopy, X-Ray photoelectron spectroscopy (XPS), Diffuse reflectance infrared Fourier transmission spectroscopy (DRIFTS), Scanning electrons microscopy (SEM) collected for selected samples and BET surface area analysis.

2.2 General catalyst preparation

Many researchers have extensively studied different methods of gold catalyst preparation and the activity of the gold catalyst has been reported to be strongly depending on the method of preparation. In other words, the catalytic performance of the gold supported on metal oxides catalyst is highly sensitive to preparation procedure. Hence, in this study, two important methods for preparation of gold catalyst were used: deposition precipitation method (DP) and Impregnation (by incipient wetness) method (IW).

2.2.1 Support

It has been accepted that gold when highly dispersed over supports such as TiO_2 shows unusual catalytic properties. Some of the reactions catalyzed by supported Au particles include CO oxidation at temperature as low as -78°C [1-4] and propylene epoxidation [5]. The catalytic activity of the gold catalysts strongly depends on the size and structure of the Au particles supported on oxides[6-7].

The metal oxide support used in this research was TiO_2 P-25 from Degussa, with a BET surface area of 50 m^2/g and an isoelectronic point of $3.5<pH<4.5$. Haruta et al.[2], have found that nano-size particles of gold deposited on TiO_2 P-25 can exhibit surprisingly high catalytic activity and studied this support and they found that it is composed of anatase + rutile in separate phases at a ratio of anatase/rutile = ~3.. However, other supports used in these studies, include γ-Al_2O_3 and SiO_2 with isoelectronic point (IEP). Extensive literature, have reported the activity of such catalysts, example, for γ-Al_2O_3, [8-10] and SiO_2.[11]

2.2.2 Deposition Precipitation

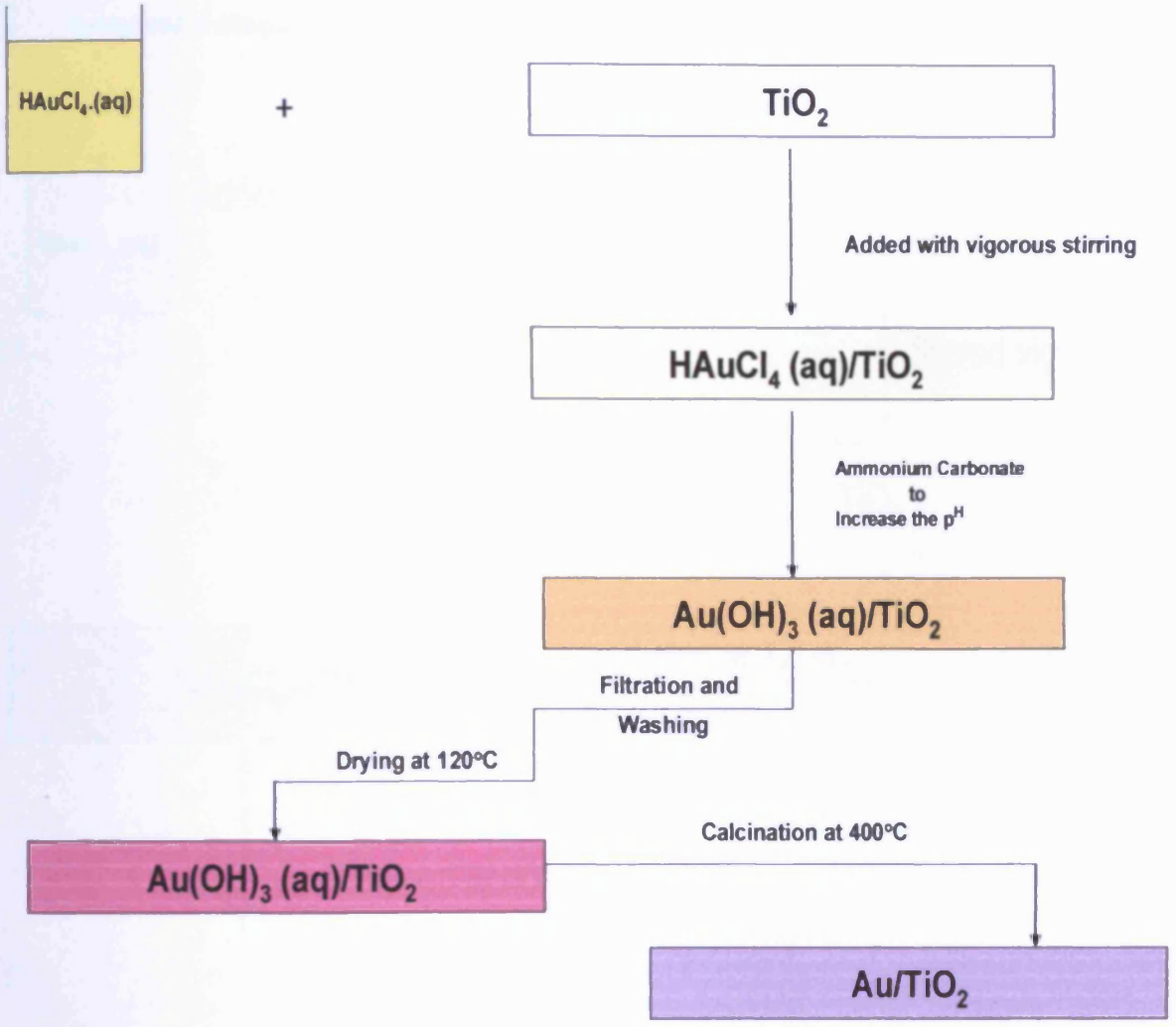

Figure 2-1: Deposition precipitation method (DP)

In this method, the TiO_2 (Degussa) was added to an aqueous solution of $HAuCl_4.3H_2O$ with vigorous stirring and the pH of the suspension was adjusted to 8 by addition of 0.1M Na_2CO_3. The mixture was aged with continued stirring for 2 hours. The precipitate produced as a result of deposition of gold hydroxide on the surface of metal oxide support was filtered and washed carefully with deionised water until all the chloride ions were removed. The sample was dried overnight in air at ambient temperature and dried again for two hours and ground using a pestle and mortar. The catalyst sample was pressed in to a disc, crushed and then sieved between 850μm and 600μm particle aggregate size.

2.2.3 Impregnation Method (IM)

Incipient wetness Method (IW)

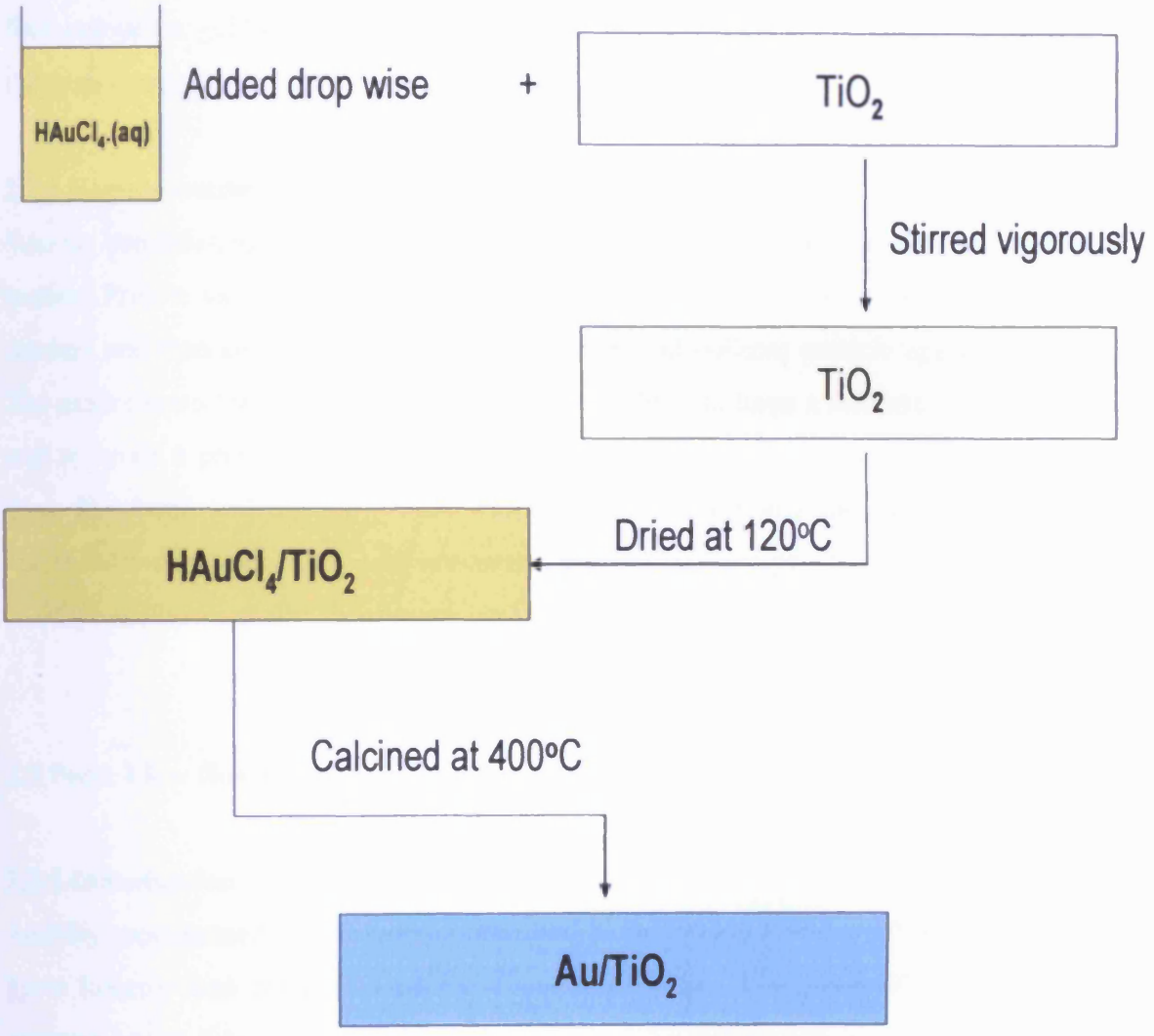

Figure 2-2: Incipient wetness method (IW)

In the incipient wetness method (IW) of impregnation, the pores of titania (TiO_2 (Degussa, treated in air at 500°C for 2h) were impregnated with a suitable volume of an aqueous solution of $HAuCl_4$ (0.705 ml/gcat in this case) until incipient wetness was achieved. The sample was dried in air for two hours and ground using a pestle and mortar. The catalyst sample was passed in to a disc, crushed and then sieved between

850μm and 600μm particle aggregate size. However, calcination at 400°C may be required especially for the high loading catalyst.

The final colour of the catalyst prepared by either deposition precipitation (DP) or incipient wetness impregnation (IW) depends on the type of support. For example, the final colour for gold on γ–Al_2O_3 is blue, while gold on SiO_2 is magenta both IW and DP respectively.

2.2.4 Sample conditioning

Sample conditioning is very important unless otherwise stated in the preparation section. Prior to use the catalyst in the reactor, 0.5-1g was ground, pressed in to a disc, crushed and then sieved to pass between 850mm and 600mm particle aggregate size. The main reason for the conditioning of the sample is to have a uniform particle size and to avoid a pressure drop across the catalyst bed, which might obstruct the gas flow. Similarly, a change in colour was observed on pressing the catalyst, which is due to increasing mixing of gold precursor, and the metal supports, which also results in different chemical and absorbency properties.

2.3 Pulse Flow Reactor

2.3.1 Introduction

Activity measurements were carried out using a Pulse Flow Reactor (PFR). The Pulse Flow Reactor was designed and constructed in house. A number of people in the research group have used the reactor in the past for different areas of research. For example, the reactor has been used by the past group members for CO oxidation over gold nanoparticles on a TiO_2 support, propene oxidation and ammoxidation, and it has also been used for NO_x reduction and storage catalysts.[12-14]

The reactor is similar to the conversional tap reactor, and it provides good kinetic and mechanistic data for catalytic reactions and allows us to test the catalyst for commercial and industrial importance.

Figure 2-3 shows the schematic diagram of the pulse flow reactor used while figures 2-4 and 2-5 show the photograph of some of components of the reactor.

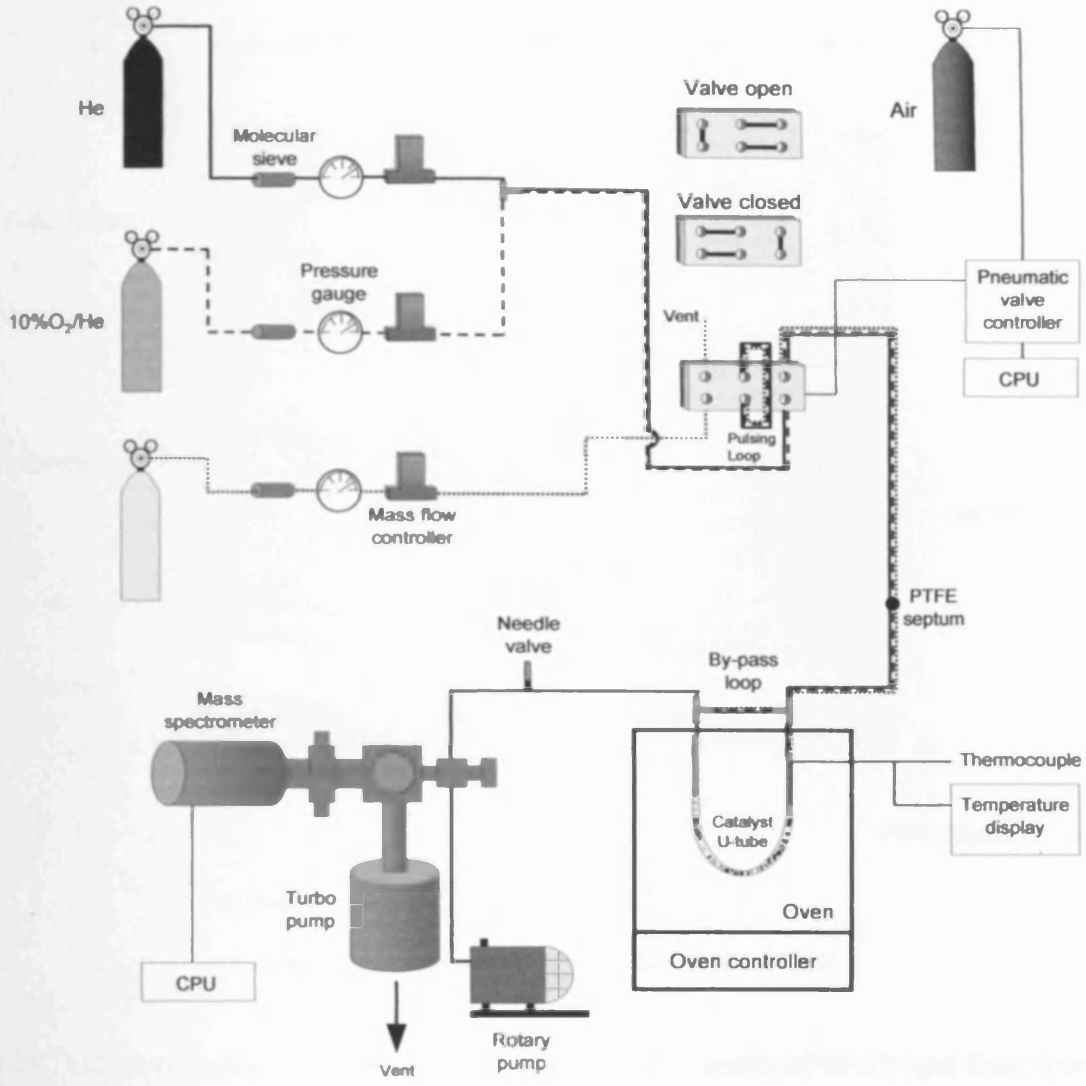

Figure 2-3: Schematic diagram of pulse flow reactor

The micro pulse flow reactor consist of a Philips PU 4500 GC oven which can be held at constant temperature or regulated at ramp between two temperatures at a specified rate. The oven consist of a stainless steel U tube (1/4" outside diameter, 0.065" thickness) held vertically containing catalyst (usually 0.5g) between the quartz wool. Two gases can pass over the catalyst bed, for example, helium, the carrier gas and O_2 (dosing gas) can mix over the catalyst bed by a means of T-piece. The two mixed gases can also react with other gases, such as CO by means of a pulsing valve, which is controlled by computer and allows the user to set the time of pulsing of the gas. However, liquids such as alcohols can mix with two gases if injected via septum periodically or continuously through Razel A-99 motorised syringe pump.

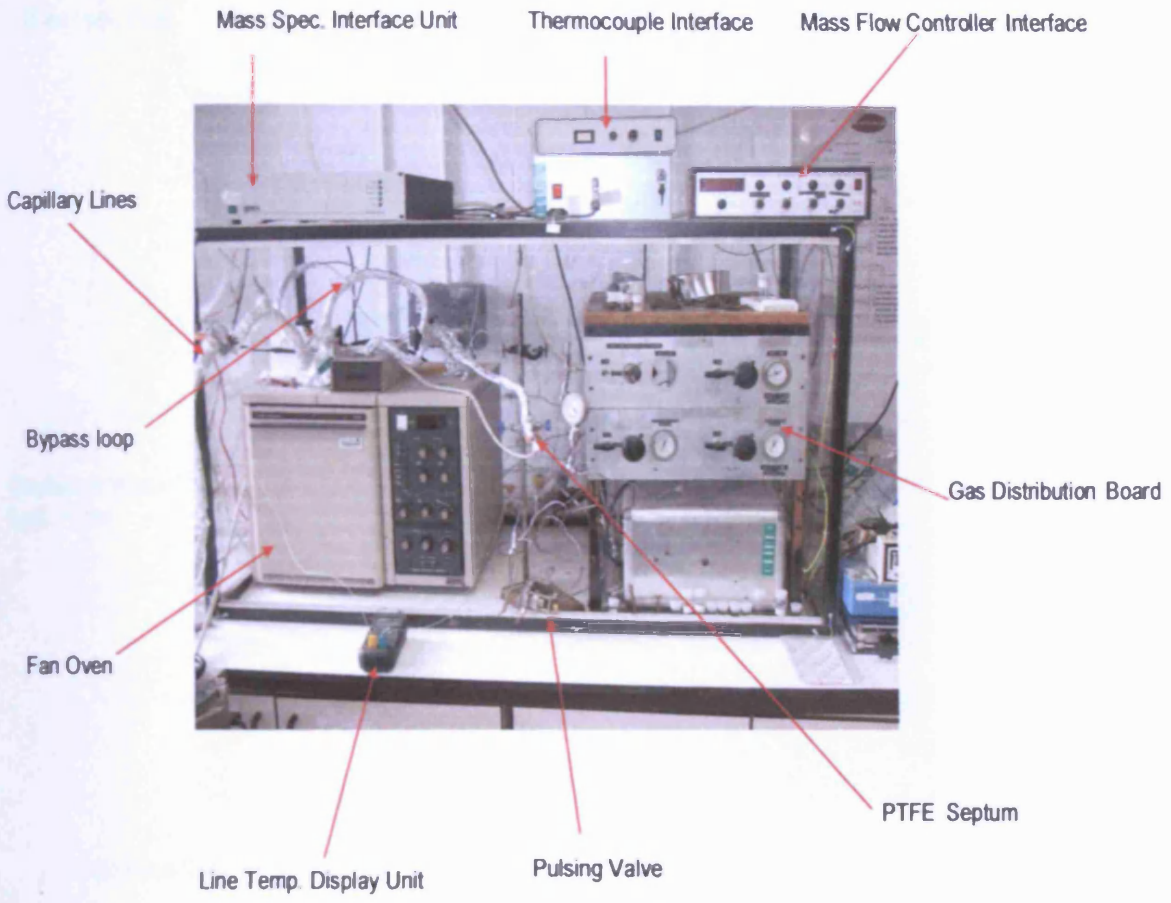

Figure 2-4: Photograph of pulse flow micro reactor

BOC Ltd supplies the gases used by the reactor with a purity of 99.5% and these gases were allowed to pass through Puritubes supplied by Phase Separation Ltd, which are filled with 5 Å molecular sieves, which allows removal of water and CO_2. The flow of the gases were controlled by mass flow controllers (Brookes 5850TR) which allows flow rate of the gases to flow within 0.1cm^3 min^{-1} and are usually calibrated using the bubble flow meter.

When the gases are mixed and reacted over the catalyst, the products flow down through the capillary tube (usually heated and depends on the type of experiment) which is controlled by a needle valve. A Leybold Heraeus Trivac rotary pump mostly vents the gases flown into the capillary tube, allowing a small fraction of it to pass through a UHV chamber containing the mass spectrometer (figure 2-5) and supported by high vacuum chamber pumped with the help of Leybold 151 turbo molecular pump assisted by an Edward 5 rotary pump.

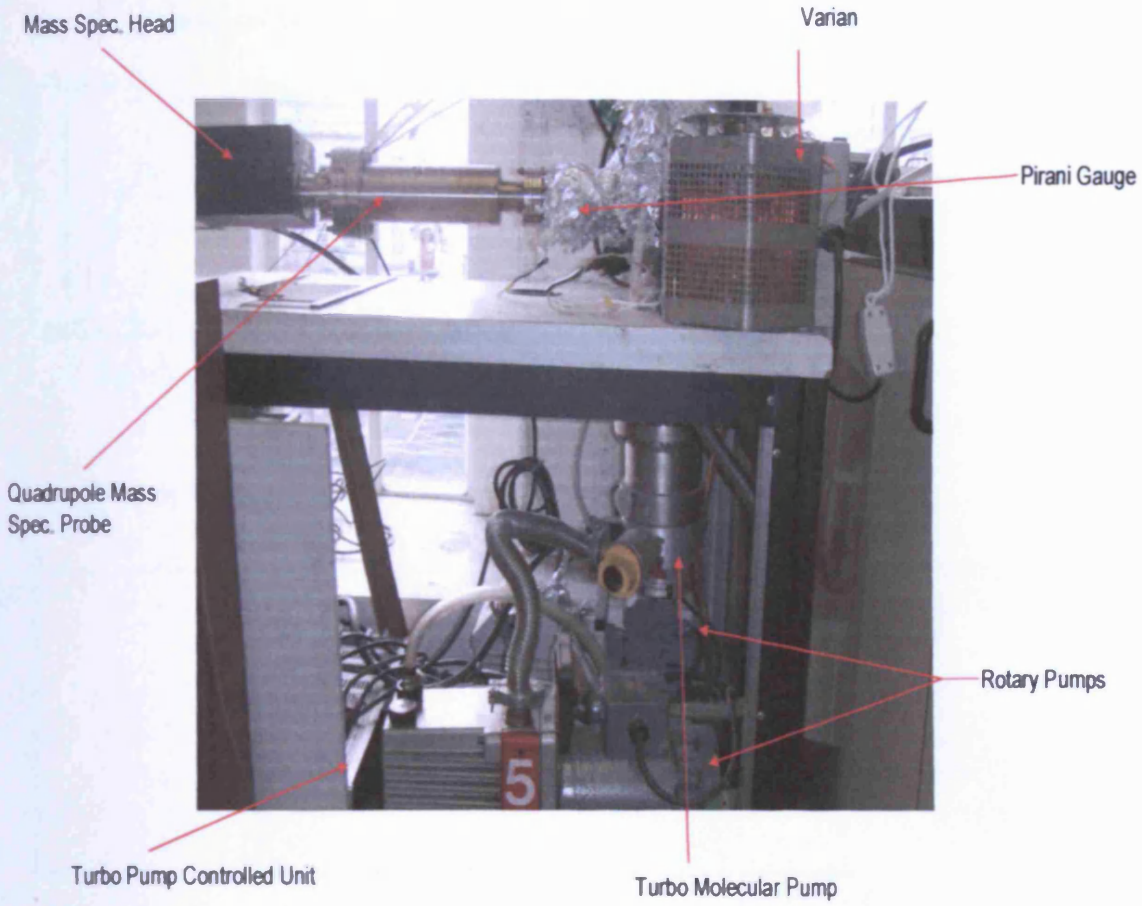

Figure 2-5: photograph of mass spectrometer components of pulse flow reactor

The output of the reaction is monitored by computer controlled Quadrupole HAL 201 mass spectrometer constructed by Hiden Analytical and allows the results to be displayed on the computer. The thermocouple inserted in the catalyst bed allows also measuring the temperature accurately and displaying on the computer. Nevertheless, the bypass injections or pulsing allows understanding the cracking patterns of the reactants or the 100% signal of unreacted / converted of the reactants.

2.3.2 Mode of operation of Pulse Flow Reactor

The pulse flow reactor can operate in three main modes (figure 2-6). In the first mode of operation, it indicates that gases can be injected or pulsed at a particular time until the breakthrough of the gas was observed (gas out), in which case an uptake can be measured. When allowed to stabilised and later heated, desorption of the products will be observed. Hence, temperature programmed desorption (TPD) may be carried and the uptake can be measured.

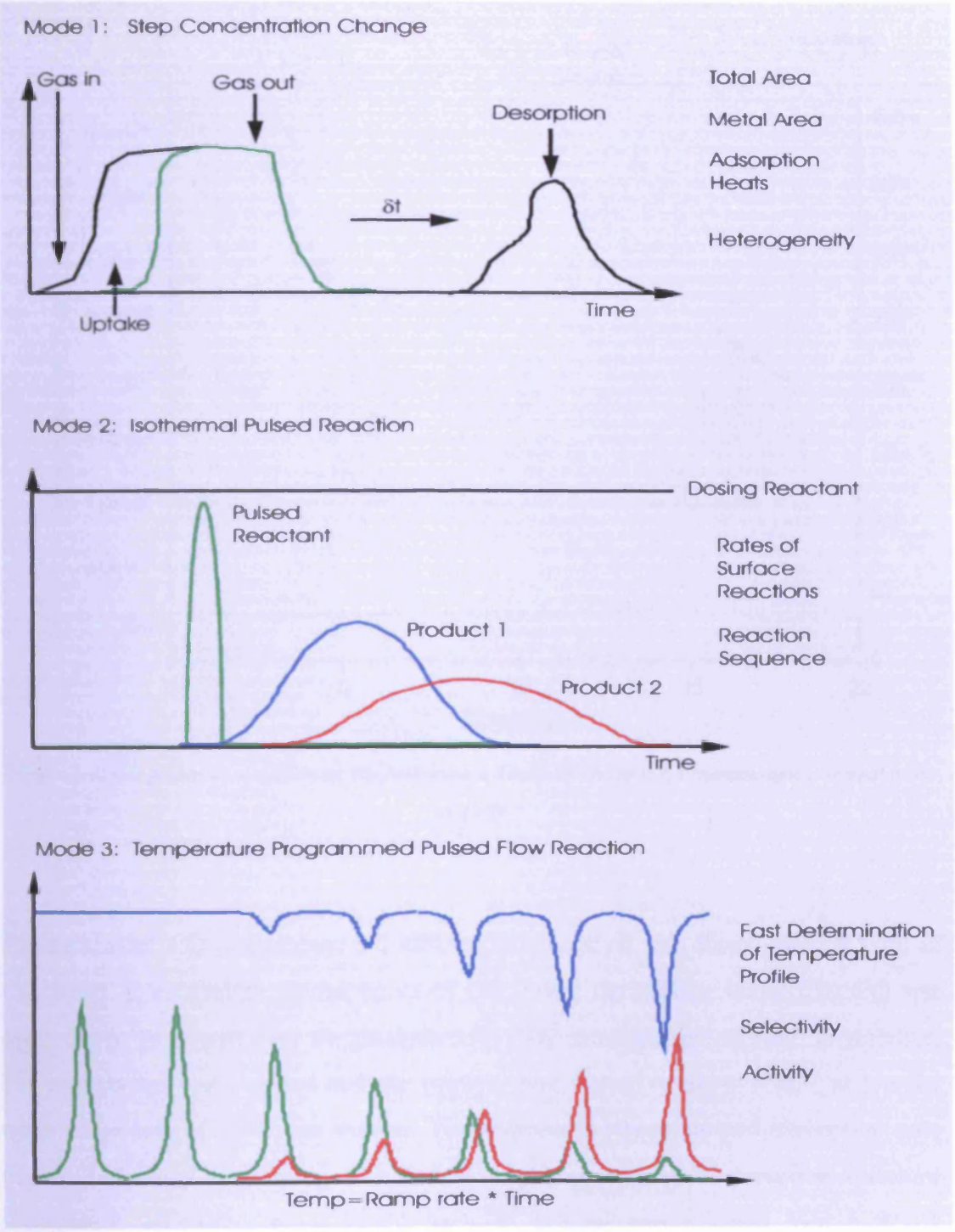

Figure 2-6: Modes of operation of pulse flow reactor

An example of the raw data obtained from this mode of operation for CO pulsed over 1wt% Au/TiO_2 catalyst (usually 0.53ml at 1-minute interval), the uptake of CO until breakthrough will be obtained as shown in figure 2-7.

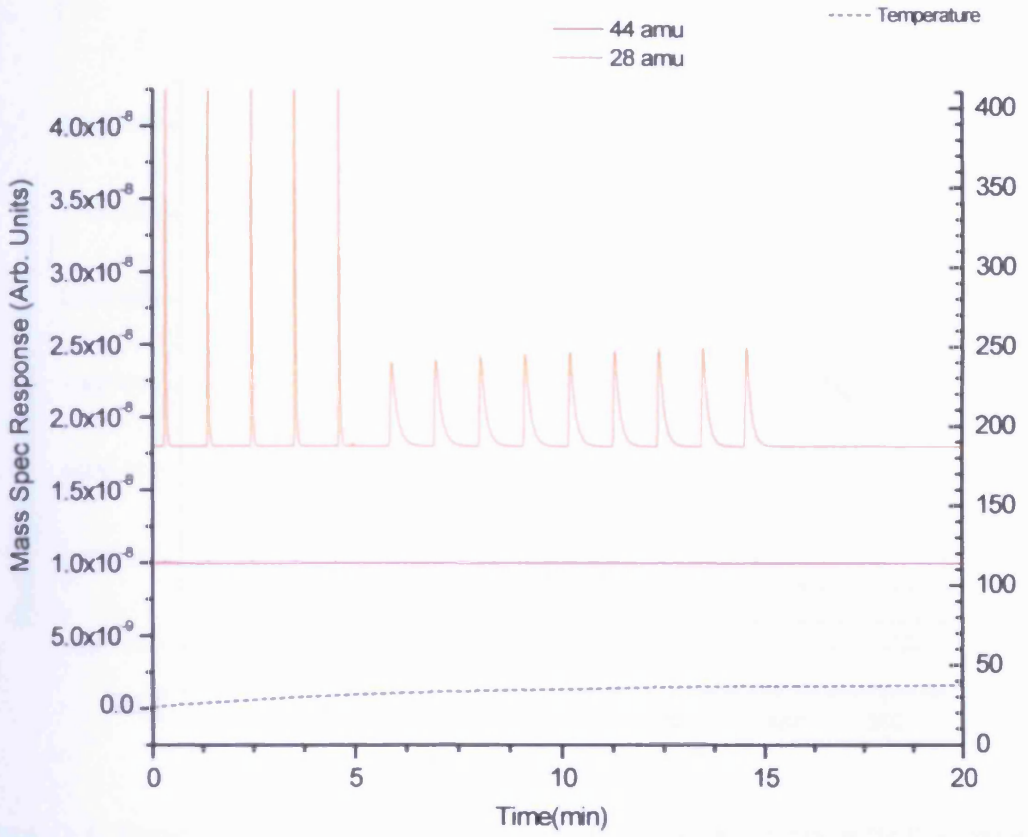

Figure 2-7: CO pulses in a stream of He flow over a 1wt%Au catalyst for uptake measurement prior to TPD

The uptake for CO pulses over a 1wt%Au/TiO_2 catalyst was found to be 0.53ml of CO, which is equivalent to one pulse of CO, using the pulsing valve. The CO was continued to be pulsed over the catalyst until fully saturated and allowed to stabilize. The experiment was stopped and the catalyst was heated to about 400°C at a usual temperature rate of 12°C per minute. The temperature-programmed desorption data (figure 2-8) show that water, CO and hydrogen were seen to desorb at different temperature. However, when liquid such as alcohol was injected over a 1%wt Au/TiO_2 catalyst (usually 1ml at 2 minutes intervals) until breakthrough, the uptake for methanol injections to breakthrough was found to be 7μl to saturate the surface (figure 2-9).

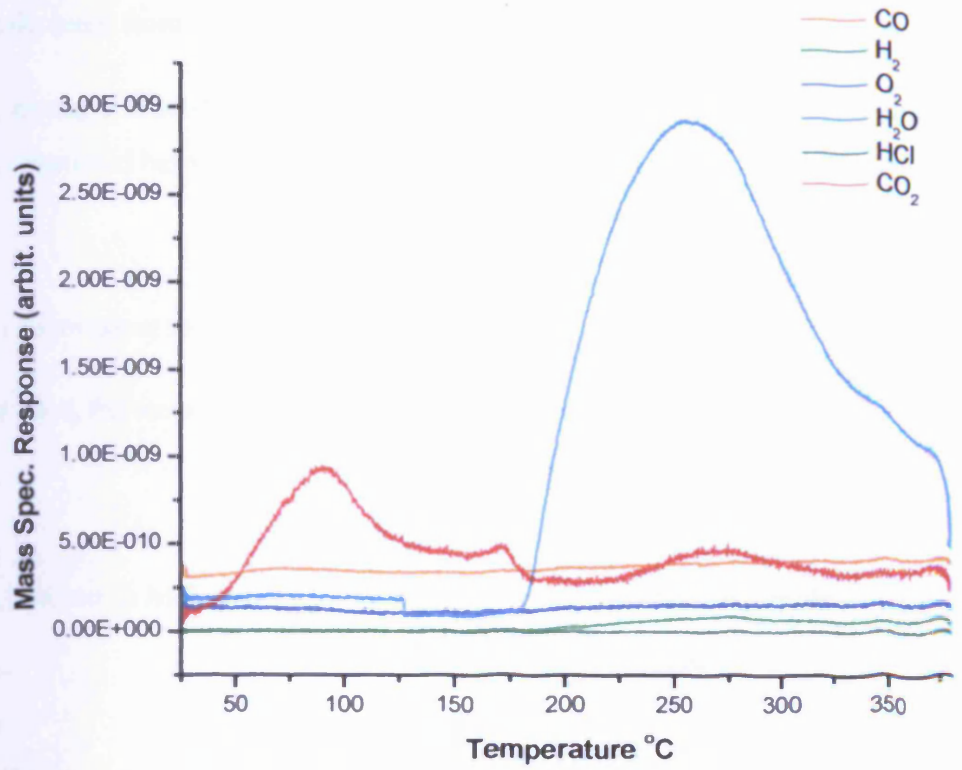

Figure 2-8: Temperature Programmed Desorption for CO pulses in a stream of He flow over a 1wt%Au/TiO_2 catalyst

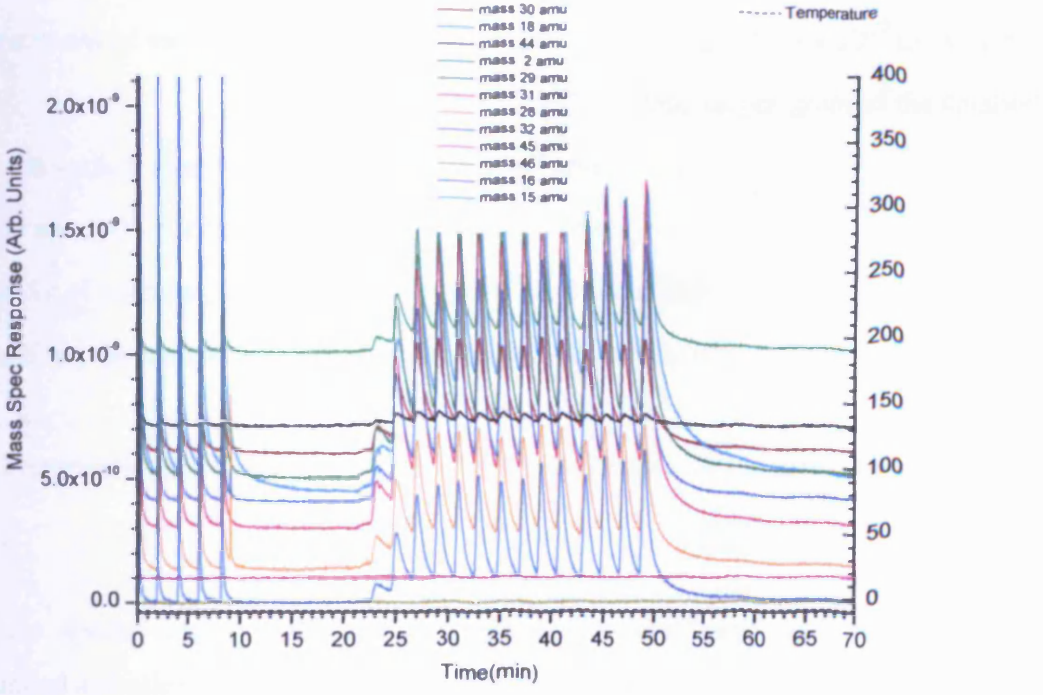

Figure 2-9: Methanol pulses in a stream of He flow over a 1wt%Au/ TiO_2 catalyst for uptake measurement prior to TPD

The amount of methanol and how many monolayers consumed before saturation can be calculated from the following:

For, example from the uptake of methanol, it was found that about 7μl of methanol was consumed before saturation.

7μl is equivalent to $7x10^{-3}cm^3$ of methanol.

Therefore, the mass of methanol = density x volume

$= 7 \times 10^{-3}cm^3 \times 0.8gm/cm^3$

$= 5.6 \times 10^{-3}gms$

But, amount in Moles = Mass in g/ Molar Mass in g/mole

$= 5.6 \times 10^{-3}gms / 32g/mole$

$= 1.75 \times 10^{-4}$ moles

Also, 1 Mole $= 6.022 \times 10^{23}$ molecules

Therefore: 1.75×10^{-4} moles $= 6 \times 10^{23} \times 1.75 \times 10^{-4}$ molecules

$= 1.05 \times 10^{20}$ molecules

The amount of methanol adsorbed in ½ g of the catalyst is 1.05×10^{20} molecules.

The amount of methanol adsorbed in 1g of the catalyst is $2 \times 1.05 \times 10^{20}$ molecules

$= 2.10 \times 10^{20}$ molecules per gram of the catalyst.

But the surface area of the catalyst is 50 m^2g^{-1} and

There are $\sim 10^{19}$ surface atoms in $1m^2$ for a material

So in 1g of material, we have about 5×10^{20} surface atoms.

Therefore, the methanol molecules per surface atom =2.10/5

= 0.4

This represents about half monolayer of methanol consumed before saturation

As the uptake was measured, the injection was continued until the surface was saturated and allowed to stabilize for some period and the experiment was stopped and new experiment was employed to carry out the TPD (figure 2-10).

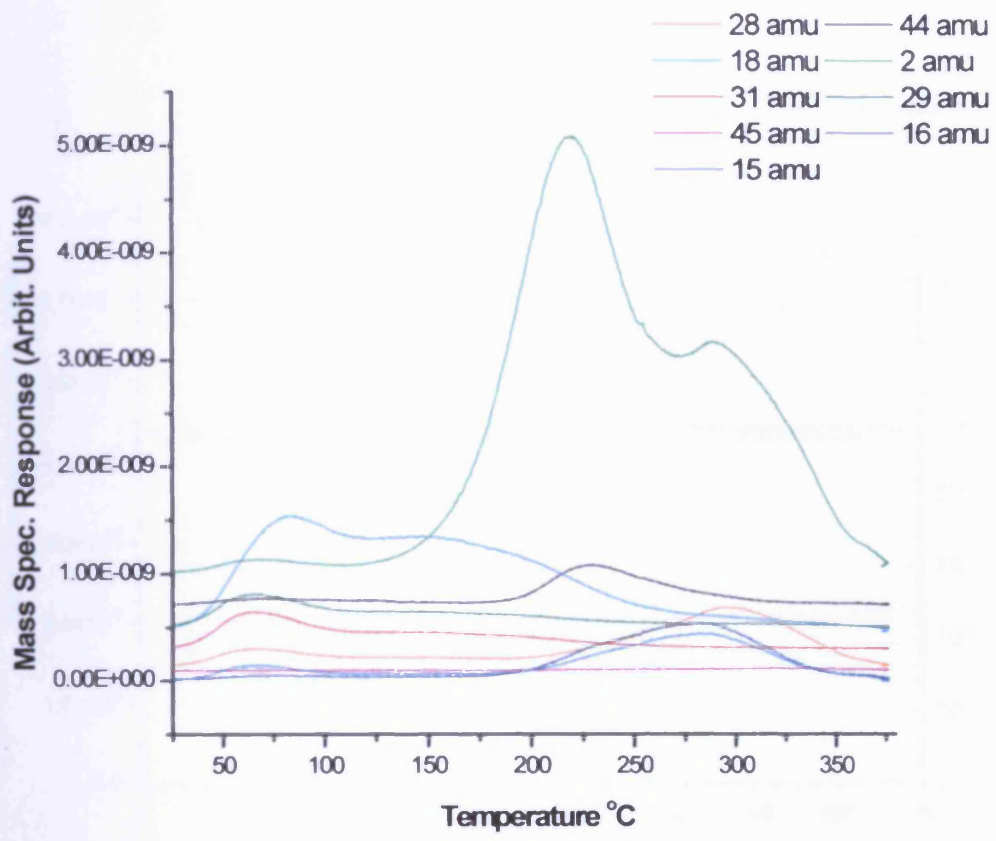

Figure 2-10: Temperature Programmed Desorption for methanol pulses in a stream of He flow over a 1wt% Au/TiO_2 catalyst

The temperature programmed desorption data show that at low temperature, water and molecular methanol (appearance of mass 18 and 31 amu signals) was desorbed and as the temperature increased to 230°C, CO_2 and hydrogen (presence of mass 44 and 2 amu signals). However, as the temperature increased to 280°C, the appearance of mass 16 and 15 amu signals confirmed the presence of methane due to deoxygenation of methanol and as the temperature reached 300°C, CO and hydrogen was desorbed (appearance of mass 28 and 2 amu signals) due to dehydrogenation of methanol at this temperature.

Another mode of operation of the pulse flow reactor is the isothermal pulse reaction, which allows understanding the rate of surface reaction changes with time and the sequence of product distribution changes and formation with time. It is also a good technique, in which it gives an insight of the changes of the conversion and selectivity

with time. It involved injection or pulsing of the reactant at a particular set temperature. Figures 2-11 and 2-13 show examples of this technique for CO oxidation and methanol isothermal reaction at 100°C temperature.

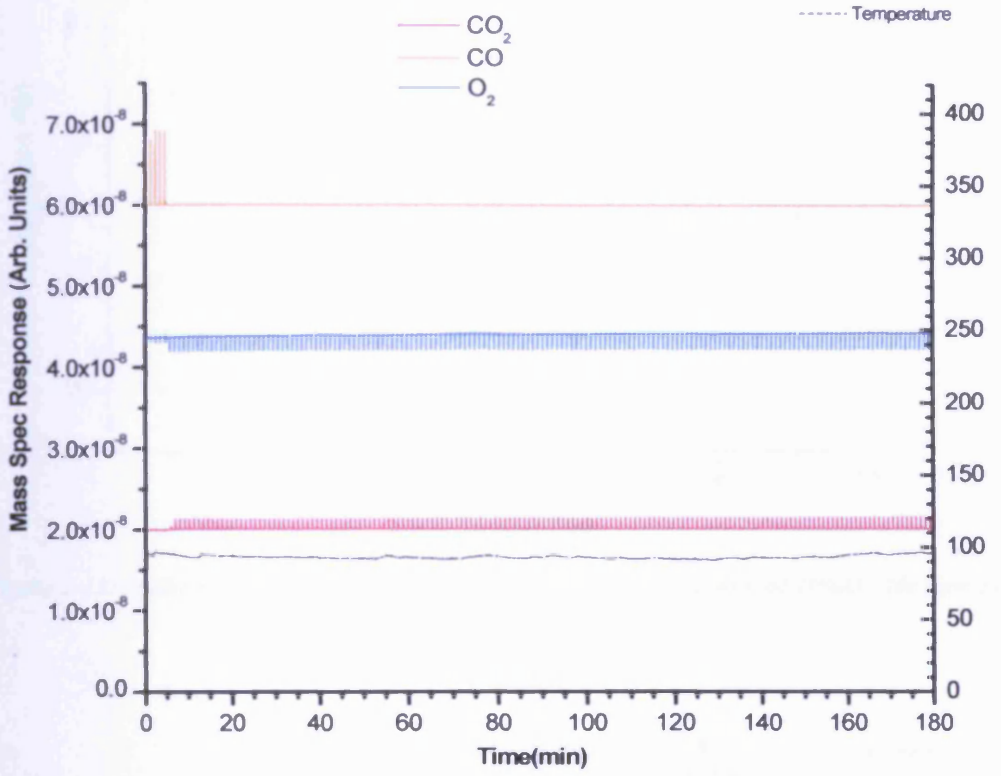

Figure 2-11: Isothermal pulse flow reaction for CO pulses in a stream of 10%O_2/ He flow over a 1wt% Au/TiO_2 catalyst

Since CO oxidation reaction involved only one product, pulsing of CO isothermally over a Au/TiO_2 catalyst held at constant temperature can give an insight of how the activity of CO_2 produced changes with time (figure 2-11) and the raw data can be analysed and integrated as shown (figure 2-12).

Similarly, when the catalyst was held at constant temperature (isothermally) and alcohol (example methanol) was injected periodically, the raw data can be presented as shown in figure 2-13. When the data was integrated and analysed as discussed fully in third mode of operation of the pulse flow reactor and the result can be presented as shown in figure (2-14).

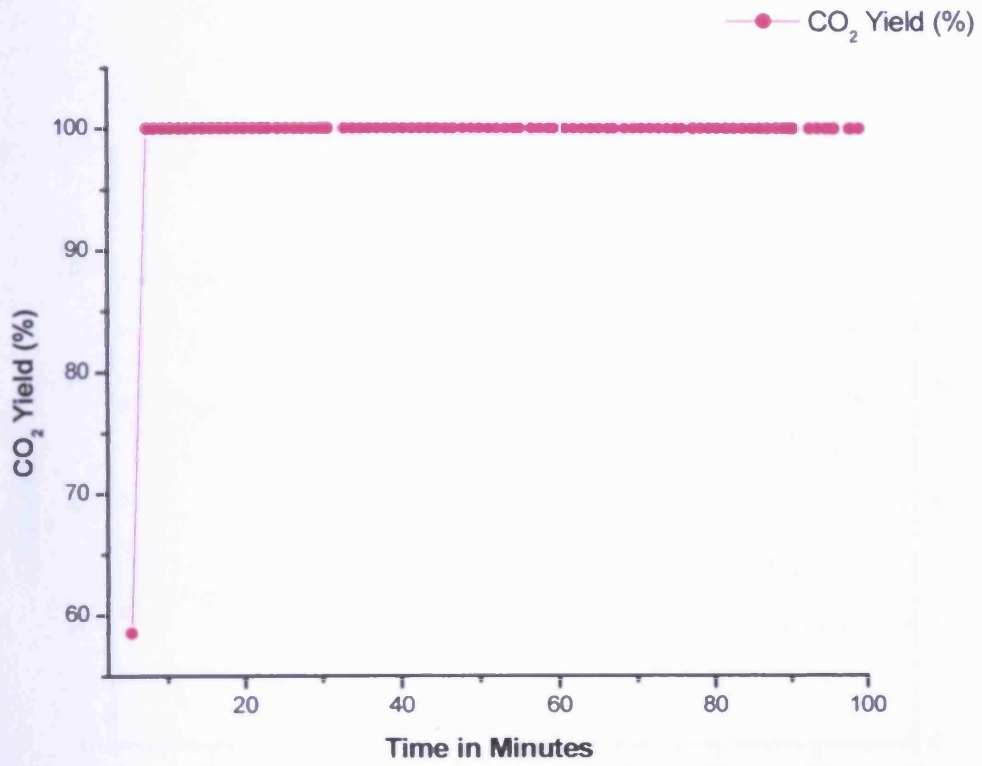

Figure 2-12: Isothermal pulse flow reaction for CO pulses in a stream of 10%O_2/ He flow over a 1wt% Au/TiO_2 catalyst

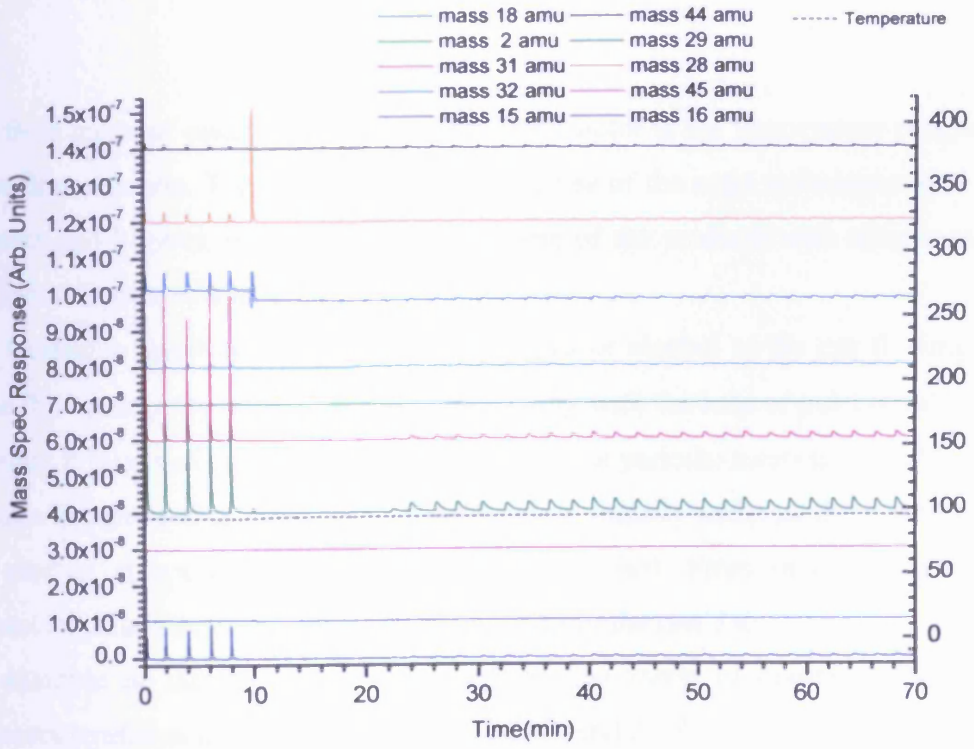

Figure 2-13: : Typical set data obtained in a single run for isothermal pulse flow reaction for methanol pulses in a stream of 10%O_2/He flow over a 1wt% Au/TiO_2 catalyst

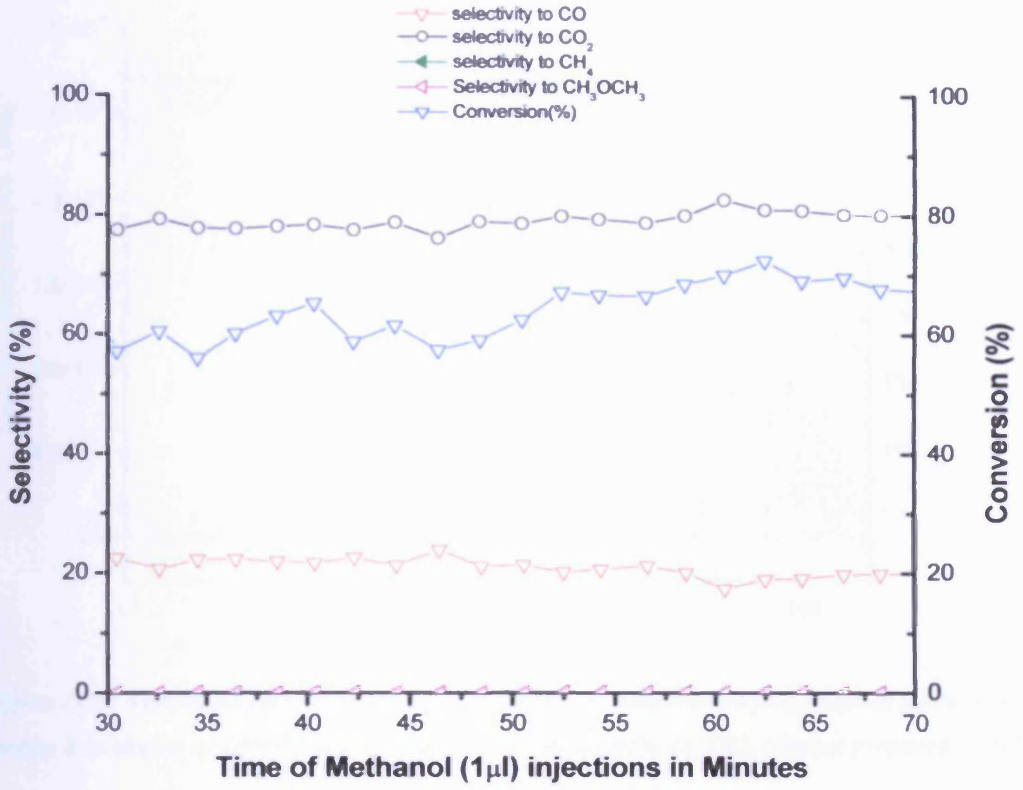

Figure 2-14: Selectivity and Conversion with temperature for methanol Isothermal pulse flow reaction in a stream of 10%O_2/ He flow (aerobic) over a 1wt% Au/TiO_2 catalyst

The third mode of operation of the pulse flow reactor is the temperature programmed pulse flow reaction. This mode of operation is one of the main techniques used in this research and it gives an insight of the variation of the products with temperature and the light off point of a reaction.

The technique involved the introduction the gas or alcohol to the gas flowing in the pulse flow reactor by pulsing or injection usually with the help of pulsing valve or 1μl syringe. It involved introducing the gas or liquid at periodic intervals (usually 1 and 2 minutes for gas and alcohol respectively), while linearly ramping the temperature of the catalyst at specified rate (usually 8°C per min). From this technique, yield, conversion, and selectivity can be determined from the raw data.

An example of the raw data obtained from this mode of operation for CO and methanol oxidation are presented in figures 2-15 and 2-17 respectively.

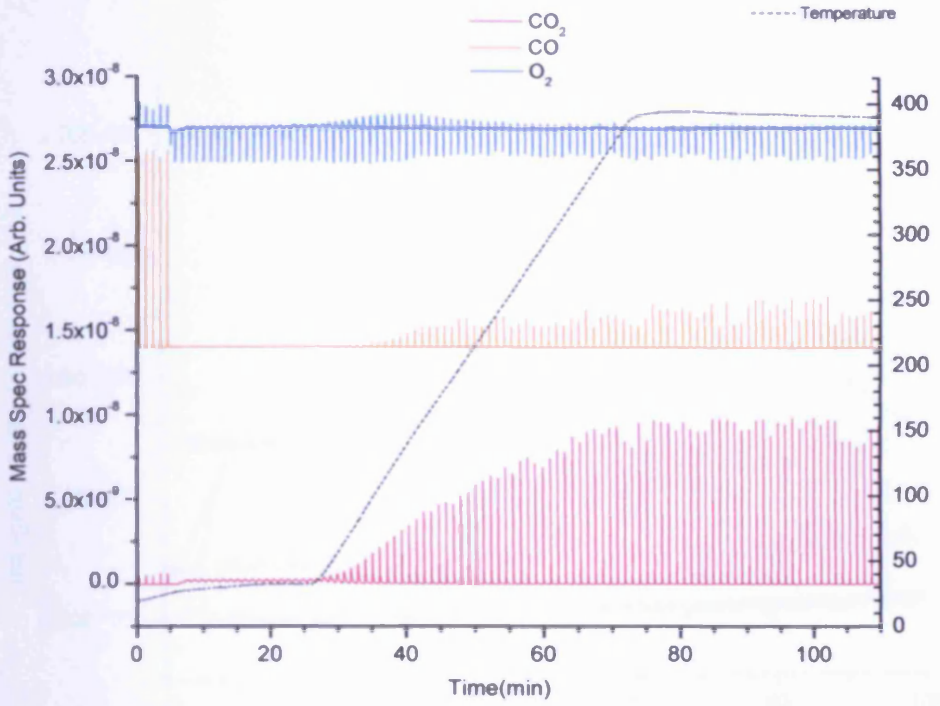

Figure 2-15: Typical set data obtained in a single run of temperature programmed pulse flow reaction in a stream of 10%O$_2$/ He flow (aerobic) over a 1wt% Au/TiO$_2$ catalyst prepared by DP method

One of the important advantages of this mode of operation is that the light-off point can easily be determined and insights into reaction kinetic and mechanism can be obtained. When the data raw data was collected, the next step was to obtain the raw peak integrals (figure 2-16). From the raw peak integrals, the reaction coordinate for CO oxidation can be understand and from there, the CO integral which corresponds to 100% conversion of CO to CO_2 can be determined and corresponds to the area integral through bypass or the peak area integral of CO_2 with constant peak area integral value of CO_2 (figure 2-16). However, from the raw data area integral, the CO_2 yield and the conversion of CO can also be determined.

The yield (%) of CO_2 as shown in figure (2-17) was calculated using the following formula:

$$\text{Yield } CO_2\ (\%) = (A_{CO2}/A_{CO2,\,100\%})*100 \qquad (2\text{-}1)$$

A_{CO2} = peak area of CO_2

$A_{CO2,\,100\%}$ = peak area of CO_2 corresponding to 100% conversion of CO

These formulas rely on a linearity of mass spectrometer signal with the amount of gas pulsed or injected on stream.

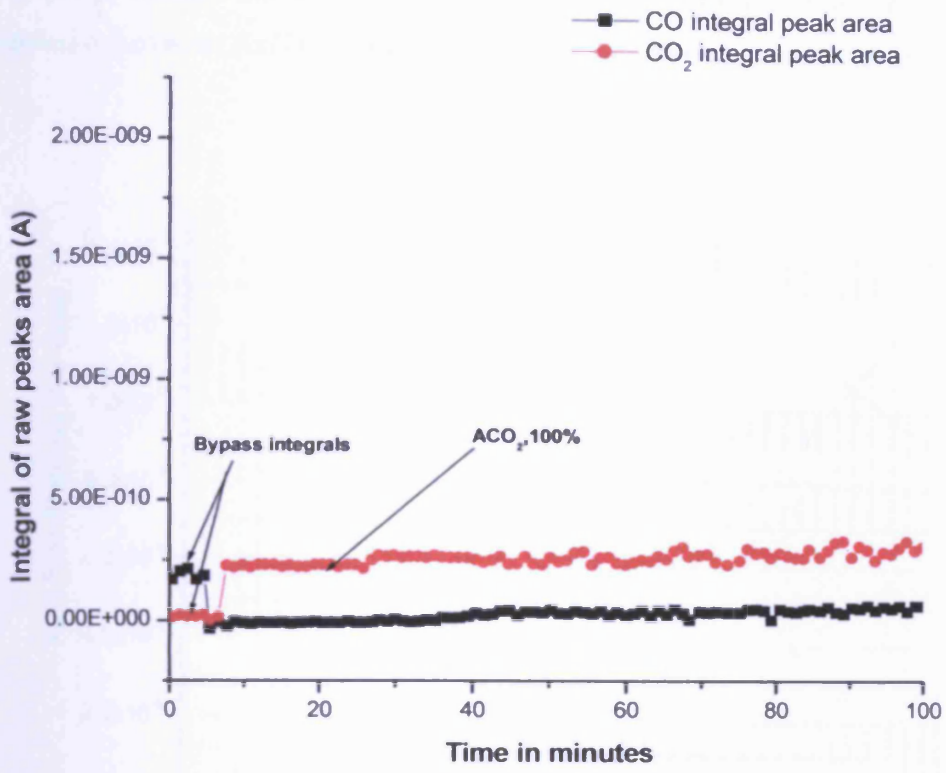

Figure 2-16: Raw data peak integral areas obtained in a single run of temperature programmed pulse flow reaction for CO in a stream of 10%O_2/ He flow (aerobic) over a 1wt% Au/TiO_2 catalyst prepared by DP method

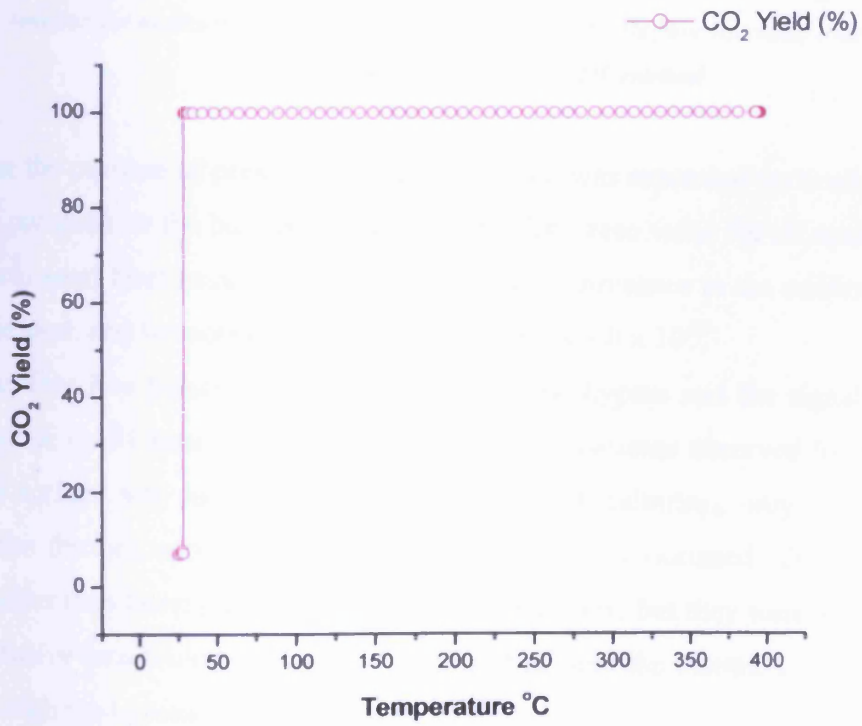

Figure 2-17: CO_2 Yield obtained in a single run of temperature programmed pulse flow reaction in a stream of 10%O_2/ He flow (aerobic) over a 1wt% Au/TiO_2 catalyst prepared by DP method

Similarly, when a temperature programmed pulse flow reaction for methanol was carried out over an Au/TiO_2 catalyst; the raw data can be presented as follows:

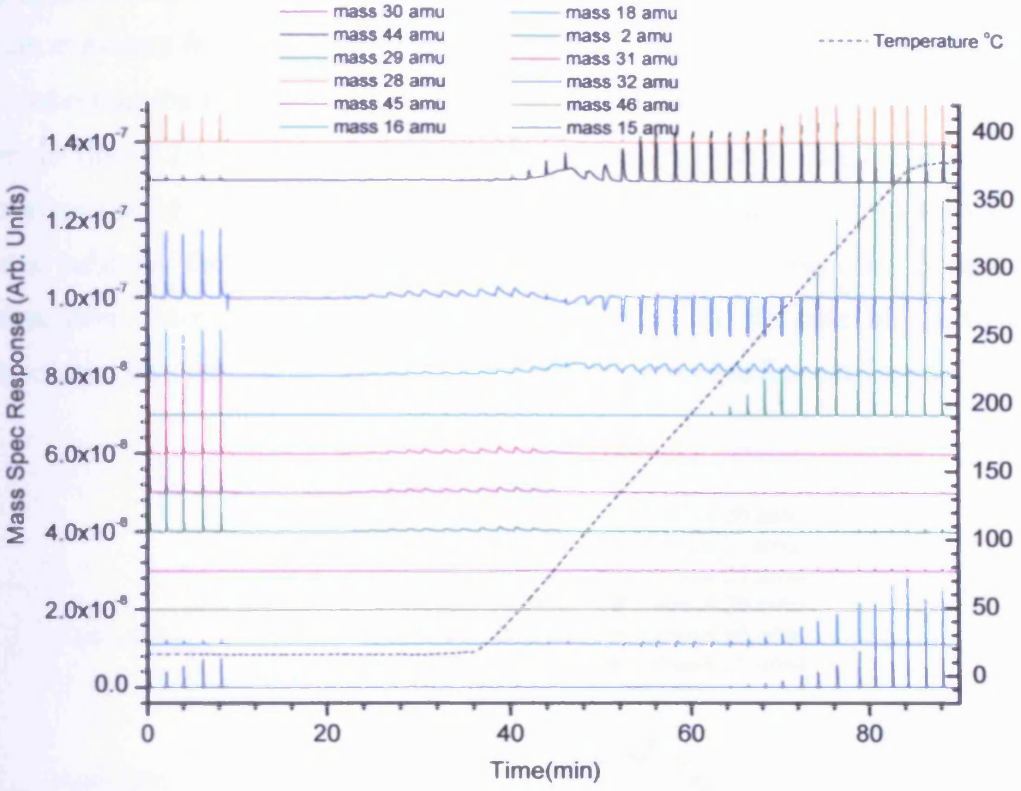

Figure 2-18: Typical data set obtained in a single run of temperature programmed pulse flow reaction for methanol injections in a stream of 10%O_2/ He flow (aerobic) over a 1wt% Au/TiO_2 catalyst prepared by DP method

For the purpose of presentation, the raw data was separated vertically by the addition of constants to the baseline signal and the time zero value for all masses is effectively zero, apart from mass 32, due to some oxygen presence in the continuous gas flow in this case, and the constant added to this mass is 9.0×10^{-8}.

The first five pulses of injection indicates the bypass and the signals obtained apart from mass 31 amu gives the idea of cracking patterns observed for methanol. When the surface was saturated (at approximately 20 minutes), only methanol molecules broke through and no conversion of the methanol occurred. The peaks were much smaller than those passing through the bypass were, but they were also broader, due to diffusive broadening through the catalyst bed, and the integrals were similar to those through the bypass.

As the temperature was increased to about 100°C, 100% conversion of methanol was obtained (loss of the 31 and 29 amu signals), and two stages of CO_2 production

occurred. In the first stage, (40-50 minutes- type I CO_2), there was slow CO_2 evolution, together with slow uptake of oxygen after each pulse injection. When the temperature reached ~ 150°C, the production of CO_2 and uptake of O_2 occurred at a fast rate as evident from the sharp peaks (type II CO_2) (from 60 to upward minutes).

After collecting the raw data, the next step is to find the raw peak area integrals as shown in figure 2-19. From the raw data integral, it could be seen that a lot of information can be collected. For, example the peak area integrals from zero to 10 minutes indicates the peak areas of methanol injections through the bypass. In addition, from there, the peak area integrals observed are the cracking pattern of methanol, and the contribution of each compound to each mass line can be removed.

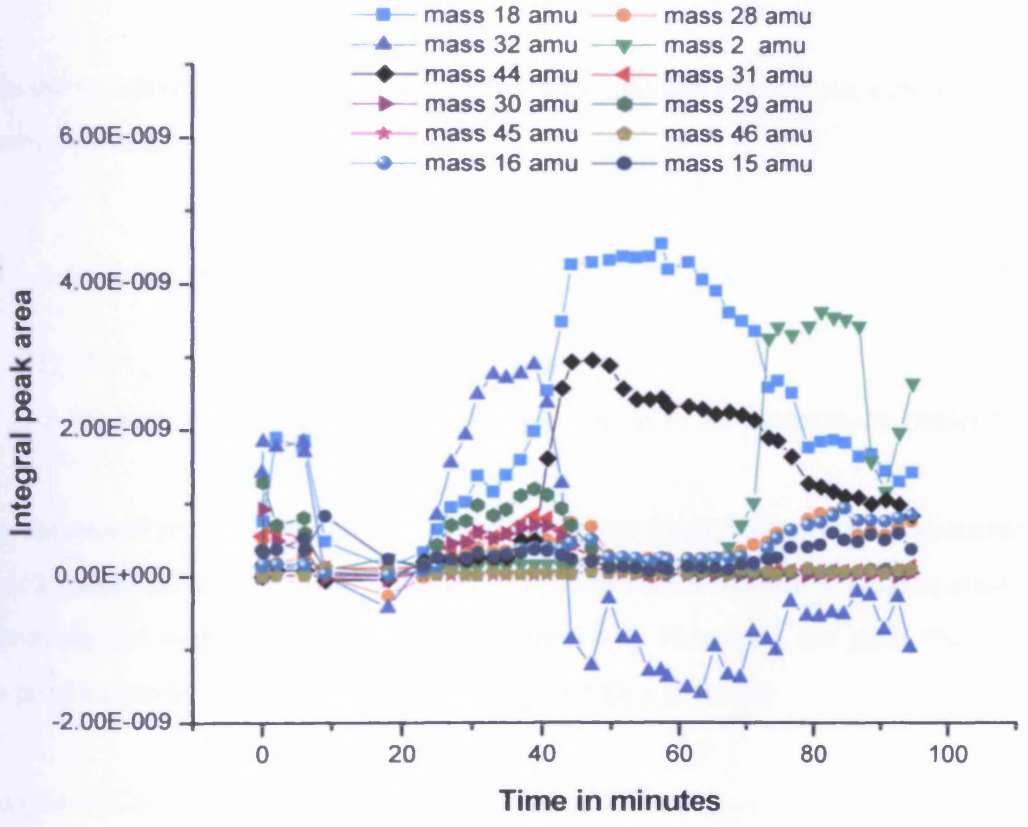

Figure 2-19: Raw data peak integral areas obtained in a single run of temperature programmed pulse flow reaction for methanol in a stream of 10%O_2/ He flow (aerobic) over a 1wt% Au/TiO_2 catalyst prepared by DP method

For example, we observe that methanol contributed to some other masses such as CO looking at the first five bypass injections. This contribution of methanol can be estimated and removed by calibration. The actual CO can be determined by removing

the contribution due to methanol, CO_2 and dimethyl ether to the 28 amu signals, leaving the rest of the portion to be actual CO. Once the integrals of the compounds are determined, they are further adjusted for sensitivity of the mass spectrometer. As soon as this has been done a precise composition of, each pulses or injection is determined. The methanol conversion (equation 2-2) and selectivity (equation 2-3) to each compound can be calculated from the following formula:

$$\text{Conversion (\%)} = (A_O/A_{U,\,100\%})*100 \quad \text{.....(.2-2)}$$

A_O = peak area of methanol observed

$A_{U,\,100\%}$ = peak area of methanol through bypass corresponding to 100% unreacted methanol

While the selectivity of the catalyst to each compound can also be calculated from the following formula:

$$\text{Selectivity}_c\ (\%) = \left[\frac{\text{Product}_c}{\Sigma\ \text{Products}}\right]*100 \quad \text{.....(2-3)}$$

Product_c = Actual peak area of a product

Σ Products = Total sum of the actual peak areas of all the products present

Once, the selectivity and the conversion of all the products observed were determined for each pulse, the next step is plotting conversion/selectivity (on y-axis) against the temperature (on x-axis) of the reaction (figure 2-20). However, the yield (%) of the main product can also be calculated from the following formula:

$$\text{Yield (\%)} = (\text{Conversion (\%)} \times \text{Selectivity (\%)}) / 100 \quad \text{.....(2-4)}$$

The temperature programmed pulse flow reactor used in these studies has a great advantage over typical continuous flow reactors, because the speed of analysis of mass spectrometer is much higher than a gas chromatograph. This technique gives an insight of small changes on the catalytic properties of the catalysts by recording changes in the activity in time. Many data can also be recorded in a short period.

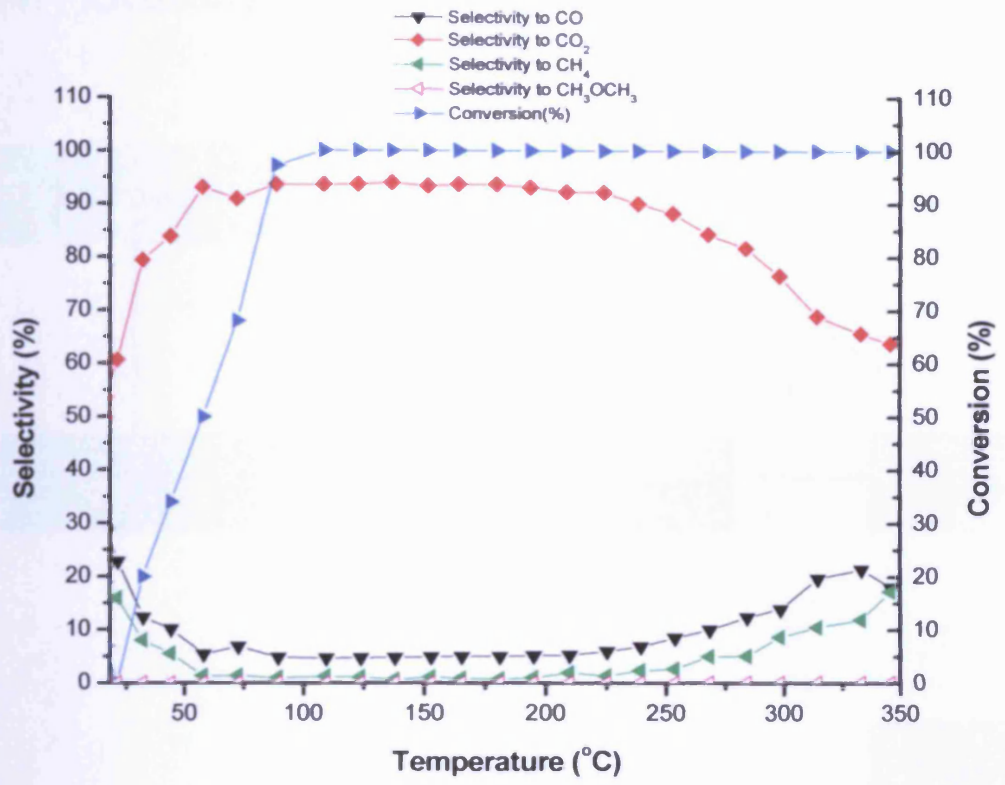

Figure 2-20: Selectivity and conversion with temperature of temperature programmed pulse flow reaction for methanol injections in a stream of 10%O_2/ He flow (aerobic) over a 1wt% Au/TiO_2 catalyst prepared by DP method

2.4.1 Quadrupole mass spectrometer

Eugen Goldstein first developed a mass spectrometry in 1886, later modified by Arthur Jeffery Dempster and F. W.Aston in 1918 and 1919 respectively. Mass Spectrometry is an analytical technique that measures the mass to charge ratio of a charged particle [15]. It is used to identify the composition of a sample by generating a mass spectrum representing the masses of the sample elemental composition. Generally, mass spectrometers consist of the following basic parts: an ion source; a mass analyser and a detector system. The stages during the operation of a mass spectrometer are:

(i) Production of ions from the sample

(ii) Separation of ion with different masses

(iii) Detection of the number of ions of each mass produced

(iv) Collection of data to generate the mass spectrum

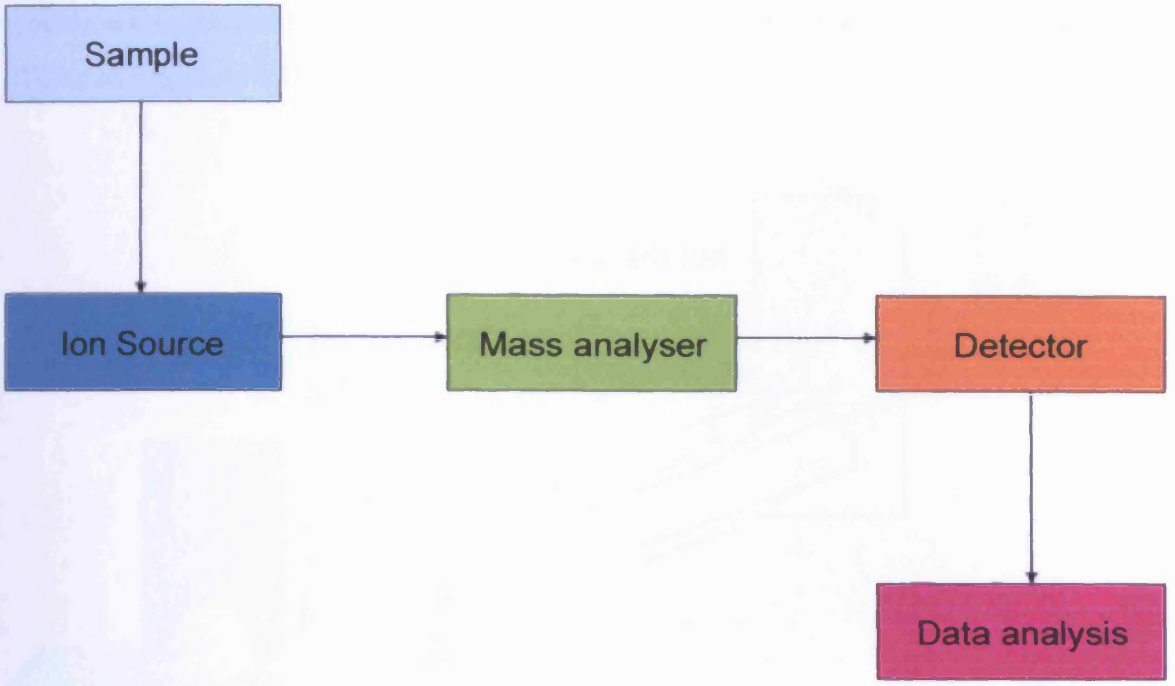

Figure 2-21: Main steps of measuring with a mass spectrometer

Mass spectrometry is a good technique that is capable for the following applications:

(i) Identifying unknown compounds by the mass of the compound molecules or their fragments

(ii) Determining the isotopic composition of elements in a compound

(iii) Determining the structure of a compound by observing its fragments

(iv) Quantifying the amount of a compound in a sample using carefully designed methods

(v) Studying the fundamentals of gas phase ion chemistry

(vi) Determining other important physical, chemical or even biological properties of compounds with a variety of other approaches.

The Quadrupole mass spectrometer acts as a mass analyzer. It is a component of the instrument responsible for the filtering of sample ions based on their mass to

charge ratio (m/z). The quadrupole mass spectrometer used in this study consists of four parallel cylindrical stainless steel metal rods, arranged symmetrically relative to the molecular fight path (figure 2-22), to produce the variation in potential required to give the electromagnetic fields. Molecules enter the mass spectrometer and are bombarded with electrons emitted from a source filament (thoriated tungsten, 0.15 mm diameter),

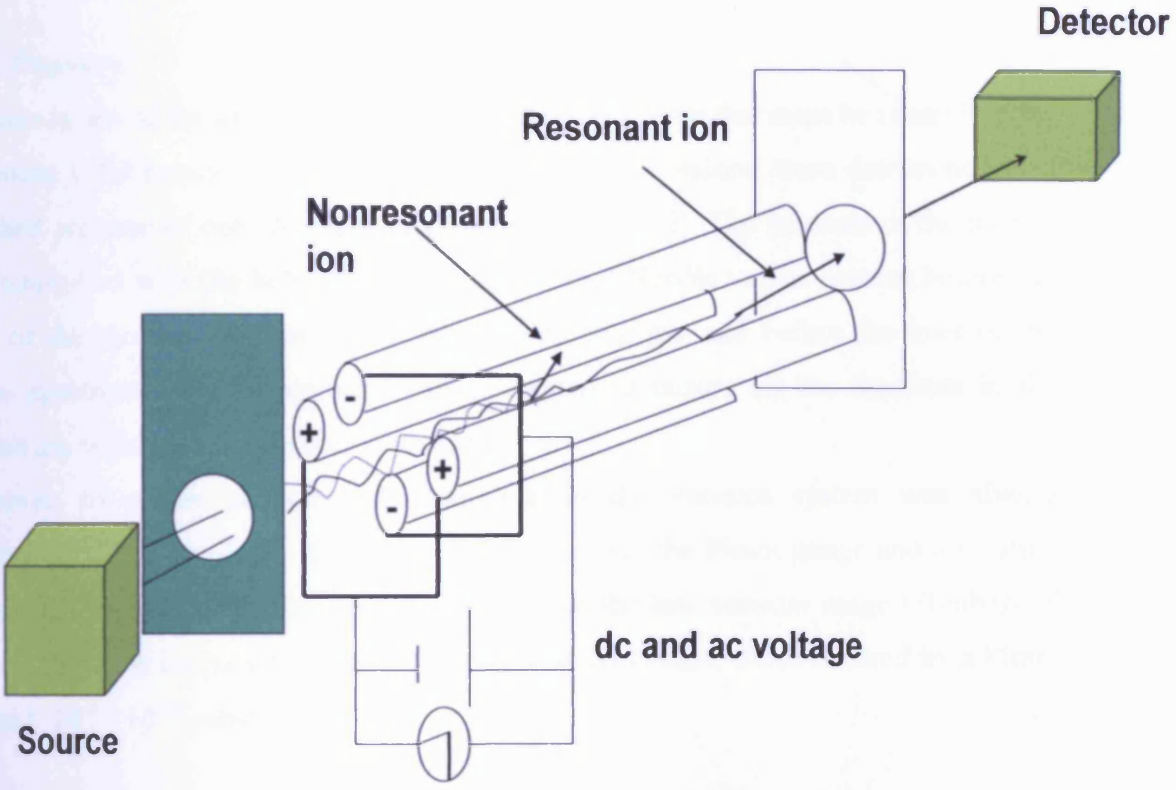

Figure 2-22: Schematic set up diagram of quadrupole mass spectrometer

A quadrupole mass analyzer is essentially a mass filter that is capable of transmitting only the ion of choice. The mass spectrum is obtained by scanning through the mass range of interest over time. Each opposing rod pair is connected together electrically and a radio frequency voltage is applied between one pair of rods, and the other. A direct current voltage is then superimposed on the R.F. voltage. Ions travel down the quadrupole in between the rods. Only ions of a certain mass –to-charge ratio will reach the detector for a given ratio of voltages: other ions have unstable trajectories and will collide with the rods. This allows selection of a particular ion, or scanning by varying the voltages.

Mass spectrometers are not commonly as accurate as other equipments for analysis such as gas chromatograph. Calibrations were always applied that took in to account daily changes in the sensitivity of the mass spectrometer. However, prior to any data acquisition from the reactor, it is important to note the reliability of the data and some operating variables are controlled:

2.4.2 Pressure

Pressure is one of the important variables in the experiment that must be controlled for obtaining valid results. In this research, all the data obtained were determined at a constant pressure of one atmospheric pressure (~14.7 psi). The pressure of the reactor was controlled with the help of pressure gauge and Needle valves present before the inlet of the catalyst bed from the dosing or pulsing gas and before the inlet of the mass- spectrometer. The pressure was calibrated to ensure all the reactants in the system are within one atmospheric pressure.

However, to ensure accuracy, the pressure in the vacuum system was always monitored with help of two different pressure gauges: the Pirani gauge and ionisation gauge. The former is used to measure pressure in the low vacuum range (30mbar-10^{-3}mbar) while the ionisation gauge measures pressures below those covered by a Pirani gauge (10^{-3} - 10^{-11} mbar).

2.4.3 Flow rate

The flow rate of each gas flowing in the reactor was controlled with help of mass flow controllers. The mass flow controllers are calibrated with the help of a bubble meter attached to it just before the reactor. The conditions under which this calibration carried out are at one atmospheric pressure and the temperature being 25°C. The flow rate of the gases was determined by setting the mass flow controllers and measures the gas flow rate. The data obtained were used to plot a graph of volume of gas flow rate versus settings of the mass flow controllers as shown (figure 2-23).

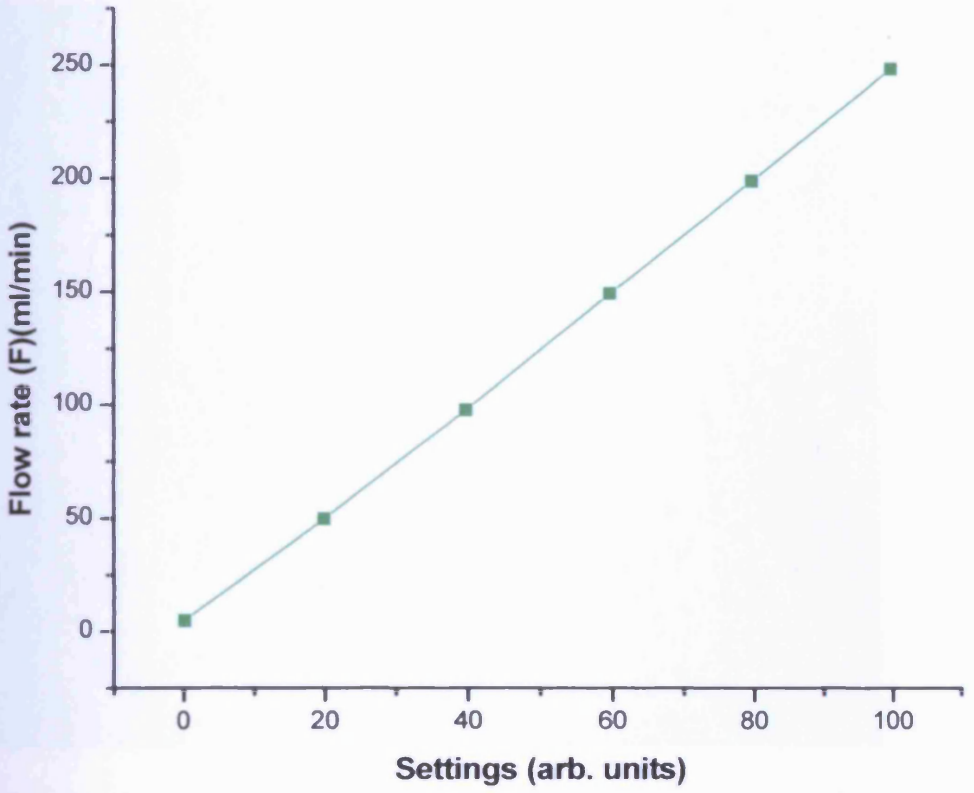

Figure 2-23: Calibration in Helium flow

The slope of the graph does not change with time but the ordinate is prone to errors. Thus, calibration was performed on regular basis, usually every three to six months.

2.4.4 Pulse volume

In order to determine the precise volume of the pulsing loop, some experiments were designed. Firstly, the pulsing loop was removed from the reactor and toluene and water were injected just to fill it several times each in order to get an average volume (figure 2-24 and 2-25) respectively.

The experiments show that toluene shows more precise results than water probably due to lower surface tension and with lower standard deviation. The average volume of the loop shown by the toluene and water is 0.53 and 0.498 cm^3 respectively. The results shown by the former are consistent with specification provided by the manufacturers. The average volume of the loop was found to be approximately 0.53cm^3. However, the volume of the pulsing loop can also be determined by measuring the inner diameter and the length of the loop.

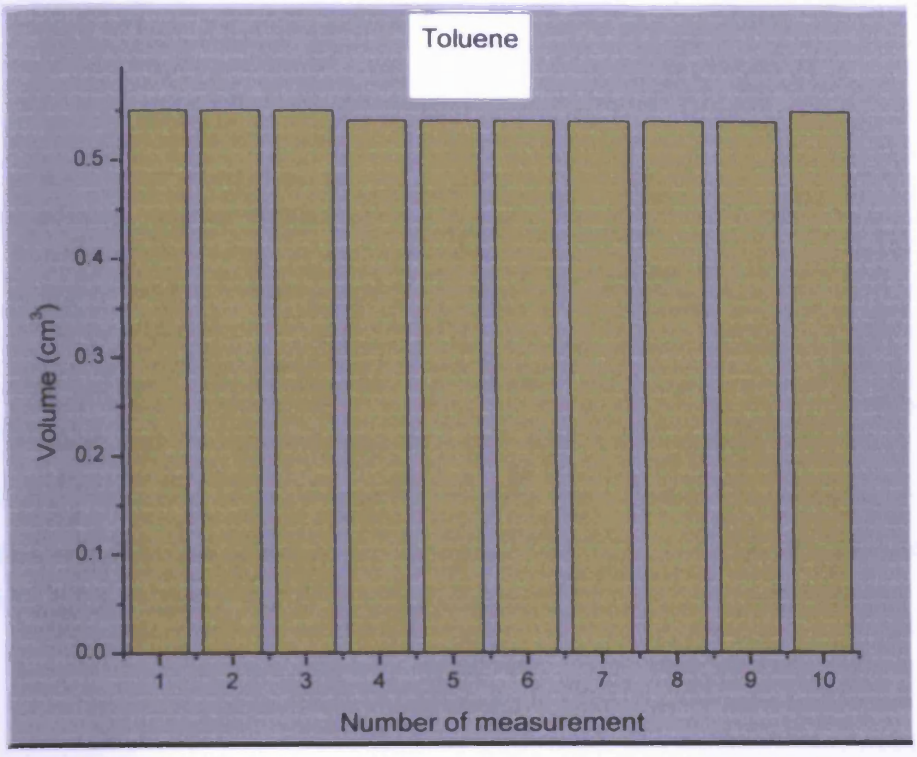

Figure 2-24: Toluene measurement for determination of pulsing loop volume

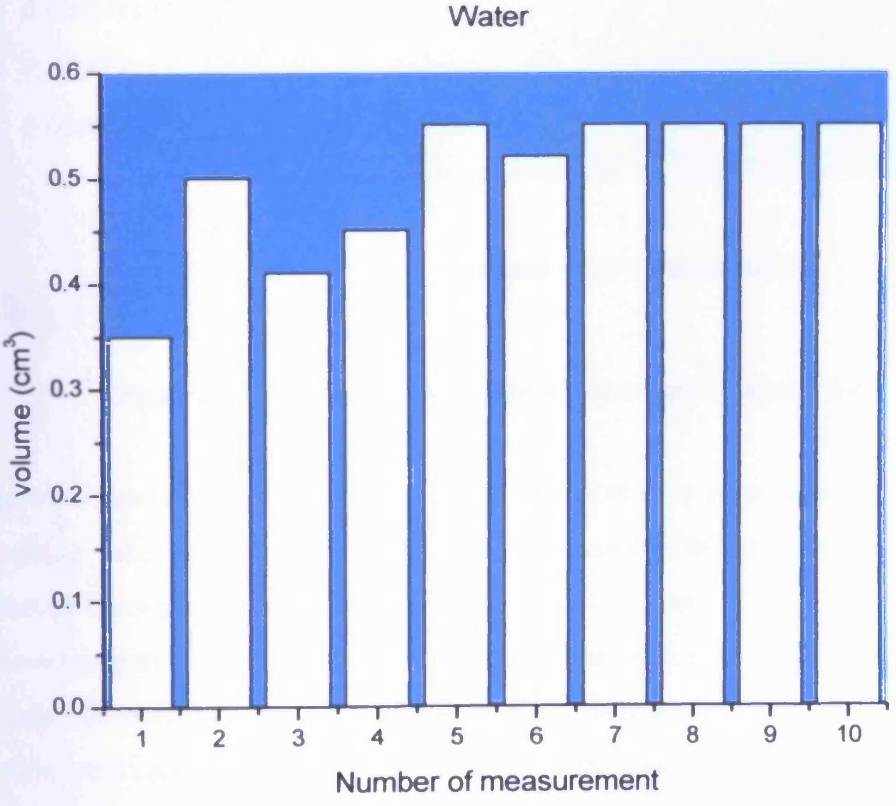

Figure 2-25: Water measurement for determination of pulsing loop volume

The volume of the gas can be estimated by using the perfect gas equation:

$$PV=nRT \qquad 2\text{-}5$$

Where P = 1 atm; V = 0.53 cm^3; R = 8.31451 $Jmol^{-1}K^{-1}$; T = 298 K

Giving n= 0.0217 moles

2.4.5 Peak area of the pulsing or injected gas or liquid

The peak area of the pulsing gas and liquid are usually calibrated by injecting different volumes of gas or liquid through the septum. The peak areas obtained are usually recorded in order to test the linearity of the injected gas or liquid as shown in CO and methanol calibration peaks, figures 2-26 and 2-27 respectively.

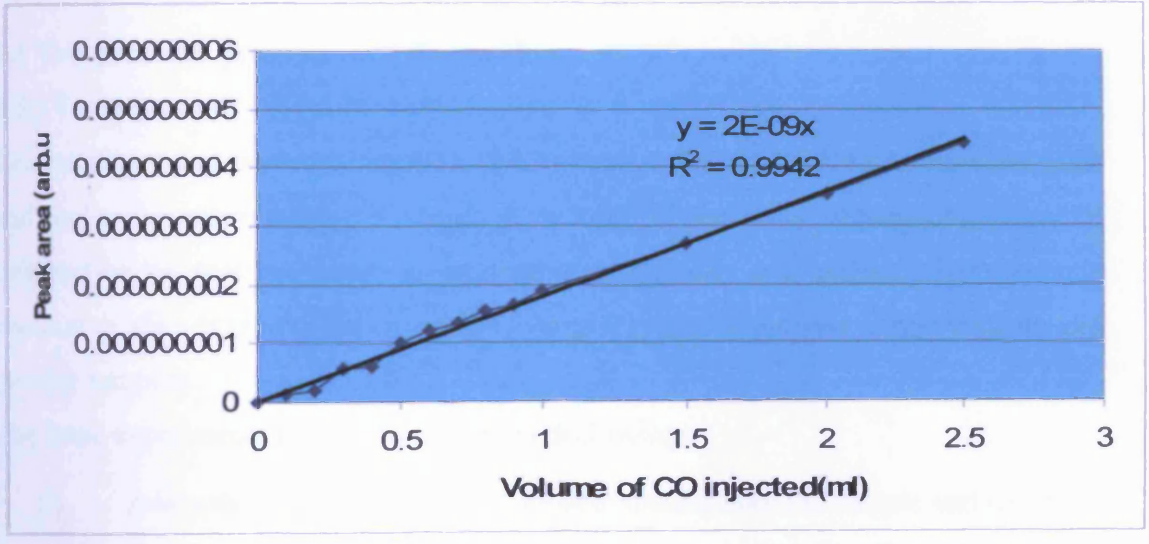

Figure 2-26: Peak area observed against volume of CO injected (ml)

Despite the manual injection of CO, several attempts have been done with the help of the pulsing valve to inject CO, and peaks corresponded with the manual injection of CO though the septum and the average peak area was found to be 1.02E-9.

The average peak area obtained correlates with the peak area of pulsing loop volume (0.53ml). However, in the case of liquid such methanol, several different sizes of injection were carried out to test the linearity of the peak area produced with different sizes of methanol injections (figure 2-27).

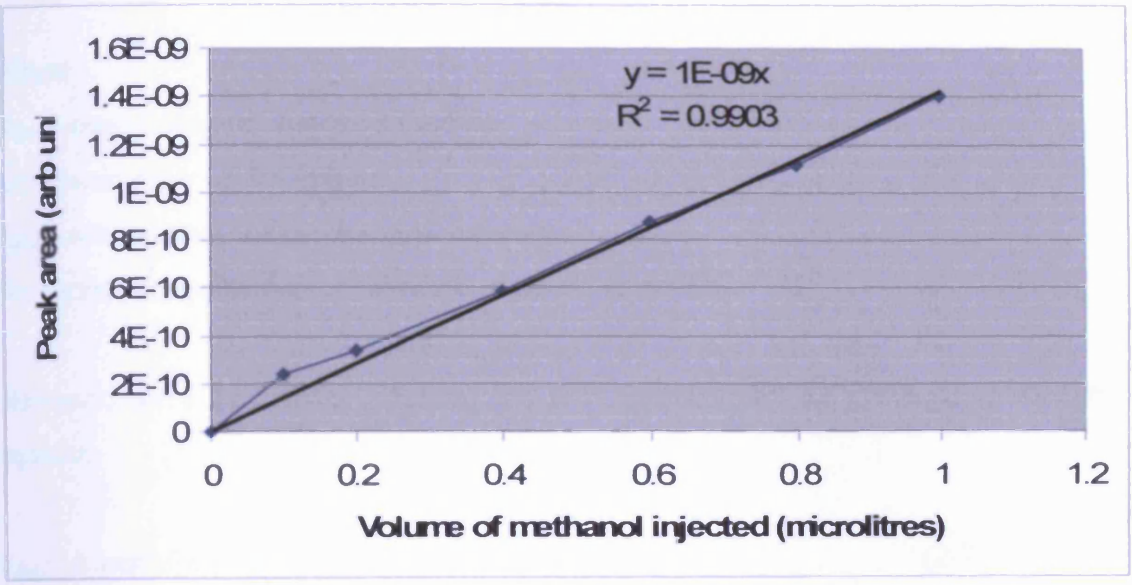

Figure 2-27: Peak area observed against volume of Methanol injected (μl)

2.5 Temperature programmed desorption

2.5.1 Introduction

Temperature programmed desorption (TPD) is a used to study about surface reactions and molecular adsorption on surfaces. It is a useful technique, which provides vital information on reaction kinetics, adsorption probability and surface coverage in a reaction profile. It is applicable to many ranges of materials, like single crystals and powder samples.

The basic experiments in TPD involved the followings:

(i) Adsorption of one or more molecular species onto the sample surface at low temperature (frequently 300 K, but sometimes sub-ambient)

(ii) Heating of the sample in a controlled manner (preferably to give a linear temperature ramp) whilst monitoring the evolution of adsorbed species from the surface back into the gas phase.

2.5.2 TPD Theory

The rate of desorption of an adsorbate from a surface with increasing temperature can be expressed as follows:

$$R_{des} = k_{des}N^{x} \qquad (2\text{-}6)$$

Where

R_{des} = rate of desorption of an adsorbate

x = kinetic order of desorption

k_{des} = rate constant for the desorption process

N= surface concentration or coverage of adsorbed species

However, for a first order reaction, the rate constant can be given by Arrhenius equation

$$k_{des} = A.\exp(-Ea_{des}/RT) \qquad (2\text{-}7)$$

Ea_{des} = the activation energy for desorption

A = the pre-exponential factor; this can also be considered to be the "attempt frequency", ν, at overcoming the barrier to desorption

R = the gas constant and,

T = the temperature in Kelvin

At low temperature, the surface concentration or the coverage remain constant so that equation 2-7 can be considered as equation of straight line and hence Arrhenius plot of (ln) of rate of desorption (R_{des}) against 1/T in Kelvin will be plotted and activation energy (Ea_{des}) and pre- exponential factor can be derived from the slope and the intercept of the graph respectively.

This then gives the following general expression for the rate of desorption

$$R_{des} = -dN/dt = \nu N^{x} .\exp(-Ea_{des}/RT) \qquad (2\text{-}8)$$

Similarly, in a TPD experiments in which the temperature increased linearly with time from initial temperature T_o, then:

$$T = T_o + \beta.t \quad \text{and} \quad dT = \beta \, . \, dt \qquad (2\text{-}9)$$

The intensity of the desorption signal (I(T)) is directly proportional to the rate of desorption; by combining equations (2-8 and 2-9), we have:

$$I(T) \alpha dN/dt = \nu N^x .\exp(-Ea_{des}/RT) \quad \ldots\ldots (2\text{-}10)$$

The equation derived (2-10), could be used to determine the activation energy for desorption by using the temperature at which the desorption maximum occurs as follows:

For a first order process:

$$Ea_{des}/(RT_p^2) = \underline{\nu}.\exp(-Ea_{des}/RT_p) \quad \ldots\ldots (2\text{-}11)$$

$$\beta$$

Where:

T_p = the temperature at which peak desorption occurs for a specific adsorbate

β = the heating rate of the process

ν = the pre-exponential factor assumed to be 10^{13} s^{-1}.

This is the Redhead equation.

2.5.3 TPD Experimental

The equipment and method used to carry out temperature programmed desorption experiments in this research has been described fully in section 2.3 of this chapter.

2.6 BET Surface area measurement

2.6.1 Introduction

The BET method is a very well known procedure for measuring the physical adsorption of gas molecules on a solid surface. It is widely used in many research and industry for measuring the specific surface area of a material. The BET procedure has been well described by many authors (5-8). The BET is an abbreviation of the first initials of the family names of Stephen Brunauer, Paul Hugh Emmett and Edward Teller, who first published BET theory in 1938.[16]

2.6.2 BET theory

The BET theory takes account of multilayer adsorption. It has been observed that if the latent heat of vaporization of a system is significantly high compared to the heat of adsorption, adsorption will occur at temperatures higher than the boiling point of the

adsorbate and the formation of multilayers becomes very unlikely. Nevertheless, when the heat of adsorption and the latent heat of vaporization are similar, a low temperature is required to bring about considerable adsorption in the first layer and under these conditions; the possibility of multi layer formation becomes significant.
BET theory is an extension of Langmuir theory as described in chapter 1, which is theory for monolayer molecular adsorption with the following assumption that:

(i) there is no interaction between each adsorption layer; i.e.the heat of adsorption for the first layer, ΔH_1 is characteristic of the adsorbate/ adsorbent system.

(ii) gas molecules physically adsorb on a solid in layers infinitely; i.e. each layer of adsorbate is considered to be a Langmuir monolayer and must be completed before the next layer.

(iii) the Langmuir theory can be applied to each layer; i.e. the heat of adsorption for subsequent layers equals the heat of condensation (liquefaction), ΔH_L.

This implies that, $\Delta H_2 = \Delta H_3 = \Delta H_4 = \ldots\ldots\ldots\ldots = \Delta H_L$

The resultant BET equation could be written as follows:

$$\frac{V}{V_m} = \frac{CZ}{(1-Z)(1-(1-C)Z)} \qquad Z = \frac{p}{p_o} \quad \ldots\ldots\ldots (2\text{-}12)$$

Where:
V = the total volume of the adsorbed gas in cm^{-3} at STP,
V_m = the volume of monolayer of adsorbed gas corresponding to monolayer coverage in cm^{-3} at STP,
p = the equilibrium pressure for a particular surface coverage (at the temperature of adsorption)
p_o = the saturation vapour pressure of adsorbate at the temperature of adsorption

and *C* known as BET constant and expressed as:

$$c = e^{(\Delta H_1 - \Delta H_L)/RT} \quad \text{.....(2-13)}$$

Where;

ΔH_1= the enthalpy of adsorption of first layer

ΔH_L = the enthalpy of adsorption of second layer and higher layer and is equal to enthalpy of liquefaction

R = the gas constant and T is the temperature.

If $\Delta H_1 >> \Delta H_L$, the BET isotherm is reduced to the Langmuir isotherm.

Rearranging equation 2- 12, we have

$$\frac{1}{V[(p_o / p) - 1]} = \frac{C-1}{V_m C} + \frac{1}{V_m C} \quad \text{.....(2-14)}$$

From equation 2-11, it indicates that an adsorption isotherm can be plotted as a straight-line graph.with $1 / v[(P_0 / P) - 1]$ on the y-axis and P / P_0 on the x-axis according to experimental results. The slope = $\frac{C-1}{V_m C}$ and the intercept = $\frac{1}{V_m C}$.

The useful region of the plot is only from p/p_o = 0.05 to 0.35 and from the value of the slope and the intercept the monolayer adsorbed gas capacity can be calculated and the surface area of solid can be determined by physical adsorption of gas molecules.

The determination of the surface area is based on the following principle: A gas close to its boiling point will concentrate (physisorb) at the surface of the solid at a pressure, P, lower than its saturated pressure Po. From the monolayer coverage and the known cross section of an adsorbing molecule, it is possible to determine the total surface area as shown below:

If liquid N_2 is used for analysis, it implies that at its temperature, each N_2 molecule covers about 16.2 $Å^2$. From the value of molecules in a statistical monolayer,

Surface area, (m^2/g) =

$(1m^2/ 10^{20} Å^2)(16.2Å^2/N_2)(6.023x\ 10^{23}N_2/22400cc\text{-}STP)(V_m, cc\text{-}STP/W_{cat}, g)$

The BET technique involves the use of volumetric or mass devices to determine the amount of gas desorbed (V in cc-STP) as a function of relative pressure (P/P_o) in the range 0.05-0.35. The data is plotted according to the linear BET equation to obtain V_m and C, from which the surface area can be calculated.

2.6.3 BET Experimental

The BET surface area was determined using A CE instruments QSurf M1 in a flow method as shown (figure 2-28)

In this method, about 2g of sample is weighed and added to a sample holder of a known weight. The sample holder was then connected to one of the degas stations. The degas station of the machine contained a nitrogen and helium mixture and was allowed to pass over the catalyst while heating at 120°C for one hour to remove surface moisture. . The thermal conductivity detector (TCD) was first calibrated by sampling a known amount of N_2 gas. The sample was then removed and move to the measuring bay of the instrument, where using a nitrogen and helium fractional mixture six measurements were made at p/p_o = 0.10, 0.14, 0.18, 0.22, 0.26 and 0.30. The sample was then immersed into a liquid nitrogen bath to allow nitrogen helium flow being adsorb onto the surface.

The sample was then removed from the bath and heated; upon heating, the N_2 adsorbed was desorbed from the surface. The LCD measures the amount of N_2 desorbed by comparing the N_2 in the exit to that enters the sample. This procedure was repeated for each six fractional mixtures of nitrogen and helium mixtures, the new weight was entered in to the controlling computer, and the surface area was measured automatically in meters squared per gram of sample

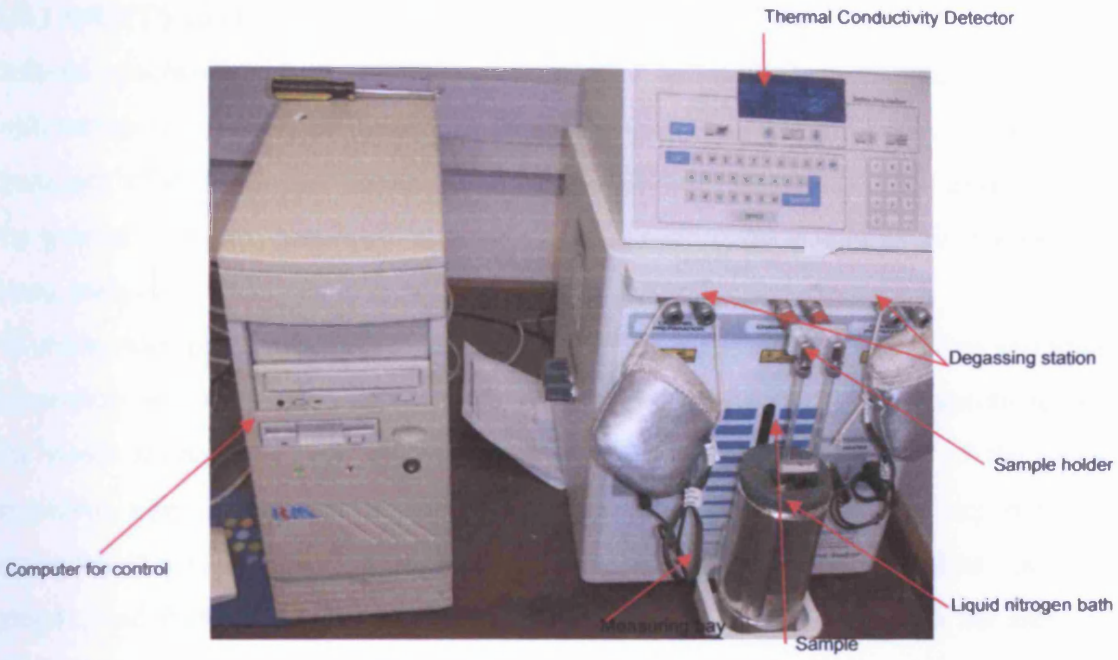

Figure 2-28: Photograph of CE instrument QSurf M1

Each time, the BET machine is always calibrated using carbon black sample of known surface area of $22.4 m^2 g^{-1}$.

2.7.1 Diffuse Reflectance Infrared Fourier Transmission Spectroscopy (DRIFTS)

2.7.1 Introduction to DRIFTS

Diffuse Reflectance Infrared Fourier Transmission Spectroscopy is a very common technique used to study the surface composition of the catalyst, the reactants and adsorbed species. In- situ DRIFTS is vital for the study of the catalyst. It main uses include determination of the adsorbed species etc. The technique is advantageous as the scattered radiation absorbed by the powdered sample is collected by an ellipsoidal mirror and focused on the detector.

2.7.2 DRIFTS theory

Infrared spectroscopy involves the interaction of infrared electromagnetic radiation with substances. It involves absorption or transmission of radiation by the sample. The frequency of absorption or transmission of IR radiation can also be used to determine the type of substance present in a sample by correlating the bonds within the sample being analyzed.

In absorption spectroscopy, the intensity of a beam of light measured before and after interaction with a sample is compared. When combined with the term spectroscopy, the words transmission and remission refer to the direction of travel of the beam measured after absorption to that before. The descriptions of the experimental arrangement usually assume that there is a unique direction of light incident upon the sample, and that a plane perpendicular to this direction passes through the sample. Light that is scattered from the sample toward a detector on the opposite side of the sample is said to be detected in transmission and treated according to the theory of transmission spectroscopy. Light that is scattered from the sample toward a detector on the same side of the sample is said to be detected in remission and it is this light that is the subject of remission spectroscopy. The remitted radiation may be composed of two kinds of radiation referred to as specular reflection (when the angle of reflection is equal to the angle of incidence) and diffuse reflection (at all other angles) as shown (figure 2-29).

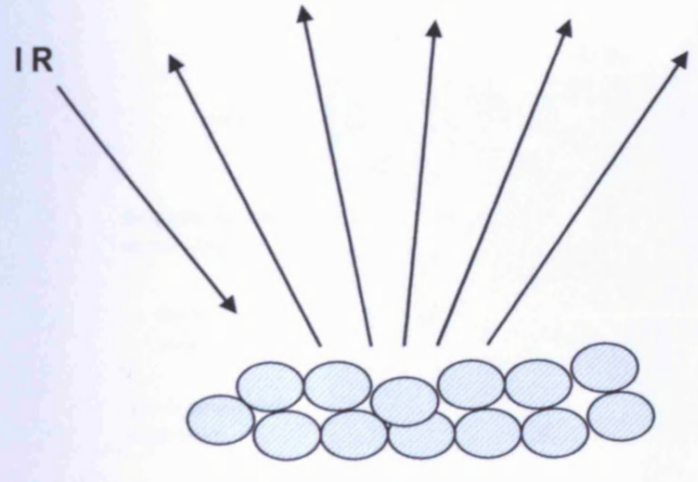

Figure 2-29: Diffuse Reflectance

In-situ DRIFTS measurements, can be made on loose powders, with the advantage that not only the tedious preparation of wafers is unnecessary but also that diffusion limitations associated with tightly pressed samples are avoided. As earlier mentioned,

the scattered radiation is collected by an ellipsoidal mirror and focused on the detector. The infrared absorption spectrum is described by the Kubelka-Munk function:

$$\frac{K}{S} = \frac{(1-R)^2}{2R} = F(R) \qquad \text{..... (2-15)}$$

Where:

K = the absorption coefficient, a function of the frequency ν

S = the scattering coefficient

R = the reflectivity of a sample, measured as a function of ν (or known as reflectance)

F(R) = the K-M spectrum.

2.7.3 DRIFTS Experimental

In-situ IR measurements were performed in a DRIFTS configuration with a Perkin-Elmer System 2000 FT-IR spectrometer, equipped with a MCT detector. The infrared comes from the source *via* a selector diffuse accessory (Specac). The accessory consist of a series of mirrors (figure 2-29), which reflect the infrared radiation as it comes from all angles from the catalyst (in powdered form) and directed it on to the detector of the machine.

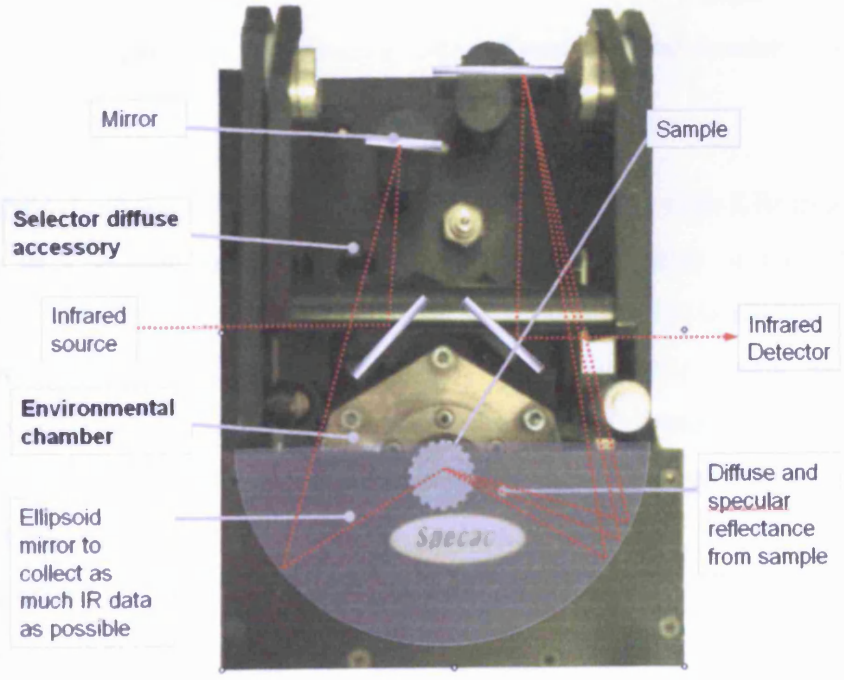

Figure 2-30: Photograph of DRIFTS accessories

This set- up allows measurements in a continuous flow of gas mixtures, in which the catalyst in the environmental chamber (Specac) allows gases to pass over the catalyst, which is heated, to the required temperature (figure 2-31). The catalyst in the environmental chamber sits directly below a ZnSe window with range from 500cm^{-1} to 20000cm^{-1}. The machine is controlled using Perkin- Elmer software (Spectrum for windows, V1.30).

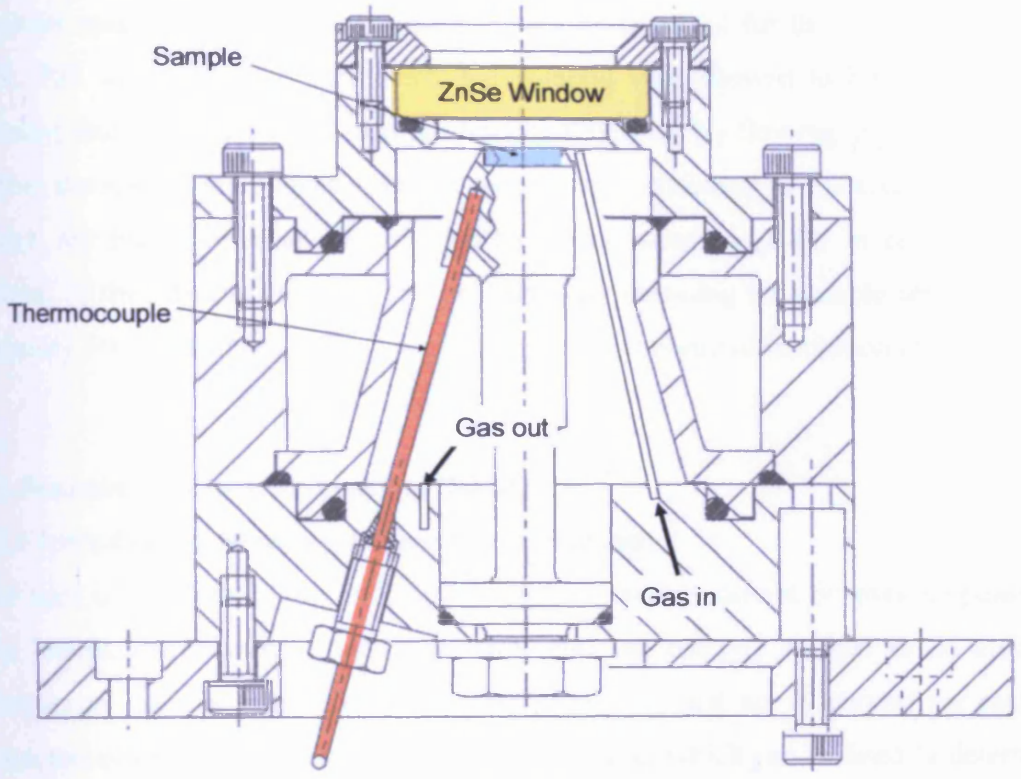

Figure 2-31: Photograph of DRIFTS environmental chamber

Prior to the experiment, the catalyst sample was ground up with KBr in a 1:1 mixture and place in a sample holder of the environmental chamber of the DRIFTS. The sample was heated in oxygen for 1 hour and allowed to cool to room temperature. The background spectrum of the clean catalyst was taken and the sample to be analysed (example methanol) was introduced at room temperature. It was allowed to stabilize in pressure and then nitrogen was subsequently introduced to purge the gas phase species (example CO_2 etc) before the spectra were taken.

However, prior to spectra acquisition, background spectra recorded on the clean catalyst at reaction temperature in a flow of nitrogen, were used for normalization by dividing the sample spectra by the background reference. The spectral contributions of

the gas phase were removed by a reference spectrum recorded over an inert carrier under similar conditions, which left only adsorbed species spectra. Finally, as the spectra of adsorbed species were determined at room temperature, the catalyst was then heated to 100°C for 10 minutes before allowed to cool to room temperature with N_2 gas was allowed to flow into the chamber in order to purge the gaseous species. Similarly, the spectra were taken by subtracting the contribution of spectra due to gaseous species from the background. This was repeated for the catalyst heated to 200, 300, and 400°C; in each case, the catalyst was allowed to be heated for 10 minutes and allowed to cool to room temperature with N_2 flowing in to the chamber before the spectra were taken. The intensities were evaluated in Kubelka-Munk units, which are linearly related to the adsorbate concentration (100). In each case, the spectra of the adsorbed species were obtained by scanning the sample several times, typically 500 scans (acquisition time ~4minutes) at a nominal resolution of $16cm^{-1}$.

2.8. Scanning electron microscopy (SEM)

2.8.1 Introduction to scanning electron microscopy

The uses of electron beams in catalytic surface studies cannot be over emphasised. The interaction between primary electron and the catalyst surface in an electron microscope leads to a number of detectable signals that are important for catalyst characterisation. Electron microscopy is a technique, which can be used to determine the size and shape of the catalyst particles. It can also give information on the composition and internal structure of the particles[18].

In electron microscopy, when a sample is irradiated with a primary electron beam, we can detect the characteristic X-rays, which are produced by the interaction of the electrons with the sample, and the electrons, which are diffracted by the sample if these are favourably oriented towards the beam, enabling one to obtain crystallographic information. The electron may also collide with sample atoms and be scattered back or lead to X-ray emission and Auger electron emission in the relaxation of core- ionised atoms (figure 20-32).

Scanning electron microscopy (SEM) is a very widely used technique to study surface topography and the surface feature of powders or solid catalysts. The SEM technique is used to complement optical microscopy, which uses light to produce an image. The SEM instruments have definite three-dimensional quality due to the depth of focus of

these instruments. In SEM, electrons are use to produce an image. The main advantage of SEM includes high resolution, larger depth of focus, greater magnification and simple sample preparation and observation.

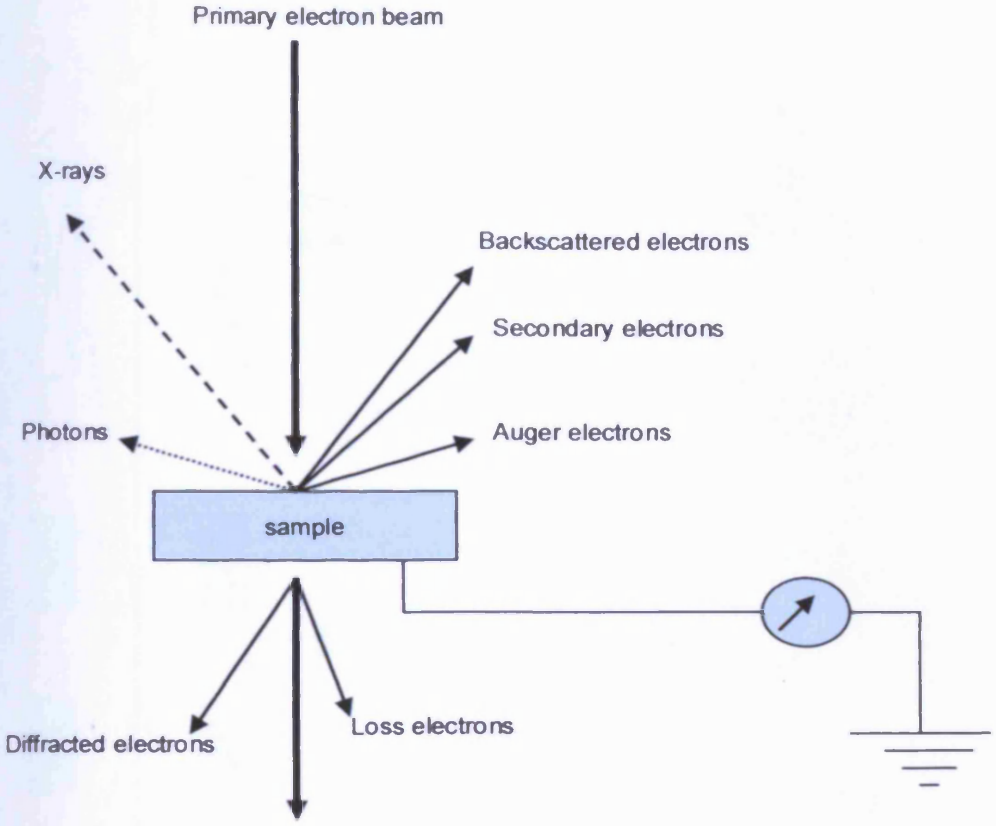

Figure 2-32: Interaction of electrons with sample

2.8.2 SEM theory

The SEM technique consists of an instrument in which the beam of electrons is produce from an electron gun. The electrons travel vertically through the column of the microscope and the beam is focused to a small spot (50-100 Å) in diameter on to the sample surface by electromagnetic lenses (or condenser).. The beam of electrons scans the sample rather like the spot on the television screen. The interaction of the primary beam of electrons with the sample results in the emission of x- rays and secondary electrons. The SEM is capable of producing high-resolution images of a sample surface. Characteristic x-rays are emitted when the primary beam causes the ejection of inner shell electrons from the sample and are used to determine the elemental composition of the sample. The secondary electrons emitted from the

sample may be used alone to form an image which is displayed on a screen while the X- rays are used for chemical analysis of the sample.

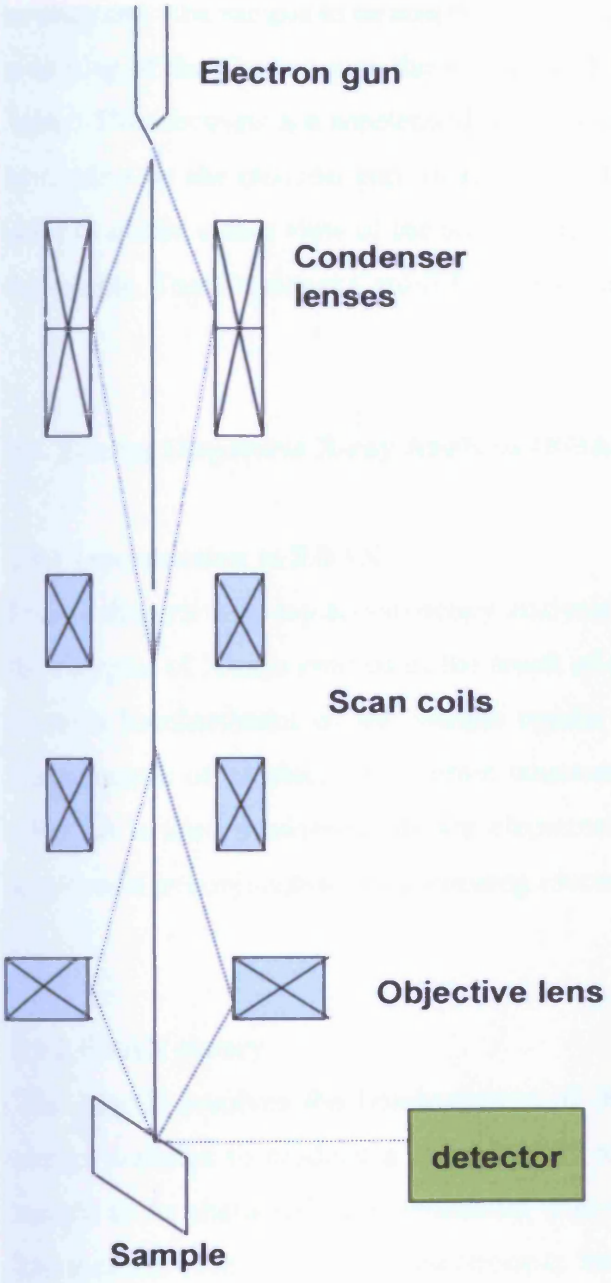

Figure 2-33: Schematic representation of Scanning Electron Microscopy instrument

2.8.3 SEM Experimental

The SEM instrument used in this study is Oxford EVO 40 system. The instrument is composed of an electron gun with a tungsten filament and anode. It also consists of

two condenser or magnetic lenses and a detector, which analyses the X-rays and secondary electrons emitted from the interaction of electron beams and the sample to be analysed. The sample to be analysed was first placed in a sample chamber and prior to turning of the electron gun, the whole SEM equipment was evacuated to 10^{-5} to 10^{-6}mbar. The electrons are accelerated with enough voltage to pass through the sample by turning on the electron gun. Images were taken at high and low magnification in order to obtain closer view of the surface and understand the nature of particle size of the sample. Tom Davies at Cardiff University obtained the SEM images.

2.9. Energy Dispersive X-ray Analysis (EDAX)

2.9.1 Introduction to EDAX

Energy dispersive X-ray spectroscopy analysis (EDAX) is the technique of measuring the energies of X-rays emitted as the result of electron bombardment of a sample. The electron bombardment of the sample results in the emission of X-rays, which are characteristic of an element's atomic structure and are uniquely different from each other[19].It is used predominantly for elemental analysis or chemical characterization, and is used in conjunction with scanning electron microscopy.

2.9.2 EDAX theory

The EDAX involves the bombardment of the sample with a high-energy beam of charge particles to produce a characteristic x-rays from the sample. To do that, the sample to be characterised is irradiated with electrons, protons, or a beam of x-rays. The incident beam may cause electrons to be ejected from an inner shell of an atom resulting in the formation of electron hole in that shell. As a result, an electron from the higher energy (outer shell) fills the hole and an X-ray or Auger electron is emitted. The energy of the X-ray photon is the difference in energy between the excited state energy level and the ground state energy level. The energies of these x-rays are characteristic of the element from which they are emitted. The x-rays are detected by a detector (usually SiLi) and analysed.

2.9.3 EDAX Experimental set-up

The same instrument used in SEM was used for the EDAX measurements. The EDAX results of the catalysts were measured using X- rays emitted by the sample in accordance with SEM experimental method as described in section 2.8.3.Tom Davies at Cardiff University obtained the EDAX results.

2.10 Raman spectroscopy

2.10.1 Introduction to Raman spectroscopy

Raman spectroscopy measures the changes of the frequency of radiation observed when a monochromatic beam is incident on the sample. The incident beam strikes the molecules of the samples and makes them excited and the radiation, which is scattered perpendicular to the incident beam, was monitored and used for characterisation. Raman Spectroscopy is based on the Raman Effect, which is the inelastic scattering of the radiation by molecules, so that a small fraction of about 1 in10^7 can be observed. Indian physicist, C.V Raman first discovered the technique in 1928.[20-23]

2.10.2 Raman spectroscopy theory

Raman spectroscopy is a very widely used technique and has been extensively covered in the literature[14-17]. It occurs because of the interaction between the molecules of irradiated sample with the monochromatic incident radiation. This causes excitation or light scattering. The scattered photons may be elastic (the same wavelength with as the incident light) or inelastic (at wavelength different to the exciting light). The elastic scattering is termed Rayleigh scattering while the inelastic is known as the Raman scattering (figure 2-34). The difference between the energy of the incident and Raman scattered light corresponds to the energy involved in changing the Vibrational motion of the molecules and is known as the Raman shift.

When the incident photons strike the molecules of the sample, the molecules are excited and upon retuning, some energy was given up and arrives to a Vibrational energy level lower than its initial state. The spectra observed is known as the stoke lines while in some cases, the energy is gained to the excited molecules and causes

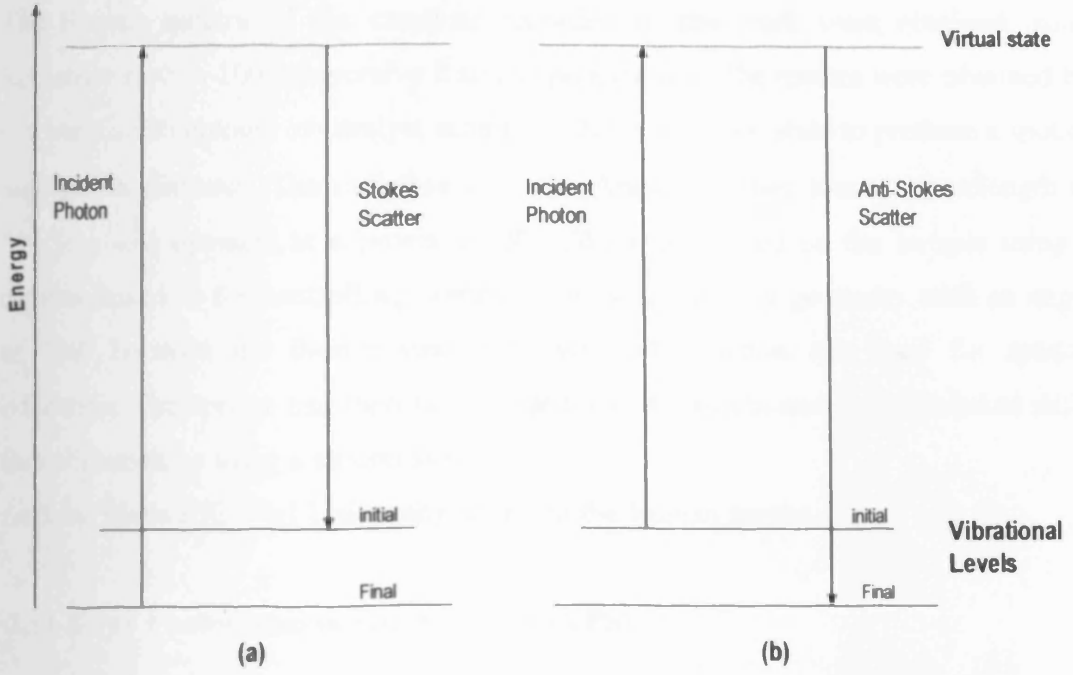

Figure 2-34: Schematic representation of energy diagram for Raman scattering

the moving to a higher unstable state by interacting with the incident photon and leading to spectra known as anti-stokes lines. The stoke lines are higher in the intensity than the anti-stokes lines. As indicated (figure 2-33), the energy difference between the incident and scattered photons is represented by the arrow lengths.

The energy difference between the initial and final Vibrational levels or Raman shift in wave numbers (cm^{-1}) is calculated as in equation (2-33), represents the signal observed, and corresponds with Vibrational or rotational mode of a molecule in a sample.

$$\text{Raman shift} = \frac{1}{\lambda incident} - \frac{1}{\lambda scattered} = (cm^{-1}) \quad \ldots\ldots\ldots\ldots\ldots\ldots\ldots\ldots\ldots\ldots \text{(2-16)}$$

A Raman spectrum is obtained by plotting the detected number of photons (intensity) against Raman shift from the incident monochromatic beam.

2.10.3 Raman spectroscopy Experimental

The Raman spectra of the catalysts recorded in this work were obtained using Renishaw system-1000 dispersive Raman spectroscope. The spectra were obtained by placing a small amount of catalyst sample on the microscope slide to produce a spot of *ca.* 3μm in diameter. The radiation from the Argon ion laser source (wavelength of 514.5nm and operated at a power of 20 mW) was focused on the sample using a camera linked to the controlling computer. A backscattering geometry with an angle of 180° between the illuminating and collected radiation was used for spectra collection. The spectra can then be recorded and the spectrometer was checked daily for calibration by using a silicon standard.

Andrew Watts at Cardiff University obtained the Raman spectra.

2.11 X-ray Photoemission Spectroscopy (XPS)

2.11.1 Introduction to XPS

Siegbahn in 1967, published a comprehensive study of XPS which summarised the recognition and uses of XPS.[24] XPS is a surface technique used to determine the elemental composition, chemical state, electronic state and empirical formula of the elements that exist within the sample. The XPS concept was based on photoelectric effect as outlined by Einstein in 1905 in which use photons to describe the ejection of electrons from a surface when photons impinge upon it.[17, 19]

2.11.2 XPS theory

The XPS phenomenon is based on the Einstein photoelectric effect as mentioned earlier. It involves using x-rays (usually Mg Kα, 1254eV or Al Kα, 1487eV monochromatic radiation) with sufficient energy ($h\nu$) to lead to ionization and emission of core electron or valence electron or inner shell with binding energy (BE) and kinetic energy (KE). An appropriate instrument is used to measure the kinetic energy distribution of the emitted photoelectrons (the number of emitted electrons as a function of their kinetic energy).

The overall process involved may be represented as follows:

$$A + h\nu \rightarrow A^{+} + e- \quad \text{..... (2-17) (a)}$$

From the conservation of energy:

$$E(A) + h\nu = E(A^+) + E(e\text{-}) \quad \text{..... (2-17) (b)}$$

But since the energy is in form of K.E, equation (b) can be written as

$$KE = h\nu - (E(A^+) - E(A)) \quad \text{.....(2-17) (c)}$$

The final term in the bracket, (equation c) represents the Binding Energy and equation (c) can be written as

$$KE = h\nu - BE \quad \text{.....(2-17) (e)}$$

The kinetic energy and binding energy of each emitted electron is characteristic of the atom or element from which it is emitted. Each atom can give rise to several characteristic binding energy corresponding to the emission of electrons from different energy levels in the atom.

However, the emission of primary electrons from an atom A, leads to the creation of vacancies and the ionized atom is said to be in the excited state, A^{+*}. The transition of an electron to a lower energy level accompanies the decay of the excited ion, which either results also in energy evolution in form of x-rays or can be transferred to another electron in the same atom, which is ejected, and such secondary ionised electrons are known as Auger electrons. The XPS process can be written as follows:

$$A + \text{X-rays} \longrightarrow A^{+*} + e \text{ (Primary electron)}$$

$$A^{+*} \longrightarrow A^{+} + h\nu \text{ (X-rays)}$$

$$A{+*} \longrightarrow A^{++} + e \text{ (Auger electron)}$$

It has been observed that when dealing with multi component catalysts, the XPS spectrum seemed to be complex. Nevertheless, with the help of the XPS data table and atlases of binding energy, one can easily identify the peaks from the Binding Energy, and Auger transition of the resulting XPS spectrum. However, there are some limitations, which must be bear in mind when investigating on gold catalysts, especially, the oxidation state of gold. The presence of insulating samples may shifts the binding energies due to charging as reported by Galvagno *et al.*[28], which observed gold signal as high as 5-8 eV on gold catalyst. Secondly, there is uncertainty in fixing the binding energies in an accurate manner due to differential charging. Several methods were available for fixing the value zero of the biding energy, but still lack of

consensus on the acceptable one. However, the use of adventitious Cls as a reference is the most common method.

Several other problems are associated with correct determination of gold such as the X-rays exposure on the XPS may induce reduction of gold as reported by Lucchesi *et al.* [29] on Au/Al_2O_3 samples. It has been also observed that there are significant gold binding energy shifts for particles with diameter <10nm[30]. However, a shift of binding energy of gold of values lower than 84 eV were observed and these effect, depends on the pre- treatment conditions and the oxides support. Similarly, oxygen and hydrogen treatment increases and lowers the binding energy respectively. These effects are related to charge transfer from the support to gold, size and geometric effects. Similarly, the XPS Au signal is sensitive to chemical surroundings and Au/Ti ratio[31]

The detection depth for the Au 4*f*, O, 1s and Ti 2p spectra can be estimated by determining the mean free path of the photoelectrons in solid *via* the so called ' universal curve'[32]. For the gold spectra, the kinetic energy of the photoelectrons is about 1030 eV, which results in a mean free path of about 2nm. For the O 1s and Ti 2p spectra the kinetic energies are ~960 eV and 1030 eV respectively, which results in a mean free path of ~ 1.4nm.

Shirley background subtractions were performed[33, 34] and peak fitting using ESCA XPS fit program. Fits of the Au 4*f* peaks were performed based on the following assumption:

(i) the difference between Au $4f_{7/2}$ and Au $4f_{5/2}$ was set to 3.67 eV,

(ii) the integral intensity of the Au $4f_{5/2}$ is three quarters of that Au $4f_{7/2}$ peak, and

(iii) the peak widths (FWHM) for both peaks, Au $4f_{7/2}$ and Au $4f_{5/2}$, are equal. The FWHM of Au^0 was 0.8 to 1.0 eV; those of Au^{x+} were fixed to 2.2 eV. Further more, the Lorenz- Gauss ratio for each Au species was kept constant

2.11.3 XPS Experimental

The XPS instrument used in this study is a Kratos Axis Ultra DLD spectrometer as shown in figure 2-35. The machine is fitted with a monochromatic AlKα radiation source, refocusing lens to give high-resolution XPS and analyser pass energies of 160eV (survey scans) or 40 eV (detail scans). Binding energies were referenced to the

C (1s) peak from adventitious carbonaceous contamination, assumed to have a binding energy of 284.7eV. Dr Albert Carley and Dr D. Morgan of Cardiff University carried out the XPS analysis.

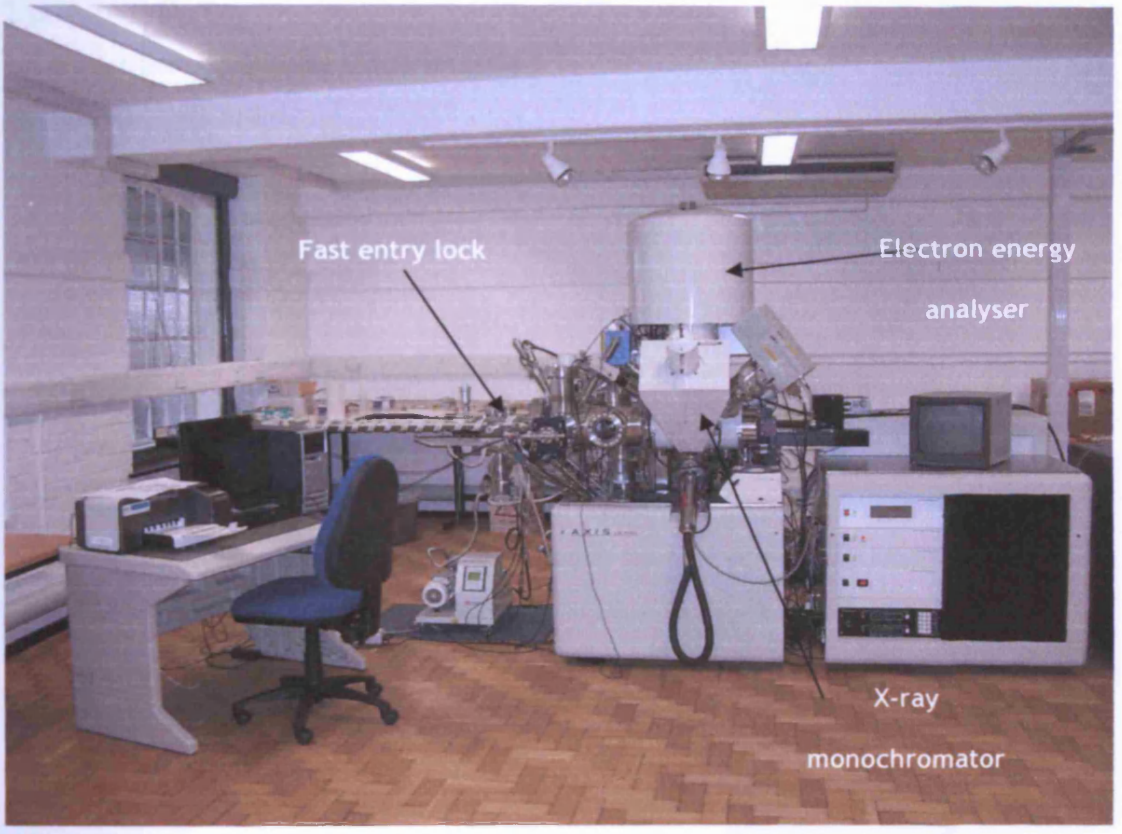

Figure 2-35: Photograph of the ***Kratos Axis Ultra DLD spectrometer***

2.12 X–ray Diffraction (XRD)

2.12.1 Introduction to XRD

X-ray Diffraction (XRD) is another very important technique whereby x-rays are used to identify inorganic materials that are non- molecular and crystalline. In addition to the identification of materials, it also used to identify bulk phases by given information about the arrangement of atoms in materials [18-19, 25-27] to monitor the kinetics of bulk transformations and to estimate particle sizes. XRD is a rapid and non-destructive method and is widely used to determine the structure of the large variety of molecules or compounds. Each crystalline solid has a unique XRD pattern,

which is used as fingerprint for its identification. The XRD is based on the discovery in 1913 that cleavage faces of crystals appear to reflect X-ray beams at certain angles of incidence (θ), known as Bragg's Law.

2.12.2 XRD theory

As earlier mentioned, the XRD technique was based on Bragg's Law. Bragg's Law can be written as follows:

$$n\lambda = 2d \sin \theta \qquad (2\text{-}18)$$

Where:

θ = angle of incidence of X-rays

λ = wavelength of the x-rays

d = distance between the atomic layers in the crystal

Bragg's equation can be derived and depends on the conditions necessary to make phases of beams coincide when the angle of incident equals to reflecting angle.

The rays of the incident beam are always in phase and parallel up to the point at which the top beam strikes the top layer at atom X (figure 2-36). The second beam

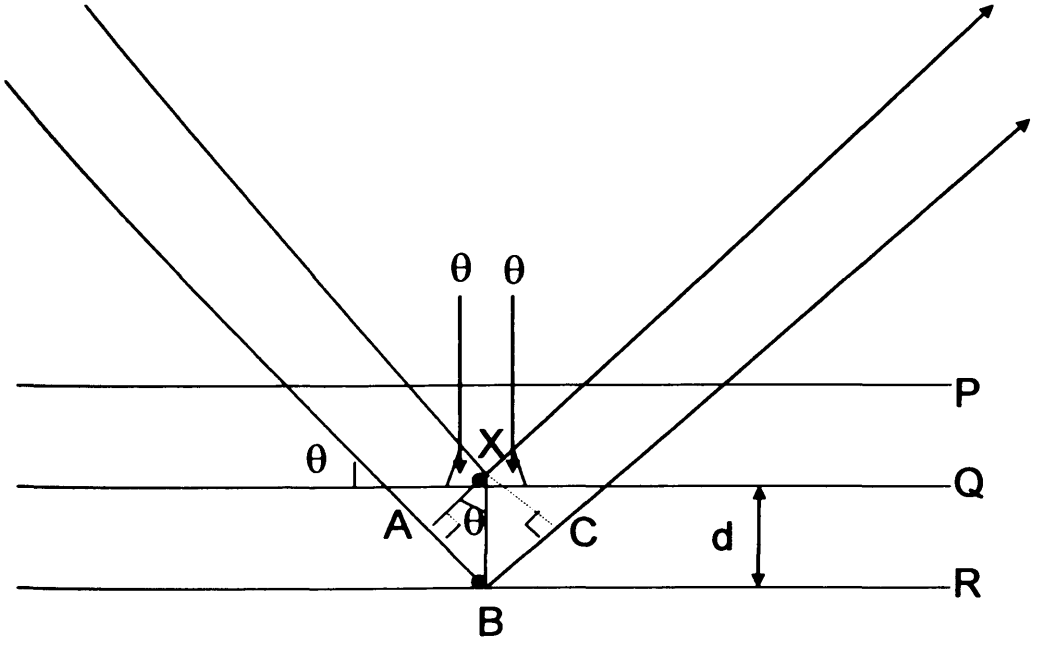

Figure 2-36: Schematic representation of illustration of Bragg's Laws

continues to the next layer where it is scattered by atom B. The second beam must be travel the extra distance AB + BC if the two beams are to continue travelling adjacent and parallel. This extra distance must be an integral (n) multiple numbers of wavelengths (λ) for phases of the two beams to be the same:

$$n\lambda = AB + BC \qquad (2\text{-}19)$$

From figure 2-36, in the right-angled triangle ABX, d can be regarded as the hypotenuse, and we can use trigonometry to relate d and θ to the distance (AB + BC). The distance AB is opposite θ so,

$$AB = d \sin\theta \qquad (2\text{-}20)$$

Because AB= BC equation (2-19) becomes,

$$n\lambda = 2AB \qquad (2\text{–}21)$$

Substituting equation 2-20 in equation 2-21, we have,

$$n\lambda = 2\, d \sin\theta \qquad (2\text{-}22)$$

From the illustration above (figure 2-36), Bragg's Law has been derived and the location of the surface does not change the derivation of Bragg's Law.

Generally, X-rays are produce from the collision of high-energy charged particles (e.g. electrons accelerated at 30,000V) with matter. The resulting X-ray spectra are usually composed of a broad of wavelength known as white radiation and a number of fixed or monochromatic wavelengths. White radiation formation occurs when electrons are slowed down or stopped by the collision and some of the lost energy changes in to electromagnetic radiation.

Once the monochromatic Cu Kα radiation (X-ray beam) produced is incident on the sample, it is being diffracts (scatters and reflects). The detector picks up the diffracted X-rays and the diffraction pattern consists of spots for single crystals and concentric circles for powdered samples as used in this research. These correspond to the regions of constructive interference and for constructive interference of the diffracted X-rays to be observed, the Bragg's equation must be satisfied (2-22).

2.12.3 XRD Experimental

In this work, powdered X-ray diffractometer was used to identify the crystalline phases present in the catalyst. The powdered diffractometer used is an Enraf Nnious PSD 120 diffractometer with monochromatic Cu Kα source operated at 1.2KW (40KeV and 30mA).In each case, the sample was placed in a sample holder and rotates as the X-rays struck the sample. The experimental patterns were calibrated against silicon standard and by matching the experimental patterns to the JCPDS powder diffraction data.

2.13 References

1. M. Haruta, T. Akita, P. Lu, S. Ichikawa and K. Tanaka, *Surface Interface Anal.*,**31** 73.(2001).
2. M. Haruta, *Catalysis Today* **36**, 153 (1997)
3. *in Conference Gold* - Vancouver (2003).
4. M. Haruta, N. Yamada, T. Kobayashi and S. Iijima, *J. Catal.*, 11 (1989).
5. T. Hayashi, K. Tanaka, and M. Haruta., *J. Catal.*, **178**, 566 (1989).
6. G.C Bond, and D. T.Thompson, *Gold Bull,* **33,** 41, (2000).
7. M. Haruta, *Chemical Record,* **3,** 75, (2003).
8. J. H. Liu, A. Q. Wang, A. Q. Y.S. Chi, Y.S. Lin, H.P. Mou,. *J. Phys. Chem.* B. **40,**109 (2005).
9. M. Date, M. Okumura, S. Tsubota, M. Haruta,. *Angew. Chem. Int. Edu.* **2004,** 43 2129.
10. S. H. Overbury; L. Ortiz- Soko, H. G. Zhu, B. Lee, M. D. Amiridis, S. Dai. *Catal. Lett.* **2004, 99** 95
11. A. Knell. P. Barnickel, A. Baiker, A. Wokaum,. *J. Catal.* **137,** 306, (1992).
12. D. James. E. Fourre, M. Ishii, and M. Bowker,. *Applied Catalysis, B: Envirnmental* , **45,** 147 (2003).
13. J. M. C. Soares; P. Moralla; A. Crossley; P. Harris; and M. Bowker; *J. of Catalysis*, **17,** 219, (2003).
14. D. James; Selective Propene Oxidation on Metal Oxide Catalysts. PhD, University of Reading, (2002).
15. S. O. David (2000). Mass spectrometry desk reference. Pittsburgh: Global View Pub ISBN 0-9660813-2-3.

16. S. Branauer; P. H. Emmett; E. Teller., *Journal of American Chemical Society* **60**, 309(1938).
17. B. Grzybowska- Swierkosz, *Topic in Catalysis* 11/12 23 2000.
18. A. R. West., *Basic Solid State Chemistry*, 2nd Edition, 1999, john Wiley and Sons, 125-160.
19. J. W. Niemantsverdriet, *Spectroscopy in Catalysis*: an introduction, (2005), 165-192.
20. G. Herzberg, *Infrared and Raman Spectra of Polyatomic Molecules*, Vanostrand Reinhold, NY, (1945).
21. N. B. Colthup, S. E. Wiberley and L. H. Daly.' *Introduction to Infrared and Raman Spectroscopy*, Academic Press, New York and London (1964).
22. J. M. Brown, *Molecular Spectroscopy*, Oxford Chemistry Primer, (1998).
23. P. W. Atkins,. *The Elements of Physical Chemistry*, (2000).
24. K. Siegbahn; *et al; Nova Acta Regiae Societatis Scientiarum Upsaliensis*, **20** 282, (1967).
25. J. P. Glusker, M. Lewis., M. Rossi., *Crystal Structure Analysis for Chemist and Biologists*, VCH Publishers, NY: 1994, ISBN 0471185434.
26. J. Drenth; *Principle of Protein X-ray Crystallography*, Springer P. Verlag Inc. NY: 1999, ISBN 0387985875.
27. G. Rhodes; *Crystallography Made Crystal Clear,* Academic Press, C.A: 2000, ISBN 0125870728
28. S. Galvagno, C. Milone, A. Donato, G. Neri, F. Neri and A.M. Visco, *Phys. Chem. Chem. Phys.*, **1**, 2869 (1999)
29. P. Claus, J. Radnik and C. Mohr, *Phys. Chem. Chem. Phys.*, **5**, 172 (2003)
30. C.A. Lucchesi, J.E. Lester and M. Batista-Leal, *J. Electron Spectroscopy and Related Phenomena* **11**, 333 (1977)
31. S. Ferrer and C. Ocal, *Surface Science* , **191**, 147 (1987)
32. G. A. Somorjai, '*introduction to Surface Science and Catalysis*' John Wiley and Sons, New York (1994)
33. D. A Shirley, *Phys. Rev.* B **5** 4709 (1972)
34. D. Briggs and M. P. Seah, '*Practical Surface Analysis- Auger and X-Ray Photoelectron Spectroscopy*' 2nd Ed., John Wiley & Sons, Chichester (1990)

Chapter 3- Gold catalyst for CO oxidation

3.1 Introduction

This chapter deals with the properties of gold and its synergies when supported over metal oxides with respect to CO oxidation. Factors investigated are catalyst preparation, different experimental conditions i.e. in aerobic (in the presence of oxygen) and anaerobic (in the absence of oxygen, i.e. in a flow of He alone) conditions were also investigated in order to gain an insight of the mechanism of CO oxidation over a gold supported on titania and other metal oxides.

The results obtained are extensively discussed and compared with the standard catalyst of the World gold council. The understanding of the activity of the catalyst and the variables monitored, coupled with characterization techniques using some analytical instruments such as XPS, XRD, Raman, SEM and Edax, the mechanism of the oxidation of CO over Au/TiO_2 catalyst was proposed as well.

3.2 Carbon Monoxide Oxidation

The catalytic oxidation of CO on gold supported on some metal oxides surfaces has gained increasing importance in recent years in industrial chemistry and, in particular, in automotive emission control. Catalysed CO oxidation is one of the possible future prospects for gold.

3.3 Carbon Monoxide oxidation on Gold

Gold has been regarded as a very inert metal. Consequently, the bonds between gold surfaces and adsorbate, such as CO and CO_2 are very weak. Unlike the considerably stronger CO adsorption on palladium and platinum, it is reported that the bond between CO and the gold surface is almost entirely due to electron donation from molecular CO to the metal. The σ-bond between CO and gold weakens when the coverage increases. Consequently, a lower 'direct donation' contribution to the Au-CO bond strength causes a stronger C-O bond.

In the low temperature range (*i.e.* 200K), CO oxidation catalyst with a highly dispersed gold phase are superior (with respect to activity) to the most active palladium, platinum or silver catalysts.

Highly dispersed, metal oxide supported gold catalysts were found to catalyse various oxidation and hydrogenation reactions, in particular the CO oxidation, already at low temperatures. [1-4] It was further found that in addition to catalyst dispersion also the

procedures for catalyst preparation and conditioning, and the nature of the oxide support play an important role, and it was possible to distinguish between 'active' easily reducible supports and the less active ('inert'), stable oxides [5].

One of the most active support materials is titanium oxide (TiO_2). For instance, Au/TiO_2 catalysts were reported to be an active catalyst for CO oxidation even at 90K[6]. The Au/TiO_2 catalysts (with gold particles sizes 1~10nm) are mostly prepared by coprecipitation or by deposition precipitation followed by calcination in air at temperatures between 120°C and 400°C [7-12].

The highly dispersed metal oxide supported gold catalysts are active and selective for CO oxidation in the low temperature region.[13-15] The term 'low temperature CO oxidation' is not commonly used for the temperature range from -65°C to 150°C [16] is denoted 'low temperature CO oxidation'.

Masatake Haruta was the first to show that CO oxidation can be performed at ambient temperatures using gold dispersed on oxide surfaces. Many researchers are now using CO oxidation as a standard test reaction, and this early work has been extensively reviewed [17-18].

The origin of the highly active Au/MeO_x, especially the Au/TiO_2 catalyst, is still discussed controversially. As a rough outline the different suggestions include (i) the reaction taking place at the interface of the gold particles and the metal oxide, [11, 19-20] (ii) the higher amount of low-coordinated, active gold atoms in small particles. [21-23] (iii) a substrate induced modification of the Au-Au distances, [24,25] and (iv) a quantum size effect, which correlates with the thickness of gold clusters. [26] In detail, the mechanism was studied on model catalyst and directly on the highly dispersed catalysts. The purpose of studies with model catalyst is to understand in the atomic scale, how the catalysts work, i.e., to identify active sites and the detection of reaction intermediates. Concerning the CO oxidation catalysed by Au/TiO_2, model studies were performed on gold single crystals and gold deposited on TiO_2 single crystals or films [25]. On a $Mo(112)(8x2)\text{-}TiO_x$ model catalyst the gold bilayer structure was reported to be significantly more active than the monolayer gold. [27] CO and oxygen adsorption and CO oxidation on Au (110)-(1x2) was studied intensively by Gottfried et al. [28]. The most significant findings were that (i) physiosorbed molecular oxygen has to be activated either by electron or photon impact in order to obtain chemisorbed oxygen (ii) CO adsorbs non dissociatively and (iii) CO can only be oxidised on an oxygen-precovered (chemisorbed oxygen) gold (110)-(1x2) surface. Mullins *et al.* [29]

studied oxygen adsorption on a different gold surface, Au (111). They found evidence for the recombination of oxygen atoms to $O_{2\ ad}$, when the oxygen atoms were deposited on the surface by exposing the sample to a plasma-jet (the plasma jet had ~40% dissociation fraction). They reported the same for an Au/TiO_2 (110) model catalyst.[30] The adsorption of excited molecular oxygen were not excluded, but they did not present direct evidence. Furthermore, they observed significant CO oxidation, when directing a CO beam ($p_{co}=10^{-7}$ to 10^{-6}mbar) on to the model catalyst, which was precovered with O_{ad} .However, it has to be pointed out, that the samples were exposed to significant amounts of reactive atomic oxygen, while for powder catalysts the reaction was observed in the presence of molecular gaseous oxygen. Hence, it was questionable, whether they have a realistic model for the CO oxidation catalysed by Au/TiO_2.

3.3.1 Mechanism of CO oxidation on Gold Catalyst

The reaction mechanisms of the CO oxidation on highly disperse Au/TiO_2 catalyst was studied in numerous publications (11, 31-32). The CO oxidation results were seldom explained by a simple Langmuir-Hinshelwood mechanism for non-competitive adsorption, combined with an additional mechanism of oxygen activation [1]. This reaction mechanism comprises of the following elementary steps:

(i) $CO + * \longleftrightarrow CO*$

(ii) $O_2 + * \longleftrightarrow O_2*$

(iii) $O_2* + * \longleftrightarrow 2O*$

(iv) $O* + CO* \longleftrightarrow CO_2* + *$

(v) $CO_2* + * \longleftrightarrow CO_2 + *$

In some cases however, the CO oxidation results do not correspond with a Langmuir-Hinshelwood mechanism according to Tanielyan. Several uncertainties remain and various mechanistic models were developed. It is also not clear whether the oxygen molecule is dissociatively or non-dissociatively adsorbed, but most likely molecular oxygen is adsorbed at the perimeter interface as reported by Haruta *et al.*[4].

Boccuzzi *et al.*[31-32] intensively studied CO adsorption at 90K and room temperature by Fourier Transform Infrared Spectroscopy (FTIR). At 90K, CO adsorbs on the gold particles and on the TiO_2 support and they postulated a back spill over from the support to the gold and a key role of support oxygen vacancies in the reaction

mechanism. At room temperature, they found that CO molecules, which were adsorbed on terrace sites and on sites at the borderline of the gold particles, were active for CO oxidation. Boccuzzi proposes two different pathways for the oxidation of carbon monoxide. First, oxygen (activated on the surface of metallic gold particles) leading to the formation of CO_2. Boccuzzi considers this mechanism to be the most important for low- temperature CO oxidation

Second, oxygen activates CO, or it enhances the reaction rate of CO species (which were adsorbed at the border of the gold particles) with the lattice oxygen. This slow, induced oxidation by surface lattice oxygen of the support results mainly in carbonates[32]. The suggestion of lattice oxygen participating in the reaction contradicts results of Maciejewski *et al.*[33] and Grunwald *et al.* [11] Maciejewski *et al.* [33] excluded Marsvan-Krevelen mechanism and postulated a reaction between adsorbed CO and molecularly adsorbed oxygen. Grunwald *et al.* detected CO adsorption on gold particles and concluded oxygen adsorption on TiO_2 vacancy sites from Thermal Desorption Spectroscopy (TDS) experiment. Without giving experimental evidence, they suggested the reaction takes place on the gold particles after an O_2- spill-over from TiO_2 support to the gold particles.

Haruta showed that three-temperature regions exist where different kinetics (*e.g.* different rates and apparent activation energies) apply. He proposes potential pathways for the oxidation of CO as shown by figure 3-2.The mechanisms of CO oxidation that have been devised to involved only the gold component are less complicated than those where the support is also implicated. Some of the mechanisms that involved gold alone, were reported by many researchers,

H. H Kung, M.C.Kung and C.K. Costello [34] proposed a model based on the assumption that reactive ionic gold species (i.e. Au^{I} -OH) are present. Figure 3-1 indicates that hydroxyl carbonyl is oxidised to bicarbonates, which is then decarboxylated to Au^{I}-OH and CO_2. The active site is an ensemble of metallic Au atoms and Au-OH. Metallic Au atoms are responsible for activation of oxygen, probably at steps or corner sites.

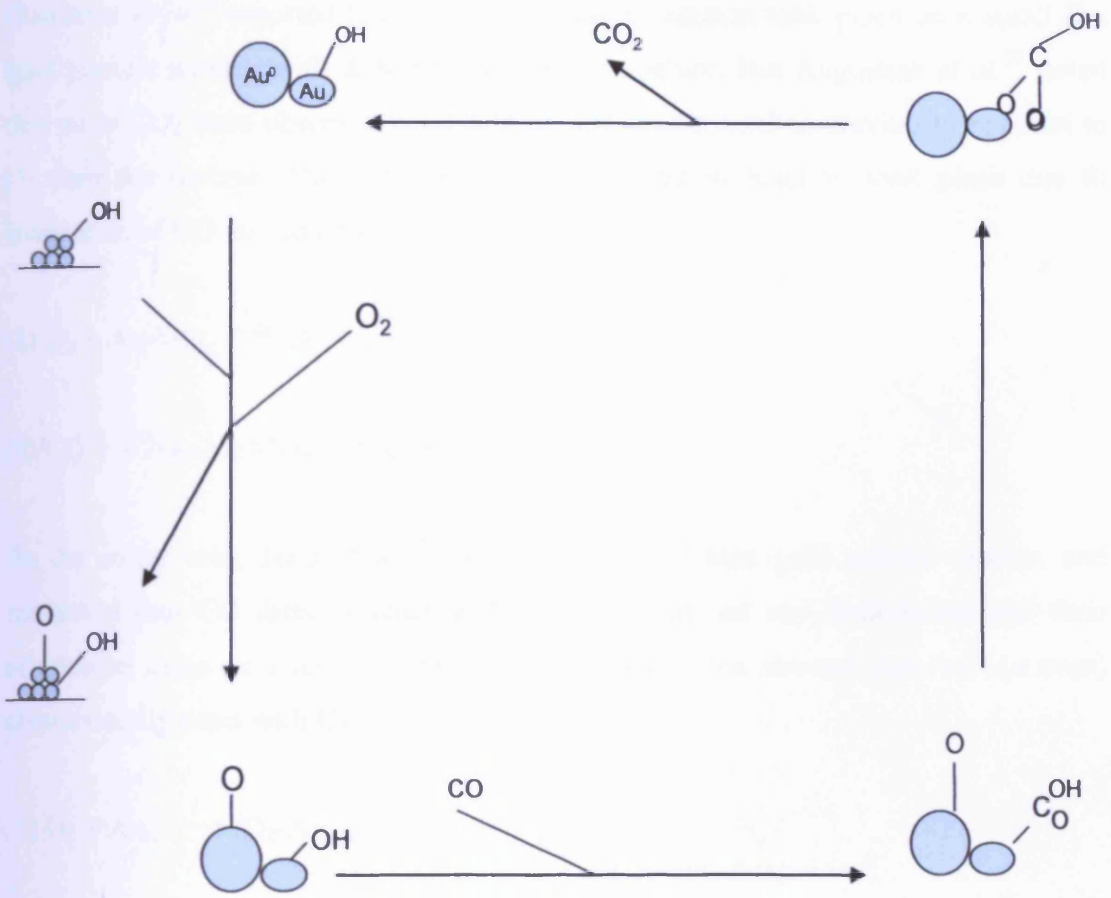

Figure 3-1: The Kung Mechanism of CO oxidation[34]

The simplified version of the mechanism (figure 3-1) can also be presented as follows:

(1) $O\text{-}Au^0\text{-}Au^I\text{-}OH^- + CO \rightarrow O\text{-}Au^0\text{-}Au^I\text{-}COOH^-$

(2) $O\text{-}Au^0\text{-}Au^I\text{-}COOH^- \rightarrow Au^0\text{-}Au^I\text{-}COOOH^-$

(3) $Au^0\text{-}Au^I\text{-}COOOH^- \rightarrow Au^0\text{-}Au^I\text{-}OH^- + CO_2$

(4) $Au^0\text{-}Au^I\text{-}OH^- + 1/2\ O_2 \rightarrow O\text{-}Au^0\text{-}Au^I\text{-}OH^-$

Similarly, Norskov *et al.*[35] reported that the CO oxidation reaction took place on gold surface defect sites and postulated the following mechanism reaction as:

(1) $CO + Au \rightarrow CO\text{-}Au$

(2) $O_2 + Au \rightarrow 2O\text{-}Au$

(3) $CO\text{-}Au + O\text{-}Au \rightarrow CO_2$

Goodman *et al.*[36] reported that the CO oxidation reaction took place on a small flat gold particle surface with different electronic structure. But Augustine *et al.*[37] noted that more CO_2 were observed when CO passed over a catalyst previously exposed to O_2 than the reverse. They claimed the CO oxidation reaction took place due to interaction of CO and adsorbed O_2 not the opposite.

(1) $O_2 + Au/MO_x \longrightarrow O_2\text{-}Au/MO_x$

(2) $CO + 1/2O_2\text{-}Au/MO_x \longrightarrow CO_2 + Au/MO_x$

In the same vein, Jena et al.[38] investigated small size gold anionic cluster, and suggested that CO directly react with oxygen with out any dissociation and their conclusion came as a result of mass spectra data which showed that Au^{n-} (n even) clusters easily react with O_2.

(1) $O_2 + Au_n^- \longrightarrow O_2\text{-}Au_n^-$

(2) $CO + 1/2O_2\text{-}Au_n^- \longrightarrow CO_2 + Au_n^-$

The Discrete Fourier Transform (DFT) calculations on Au12 and Au34 particles and on stepped Au (211) and (221) surfaces lead to the proposal of an Eley- Rideal type of mechanism[39], in which gaseous oxygen reacts with carbon monoxide adsorbed on gold, through the formation of metastable O-O-CO intermediate complex:

$O_2 + CO^* \longrightarrow CO_2 + O^*$ (slow reaction)

The extra oxygen atom adsorbed on gold then reacting quickly with a second CO molecule:

$O^* + CO \longrightarrow CO_2$ (fast reaction)

There are a number of publications that involved the role of the support and the gold for CO oxidation reaction. The mechanisms, which involved the role of the supports, are:

According to Vannice *et al.* [40], a mechanism in which CO was adsorbed on gold and the oxygen adsorbs on the support. Based on their assumption, they conclude that the reaction took place at the interface and the model is a non-competitive Langmuir-Hinshelwood one

(1) $CO + Au \rightarrow CO\text{-}Au$

(2) $CO\text{-}Au + O\text{-}MO_x(i) \rightarrow CO_2$

(3) $O_2 + MO_x(i) \rightarrow O_2\text{-}MO_x(i)$

i - interface MO_x - metal oxide support

Iwasawa *et al.*[41] studied the CO oxidation reaction over $Au/Ti(OH)_4$ by oxygen isotopic exchange using FTIR, O_2 TPD, ESR etc, they pointed out that CO was adsorbs on gold metallic particles and O_2^- adsorbed on oxygen vacancies at the surface adjacent to the Au particles and based on that, they proposed a mechanism as follows:

(1) $CO + Au \rightarrow CO\text{-}Au$

(2) $O_2 + \square \rightarrow O_2^*$

(3) $2CO\text{-}Au + O_2^* \rightarrow 2CO_2$

□ - Oxygen vacancy in the support * - negatively charged molecule

The authors reported similar studies on $Au/Fe(OH)_3$ and proposed the following mechanism:

(1) $CO + Au \longleftrightarrow CO\text{-}Au$

(2) $O_2 + V_s(i) + e^- \rightarrow O_2^-\text{-}V_s(i)$

(3) $CO\text{-}Au + O_2^-\text{-}V_s(i) \rightarrow CO_2 + Au + O^-\text{-}V_s(i)$ slow step

(4) $CO\text{-}Au + O^-\text{-}V_s(i) \rightarrow CO_2 + Au + e^- + V_s(i)$

$V_s(i)$ - Oxygen vacancy in the support at the interface with gold

There are number of studies of CO reaction mechanism that involved gold and support over Au/TiO_2 catalyst; among them is one due Baiker *et al.*[42]. They proposed the CO

oxidation mechanism based on the DRIFTS and Pulse Thermal Analysis data as follows:

(1) $CO + Au \longleftrightarrow CO\text{-}Au$ (reversible adsorption on gold sites)

(2) $O_2 + \square + e^- \rightarrow O_2^-\text{-}\square$ (strongly dependant on support – irreversible)

(3) $2Au + O_2^-\text{-}\square \longleftrightarrow 2Au\text{-}O + \square + e^-$ (spill over, dependant on particle size)

(4) $CO\text{-}Au + Au\text{-}O \longleftrightarrow 2Au + CO_2$ (fast reaction)

□ - Vacancy on TiO_2

Haruta postulated a model in which bidentate carbonates adsorbed on the support are important intermediates for CO_2 formation[43]:

(i) $CO + {}^*Au \longleftrightarrow CO\text{-}{}^*Au$

(ii) $O_2 + {}^*sup + e^- \longleftrightarrow O_2^-\text{-}{}^*sup$

(iii) $CO^{-*}Au + O_2\text{-}{}^*sup \longleftrightarrow CO_3^-{}^*sup + {}^*Au + e^-$

(iv) $CO_3^-{}^*sup + {}^*sup \longleftrightarrow CO_2^-{}^*sup + O^-{}^*sup$

(v) $CO_2^-{}^*sup \longleftrightarrow CO_2 + {}^*sup$

(vi) $2\,O^-{}^*sup \longleftrightarrow O_2 + 2{}^*sup$

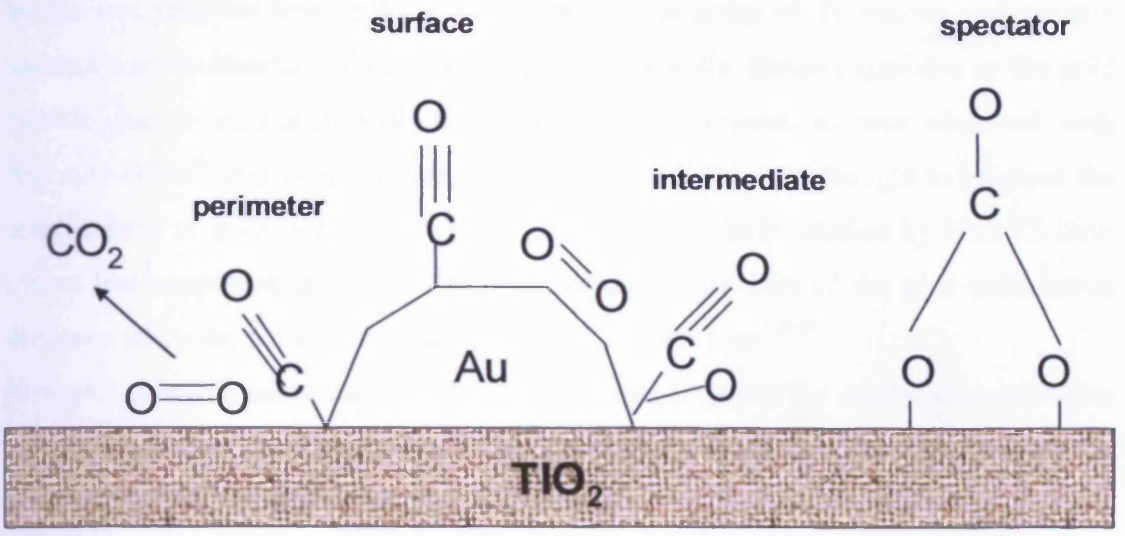

Figure 3-2: Mechanism proposed by Haruta et al[43].

G.C.Bond and D.T.Thampson proposed the following mechanism, involving gold-hydroxide groups.[44]

(i) $Au^0 + CO \rightarrow CO\text{-}*Au^0$

(ii) $Au^3 + OH^-* \rightarrow OH^-*Au^2$

(iii) $CO\text{-}*Au^0 + OH^-*Au^2 \rightarrow COOH^-*Au^2 + *Au^0$

(iv) $O_2 + sup + e^- \rightarrow O_2\text{-}*sup$

(v) $COOH^-*Au^2 + O_2\text{--}*sup \rightarrow *Au^2 + CO_2 + HO_2^-*sup$

(vi) $COOH^-*Au^2 + HO_2\text{-}*sup \rightarrow Au^2 + CO_2 + 2OH^-*sup + sup$

(vii) $*Au^2 + *sup + e^- \rightarrow *Au^3 + *sup$

There have been a number of CO oxidation reactions on Au/TiO_2 support. A number of the publication supported the idea of a Langmuir- Hinshelwood mechanism; [39,45,46,47], oxygen molecules adsorb at the particles edge, the O-O bond being stretched

by electron transfer from gold, initiated by the presence of Ti cations and oxygen vacancies at the interface. Other reactions [48, 49] show the lattice expansion in the gold particle due to mismatch with the lattice of the support, as was observed with Au/MgO (100)[50] and with Au/ anatase-TiO_2 (110); [51] this was thought to increase the effectiveness of gold in catalysing CO oxidation. Similarly, studies by EXAFS have shown that supported gold particles demonstrate contraction of the gold-gold lattice distances when the particle size becomes smaller than 3nm [52-54].

However, J.M.C.Soarers and Bowker *et al.*[55] also reported the catalytic contribution for CO oxidation in our group earlier. The study particularly focused on catalytic and non- catalytic CO oxidation on Au/TiO_2 catalysts.

They point out that during this reaction, the formation of oxidic states on the surface of these Au/TiO_2 catalysts occurs. This results in stoichiometric, non-catalytic reaction with CO to produce CO_2.

The experiment performed by Soares on CO oxidation using an Au/TiO_2 catalyst (prepared by impregnation method), give data showing non -catalytic and non-catalytic behaviour. In the first experimental stages (at low temperature), there was 100% conversion of CO into CO_2 but no oxygen was consumed. It also proved that the oxygen provided came from the catalyst sample itself. In the final stage of the reaction (at 573/673K), the real catalytic oxidation began.

They concluded, after further experiments, that it might be at low loadings that all the Au is strongly associated to the support layer, even resulting in Au oxidation. At increased loading, it may be that Au particles are formed, in which the top layer is not strongly bound to the surface.

In the next experiments, Au/TiO_2 prepared by deposition precipitation was used. It is also known that catalysts prepared by this method are more active than catalysts prepared by impregnation. They show catalytic activity for CO oxidation even at room temperature.

Using many analysis techniques Soares still was not able to clearly point out the nature of the active Au particle responsible for the catalytic reaction. He concluded that CO could be oxidised by Au/TiO_2, prepared by both incipient wetness and deposition precipitation. The latter catalyst however, is much more active for the steady state catalysis. Results have shown at least two ways in with CO can be oxidised by gold through the preparation of the catalysts and catalytic reaction mediated by gold.

Besides, the reaction mechanism, the adsorption and activation of oxygen is discussed controversially. Some researchers postulates O_2 adsorption and activation on the TiO_2 support, [8,11,33,41] mostly with the build-up of O_{2ad}^- -species. These species were detected with electron paramagnetic resonance by Okumura *et al.* (as well as its stabilization by the TiO_2 support), but they excluded its participation in the reaction mechanism. [56] The build-up of an active O_2^- species on the TiO_2 support contradicts the conclusions made by Iizuka *et al.*[9, 30]. In the first study, [9] they circulated CO over Au, TiO_2 and Au/TiO_2 sample, which were precovered with oxygen, and obtained significantly higher amounts of CO_2 on the Au/TiO_2 and Au samples than on the TiO_2 samples. From this results, they concluded, that during CO oxidation on Au/TiO_2 catalysts, the active oxygen is adsorbed on the gold particles. Since CO oxidation is normally performed with simultaneous introduction of gaseous CO and O_2, it is questionable, whether their experiments contribute results for this condition. In a later study, [57] they specified that the oxidation rate is significantly higher, if O_2 is present in the gas phase. They suggested that the gas phase O_2 is directly activated on the surface of the deposited gold particles or their perimeter, without contacting the TiO_2 support. However, no experimental evidence for this suggestion were given. Theoretical studies have revealed that on defective TiO_2 surfaces, oxygen vacancies can stabilize Au atoms and Au clusters, [58, 59] as well as adsorbed molecular oxygen, whose dissociation is enhanced on these vacancies [60].

3.3.2 Kinetics for CO oxidation on Gold Catalyst

The CO reaction kinetics on highly dispersed catalysts are usually studied at atmospheric pressure by varying the CO and O_2 concentrations or partial pressures in the gas mixtures. There is a lot of controversy regarding the order of the reaction and the apparent activation energy. The order and the activation energy are important as they supply valuable information on reaction mechanism; as more than any other technique they indicate directly of what is occurring at the active centres; and the differences in their values ought to reveal changes in mechanism.

The value of the order with respect to CO ranges between 0.05 and 0.5 and that of O_2 between 0 and 0.24 for low temperature CO oxidation on supported gold catalyst, with an activation energy value ranging from 2.1 to 54 KJ/mol. This means that the values strongly vary with catalyst composition and the temperature range used. Possibly

dissimilar reaction pathways exist for CO oxidation on different catalyst types and temperature regions.

The kinetics of these catalysts are independent of the CO concentration and only slightly dependent of the O_2 concentration. This suggests that nearly the entire surface is saturated with adsorbed CO and O_2, and that the reaction is the rate –determining step.[61]

Similarly, the oxygen needed for the reaction is thought to come either from the oxide lattice or from the gas phase. Molecular oxygen adsorbed on gold can easily oxidise near the gold particles, preferentially along the gold/ oxide interface. The oxygen adsorbed on gold can easily oxidise adsorbed CO to CO_2. However, unfortunately, no experimental data about O_2 adsorption on the catalytic surface is known.

3. 3.3 Oxidation state of Gold

The oxidation state of gold has been one of the crucial issues with regard of current research on the principle factors responsible for the activity and inactivity of the gold catalysts for carbon monoxide oxidation. The oxidation state of gold in the active centre is one of the major causes of disagreement as inferred by several methods such as XRD, XPS, and EXAFS etc. Several different kinds of gold species have been identified using FTIR studied of chemisorbed carbon monoxide; [62] these include Au^0, in high or low coordination, "positively polarized" gold atoms at the periphery, [16, 62] and gold species on which both carbon monoxide and oxygen atoms are adsorbed. [63]

The oxidation state of gold have been determined or confirmed by many authors, by considering the effect of pre-treatment on activity; according to many authors, calcination of the catalyst in air is sometimes beneficial, unnecessary, or harmful and can lead to decomposition of the oxidized gold species to Au^0 due to instability in air when the temperature is increased. The decomposition of the gold species leads to loss of chemisorption ability and catalytic activity. [64] Several authors reported the oxidation state of gold to be either as Au^0, or Au^{n+} and some reported to be Au^{n-}.

3.3.4 Research controversy and gaps in the literature

CO oxidation reaction has been regarded as one of the simplest reaction in heterogeneous catalysis. However, the understanding the reaction involved and the mechanism of the reaction is a very difficult task. The literatures were reviewed with respect to reaction Mechanisms of CO oxidation over gold catalyst supported on

different metal oxide. However, they are still subject of controversy due to lack of enough consistent kinetic evidence as the mechanism may differ from one catalyst to another because of the different activation energies and orders of reaction obtained by different authors. Some of the above mechanisms are more simplified than others. While other mechanisms involved intermediate species (e.g. carbonate, formate, hydroxyl groups, etc.).

However, the following have been observed as a consensus as the factors responsible for the oxidation of CO over gold catalyst supported onto different metal oxides:

1. Large supported gold particles and unsupported gold in the form of sponge, wire, and powder are weakly active for CO oxidation.[65-67] While, the small or fine gold powder (mean particle size 76nm) shows activity in the range 249-294K.[9]
2. Choice of the support is another important factor. The CO oxidation reaction success depends on using an oxide of the transition Series elements[10]. Many authors recommended titanium and iron as the most interest and very effective for CO oxidation.[1] Many authors included that of alumina and silica but are very less efficient. [68, 69, 70]
3. Good method of preparation is another important issue for CO oxidation. Methods of preparation such as impregnation and ion exchange have proved to be insufficient for CO oxidation. [31, 40, 71, 72, 73, 74] However, successive calcination and reduction have reported to generate good activity for CO oxidation.[40].
4. Good activity of the catalyst for CO oxidation were found for most metal oxide supported on small gold particles less than 5nm in size, with the highest rates being shown at sizes of about 2-3nm. [3,30-31, 40]
5. Presence of moisture and hydrogen in the reacting system has been found to enhance the CO oxidation over gold supported on metal oxides [47, 76, 77].
6. Another crucial factor is the mode of pre-treatment of the catalyst before use. Catalysts calcined in air show good activity for CO oxidation while reduction of the catalyst is not helpful.

However, there is still much to do concerning the gold catalysis with respect to CO oxidation, as there are a lot of questions and controversy, which need clarification such as:

1. Why the activity of the catalyst is sensitive to methods of preparation and pre-treatment? In what circumstances are the methods and pre-treatment desirable and what the best conditions to use?
2. What is low temperature CO oxidation and what gold species is active at low temperature? Is it (Au^0, Au^{n+} or both)?
3. Does the activity of the catalyst increase or decrease with time on stream before attaining a steady state?
4. Do the kinetic parameters (order of reaction, activation energy etc) supposed to be varied and what factors are responsible for that?
5. How does effectively gold itself catalyse oxidation of carbon monoxide.
6. How do chlorine and other impurities poison the catalysts?
7. From all the different interpretations of the low particle size effect, which one(s) explain conveniently the low temperature activity

The above-mentioned approaches are necessary and the purpose of this thesis will be to give further insight to these questions. As mentioned at the beginning of the introduction, the objective of this work was to investigate the CO oxidation on highly dispersed gold catalyst at low temperature, which includes the characterization of the samples as well as kinetics and Mechanistic investigations.

3.4 Results and discussions

3.4.1 Deposition Precipitation

A set of samples was prepared by the DP method as outlined in the experimental section (chapter II). The samples studied are shown in table 3-1.

S/N	Code	Metal oxide	L/NL (Wt %)	Colour	Tc (°C)	pH control	
						pH	Compound
1	Audpco1	TiO_2	*0.5	Light blue	120	8	Na_2CO_3
2	Audpco2	TiO_2	*1.0	Light blue	120	8	Na_2CO_3
3	Audpco2	TiO_2	*1.0	Light blue	400	8	Na_2CO_3
4	Audpco3	TiO_2	*3.0	Blue/ Violet	120	8	Na_2CO_3

5	Audpco4	TiO_2	*5.0	Blue/ Violet	120	8	Na_2CO_3
6	Audpco5	TiO_2	*20.0	Blue/ Violet	120	8	Na_2CO_3
7	Audpco6	Al_2O_3	*1.0	Light white	120	8	Na_2CO_3
8	Audpco6	SiO_2	*1.0	Light white	120	8	Na_2CO_3

*The Au loading (L) is unknown for these samples but it is always less than the nominal loading (NL) and Tc is pre-treatment temperature

Table 3-1: Deposition precipitation samples

3.4.1.1 Activity studies

3.4.1.1.1Transient activity test

A freshly prepared 1wt% Au/TiO_2 catalyst was prepared using Deposition precipitation method with washing with either water or Na_2CO_3, dried in air at $120^{O}C$ was tested in the Pulse Flow Reactor in order to understand the activity of the catalyst and how the CO oxidation reaction takes place. Figure 3-3 shows the first run of a temperature programmed pulse flow reaction where CO oxidation takes place in a flow of $10\%O_2$/He.

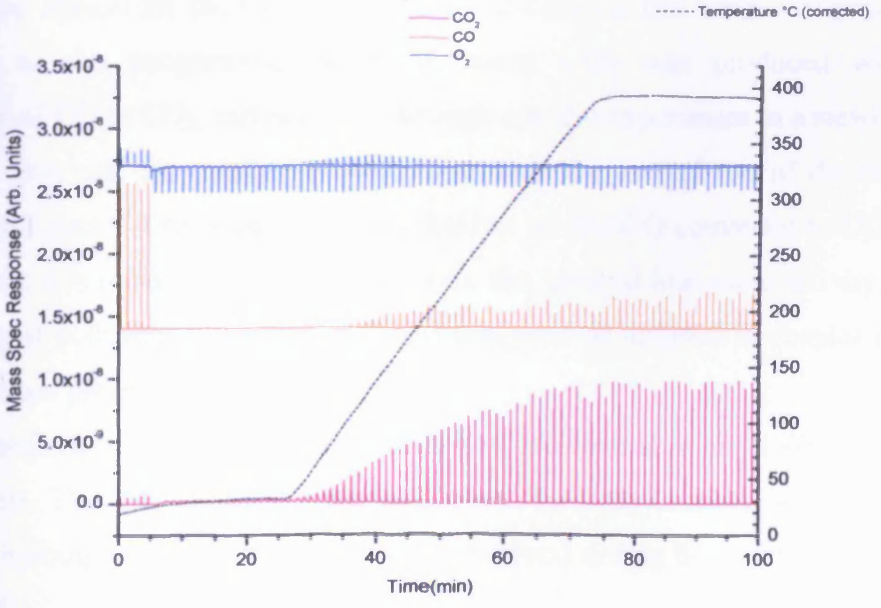

Figure 3-3: Temperature programmed pulse flow reaction for CO in a stream of $10\%O_2$/He flow over a 1wt% Au/TiO_2 catalyst dried at $120^{o}C$ in air.(1^{st} run)

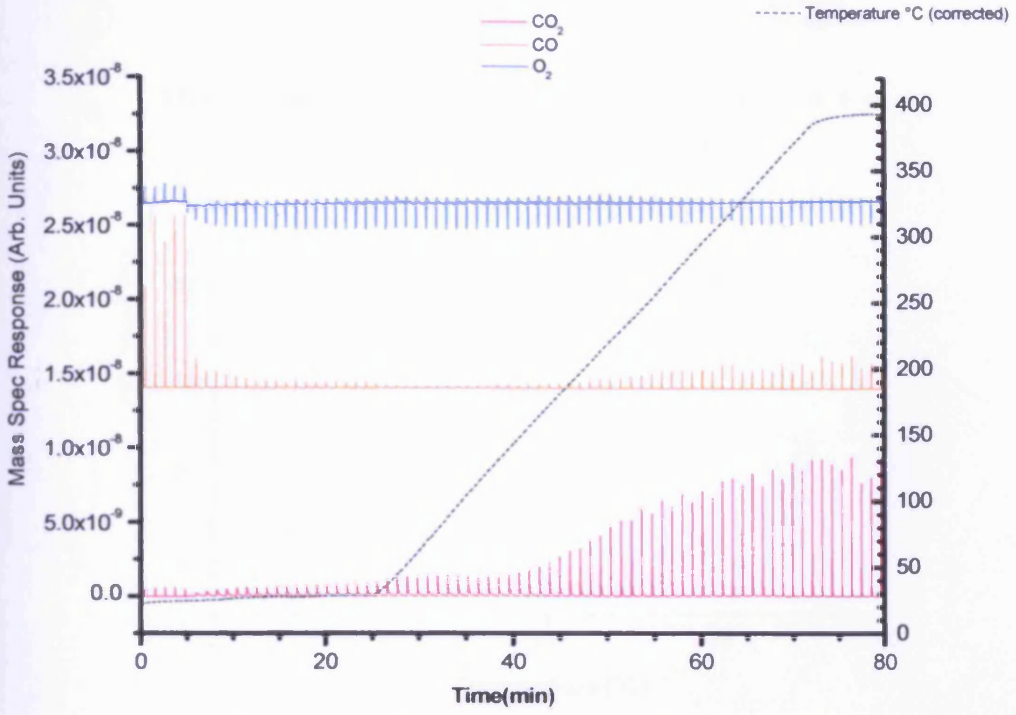

Figure 3-4: Temperature programmed pulse flow reaction for CO in a stream of 10%O_2/He flow over a 1wt% Au/TiO_2 catalyst dried at 120°C in air.(2^{nd} run)

During the first run (Figure 3-3), high conversion of CO was observed at room temperature, almost all the CO pulsed over the catalyst has been converted to CO_2. However, as the temperature increased, more CO_2 was produced with 100% conversion of CO to CO_2, and continue through out the experiment in a steady state.

After the first run, the catalyst cooled down and the second run of the experiment carried out, figure 3-4 obtained. It shows that not all the CO converted to CO_2 at room temperature; this is because after the first run, the catalyst lost some activity. The raw peak areas of both runs was integrated and analysed as outlined in chapter II and the CO_2 yields are presented in 3-5.

Similar results were obtained when the catalyst pre-treated in air at 400°C before the activity test. The CO oxidation reaction over Au/TiO_2 catalyst occurred with no evolution hydrogen gas but with some water evolved during the course of the reaction (figure 3-6).

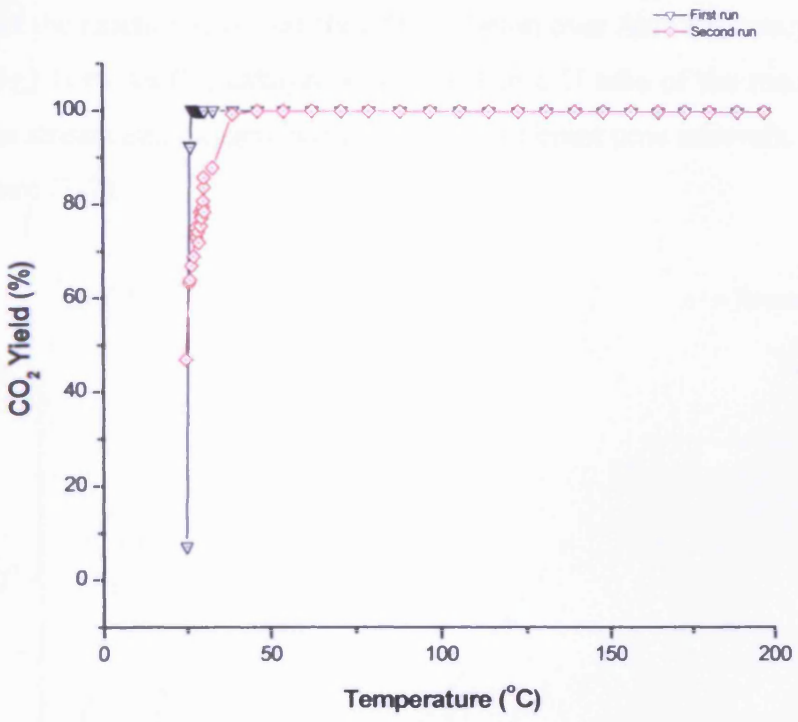

Figure 3-5: CO_2 yield (%) with temperature for CO pulses in a stream of 10%O_2/He flow over a 1%wt Au/TiO_2 catalyst dried at 120°C in air.(1st and 2nd run)

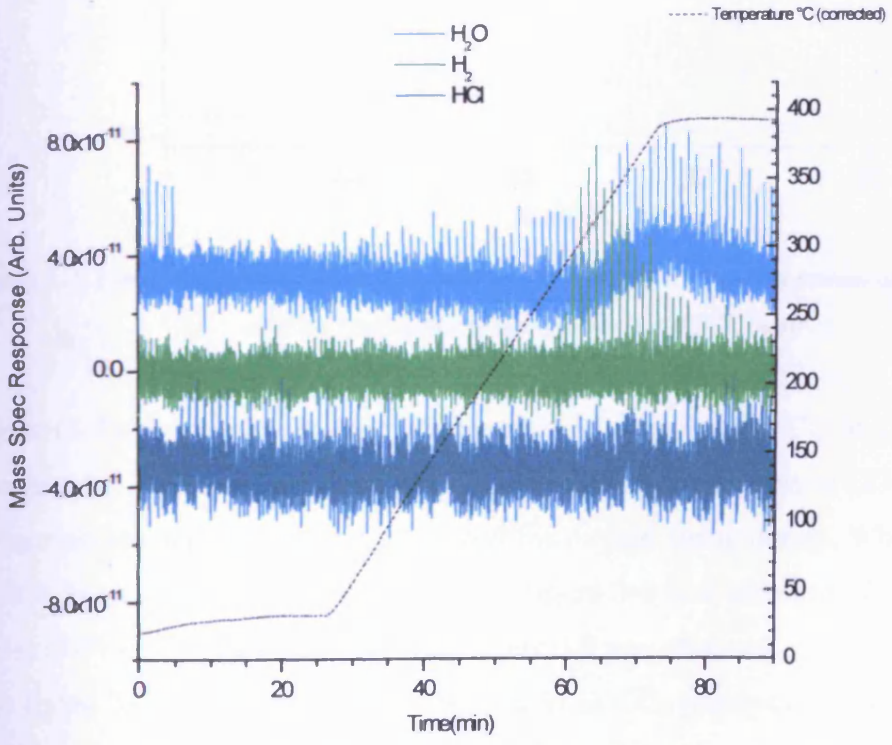

Figure 3-6: Water production for CO pulses in a stream of10%O_2 He flow over a 1%Au/TiO_2 catalyst dried at 120°C in air. (First run)

3.4.1.1.2 Continuous CO oxidation over Au/TiO_2 catalyst

To understand the reaction involved for CO oxidation over Au/TiO_2 catalyst, a freshly prepared (0.5g) 1wt% Au/TiO_2 catalyst was loaded in a U tube of the reactor with CO flowing in the stream and oxygen being pulsed at different time intervals. The result is shown in figure (3-7).

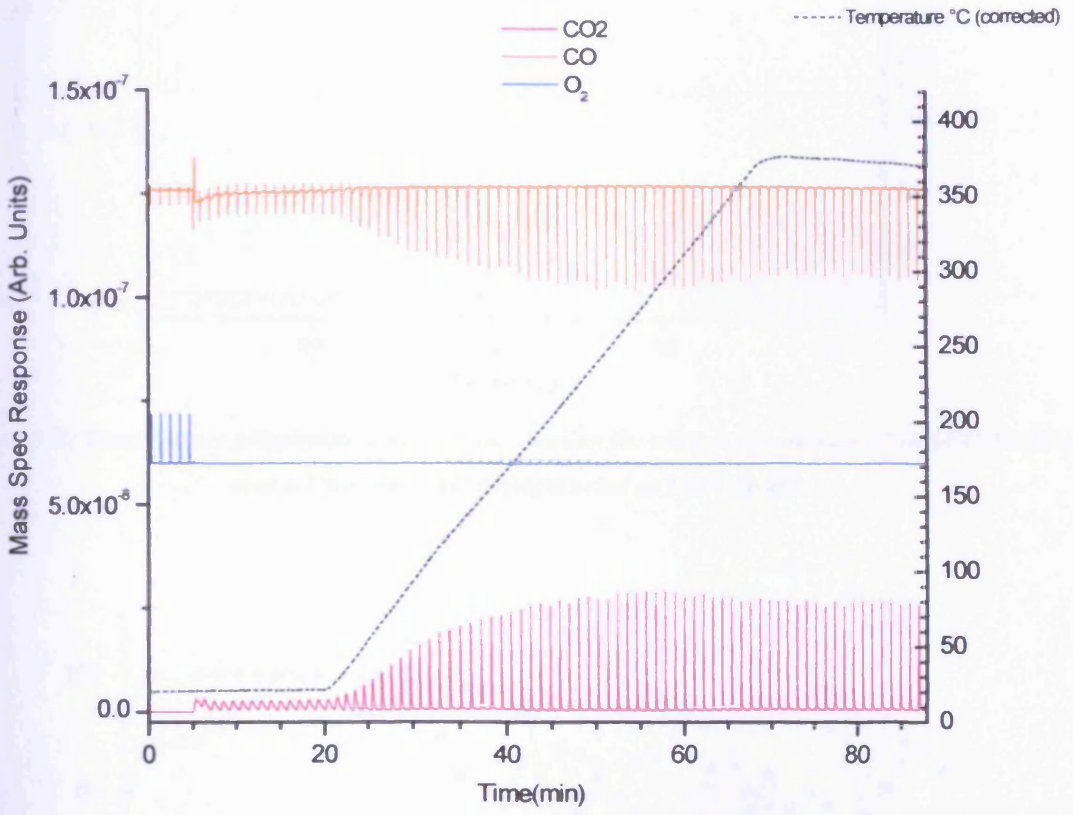

Figure 3-7: Temperature programmed pulse flow reaction for oxygen in a stream of 10%CO/He flow over a 1%wt Au/TiO_2 catalyst dried at 120°C in air

Figure (3-7) shows almost 100% conversion of oxygen with CO to CO_2 at ambient temperature. When the temperature was increased, more signals of CO_2 observed due to reaction between CO in the stream and the oxygen being pulsed. When the first run cooled down and second run carried out, figure 3-8 was obtained. When the data in figure (3-7) and (3-8) were integrated, figure 3-9 was obtained.

The figure 3-7 (first run), shows 100% yield of CO_2 observed at room temperature, continues in a steady state, and drops slightly as the temperature increased. However, similar patterns were observed for the second run but 100% to CO_2 was observed at lower temperature than the first run.

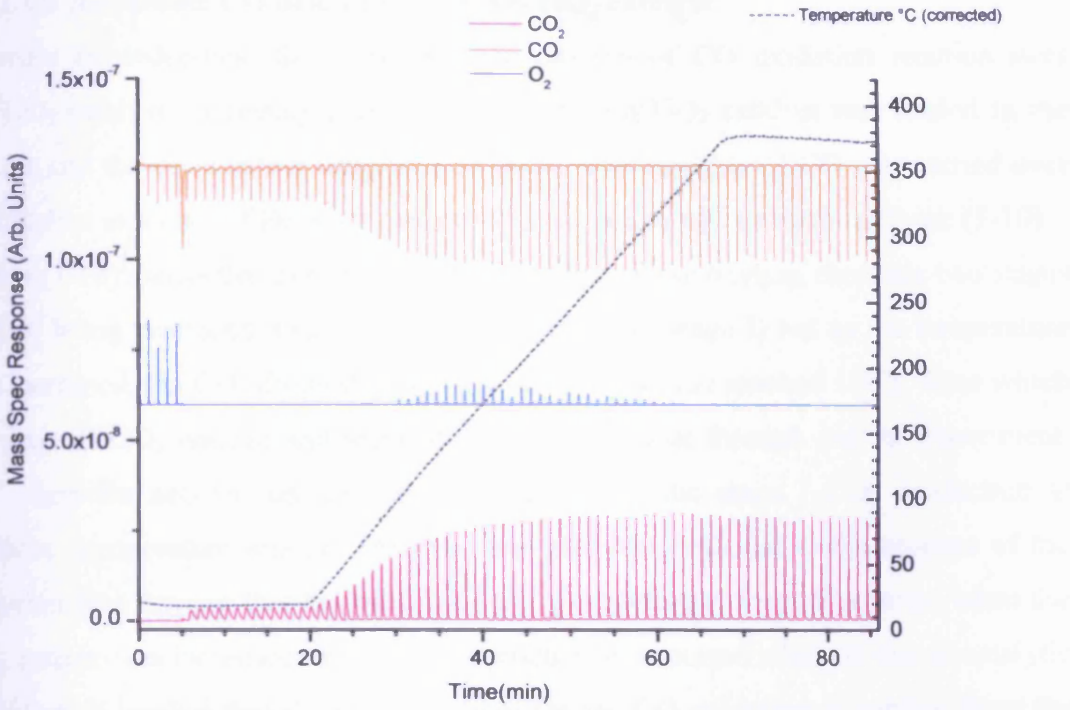

Figure 3-8: Temperature programmed pulse flow reaction for oxygen in a stream of 10%CO/He flow over a 1%wt Au/TiO_2 catalyst dried at 120°C in air

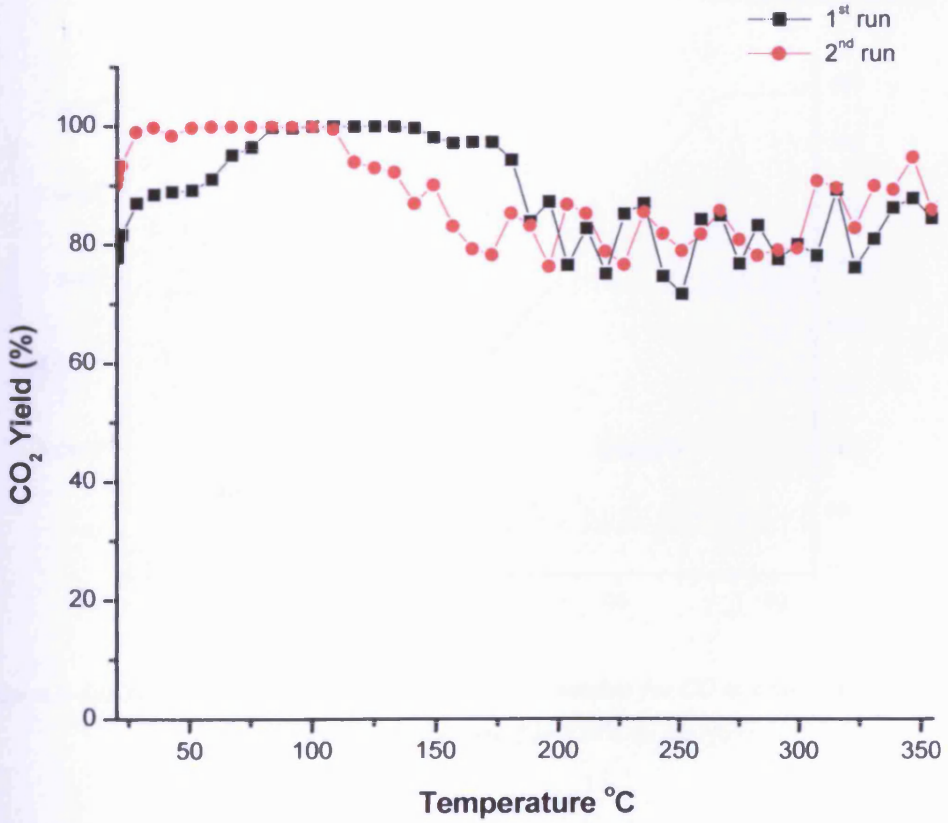

Figure 3-9: CO_2 yield (%) with temperature for oxygen pulses in a stream of 10%CO/He flow over a 1%wt Au/TiO_2 catalyst dried at 120°C in air.(1st and 2nd run)

3.4.1.1.3 Anaerobic CO oxidation over Au/TiO_2 catalyst

In order to understand the active surface oxygen of CO oxidation reaction over Au/TiO_2 catalyst , a freshly prepared DP 1wt% Au/TiO_2 catalyst was loaded in the reactor and the temperature programmed pulse flow reaction of CO was carried over the catalyst in a flow of He alone (anaerobic) and the result is shown in figure (3-10). Figure (3-10) shows that even in the absence of gas phase oxygen, there are two stages of CO_2 being produced. One at ambient temperature (stage I) but as the temperature was increased, the CO_2 drops slightly until the temperature reached 100°C from which the stage II CO_2 emerge and remained in a steady state through out the experiment. But when the second run was done (figure 3-11), the stage I CO_2 production at ambient temperature was not observed and may be attributed to the absence of the active surface oxygen that has been used off and no longer there. However, when the temperature was increased, stage II CO_2 production occurred which is due to catalytic activities. It implies that the active oxygen for the CO oxidation is coming from the sample not due to catalytic activity.

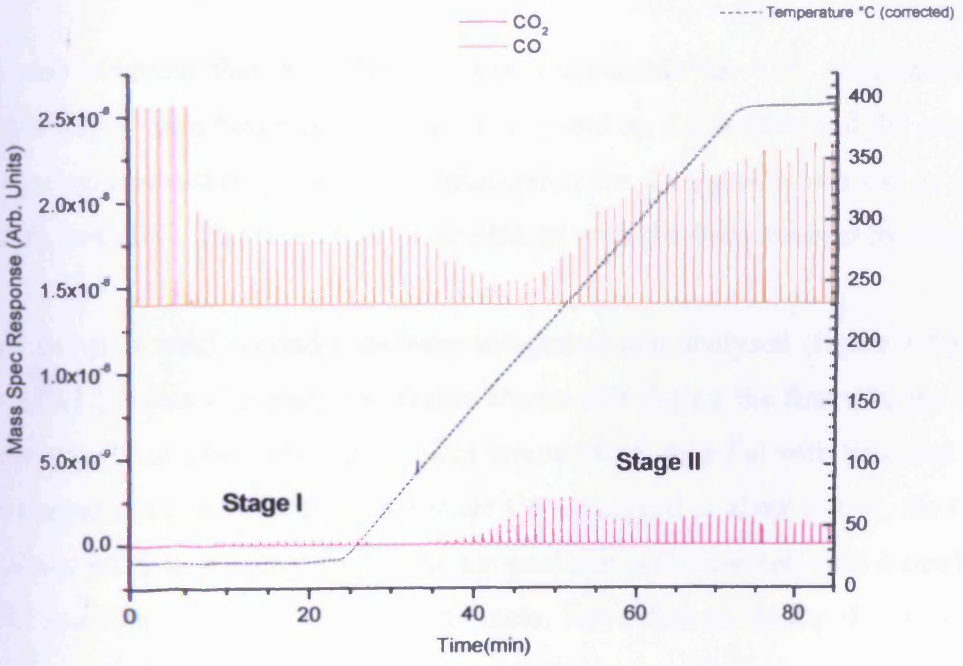

Figure 3-10: Temperature programmed pulse flow reaction for CO in a stream of He flow over a 1wt% Au/TiO_2 catalyst dried at 120°C in air (first run)

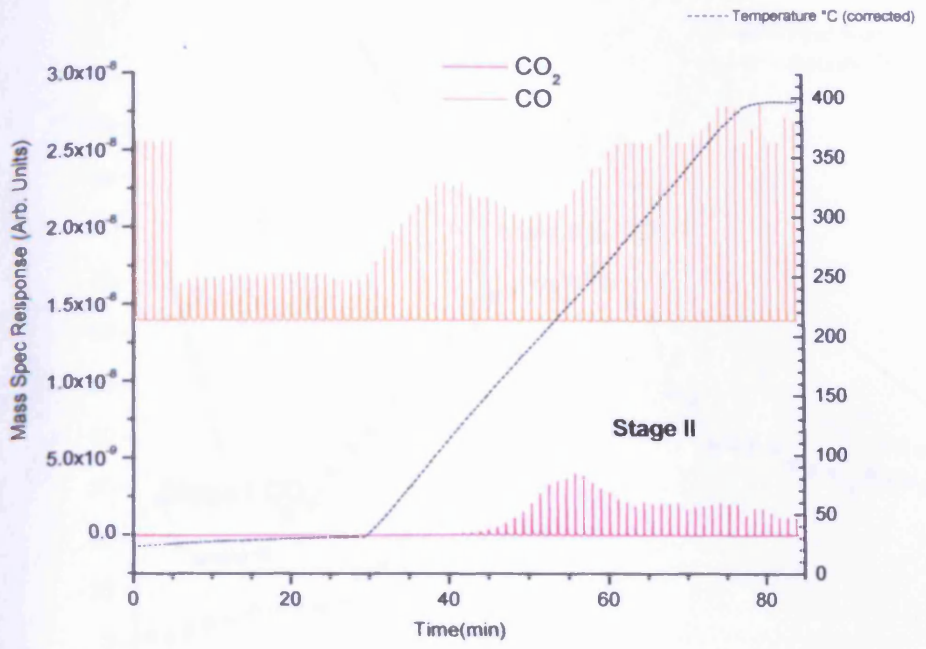

Figure 3-11: Temperature programmed pulse flow reaction for CO in a stream of He flow over a 1wt% Au/TiO_2 catalyst dried at 120°C in air (second run)

it is also evident that the active oxygen responsible for CO_2 produced (First and Second stage) are two types, one loosely bound on the surface and the other the gas phase oxygen must be present for consumption for CO_2 production and is due to true catalytic activity. The results are in agreement with the data obtained by Jorge *et al.*[21]

When the first and second runs were integrated and analysed (figure 3-10 to 3-11), figure (3-12) was obtained. The figure shows that during the first run, the CO_2 yield for the stage I is about 30% at ambient temperature, then fall with time and increased with temperature. However, as the stage CO_2 emerged at about 200°C, the CO_2 Yield was about 98% and then drops as the temperature was increased until it reached about 300°C and then continues in a steady state. Nevertheless, during the second stage I CO_2 was not observed at ambient temperature because the active surface oxygen was used during the first run and as the temperature was increased to 200°C, more CO_2 (stage II) was obtained with yield value of 98%, higher than the first run. The CO_2 yield (stage II) has been due to catalytic reaction involving the support oxygen and CO as confirmed by the XPS, which only shows reduction of support surface

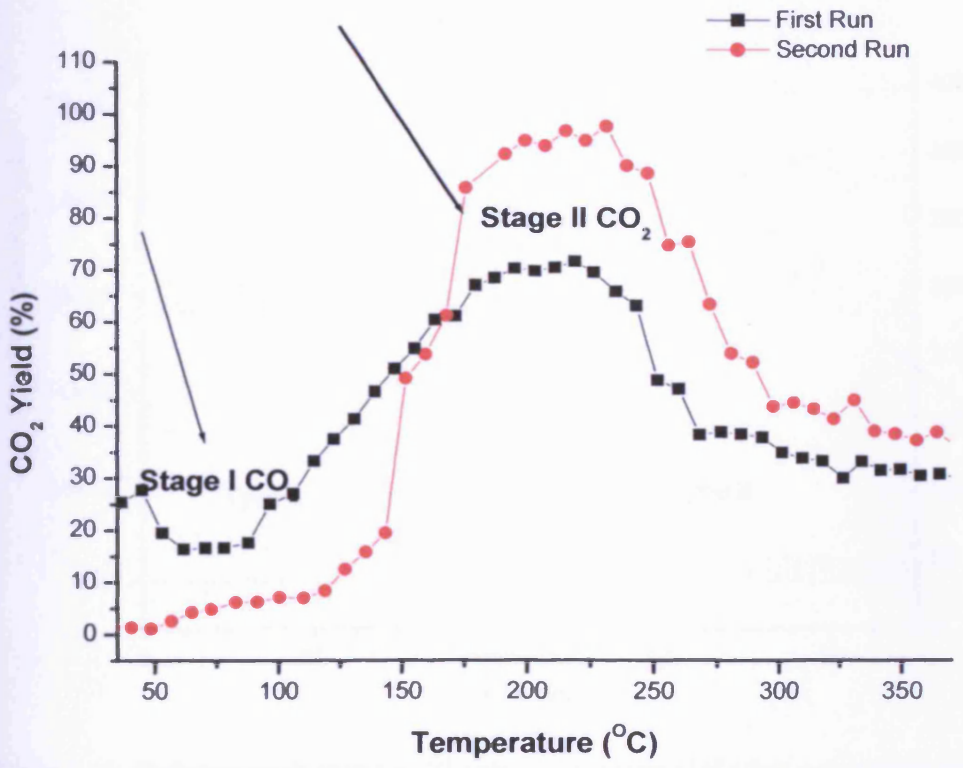

Figure 3-12: CO_2 yield (%) for CO pulses in a stream of He flow over a 1wt% Au/TiO_2 catalyst dried at 120°C in air. (First and second run)

However, the anaerobic CO oxidation over a 1wt% Au/TiO_2 catalyst produced CO_2 together with a massive production of hydrogen. The hydrogen production was observed in the first and with the highest production observed in the second run experiment of the anaerobic CO oxidation reaction over a 1wt% Au/TiO_2 catalyst (figure 3-13).

The hydrogen produced may be due to the following reactions either between the hydroxides of the catalyst or due to water gas shift as shown below in equation 1 and 2:

1. $Au(OH)_3 \longrightarrow Au^{3+} + 3OH^-$

$2OH + 2CO \longrightarrow 2CO_2 + H_2$

2. $CO + H_2O \longrightarrow CO_2 + H_2$

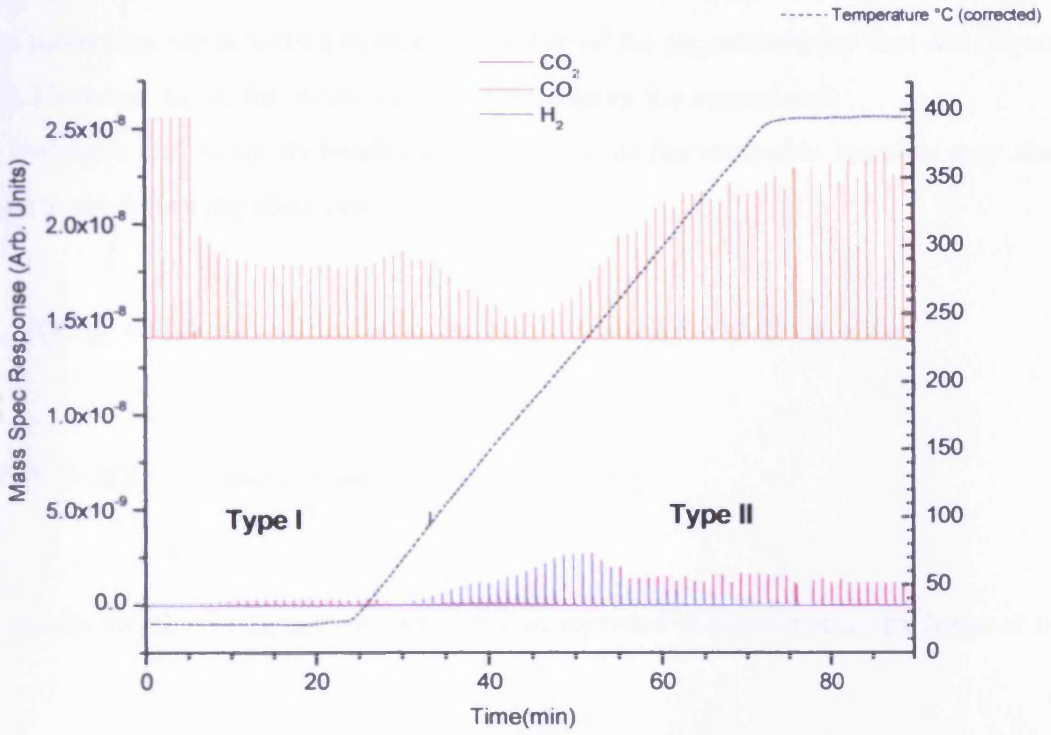

Figure 3-13: Hydrogen production for CO pulses in a stream of He flow over a 1w%t Au/TiO_2 catalyst dried at 120°C in air. (First run)

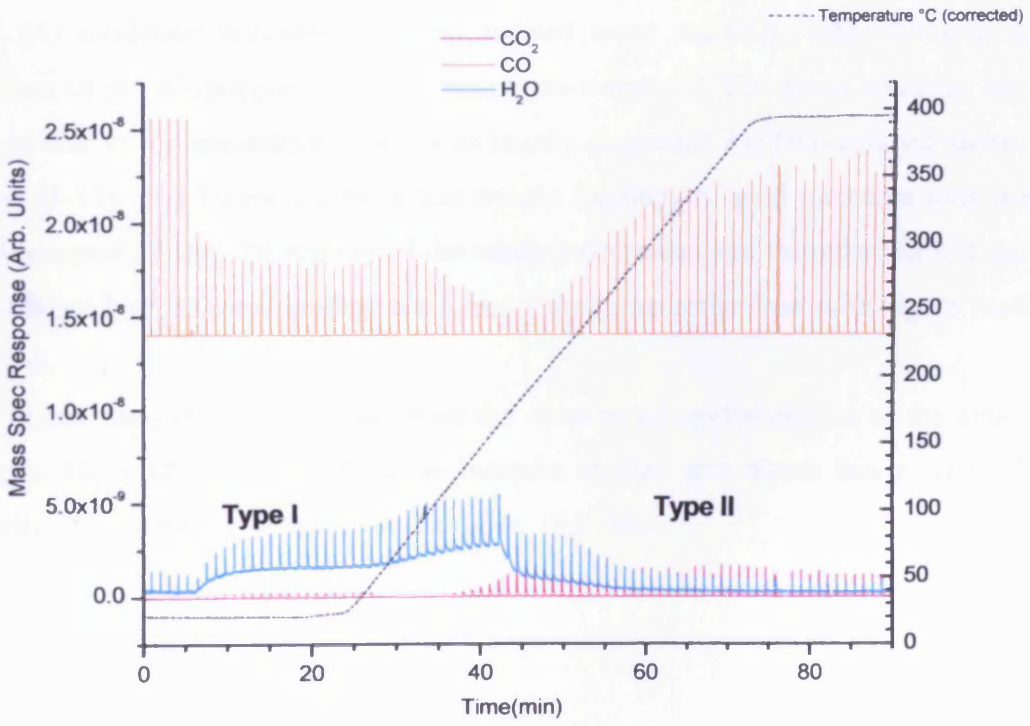

Figure 3-14: Water production for CO pulses in a stream of He flow over a 1wt% Au/TiO_2 catalyst dried at 120°C in air. (First run)

It was observed that, during anaerobic CO oxidation over a 1wt% Au/TiO_2 catalyst, water molecules are desorbed during the course of the experiment for first run (figure 3-14). However, no water molecules observed during the second run.

The hydrogen and water molecules produced due to the anaerobic reaction may also be due to the following reactions

1. $Au(OH)_3 + CO \longrightarrow Au^{3+} + H_2O + OH^- + CO_2$

2. $2OH + 2CO \longrightarrow CO_2 + H_2$

The results are also in agreement with data as reported in the literature by Jorge *et al.* [21]

3.4.1.1.4 Effect of weight loadings of Au over Au/TiO_2 catalyst

The CO oxidation reaction was investigated over Au/TiO_2, with different gold loadings over TiO_2 support under different pre-treatment. The result obtained for the CO oxidation for uncalcined catalyst of highly dispersed Au/TiO_2 catalyst shown in figure (3-15). The figure shows as the weight loadings of gold increases over metal oxide support (TiO_2), the activity of the catalyst decreases and from the result it shows that the catalyst with low loading are found to be more active than with higher loading catalyst.

The higher the gold loadings the more the chances of agglomeration of the catalyst. Making the gold catalyst to become increase in size and shows less activity. The activity of the catalyst increases in the order, 1>3>5%.

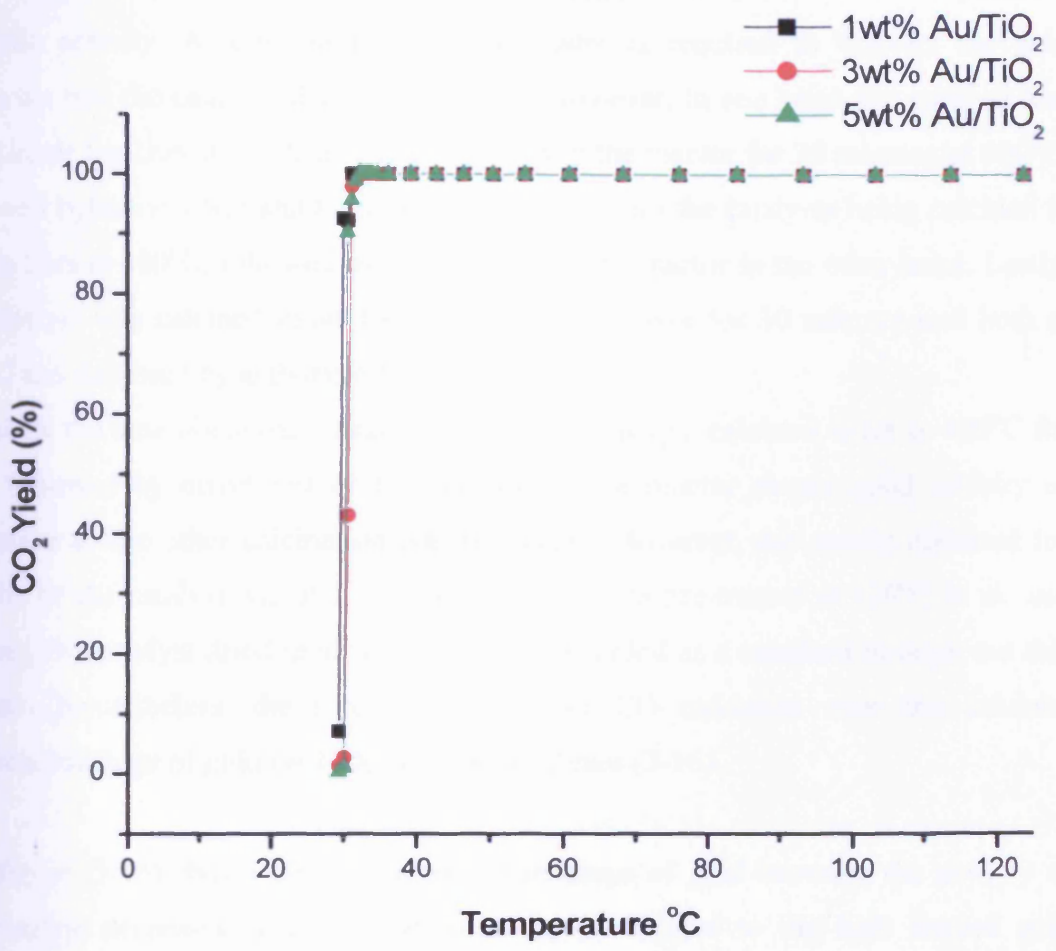

Figure 3-15: Comparison of CO_2 yield (%) with temperature for CO in a stream of 10%eO_2/ He flow over different gold loadings supported onTiO_2 catalysts dried at 120°C in air

3.4.1.1.5 Effect of calcination of Au/TiO_2 catalyst

Calcination of a highly dispersed gold supported on metal oxide catalyst, have been shown by many researchers to enhance or decrease the activity of the catalyst for CO oxidation. There are a lot questions regarding calcination of the CO catalyst, that under what circumstances is calcination desirable and what is the best condition to use? To answer these questions, the catalyst was subjected to a number of pre-treatment conditions in order to get an insight on the best condition of the catalyst for CO oxidation.

The catalyst pre-treatment controls the gold particle size, and thus the potential catalytic activity. A low calcination temperature is required to convert the gold precursor into the catalytically active species. However, in one hand, the catalyst was dried in air for 2hrs at 120°C and then calcined in the reactor for 30 minutes at 400°C, followed by activity test and these were compared with the catalysts being calcined in air for 2hrs at 400°C, followed by a direct test in the reactor in the other hand. Lastly, the catalyst was calcined in air for 2hrs and in a reactor for 30 minutes and both at 400°C and followed by activity test.

Based on the data obtained, it was found that the catalyst calcined in air at 400°C for 2hrs followed by direct test of the catalyst in the reactor shows good activity as compared to the other calcination pre-treatments. However, the results obtained for activity of the catalyst was still less than the catalysts pre-treated at 120°C in air and for that, the catalyst dried in air at 120°C was regarded as a standard through out this chapter. Nevertheless, the results obtained for CO oxidation over the calcined different loadings of gold on TiO_2 is shown in figure (3-16).

The figure (3-16) shows that as the weight loadings of gold increase, the activity of the catalyst decreases. The calcination is more effective to the high loaded gold catalyst, as compared to the low loaded gold catalyst as the calcination of gold catalysts results in a large gold particle size and subsequently makes the catalyst less active[81].

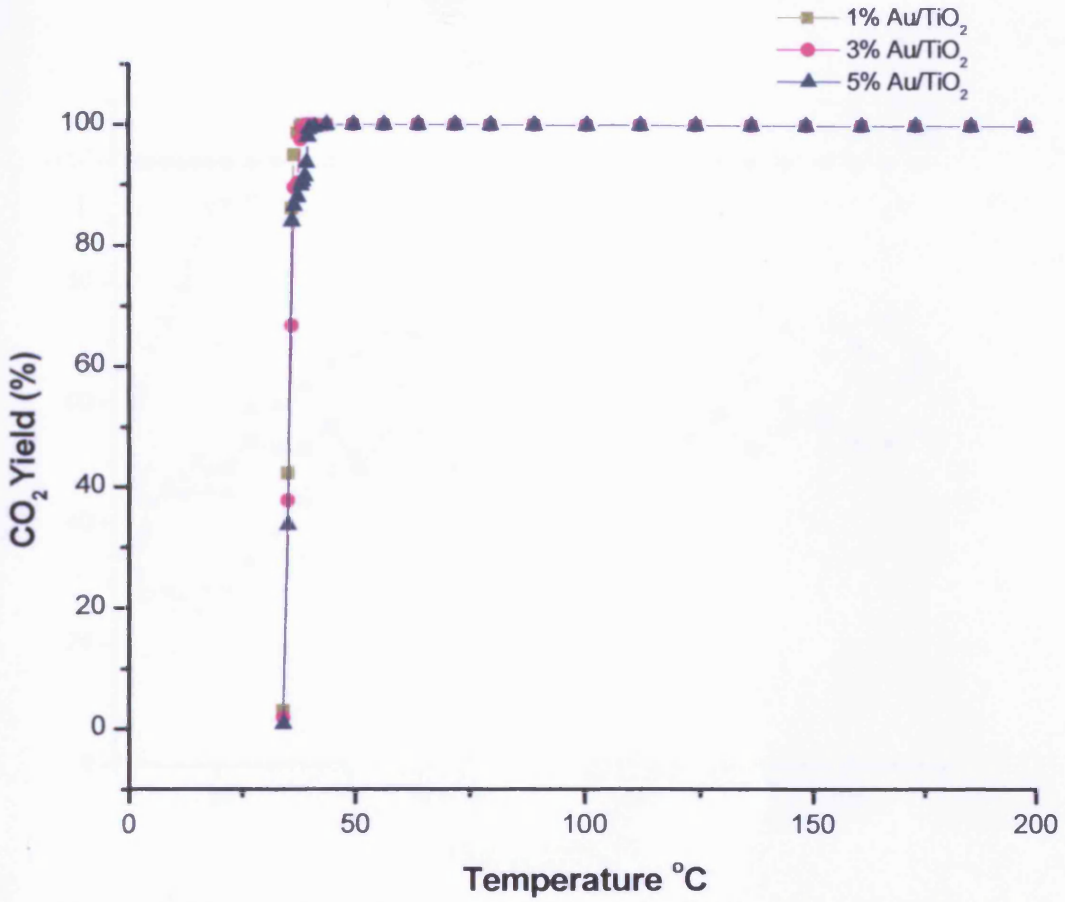

Figure 3.16: Comparison of CO_2 yield (%) with temperature for CO pulses in a stream of 10%eO_2/ He flow over different calcined gold loadings of Au/TiO_2 catalysts calcined at 400°C in air

3.4. 1.1.6 Effect of varying the Au/TiO_2 catalyst loadings

The effect of different catalyst loadings has been investigated in order to get an insight to the activity of these different catalysts with respect to CO conversion to CO_2. To deduce that a number of different freshly prepared 1wt% Au/TiO_2 catalysts were loaded in the reactor as 0.05, 0.2, 0.3, 0.4 and 0.5g were compared and the data obtained shown in figure (3-17). The results show that 0.1g of a freshly prepared 1wt% Au/TiO_2 catalyst shows low CO_2 yield at room temperature (< 38%). However, as the temperature was increased to 100°C, the yield of CO_2 begins to increase and become steady with CO_2 being ~50%.

The CO oxidation observed for 0.2g of the loaded catalyst is similar in activity with that of 0.1g with CO_2 being 38% and as the temperature was increased to 100°C, CO_2 yield increased remarkably to about 60% and continue in a steady state through out the experiment.

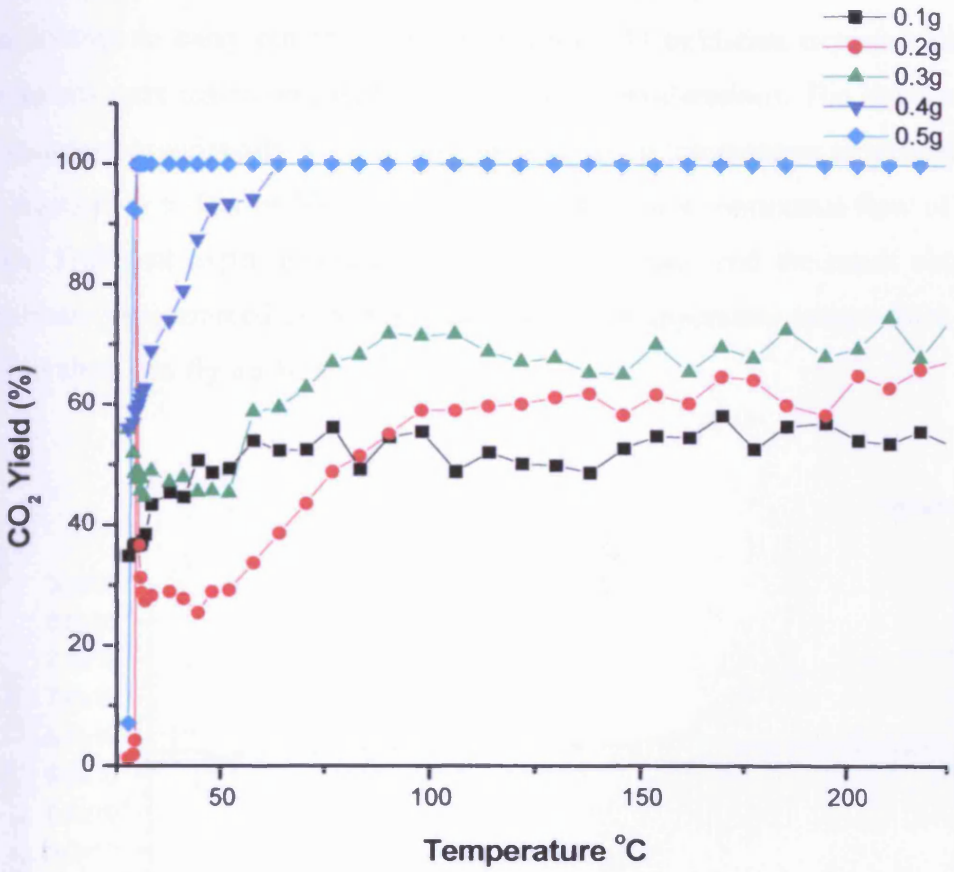

Figure 3-17: Comparison of CO_2 yield (%) with temperature for CO in a stream of 10%O_2/ He flow over different loadings of Au/TiO_2 catalysts dried at 120°C in air

However, the activity of 0.3g of the loaded catalyst of 1%wt Au/TiO_2 shows a little bit higher CO conversion to CO_2 than 0.1 and 0.2g of the catalyst with CO_2 yield being almost 50% at room temperature. Nevertheless, as the temperature was increased to 100°C, the CO_2 yield increased to 70% then drops and continues in a steady state with a value being ~65%.

Similarly, the CO oxidation to CO_2 observed at room temperature for 0.4g and 0.5g of the loaded catalyst of 1wt% Au/TiO_2 catalyst was 60 and 100% respectively. However, when the temperature was increased to 50°C, the CO_2 yield for 0.4g loaded catalyst was almost 90% and by the time, the temperature reached 70°C, already, the conversion of CO was 100% to CO_2 and continues in a steady state through out the experiment.

Therefore, the CO oxidation reaction to CO_2 over a freshly prepared 1wt% Au/TiO_2 catalyst increases with the high loading of the catalyst in the reactor.

3.4.1.1.7 Low temperature CO oxidation over Au/TiO_2

In an attempt to carry out the low temperature CO oxidation experiments, several experiments were carried out with great care and considerations. The low temperature CO oxidation experiments were carried out, one using temperature programmed pulse flow reaction in a flow of $10\%O_2$/He, and the other in a continuous flow of both CO and O_2. Different experimental parameters were varied, and the result obtained for temperature programmed pulse flow reaction with temperature ranges from -50°C to 100°C is shown in figure 3-18.

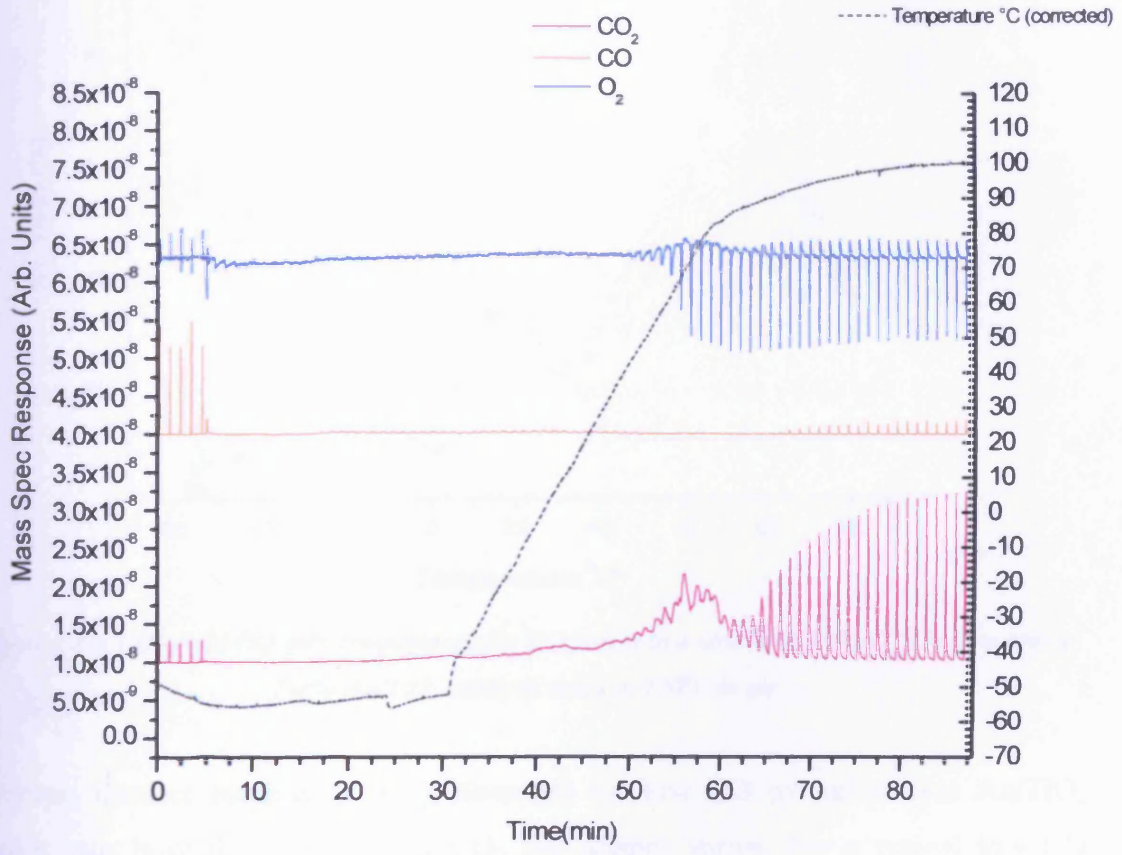

Figure 3-18: Low temperature programmed pulse flow reaction for CO in a stream of $10\%eO_2$/ He flow over a 1wt% Au/TiO_2 catalysts dried at 120°C in air

From figure 3-18, it shows that no CO_2 was produced at lower temperature; the actual break through of CO_2 took place at about 20°C. Several techniques were employed in order to investigate the reason behind this observation. However, it was concluded that at lower temperature the CO_2 produced are being poisoned on the surface of the catalyst, presumably, the freezing point temperature of a dried ice was lower than that

of CO_2. Hence solidified the CO_2 produced which later desorbed after heating the catalyst. When the data in figure 3-18 were integrated and analysed, figure 3-19 was obtained. The figure shows low yield of CO_2 at low temperature due to poisoning of CO_2, but when the temperature was raised the CO_2 yield begins to increase due to desorption of CO_2 at relatively high temperature (20°C) and 100% conversion was observed at approximately 80°C.

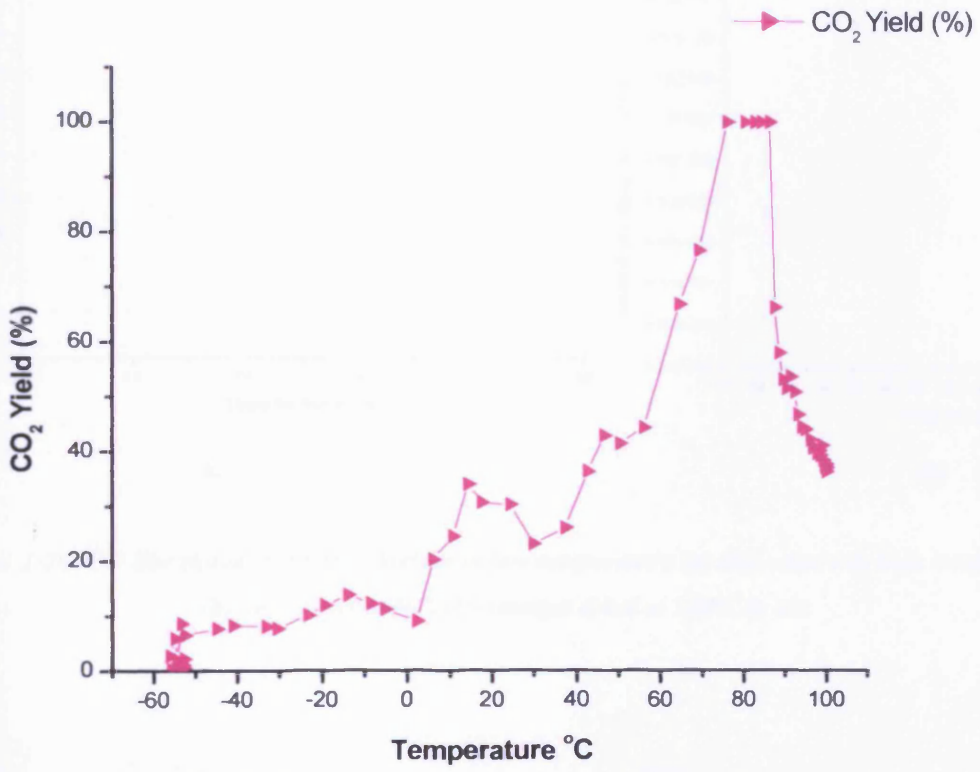

Figure 3-19: CO_2 yield (%) with temperature for CO pulses in a stream of 10%eO_2/ He flow over a 1wt% Au/TiO_2 catalysts dried at 120°C in air

However, another interesting thing observed for low CO oxidation over Au/TiO_2 catalyst was how the CO, O_2 and CO_2 line shapes varies. For a typical low CO oxidation over a 1wt% Au/TiO_2 catalyst, such as in figure (3-18). The CO line shape was observed to be short, broaden and a little bit wider than the normal CO peaks at room temperature. The short and broad peaks for CO observed may be due to low desorption of adsorbed CO at low temperature. Nevertheless, when the temperature was relatively increased, the CO peaks sharpened and narrowered and this was as a result of fast desorption and due to cracking of CO_2 (mass 28 amu signals) as evident in figure 3-20a and b.

The long height and sharp peaks observed for CO_2 at relatively high temperature will be due to the fast desorption of CO_2 adsorbed on the surface of the catalyst at that temperature as in figure 3-21a and b.

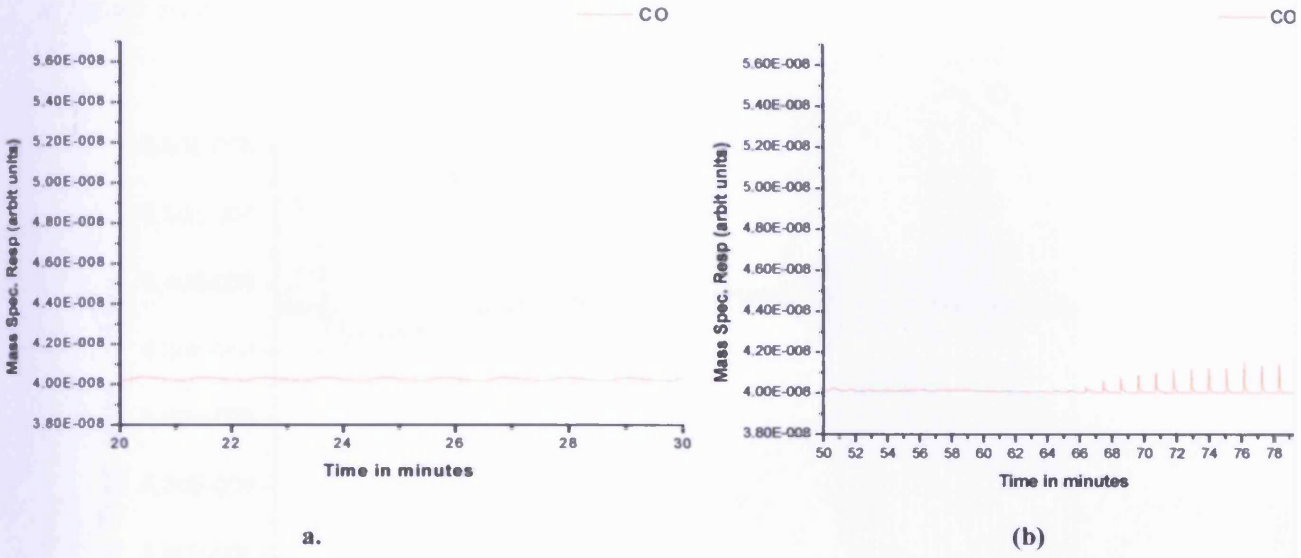

Figure 3-20: CO line shapes for CO oxidation at low temperature (a) and relatively high temperature (b) over a 1wt% Au/TiO_2 catalyst dried at 120°C in air

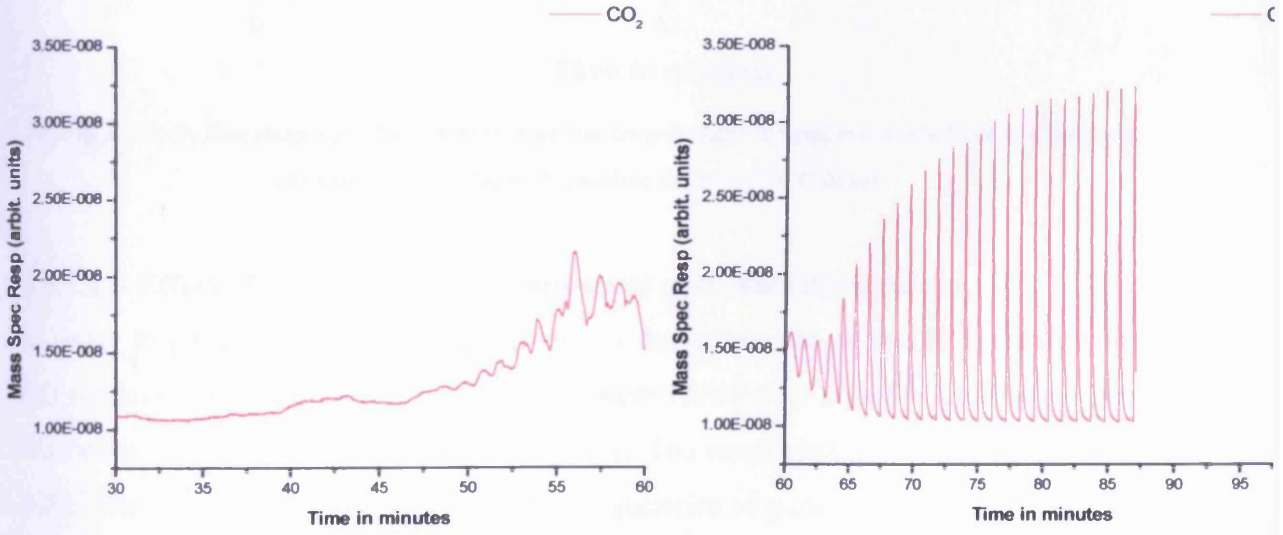

Figure 3-21: CO_2 line shapes for CO oxidation at low temperature (a) and relatively high temperature (b) over a 1wt% Au/TiO_2 catalyst dried at 120°C in air

In the same vein, the peak intensities observed for oxygen at low temperature seems to show very low adsorption of oxygen and the uptake observed to be slow and very small. The intensity of the peaks observed at that temperature seems very short and broad but as the temperature was increased, more O_2 uptake was observed with very deep peak intensity due to fast up take of O_2 at that particular temperature as evident in figure 3-22.

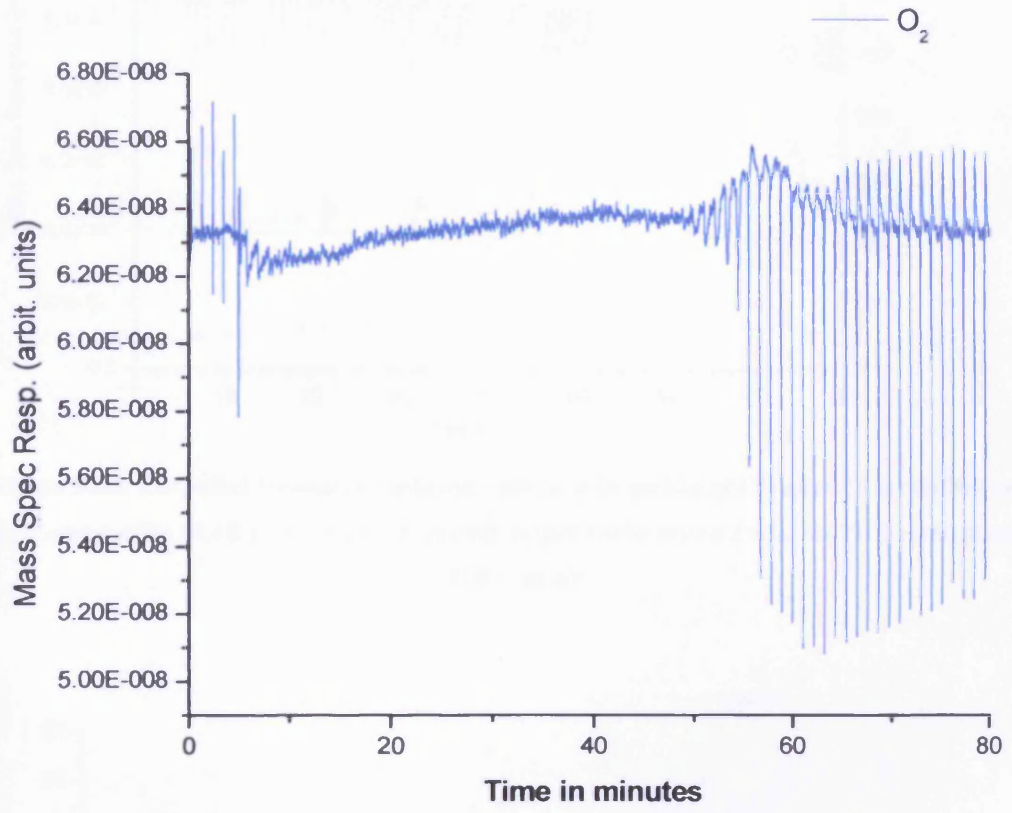

Figure 3-22: O_2 line shapes for CO oxidation at low temperature (a) and relatively high temperature (b) over a 1wt% Au/TiO_2 catalyst dried at 120°C in air

3.4.1.1.8 Effect of variation of CO frequencies over Au/TiO_2 catalyst

In order to get an insight on what happens in the active site on Au/TiO_2 catalyst for CO oxidation, the frequencies of CO pulses were varied over a 1wt% Au/TiO_2 catalyst with constant flow of 10%O_2/He in the stream. The result obtained is shown in figure 3-23. The figure shows that the more the frequencies of pulses of CO, the more CO_2 produced. When the heights of CO_2 produced plotted against relative amount of CO flow, figure 3-24 obtained. The figure (3-24) shows direct proportionality between the CO_2 with relative amount of oxygen. The more the frequency of CO pulses, the more

the CO_2 produced. Less CO_2 were observed with CO pulses at every 60 seconds while for CO pulses in every 5 seconds more CO_2 observed.

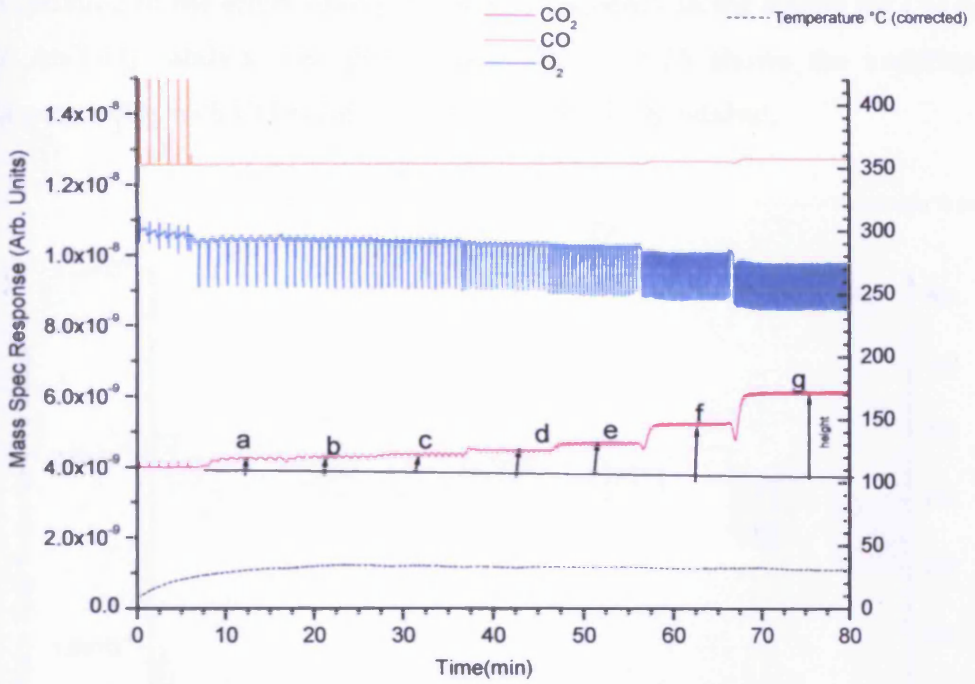

Figure 3-23: CO pulses frequency variation with time (a=pulses of CO after 60 second/ml and b,c,d,e,f and g-after 50,40,30,20,10 and 5 seconds respectively) over a 1wt% Au/TiO_2 catalyst dried at 120°C in air

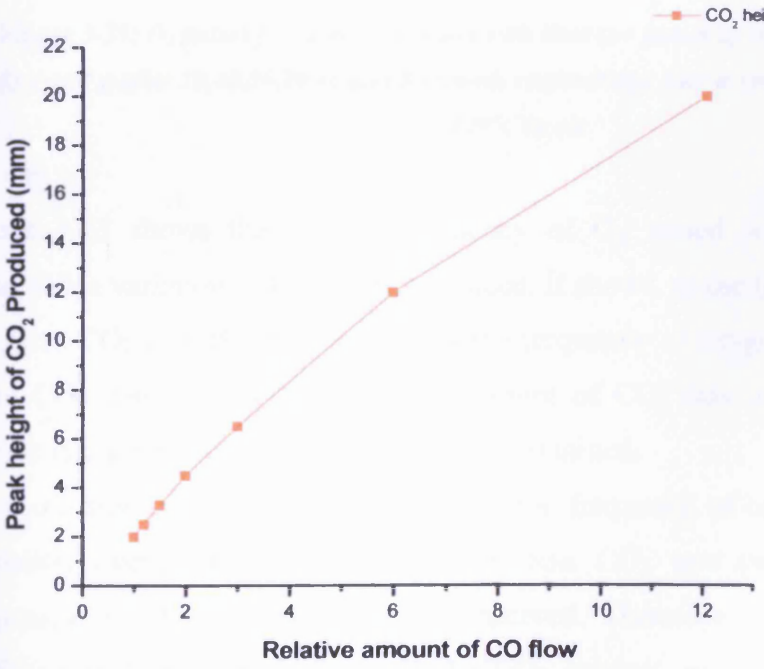

Figure 3-24: CO_2 peak height produced with relative amount of CO flow for CO oxidation over a 1wt % Au/TiO_2 catalyst dried at 120°C in air

3.4.1.1.9 Effect of variation of O_2 frequencies for CO oxidation over Au/TiO_2 catalyst

The variation of the effect of oxygen pulses frequency in the stream for CO oxidation over Au/TiO_2 catalyst was also studied. Figure 3-25 shows the variation of the frequency of O_2 with CO pulses over a 1wt% Au/TiO_2 catalyst.

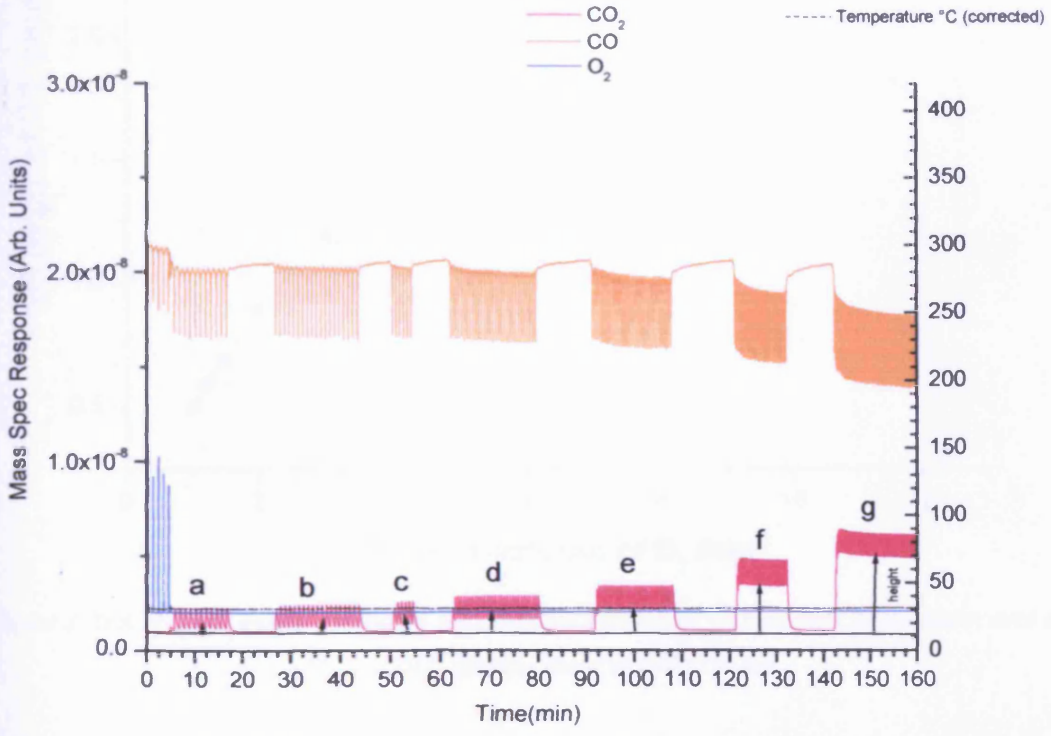

Figure 3-25: O_2 pulses frequency variation with time (a= pulses of O_2 after 60 second/ml and b,c,d,e,f and g-after 50,40,30,20,10 and 5 seconds respectively) over a 1wt% Au/TiO_2 catalyst dried at 120°C in air

Figure 3-25 shows that as the frequency of O_2 varied with continuous flow of 10%CO/He variation of CO_2 were produced. It shows, as the frequency of oxygen was low, less CO_2 was observed and when the frequency of oxygen increases per second, more CO_2 was observed. If the peak height of CO_2 data in figure 3-25 is plotted against relative flow oxygen, figure 3-26 is obtained.

From the figure (3-26), it shows that, as the frequency of oxygen was low for CO oxidation over 1wt% Au/TiO_2 catalyst, less CO_2 was produced and when the frequency was high, more CO_2 was observed. Therefore, it indicated that for CO oxidation to take place over 1wt% Au/TiO_2 catalyst, more frequent oxygen pulses were needed in order to get the desired product.

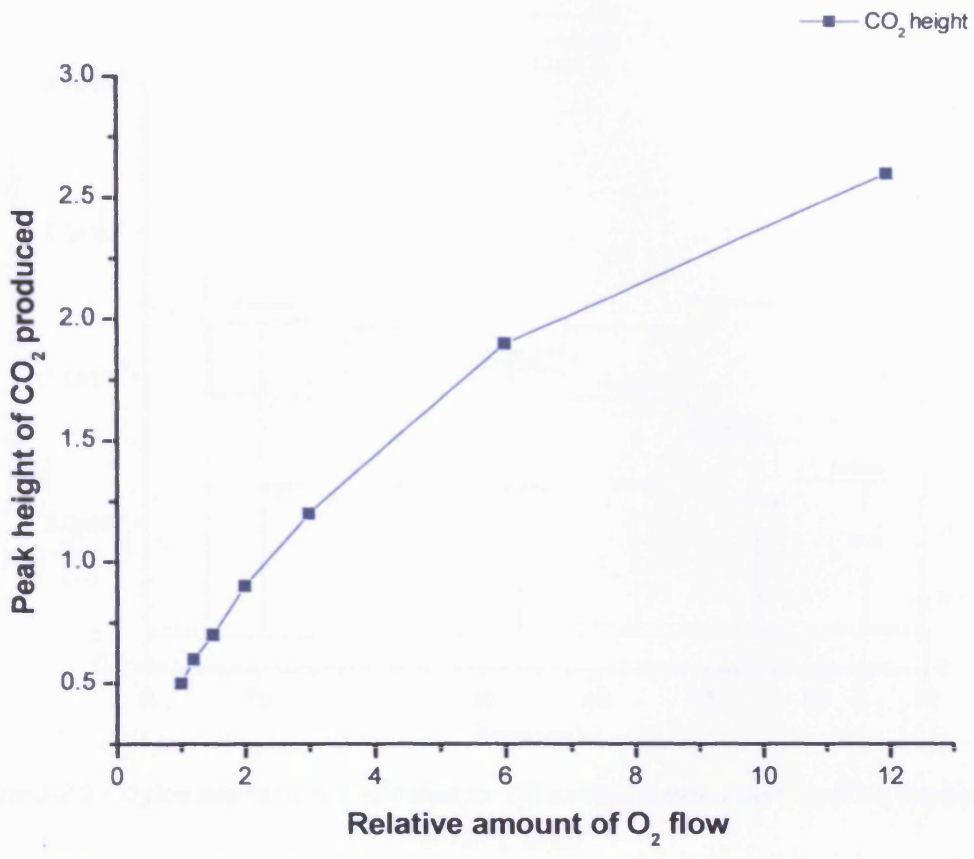

Figure 3-26:CO_2 peak height produced with relative amount of O_2 flow for CO oxidation over a 1wt% Au/TiO_2 catalyst dried at 120°C in air

3.4.1.1.10 Effect of variation of CO and O_2 flow for CO oxidation over Au/TiO_2 catalyst

When the contact time or the flow rate of the reactants in a gaseous catalytic reaction was increased or decreased, the rate of the products reaction was also highly affected. To explore the effect of the variation of the flow rate of CO and O_2 gas flow in the stream for CO oxidation over Au/TiO_2 catalyst, CO oxidation reaction was carried out in a continuous flow of CO and O_2 at the rate of 30ml per minute over a 1wt% Au/TiO_2 catalyst (Figure 3-27).

The figure (3-27) shows that as the CO flow rate decreases from 30-25 ml/minute less CO_2 signals were observed. It indicates as the flow rate of CO_2 decreases, less CO_2 were observed. When the relative flow of CO plotted against peaks height of CO_2 produced, figure 3-28 was obtained.

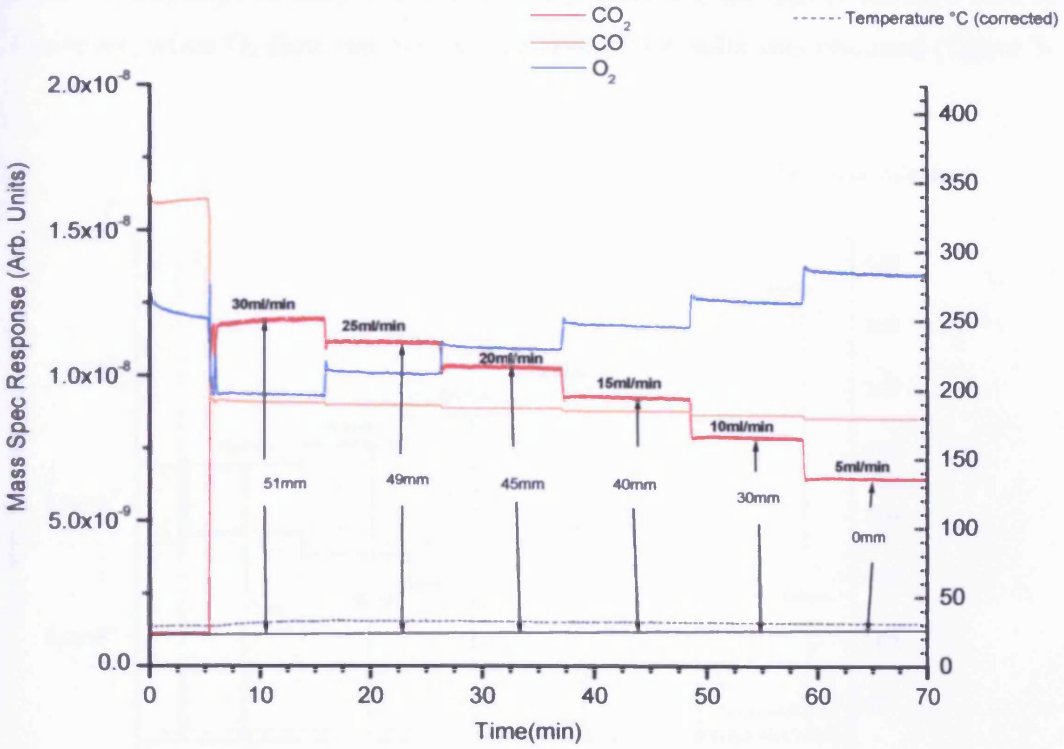

Figure 3-27: CO flow rate variation with time for CO oxidation over a 1wt% Au/TiO_2 catalyst dried at 120°C in air

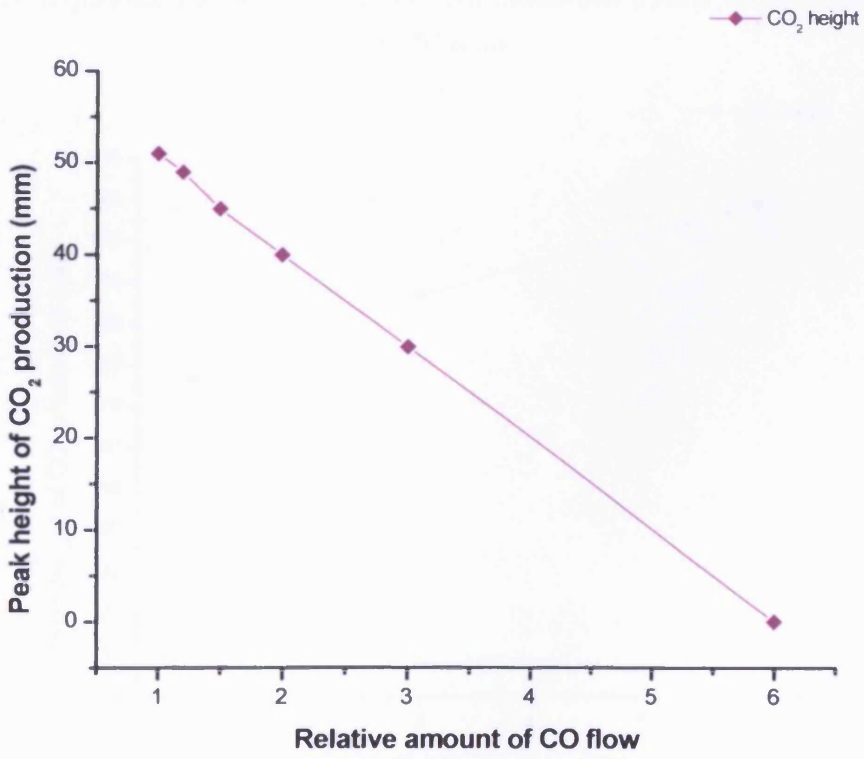

Figure 3-28:CO_2 peak height produced with relative amount of CO flow for CO oxidation over a 1w%t Au/TiO_2 catalyst dried at 120°C in air

The figure (3-28) implies that the more the CO_2 observed, the higher the flow rate of CO. However, when O_2 flow rate was varied, (similar results was obtained (figure 3-29).

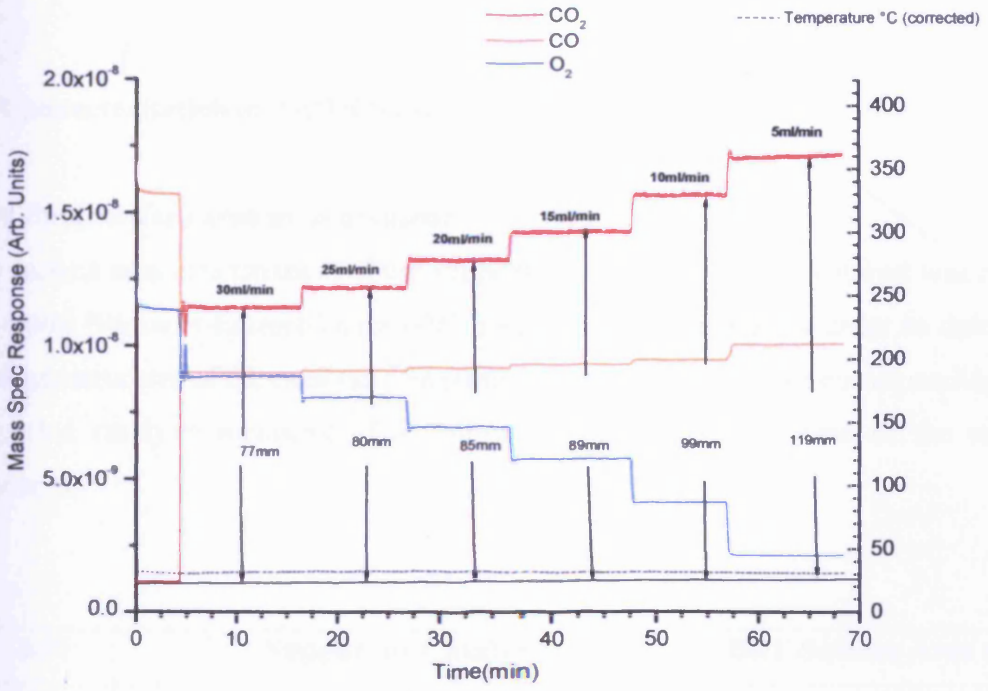

Figure 3-29: O_2 flow rate variation with time for CO oxidation over a 1wt% Au/TiO_2 catalyst dried at 120°C in air

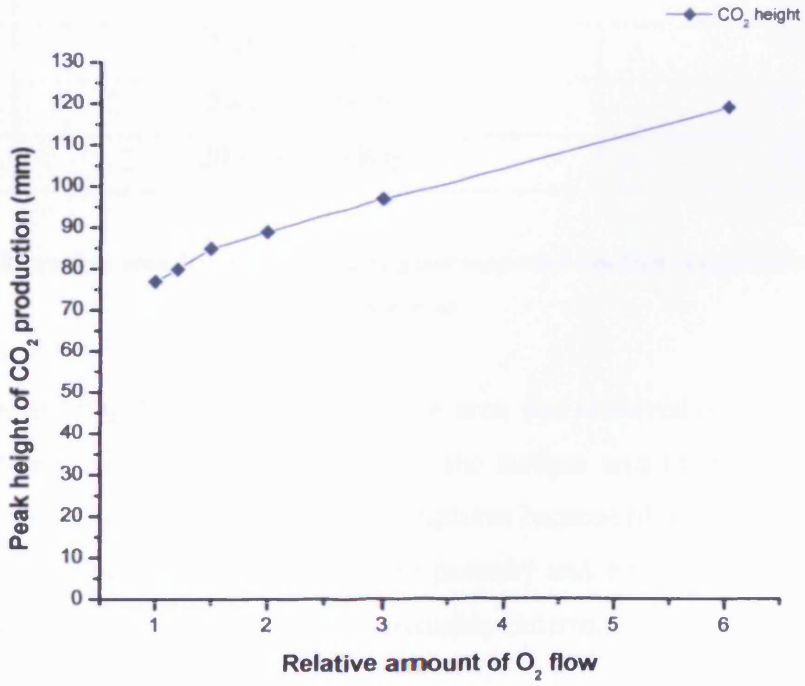

Figure 3-30:CO_2 peak height produced with relative amount of O_2 flow for CO oxidation over a 1wt% Au/TiO_2 catalyst dried at 120°C in air

When the relative flow rate of oxygen was plotted against peaks height of CO_2 produced, figure 3-30 was obtained. The figure (3-30) shows that the CO_2 production depends on O_2 present in the reacting system.

3.5 Characterisation of Au/TiO_2 catalyst

3.5.1 BET surface area measurement

The surface area measurement of the supports and gold supported catalyst was carried out using Brunauer-Emmet-Teller (BET) surface area method in order to determine the microstructure of the catalyst. The surface area of TiO_2 and the corresponding gold supported catalysts measured. The following are the surface area of the catalyst measured:

S/N	Support or Catalyst	BET Surface Area m^2g^{-1}
1	TiO_2	48
2	0.5wt%Au/TiO_2	50
3	1wt%Au/TiO_2	51
4	3wt%Au/TiO_2	51
5	5wt%Au/TiO_2	51
6	20wt%Au/TiO_2	52

Table 3-2: BET surface area for the support and gold supported catalysts of deposition precipitation method

As always with TiO_2 (Degussa), high surface area was observed due to its nature and property. When gold was loaded on TiO_2, the surface area of the catalyst may be higher than the TiO_2 as reported in many literatures because of the increase in the sizes of micro pores in the support material. The porosity and size of the support particles relative to the size of TiO_2 particles presumably determine the surface area of each catalyst.

3.5.2 XRD

X- ray diffraction was employed to identify the crystalline phases present in the catalyst. Figure (3-31) shows the X-ray diffraction patterns of TiO_2, and uncalcined 0.5, 1, 3, 5 and 20wt% Au/TiO_2 catalysts. The results indicates the X-ray diffraction of TiO_2 alone, with the peaks corresponding to a mixture of anatase and rutile (both tetragonal), but the anatase phase has dominated the rutile phase as expected. Weak XRD peaks of gold were observed. The low peaks of gold on the catalyst might be due to intense peaks of TiO_2, which merged, with gold peaks. In particular the $2\theta = 38.2^o$ is position very close to anatase peak $2\theta = 38.5^o$

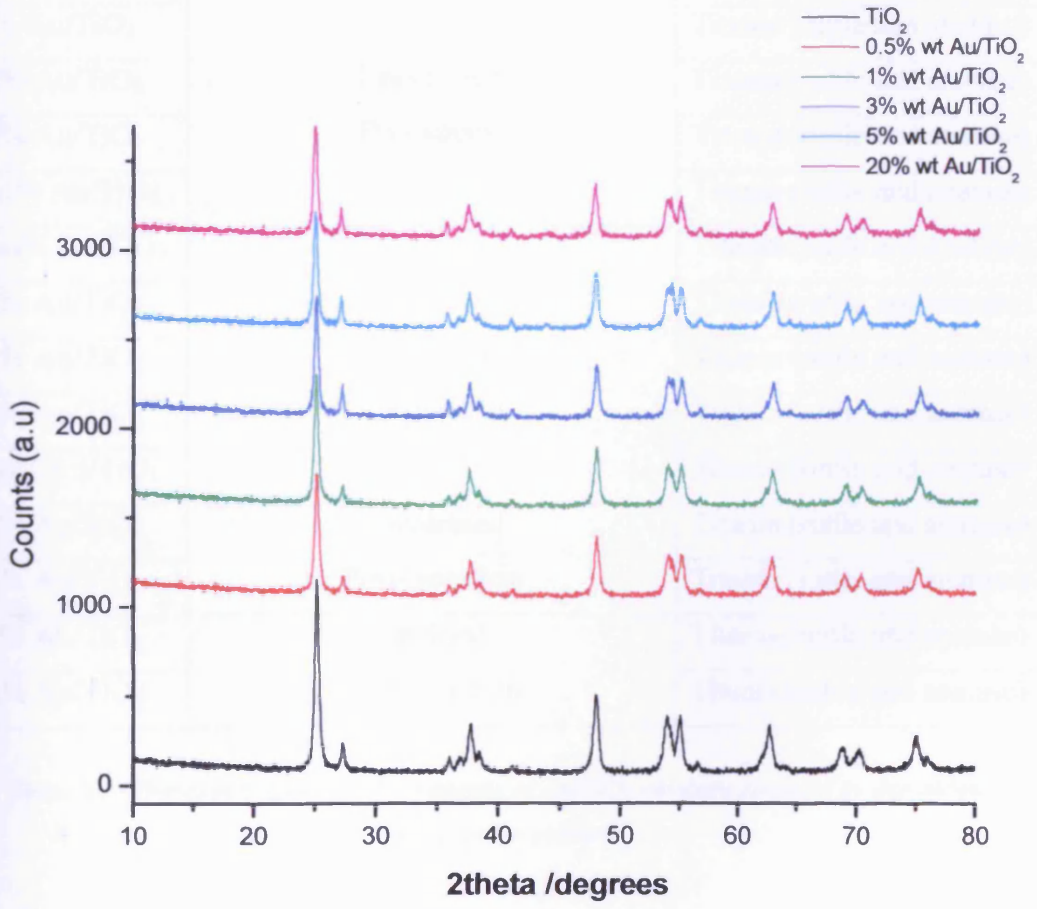

Figure 3-31: XRD patterns for TiO_2 and different weight loadings of uncalcined Au/TiO_2 catalysts

Another important characteristics peaks of Au as reported in the literature[77], particularly at $2\theta = 44.4^o$ and 64.5^o were not observed in the spectra. This may also be due to low or smaller size of gold, which is too small and difficulty to be detected by the X-ray diffraction machine.

The same was observed in the case of uncalcined and calcined catalyst. According to Chang *et al.*[69].The limitation of XRD for reduced gold crystallites corresponds to a particle size smaller than to 5nm in diameter. No transformations of the phases were observed after calcination at 400°C. However, the XRD analysis results were summarised in table 3-3 and figure 3-32 to 3-33. The results revealed that diffraction peaks observed for all the calcined and post CO reactor catalyst in both aerobic and anaerobic reactions were representative of TiO_2 (dominated by rutile and anatase);

Catalysts	Type	Phases identified
0.5wt% Au/TiO_2	Uncalcined Pre-reactor	Titania (rutile and anatase)
1wt% Au/TiO_2		Titania (rutile and anatase)
3 wt% Au/TiO_2		Titania (rutile and anatase)
5 wt% Au/TiO_2		Titania (rutile and anatase)
20 wt% Au/TiO_2		Titania (rutile and anatase)
0.5 wt% Au/TiO_2	Calcined Pre-reactor	Titania (rutile and anatase)
1 wt% Au/TiO_2		Titania (rutile and anatase)
3 wt% Au/TiO_2		Titania (rutile and anatase)
5 wt% Au/TiO_2		Titania (rutile and anatase)
20 wt% Au/TiO_2		Titania (rutile and anatase)
1 wt% Au/TiO_2	Uncalcined Post- reaction	Titania (rutile and anatase)
1 wt% Au/TiO_2		Titania (rutile and anatase)
3 wt% Au/TiO_2	calcined Post- reaction	Titania (rutile and anatase)
5 wt% Au/TiO_2		Titania (rutile and anatase)

Table 3-3: Phases identified in XRD patterns of Au/TiO_2 catalysts prepared by deposition precipitation method

The absence of diffraction from gold in all catalysts can be attributed to a low loading of gold or presence of phases that are not detectable due to their high dispersion of gold on the catalyst.

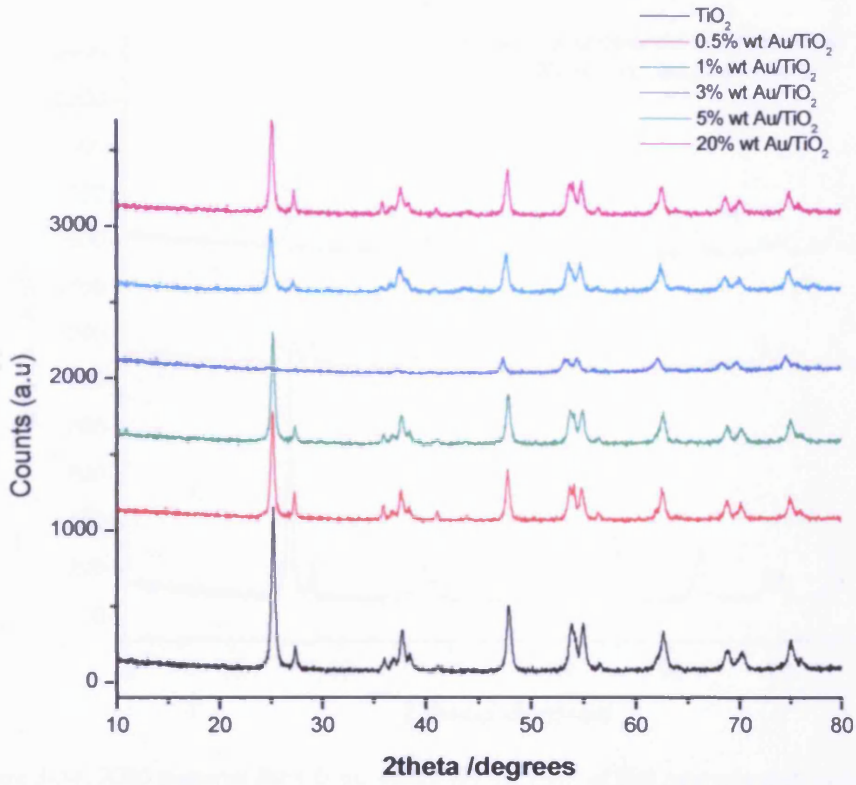

Figure 3-32: XRD patterns for TiO_2 and different weight loadings of calcined Au/TiO_2 catalysts

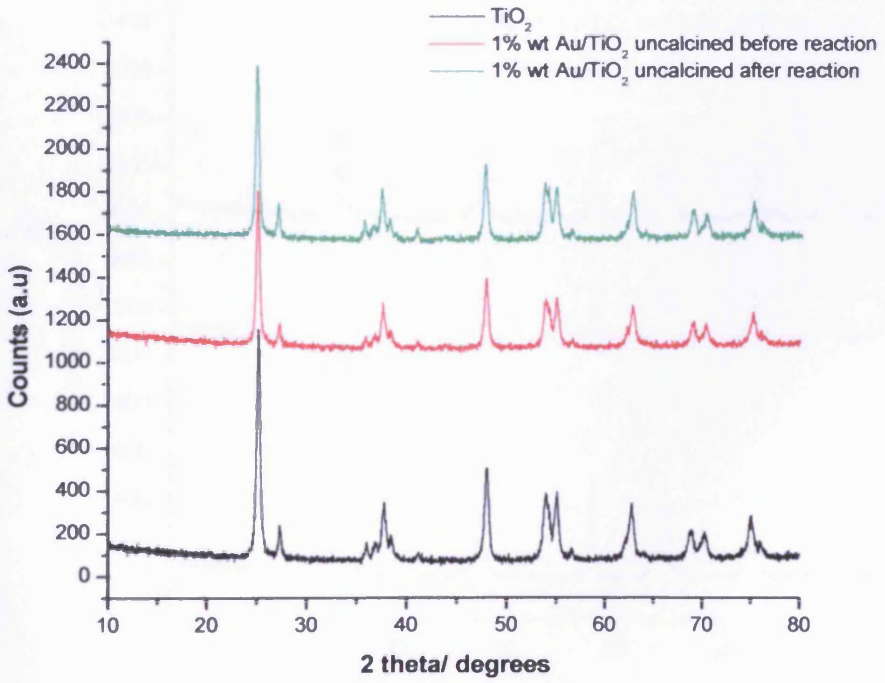

Figure 3-33: XRD patterns for CO oxidation (in the flow of 10%O_2/He) post reaction over TiO_2 and different weight loadings of uncalcined Au/TiO_2 catalysts

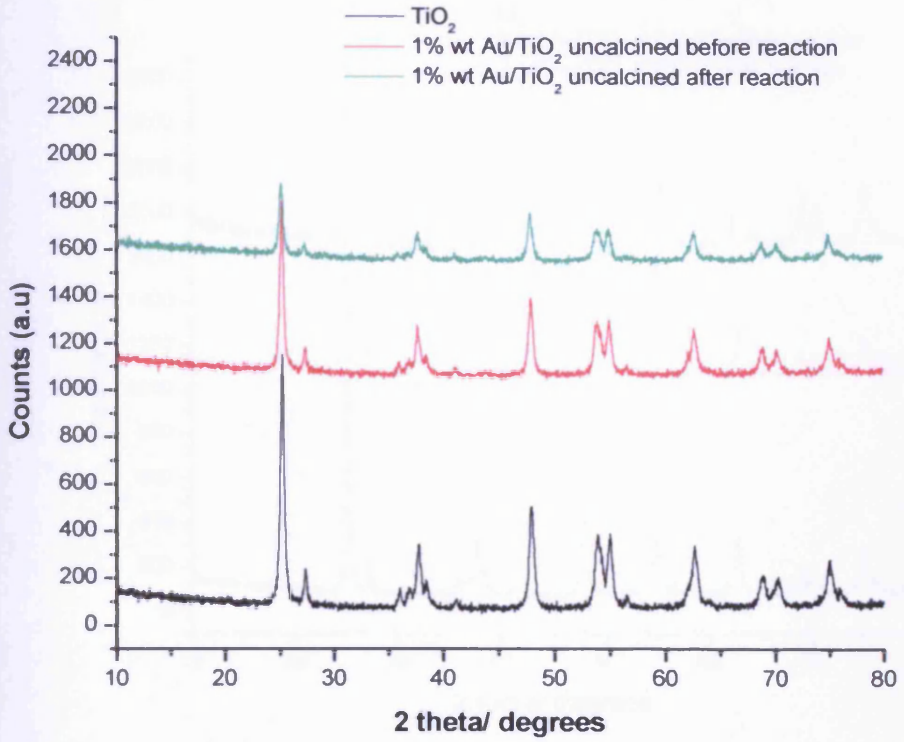

Figure 3-34: XRD patterns for CO oxidation (in the flow of He) post reaction over TiO_2 and different weight loadings of uncalcined Au/TiO_2 catalysts

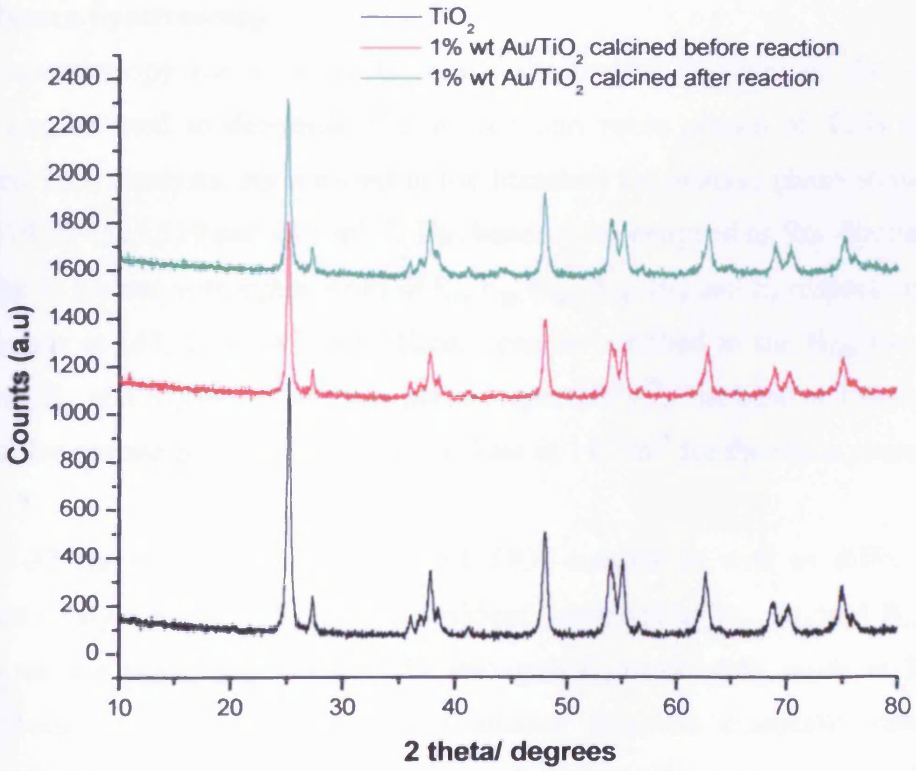

Figure 3-35: XRD patterns for CO oxidation (in the flow of 10%O_2/ He) post reaction over TiO_2 and different weight loadings of calcined Au/TiO_2 catalysts

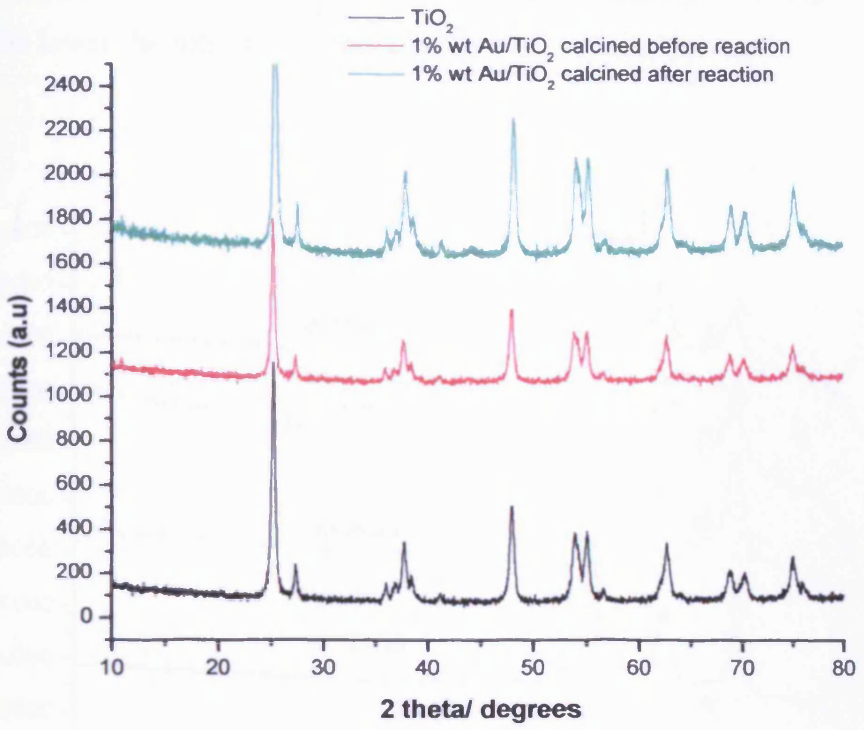

Figure 3-36: XRD patterns for CO oxidation (in the flow of He) post reaction over TiO_2 and different weight loadings of calcined Au/TiO_2 catalysts

3.5. 3 Raman Spectroscopy

Raman spectroscopy can used to determine the crystal structure of the catalysts. Raman can be used to determine the anatase and rutile phases of TiO_2 and gold supported TiO_2 catalysts. As reported in the literature the anatase phase shows bands at 144,179,399,515,519 and 639cm[1 78]. The bands were assigned as Six -Raman active bands due to anatase with symmetries of E_g, E_g, B_{1g}, A_{1g}, B_{1g} and E_g respectively[79].

Rutile bands at 143, 234, 447 and 612cm^{-1} can be ascribed to the B_{1g}, two-photon scattering, E_g, and A_{1g} modes of rutile phase respectively[79]. The band at 144cm^{-1} is the strongest for anatase phase while is the weakest at 143cm^{-1} for the rutile phase, figure 3-37.

Figure 3-37 shows the Raman spectra of TiO_2 catalyst as well as different gold supported catalyst on TiO_2 395, 510 and 635cm^{-1} assigned to B_{1g}, A_{1g} and B_{2g} modes of TiO_2 anatase phase respectively. The strongest E_g mode at E_g mode at 145cm^{-1}, arising from the extension vibration of anatase structure drastically reduced in intensity due to the presence of nanoparticles of gold on TiO_2 surface. It has also been observed that the reduced intensities of other modes such as B_{1g}, A_{1g}, and B_{2g} as

evident in figure 3-37 are as result of different gold loadings (the higher the gold loadings, the lower the intensity of the peaks)

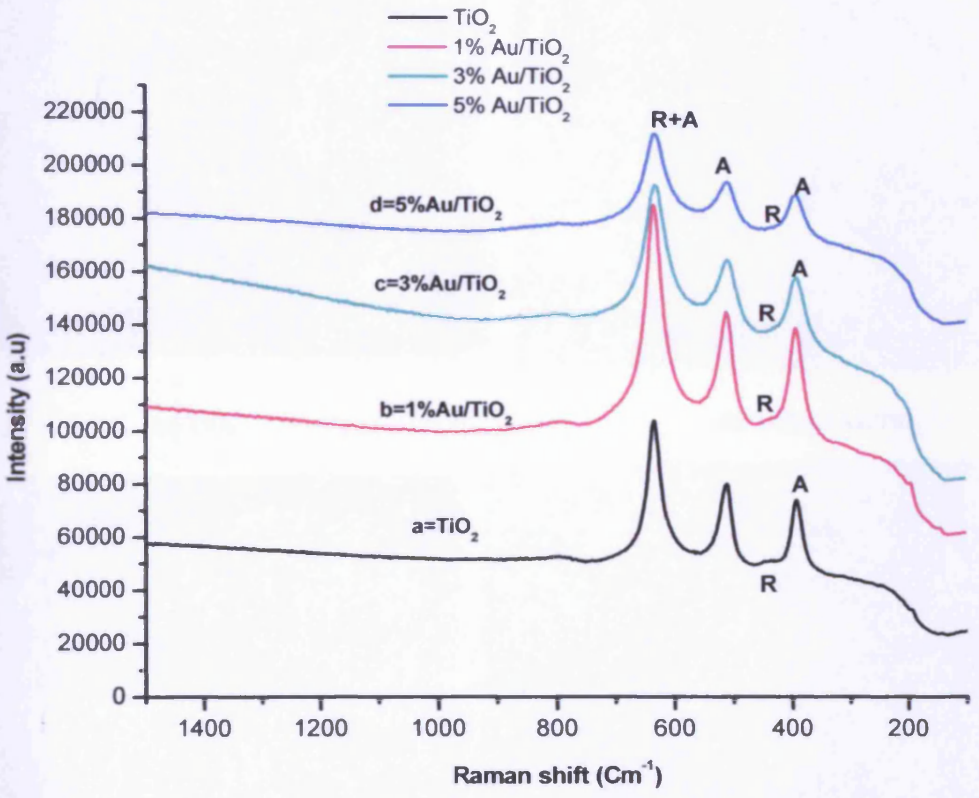

Figure 3-37: Raman spectra of TiO_2 and different loadings of Au/TiO_2 catalysts (uncalcined) with A= anatase and R= rutile phases respectively

As the gold loading increases, the intensities of the peaks decrease as shown (figure 3-37, from b-d) and similar results were obtained even when the catalyst was calcined. It also implies that the presence of the gold reduces the intensities of rutile and anatase phases as depicted in figure 3-37.

3.5.4 SEM

Figure 3-38 shows the SEM images for TiO_2 alone (a) and uncalcined Au/TiO_2 catalyst dried at 120°C for 2h. The figure shows the uncalcined Au/TiO_2 catalyst (ranges from 0.5wt%, 1wt%, 3wt%, and 5wt% of gold loadings) demonstrated a mark similarity in morphology (porous irregular gold particles of varying sizes < 1.7μm to approximately 4.5μm). While the morphology exhibited by 20wt% gold loading catalyst shows difference in morphology forming larger lumps of irregular particles, presumably the particles of this catalyst was agglomerated. The similarities in

morphology exhibited by most of these catalysts are consistent with its high surface area and small crystallite size (from the XRD) due to low loadings of gold.

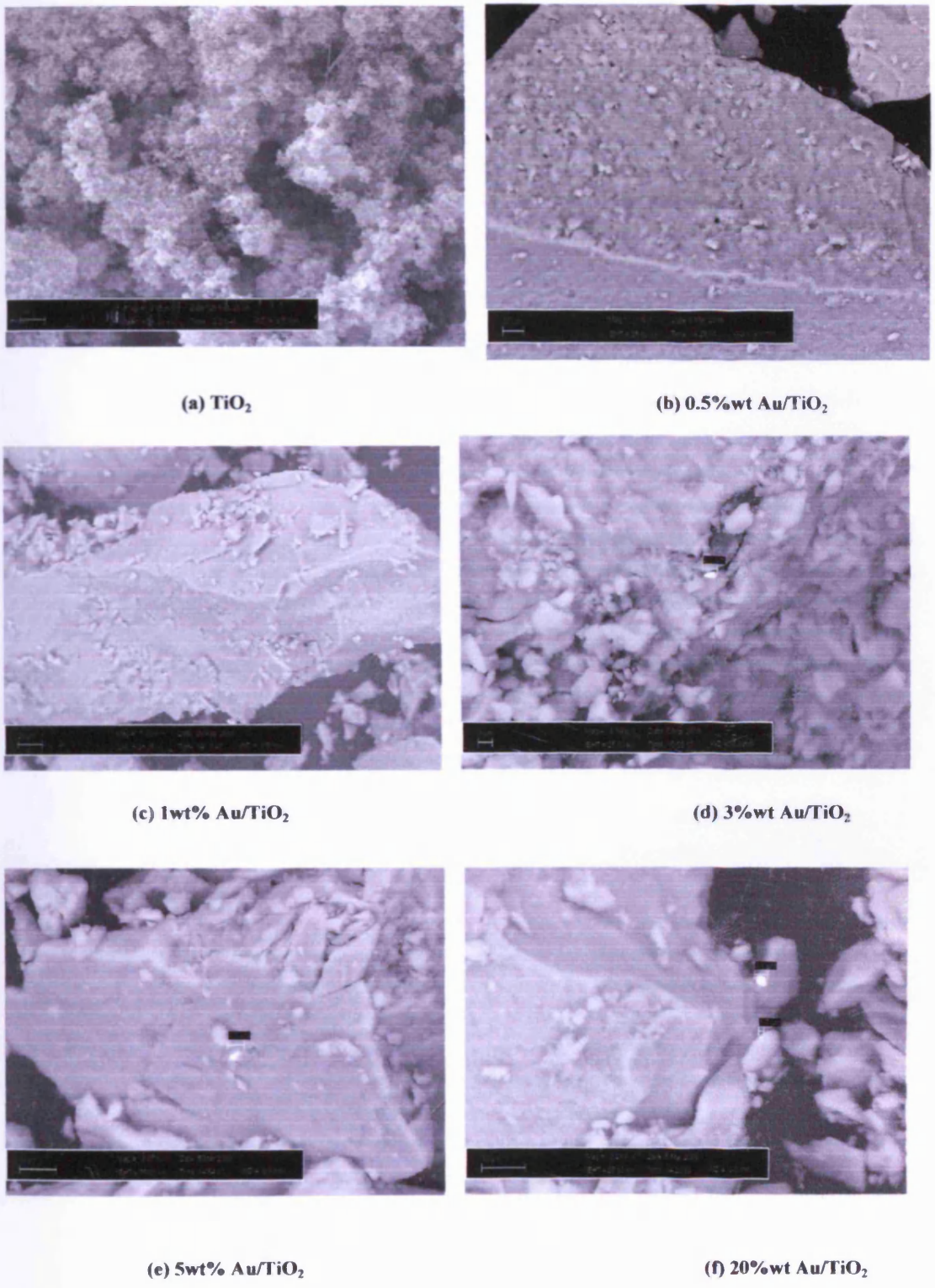

(a) TiO_2 (b) 0.5%wt Au/TiO_2

(c) 1wt% Au/TiO_2 (d) 3%wt Au/TiO_2

(e) 5wt% Au/TiO_2 (f) 20%wt Au/TiO_2

Figure 3-38: Scanning Electron Microscopy of TiO_2 and different loadings of Au/TiO_2 catalysts (uncalcined) prepared by deposition precipitation.

However, figure 3-39 shows also the SEM images for Au/TiO_2 catalysts calcined at 400°C for 2h. The figure shows different loadings of gold range from 0.5wt%, 1wt%, 3wt%, 5wt% and 20%wt supported on TiO_2. The images from the figure, the catalysts demonstrated a mark similarity in morphology (porous irregular particles of varying sizes<1.2μm to approximately 2.5μm of gold). The morphology of the uncalcined and

(g) 0.5wt% Au/TiO_2

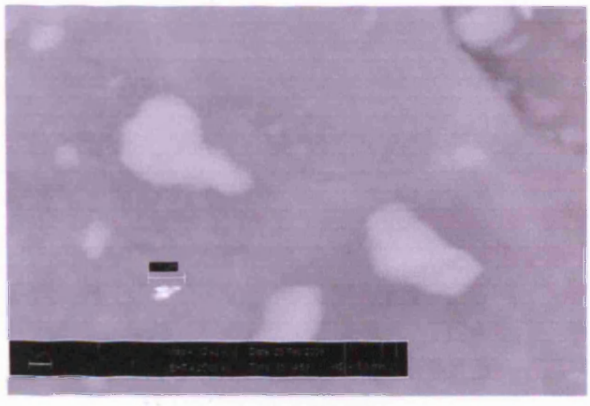

(h) 1wt% Au/TiO_2

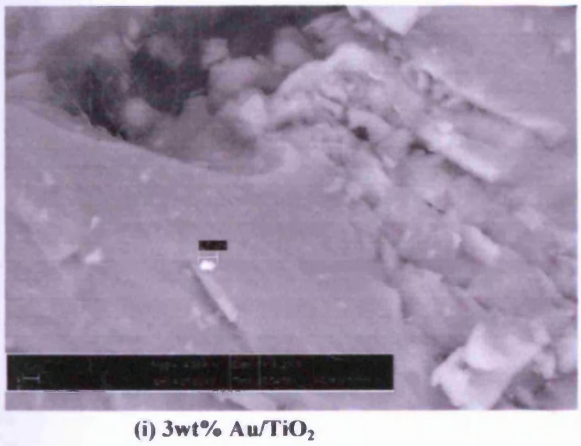

(i) 3wt% Au/TiO_2

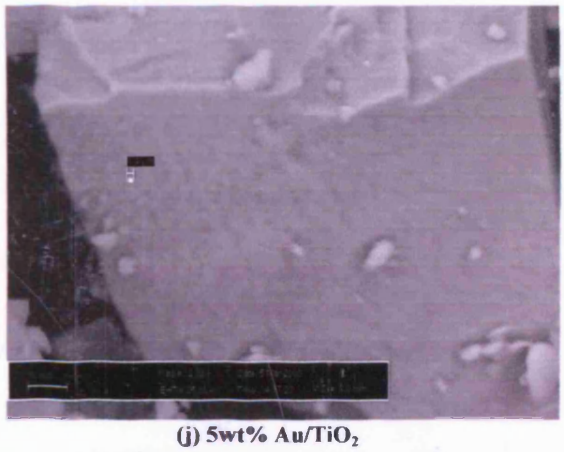

(j) 5wt% Au/TiO_2

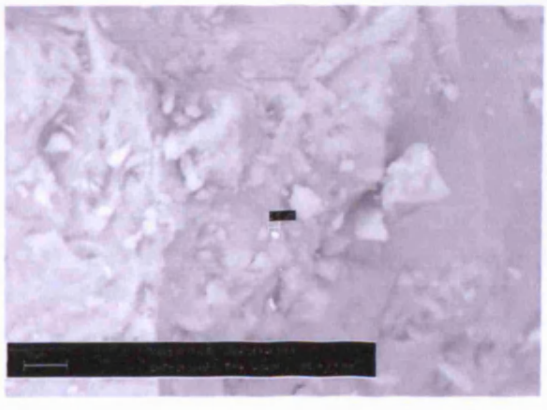

(k) 20wt% Au/TiO_2

Figure 3-39: Scanning Electron Microscopy of different loadings of Au/TiO_2 catalysts (uncalcined) prepared by deposition precipitation

calcined catalysts of Au/TiO_2 varied slightly from each other with small gold particles observed with uncalcined Au/TiO_2 catalysts. Similarly, SEM images of aerobic CO oxidation (in a flow of $10\%O_2$/He) of uncalcined and calcined post reactor catalyst of a 1wt% Au/TiO_2 is presented in figure 3-40. The figure (3-40) reveals a change in morphology and particle size after aerobic CO oxidation reaction. It demonstrates difference in morphology (porous irregular particles of varying sizes<1.0μm to approximately 1.7μm). The morphology of the aerobic post reactor uncalcined catalyst varied greatly from that of catalyst calcined aerobic post reactor (dense irregular particles).

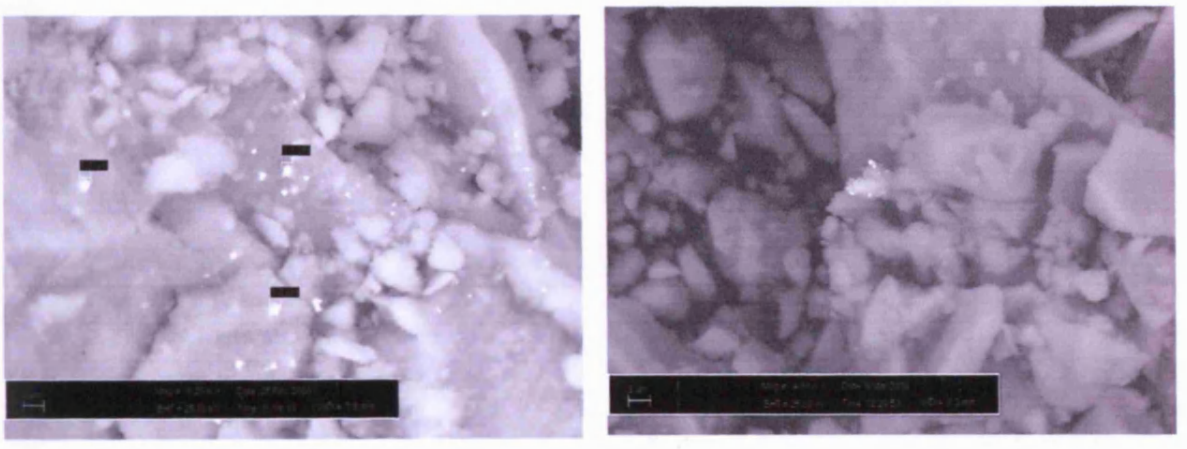

(a) *(b)*

Figure 3-40: Scanning Electron Microscopy of a 1wt% Au/TiO_2 post reactor aerobic CO oxidation catalysts (uncalcined= a and calcined =b) prepared by deposition precipitation

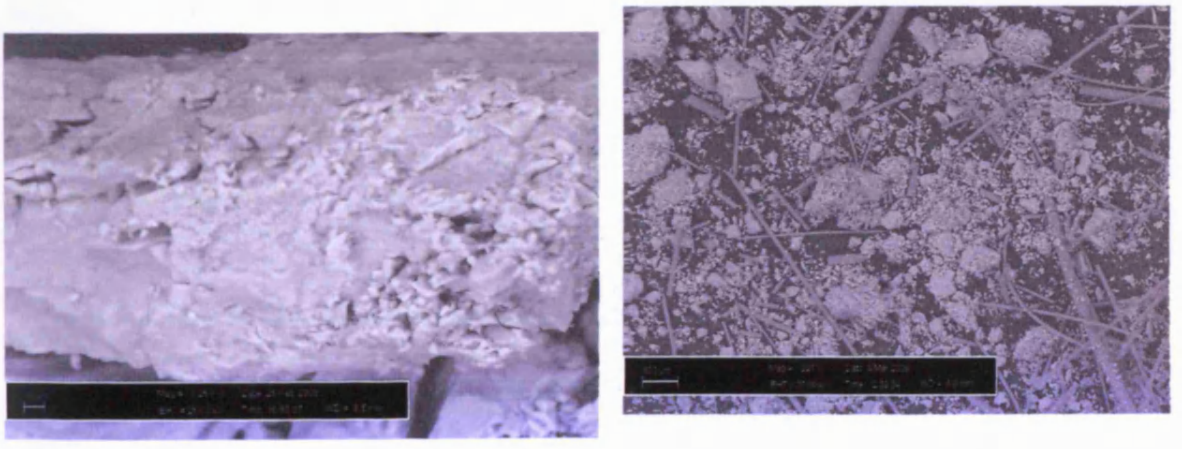

(a) *(b)*

Figure 3-41: Scanning Electron Microscopy of a 1wt% Au/TiO_2 post reactor anaerobic CO oxidation catalysts (uncalcined= a and calcined =b) prepared by deposition precipitation

The post reactor scanning electron microscopy images of anaerobic CO oxidation (in a flow of He alone) uncalcined and calcined 1wt% Au/TiO_2 catalyst is illustrated in figure 3-41. The figure shows images with a variation in morphology of uncalcined and calcined. The morphology of the former shows dense irregular particles while the latter exhibits porous irregular particles.

3.5.5 XPS

To understand the oxidation state of the catalyst and the surface interaction between nanoparticles of gold and the support in Au/TiO_2 catalyst for pre- reactor catalyst (washed and unwashed) and calcined catalyst, the technique of X-ray Photoelectron spectroscopy (XPS) was employed.

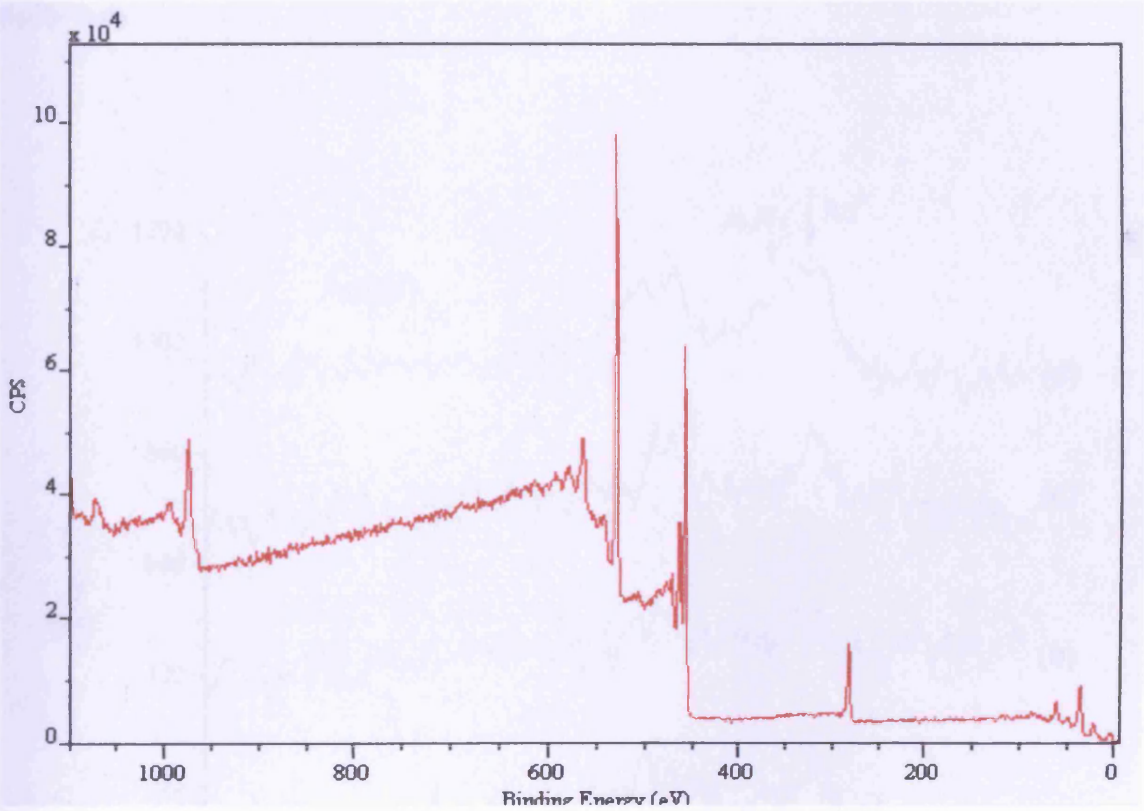

Figure 3-42: XPS of 1wt% Au/TiO_2 and TiO_2 (Uncalcined) prepared by Deposition precipitation

Shown in figure 3-42 are the XPS details for the catalysts studied. By cross referencing the corrected binding energies with known values, demonstrate that all the pre-reactor catalyst prepared by deposition precipitation have gold present as a combination of components. From the figure (3-42), it indicates that most of the Au 4*f* envelopes are situated around 85 eV for the $4f_{7/2}$ peak, while small amount was seen at

about 83eV. These confirmed the existence of gold in the oxidation as Au^0 and Au^{x+}. It should be noted here that correction was made against the O 1s value of 530.4 eV for all catalysts[33], as some catalyst present more than one carbonaceous species.

Catalysts prepared by deposition precipitation dried at 120°C and 400°C present surface gold as Au^0 and Au^{x+} oxidation. This is contrary to the predicted oxidation state of gold in $HAuCl_4$ which is 3+ and the Au^{x+} signal observed may probably come from a reaction between the $HAuCl_4$ and the support material.

However, as the loading of gold increases in the catalyst, the intensity of the spectrum increases, indicating the presence of high amount of gold on the surface. Furthermore, the XPS data also indicates that the nominal loading on gold in each catalyst was not obtained as most of the gold has been washed off by filtration during the preparation (table 3-4).

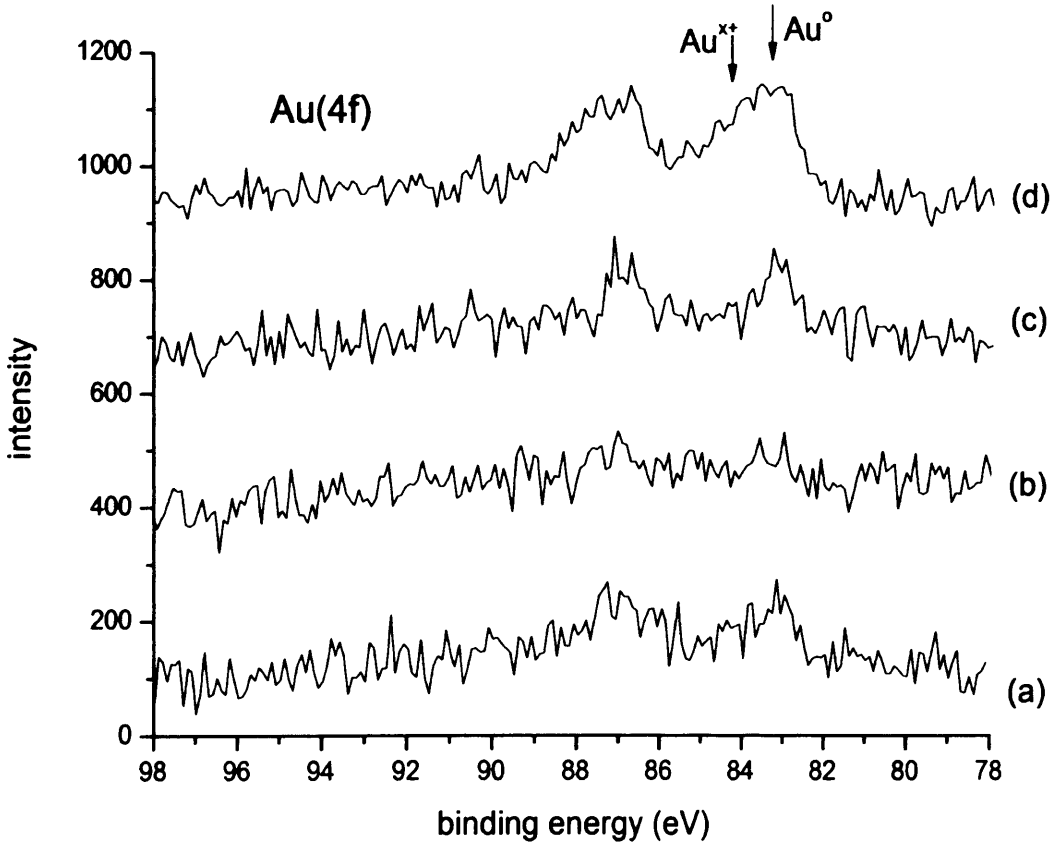

Figure 3-43: Au(4f) spectrum for (a)0.5wt% Au/TiO_2 (uncalcined), (b) 0.5wt% Au/TiO_2 (calcined),(c) 1wt% Au/TiO_2 (unwashed and uncalcined) and (d) 20wt% Au/TiO_2 (uncalcined) catalysts

Sample	Atom %				Wt%
	Au	Si	Ti	O	Au
(a)	<0.1	-	31.0	69.0	<0.8
(b)	<0.1	-	33.1	66.9	<0.8
(c)	<0.1	-	32.9	67.1	<0.8
(d)	0.25	-	29.5	70.2	2.1

Table 3-5: Elemental composition for (a)0.5wt% Au/TiO_2 (uncalcined), (b) 0.5wt% Au/TiO_2 (calcined),(c) 1wt% Au/TiO_2 (unwashed and uncalcined) and (d) 20wt% Au/TiO_2 (uncalcined) catalysts

The XPS data for the post reactor catalyst (figure 3-44) indicates that most of the Au 4*f* envelopes are situated around 87 eV for the $4f_{7/2}$ peak while the rest was observed at about 83eV. These features confirmed the presence of gold in the oxidation state as Au^0 and Au^{x+}. The gold oxidation remained unchanged even after aerobic (in the presence of $10\%O_2$/He) and anaerobic (in the presence of He alone) CO oxidation reaction.

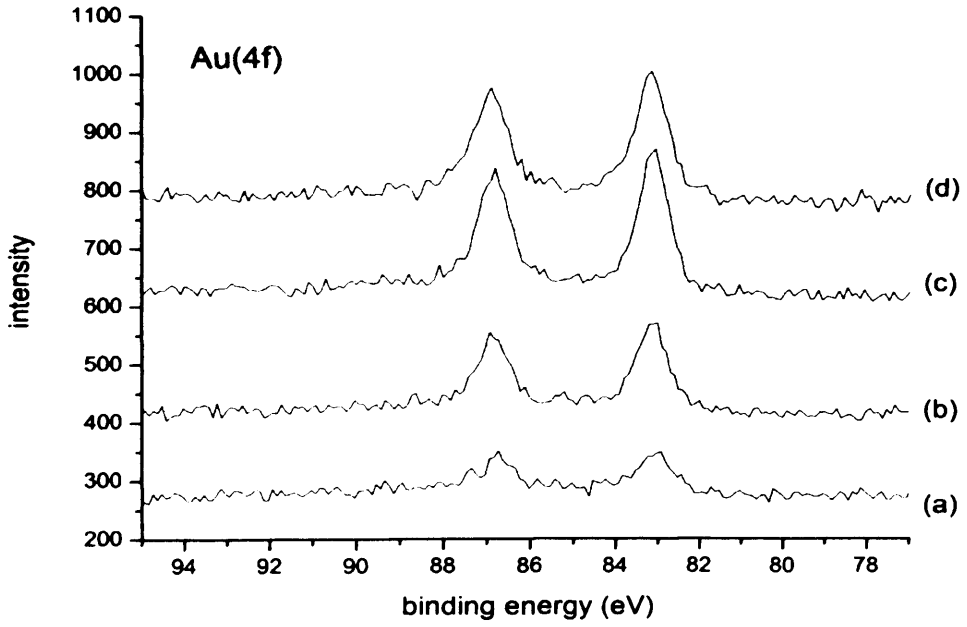

Figure 3-44: Au (4f) spectrum for (a) 1wt% Au/TiO_2 (uncalcined) aerobic, (b) 1wt% Au/TiO_2 (uncalcined) anaerobic,(c) 1wt% Au/TiO_2 (calcined) aerobic and (d)1wt% Au/TiO_2 (calcined) anaerobic post reactor catalysts

3.5.6 EDAX

Table 3-6 shows the EDAX results of uncalcined catalysts from 0.5wt%, 1wt%, 3wt%, 5wt% and 20wt% of gold supported on TiO_2 prepared by deposition precipitation. The "bulk" refers to a bulk analysis of the entire material whereas "spot" is a spot analysis of an approximately micron square area. Table 3-6 shows the EDAX result details of 0.5%wt uncalcined catalyst of Au/TiO_2. The main elemental composition of the bulk analysis of the catalyst indicates that the catalyst contained 31.5%, 37.2% and 31.3% of C, O and Ti respectively. The bulk analysis shows that TiO_2 is the main component with some carbon contamination in the bulk, while the spot shows Ti and Au as the element seen on the spot analysis of the catalyst, with 99.6% and 0.4% being the weight % of Ti and Au respectively.

S/N	Sample	Type	Elements	App Conc	Intensity Corrn	Weight %	Weight% Sigma	Atomic %
1	0.5%wtAu/TiO_2	**Bulk**	C K	18.6	0.9	31.5	0.5	46.8
			O K	6.6	0.3	37.2	0.5	41.6
			Ti K	18.5	0.9	31.3	0.3	11.6
			Totals			**100.00**		
2	0.5%wtAu/TiO_2	**Spot**	Ti K	40.5	1.0	99.6	0.1	99.9
			Au M	0.2	0.9	0.4	0.1	0.1
			Totals			**100.00**		

Table 3-6: EDAX result for uncalcined 0.5wt% Au/TiO_2 catalyst prepared by deposition precipitation

SNO	Sample	Type	Elements	App Conc	Intensity Corrn	Weight %	Weight% Sigma	Atomic %
1	1%wtAu/TiO_2	**Bulk**	O K	5.7	0.3	47.9	0.6	73.3
			Ti K	21.9	0.9	52.1	0.6	26.7
			Totals			**100.00**		
2	1%wtAu/TiO_2	**Spot**	O K	13.4	0.3	47.4	0.3	73.1
			Ti K	52.6	0.9	52.3	0.3	26.9
			Au M	0.3	0.9	0.3	0.1	0.1
			Totals			**100.00**		

Table 3-7: EDAX result for uncalcined 1wt% Au/TiO_2 catalyst prepared by deposition precipitation

Similarly, table 3-7 shows the bulk analysis of the uncalcined 1wt% Au/TiO_2 catalyst prepared by deposition precipitation, it shows that the bulk elemental composition of the catalyst are Ti, O, and Si, with weight % of 52.0, 47.9 and 0.1% respectively. The presence of the Si may be due to contamination of the catalyst with silica. However, the spot analysis shows that O, Ti and Au are the main composition elements observed on the spot, with O, Ti and Au weight % being 45.1, 54.6 and 0.3 % respectively.
However, careful analysis of the EDAX results of 0.5, 1, 3, 5 and 20wt% (table 3-6 to 3-10) of Au over TiO_2 support shows that all the catalysts are free from chloride, indicating no possible contamination of the catalyst with chloride or no possible detected level of chloride left on the catalyst. The results of the uncalcined samples of the Au/TiO_2 catalyst also

SNO	Sample	Type	Elements	App Conc	Intensity Corrn	Weight %	Weight% Sigma	Atomic %
		Bulk	O K	6.5	0.3	47.9	0.5	73.3
			Si K	0.04	0.7	0.1	0.03	0.1

1	3%wtAu/TiO_2		Ti K	24.9	0.9	52.0	0.4	26.6
			Totals			**100.00**		
2	3%wtAu/TiO_2	**Spot**	O K	6.9	0.2	45.1	0.5	71.2
			Ti K	31.0	0.9	54.6	0.4	28.7
			Au M	0.1	0.9	0.3	0.1	0.03
			Totals			**100.00**		

Table 3-8: EDAX result for uncalcined 3wt% Au/TiO_2 catalyst prepared by deposition precipitation

SNO	Sample	Type	Elements	App Conc	Intensity Corrn	Weight %	Weight% Sigma	Atomic %
1	5%wtAu/TiO_2	**Bulk**	O K	6.4	0.3	48.7	0.5	74.0
			Ti K	23.6	0.9	51.3	0.5	26.0
			Totals			**100.00**		
2	5%wtAu/TiO_2	**Spot**	O K	7.0	0.2	39.7	0.6	66.8
			Ti K	41.2	0.9	58.7	0.6	33.0
			Au M	1.1	0.9	1.6	0.1	0.2
			Totals			**100.00**		

Table 3-9: EDAX result for uncalcined 5wt% Au/TiO_2 catalyst prepared by deposition precipitation

shows that the main elemental composition in the bulk are purely Ti , O and some contaminants which can be C or Si while on the spot are mainly Ti, O and Au, indicating the Au is mainly on the surface of the support (TiO_2). Similar EDAX results were obtained for calcined samples of Au/TiO_2 catalyst.

SNO	Sample	Type	Elements	App Conc	Intensity Corrn	Weight %	Weight% Sigma	Atomic %
1	20%wtAu/TiO_2	Bulk	O K	4.4	0.3	49.9	0.9	74.8
			Si K	0.1	0.7	0.5	0.1	0.4
			Ti K	15.0	0.9	49.6	0.9	24.8
			Totals			**100.00**		
2	20%wtAu/TiO_2	Spot	O K	9.6	0.2	39.4	0.5	66.2
			Ti K	57.5	0.9	60.0	0.5	33.7
			Au M	0.5	0.9	0.6	0.09	0.1
			Totals			**100.00**		

Table 3-10: EDAX result for uncalcined 20wt% Au/TiO_2 catalyst prepared by deposition precipitation

3.6 Comparison of standard Au/TiO_2 catalyst with WGC catalyst

The World Gold Council catalyst was compared with respect to CO oxidation over Au/TiO_2 catalyst in a pulsing and continuous flow of CO. The study carried out using temperature programmed pulse flow reaction at normal and relatively low temperature shows that both catalysts are active at room temperature (figure 3-46-47).

When the data in figures 3-45 to 46 was integrated and analysed, figure 3-47 was obtained. The figure (3-47) shows that light off temperature of World Gold Council catalyst was observed to be higher and 100% conversion attained at room temperature in both catalysts in the first run and continues steadily through out the experiment. When the second run was compared, the catalysts both show 100% conversion at room temperature but the activity drops with increase in temperature for World Gold Council catalyst as evident when the temperature reached 100°C.

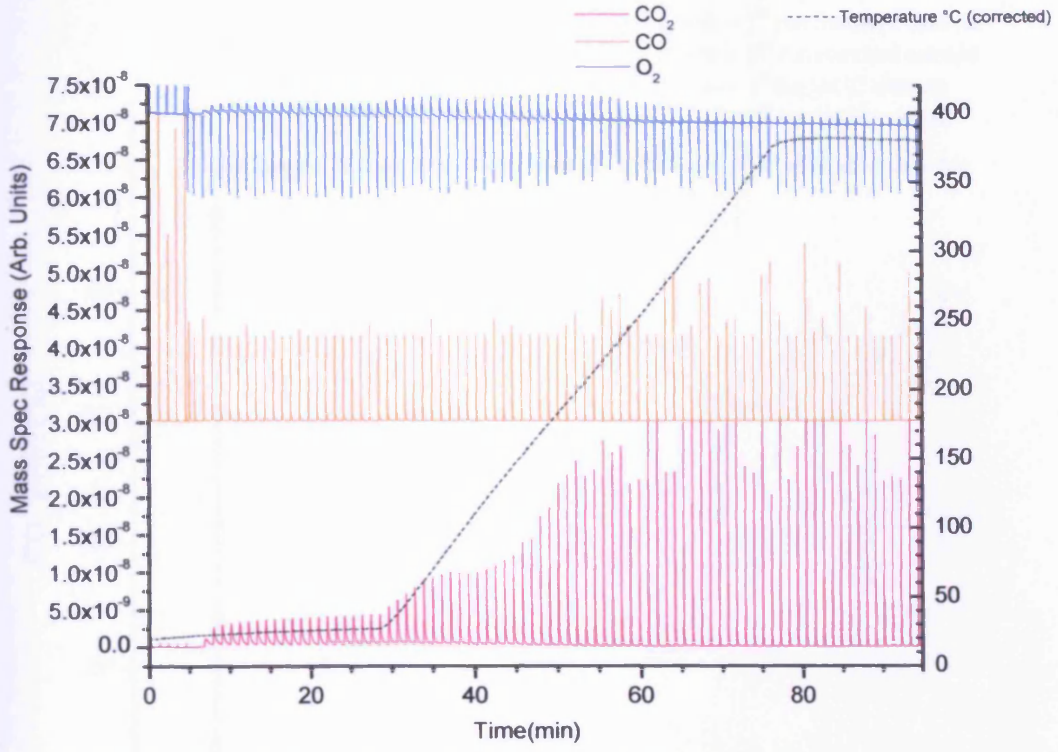

Figure 3-45: Temperature programmed pulse flow reaction for CO in a stream of 10%eO$_2$/ He flow over a WGC Au/TiO$_2$ catalyst (first run)

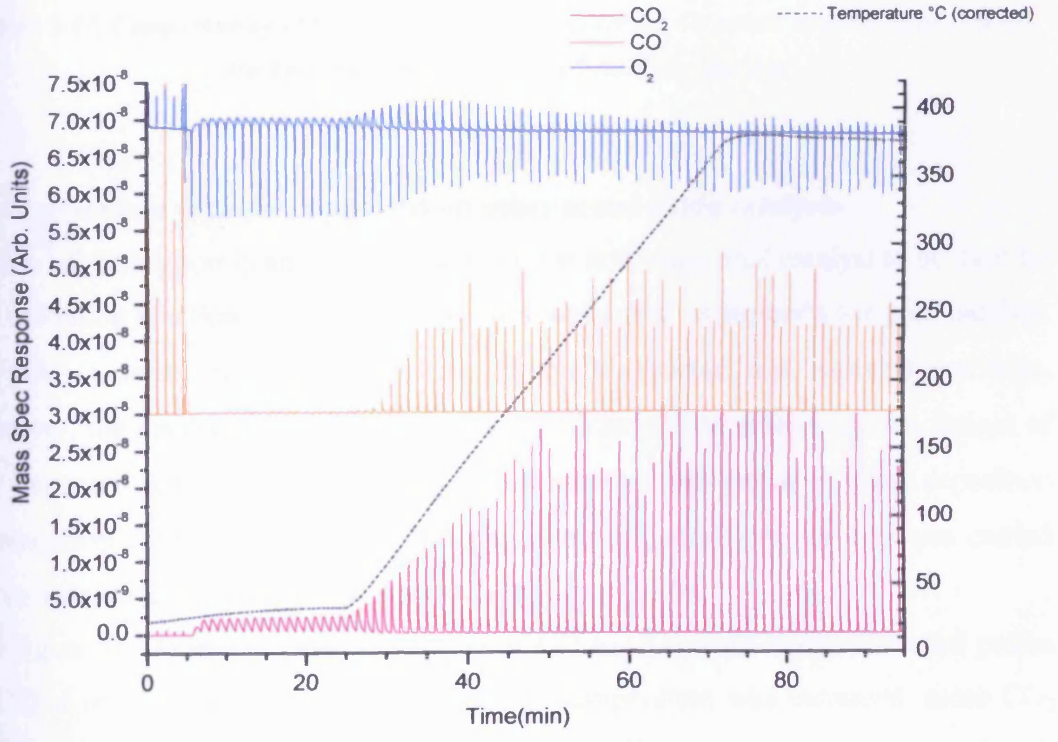

Figure 3-46: Temperature programmed pulse flow reaction for CO in a stream of 10%eO$_2$/ He flow over a WGC Au/TiO$_2$ catalyst (second run)

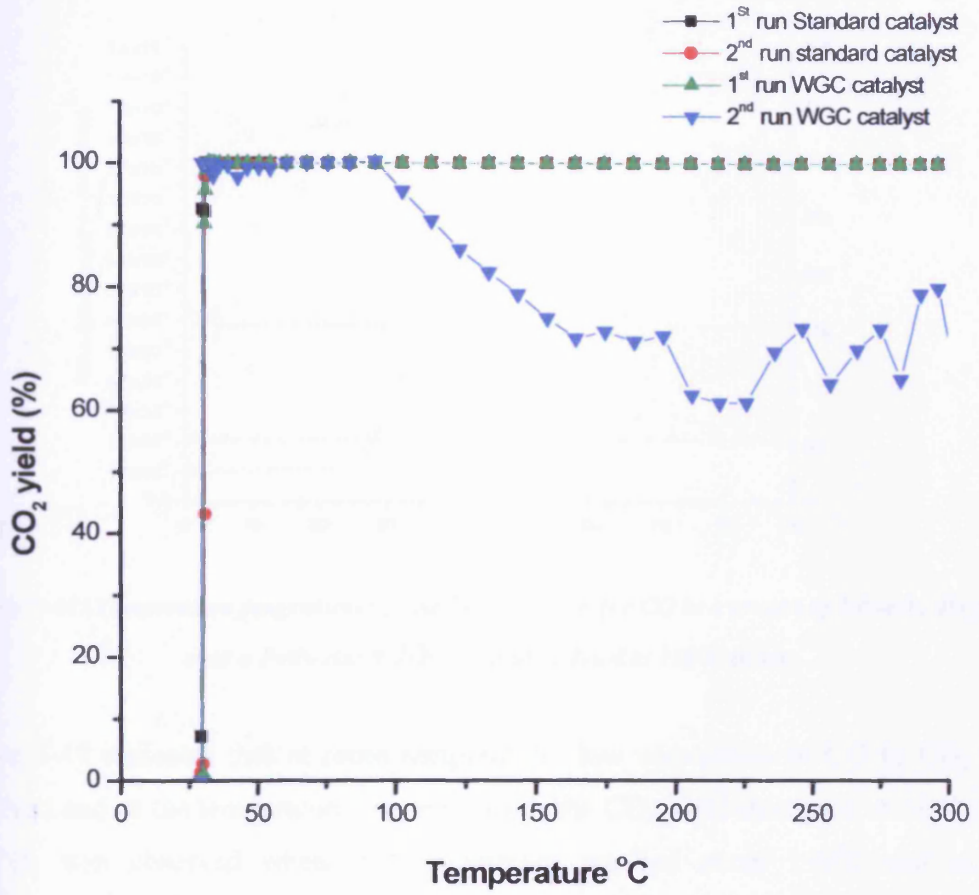

Figure 3-47: Comparison of CO_2 yield (%) with temperature for CO pulses in a stream of 10%eO_2/ He flow over standard and WGC Au/TiO_2 catalysts

3.7 Comparison with Au supported on other metal oxide catalysts

Choice of the support is another crucial issue for gold supported catalyst to be used for CO oxidation reaction. Several metal oxides were used as supports for gold catalyst. Au/ γ-Al_2O_3 were one of the supports, although reported with variable activities. However, the results proved efficient or less efficient [15]. In order to get an insight of CO oxidation reaction, a 1wt% Au/ γ-Al_2O_3 catalyst was prepared using deposition precipitation method .The temperature programmed pulse flow reaction was carried out in order to test the activity of the catalyst (figure 3-48).

The figure (3-48) shows little conversion of CO to CO_2, with many unreacted pulses of CO at room temperature. However, as the temperature was increased, more CO_2 peaks were observed. When the data in figure 3-48 were integrated and analysed, figure 3-49 was obtained.

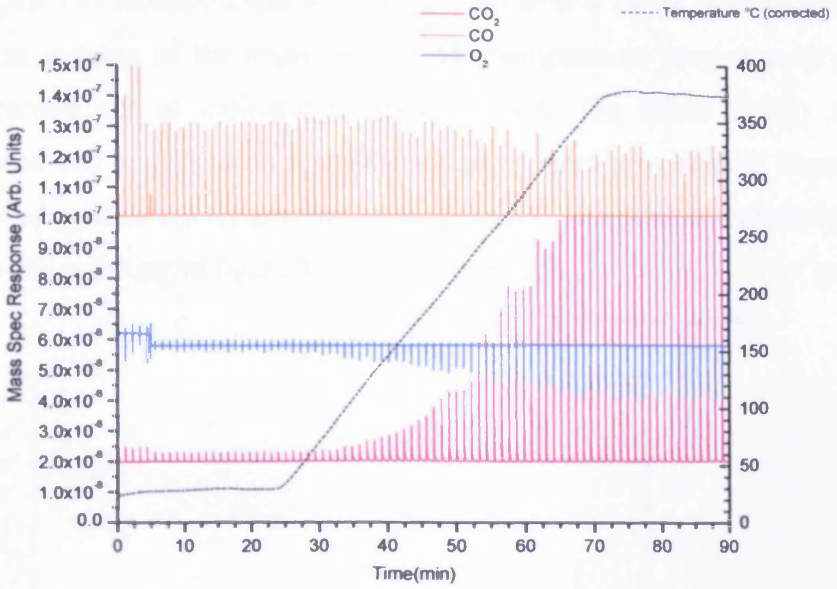

Figure 3-48: Temperature programmed pulse flow reaction for CO in a stream of 10%eO₂/ He flow over a 1wt% Au/ γ-Al_2O_3 catalyst dried at 120°C in air

Figure 3-49 indicates that at room temperature, low conversion of CO to CO_2 was observed and as the temperature was increased, the CO_2 yield increased. A 50% yield of CO_2 was observed when the temperature reached about 190°C and as the temperature reached 320°C, 100% yield of CO_2 was attained. This has proved less efficiency of Au/ γ-Al_2O_3 than Au/TiO_2 catalyst for CO oxidation.

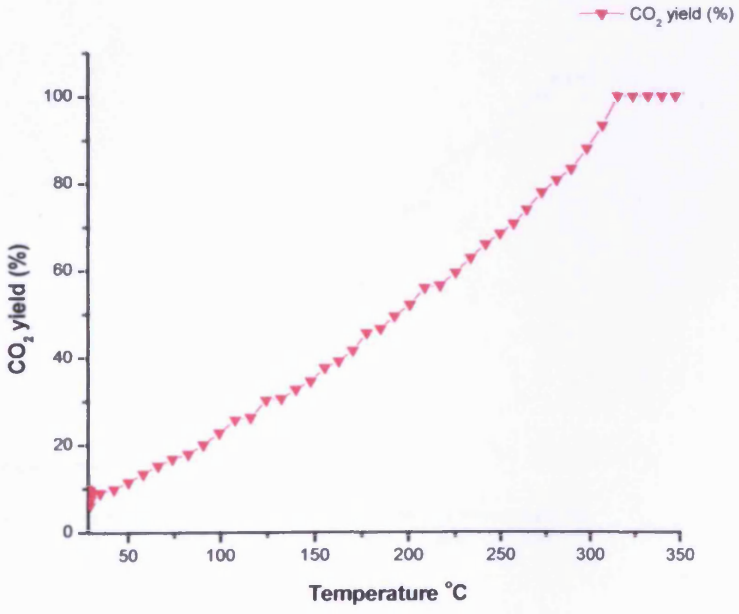

Figure 3-49: CO_2 yield (%) with temperature for CO pulses in a stream of 10%eO₂/ He flow over standard a 1wt% Au/ γ-Al_2O_3 catalyst dried at 120°C in air

Similarly, the CO oxidation was also carried out over a 1wt% Au/ γ-Al_2O_3 prepared by incipient wetness of the impregnation. The temperature programmed pulse flow reaction carried out as indicated in figure (3-50). The figure (3-50) shows low conversion of CO to CO_2, with low CO_2 signal at room temperature, however, more CO_2 was observed as the temperature was increased. Integration and analysis of data in figure 3-50, resulting in figure 3-51 being obtained.

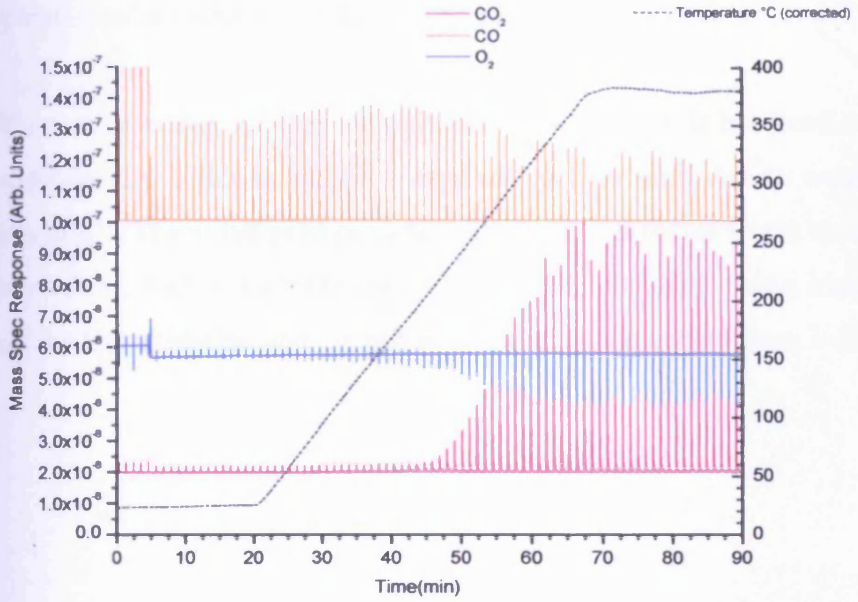

Figure 3-50: Temperature programmed pulse flow reaction for CO in a stream of 10%eO2/ He flow over a 1wt% Au/ γ-Al_2O_3 catalyst dried at 120°C in air (IW)

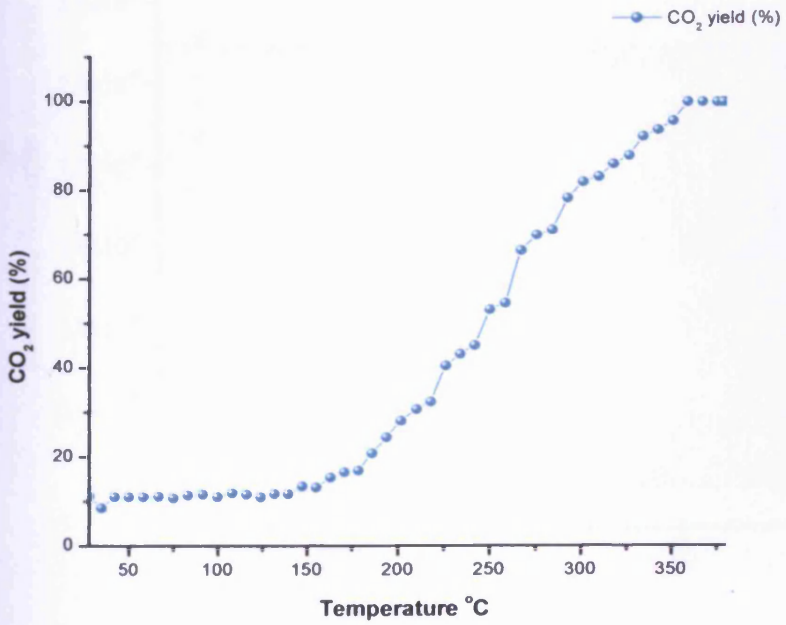

Figure 3-51: CO_2 yield (%) with temperature for CO pulses in a stream of 10%eO2/ He flow over a 1wt % Au/ γ-Al_2O_3 catalysts dried at 120°C in air (I W)

The analysis of figure 3-51 shows that at room temperature, about 11% of CO_2 yield was observed and as the temperature increases, the yield of CO_2 increases , with 50% of CO_2 yield being attained at 230°C, a little higher temperature than the similar catalyst prepare by deposition precipitation method. However, 100% of CO_2 yield observed as the temperature reached 350°C.The results shows that Au/Al_2O_3 catalyst prepared by deposition precipitation is better in activity for CO oxidation than the prepared similar catalyst by incipient wetness.

In the same manner, another support employed (SiO_2). It has been reported by many researchers that Silica is the least used support for gold due to weak metal –support interaction[41]. The small gold particles size is very difficult to get as they sinter easily. Nevertheless, 1wt% Au/SiO_2 catalyst was also prepared using incipient wetness to study the CO oxidation and the result obtained is shown in figure 3-52.

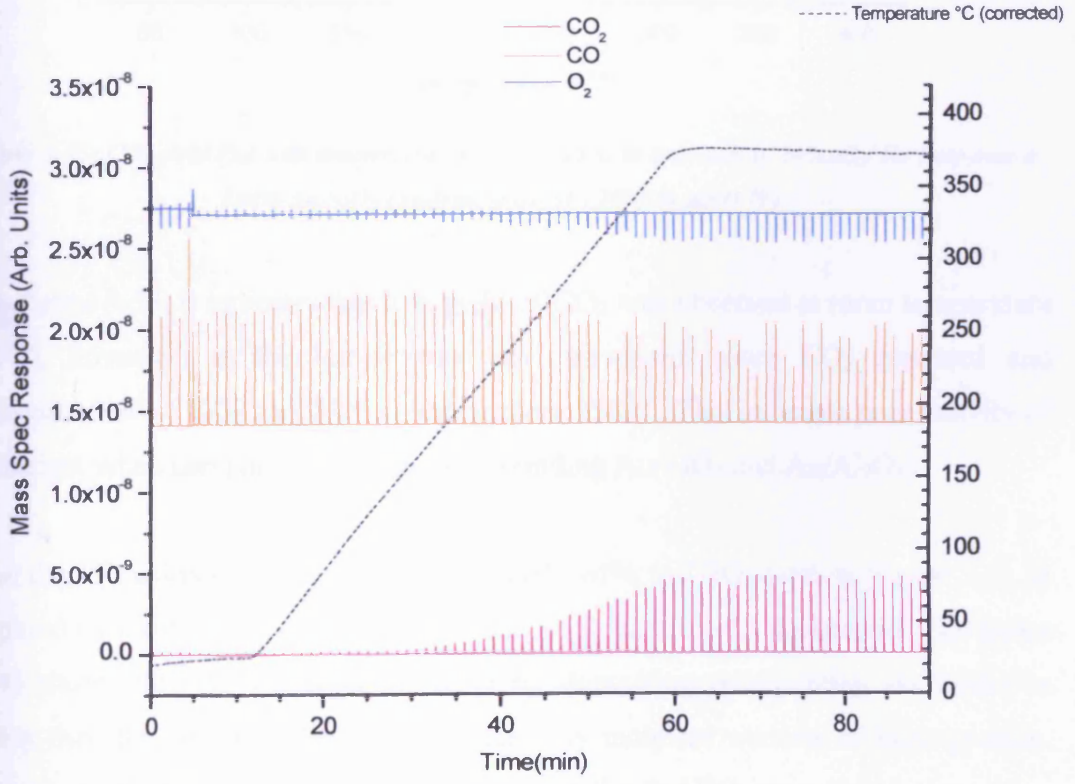

Figure 3-52: Temperature programmed pulse flow reaction for CO in a stream of 10%eO_2/ He flow over a 1wt% Au/SiO_2 catalyst dried at 120°C in air (IW)

Figure 3-52, shows that not much signals for CO_2 observed at room temperature, however as the temperature was increased, more CO_2 appeared. Figure 3-53 shows the integrated and analysed data of figure 3-52.

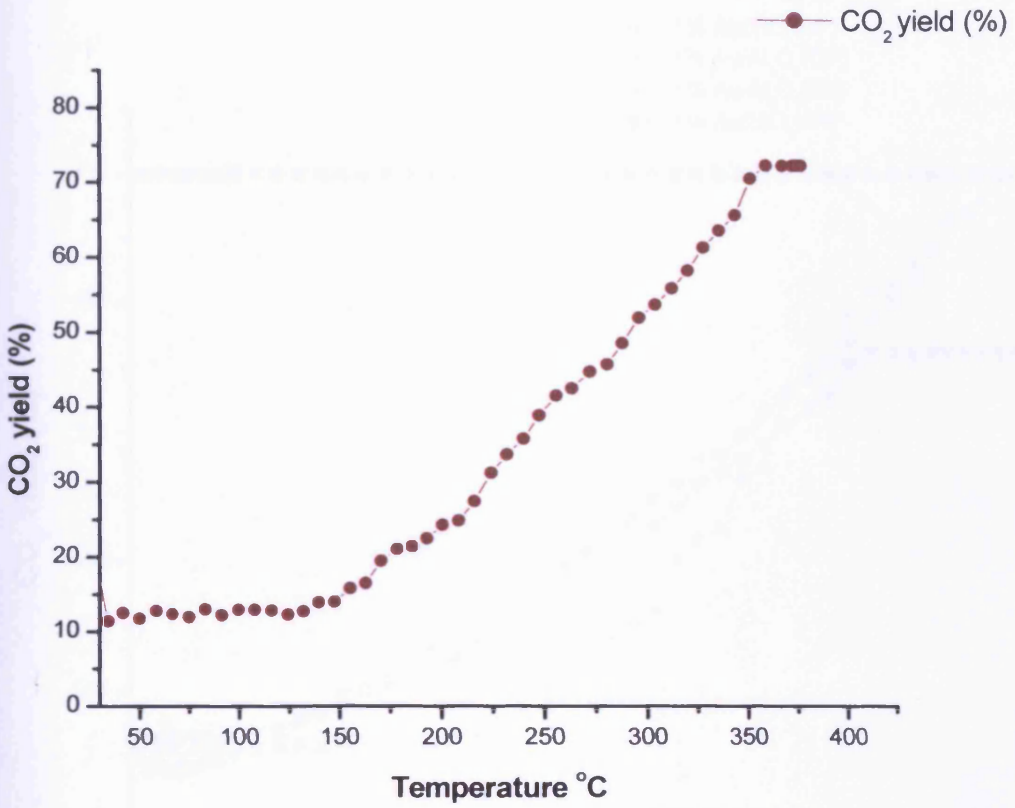

Figure 3-53: CO_2 yield (%) with temperature for CO pulses in a stream of 10%eO_2/ He flow over a 1wt% Au/SiO_2 catalysts dried at 120°C in air (I W)

From figure 3-53, it indicates that low yield of CO_2 was observed at room temperature (<10%), however, as the temperature was increased, more CO_2 appeared and maximum yield of CO_2 was 75% at temperature 350°C. This indicates poor activity of the catalyst when compared with the corresponding Au/TiO_2 and Au/Al_2O_3.

When the CO oxidation data in the first run of 1wt% Au/TiO_2 catalyst (figure 3-3), is compared with data in figure (3-48, 3-51 and 3-53), figure 3-55 is obtained. The figure (3-54) shows that the catalysts prepared by deposition precipitation are better in activity then the corresponding catalyst made by incipient wetness of impregnation. However, more activity observed for the case of the Au/TiO_2 prepared by deposition precipitation then the corresponding catalyst of Au/ γ-Al_2O_3.

The order of the activity of the catalysts with respect to CO oxidation is as follows

Au/TiO_2 (**DP**)>Au/Al_2O_3 (**DP**)>Au/γ-Al_2O_3 (**IW**)>Au/SiO_2 (**IW**)

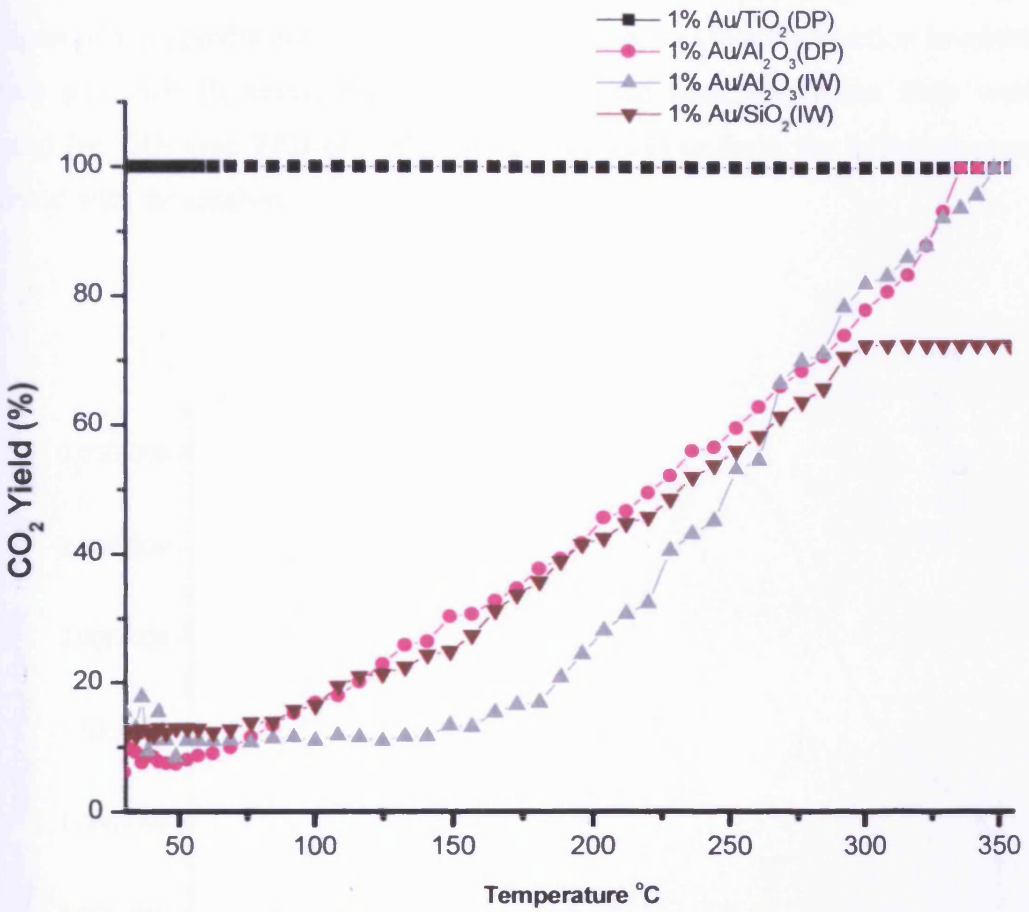

Figure 3-54: Comparison of CO_2 yield (%) with temperature for CO pulses in a stream of 10%eO_2/ He flow over Au supported on different metal oxide catalysts with different preparation methods

3.8 Temperature Programmed Desorption of CO over Au/TiO_2 catalyst

Knowledge of the activation energy and the adsorbed species are one of the vital tools for estimation or determining the mechanism of the reaction. The temperature programmed reaction desorption can be used to estimate the activation energy of desorption and to determine the adsorbed species on the surface. Several mechanisms revealed the adsorption of CO O_2 and CO_2 on the surface of the catalyst before desorbing to CO_2[11, 31-32].

1wt% Au/TiO_2 catalyst was used in order to explore the temperature programmed desorption of CO over Au/TiO_2 catalyst. Figure 3-55 shows the TPD of CO after

pulses in a stream of He Flow over a 1wt% Au/TiO_2 catalyst. The figure (3-55) indicates that the CO_2 produced over Au/TiO_2 has two desorption peaks, one at lower temperature with maximum desorption peak centred at 80°C, and the other at high temperature with peak centred at 270°C.The high temperature desorption of CO_2 is accompanied with production of hydrogen , which implies that the reaction involved, is water gas shift However, the hydrogen desorbed may also come from water produced by TiO_2 (see TPD of TiO_2 alone, page 154) or from the hydroxyl group associated with the catalyst.

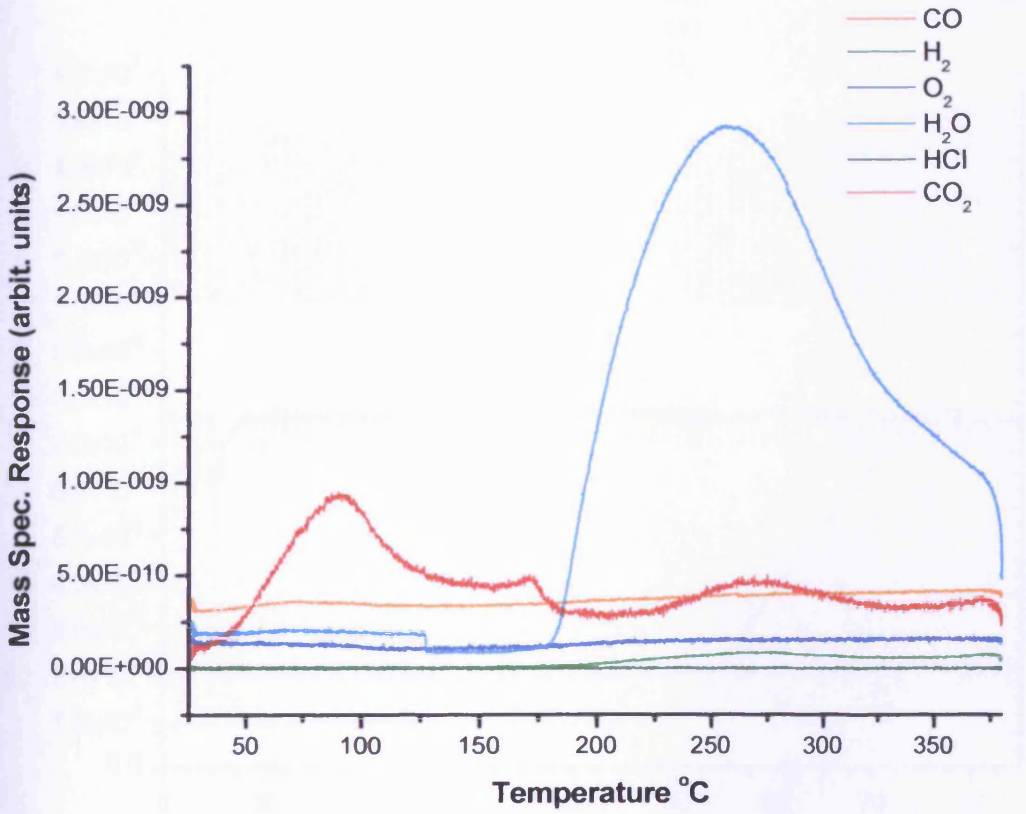

Figure 3-55: Temperature Programmed Desorption for CO pulses in a stream of He flow over a 1wt% Au/TiO_2 catalyst prepared by deposition precipitation method

Similarly, a broad peak of water observed at high temperature, presumably comes from TiO_2. The TPD also shows no desorption of oxygen, and HCl desorption peak was also not observed which indicates the catalyst is free from chloride ion.

3.9 Control experiments

Blank control experiments were performed to aid analysis of the data. Figure 3- 56 shows the temperature-programmed pulse flow reaction of CO in a stream of 10%O_2/He gas flow over an empty U tube. The data shows no CO_2 reasonable CO_2 peaks observed at room temperature and at high temperature. When the data was integrated and analysed figure, 3-57 obtained. The figure shows the CO_2 yield seem to be negligible, with yield value of CO_2 being not more than 8%.

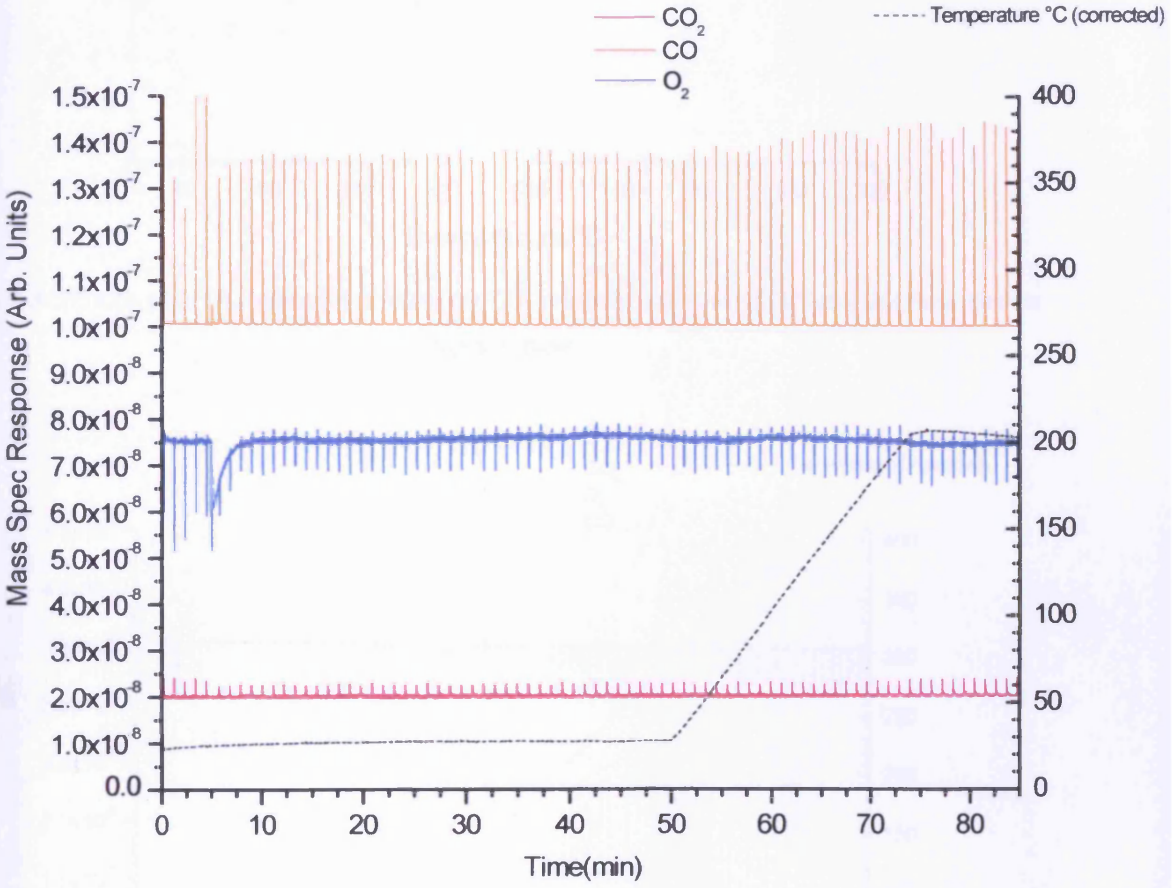

Figure 3-56: Temperature programmed pulse flow reaction for CO in a stream of 10%O_2/ He flow over an empty U tube

However, when TiO_2 was used as a catalyst alone for aerobic (in 10%O_2/He flow) CO oxidation (figure 3-58), low intensity CO_2 peaks were observed at room temperature. However, as the temperature was increased, more intense CO_2 peaks observed.

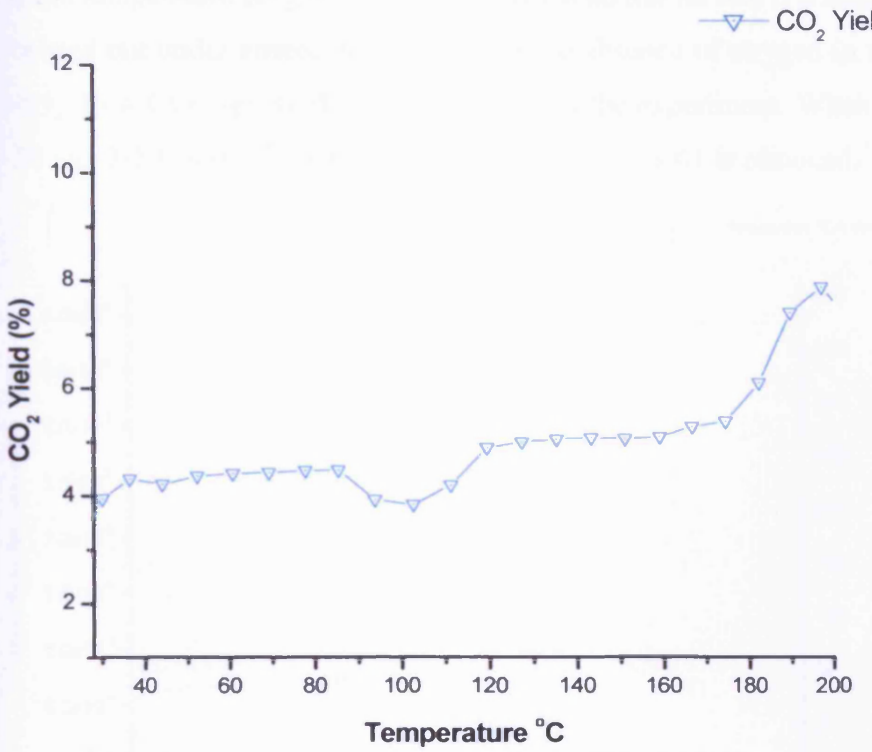

Figure 3-57: CO_2 yield (%) with temperature for CO pulses in a stream of 10%eO_2/ He flow over an empty U tube

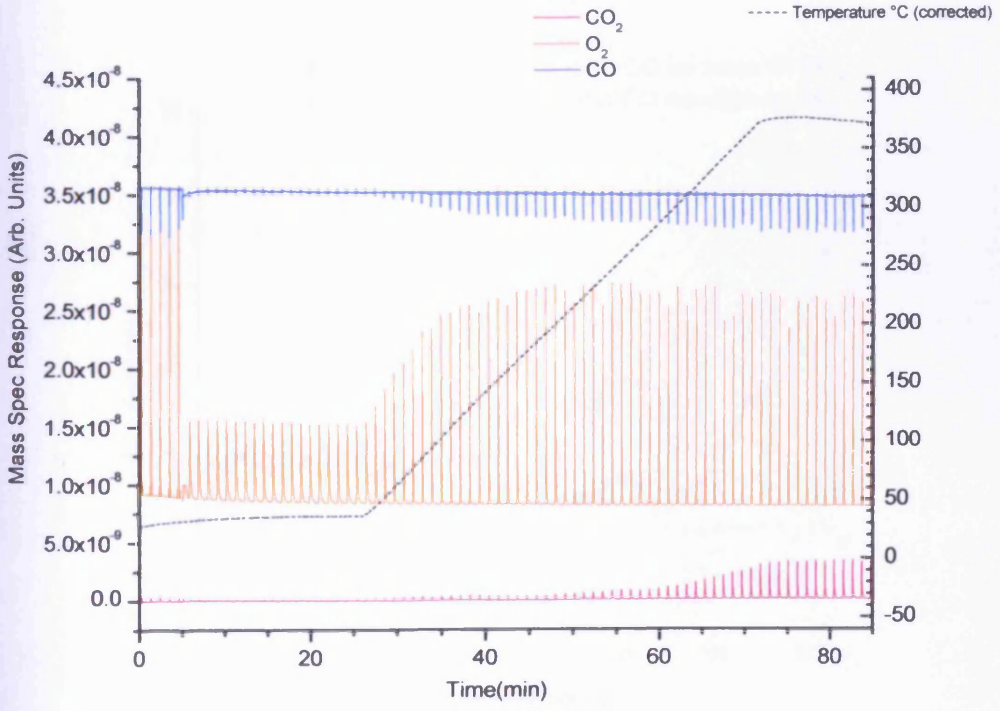

Figure 3-58: Temperature programmed pulse flow reaction for CO in a stream of 10%O_2/ He flow over a TiO_2 catalyst

However, the temperature programmed pulse flow reaction for CO reaction over TiO_2 catalyst carried out under anaerobic reaction (in the absence of oxygen in the stream) (figure 3-59). Low CO_2 signals observed through out the experiment. When the data in figure 3-58 and 3-59 were integrated and analysed, figure 3-61 is obtained.

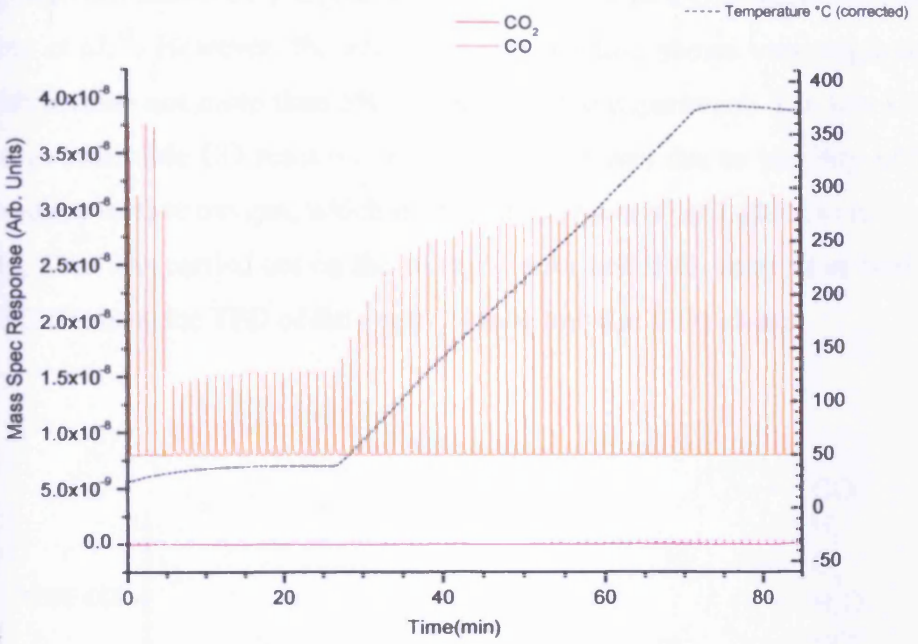

Figure 3-59: Temperature programmed pulse flow reaction for CO in a stream of He flow over a TiO_2 catalyst

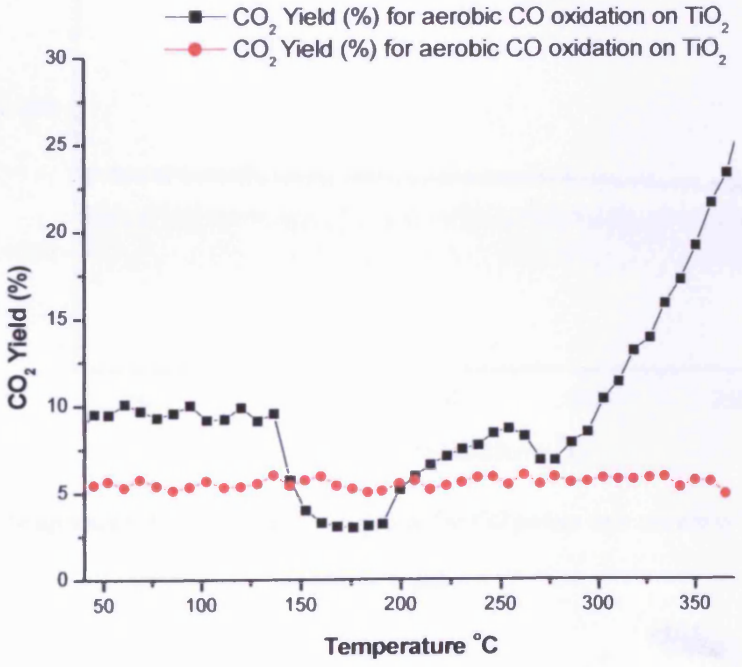

Figure 3-60: Comparison of CO_2 yield (%) with temperature for CO pulses in a stream of 10%eO2/ He (aerobic) and He (anaerobic) flow over TiO_2 catalyst

Figure 3-60 shows that low yield of CO_2 was observed for aerobic CO oxidation and with yield value for CO_2 at room temperature being almost 10%, but as the temperature was increased, the CO_2 yield increased with value being 25% at 350°C. The low yield of CO_2 observed for TiO_2 catalyst was due to intrinsic nature of it. This type of properties shown by TiO_2 makes it inactive for low CO oxidation as concluded by Haruta *et al.*[57]. However, the anaerobic CO reaction shows very negligible CO_2 yield with a value not more than 5% through out the experiment. The low CO_2 yield observed in anaerobic CO reaction on TiO_2 catalyst was due to inability of TiO_2 to produce active surface oxygen, which is only present when gold added to it.

Similarly, TPD was carried out on the empty U tube and TiO_2 catalyst as well. Figure 3-61 and 3-62 show the TPD of the empty U tube and the TiO_2 alone.

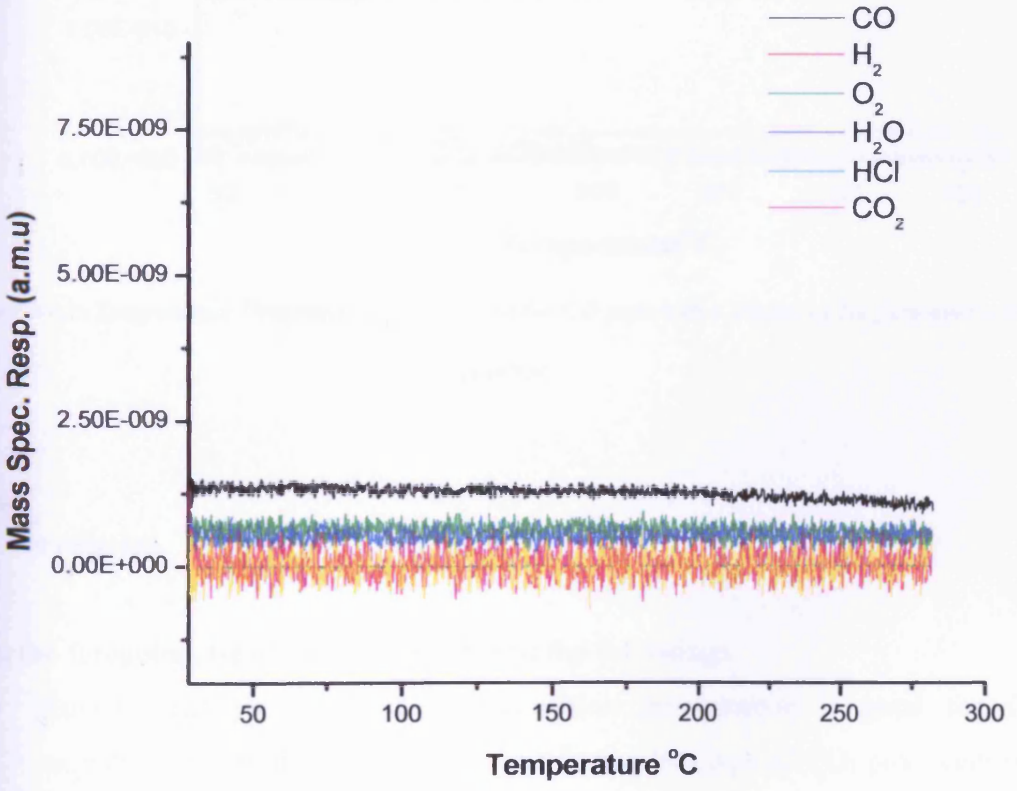

Figure 3-61: Temperature Programmed Desorption for CO pulses in a stream of He flow over an empty U tube

The TPD for TiO_2 (figure 3-62) shows that no oxygen and CO_2 were desorbs at room temperature or high temperature. However, an appreciable amount of water was

desorbed at high temperature with desorption peak centred at 320°C, presumably due to water gas shift occurring on the TiO_2 surface.

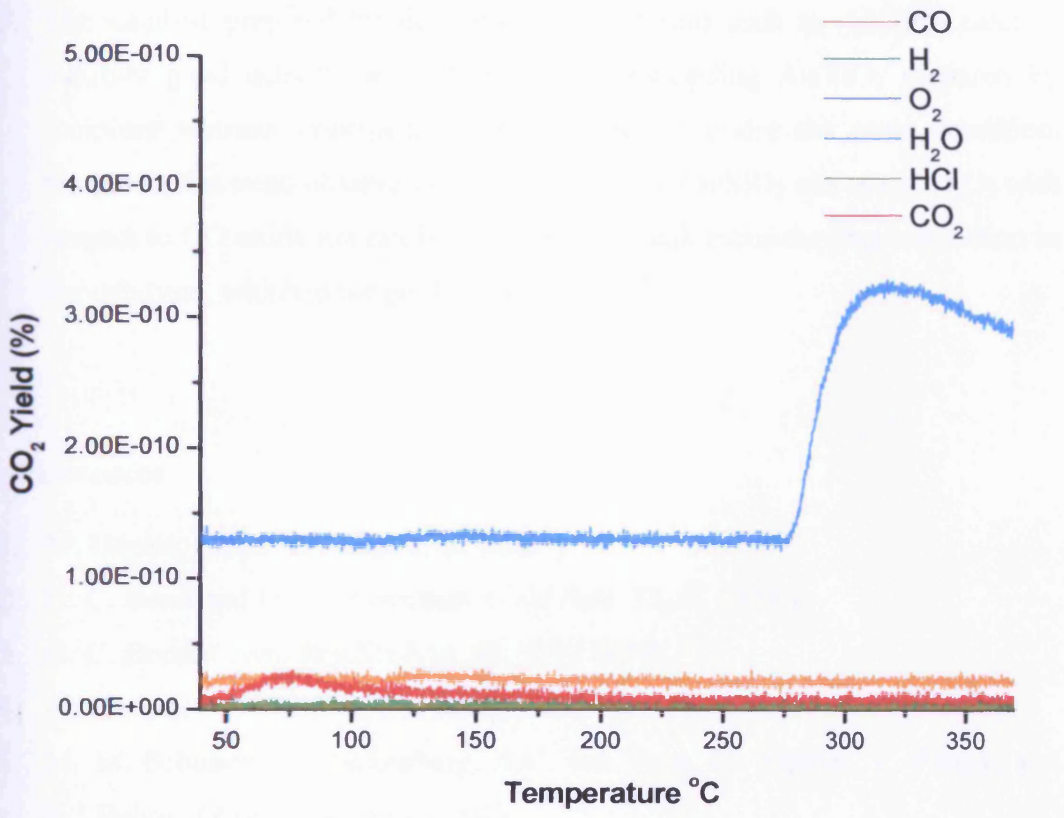

Figure 3-62: Temperature Programmed Desorption for CO pulses in a stream of He flow over a TiO_2 catalyst

3.10 Conclusion

From the foregoing, we are able to understand the followings

1. Au/TiO_2 catalyst prepared by deposition precipitation is good for CO oxidation. It was also possible to identify that two type of CO_2 produced; one at low temperature (stage I CO_2) and the other at relatively high temperature (stage II CO_2). Both types of CO_2 produced, with stage I CO_2 due to stoichiometric reaction and the other (stage II CO_2) due to catalytic reaction.
2. Both types of CO_2 produced are observed for the catalyst pre-treated in air at 120°C or 400°C. However, the catalyst of Au/TiO_2 prepared by deposition pre-treated in air at 120°C shows better activity with respect to CO oxidation.

3. Two types of CO_2 produced (stage I and stage II), which are due to stoichiometric and the other due to catalytic reaction respectively.
4. The higher the flow rate of CO and O_2, the more the oxidation of CO to CO_2.
5. The catalyst prepared by deposition precipitation such as Au/TiO_2 catalyst exhibits good activity better than the corresponding Au/TiO_2 prepared by incipient wetness impregnation and pre-treated under the same condition. However, the trend observed for low activity of Au/SiO_2 and $Au/g\text{-}Al_2O_3$ with respect to CO oxidation can be attributed to weak metal-support interaction in the catalysts, which make gold to sinter easily[80].

3.11 References

1. M. Haruta, *Catal.Surf.,Jap.* **1,** 61 (1997).
2. G. C. Bond and D. T. Thompson, *Gold Bull.* **33,** 41 (2000).
3. G. C. Bond, *Catal. Rev.Sci.Eng.* **41,** 319 (1999).
4. M. Haruta, *CATECH* **6,** 102 (2002).
5. M. M. Schubert, S. Hackenberg, A.C. van Veen, M. Muhler, V. Plazak, and R.J.Behm, *J.Catal.* **197,** 113 (2001).
6. F. Boccuzzi and A. Chiorino, *J. Phys.Chem. B* **104,** 5414 (2000).
7. G. R. Bamwenda, S.Tsubota, T. Nakamura, and M. Haruta, *Catal.Lett.* **44,** 83 (1997).
8. M. Haruta, S. Tsubota, T. Kobayashi, H. Kageyama, M. J. Genet, and B. Delmon, *J. Catal.* **144,** 175 (1993).
9. Y. Iizuka, H. Fujiki, N. Yamauchi, T.Chijjiwa, S. Arai, S. Tsubota, and M.Haruta, *Catal., Today* **36,** 115 (1997)
10. A. I. Kozlov, A. P. Kozlov, H. Liu and Y. Iwasawa, *Appl. Catal., A* **182,** 9 (1999)
11. J.-D.Grunwaldt and A. Baiker, *J.Phys.Chem. B.* **103,** 1002 (1999)
12. F. Boccuzzi and A. Chiorino, M. Manzoli, P. Lu, T. Akita, S. Ichikawa, and M. Haruta, *J. Catal.* **202,** 256 (2001).
13. M.J. Kahlich, H. A. Gasteiger, and R. J. Behm., *J. Catal.,* **182,** 430 (1999).
14. G. Avgouropoulos, T. Ioannides, Ch. Papadopoulou, J. Batista, S. Hocevar, and H.K.Matralis, *Catal. Today* **75,** 157 (2002)

15. T. V.Choudhary, C. Sivadinarawa, C.C.Chusuei, A.K.Darye, J.P.Facker, and D.W.Goodman, *J.Catal.* **207,** 247 (2002).

16. J-D.Grunwaldt, C.Kiener, C. Wogerbauer, and A. Baiker, *J.Catal.* **181,** 223 (1999).

17. G. C. Bond, *Catal. Today* **72** 5 (2002).

18. D.T Thompson, *Appl.Catal.A* **243**,201 (2003).

19. S. D. Lin, M.A. Bollinger, and M. A. Vannice, *Catal. Lett,* **17,** 245 (1993).

20. A. Sanchez, S. Abbet, U. Heiz, W.-D. Schneider, H. Hakkinen, R. N. Barnett, and U. L andman, *J. Phys. Chem.A* **103,** 9573 (1999)

21. F. Boccuzzi, G.Cerrato, F.Pinna, and G.Strukul, *J.Phys.Chem.B* **102,** 5733 (1998)

22. M. Ruff, S. Frey, B. Gleich, and R.J.Behm, *Appl. Phys. A* **66,** S513 (1998).

23. M. Mavrikakis, P. Stoltze, and J. K. Norskov, *Catal. Lett.* **64,** 101 (200)

24. S. Giorgio, C.R. Henry, B. Pauwels, and G. Van Tendeloo, *Mater. Sci. Eng., A* **A297,** 197 (2000)

25. R. Meyer, C. Lemire, S.K.Shaikhutdinov, and H. –J. Freund, *Gold Bull.***37,** 72 (2004)

26. M. Valden, D. Lai, and D. W. Goodman, *Science* 281, 1647 (1998).

27. M. S.Chen and D. W. Goodman, *Science* **306,** 252 (2004).

28. J. M. Gottfried and K. J. Schmidt, S. L. M. Schroeder, and K. Christmann, *Surf. Sci.* **536** 206 (2003

29. J. D. Stiehl, T. S. Kim, S. M.McClure, and C. B. Muillins, *J. Am. Chem. Soc.* **126,** 1606 (2004).

30. X. Lai, T. P. St. Clair, M. Valden, and D. W. Goodmann, Prog. *Surf. Sci.*, **59,** 25 (1998).

31. M. Monzali, A. Chiorino, and F. Boccuzzi, *Surf. Sci.* **532-535,** 377 (2003).

32. F. Boccuzzi, A. Chiorino, S. Tsubota, and M. Haruta, *J. Phys. Chem.* **100,** 3625 (1996).

33. M. Maciejewski, P. Fabrizioli, J-D.Grunwaldt, O. S.Becker, and A. Baiker, *Phys. Chem. Chem. Phys.* **3,** 3846 (2001).

34. H. H. Kung and C. K. Costello, *J. Catal.*, **216,** 1-2 (2003), 425-432

35. J.K. Norskov, P. Stoltze and M. Mavrikakis, *Catalysis Letters*, 64, 101 (2000).

36. D.W. Goodman, M. Valden, S. Pak and X. Lai, *Catalysis Letters,* 56, 7 (1998).

37. R.L. Augustine and S.K. Tanielyan, *Applied Catalysis A: General*, **85**, 73 (1992).

38. P. Jena, D. Stolcic, M. Fischer, G. Gantefor, Y.D. Kim and Q. Sun, *J. Amer. Chem. Soc.* 2003, **1248.5**, 28

39. Z.-P.Liu, P. Hu and A. Alavi, J. Am. Chem. Soc.**124,** 14770 (2002)

40. M.A. Vannice and M. Bollinger, *Appl. Catalysis B: Environmental*, **8**, 417 (1996).

41. Y. Iwasawa, H. Liu, A.I. Kozlov, A.P. Kozlova, T. Shido and K. Asakura, J. Catalysis, **185**, 252 (1999).

42. A. Baiker and J.-D. Grunwaldt, *J. Phys.Chem B,* 103, 1002 (1999).

43. M. Haruta, J. New Mater. *Electrochem. Systems* **7,** 163 (2004).

44. .G.C.Bond and D.T.Thompson, *Gold Bull.*,2000,**33**,41

45. Z.-P. Liu, X.-Q.Gong, J. Kohanoff, C. Sanchez and P. Hu, *Phys. Rev. Lett.*, **91,** 266102 (2003).

46. L. M. Molina and B. Hammer, *Appl. Catal.,A:* Gen.,**291,** 21 (2005).

47. M. Haruta, M. Date, Y. Iisuka and F. Manzoli, D. Andreeva and T. Tabakova, *J. Catal.*. **43,** 125 (2001).

48. M..Mavrikakis, P. Stoltze and J. K. Noskov, *Catal. Lett.* **64,** 101 (2000).

49. Y. Xu and M. Mavrikakis, *J.Phys. Chem. B.***107,** 9298 (2003).

50. S. Giorgio, C. Chapon, C.R. Henry, G. Nihoul and J.M. Penisson, *Phil. Mag. A* **64,** 87 (1991).

51. S. Giorgio, C. R. Henry, B. Pauwels and G. P. Tenderloo, *Mater.Sci.Eng. A.* **297,** (2001).

52. V. Schwartz, D.R. Mullins, W. Yan, B. Chen, S. Dai and S. H. Overbury, *J. Phys. Chem. B* **108,** 15782 (2004).

53. J. H. Yang, J. D. Henao, M.C. Raphulu, Y.Wang, T Caputo, A.J. Groszek, M. C.Kung, M. Scurrell, J. T. Miller and H. H. Kung, *J.Phys. Chem. B.* **109,** 10319 (2005).

54. J. T. Miller, A. J. Kropf, Y. Zha, J. R. Regalbuto, L. Delannoy, C. Louis, E. Bus and J. A. van Bokhoven, *J. Catal.* **240,** 222 (2006).

55. J. M.C. Soares, P. Morrall et. *J. Catal.* **219,** (2003) 17-24.

56. M. Okumura, J. M. Coronado, J. Soria, M. Haruta, and J. Cones, *J. Catal.* **203,** 168 (2001).

57. Y.Iizuka, T.Tode, T. Takao, K. Yatsu, T. Takeuchi, S. Tsubota, and M. Haruta, *J. Catal.* **187,** 50 (1999).

58. E. Wahlstrom, N. Lopez, R. Schaub, P. Thostrup, A. Ronnau, C. Africh, E. Laegsgaard, J.K.Norskov, and F.Besenbacher, *Phys. Rev. Lett.* **90,** 261011 (2003)

59. N. Lopez, J. K. Norskov, T. V. W. Janssens, A. Carlsson, A. Puig-Molina, B.S.Clausen, and J.-D. Grunwaldt, *J. Catal.* **225,** 86 (2004).

60. U. Diebold, *Surf.Sci. Rept.* **48,** 53 (2003).

61. Masatake Haruta, *Cattech.* **6,** 3 (2002).

62. (a) M. A. P. Dekkers, M. J. Lippits and B. E. Nieuwenhuys, *Catal. Lette.*, **56,** 195 (1998). (b) M. A. P. Dekkers, M. J. Lippits and B. E. Nieuwenhuys, *Catal. Today*, **54,** 381 (1998).

63. G. C. Bond and D. T. Thompson, *Cat. Rev. Sci. Eng*, **41,** 319 (1999).

64. E. D. Park and I. S. Lee, *J. Catal.*, **186,** 1 (1999).

65. N. W.Cant and W. K. Hall, *J. Phys. Chem,* **75,** 2914 (1971).

66. S. D. Lin, M. Billinger and M. A. Vannice, *Catal. Lett.* **17,** 245 (1993).

67. W. A. Bone and G. W. Andrew, *Proc. Roy. Soc.(*London), **109A,** 459, (1925).

68. "The abilities and Potential of Gold as a Catalyst", Report of the National Research Institute, Osaka, Japan, (1999).

69. C. K. Chang, Y. J. Chen and C. T. Yech, *Appl. Catal. Lett.*, **174,** 13 (1998).

70. Y. Yuan, K. Asakura, A. P. Kozlova, H. Wan, K. Tsai and Y. Iwasawa, *Catal. Today,* **44,** 333 (1998).

71. A. M.Visco, F. Neri, G. Neri, A. Donato, C. Milone and S. Galvagno, *Phys. Chem. Chem. Phys.* **1,** 2869 (1999).

72. N. J. Osipoff and N. W. Cant, *Topics in Catalysis,* **8,** 161 (1999).

73. K. –H. Choi, B. –Y. Koi and H. –I. Lee, *Catal. Today,* **44,** 205 (1998).

74. Haoguo Zhu, Zhen Ma, Jason C. Clark, Zhengwei Pan, Steven H. Overbury and Sheng Dai, *Applied Catalysis* A: General, Volume **326,** Issue 1, 89-99 (2007).

75. C. Ozdemir, A. N. Akin, and R. Yildrim, *Appl. Catal.*, A **258,** 145 (2004).

76. D. Tibileti, E. A. B.Graaf, S.P. Teh, G. Rothen berg, D. Farrusseng and C. Mirodates, *J. Catal.*, **225,** 2 (2004).

77. M.M. Schubert, V. Plzak, J. Garche and R.J. Behm, *Catal. Lett.* **76,** 43 (2001).

78. Ohsaka, T.Izumi, F;Fujiki, Y.J *Raman Spectrosc,* **7,** 321 (1978).

79. Chaves, A:Katiyan, K.S;Porto,S.P.S .*Phys.Rev.*, **10,**3522 (1974).

80. Y. Yuan, K. Asakura, H. Wan, K. Tsai and Y. Iwasawa, *Catal. Letter.* **42**, 15 (1996)

81. S. Tsubota, T. Nakamura, K. Tanaka and M. Haruta; *Catal Letter.* **56,** 131 (1998)

Chapter 4- Gold catalysts for Methanol oxidation

4.1 Introduction

This chapter deals with the methanol oxidation over gold supported on Titania. Factors, such as catalyst preparation, reaction conditions, calcinations and drying temperatures were investigated. The pulsing or injection of methanol in a Temperature Programmed Reaction, isothermally in a continuous flow of a gas both aerobically (in the presence of oxygen) and anaerobically (in the absence of oxygen, *i.e.* in a flow of He alone) were also explored in order to gain insight in to the requirements for methanol oxidation over gold supported Titania.

The results obtained, were compared with the standard catalyst of the World Gold Council (WGC) in order to understand the activity of our catalysts. In order to understand these variables mentioned earlier, characterization techniques such as XPS, XRD, SEM, EDAX, Raman and DRIFTS were used and the mechanism of the oxidation of methanol over Au/TiO_2 catalysts proposed.

4.2 Brief introduction to the uses of methanol

Methanol is one of the most important chemical intermediates used in industrial chemistry. It is the starting reactant for the synthesis of various products, including hydrocarbons and mild oxidation products. Among the oxidation processes, formaldehyde production for the synthesis of phenolic resins [3] is largely predominant. Industrially, the oxidative dehydrogenation of methanol to formaldehyde is carried out both on silver and on ferric molybdate catalysts. [3-4] Although the ferric molybdate catalyst has been known since 1931 from the work of Adkins and Peterson [3], the industrial process was only developed on a large scale in the sixties.

Recently, it has been reported that methyl formate could be directly produced with high selectivity and yield, by catalytic methanol oxidation on V-Ti oxides [3-4], and Sn-Mo oxides. [2] This versatile product is of great interest for industry since it can be transformed into N-N dimethyl formamide or acetc acid [3].The methanol oxidation can lead to various products depending on the catalyst, reaction temperature, conversion and reactant partial pressure. [4, 5]

The main reaction product cited in the literature is formaldehyde (CH_2O), because of its industrial interest. However, it is also reported that important amounts of dimethyl ether (CH_3OCH_3), methyl formate ($HCOOCH_3$), methylal ($(CH_3O)_2CH_2$) and carbon oxides can be formed during the methanol oxidation. Surprisingly, the formation of

formic acid (HCOOH) is rarely observed. [6, 7] This product is considered as an intermediate in the formation of methyl formate [8&1] or carbon oxides.

It has been observed that gold is the least active among the noble metals group, but when highly dispersed on a reducible metal support such as TiO_2 it can exhibit surprisingly high activity for CO oxidation at low temperature.[10] Taking into consideration the low melting point and weak nature of chemisorption on gold, low-temperature catalytic combustion appears to be one of the most prosperous fields of applications for the supported gold catalyst.

Therefore, since methanol is readily combusted with noble metals and convertible into CO and H_2 by decomposition or reforming, it is expected that methanol will expand its usage as a clean fuel and a new energy carrier for hydrogen.

Several products such as formaldehyde, di-methyl ether, formic acid, etc have been reported to be part of methanol oxidation, though few reports were published about methanol oxidation over Au/ TiO_2.

4.3 Preparation of the catalyst.

The catalyst was prepared in a similar way as reported previously (*i.e.*, deposition precipitation method as discussed in Chapter 2).

The catalysts prepared were of two types: one catalyst was dried at 120°C and the other calcined at 400°C, in each case for 2hrs before loading in to the U tube of an oven of the reactor as described in Chapter 2. Both of these catalysts were subjected to various pre- treatments and were investigated under aerobic and anaerobic conditions.

4.4 Results and Discussion

4.5 Temperature Programmed Pulse Flow Reactions

4.5.1 Activity Test.

4.5.1.1 Uncalcined catalyst.

In order to understand the activity of the catalyst, a freshly prepared 1wt% Au/TiO_2 uncalcined sample of the catalyst dried at 120°C in air was used. It was then loaded in a pulse flow reactor in the presence of 10% O_2/He flow of gas at rate of 30ml per minute. The lines of the flow gas were heated to 80°C and injections of methanol were

done over the bypass and the catalyst. In each experiment in our investigations, different masses were monitored with respect to methanol oxidation. Table 1 below shows the masses monitored using the quadrupole mass spectrometer:

S NO	MASS	PRODUCT NAME
1	2	Hydrogen (H_2)
2	15 and 16	Methane (CH_4)
3	18	Water (H_2O)
4	28	Carbon monoxide (CO) and Nitrogen (N_2)
5	29	Formaldehyde (CH_2O) and Methanol (CH_3OH)
6	30	Formaldehyde (CH_2O)
7	31	Methanol (CH_3OH)
8	32	Oxygen(O_2) and Methanol (CH_3OH)
9	45	Dimethyl ether ($(CH_3)_2O$)
10	46	Formic acid (COOH)

Table4- 1: Masses monitored in methanol oxidation over a 1wt% Au/TiO_2 catalyst

The masses monitored were chosen because methanol can be dehydrogenated to produce H_2, and CO in the presence of oxygen (oxidation) or it may be decomposed to produce CO, H_2 and sometime CO_2. Methanol can also be partially oxidised to formaldehyde, or can even to formic acid.

The loaded catalyst (surface area of $50m^2/g$) loaded in a U tube of an oven of the reactor was heated at 120°C for 30 minutes in a flow of oxygen at a rate of 30ml per minute in the gas phase (aerobically) as described earlier in Chapter. Figure (4-1) below indicates the signals obtained for the different masses when methanol was subjected to a temperature controlled pulse programmed reaction. Methanol was allowed to be injected through the by pass and then switched over the catalyst.

The resulting first five pulses were detected through the by pass, and 100 percent of un-reacted methanol was detected. The first peaks observed, after the five by-pass injections (mass 31 and 29 a.m.u signals); represent 100% percent of un-reacted methanol. Although the peak is short and broad in size when compared with the by pass peaks. However, when the peaks are integrated, they are the same intensity as the peak through the by-pass and from the same figure (4-1); it indicates that about 7μl of methanol saturated the surface.

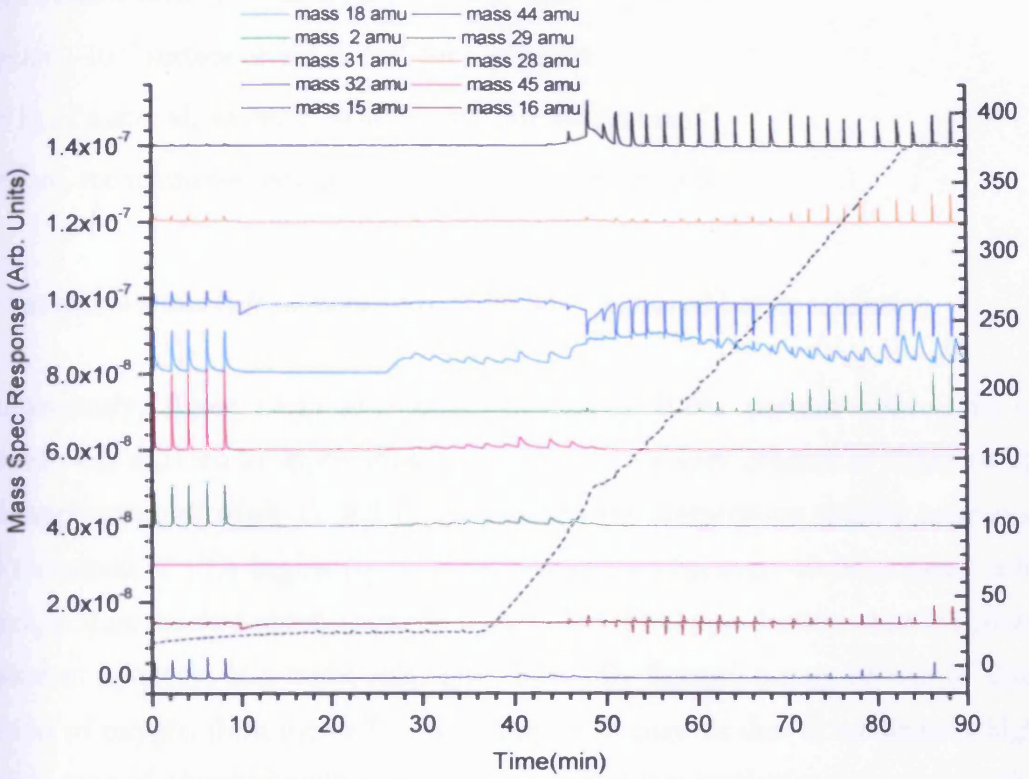

Figure 4-1: Temperature Programmed Pulse Flow Reaction of methanol oxidation over a 1wt% Au/TiO_2 catalyst dried at120 °C in air (First run)

7μl is equivalent to $7x10^{-3}cm^3$ of methanol.

Therefore, the mass of methanol = density x volume

$= 7 \times 10^{-3}cm^3 \times 0.8gm/cm^3$

$= 5.6 \times 10^{-3}gms$

But, Amount in Moles = Mass in g/ Molar Mass in g/mole

$= 5.6 \times 10^{-3}gms /32g/mole$

$= 1.75 \times 10^{-4}$ moles

Also, 1 Mole $= 6.022 \times 10^{23}$ molecules

Therefore: 1.75×10^{-4} $= 6 \times 10^{23} \times 1.75 \times 10^{-4}$ molecules

$= 1.05 \times 10^{20}$ molecules

The amount of methanol adsorbed in ½ g of the catalyst is 1.05×10^{20} molecules.

The amount of methanol adsorbed in 1g of the catalyst is $2 \times 1.05 \times 10^{20}$ molecules

$= 2.10 \times 10^{20}$ molecules per gram of the catalyst.

But the surface area of the catalyst is 50 m^2g^{-1} and

There are ~10^{19} surface atoms in 1m^2 for a material

So in 1g of material, we have about 5 x 10^{20} surface atoms.

Therefore, the methanol molecules per surface atom =2.10/5

= 0.4

This represents about half monolayer of methanol consumed before saturation.

Simultaneously, figure (4-1) also indicates that a 100% percent conversion of methanol was attained at approximately 100°C. This is very evident in figure (4-1): the disappearance of mass 31 and 29 amu and as the temperature slightly increases, slow formation of CO_2 begins (type I CO_2 production) between 40-50 minutes until the temperature reached about 150°C in which type II CO_2 production occurred (from 50 minutes upwards) at a faster rate. The slow CO_2 formation may be due to slow diffusion of oxygen from the bulk of the support or may be due to moderately high retention time of adsorbed methanol on the surface at that particular temperature. The oxygen diffusing from the bulk is being replaced by the oxygen gas in the stream and both the two types of CO_2 produced (type I and II) are due to catalytic reactions as can be clearly seen from figure (4-1).

The type I CO_2 occurred at low temperature and evolved at a very slow rate due to slow uptake of oxygen (mass 32 amu signal) from the stream, while for type II CO_2, the oxygen up take occurred at a faster rate as evident at a temperature150°C (figure (4-1). The two types of CO_2 produced are due to catalytic reaction in which the oxygen that comes from the TiO_2 is being replaced by the gas phase oxygen, which comes from the flow gas in the stream.

However, as the temperature reached about 170°C, dehydrogenation begins in which CO, H_2 are produced, and both are produced at a faster rate. The CO_2 production decreases and more CO is produced at a faster rate and as the temperature reached about 280°C, de-oxygenation occurred which leads to the production of methane.

When the data (figure 4-1) was integrated, it leads to the following data as shown in figure (4-2) below:

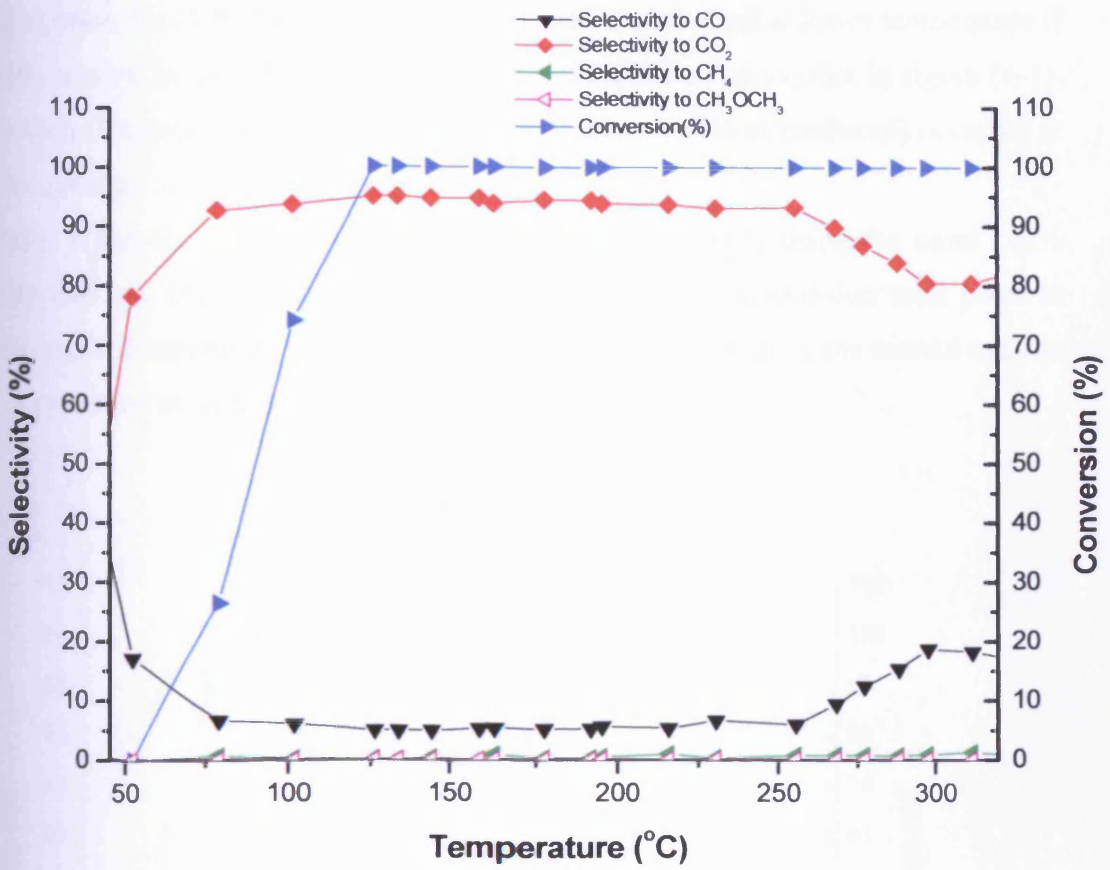

Figure 4-2: Selectivity and conversion for methanol oxidation over a 1wt% Au/TiO_2 catalyst dried at 120°C (First run)

From figure (4-2), it is possible to see that as the methanol is saturated on the surface at room temperature; the slow CO_2 production (type II) begins from when the conversion of methanol was only (>10%) and continued till the selectivity of CO_2 reached about 90% as the conversion of methanol was only 25%. When the conversion of methanol reached about 100%, already the CO_2 selectivity was 90% and the temperature was about 125°C. The selectivity to CO_2 remains steady until the temperature reached about 250°C. The CO_2 selectivity then drops, and the selectivity to CO begin to increase due to dehydrogenation of the methanol on the surface of the catalyst. The CO selectivity continues to increase and methane selectivity begins to increase due to de-oxygenation of the methanol at that particular temperature. Although the selectivity to methane is minimal (>10%), the results indicate that the Au/TiO_2 catalyst is a good combustor of methanol at very low temperature. It also makes possible to understand that methanol oxidation over Au/TiO_2 was a complete oxidation reaction. The role of Au on this reaction was to lower the activation energy

of the reaction, (i.e. 100% conversion of methanol was attained at lower temperature if Au/TiO_2 catalyst is used than when TiO_2 was used alone) as evident in figure (4-1). When TiO_2 (Degussa) was used alone the conversion (100% of methanol) occurred at high temperature as will be shown subsequently.

Similarly, if the second run of the reaction was carried out re-using the same 1wt% Au/TiO_2 catalyst, the results seem to be identical but the conversion took place at slightly higher temperature than the first run. The data obtained for the second run can also be presented as follows:

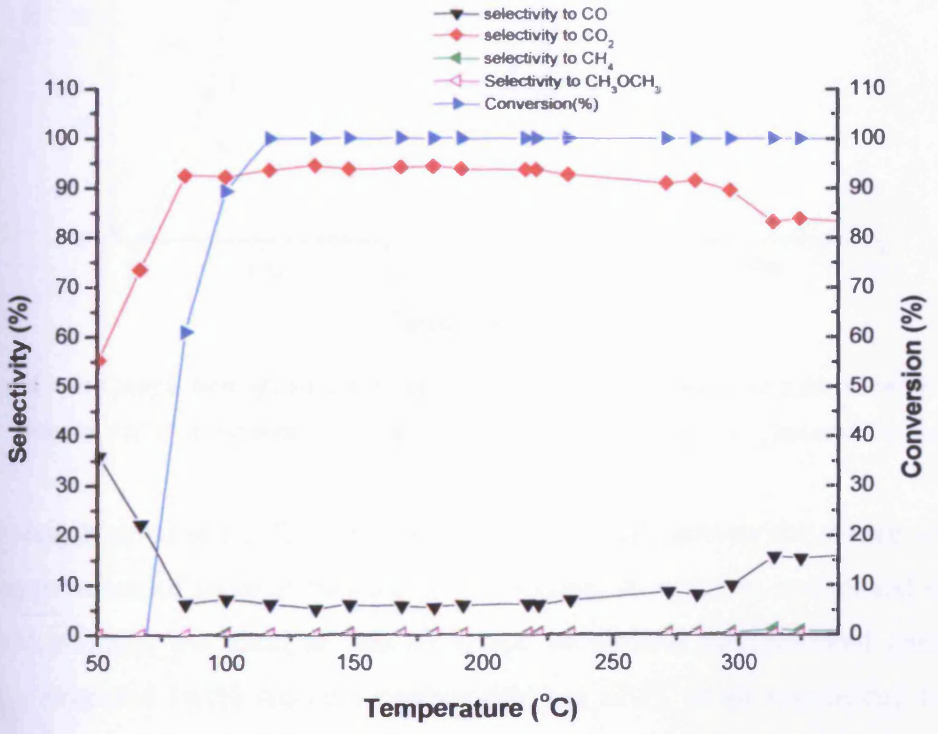

Figure 4- 3: Selectivity and conversion for methanol oxidation over a 1wt% Au/TiO_2 catalyst dried at 120°C (Second run)

100% conversion of methanol starts at about 125°C in figure (4-2) for the first run while 100% conversion was attained at about 130°C in figure (4-3) for the second run. When both data are gathered, significant information may be obtained as shown in figure (4-4).

From figure (4-4), it could be seen that 100% methanol conversion was attained at lower temperature for the first run while it occurred at little higher temperature for the second run.

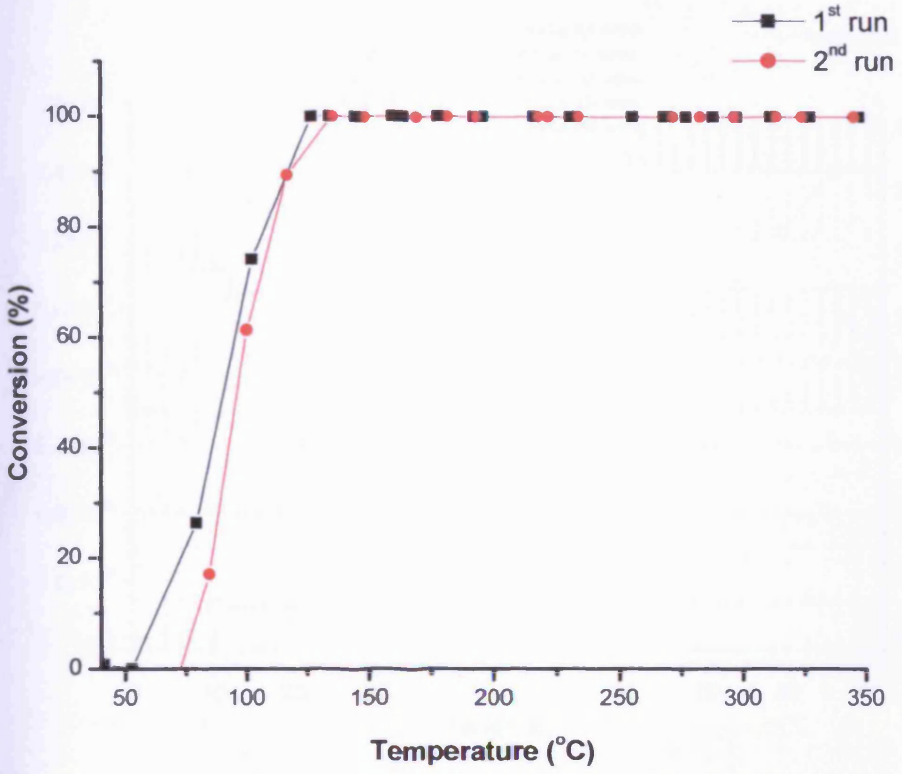

Figure 4-4: Comparison of conversion data for methanol oxidation over a 1wt% Au/TiO_2 catalyst dried at 120°C in air then heated at 120°C in 10%O_2/He flow for (first and Second run)

The catalyst dried at 120°C (first run) clearly has high activity for methanol oxidation in the presence of oxygen flowing in the stream. In order to understand the role of surface oxygen, the catalyst was subjected to various pre-treatment conditions. A freshly prepared 1wt% Au/TiO_2 catalyst dried at 120°C in air was loaded in a reactor and heated at 400°C in a 10%O_2/He flow at a rate of 30ml per minutes. The reaction was subjected to first and second run experiments and the following data were obtained figure (4-5).100% conversion of methanol occurred at about 126°C with type I CO_2 selectivity being observed at temperature (~100°C). The type I selectivity continues until type II CO_2 production begins and continue also in a steady state until the temperature reached about 320°C at which the dehydrogenation begins leading to CO production at that temperature. However, as de-oxygenation begins little methane was observed to be evolved at about 340°C and the methane selectivity was less than 10% as shown in figure (4-6).

When the catalyst was cooled after the first experiment and second run was carried out, the data were obtained shown in figure (4-7).

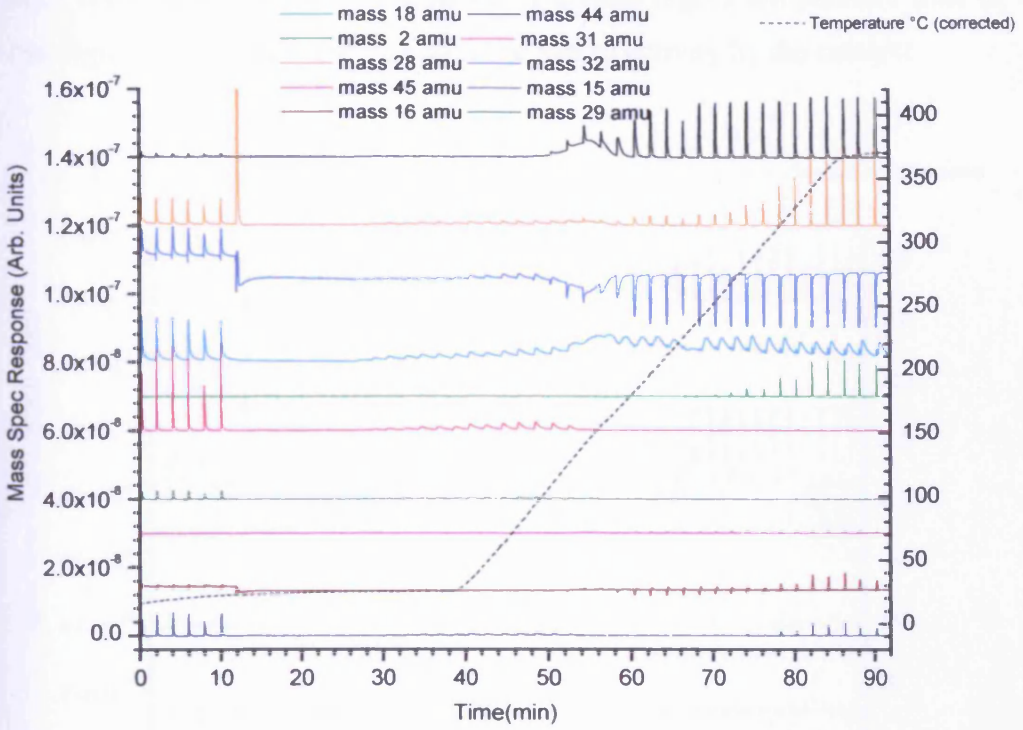

Figure 4-5: Temperature Programmed Pulse Flow Reaction of methanol oxidation over a 1wt% Au/TiO_2 catalyst dried a t 120 °C in air (un calcined) and heated in 10% O_2/He in a reactor at 400 °C (1^{st} run)

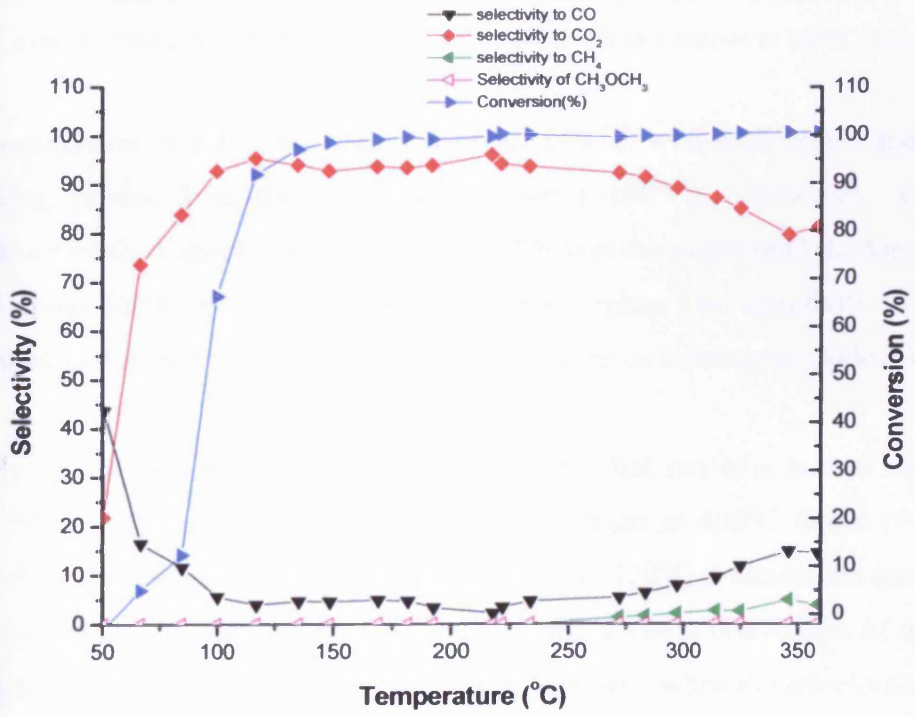

Figure 4-6: Selectivity and conversion for methanol oxidation over a 1wt% Au/TiO_2 catalyst dried at 120°C and heated in 10% O_2 /him in a reactor at 400 °C (First run)

Similarly, the second run figure (4-7) was obtained, and the figure shows that methanol conversion (100%) was attained at a little higher temperature than in the first run, figure (4-6) which also indicates the lost of activity by the catalyst.

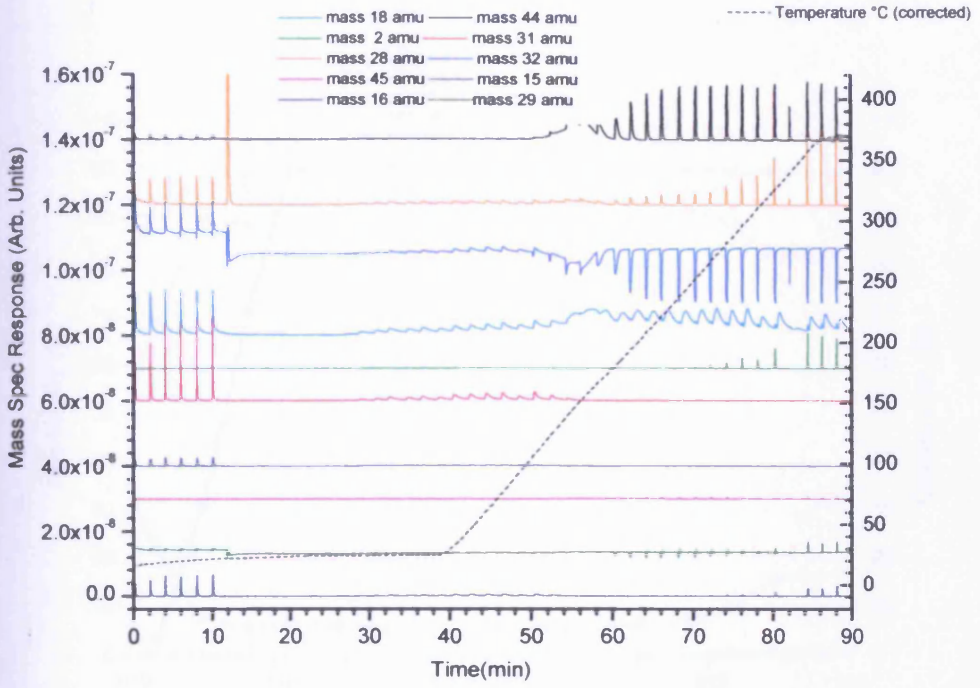

Figure 4-7: Temperature Programmed Pulse Flow Reaction of methanol oxidation over a 1wt% Au/TiO_2 catalyst dried at 120 °C in air and heated in 10%O_2/He in a reactor at 400 °C (Second run)

100% conversion of methanol begins at about 140 °C with both type I and type II CO_2 being produced at the same temperature (~100°C). However, when the temperature reached about 150°C, the type II CO_2 was dominant until the temperature reached about 300°C in which the deoxygenation begins. The selectivity to Type II CO_2 begins to decrease and methane selectivity begins to increase as evident in figure (4-6).

Similarly, if the two sets of data were compared, (first run of a heated catalyst at 120°C (figure 4-2) and the first run of heated catalyst at 400°C figure (4-5). The figures show that the activity of the catalyst heated at 120°C is almost the same as for the catalyst heated at 400°C because, in both cases, a 100% conversion of methanol was reached in the same temperature (~125°C). However, when the selectivities of the various products were analysed, it is indicates that almost all the products emerged at the same temperature. Thus, we conclude that if the catalyst is un-calcined, (heated at

120°C or 400°C) in a flow of 10%O_2/He, the same product distribution will be observed (figure 4-4 and 4-2). When the second run experiment was done, the activity of the catalyst is reduced with a 100% conversion of methanol being attained at somewhat higher temperature than in the first run of the experiment.

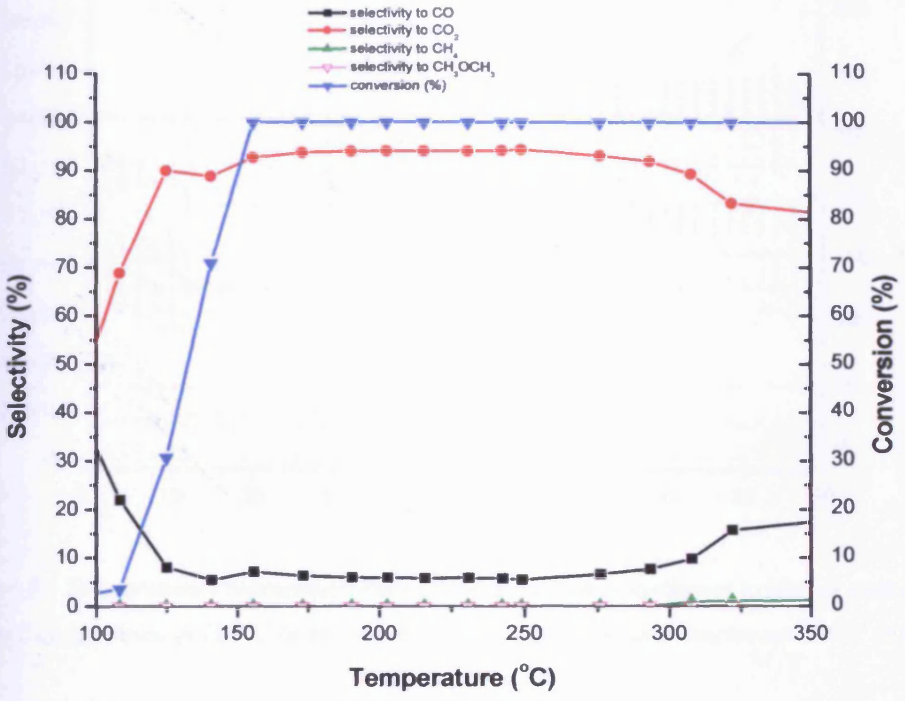

Figure 4-8: Selectivity and conversion for methanol oxidation over a 1wt% Au/TiO_2 catalyst dried at 120°C and heated in 10%O_2/He in a reactor at 400°C (Second run)

4.5.1.2 Calcined catalyst.

In order to understand the reactivity of methanol oxidation over Au/TiO_2, catalyst, a freshly prepared 1wt% Au/TiO_2 catalyst calcined at 400°C in air was loaded in a U tube of an oven of a reactor, heated at 120°C for 30 minutes in a 10%O_2/He flowing in a stream then cooled to room temperature.

The catalyst was then subjected to Temperature-Programmed Pulse Flow Reaction in which 5µl of methanol was allowed to pass over the by-pass and then switched over the catalyst with injection of 1µl of methanol at 2 minutes intervals.

In this reaction, about the same amount (7µl) of methanol was consumed before the surface of the catalyst became saturated. When the experiment was completed, figure (4-9) was obtained. It indicates that methanol became saturated on the surface at about

25 minutes (appearance of mass 31 and 29 amu signals) and became 100% converted to another product at about 45 minutes (disappearance of mass 31 and 29 amu).

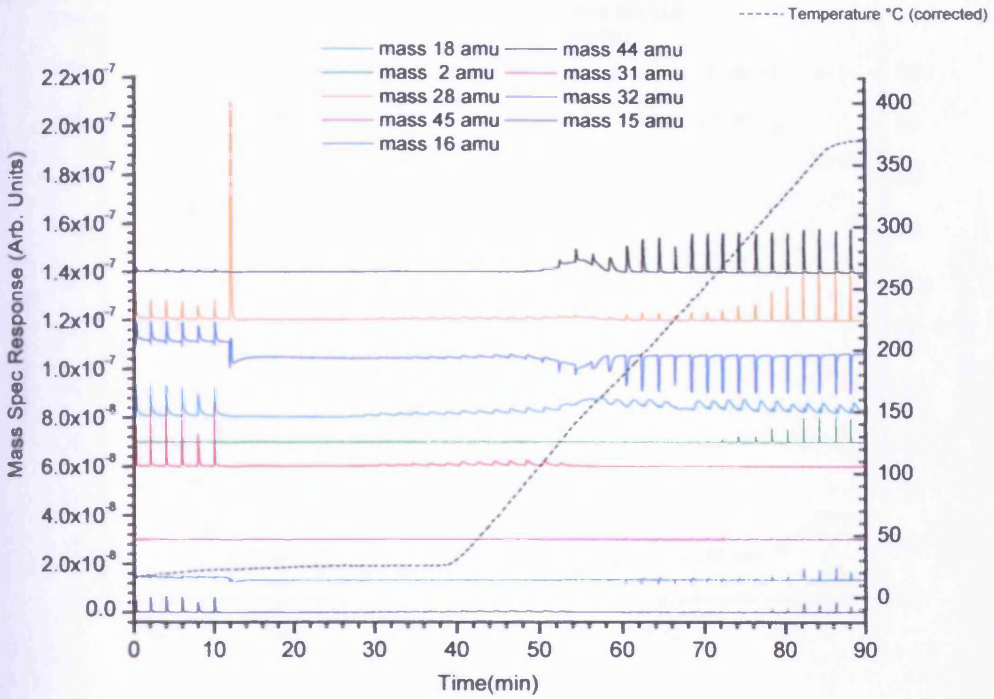

Figure 4-9: Temperature Programmed Pulse Flow Reaction of methanol oxidation over a 1wt% Au/TiO_2 Catalyst dried at 120 °C in air and heated in 10%O_2/He in a reactor at 400 °C (First run)

However, as the methanol conversion reached 100%, the slow formation of type I CO_2 begins at 40 minutes and continues until 50 minutes. Type II CO_2 then begins to emerge and continues until about 70 minutes from the beginning of the experiment, hydrogenation begins, and type II CO_2 then starts to decline due to the de-oxygenation of methanol on the catalyst at a temperature of about 300°C; CO and methane are dominant from that temperature.

When the data in figure (4-9) were integrated and analysed, we obtained the data shown in figure (4-10). The data show that 100% methanol conversion was reached at about ~118°C with CO_2 (type I) being produced when the methanol conversion was only ~50%. CO_2 produced, continues until the temperature reaches almost 91°C. The selectivity to type II CO_2 was then about 90% being produced at a fast rate and continues until ~300°C where the selectivity drops, the reaction is selective to CO due to dehydrogenation and as the temperature reached 320°C more methane production begins and continues in a steady state due to de-oxygenation of methanol at high temperature.

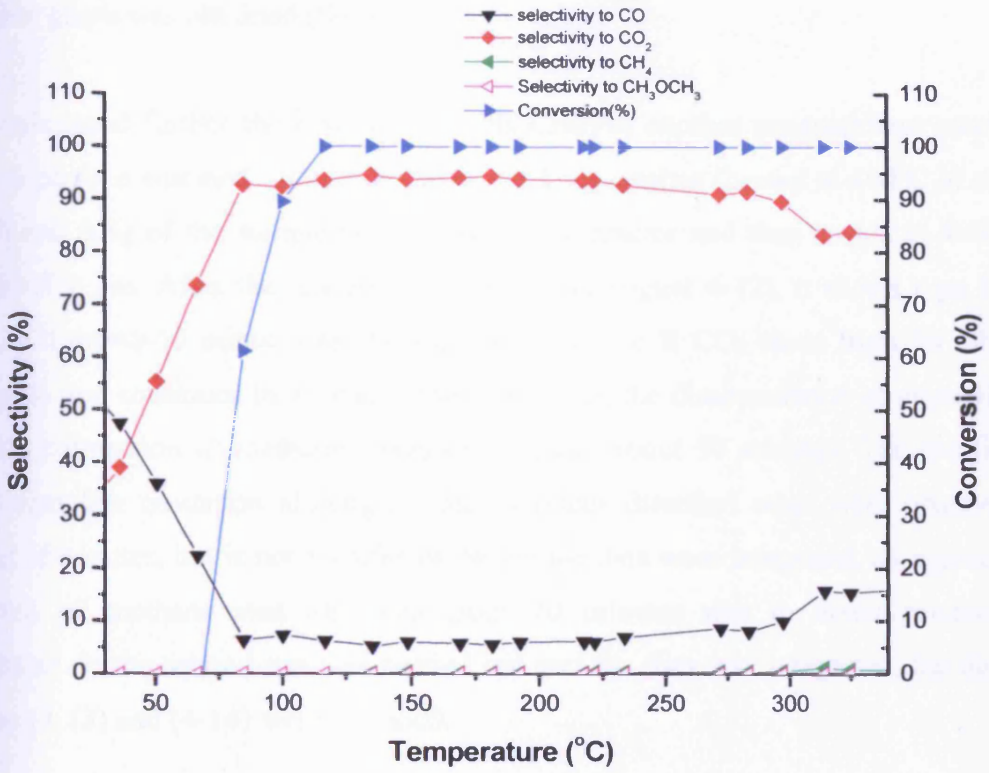

Figure 4-10: Selectivity and conversion for methanol oxidation over a 1wt% Au/TiO_2 catalyst calcined at 120°C and heated in 10%O_2/He in a reactor at 400°C (First run)

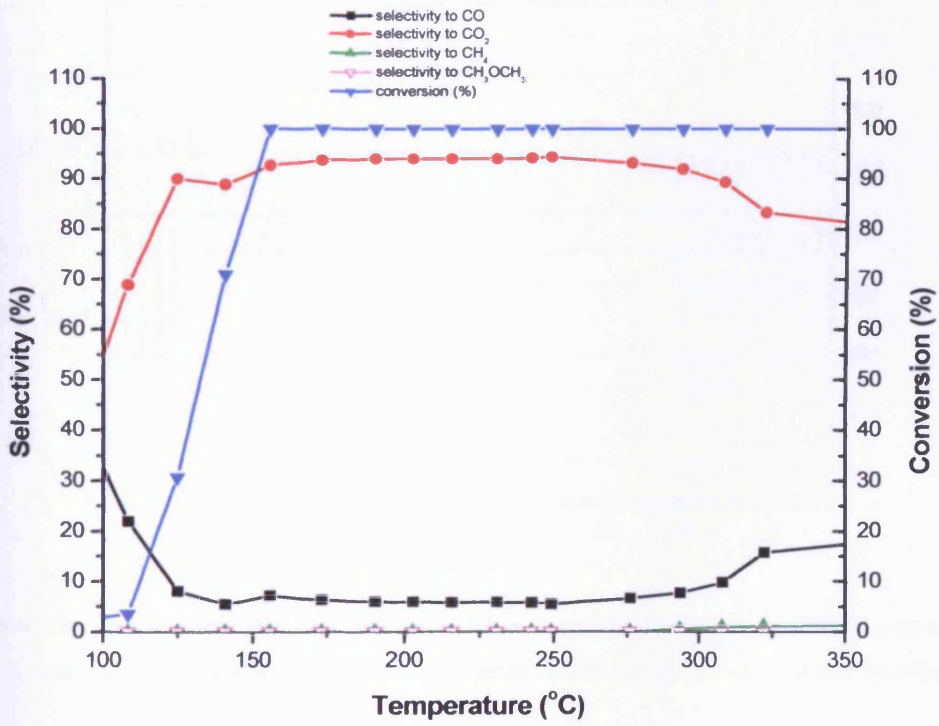

Figure 4-11: Selectivity and conversion for methanol oxidation over a 1wt% Au/TiO_2 catalyst Calcined at 120°C and heated in 10%O_2/He in a reactor at 400°C (Second run)

In the same manner, when the second run was carried out, and the data was integrated another graph was obtained (figure 4-11).

To understand further the reactivity of this catalyst, another pre-treatment condition was done on a calcined sample of 1wt% Au/TiO_2 catalyst (heated at 400°C in air for 2hrs) and 0.5g of the sample was loaded in the reactor and then heated at 400°C in 10%O_2/He gas. After the reaction with methanol (figure 4-12), it shows type I CO_2 begins from 40-50 minutes as shown, and then type II CO_2 starts from 50 minutes upwards and continues in a steady state. However, the disappearance of mass 31amu (100% conversion of methanol) was observed at about 50 minutes. The reaction is also complete oxidation although some of traces dimethyl ether were observed at about 55minutes, but is not significant. When the data were integrated, an appreciable amount of methane was observed from 70 minutes due to de-oxygenation of methanol. If the second run was carried out and the data was integrated, the data in, figure (4-13) and (4-14) were obtained.

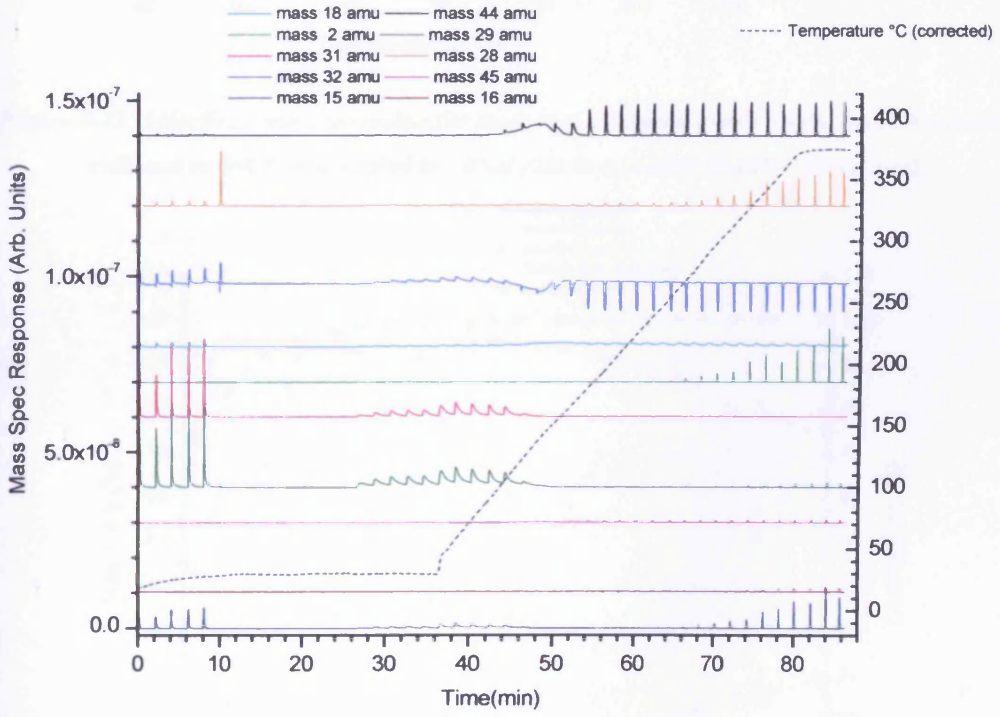

Figure 4-12: Temperature Programmed Pulse Flow Reaction of methanol oxidation over a 1wt% Au/TiO_2 Catalyst dried a t 400 °C in air and heated in 10%O_2/He in a reactor at 400 °C (First run)

From the figures (4-13), indicate that as the conversion of methanol reached 50%, the production of type I CO_2 had already begun and when it reached 100%, type II CO_2

was already in a stable state with selectivity being ~90%. The high selectivity of CO_2 type II continue in a steady state until the temperature reached 300°C. Type II CO_2 selectivity then drops to about 70% due to de-hydrogenation; however, the selectivity of methane was observed to increase, although with little selectivity being <5% as evidenced in figure (4-13) below.

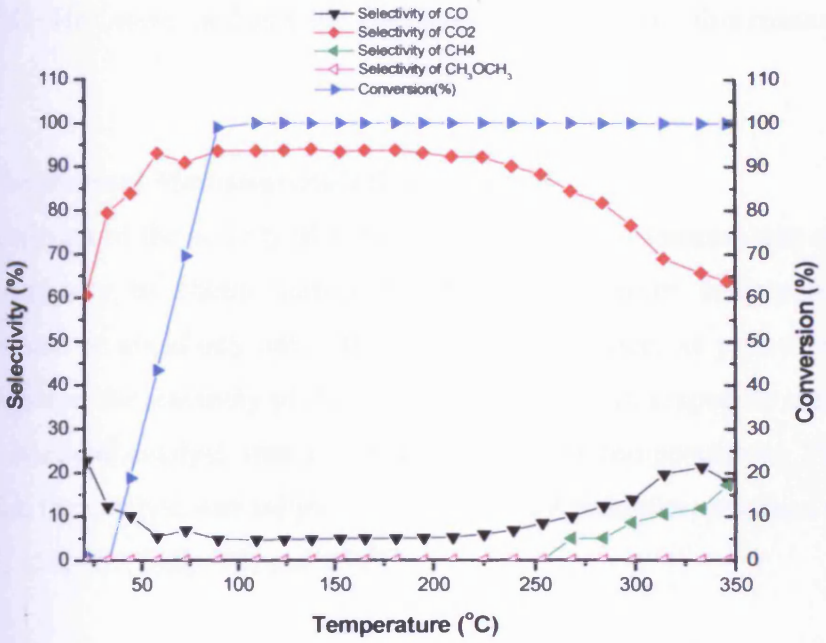

Figure 4-13: Selectivity and conversion for methanol oxidation over a 1wt% Au/TiO_2 catalyst calcined at 400°C and heated in 10%O_2/He in a reactor at 400°C (First run)

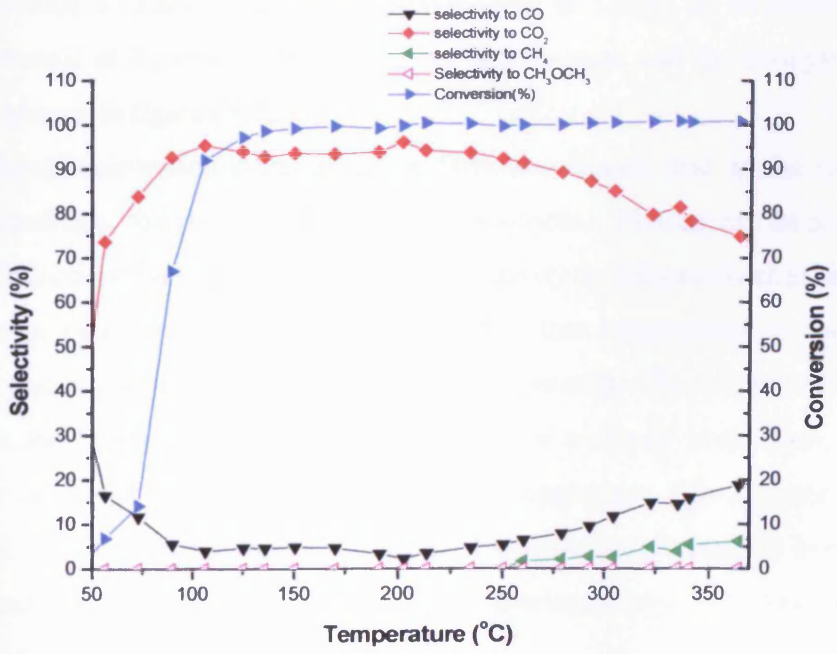

Figure 4-14: Selectivity and conversion for methanol oxidation over a 1wt% Au/TiO_2 catalyst calcined at 400°C and heated in 10%O_2/He in a reactor at 400°C (Second run)

Based on the data gathered so far, it is evident that if the catalyst is calcined in air and heated in a flow of 10%O_2/He in situ in the reactor for 30 minutes before carrying out Temperature Pulse Flow Programmed reaction, the catalyst shows good activity with respect to methanol oxidation over a 1wt% Au/TiO_2 catalyst. Hence, the most active catalyst (calcined in air at 400°C and heated in situ in the reactor in a flow of 10%O_2/He), were used as a standard catalyst through out this research.

4.6 Isothermal Methanol oxidation Reaction

Knowledge of the activity of the catalyst at different temperature makes it possible in the industry to obtain various products at different temperature. This helps to eliminate or avoid any unwanted products and hence, as part of the investigation to understand the reactivity of the Au/TiO_2 catalyst with respect to methanol oxidation, the standard catalyst was subjected to various temperatures, The temperatures to which the catalyst was subjected and methanol oxidation reaction was carried out are 100, 150, 200, 250, 300, and 350°C:

4.6.1 Isothermal methanol oxidation profile at 100°C

When the standard catalyst Au/TiO_2 was subjected at 100°C to methanol injections (1µl of methanol at 2 minutes intervals) over the by-pass and the catalyst, the result obtained is shown in figure (4-15).

Initial methanol conversion starts at about 60% conversion and as the injections of methanol continues, the conversion increases to almost ~70% as can be seen from 55 minutes of injection time. Nevertheless, the selectivity to CO_2 starts at about 73% and continues at a steady level. The CO_2 produced at this temperature is dominated by type I CO_2 that is produced at moderately low temperature. The selectivity to CO was very low at the beginning (~20%) and continues in a steady state. This has clearly indicated a complete oxidation reaction at this temperature. The methane selectivity observed at this temperature was minimal as it is only approximately less than 10% and continues in that state through out the experiment and no dimethyl ether is observed at this stage of the experiment.

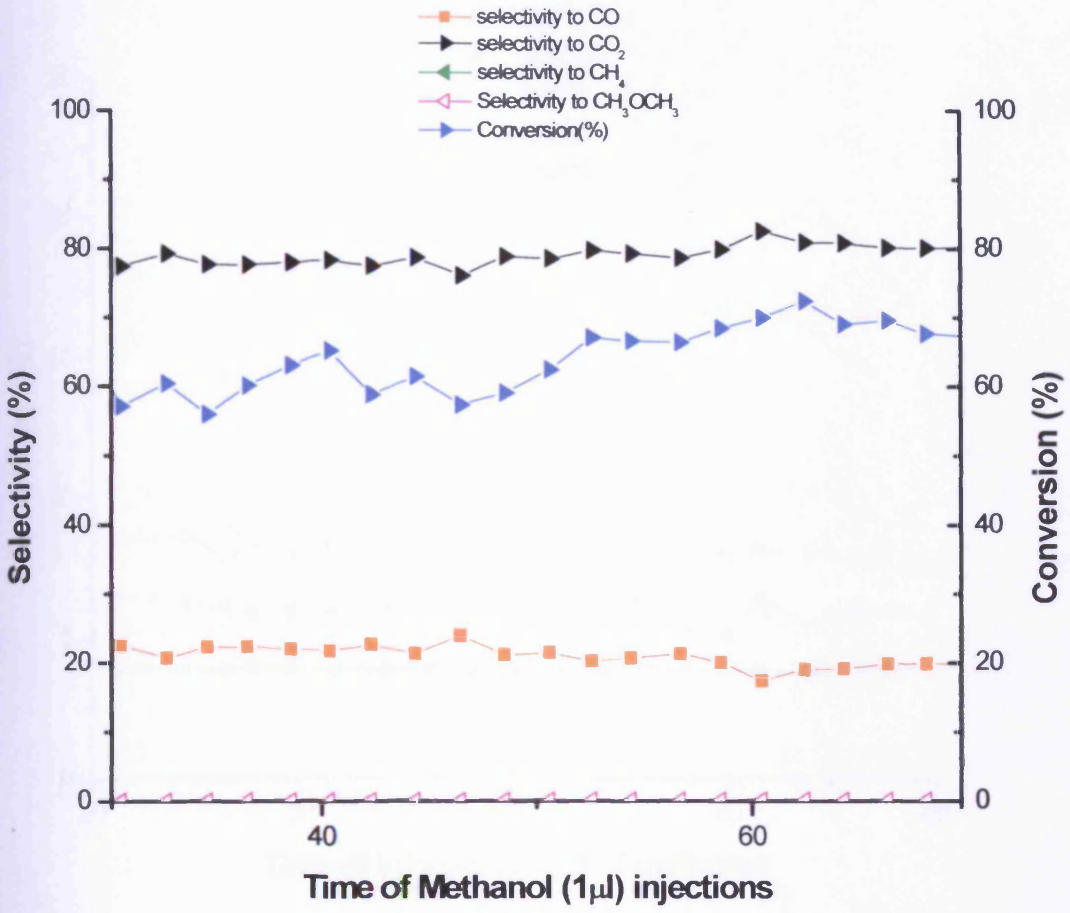

Figure 4-15 Isothermal methanol oxidation over a 1wt% Au/TiO_2 catalyst at 100°C

4.6.2 Isothermal methanol oxidation profile at 150 to 350°C

The isothermal profile data for methanol oxidation at 150°C shows that the conversion of methanol was 100% at this temperature and continues through out the course of isothermal experiments. Hence, the data presented from figure (4-16) to (4-19) show no conversion data for methanol.

When the CO selectivity data for all the isothermal experiments from 150- 350°C were gathered, figure (4-16) was obtained. The selectivity to CO at 150°C was very low compared to that for 200 to 350°C. At this temperature the CO selectivity is less than 5% but even when the temperature was raised to 300°C, low CO selectivity was observed from 200-250°C and as soon as the temperature was raised to 300°C, the CO selectivity begins to increase due to dehydrogenation of methanol at this temperature.

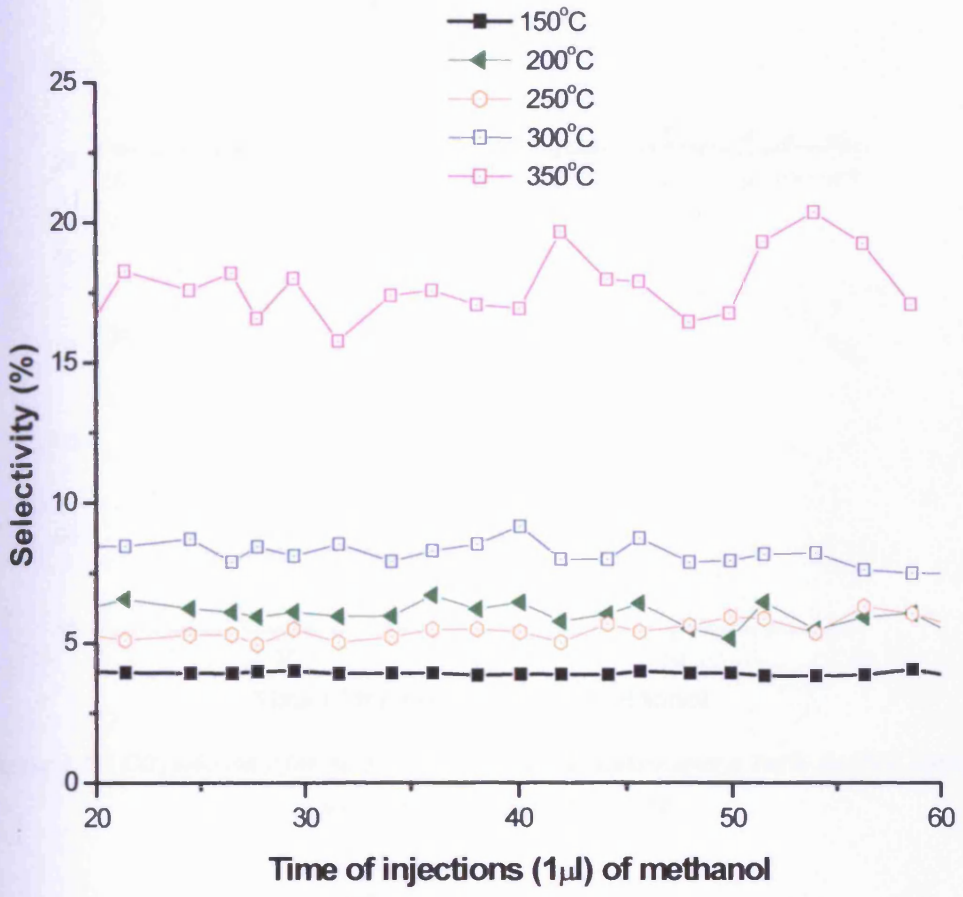

Figure 4-16: CO selectivity for isothermal methanol oxidation over a 1wt% Au/TiO_2 catalyst at temperatures from 150 to 350°C

The activity of the catalyst drops a little towards CO production and as the temperature reached 350°C, more dehydrogenation was observed and an increased selectivity towards CO. The CO selectivity at this temperature (350°C) was around 17%.

When the CO_2 selectivity data were collated for methanol isothermal oxidation reaction at a temperature from 150-350°C figure (4-17) was obtained. It shows high selectivity to CO_2 (~92%) from temperatures ranging from 150 to 250°C. As the temperature was raised from 300-350°C, the CO_2 selectivity decreases due to dehydrogenation of methanol to CO. The selectivity to CO_2 at 300 and 350°C was around 88 and 73% respectively.

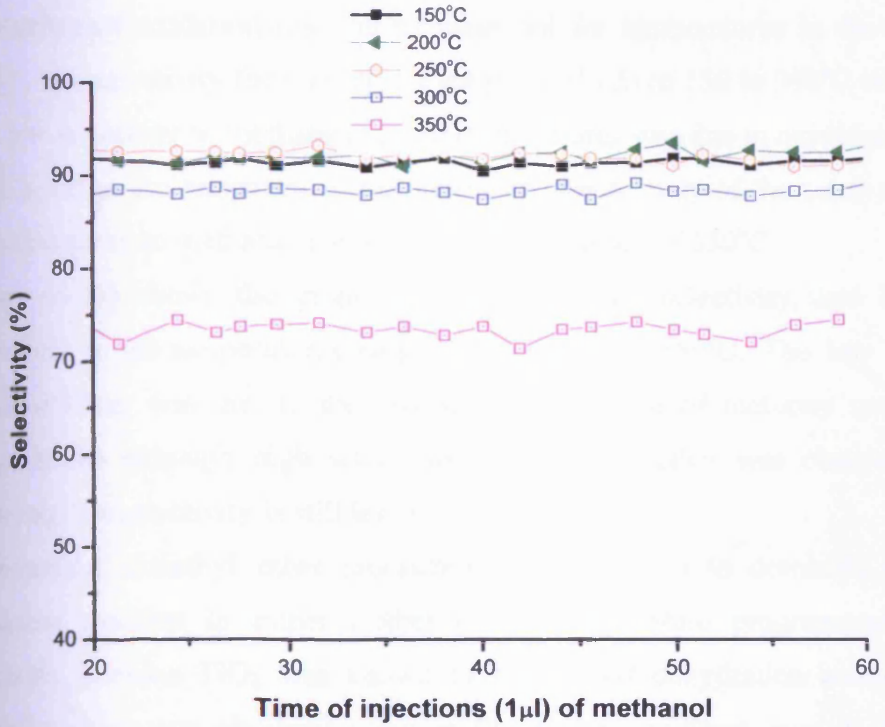

Figure 4-17: CO_2 selectivity for isothermal methanol oxidation over a 1wt% Au/TiO_2 catalyst at temperatures from 150 to 350°C

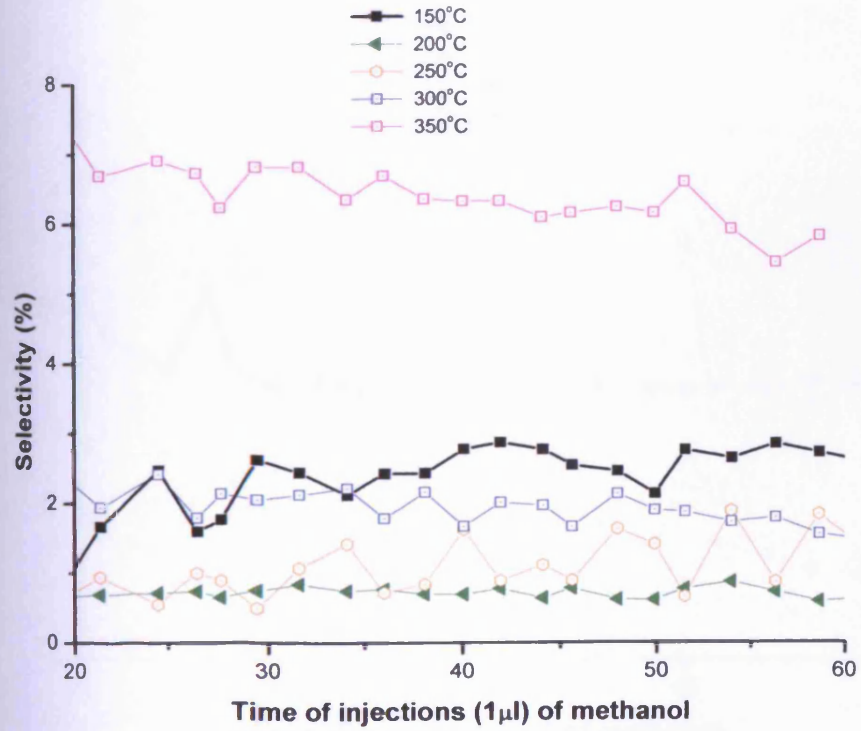

Figure 4-18: Methane selectivity for isothermal methanol oxidation over a 1wt% Au/TiO_2 catalyst at temperatures from 150 to 350°C

Similarly, figure (4-18) shows the variation of selectivity for methane production from the isothermal oxidation reaction of methanol for temperatures in the range 150 to 300°C. The selectivity for methane at temperatures from 150 to 300°C was below 5%. The low selectivity to methane at these temperatures was due to oxidation of methanol to CO_2 and as the temperature was increased, the activity of the catalyst was toward high selectivity to methane as evident at a temperature of 350°C

Figure (4-19) shows the graph for dimethyl ether selectivity, and indicates low selectivity at all temperatures ranging from 150 to 350°C. The low selectivity to dimethyl ether was due to the low surface coverage of methoxy species at these temperatures although high selectivity of dimethyl ether was observed at 350°C. However, the selectivity is still less than 10%.

In principle, dimethyl ether production was supposed to dominate the methanol oxidation reaction in either isothermal or temperature programmed pulse flow reactions, because TiO_2 was known to be a good dehydration catalyst, in which dimethyl ether was obtained when methanol was oxidised over it. However, the presence of the gold supported by TiO_2 blocked the formation of dimethyl ether and more CO_2 was evolved due to formation of formate on the surface of the catalyst

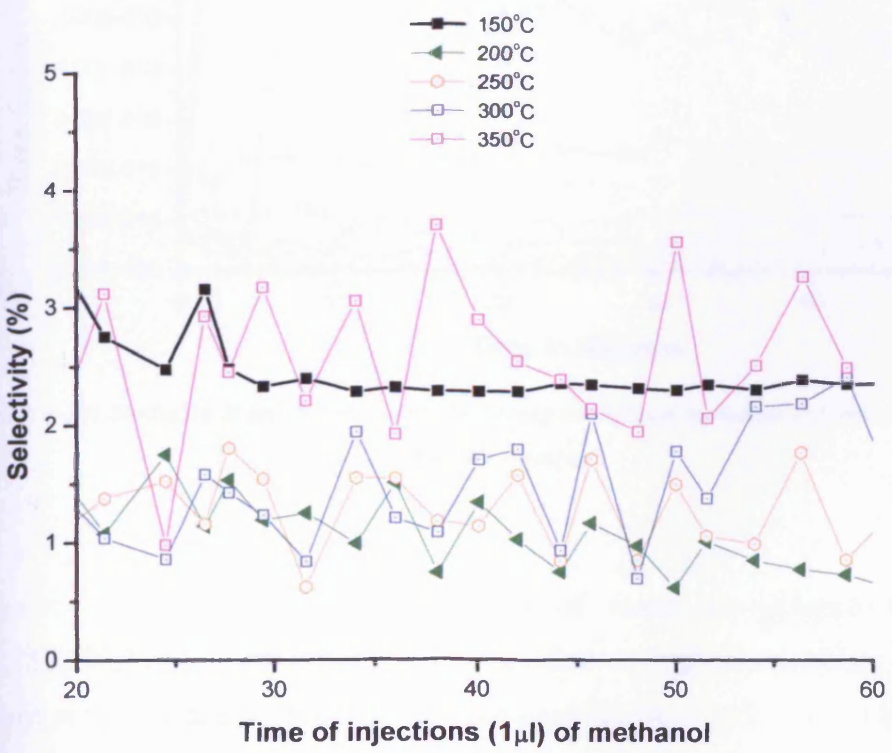

Figure 4-19: Dimethyl ether selectivity for isothermal methanol oxidation over a 1wt% Au/TiO_2 catalyst at temperatures from 150 to 350°C

4.6.3 Water and hydrogen evolution

During the course of methanol oxidation under isothermal condition over a supported gold on a single oxide titania, it was observed that the reaction is accompanied by water and hydrogen evolution as shown in figure (4-20). At a temperature of 100°C, low hydrogen production was observed and when the temperature was increased, high hydrogen production was observed especially in the temperature range 300 -350°C. This may be due to the dehydrogenation and deoxygenation of methanol, which begins at 300°C and 350°C respectively.

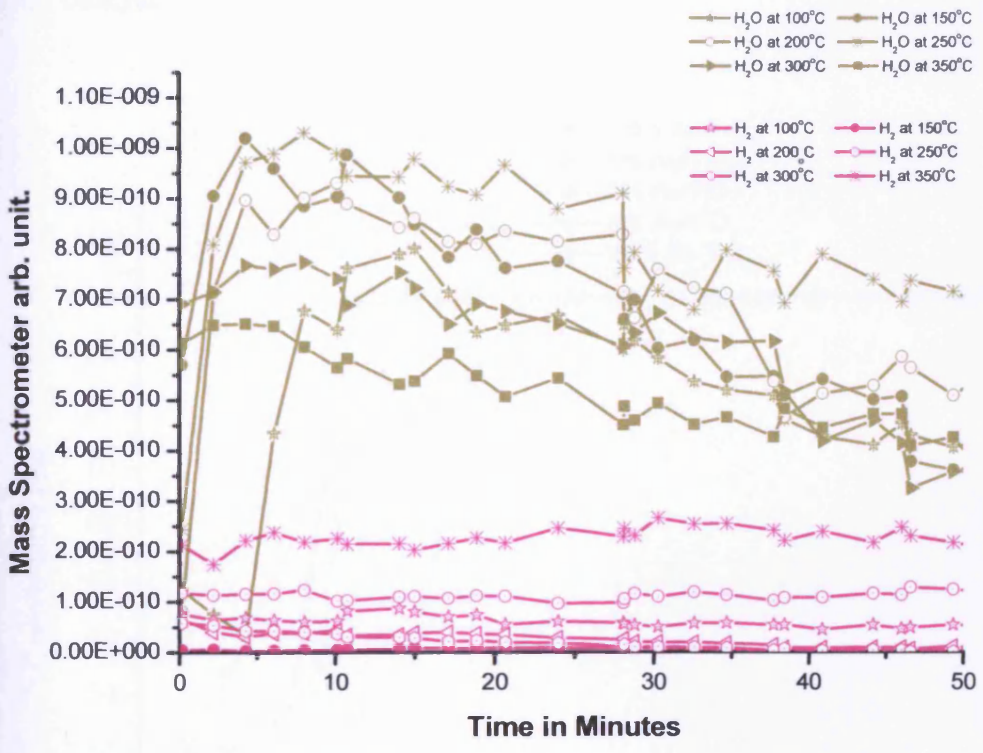

Figure 4-20: Evolution of water and hydrogen during isothermal methanol oxidation over a 1wt% Au/TiO_2 catalyst

Figure (4-20) also shows the evolution of water at different temperatures (100,150,200,250,300,350°C), and indicates that at high temperature, more water evolved at the beginning of the reaction but later decreases as is evident in the case of water evolved at 350°C and 100°C.

4.7 Variation of preparation parameters

4.7.1 Effect of weight loadings

Gold catalyst has been known to be in active. When dispersed in a large quantity over a supported metal oxide such as TiO_2, its activity tends to be reduced remarkably (i.e. as the particle size of gold increases on the support, the activity tends to be very low because of the chances of agglomeration of gold particles on the support and makes the catalyst to coagulate.

The effect of gold loading was investigated for methanol oxidation over the Au/TiO_2 catalyst and the results show very remarkable effect. The figure (4-21) indicates the conversion of methanol oxidation over different weight loadings of gold supported on the TiO_2 catalyst.

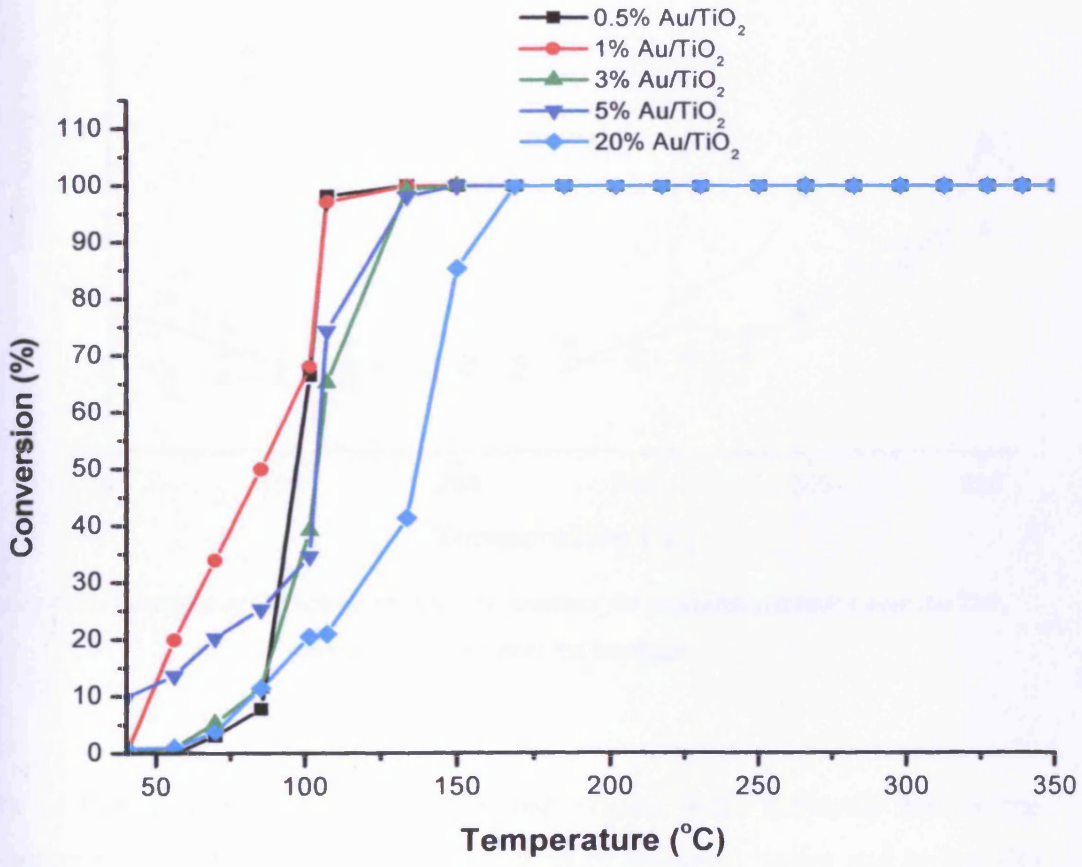

Figure 4-21: Methanol oxidation conversion over different weight loadings of a TiO_2 supported Au catalyst

The result indicates that as the weight loading of gold increases, 100% conversion of methanol was attained at higher temperature compared to the lower loadings of gold

in which 100% was attained at very low temperature, and this is evident in the gold loading of 0.5% and 1% for which 100% conversion of methanol was attained below 100°C. The low temperature methanol conversion was due to the smaller quantity of gold highly dispersed on the TiO_2 support, which was in very minute quantity. The lower the loading of gold over TiO_2 the more its activity as evident in figure (4-21) in which 100% conversion of methanol was reached as the loading of gold is low and decreases in the order 0.5>1>3>5>20%

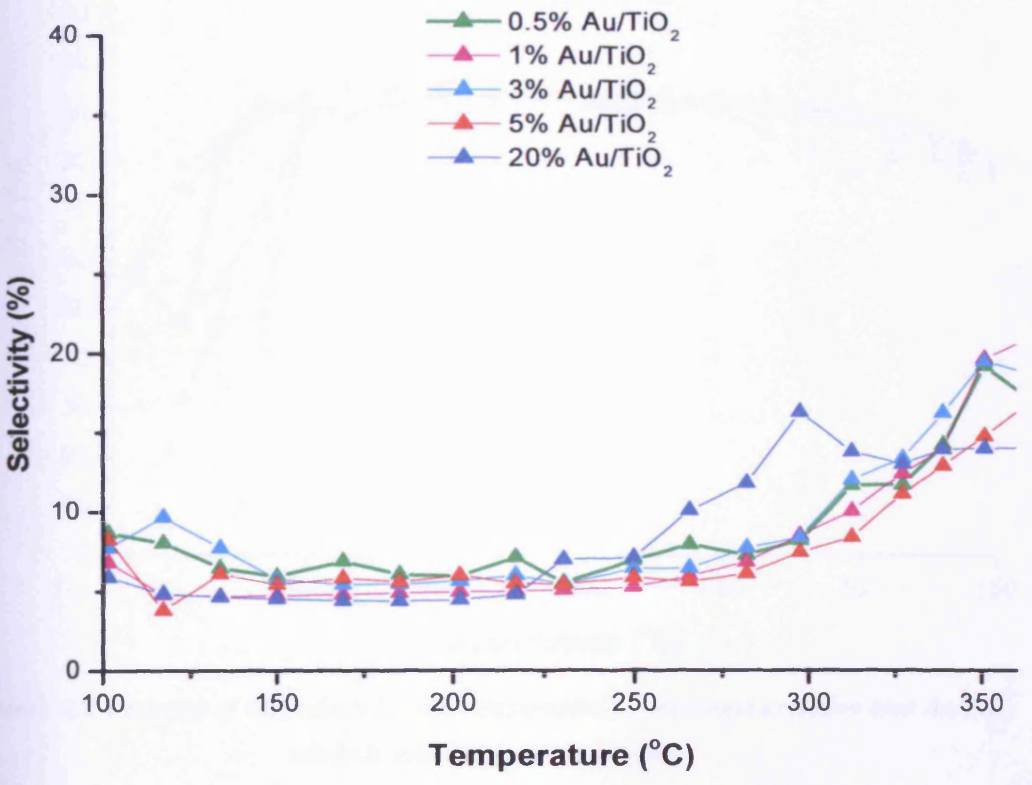

Figure 4-22: Variation of CO selectivity with temperature for methanol oxidation over Au/TiO_2 catalysts with different Au loadings

A plot of CO selectivity against temperature, (figure 4-22) indicates that as the temperature reached 250°C, the dehydrogenation of methanol begins and higher CO selectivity was observed. When the temperature was increased, the CO selectivity continued to increase. At this temperature, it is believed that the gold does not take part in the reaction and TiO_2 mainly dominates the reaction involved at this temperature, as evident when TiO_2 alone was used as a catalyst as subsequently is shown in this chapter.

As the gold loadings increase, as shown in figure (4-22), the behaviour of the catalyst changed to like TiO_2 alone. For example, 20wt% Au/ TiO_2 catalyst, high CO selectivity was observed but decreased as the temperature reached 300°C and no appreciable difference was observed for catalysts loaded from 0.5wt% to 5wt% gold.

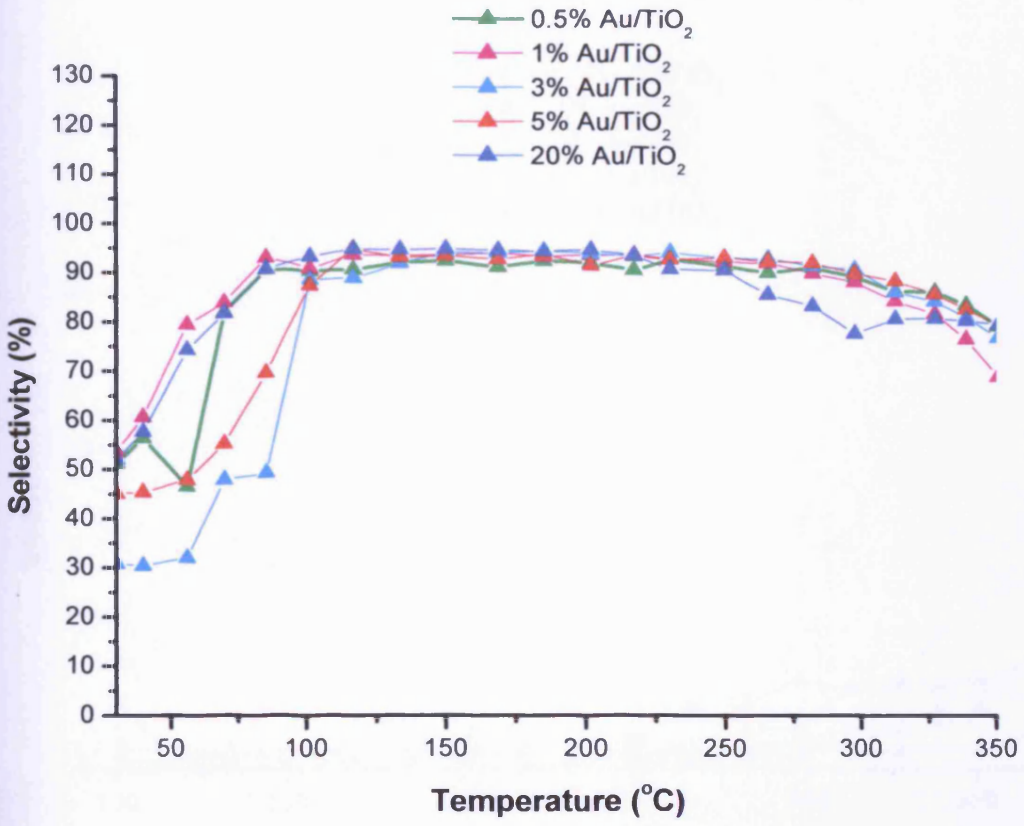

Figure 4-23: Variation of CO_2 selectivity with temperature for methanol oxidation over Au/TiO_2 catalysts with different Au loadings

Similarly, when the selectivity to CO_2 was plotted against temperature of oxidation of methanol, figure (4-23) was obtained. The figure indicates that type I CO_2 production starts at a very low temperature for all the loadings. However, when the temperature was raised to 100°C type II CO_2 evolution begins, continues in a steady state at all the loadings, and drops rapidly as the temperature reaches 250°C as in the case of 20wt% Au/TiO_2 catalyst due to dehydrogenation of methanol, as discussed earlier. However, for the rest of loadings no appreciable difference was observed as type II CO_2 production decreases at approximately 300°C to produce CO and hydrogen.

Methane selectivity increases with the increase in the weight loading of Au (figure 4-24). It was observed however, that 1wt% Au/TiO_2 tends to be more selective to methane as can be observed in the same figure.

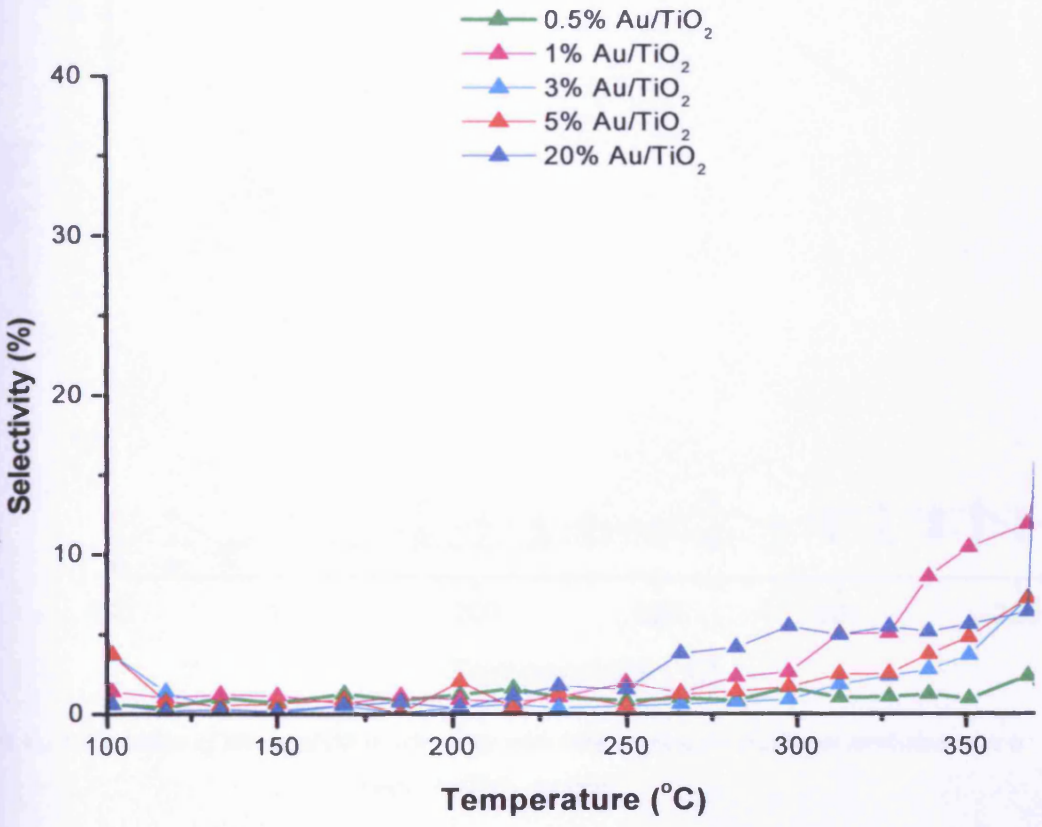

Figure 4-24: Variation of CH_4 selectivity with temperature for methanol oxidation over Au/TiO_2 catalysts with different Au weight loadings

The high selectivity of 1wt% Au/TiO_2 could be due to a high dispersion of gold on the support. The catalyst being prepared by deposition precipitation, it may be noted that not all the gold will be on the surface of the support as some appreciable amount may be removed by washing and hence, disperse itself on the surface accordingly and suitable to convert methanol at very low temperature

Figure (4-25) indicates low selectivity to dimethyl ether at all temperatures and for all the gold loadings.

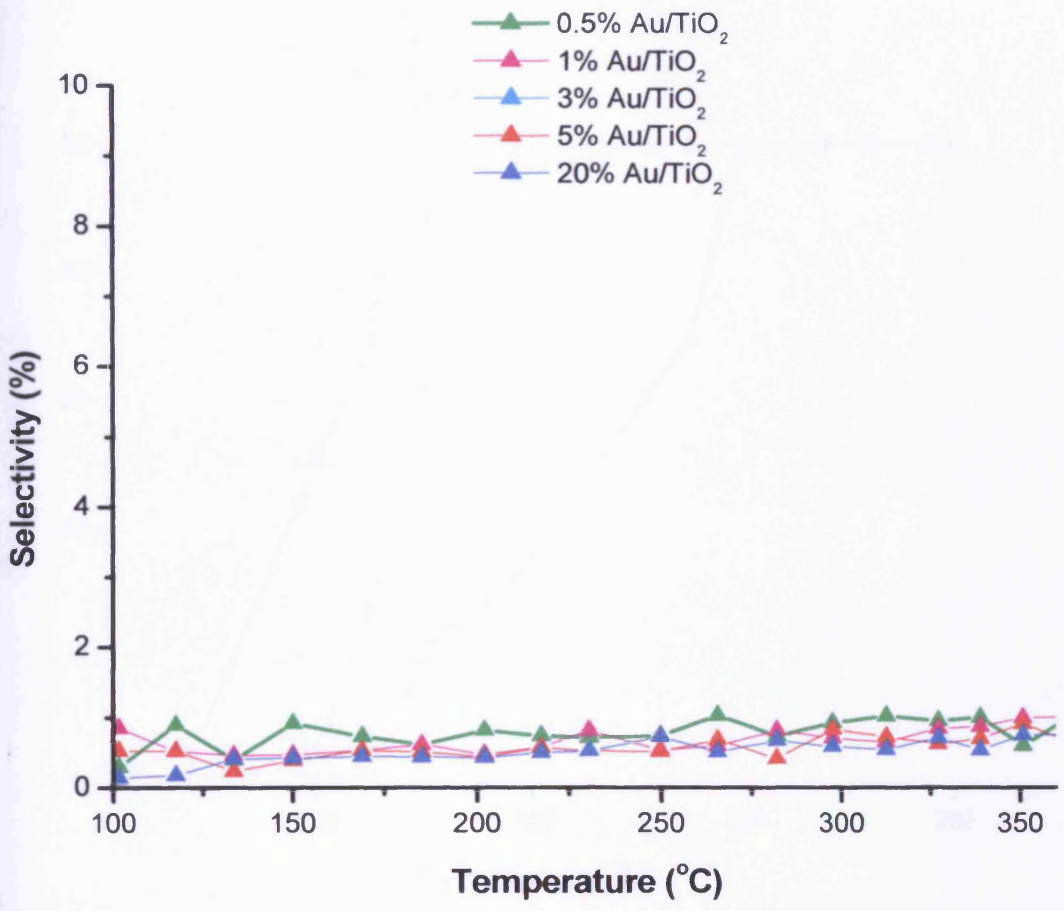

Figure 4-25: Variation of dimethyl ether selectivity with temperature for methanol oxidation over a 1wt% Au/TiO_2 catalyst

4.7.2 Effect of pH

pH is another important factor for determining catalyst activity, and must be considered during the catalyst preparation.

The role of pH in catalyst preparation of Au/TiO_2 using deposition precipitation is very crucial, the higher the pH of the solution of the preparation, the more the activity of the catalyst will be as it makes the precipitation of chloride more and can be washed away by filtration. The effect of using different pH for the preparation was investigated and the results show as follows:

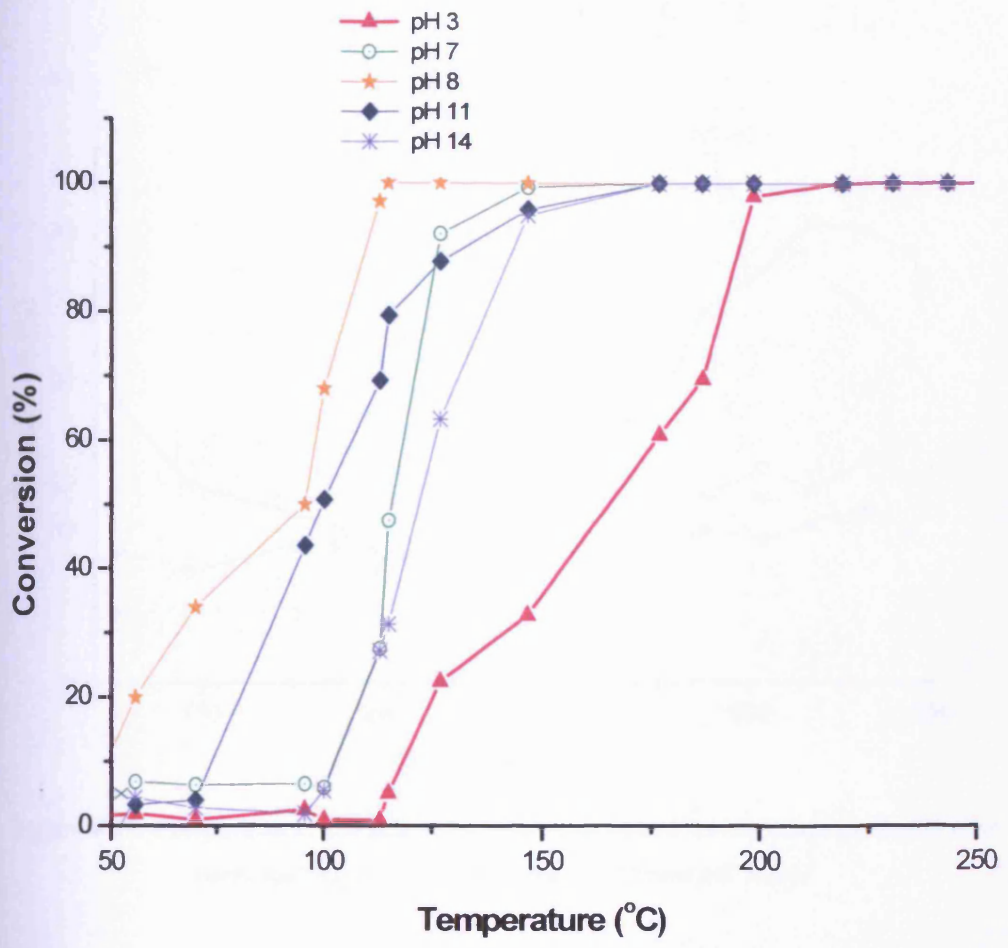

Figure 4-26: Comparison of methanol conversion with temperature over a 1wt% Au/TiO_2 catalyst prepared at different pH values

Figure (4-26) indicates the conversions of methanol of different pH values. It shows that 100% of methanol conversion was reached first by pH 8 (standard catalyst) at very low temperature. The catalyst prepared by pH 7 was the next to reach 100% conversion of methanol, followed by 11 and 14. Similarly, as the temperature increased to 200°C, 100% conversion of methanol was observed for the catalyst prepared at pH 3.These imply that at a moderately pH value like 8, the performance of the catalyst was more and when it is neutral pH 7, its performances was good but at relatively high temperature than the standard catalyst. However, at pH 11 and 14 in which the basicity was high, the activity was good at low temperature but 100% conversion was reached at relatively high temperature compared to seven. Nevertheless, at very low pH 3, the performance of the catalyst was very poor as there

was more chloride ion, which increases the sintering of gold in the catalyst, and hence the conversion was observed to be at higher temperature.

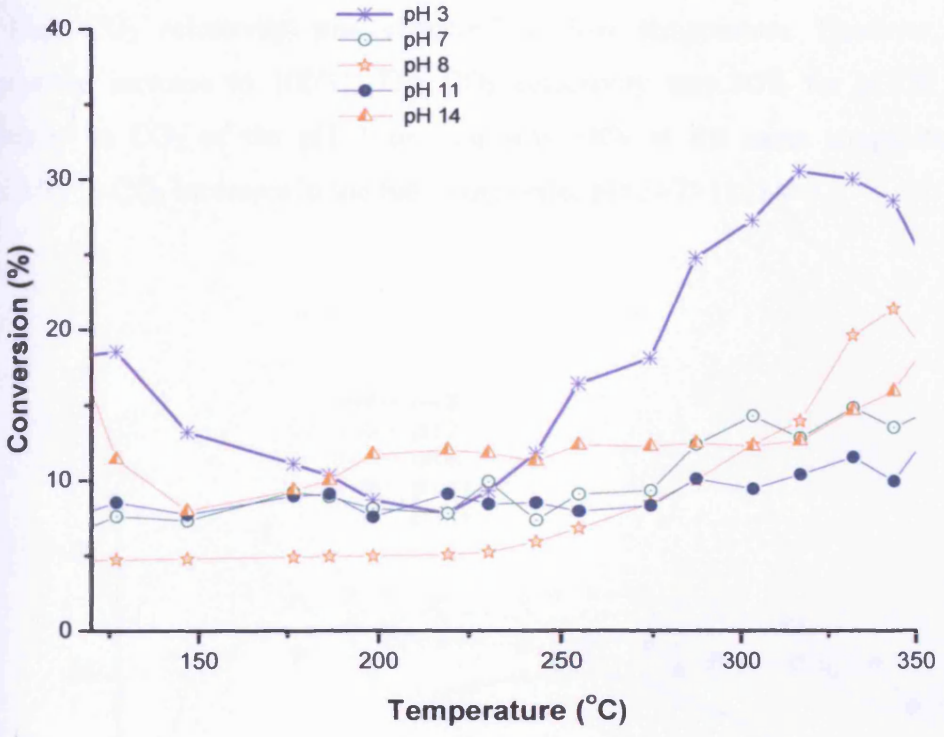

Figure 4-27: Comparison of CO selectivity with temperature for methanol oxidation over 1wt% Au/TiO_2 catalysts prepared at different pH values

Figure (4-27) shows selectivity to CO of catalysts prepared by DP at different *pH* values. It indicates that low selectivity to CO was observed at high pH (11 and 14), while at low pH (3) high selectivity to CO was observed, with selectivity being 30% .However, at a moderately high temperature (pH 8), more CO was observed but with relatively low CO selectivity than pH 3. The selectivity to CO of the moderately high pH (8) catalyst was 18%. The high CO selectivity observed at low pH was because of more chloride may be present and the catalyst behaves like TiO_2 alone. The selectivity to CO increases in the following order 3>8>11>7>14

The selectivity to CO_2 (figure 4-28) was observed to be high at low temperature, in the case of catalyst of pH 8, while at pH 3, low selectivity to CO_2 was observed at very high temperature. The presence of gold is responsible for the formation of CO_2 in the catalyst at low temperature. The result also indicates that, at low pH (3), more chlorides are in the catalyst, which enhances sintering of the gold in the catalyst, and

makes the catalyst less active at low temperature and hence low CO_2 was observed at low temperature. Nevertheless, for the catalyst with a moderate pH of 8, the chloride ions are presumably, precipitated and washed out and make the catalyst more active and high CO_2 selectivity was observed at low temperature. However, as the temperature increase to 100°C, The CO_2 selectivity was 90% for pH 8, but the selectivity to CO_2 of the pH 3 catalyst was 38% at the same temperature. The selectivity to CO_2 increases in the following order pH 8>7>11>14>3.

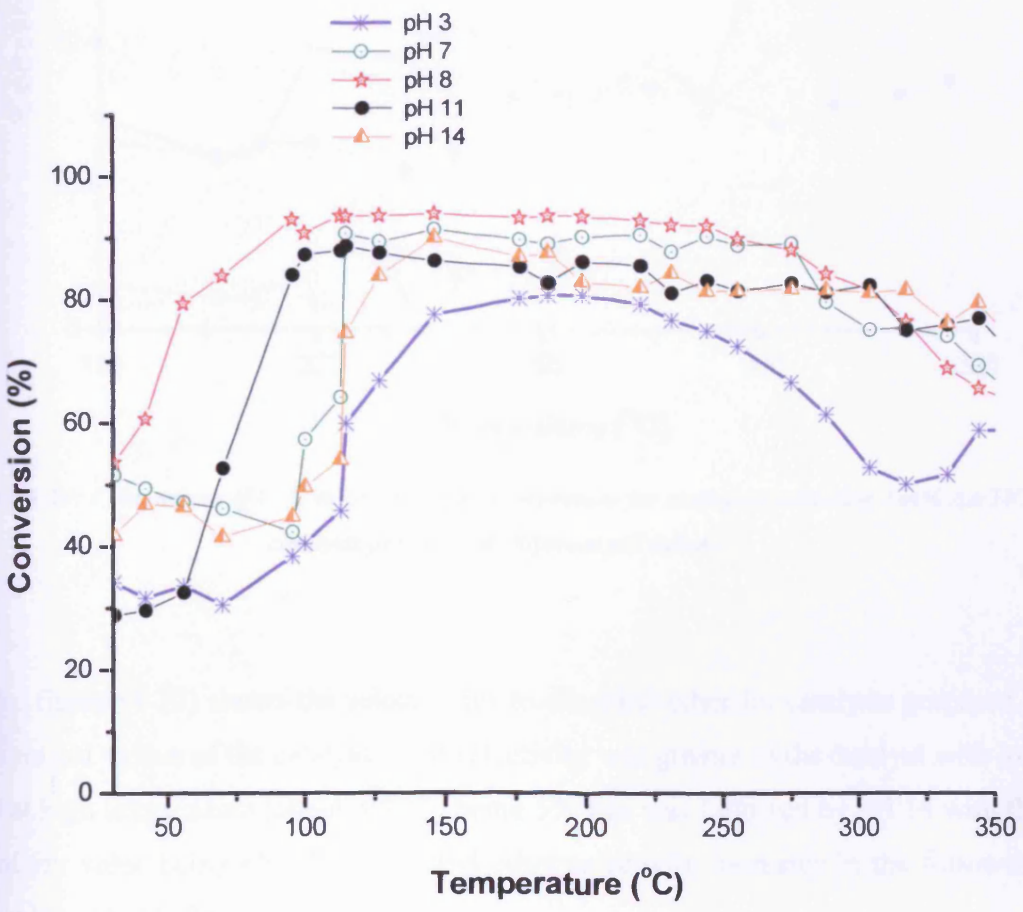

Figure 4-28: Comparison of CO_2 selectivity with temperature for methanol oxidation over 1wt% Au/TiO_2 catalysts prepared at different pH values

High methane selectivity of 20% was observed (figure 4-29) at low pH (3), followed by the catalyst with pH of 7 and 8, with selectivities being 18 and 15% respectively. The selectivity of methane increases in the following order of 3>7> 8>11>14.

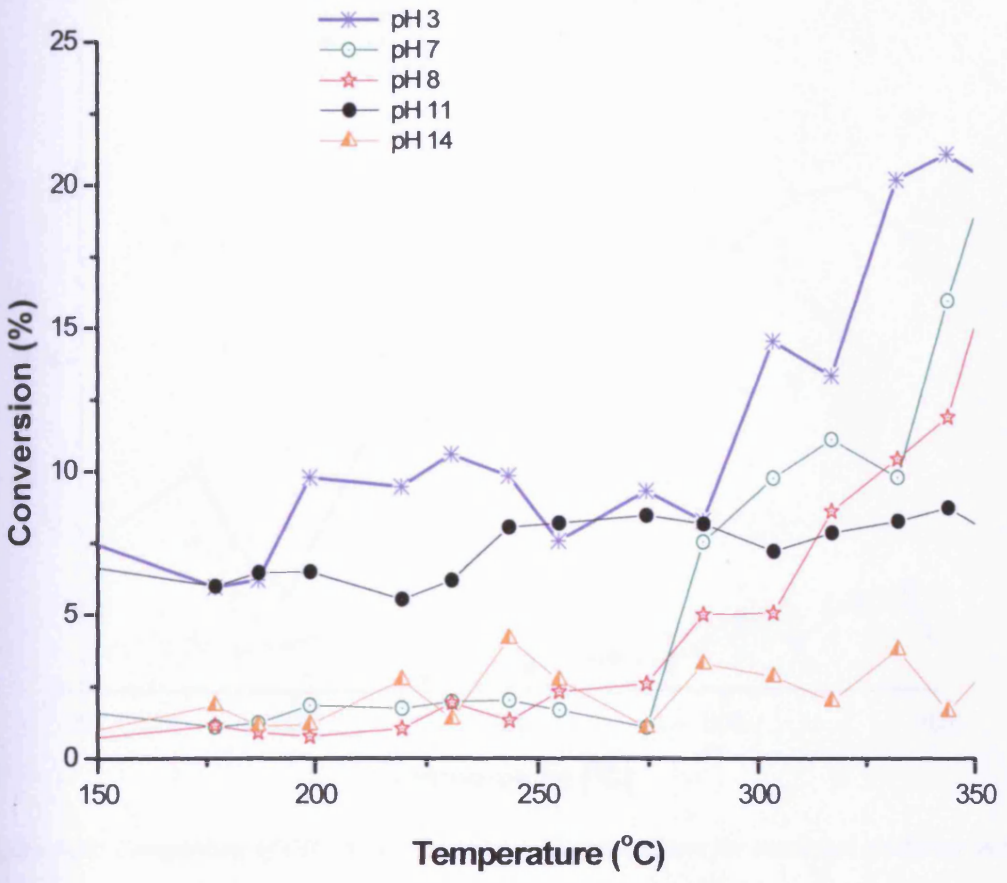

Figure 4-29: Comparison of CH_4 selectivity with temperature for methanol oxidation 1wt% Au/TiO_2 catalysts prepared at different pH values

Lastly, figure (4-30) shows the selectivities to dimethyl ether for catalysts prepared at different pH values of the catalyst. The selectivity was greater in the catalyst with low pH 3 at high temperature (about 300°C) being 5% this was followed by pH 14 with the selectivity value being 4%. The dimethyl ether selectivity increases in the following order pH3>14>11>8>7.

The order of dimethyl ether selectivity at different pH values implies that the lower the pH value, the more the deoxygenation of methanol occurs and at moderately high low and high less dimethyl ether was observed at evident in figure (4-30).

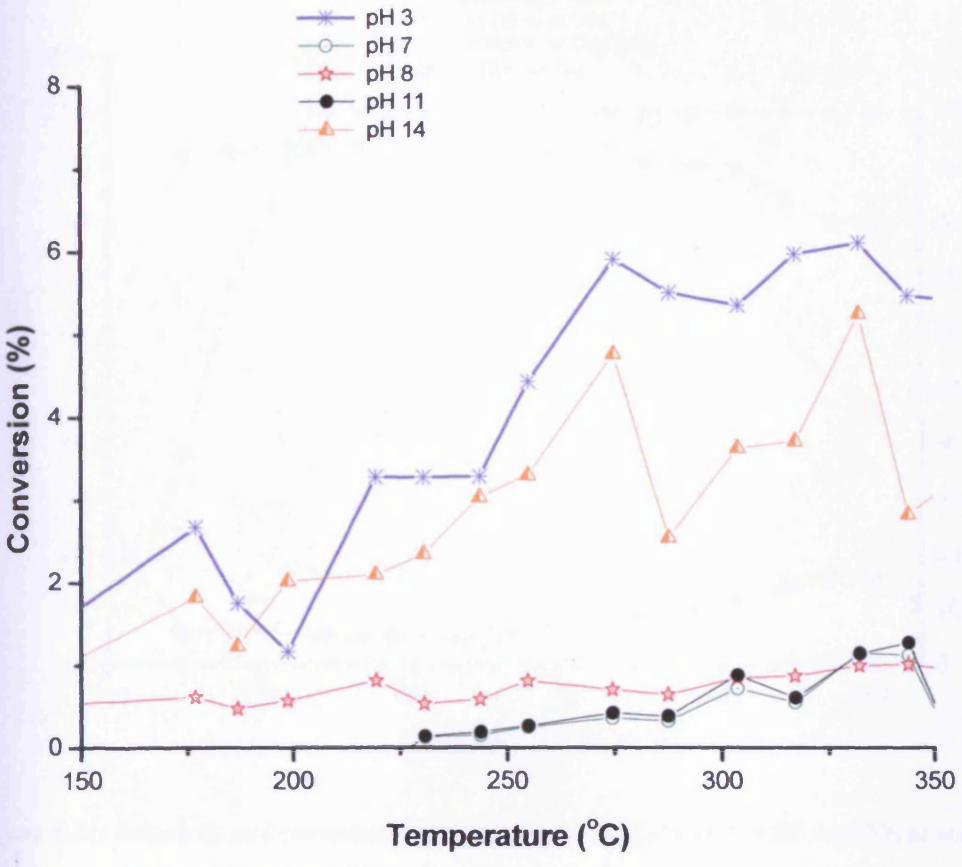

Figure 4-30: Comparison of CH_3OCH_3 selectivity with temperature for methanol oxidation over 1wt% Au/TiO_2 catalysts prepared at different pH values

4.7.3 Effect of washing of the catalyst

When the catalyst was washed during preparation, its activity was presumed to be greater and the possibility of presence of chloride in the catalyst was minimal, as the dissolved chloride will be washed away by washing the catalyst with water or Na_2CO_3. However, in order to determine the extent and the activity of the unwashed catalyst, it was prepared without washing and tested in the reactor aerobically. The result obtained is as shown in figure (4-31):

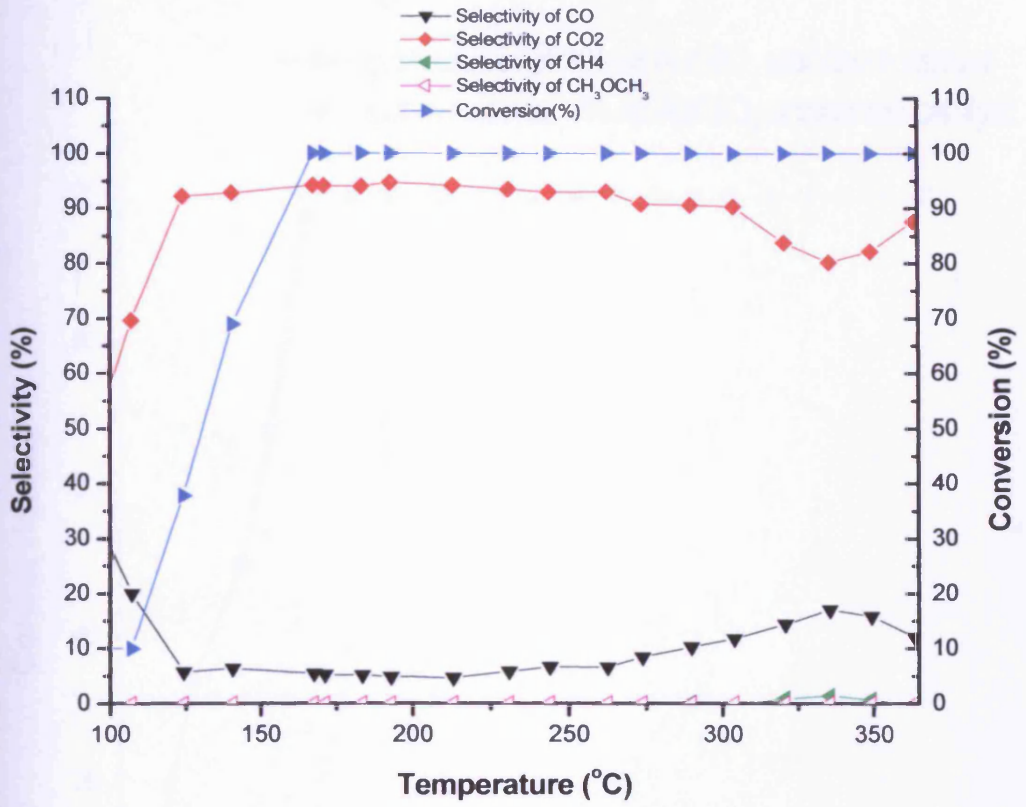

Figure 4-31: Selectivity and conversion for methanol oxidation over a 1wt% Au/TiO_2 unwashed catalyst calcined at 400°C and heated in 10%O_2/He in a reactor at 400°C

Figure (4-31) shows that complete methanol conversion was attained at very high temperature, with 100% conversion reached at about 160°C higher than when the catalyst was washed moreover, when the methanol conversion was less than 50%, already the selectivity to CO_2 was 90% with CO selectivity less than 10%. Similarly, as the temperature increased to 300°C, the CO selectivity increases and the selectivity to CO_2 decreases due to dehydrogenation and de-oxygenation; little methane selectivity was seen to increase and no dimethyl ether seen. When the standard catalyst was compared with the unwashed catalyst, a plot of conversion of methanol and selectivity data to CO, CO_2, CH_4 and CH_3OCH_3 was plotted against the temperature, as shown in figure (4-32 to 4-36)

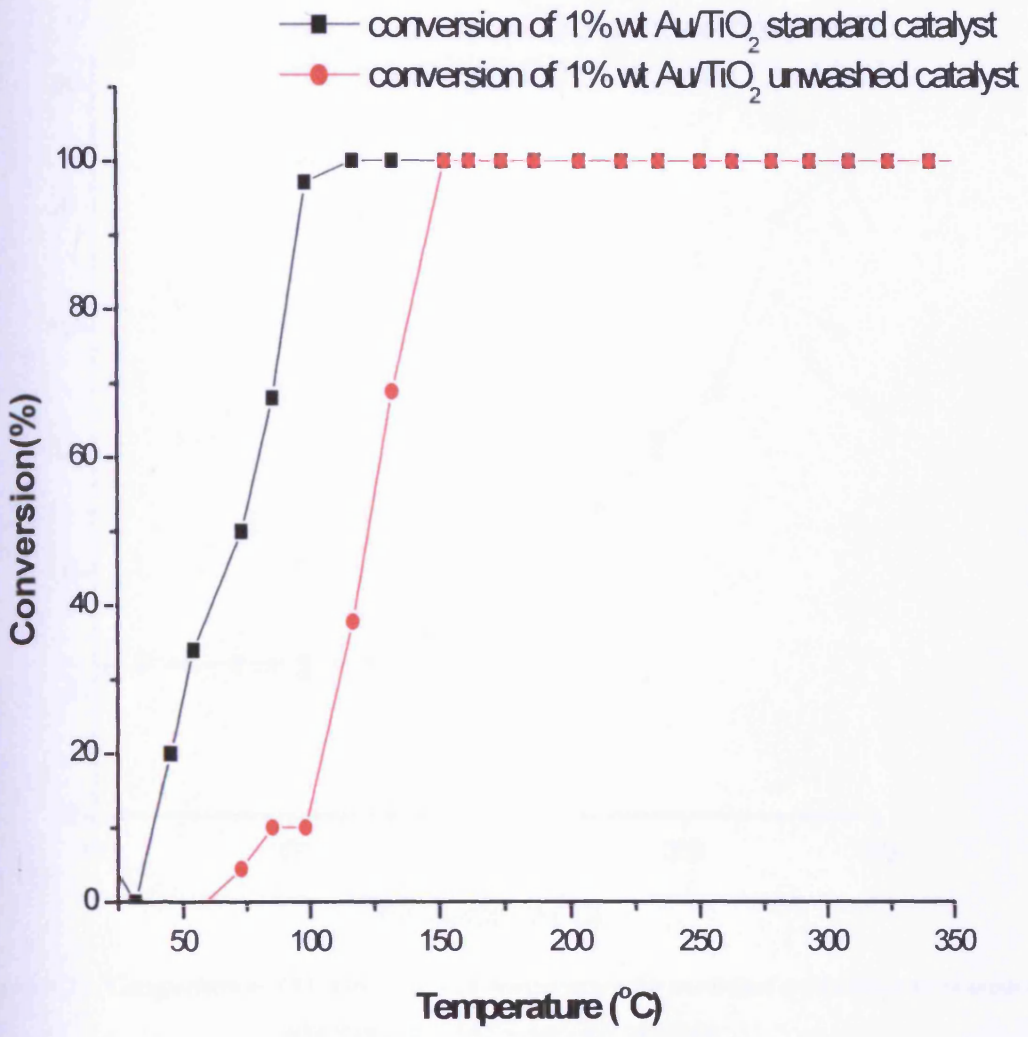

Figure 4-32: Comparison of conversion for methanol oxidation over a washed (standard) and unwashed Au supported TiO_2 catalyst

Figure (4-32) indicates methanol conversion over a standard (washed) and unwashed 1wt% Au/TiO_2 catalyst. It shows that methanol reached 100% conversion at very low temperature (80°C) in the case of washed catalyst (standard), compared with unwashed which shows that 100% methanol conversion was reached at very high temperature (~160°C), which indicates very low activity of the catalyst. This has confirmed that washing of the catalyst enhances the activity of the catalyst. It helps to reach 100% conversion quicker at very low temperature when compared with the unwashed catalysts.

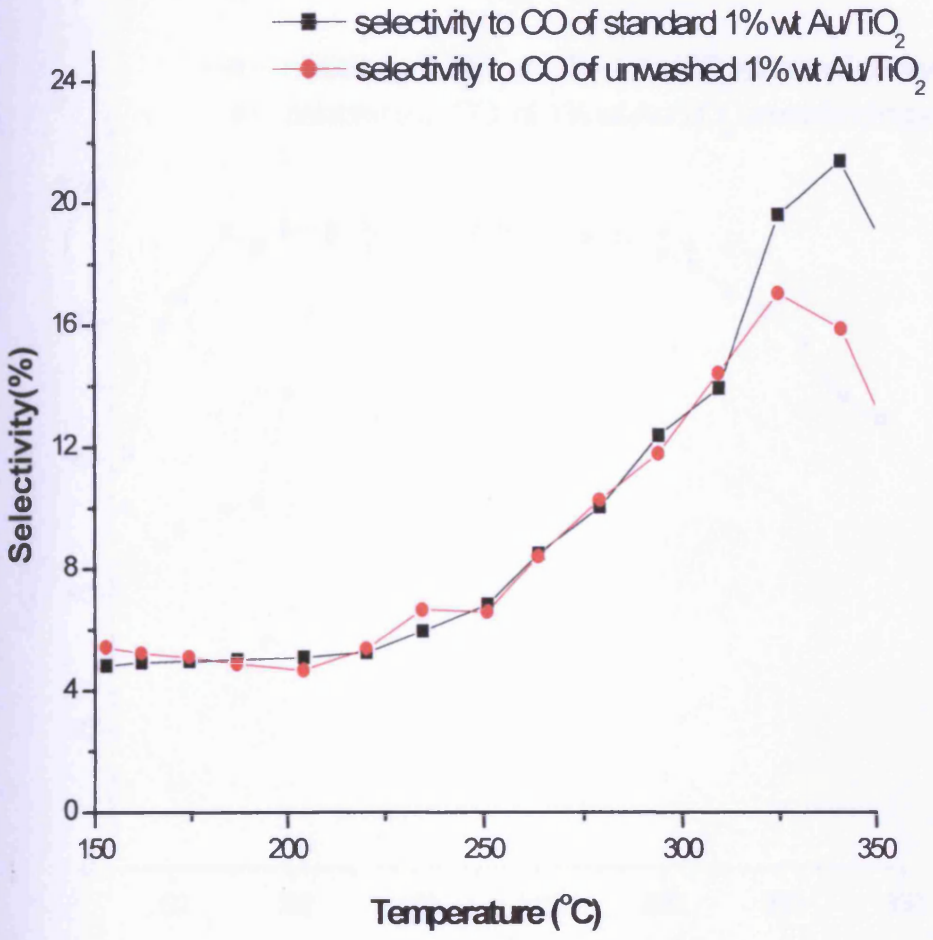

Figure 4-33: Comparison of CO selectivity with temperature for methanol oxidation over standard and unwashed 1wt% Au/TiO_2 catalysts

Similarly, it was observed (figure 4-33) a steady CO selectivity for both catalysts at 125- 250°C after which both selectivity begin to increase. However, the selectivity to CO of the washed catalyst (standard) was higher than the corresponding un-washed catalyst as evident at temperatures from 300 to 325°C.

Figure (4-34) shows the selectivity graph to CO_2 for the washed (standard) and un-washed 1wt% Au/TiO_2 catalysts. In both cases type I CO_2 start at low temperature, with the washed catalyst starting to produce type II CO_2 at very low temperature (~80°C) when compared with un washed catalyst where type II CO_2 production begins at higher temperature (~125°C). However, as the temperature reached 300°C both start to drop at the same temperature due to dehydrogenation of methanol and then continue to decrease due to de-oxygenation.

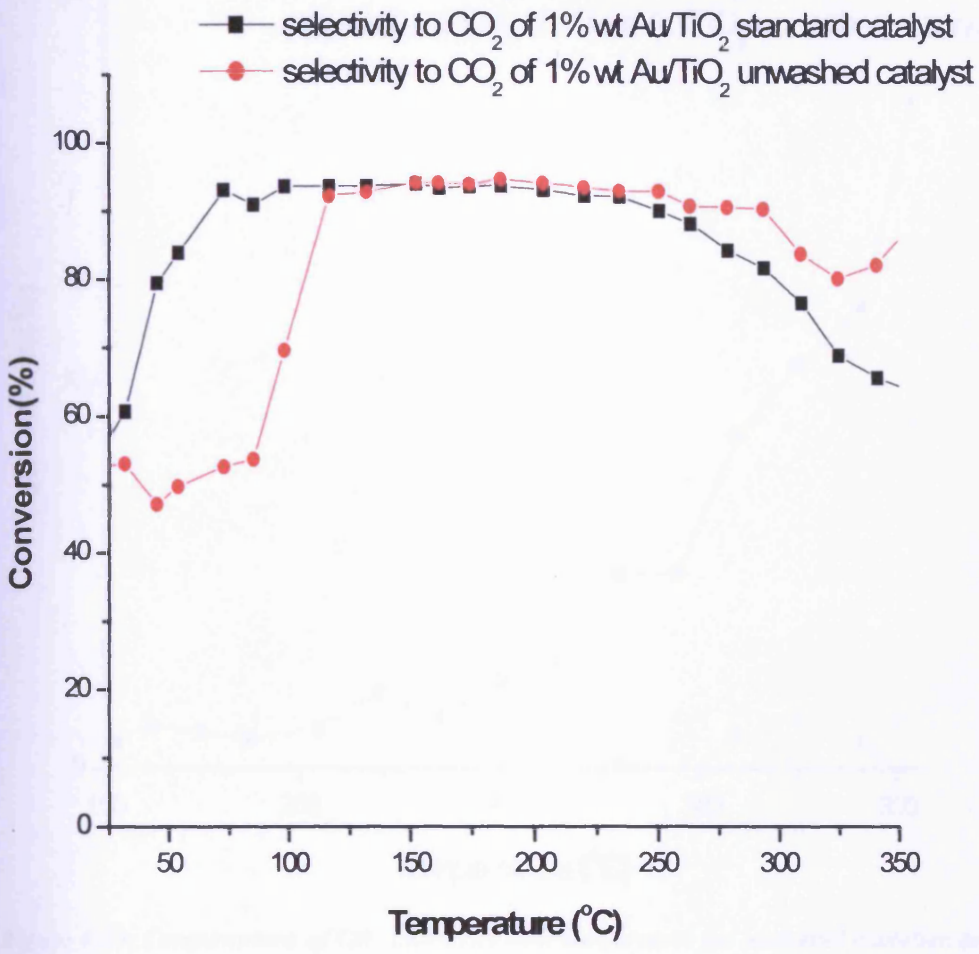

Figure 4-34: Comparison of CO_2 selectivity with temperature for methanol oxidation over standard and unwashed 1wt% Au/TiO_2 catalysts

Figure (4-35) shows that the selectivity to methane begins at a temperature of 200°C in the case of the washed catalyst and continues until the temperature reaches 300°C where the deoxygenation begins and more methane is produced at this temperature. At this temperature, the methane selectivity of an unwashed 1wt% Au/TiO_2 catalyst begins (300°C) and continues until the temperature reached 350°C where the methane selectivity drops. It is also evident that the selectivity of methane is more in the case of the washed catalyst than unwashed one.

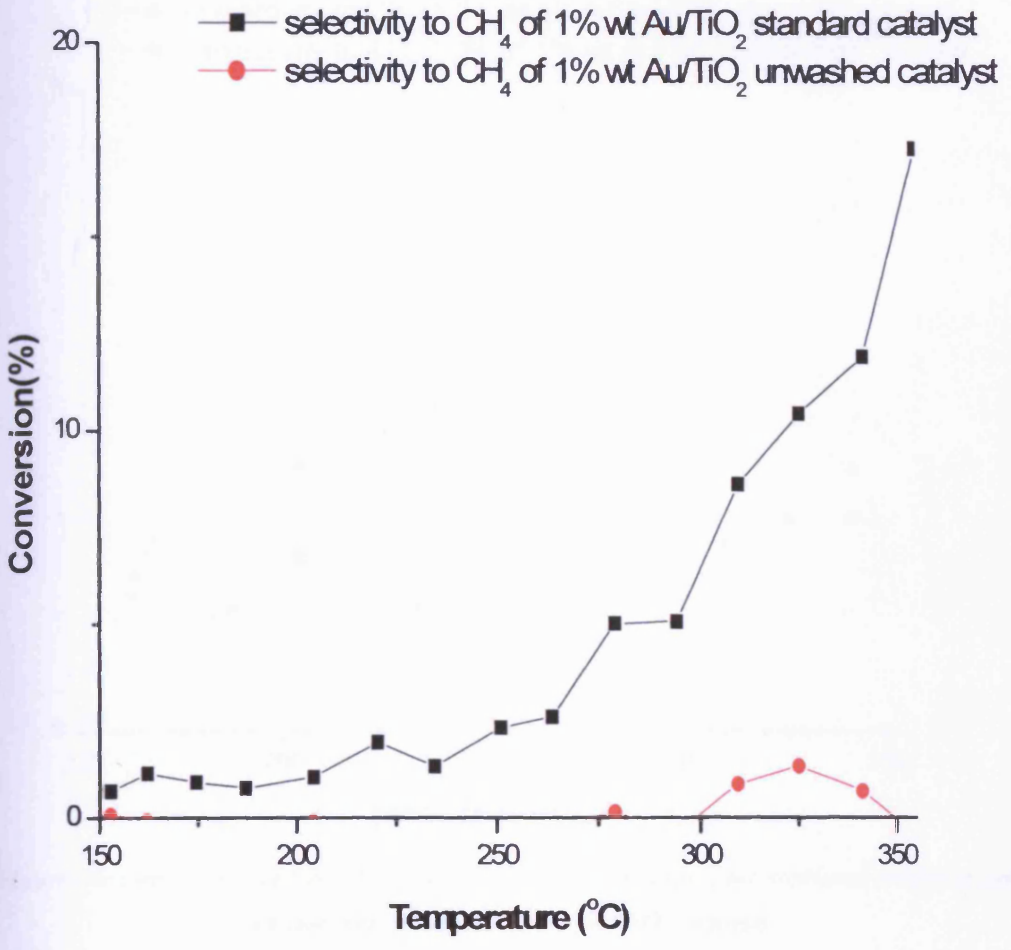

Figure 4-35: Compararison of CH_4 selectivity with temperature for methanol oxidation over standard and unwashed 1wt% Au/TiO_2 catalysts

Simultaneously, figure (4-36) shows a graph of dimethyl ether selectivity's of washed and unwashed catalyst of a 1wt% Au/TiO_2. It indicates that in both catalysts the selectivity or yield of dimethyl ether is very low almost negligible because very little dimethyl ether was produced in all cases (washed and unwashed catalyst of a 1wt% Au/TiO_2). The result was signified that washing or unwashing of the catalyst might not promote the production of dimethyl ether. probably, due to the presence of gold in both cases which found to prevent the formation of dimethyl ether in which the methoxy (CH_3O-) which is a species for the formation of dimethyl ether has either have very low coverage or short resident time on the surface of the catalyst especially when gold is present.

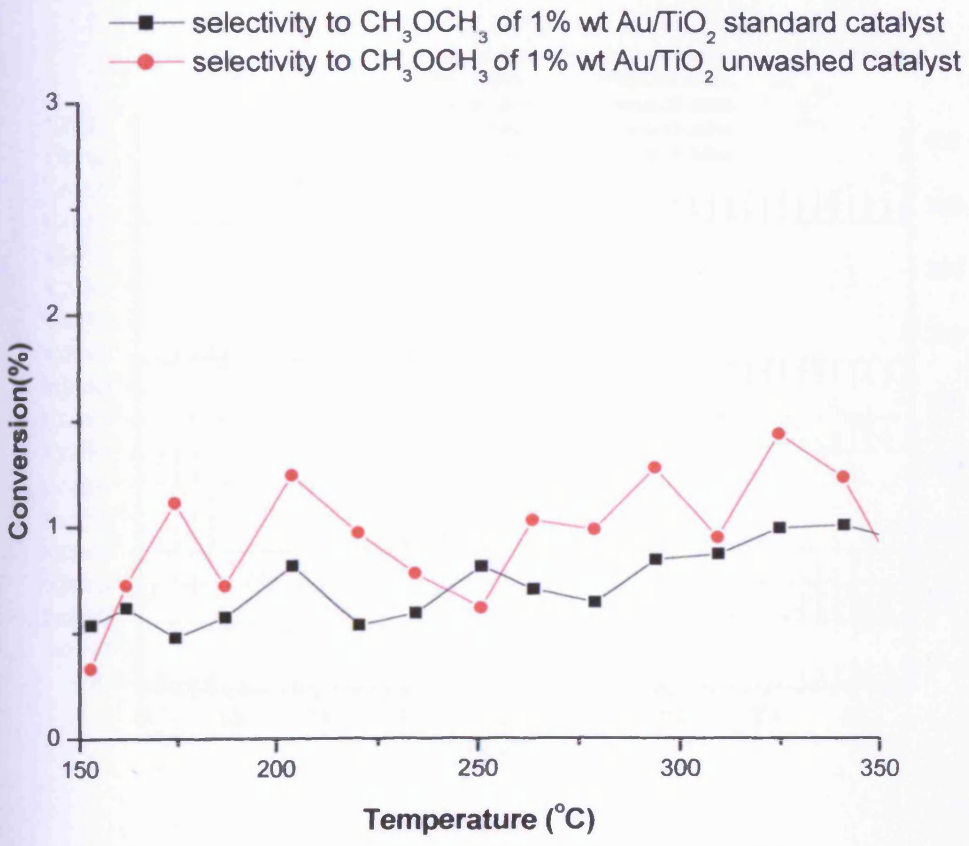

Figure 4-36: Comparison of CH_3OCH_3 selectivity with temperature for methanol oxidation over standard and unwashed 1wt% Au/TiO_2 catalysts

4.8 Kinetic Isotope Effect

The variation of one of the atom in the reaction rate of the chemical reaction in which one the atom of the reactant is being substituted by an isotope is known as Kinetic Isotope Effect, it is known as KIE. When hydrogen is replaced by a deuterium, it leads to certain changes in the reaction rate and the ratio between them determine the extent to which the reaction is modified and such modification can be used to determine the reaction mechanism.

In order to understand the reaction involved and possibly to develop a reaction mechanism for methanol oxidation over a 1wt% Au/TiO_2 catalyst, deutrated methanol was used and the kinetic effect were also monitored when the hydrogen of the methanol, was replaced as (CH_3OD) as shown below in the figure (4-37).

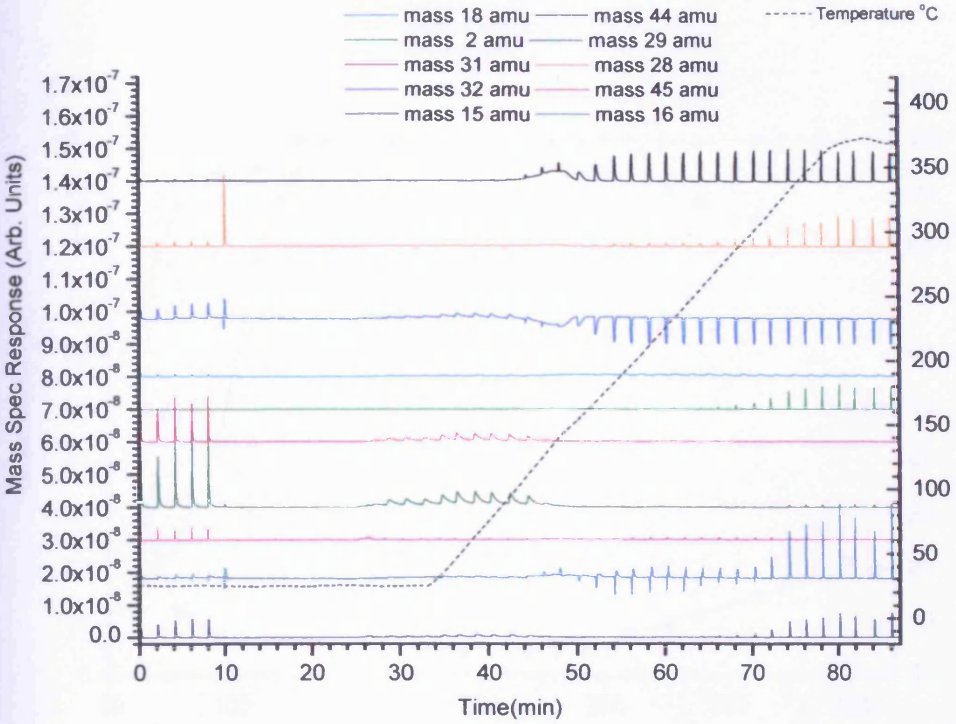

Figure 4-37: Temperature Programmed Pulse Flow Reaction for CH_3OD oxidation over a 1wt% Au/TiO_2 catalyst dried a t 400 °C in air and heated in 10%O_2/He in a reactor at 400°C

Figure (4-37) indicates the temperature programmed reaction, when CH_3OD was injected over the by- pass and the catalyst (in the same manner as reported previously in this chapter). The figure also indicates that the first pulses of injection of CH_3OD over the by- pass and indicates 100% of un-reacted CH_3OD. The disappearance of mass 31 and 29 amu indicates the 100% conversion of CH_3OD.Slow CO_2 (type I) formation starts at about 44 minutes which is slightly higher than the standard catalyst and the fast CO_2 (type II) starts at 54 minutes which is a bit longer than our standard catalyst. When the data was integrated and analysed, figure (4-38) was obtained, which indicates that 50% conversion was reached at about 120°C and the CH_3OD 100% conversion was attained at little higher temperature (about 129°C) than the standard, in which 100% was attained at about 118°C. The high temperature value for 100% conversion of CH_3OD was due to primary kinetic isotope effect, which leads to a higher activation energy, and more energy needed to break the bond and hence, attained 100% conversion at high temperature.

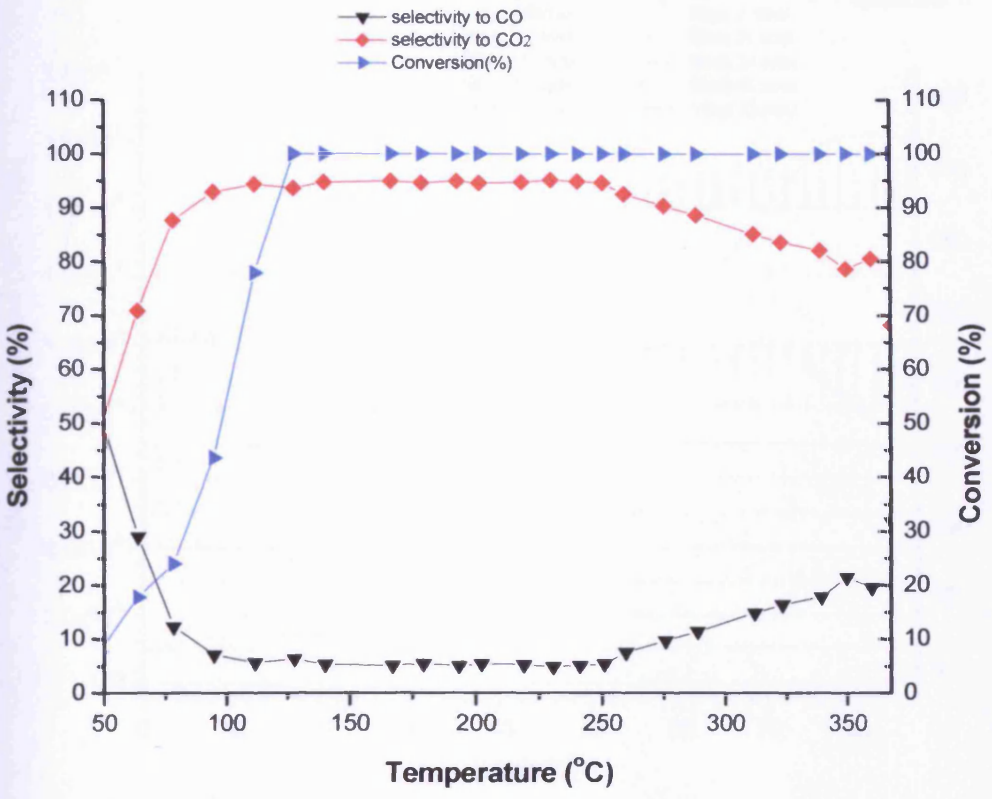

Figure 4-38: Selectivity and conversion for CH_3OD oxidation over a 1wt% Au/TiO_2 catalyst calcined at 400°C and heated in 10%O_2/He in a reactor at 400°C

In the same manner, the selectivity to CO_2 (type I) begins at about 50°C until the temperature reached 100°C when type II CO_2 begins and continues in a steady state with selectivity reaching about 90%, however, at 250°C, the CO_2 selectivity decreases in contrast with the standard catalyst where it dropped at 300°C due to dehydrogenation of methanol. However, as the selectivity to CO_2 drops, the CO selectivity increases and continue reaching about 20%; methane selectivity also increased at that temperature due to de-oxygenation, especially at 350°C.

When a high deutrated methanol was used such as CD_3OD, the results vary. Figure (4-39) indicates the temperature programmed pulse reaction of CD_3OD as described in figure (4-37). The figure indicates that the CO_2 (type I) starts earlier than expected, from 35 minutes to 50 minutes and from there type II CO_2 begins and continues in a steady state.

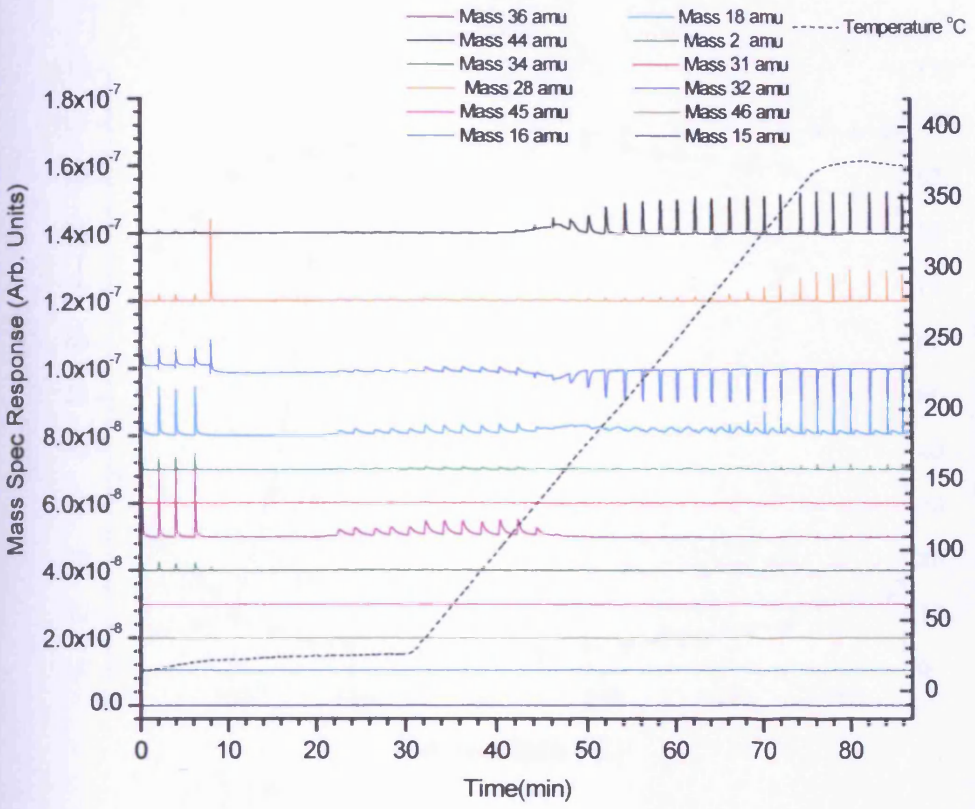

Figure 4-39: Temperature Programmed Pulse Flow Reaction for CD_3OD oxidation over a 1wt% Au/TiO_2 catalyst dried a t 400 °C in air and heated in 10%O_2/He in a reactor at 400

However, no hydrogen was observed and only deutrated water and CO was present as products. Methanol conversion varies with the product formation. A 100% conversion of methanol was attained at higher temperature more than methanol and CH_3OD (~140°C). However, the dominant products are CO_2 and CO but with low selectivity to CO_2 (<90%) when compared to its selectivity to methanol and CH_3OD as reported previously in this chapter.

Similarly, the selectivity to CO was a bit higher when compared with its value in methanol and CH_3OD. In the same manner as the CO_2 selectivity continue in a steady state until the temperature reached about 300°C, it selectivity decreases and continue to drop till the temperature reached 350°C where more decrease to CO_2 selectivity was observed and selectivity to CO increases more at this temperature. However, no dimethyl ether and methane was observed due to the absence of hydrogen.

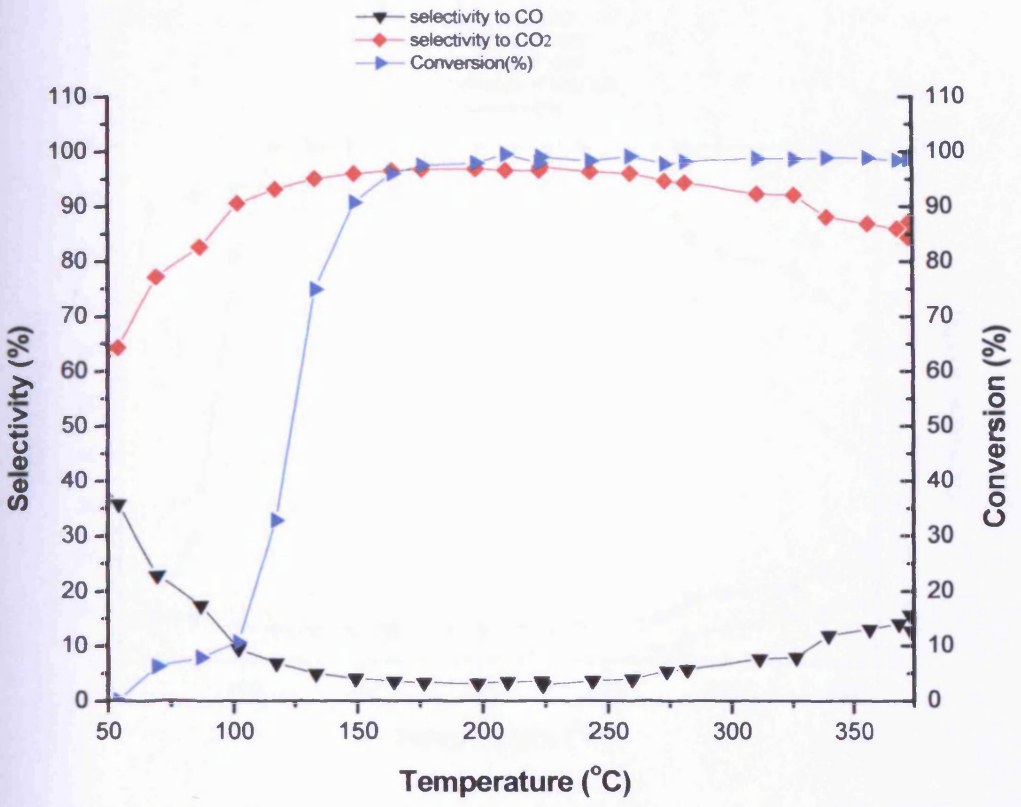

Figure 4-40: Selectivity and conversion for CD_3OD oxidation over a 1wt% Au/TiO_2 catalyst calcined at 400°C and heated in 10%O_2/He in a reactor at 400°C

The different patterns of reaction and the selectivity of the products are due to primary kinetic isotope effect, which occurs when the bond to the isotopic substitution is broken at or before the transition state.

4.9 Comparison with World Gold Council catalyst.

In order to determine the extent of the activity of our catalyst, the World Gold Council catalyst was compared with our standard catalysts (4-41).

The figure (4-41) shows a 100% conversion of methanol was attained at 112°C. It indicates that the type I CO_2 begins at low temperature (as low as even when the conversion was below 10%). Similarly, the selectivity to type II CO_2 begins when the temperature was around 70°C. When data was compared with our standard catalyst data, the results obtained are as shown in figure (4 -42).

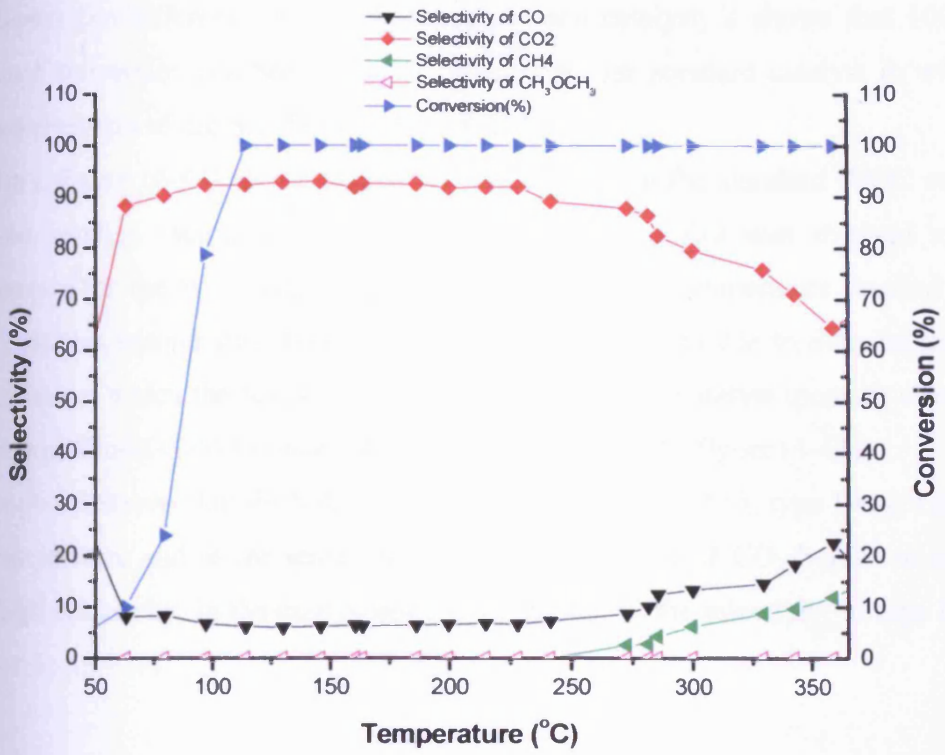

Figure 4-41: Selectivity and conversion for methanol oxidation over a 1wt% Au/TiO_2 WGC catalyst

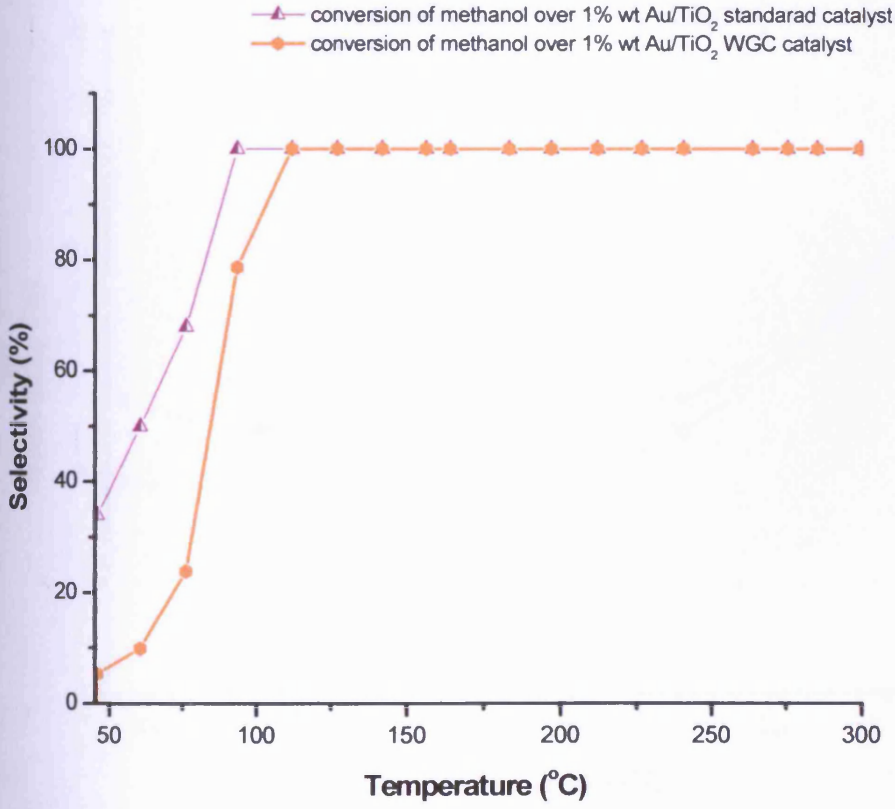

Figure 4-42: Comparison of conversion with temperature for methanol oxidation over standard and WGC Au supported TiO_2 catalysts

It indicates the difference in the activities of each catalyst; it shows that 100% of methanol conversion reached at 112°C contrary to our standard catalyst in which a 100% conversion of methanol reached at 89°C

Similarly, figure (4-43) shows selectivity to CO of both the standard WGC catalyst and our catalyst (standard). The figure indicates that CO was evolved at low temperature for the WGC catalyst and continues until the temperature reached about 300°C. At this temperature, both selectivity to CO increases due to dehydrogenation but the rate at which the selectivity to CO of our standard catalyst increase was more than that of World Gold Council catalyst as evidenced in the figure (4-43).

Figure (4-44) shows that for both catalysts the selectivity to CO_2 type I begin at very low temperature and as the temperature increases the type II CO_2 begins to emerge with high selectivity, in the case of our standard catalyst the selectivity to type II CO_2 reached about 91%.

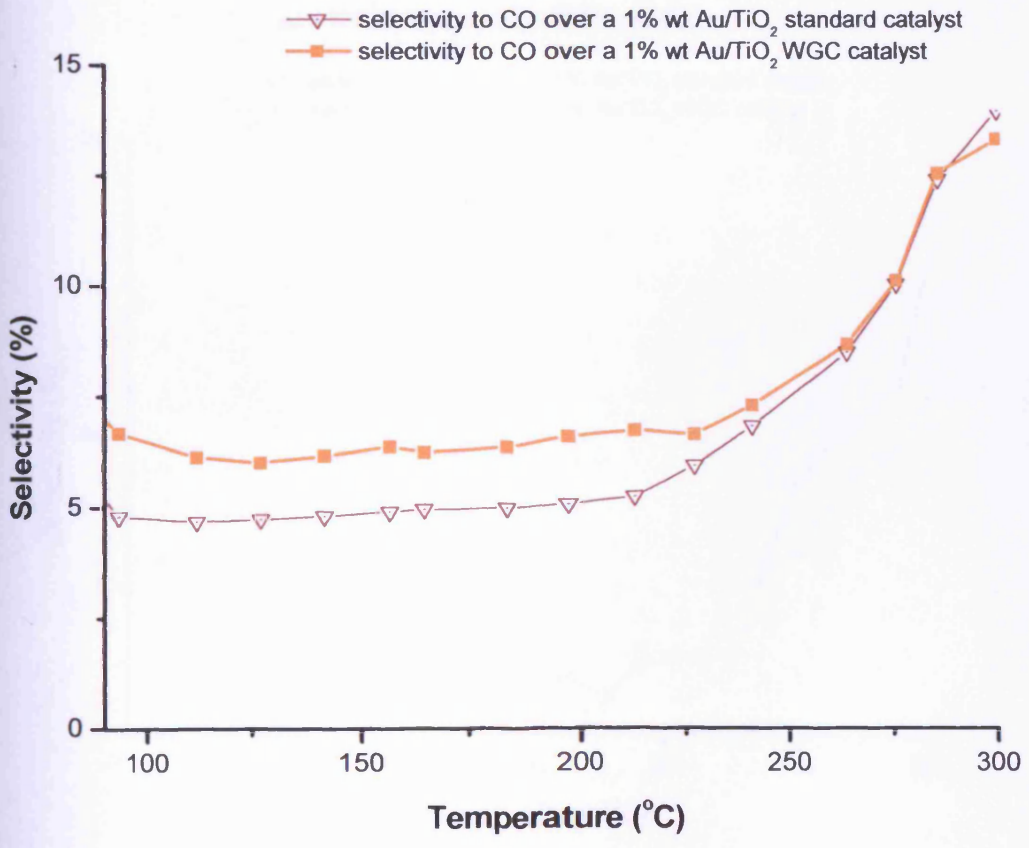

Figure 4-43: Comparison of CO selectivity with temperature for methanol oxidation over standard and WGC Au supported TiO_2 catalysts

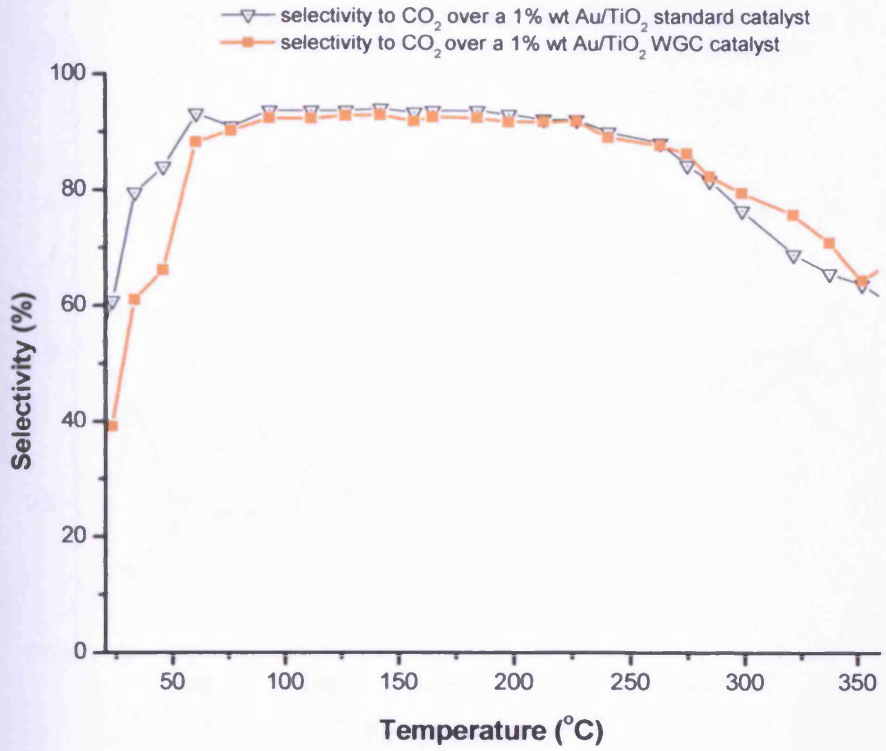

Figure 4-44: Comparison of CO_2 selectivity with temperature for methanol oxidation over standard and WGC Au supported TiO_2 catalysts

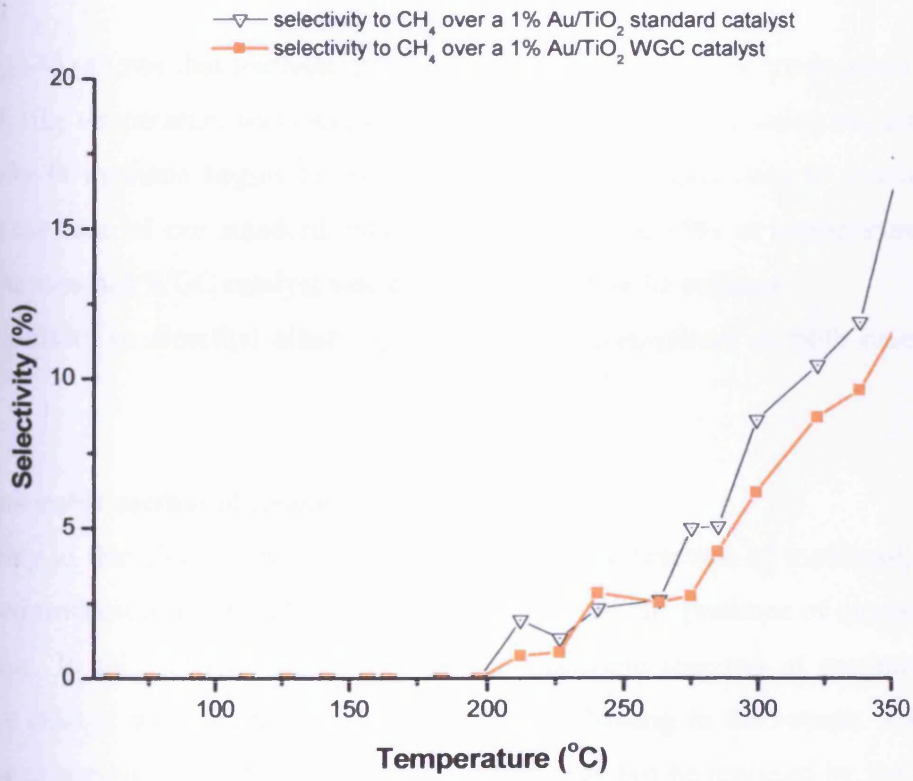

Figure 4-45: Comparison of CH_4 selectivity with temperature for methanol oxidation over standard and WGC Au supported TiO_2 catalysts

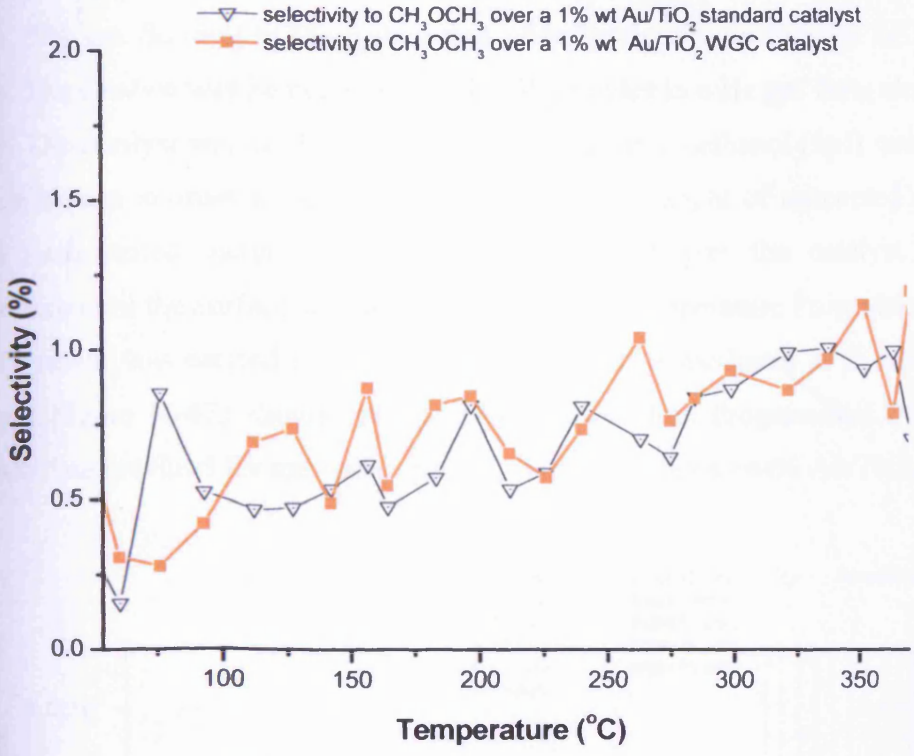

Figure 4-46: Comparison of CH_3OCH_3 selectivity with temperature for methanol conversion over a 1wt% Au/TiO_2 standard and WGC catalyst

Figure (4-45) shows that methane production begins at very low temperature in both cases .As the temperature was increased to about 300°C, deoxygenation begins and the selectivity to methane begins to increase. However, the selectivity to methane was high in the case of our standard catalyst reaching about 15% at temperature 350°C while the standard WGC catalyst was only 10% selective to methane.

The selectivity to dimethyl ether figure (4-46) is insignificant in both cases being <2%.

4.10 Anaerobic methanol reaction

Previously in this chapter, we reported on the aerobic reaction of methanol, i.e. the oxidation reaction of methanol over Au/TiO_2 catalyst in the presence of oxygen in the gas phase. In this section, we deal with the anaerobic reaction of methanol over Au/TiO_2 catalyst with out the presence of oxygen flowing in the stream. Therefore, the oxygen removed from the bulk of the support may not be replaced by the any gas presence in the reaction system.

0.5g of standard 1wt% Au/TiO_2 catalyst was loaded in the U tube of the oven of the reactor. The gas flowing in the system was only He flowing at the rate of 30ml per minute. The catalyst was heated to 400°C for 30 minutes in a He gas flow alone in the reactor. The catalyst was cooled to room temperature and methanol (1µl) was injected over the bypass in order to determine the signal peaks height of unreacted methanol (100% unconverted methanol). It was then switched over the catalyst at room temperature until the surface was saturated before the Temperature Programmed Pulse Flow Reaction was carried out with injection of 1µl of methanol at 2 minutes gap intervals. Figure (4-47) shows the anaerobic Temperature Programmed Pulse Flow Reaction data obtained for methanol oxidation reaction over a 1wt% Au/TiO_2 catalyst.

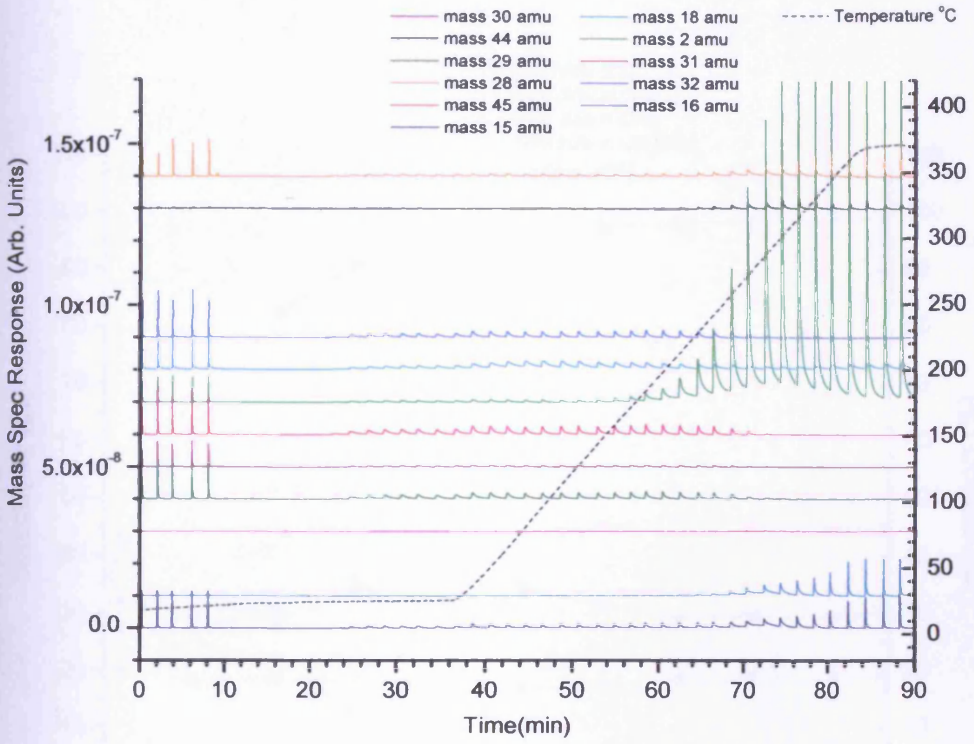

Figure 4-47: Temperature Programmed Pulse Flow Reaction for methanol anaerobic reaction over a 1wt% Au/TiO_2 catalyst

Form the data (figure 4-47) we deduce that about 7µl of methanol was taken up before the surface saturated, equivalent to the amount taken up by the surface of the catalyst at room temperature when subjected to aerobic reaction. The amount is equal to 2.1x 10^{20} molecules g^{-1} of catalyst. This in turn corresponds to about $4x10^{18}$molecules m^{-2} or about half monolayer of methanol consumed, if we assumed the total surface atom

density of $10^{19}m^{-2}$, which also implies that the surface is saturated. However, at the end of the reaction, the colour of the catalyst changed from pale blue to purple colour. Similarly, as the injections of methanol continue, (from 20-70minutes) 100% methanol conversion was reached at about 70 minutes (the disappearance of mass 31 and 29 amu). Simultaneously, the anaerobic methanol reaction indicates that methanol is being combusted to CO and H_2. The reaction involved in the anaerobic methanol reaction was dehydrogenation to CO and water (from 70minutes upwards) in which dimethyl ether was observed at 80 minutes and deoxygenation to methane (from 80 minutes up wards). However, small amount of CO_2 was observed in the anaerobic methanol oxidation. When the data in figure (4-47) was integrated and analysed, figure (4-48) was obtained:

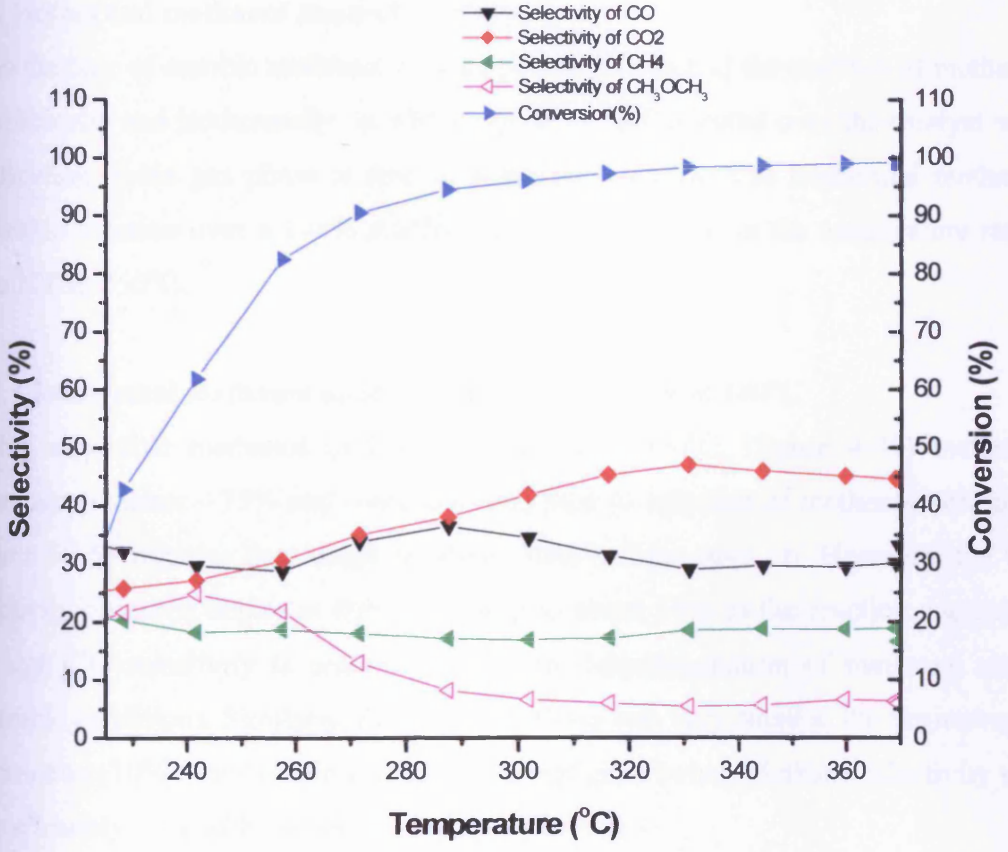

Figure 4-48: Selectivity and conversion with temperature for methanol anaerobic reaction over a 1wt% Au/TiO_2 catalyst

Figure (4-48) indicates that 100% conversion of methanol is attained at high temperature at (300°C) which is contrary to the oxidation of methanol aerobically, in which 100% conversion of methanol attained at relatively very low temperature.

However, the figures shows when methanol conversion was only 50%, the CO and CO_2 selectivity was very low until the conversion reached 80% where the selectivity of both start to increase and the temperature was about 260°C. As the temperature reached 290°C, CO selectivity begins to decrease and selectivity to CO_2 increases appreciably until the temperature reached 340°C, at which the selectivity to both became steady with 45% and 30% selectivity to CO_2 and CO respectively. It also observed that CO_2 produced was type II and no type I observed during the course of anaerobic methanol reaction. Simultaneously, the methane observed has a steady selectivity of about 20% with high dimethyl ether selectivity at 240 to 260°C due to high surface coverage and residence time of methoxy at that temperature and decreases as the temperature reached 270°C and the selectivity drops below 10%.

4.11 Isothermal methanol anaerobic reaction

As in the case of aerobic methanol oxidation, we also studied the reaction of methanol anaerobically and isothermally, in which methanol was injected over the catalyst with He flowing in the gas phase at rate of 30ml per minutes. The isothermal methanol anaerobic reaction over a 1wt% Au/TiO_2 catalyst was done in the temperature range from 100 to 350°C.

4.11.1 Isothermal methanol anaerobic reaction profile at 100°C

During anaerobic methanol isothermal reaction at 100°C, (figure 4-49) methanol conversion reaches ~ 75% and continues with time of injection of methanol until 80% at time 50-55 minutes then drops to about 70% as time goes on. However, the CO selectivity observed begins at 80% then drop to about 50% as the reaction continues; the high CO selectivity is presumably due to dehydrogenation of methanol under anaerobic conditions. Similarly, the CO_2 selectivity was very small at the beginning of the reaction (10%>) and continues to almost negligible value. Methane selectivity was approximately 10% with no dimethyl ether observed.

The profile data of methanol at 150°C is shown in figure (4-50). It shows the conversion of methanol to be 80% and continues through out the time of injections of methanol; in the same vein, the selectivity to CO drops to about 65% with CO_2 selectivity increasing to 20% and no dimethyl produced and the methane selectivity remains constant (~10%).

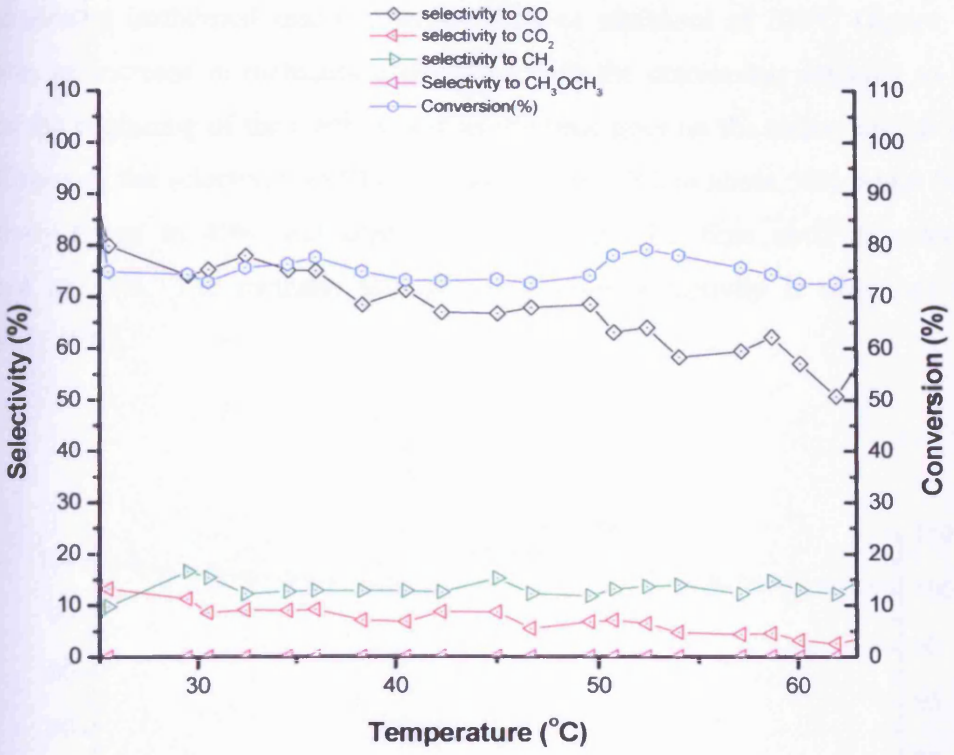

Figure 4-49: Isothermal methanol anaerobic reaction over a 1wt% Au/TiO_2 catalyst at 100°C

4.11.2 Isothermal Anaerobic Methanol Reaction Profile at 150°C

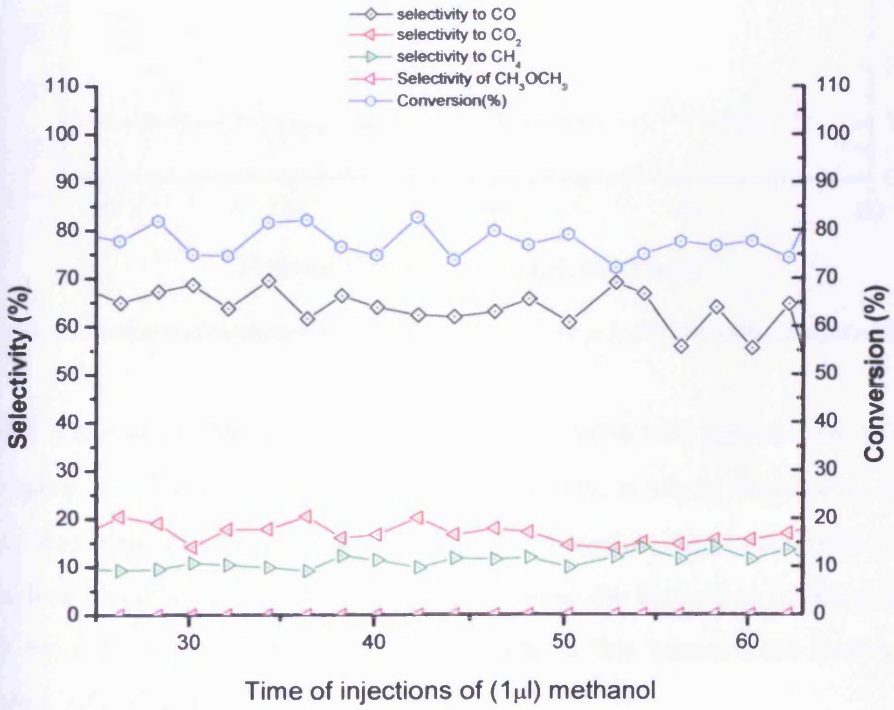

Figure 4-50: Isothermal methanol anaerobic reaction over a 1wt% Au/TiO_2 catalyst at 150°C

4.11.3 Anaerobic Isothermal methanol reaction profile at 200°C

The anaerobic isothermal reaction profile data of methanol at 200°C (figure 4-51) indicates an increase in methanol conversion with the conversion reaching to about 98% at the beginning of the reaction and as the time goes on the conversion drops by 3%. However, the selectivity to CO_2 increases from 50% to about 58% while the CO selectivity drops to 40% and continue decreasing with time until its selectivity dropped to 35%. The methane and dimethyl ether selectivity is observed to be minimal (<5%).

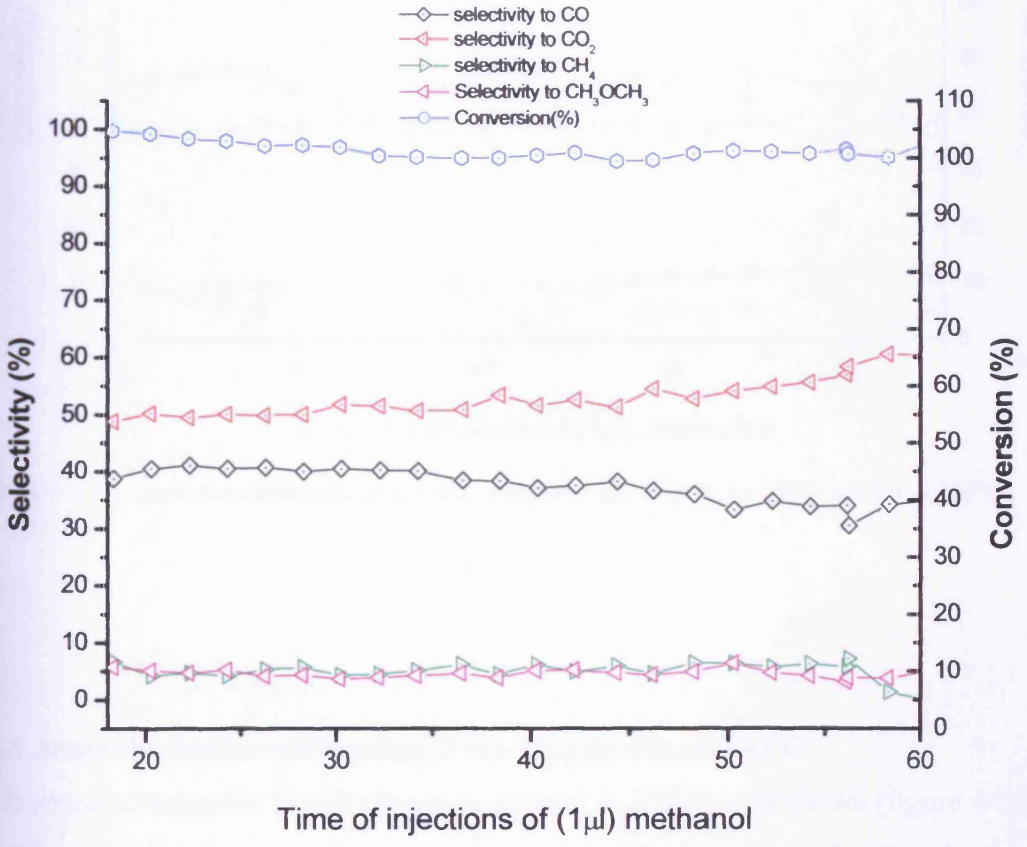

Figure 4-51: Isothermal methanol anaerobic reaction over a 1wt% Au/TiO_2 catalyst at 200°C

Figure (4-52) shows methanol conversion reaching 100% with selectivities to CO and CO_2 dropping to 37 and 47% respectively. However, a slight increase in methane selectivity was observed (from 10 to >10 %); the dimethyl ether selectivity is around 10%. The low CO and CO_2 selectivity may be due to the beginning of deoxygenation in which more methane is produced. The results at this temperature shows similar results when TiO_2 (Degussa) was used alone.

4.11.4 Anaerobic isothermal methanol reaction profile at 250°C

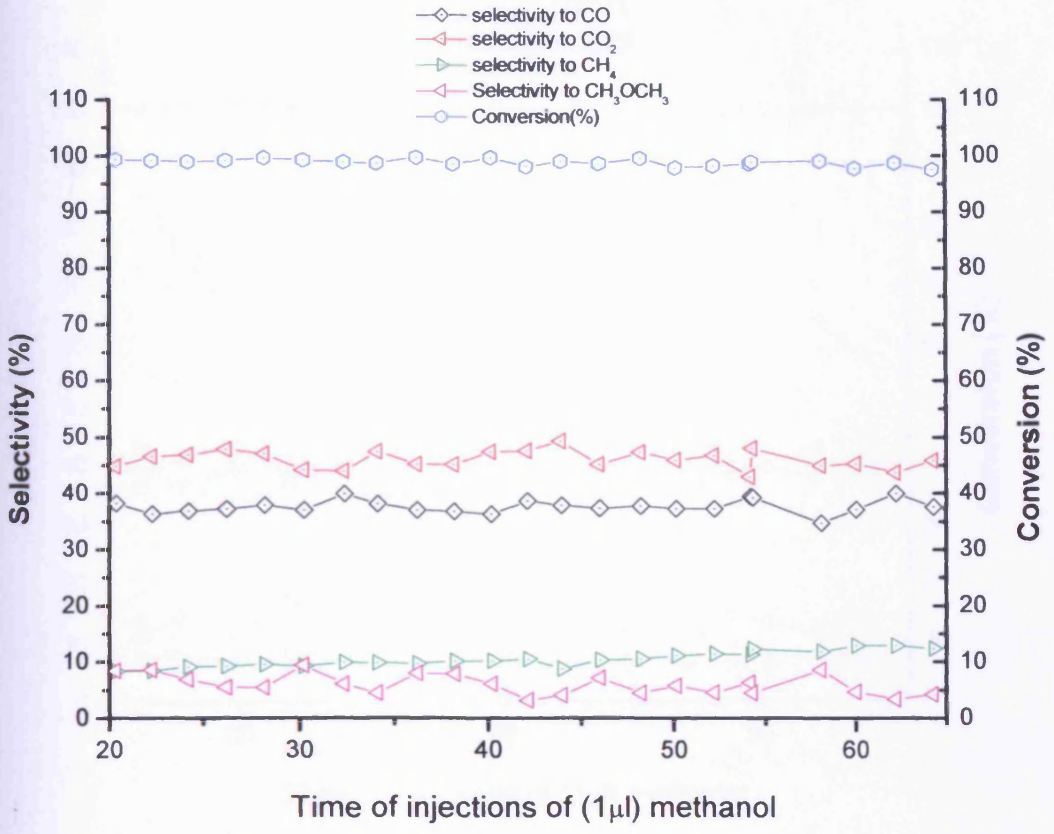

Figure 4-52: Isothermal methanol anaerobic reaction over a 1wt% Au/TiO_2 catalyst at 250°C

4.11.5 Anaerobic isothermal methanol reaction profile at 300°C

The isothermal anaerobic profile data of methanol at 300°C is as shown (figure 4-53), it indicates 100% of methanol conversion at this temperature, with CO selectivity being 42% little higher than the CO_2 which has selectivity of 38% at the beginning of the reaction. However, the CO and CO_2 selectivity was not steady with the time of injections of methanol continues especially between 50 to 60 minutes of time of injection as indicated in the figure. However, the methane selectivity in this temperature is still below 10% with dimethyl ether selectivity being 15%.

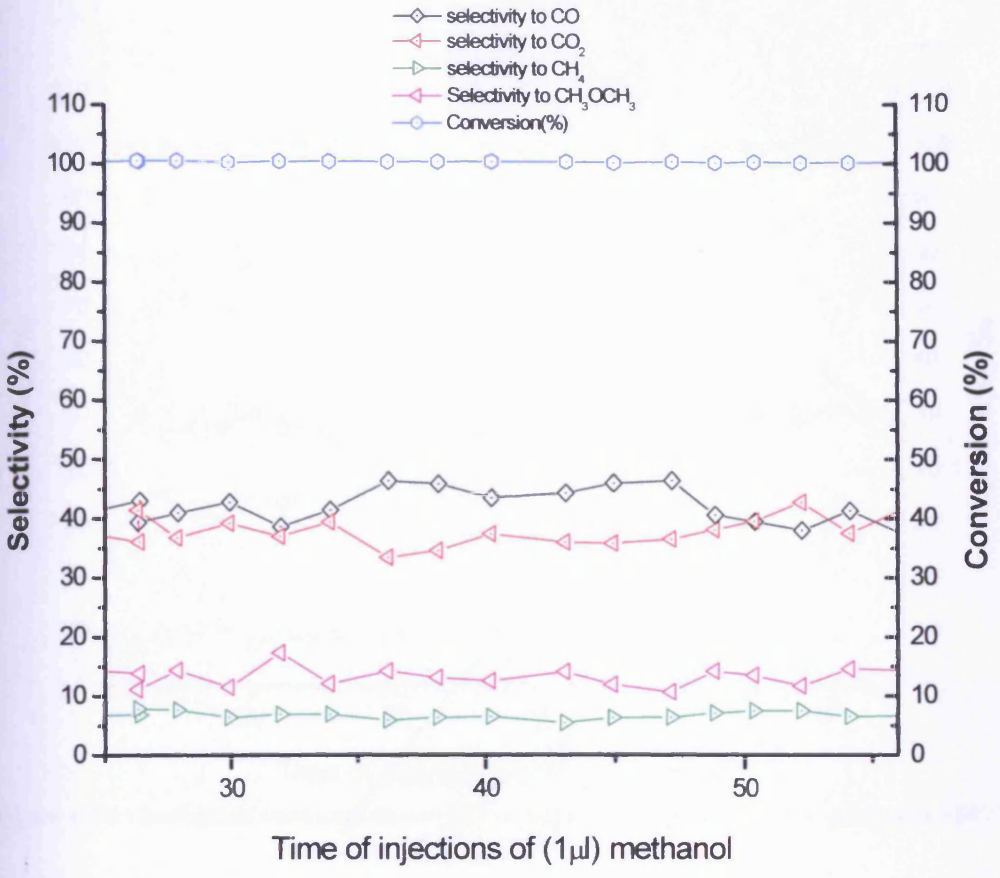

Figure 4-53: Isothermal methanol anaerobic reaction over a 1wt% Au/TiO_2 catalyst at 300°C

4.11.6 Anaerobic Isothermal methanol reaction profile at 350°C

When the profile data of methanol plotted against time of injection of methanol in anaerobic condition, figure (4-54) obtained; it shows 100% of methanol conversion, with CO selectivity being 50%, higher than CO_2 with selectivity around 40%. However, the dimethyl ether selectivity drops from 10% and decrease even below 10% as the time of injections continue. The drop of dimethyl ether selectivity was due to deoxygenation which leads to the methane produced as evident in the figure in which the selectivity increases to 10%.

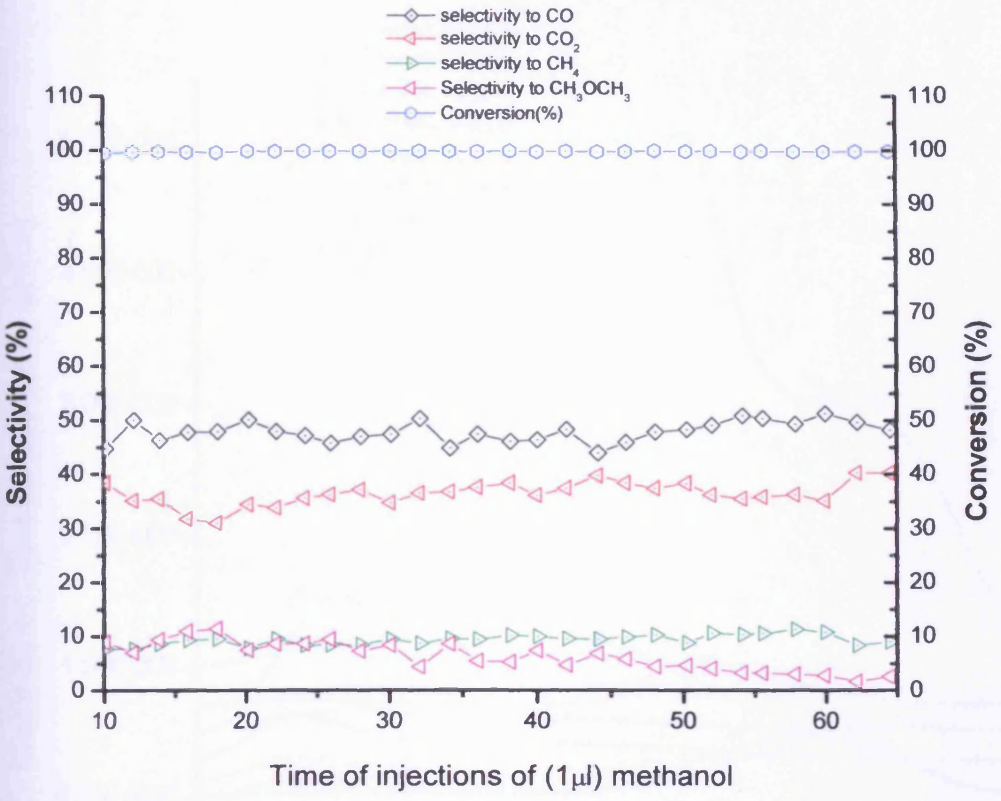

Figure 4-54: Isothermal methanol anaerobic reaction over a 1wt% Au/TiO_2 catalyst at 350°C

4.12 Methanol Temperature Programmed Desorption

Temperature Programmed Desorption profiles can be used to determine the adsorbed species on the surface of the catalyst. Knowledge of this can be used to estimate the actual activation energy and can be used to determine the mechanism of the reaction on the surface. The Temperature Programmed Reaction of methanol over an Au/TiO_2 catalyst is as shown in figure (4-55). The data shown in the figure were obtained when methanol (1μl at 2 minutes intervals) was injected over the bypass (5 times) and then switched over the catalyst with continue injections of methanol (1μl) at 2 minutes intervals until saturation. It was observed that about 7μl of methanol were taken by the surface in order to be saturated. This clearly corresponds to an uptake of half monolayer of methanol at saturation.

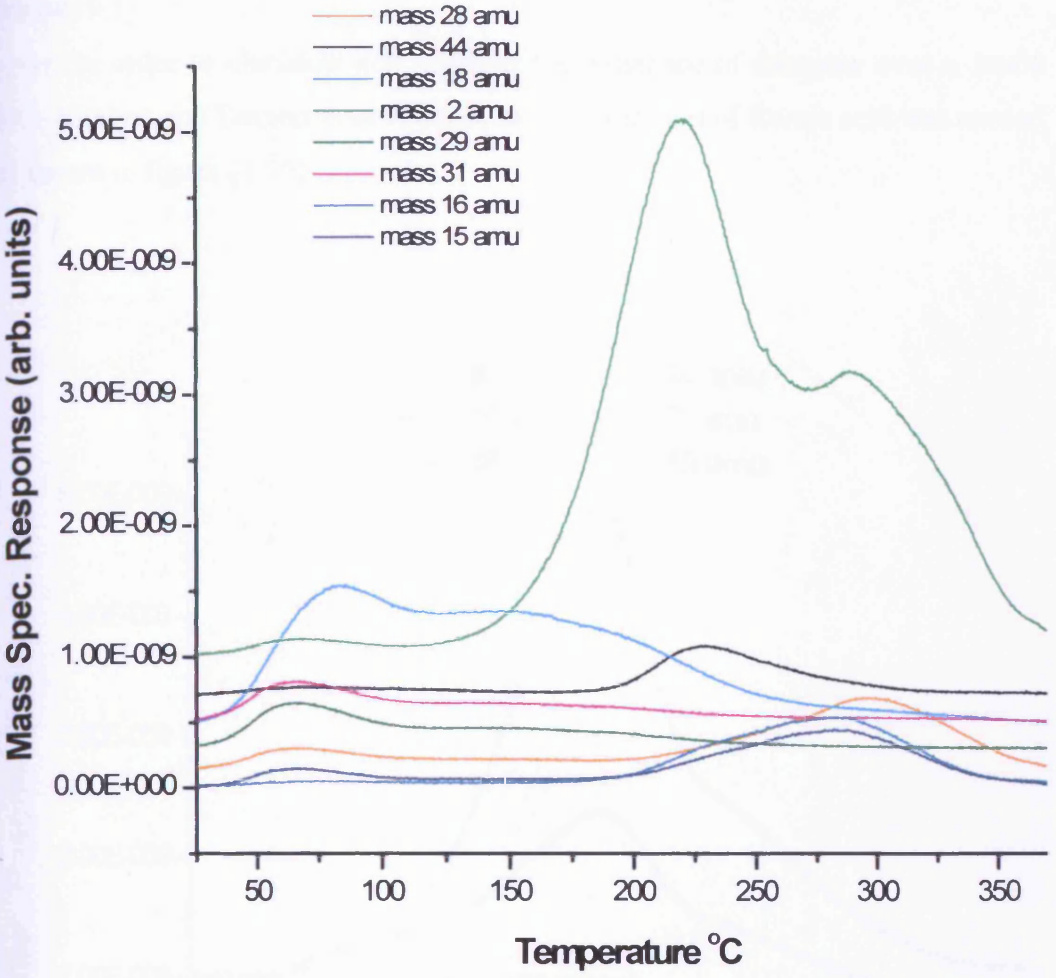

Figure 4-55: Temperature Programmed Desorption of a 1wt% Au/TiO_2 catalyst saturated with methanol at room temperature

Methanol is desorbed at lower temperature with a desorption peak centred at (~80°C) .Similarly, water is also being desorbed, one at lower temperature with desorption peaks centred at about 100°C and as the temperature was increased to about 200°C, two products of desorption were observed. Among the products of desorption are CO_2 and hydrogen and both are coincidently desorbed at the same temperature with desorption peaks centred at 250°C; this suggests the existence of formates as the active surface species for the combustion pathway for the different products obtained for methanol oxidation over Au/TiO_2.

However, as the temperature of desorption increases, methane was evolved with a desorption peak centred at 300°C and then followed by CO and hydrogen with peaks centred at about 313°C. The desorption of CO and hydrogen is similar to the peaks

obtained when methanol reaction was carried out on TiO_2 alone as described in section (4.19.1).

However, in order to elucidate and confirm the existence of formates over a 1wt% Au/TiO_2 catalyst, the Temperature Programmed Desorption of formic acid was carried out as shown in figure (4-56).

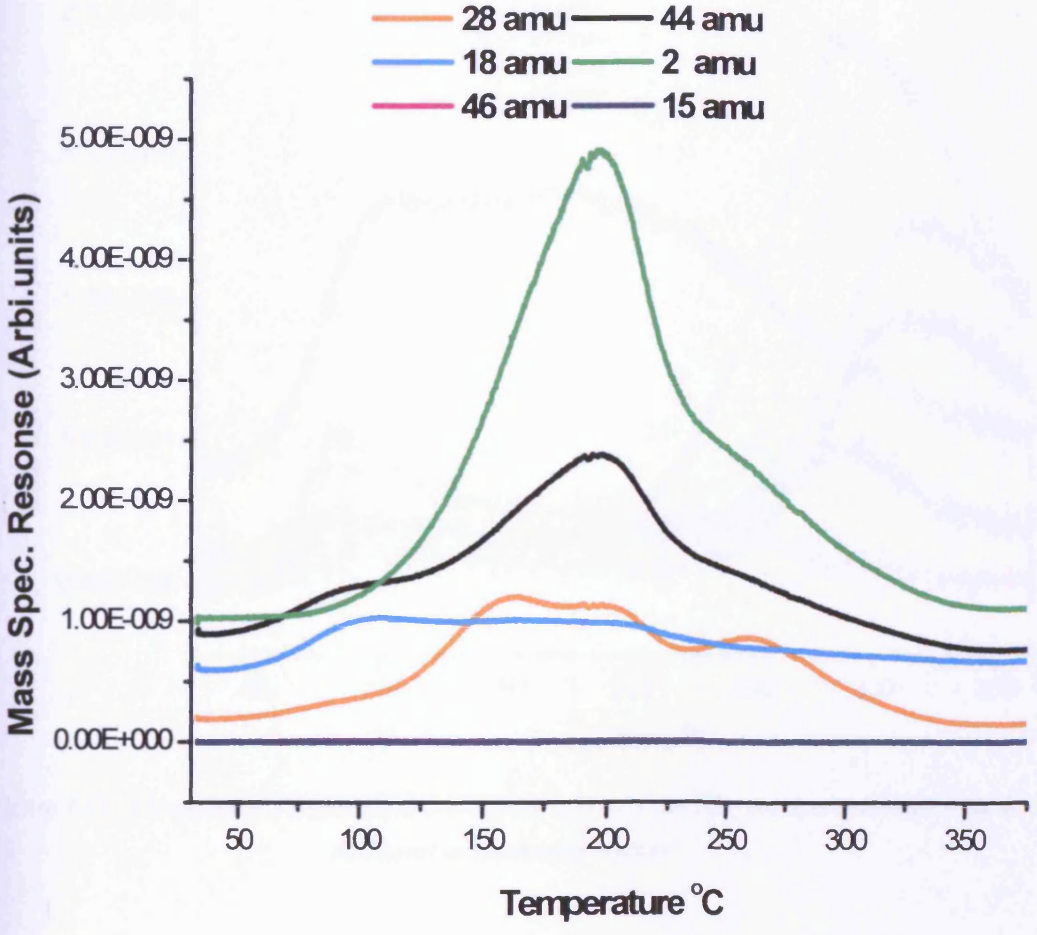

Figure 4-56: Temperature Programmed Desorption of a 1wt% Au/TiO_2 catalyst saturated with formic acid at room temperature

It indicates that the products of desorption are CO_2 and hydrogen with peaks centred at lower temperature (~197°C) than for methanol TPD. This has also confirmed that the adsorbed species present on the surface of a 1wt% Au/TiO_2 catalyst for methanol oxidation to be formates responsible for the oxidation products as previously discussed in this chapter.

Similarly, if d-methanol (CH_3OD) was used instead of methanol, the Temperature Programmed Desorption profiles were as shown (figure 4-57). CH_3OD and water are being desorbed at lower temperature similar to methanol, with desorption peak centred at (~80°C).

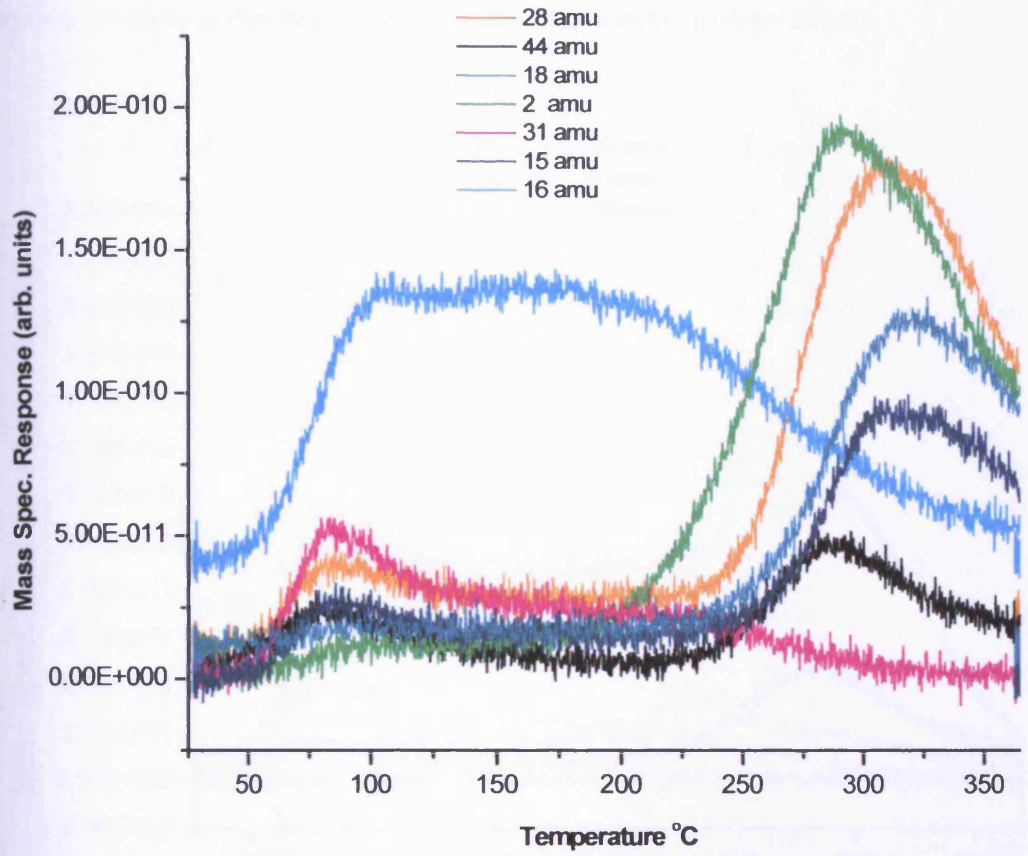

Figure 4-57: Temperature Programmed Desorption of 1wt% Au/TiO_2 catalyst saturated with d-methanol at room temperature

In the same manner, as the temperature was increased to about 300°C, two desorption products was observed, one being CO_2 and the other hydrogen both are being desorbed at the same temperature with a desorption peak centred at 288°C which is little higher than for CO_2 and hydrogen desorption when methanol TPD was used. The higher desorption temperature of CO_2 and hydrogen is due to higher activation energy due to primary kinetic isotope effect. However, at approximately 308°C the CO and methane desorption peak was observed in contrast to the peaks of CO and methane observed in figure (4-55) for methanol TPD.

The variation of desorption temperatures of the various products of methanol and d-methanol Temperature Programmed Reaction was due to a kinetic isotope effect. When d4-methnaol (CD_3OD) was used, the story is different as shown in figure (4-58). The Temperature Programmed Desorption of d_4- methanol indicates that the same products are being desorbed at the same temperature but no methane was desorbed as products due to the absence of hydrogen in the reaction. The variation of different adsorption products is due to primary or secondary kinetic isotope effects.

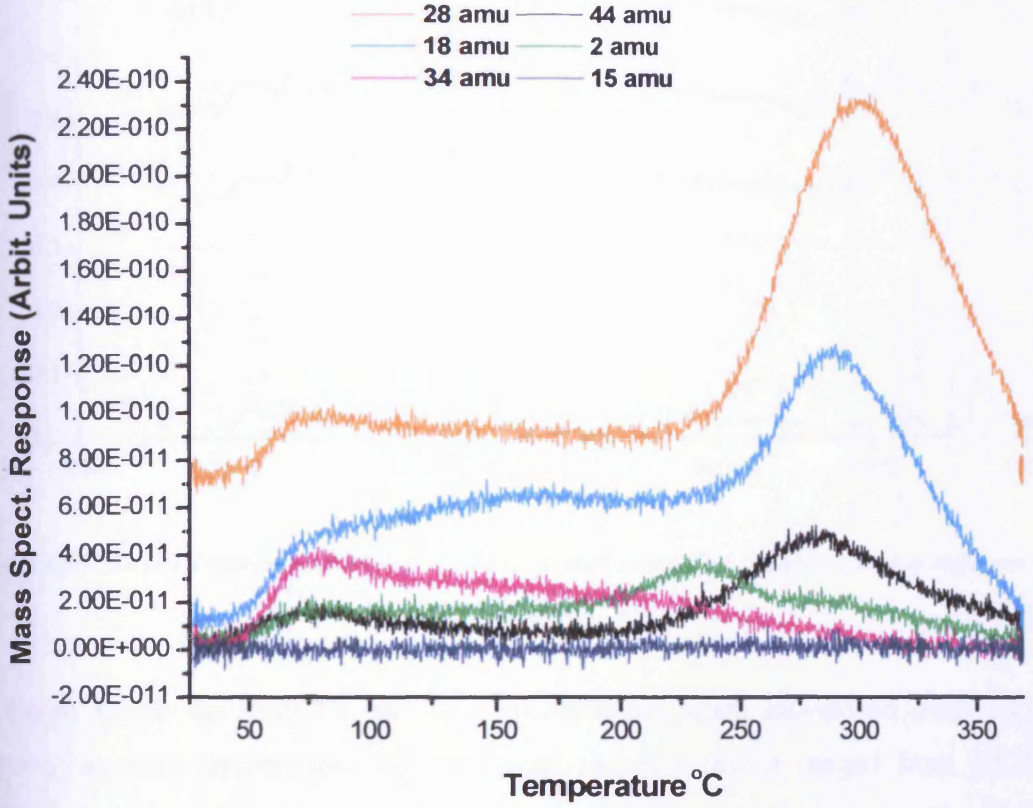

Figure 4-58: Temperature Programmed Desorption of 1wt% Au/TiO_2 catalyst saturated with d4-methanol at room temperature

4.13 Infra Red Spectroscopy

Diffused Reflectance Infra Red Fourier Transform Spectroscopy (DRIFTS as described in chapter II previously) was measured. Pure TiO_2 support was heated in the DRIFTS cell for 1 hour then cooled to room temperature in a flow of oxygen. The methanol was then introduced over the catalyst at room temperature and allowed to stabilise before nitrogen was introduced in order to purge the gaseous species.

The adsorbed species were determined at room temperature and subsequently at 100, 200, 300 and 400°C as indicated in figure (4-59)

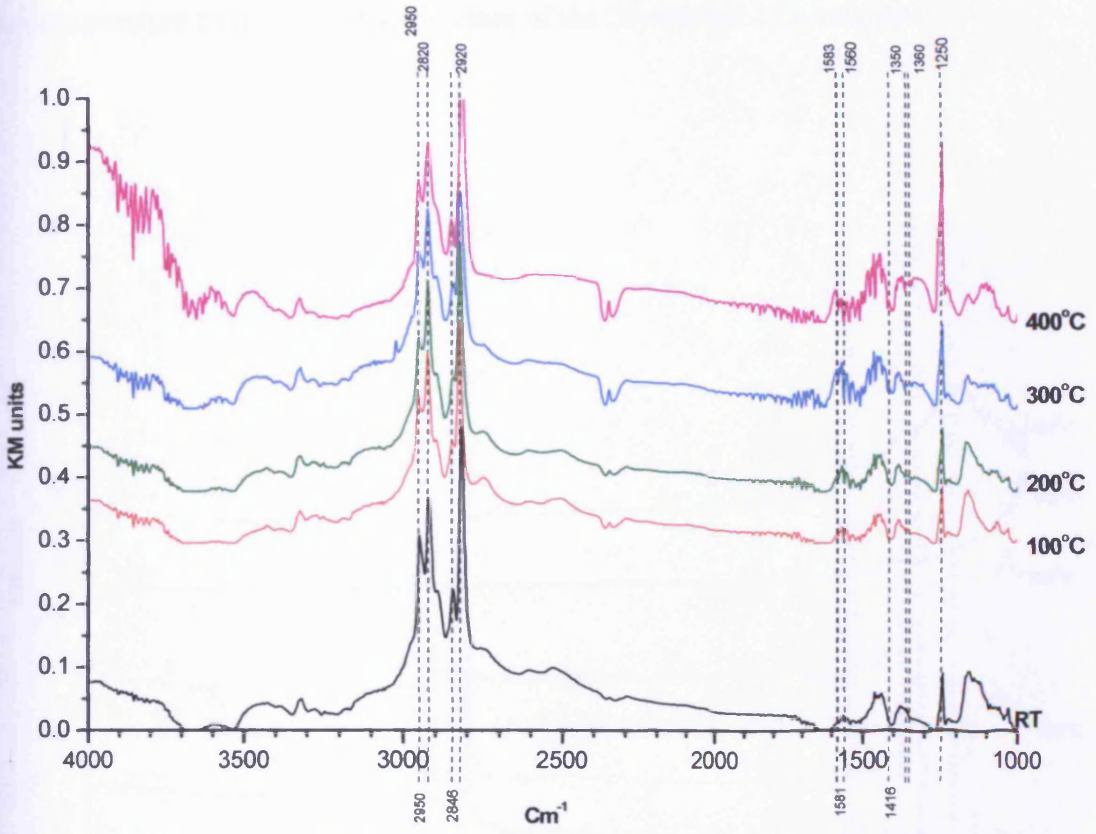

Figure 4-59: DRIFTS spectra from the adsorbed methanol over a TiO_2 catalyst a lone at different temperatures.

The figure shows the DRIFTS spectrum of methanol when introduced over TiO_2 (Degussa) at room temperature. The spectrum shows a region ranged from 1000-1700cm^{-1} and the other from 2500-3500cm^{-1}. The later region shows the C-H stretching at 2971, 2931 and 2872 cm^{-1} of the adsorbed methanol, while the band at approximately 2920 and 2820 cm^{-1} are characteristic bands of the adsorbed methoxy [19, 20]. Similarly, the band at 1460 cm^{-1} may indicate a methoxy bridged between two titanium cations. However, the bands at 2846, 1573, 1416 and 1350 cm^{-1} are the characteristic bands assigned to ν (C-H), ν_{as} (COO),σ (C-H), ν_s (COO) respectively of the adsorbed formate on TiO_2[19]. However, the band at 2950 cm^{-1} is mostly likely to be a formate, although Boccuzi[21] assigns only the band at ~2840 as due to formate on TiO_2; likewise bands in the region of 1550 and 1380 cm^{-1} are likely to be due to formate on titania. Thus, two main species appears to be dominating the titania, the

methoxy and formate, and both have considerable thermal stability. The band at 1250 cm^{-1} could be assigned to the σ (OH) of the adsorbed methanol [19].

Similarly, figure (4-60) shows the spectrum obtained when methanol was introduced at room temperature over the oxidised surface of the 20wt% Au/ TiO_2 catalyst.

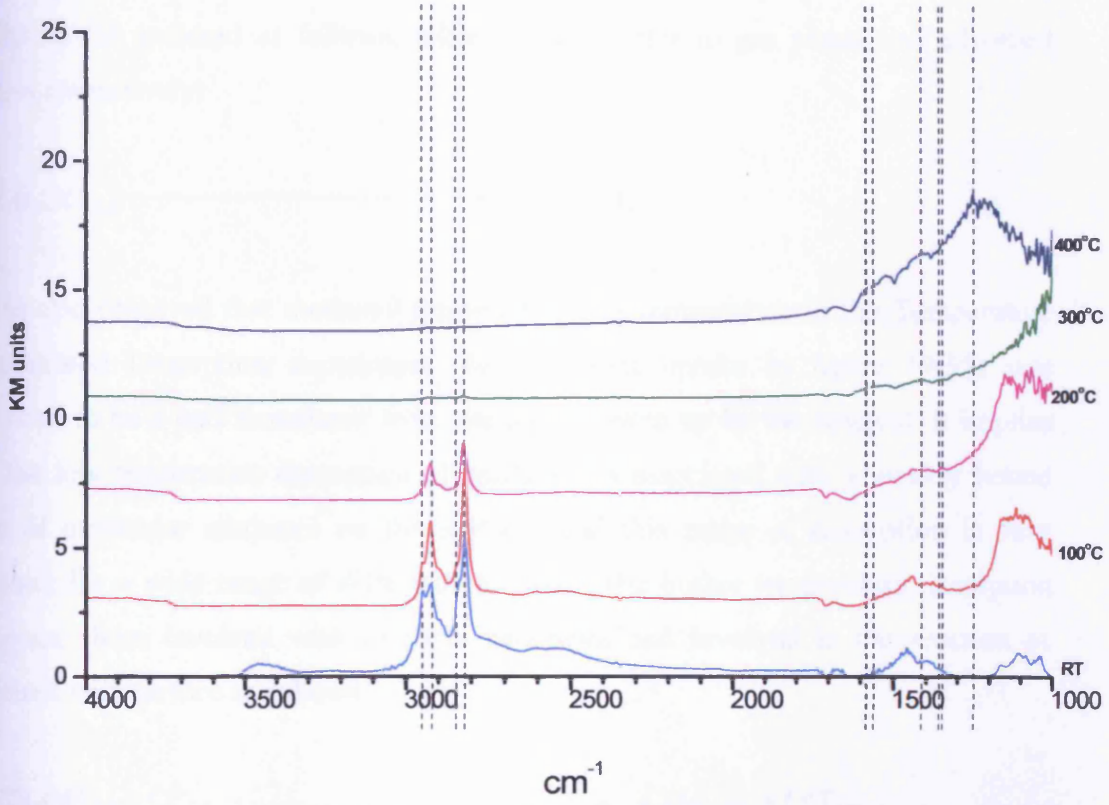

Figure 4-60: DRIFTS spectra from the adsorbed methanol over a 20wt% Au/TiO_2 catalyst at different temperatures.

Figure (4-60), shows bands in the range 1000cm^{-1} to 1700cm^{-1} and in the range 2500cm^{-1} to 3500cm^{-1}. The spectrum is similar to the TiO_2 alone but with some differences as observed with the intensities of the peaks. The high intensities may be as a result of formate formation presence due to gold and reduced coverage of methoxy species on the surface of the catalyst. The main observation is that the pair of bands at 2820,2840, 2920 and 2950 cm^{-1}, disappear upon heating to 300°C and so these may well correlate with the CO_2 and hydrogen peaks in the Temperature Programmed Desorption (figure 4-55), and with the presence of formate on TiO_2 and gold. The remaining bands are probably methoxy- derived and presumably related to

the titania species, which produce dehydrogenation and deoxygenation products at high temperature.

4.14 Mechanism of methanol oxidation over Au/TiO_2 catalyst

The mechanism of methanol oxidation over Au/TiO_2 can be proposed based on the results so far gathered as follows, where $_g$ and $_a$ refer to gas phase and adsorbed species respectively:

(a) $CH_3OH_{(g)} \longrightarrow CH3OH_{(a)}$

It was also observed that methanol desorbed at low temperature in the Temperature Programmed Desorption experiment, the methanol uptake in figure (4-55) was measured to be a half monolayer from the pulses taken up by the catalyst. It implies that the low temperature desorption of methanol is associated with a weakly bound form of molecular methanol on the surface, and this range of desorption is very common for a wide range of different catalysts. The higher temperature desorption states are those involved with catalytic processes and involved in the reaction of methanol with surface as follows:

(b) $CH_3OH_{(a)} + O^{2-}_{(a)} \longrightarrow CH_3O^-_{(a)} + OH^-_{(a)}$

(c) $CH_3OH_{(a)} + OH^-_{(a)} \longrightarrow CH_3O_{-(a)} + H_2O_{(g)}$

The steps above (b and c) indicate the various ways in which methoxy species is being form but with step b most likely to be dominant at ambient temperature for titania. Here anion vacancies are denoted as Vo^{2-}, although the electrons are more likely to be associated with cation sites, as Ti^{3+} than the vacancy itself. The presence of bands at 2920 and 2820 cm^{-1} indicate that methoxy species are formed according to steps (b, c) above.

The adsorbed methoxy formed by the reaction in (b) and (c) above is likely to be the intermediate for the formation of gas phase products as follows:

(d) $2CH_3O^-_{(a)} \longrightarrow CH_3OCH_3 + O^{2-}_{(a)}$ (very significant on TiO_2 alone)

(e) The adsorbed methoxy may also react with an oxygen vacancy on the surface and give methane, which is observed as a product at high temperature from titania, even when Au is present.

(i) $CH_3O^-_{(a)} + Vo^{2-} \longrightarrow CH_3^-{}_{(a)} + O^{2-}_{(a)}$

(ii) $CH_3^-{}_{(a)} + OH^-_{(a)} \longrightarrow CH_{4\,(g)} + O^{2-}_{(a)}$

The appearance of particular peaks, which indicates the presence of adsorbed formates species, which may be formed by the following reaction,

(f) $CH_3O^-_{(a)} + O^{2-}_{(a)} \longrightarrow H_{2\,(g)} + Vo^{2-} + HCOO^-_{(a)}$

The formates adsorbed on the catalyst surface are subsequently decomposed to give the following

(g) $2HCOO^-_{(a)} \longrightarrow 2CO_{2\,(g)} + H_{2\,(g)} + 2e^-$

These steps are similar to those proposed earlier for methanol reaction with Cu [21] and Zn [22, 23].

4.15 CHARACTERISATION OF CATALYST

4.15.1 Surface Area Measurement

Surface area measurements of the catalysts are another important technique in understanding the performance of the catalyst. The micro structural development of the BET surface area of the catalyst was measured using a Micromeretics Gemini

2360 surface area machine. The surface area of TiO_2 and that of Au/TiO_2 was measured. As always with TiO_2, high surface area was observed due to nature of the TiO_2.Based on our measurement the surface area was found to be $50m^2/g$.

4.15.2 XRD

The pre- reaction XRD data information regarding TiO_2 and Au/TiO_2 catalyst has been fully discussed in (3.5.1) of chapter 3. However, figure 4- 61 and 4-62 shows the post reaction aerobic and anaerobic for methanol reaction respectively.

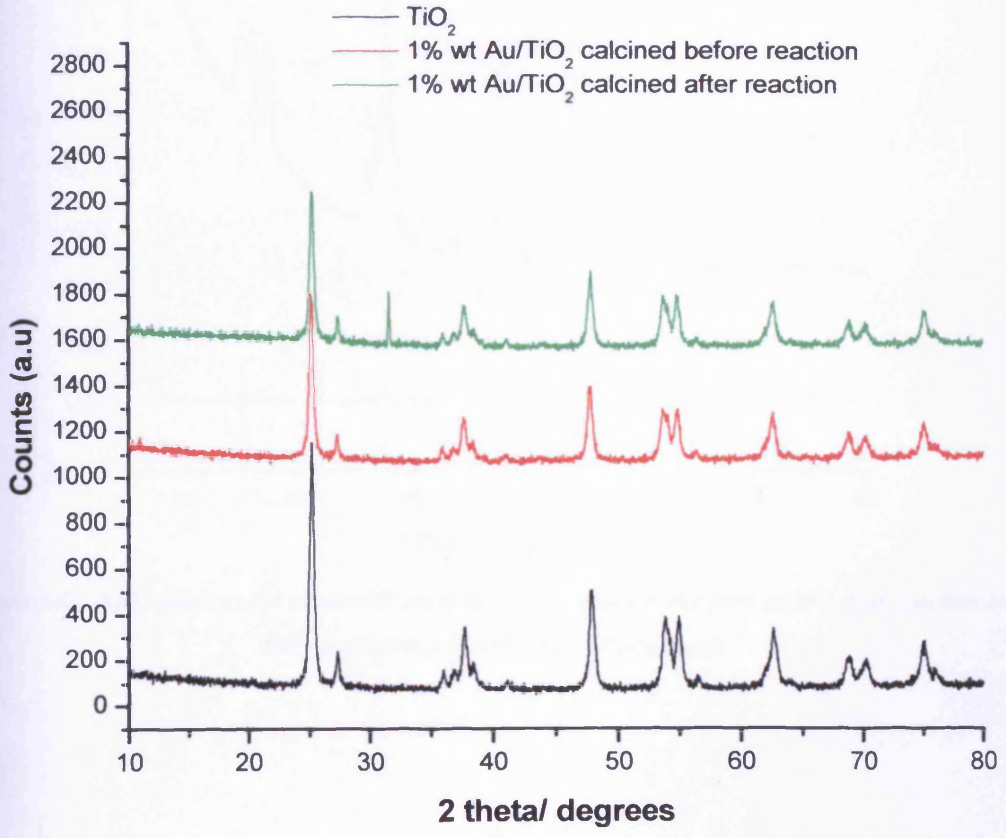

Figure 4-61: XRD patterns for aerobic methanol oxidation (in the flow of 10%O_2/ He) post reaction over TiO_2 and calcined 1wt% Au/TiO_2 catalysts

The XRD pattern of the post reactor Au/TiO_2 catalyst of methanol oxidation (figure 4-61) shows that there was no appearance of Au peaks in the post reactor. It indicates that the catalyst remained the same, even after the methanol reaction, no transformation of phases occurred. At the end of the methanol oxidation reaction

(aerobic), the main phases observed are anatase and rutile as seen in the pre-reactor catalyst.

However, when the anaerobic methanol reaction was carried, the post reactor catalyst indicated that there is increase in the phases of TiO_2 as shown by the XRD pattern of the post reactor catalyst. Both anatase and rutile phases intensities increases.

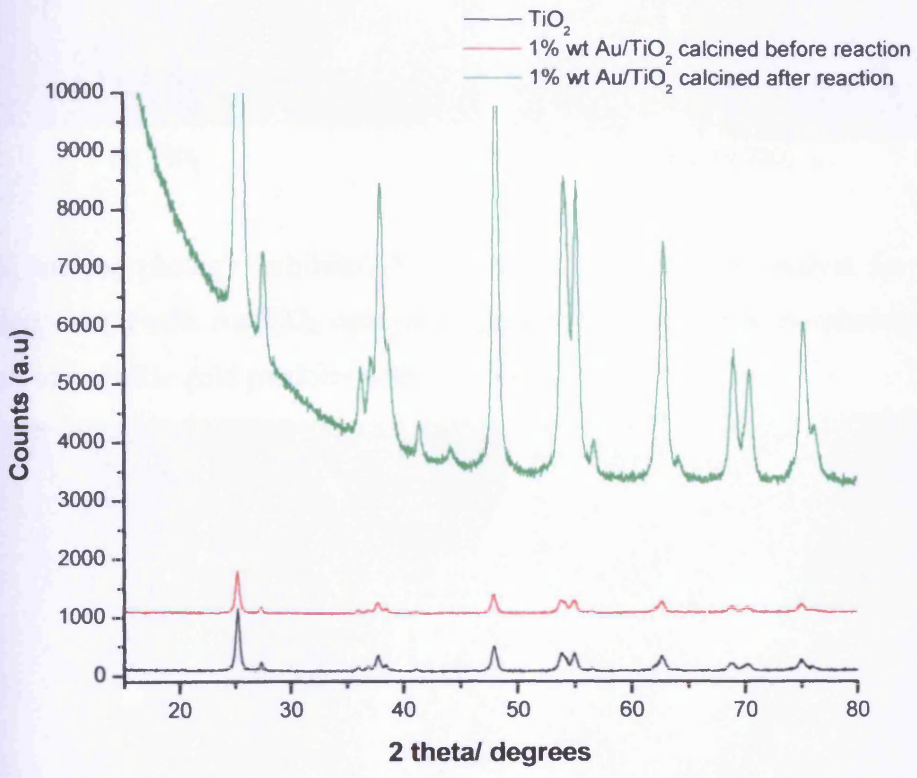

Figure 4-62: XRD patterns for anaerobic methanol oxidation (in the flow of He) post reaction over TiO_2 and calcined 1wt% Au/TiO_2 catalysts

4.15.3 SEM

Figure 4-63 shows the SEM images for TiO_2 alone (a) and (b) calcined Au/TiO_2 catalyst dried at 400°C for 2h. The post reactor calcined 1wt% Au/TiO_2 catalyst dried at 400°C for 2h (figure 4-63c). The figure shows that the methanol oxidation (aerobic) post reactor calcined 1wt% Au/TiO_2 catalyst demonstrated a morphology (porous irregular gold particles of varying sizes < 4.6μm to approximately 8.6μm).

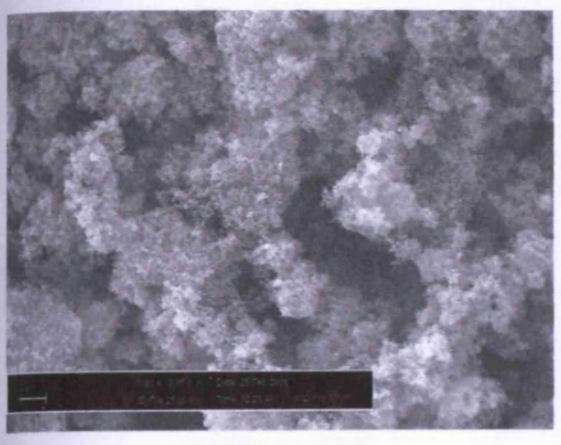

(a) TiO_2

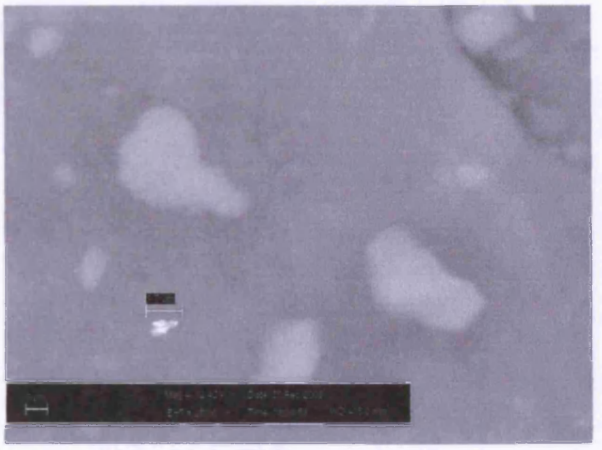

(b) *1wt% Au/TiO_2*

While the morphology exhibited by anaerobic post reactor catalyst for methanol reaction over 1wt% Au/TiO_2 catalyst (Figure 4-63d) shows a morphology forming porous of irregular gold particles with varying sizes from 1.7μm.

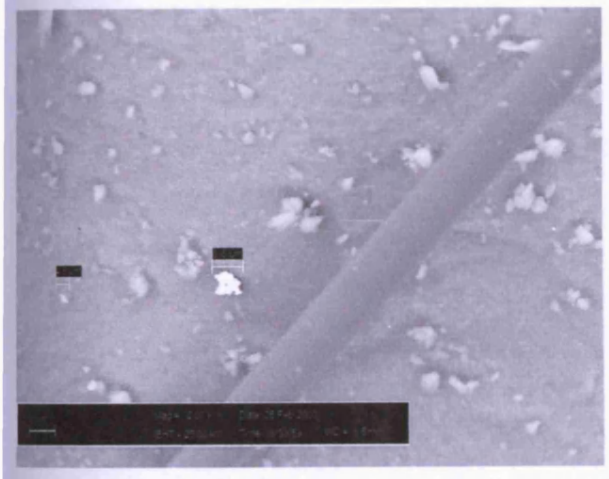

(c) *1wt% Au/TiO_2*

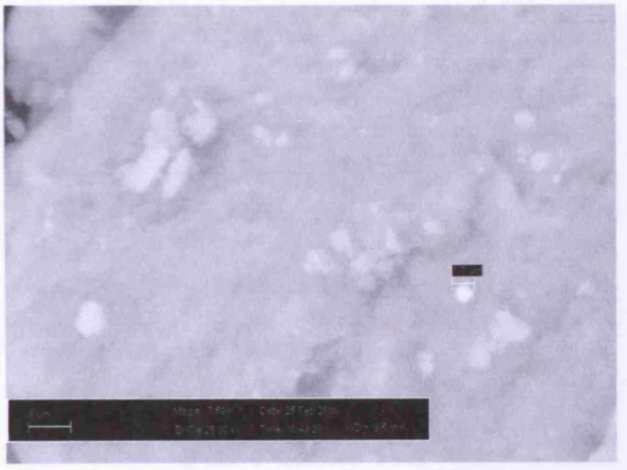

(d) *1wt% Au/TiO_2*

Figure 4-63: Scanning Electron Microscopy images for post reactor catalyst for TiO_2 (a), 1wt% Au/TiO_2 catalysts (calcined) (b), post reactor methanol oxidation (aerobic) (c) and anaerobic (d) over 1wt% Au/TiO_2 catalysts (calcined) prepared by deposition precipitation

4.15.4 XPS

The XPS spectra for the methanol oxidation (aerobic) and the anaerobic post reaction over 1wt% Au/TiO_2 catalyst is shown (figure 4-64a and b) respectively. The

figure (4-64) indicates that the Au 4*f* envelope is still around 87 eV with a small shift of 2

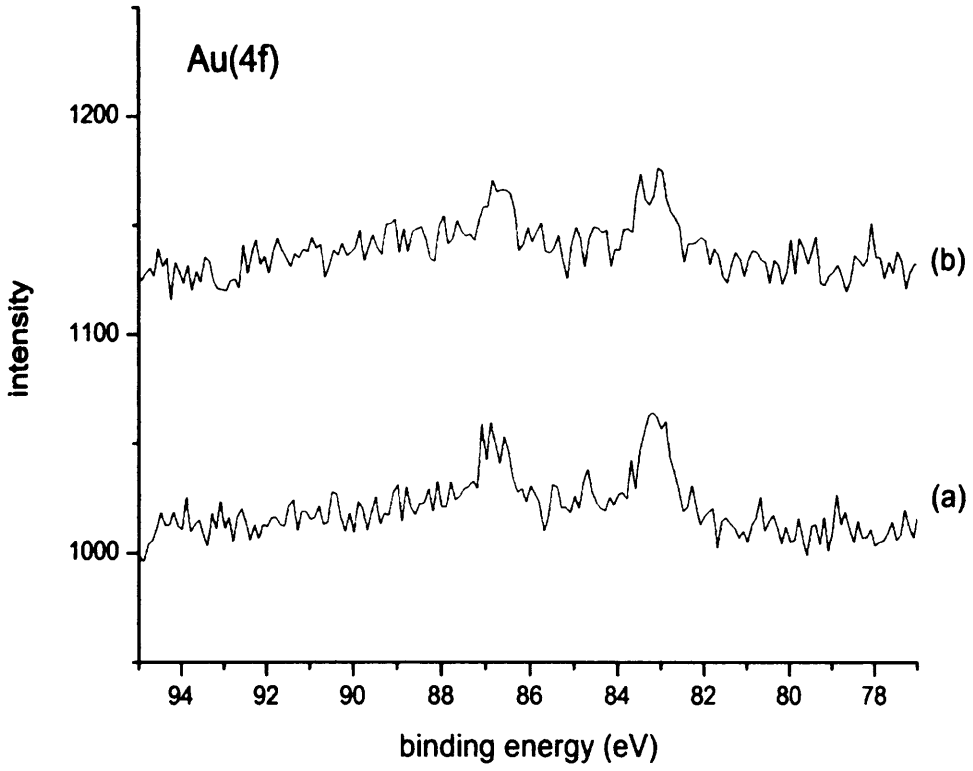

Figure 4-64: Au (4f) spectrum for (a) 1wt% Au/TiO_2 for methanol post reactor aerobic (calcined) catalyst, (b) 1wt% Au/TiO_2 for methanol post reactor anaerobic (calcined) catalysts

eV while the gold $4f_{7/2}$ peak was observed at about 83eV. These features indicate that the oxidation state of gold in the catalyst remained Au^{x+} and Au^0 and does not change even after the reaction. The existence of gold in oxidation state as Au^{x+} and Au^0 was the same in all aerobic methanol oxidation reaction and anaerobic reaction.

4. 16 Control Experiments

4.16.1 Temperature Programmed Reaction of methanol over TiO_2 catalyst

As part of a control experiment, the methanol oxidation reaction was carried over TiO_2 (Degussa) catalyst alone (figure 4-65). The reaction is a complete oxidation

reaction, with dehydration at low temperature and dehydrogenation to CO at high temperature.

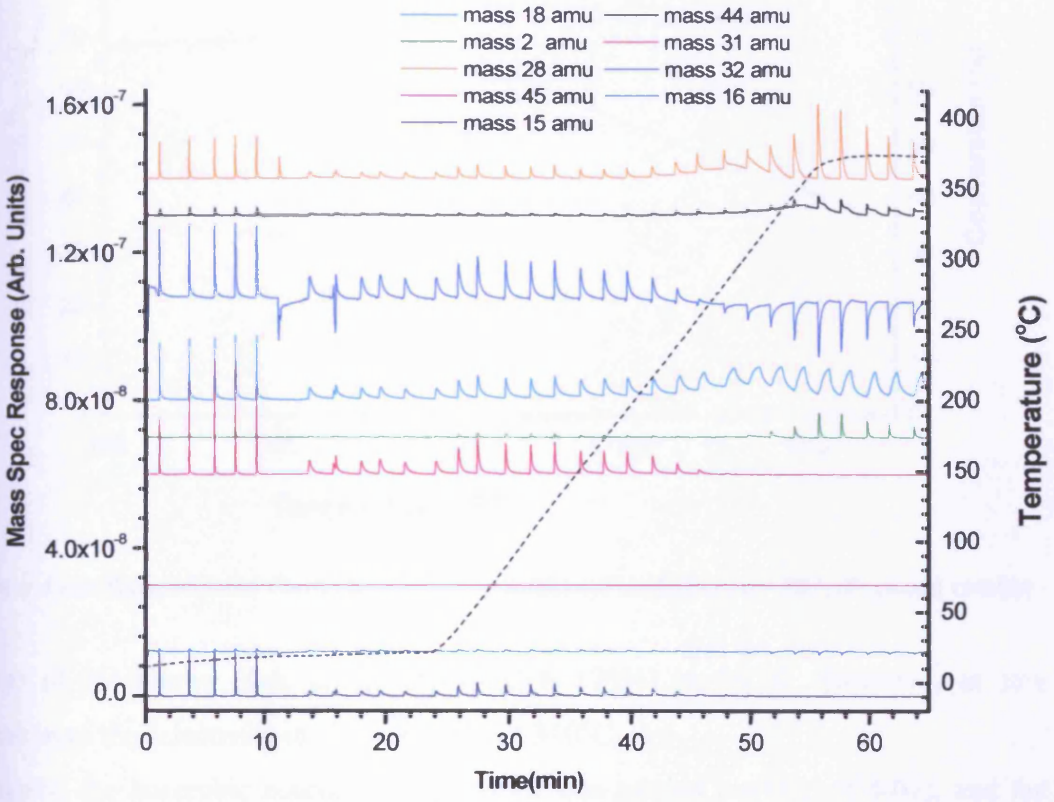

Figure 4-65: Temperature Programmed Pulse Flow Reaction of Methanol oxidation over TiO_2 (Degussa) Catalyst

Figure (4-66) shows high selectivity to CO_2 (70%) at 350°C. However, at low temperature the selectivity of CO was 50% at 310°C.

Similarly, the anaerobic reaction of methanol was carried out (figure 4-67), and the reaction involved is a complete oxidation, with dehydration at low temperature as well as dehydrogenation and deoxygenation at high temperature.

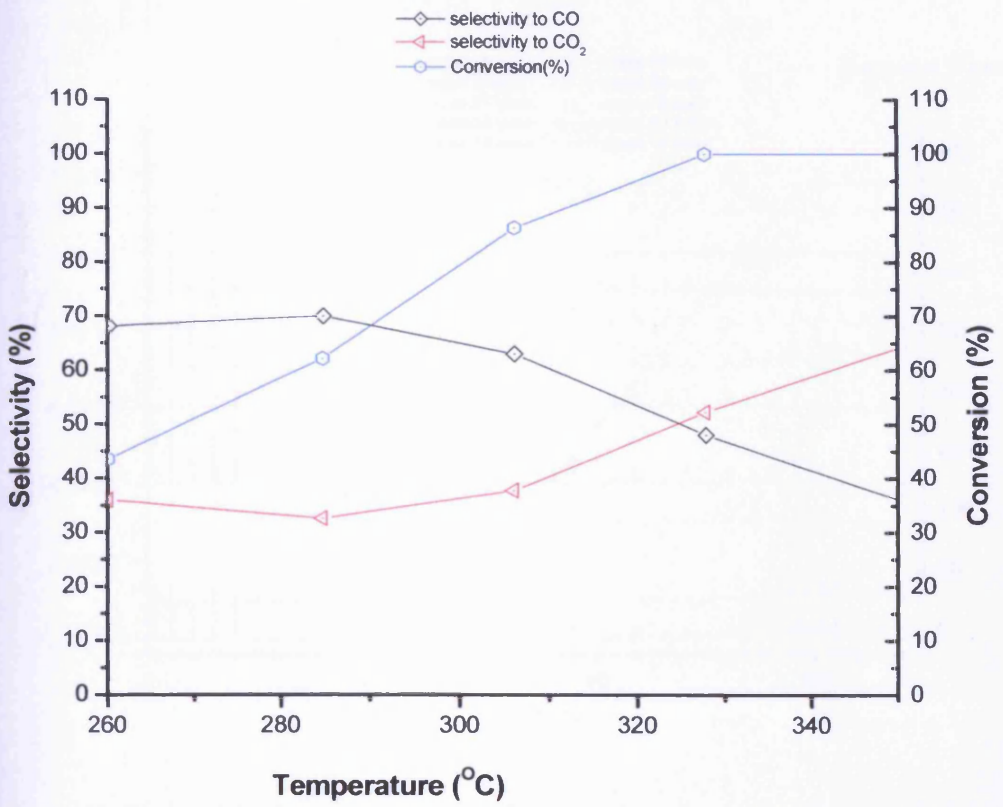

Figure 4-66: Selectivity and Conversion graph of methanol oxidation over TiO_2 (Degussa) catalyst

Figure (4-66) shows high selectivity to CO_2 (70%) at 350°C. However, at low temperature the selectivity of CO was 50% at 310°C.

Similarly, the anaerobic reaction of methanol was carried out (figure 4-67), and the reaction involved is a complete oxidation, with dehydration at low temperature as well as dehydrogenation and deoxygenation at high temperature.

Figure (4-68) shows at low temperature, more dimethyl ether selectivity was observed (80%) at 240°C with methanol conversion being 25%. The dimethyl ether selectivity drops when the temperature reached 320°C and CO and methane selectivity begin to rise and continue until the temperature reached 370°C and the conversion was 99% with CO and methane selectivity being 35% and 55% respectively.

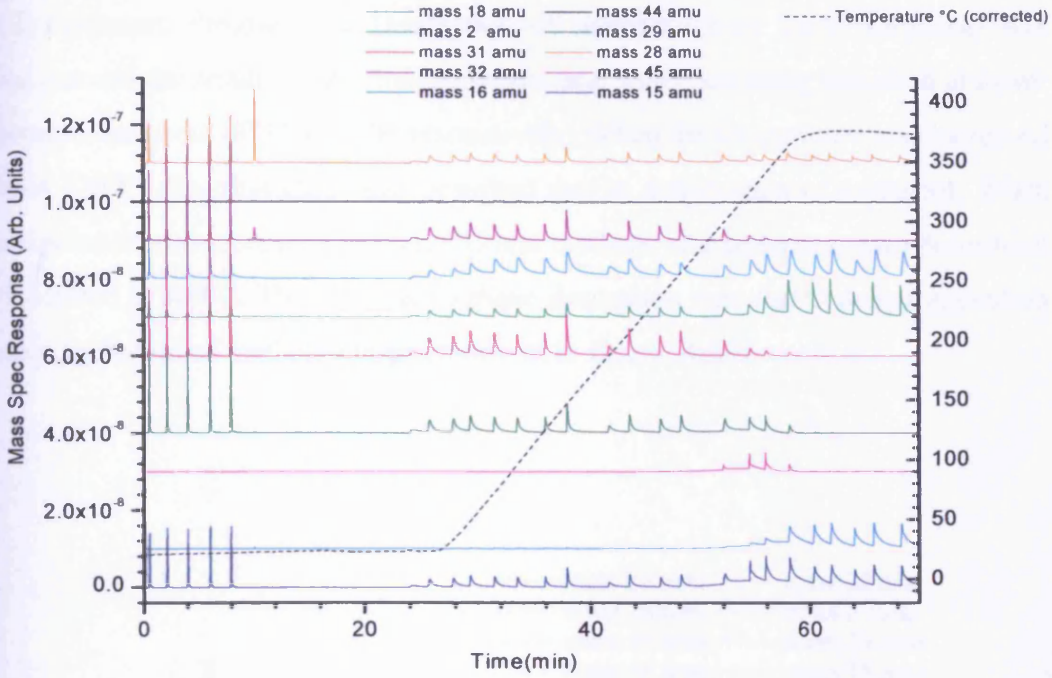

Figure 4-67: Temperature Programmed Pulse Flow Reaction of anaerobic reaction of Methanol over TiO_2 (Degussa) Catalyst

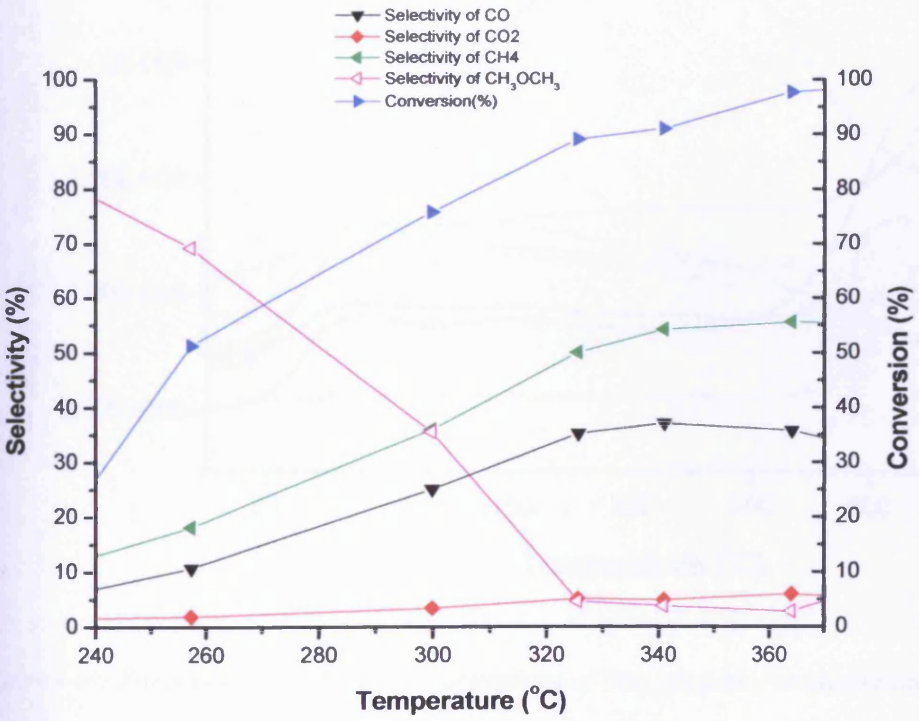

Figure 4-68: Selectivity and Conversion graph of anaerobic methanol reaction over TiO_2 (Degussa) catalyst

4.16. 2 Temperature Programmed Desorption of Methanol over TiO_2

The Temperature Programmed Desorption of methanol over TiO_2 (Degussa) was carried out and the result shows that, methanol and water are being desorbed at lower temperature (at about 80°C and 100 respectively).When the temperature was increased to about 320°C, dimethyl ether was desorbed due to dehydration of methanol. When the temperature was increased further, CO and methane was desorbed, with desorption peaks centred at 360°C. The CO and methane desorption was due to dehydrogenation and deoxygenation of methanol respectively as in figure (4-69)

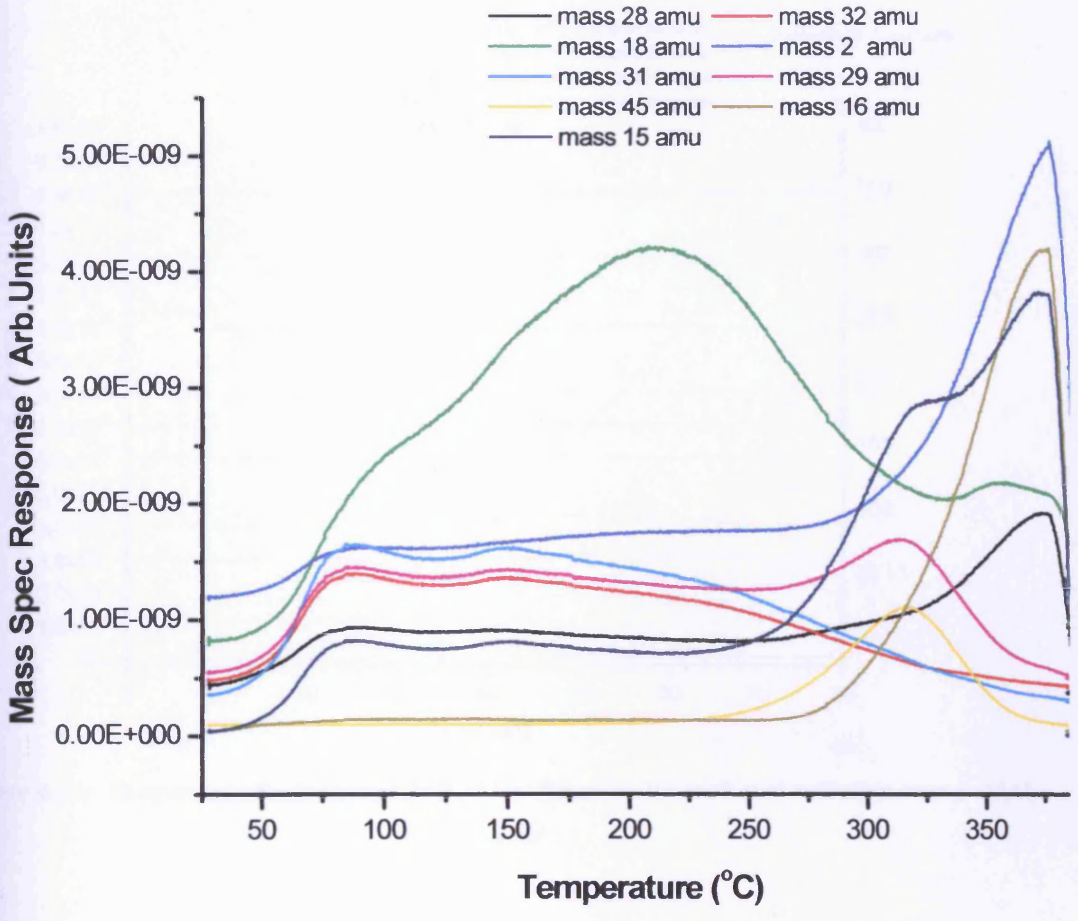

Figure 4-69: Temperature Programmed Desorption of TiO_2 (Degussa) catalyst saturated with methanol at room temperature

4.17 Methanol oxidation over Au/γ–Al_2O_3

4.17.1 Temperature Pulse Flow Reaction of methanol over a 1wt% Au//γ–Al_2O_3 catalyst

The methanol oxidation reaction was also investigated over 1wt% Au/γ-Al_2O_3. In order to understand the reaction involved and the role of the Au and the support, different preparation techniques were employed. The support (γ-Al_2O_3) alone was first investigated using Temperature Programmed Pulse Flow Reaction and Temperature Programmed Desorption in order to get an insight of the role of the support with respect to methanol oxidation.

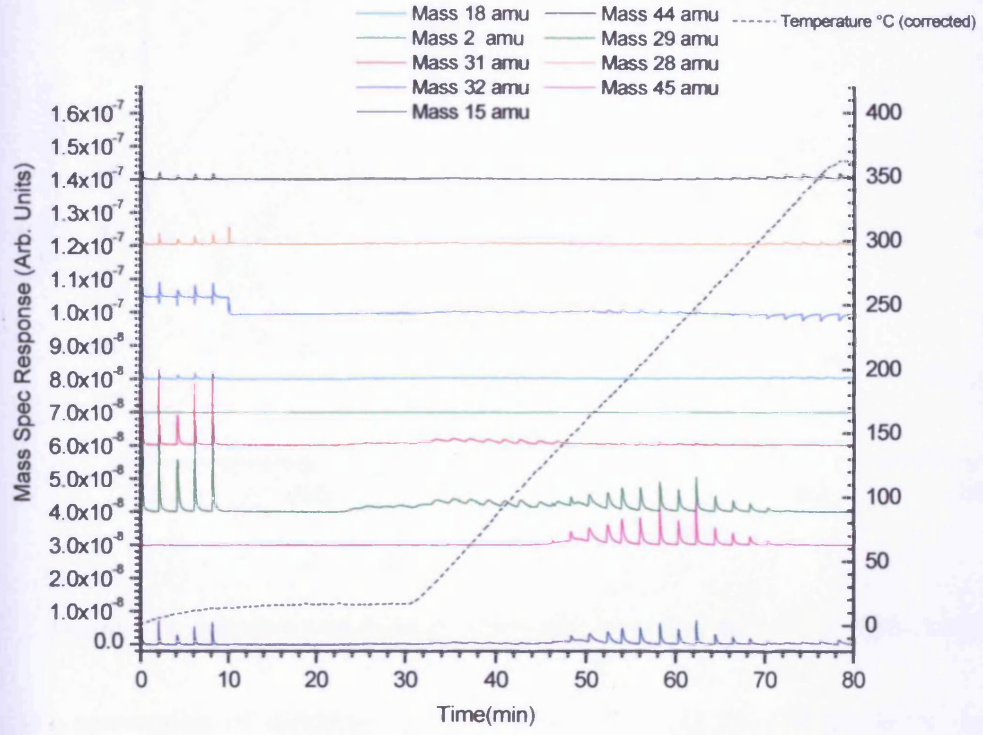

Figure 4-70: Temperature Programmed Pulse Flow Reaction for methanol oxidation over γ–Al_2O_3 Catalyst

0.5g of γ–Al_2O_3 with surface area of 128m^2/g was loaded in the U tube of the oven of the reactor and the Temperature Programmed Pulse Flow Reaction was carried out (figure 4-70).

The results in figure 4-70 indicate the saturation of methanol on the γ–Al_2O_3 surface (the appearance of mass 31 and 29 amu signals) at about 25 minutes. The amount of

methanol used to saturate the surface was about 10µl. Similarly, as the temperature was raised and the injection was continued, the dehydration to dimethyl ether begins from 50 minutes (The appearance of mass 45 and 15 amu signals). Nevertheless, the dehydration continues up to 70 minutes while the oxidation begins with CO and CO_2 being the products of oxidation. When the data was integrated and analysed, figure (4-71) will be obtained:

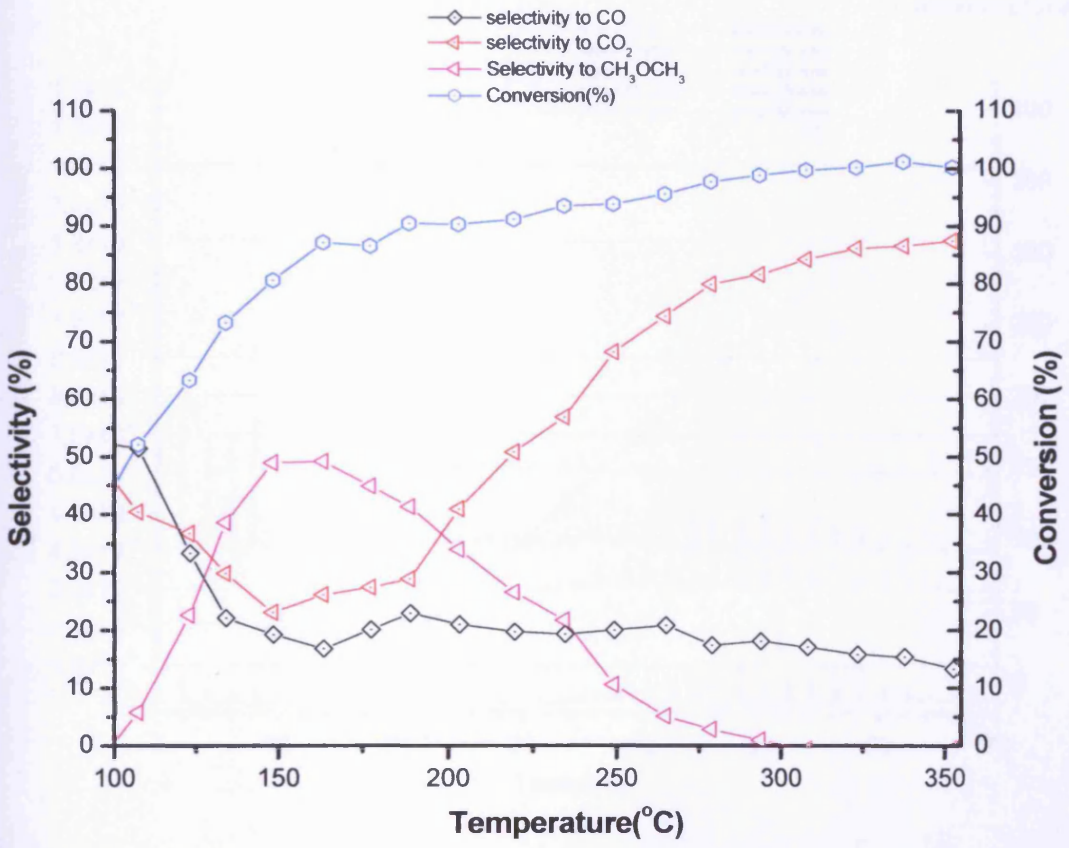

Figure 4-71: Selectivity and conversion for methanol oxidation over a γ–Al_2O_3 Catalyst

As the conversion of methanol reached 50%, dehydration and products begin to emerge and the selectivity to dimethyl start to increase. High selectivities to dimethyl ether (~50%) were observed at 150°C and the conversion of methanol was 85%. However, when the temperature was increased, dimethyl selectivity decreases as the temperature reached 300°C.Similarly, the CO_2 selectivity begin to increase as the temperature reached 180°C and continue until its selectivity was almost 89%. Simultaneously, the CO selectivity decreases at the same temperature (180°C) and continues in a steady state through out the course of the experiment. The dehydration

observed from 100 to 300°C was due to high surface coverage and retention time of methoxy species at these temperatures.

In the same manner, an anaerobic reaction of methanol over a γ–Al_2O_3 catalyst was carried out (figure 4-72).

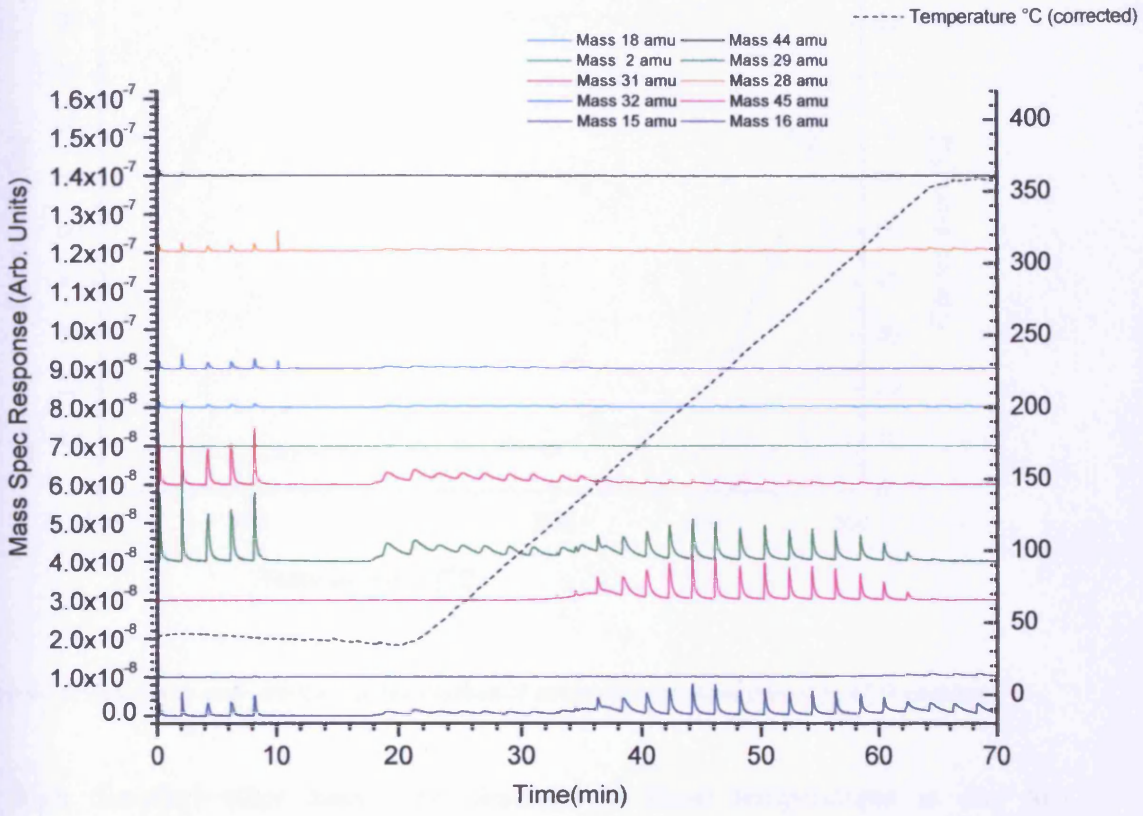

Figure 4-72: Temperature Programmed Pulse Flow Reaction for methanol anaerobic reaction over a γ–Al_2O_3 Catalyst

Figure (4-72) shows about 10µl of methanol was needed to saturate the surface; the appearance of mass 31 and 29 amu signals indicate the saturation of the catalyst at room temperature. However, after 35 minutes, dehydration to dimethyl ether begins and at 65 minutes, it stops. Deoxygenation to methane then begins and continues to increase. More CO was observed due to dehydrogenation but with less CO_2 being produced at high temperature.

Figure (4-73) shows the integrated and analysed data of figure (4-72). As the conversion of methanol was 40%, the catalyst activity was towards dimethyl ether selectivity. The dimethyl ether selectivity was 70% when the temperature was 105°C,

and as the conversion of methanol was increased to 85% the selectivity to dimethyl, ether was 86%.

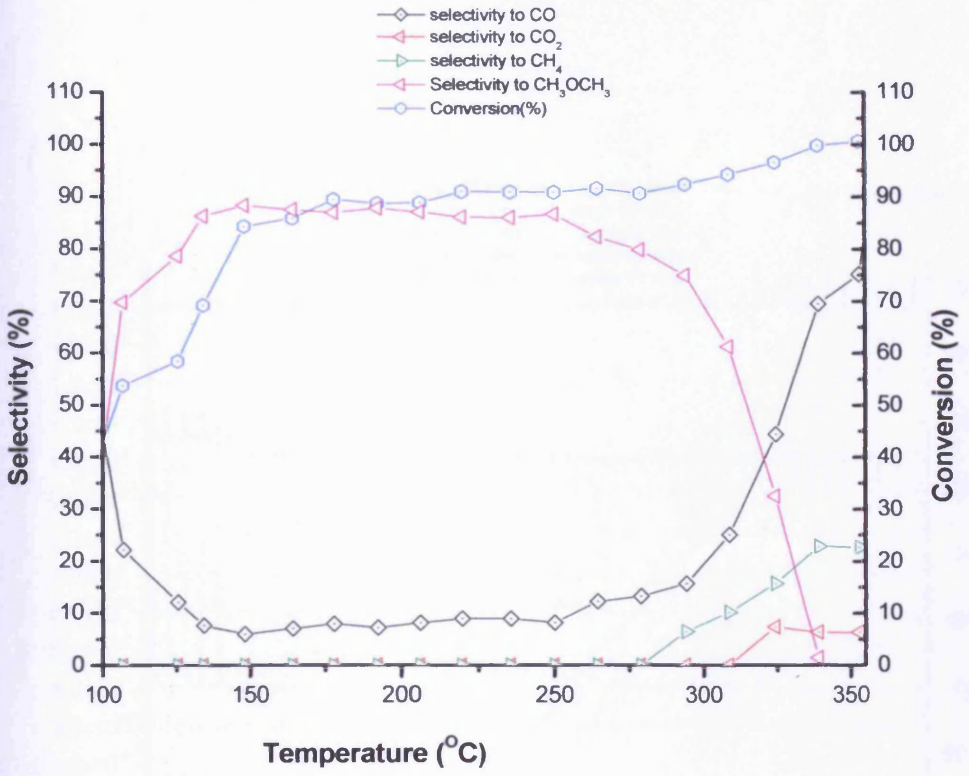

Figure 4-73: Selectivity and conversion for methanol anaerobic reaction over a γ–Al_2O_3catalyst

The high dimethyl ether selectivity observed at these temperatures is due to dehydration caused by a high surface coverage of methoxy species. The selectivity to dimethyl ether continues, and then drops and the CO selectivity begins to increase as the conversion of methanol begins to increase to 95%. Nevertheless, when the temperature reached 340°C, no dimethyl ether was seen and selectivity to CO was 75% as the conversion of methanol reached 100%. However, the increase in selectivity to CO at 250°C was accompanied by the increase in methane selectivity due to deoxygenation and CO_2. The selectivity to CO and methane was 22% and 6% respectively when methanol conversion reached 100%.

4.17.2 Temperature Programmed Reaction of methanol over *Au*/γ-Al_2O_3catalyst

A freshly 1wt% Au/γ-Al_2O_3 catalyst was prepared by two different methods; namely, deposition precipitation (DP) and the incipient wetness impregnation (IW).

4.17.3 Au/γ-Al_2O_3catalyst prepared by Deposition Precipitation

The Au/ γ-Al_2O_3 catalyst prepared by deposition precipitation shows different behaviour when subjected to Temperature Pulse Flow Reaction. (Figure 4-74).

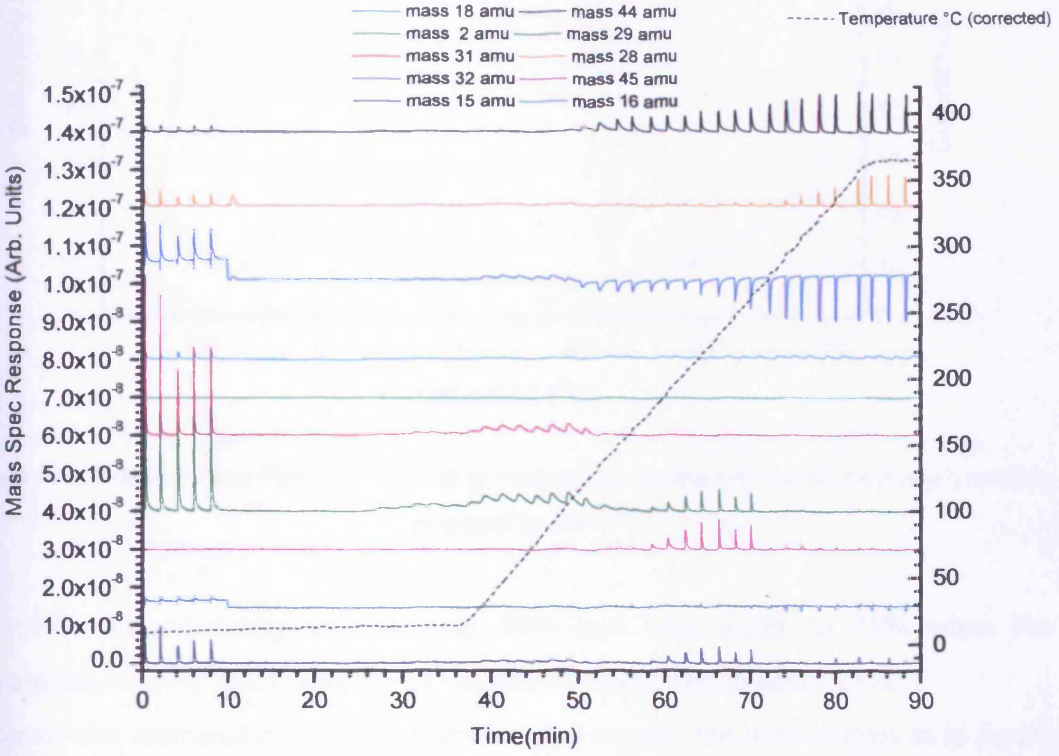

Figure 4-74: Temperature Programmed Pulse Flow Reaction form methanol oxidation over a 1wt%Au/γ–Al_2O_3 Catalyst prepared by DP

Saturation with methanol occurs at about 28 minutes (the appearance of mass 29 and 31) and at 60 to 70 minutes, the evolution of dimethyl ether was observed. The reaction was complete oxidation with CO, CO_2 and H_2O being the main products.

Figure (4-75) shows when the conversion of methanol was 50%, the activity of the catalyst was towards the CO_2 production and continues to increase until the conversion of methanol reached 100%, and then selectivity to CO_2 drops. Dehydration begins and the selectivity to dimethyl ether begins to increase until the temperature reached 250°C, although, the selectivities were very low (<10%).

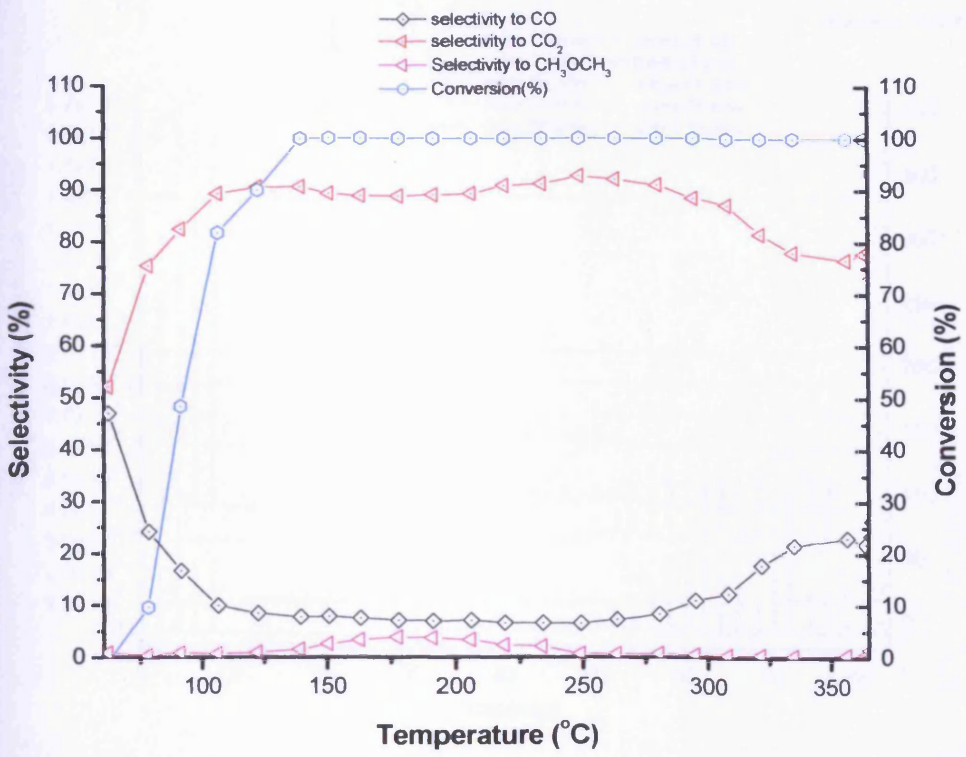

Figure 4-75: Selectivity and Conversion graph of methanol oxidation over 1wt% Au/γ–Al_2O_3 catalyst prepared by DP

At 250°C, the selectivity to CO_2 was 90% and later drops to 75% when the temperature reached 325°C and the CO selectivity increased to about 25%.

The anaerobic methanol reaction was also carried out and the result shows as in figure (4-76). It shows a dehydration and deoxygenation of methanol between 50 to 78 minutes, dehydrogenation begins, more CO was observed, and at higher temperature, the CO_2 begins to emerge, presumably due to a higher surface oxidation reaction at these temperatures.

In the same manner, when the data was integrated and analysed, figure (4-77) was obtained. The figure shows an increase in the selectivity of methane and dimethyl ether, when the conversion was only 50% and the temperature was only 130°C. However, when the conversion reached 100%, the temperature was about 180°C and the selectivity to dimethyl ether was 90%. Nevertheless, the dimethyl ether selectivity begins to decrease as the temperature reached 250°C. The CO and methane selectivity begin to increase and continue until the selectivity was 40 and 8 % respectively. CO_2 was observed to be evolved as the temperature increase to 300°C, with selectivity less than 5% and later drops as the temperature reached 350°C.

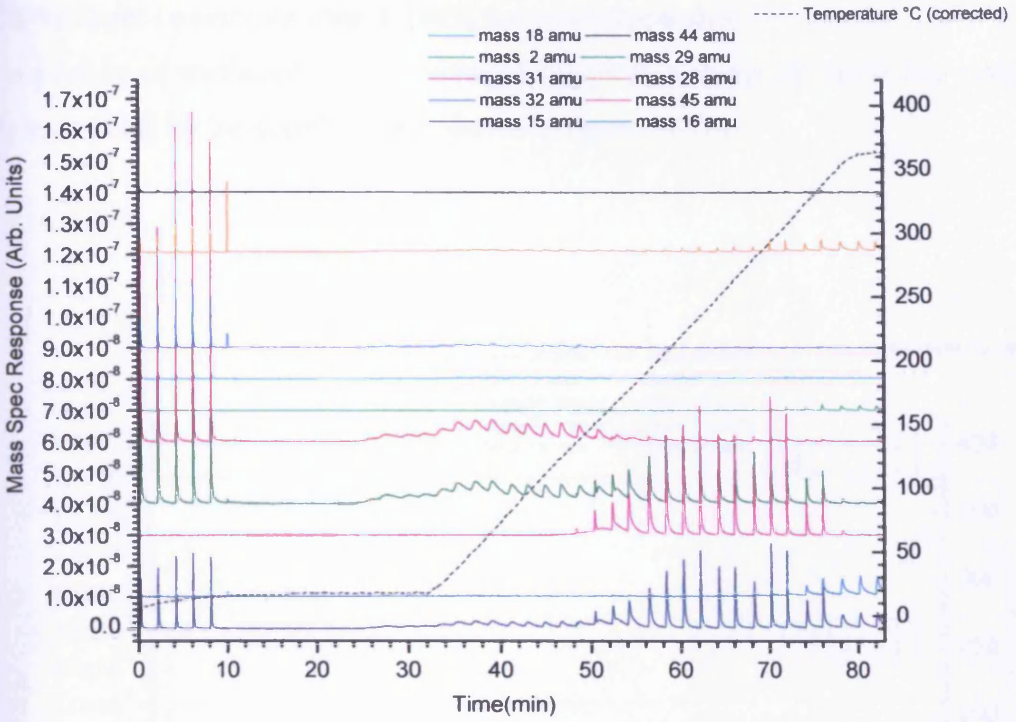

Figure 4-76: Temperature Programmed Pulse Flow Reaction for methanol anaerobic reaction over a 1wt% Au/γ–Al_2O_3 catalyst prepared by DP

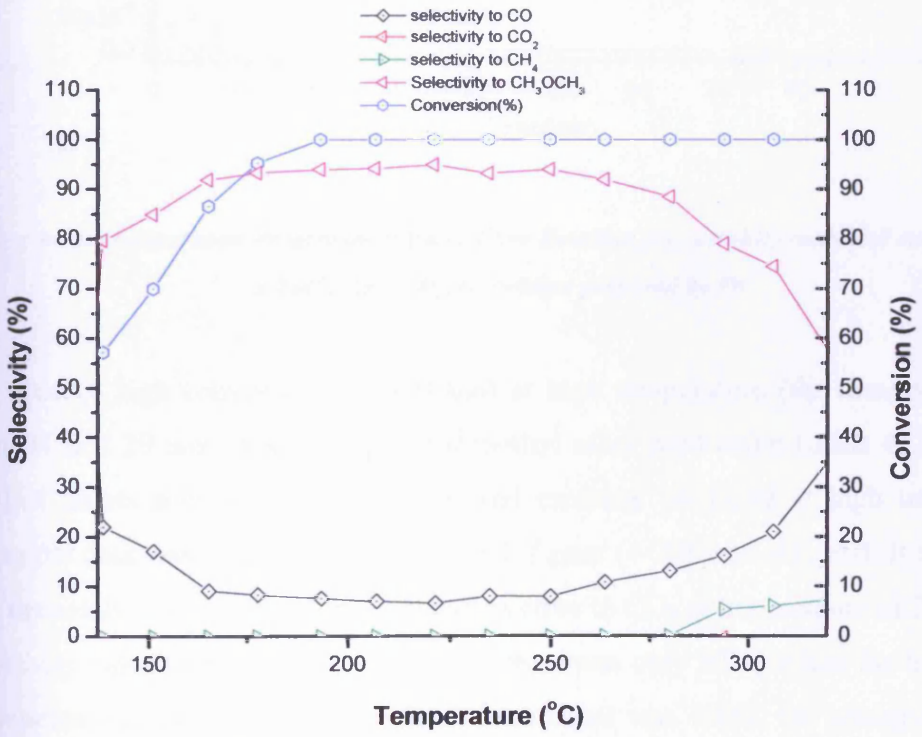

Figure 4-77: Selectivity and conversion with temperature for methanol anaerobic reaction over a 1wt% Au/γ–Al_2O_3 catalyst prepared by DP

4.17.4 Methanol oxidation over a *1wt% Au/γ–Al$_2$O$_3$* catalyst

The oxidation of methanol over a prepared incipient wetness of 1wt% Au/γ-Al_2O_3 catalyst prepared by incipient wetness shown in figure (4-78).

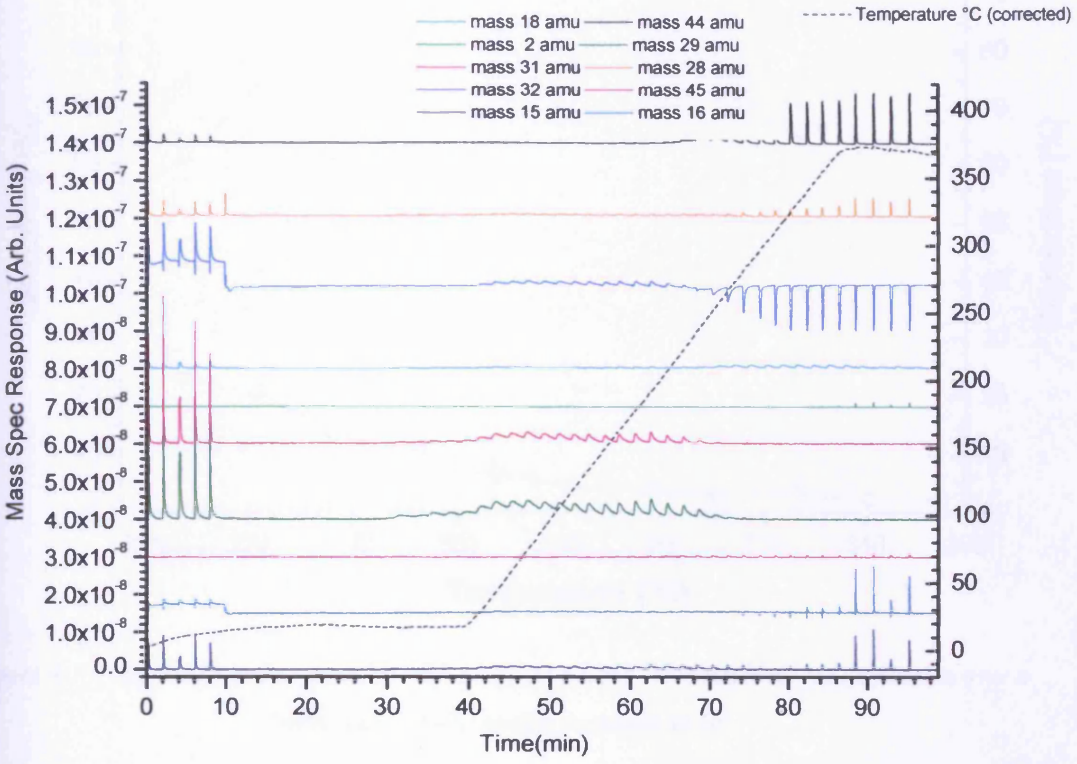

Figure 4-78: Temperature Programmed Pulse Flow Reaction for (aerobic) methanol oxidation over a 1wt% Au/γ–Al$_2$O$_3$ catalyst prepared by IW

We observe high conversion of methanol at high temperature (the disappearance of mass 31 and 29 amu) and no sign of dimethyl ether production (mass 45 amu). The catalyst shows selectivity to CO, CO_2 and methane produced at high temperature. When the data was integrated and analysed, figure (4-79) was obtained. It also shows that the catalyst activity was very much selective to CO_2 at temperature of 200°C with selectivity value being 70% and the conversion was only 50%. When the temperature was increase to 260°C, the conversion of methanol was 100%, the selectivity to CO_2 was 93% with CO selectivity being less than 5%.

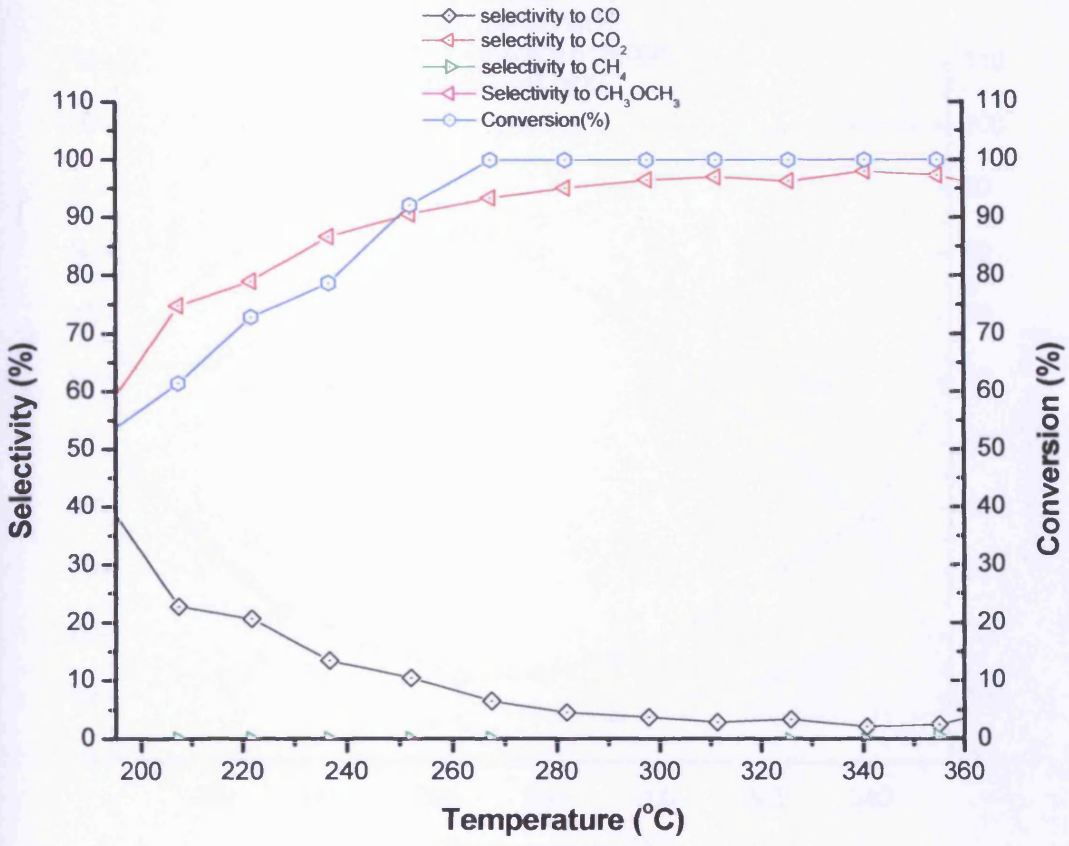

Figure 4-79: Selectivity and conversion with temperature for (aerobic) methanol oxidation over a 1wt% Au/γ–Al_2O_3 catalyst prepared by IW

Figure (4-80) shows the integrated data for methanol when reacted anaerobically over a 1wt% Au/γ-Al_2O_3 catalyst. Methanol conversion was 60% as the temperature was 200°C with selectivity to dimethyl ether of 65%. When the temperature was increased to 260°C, the dimethyl ether selectivity was high (90%) and the conversion of methanol was 80%. Nevertheless, the CO selectivity begins to increase due to dehydrogenation and as the temperature reached 280°C, the CO_2 begins to emerge and continue to increase. Simultaneously, the selectivity of methane begins to increase as the temperature reached 310°C.The selectivity to methane and CO_2 was 5 and 20% respectively and by the time when the temperature reached 350°C and methanol conversion was 100%.

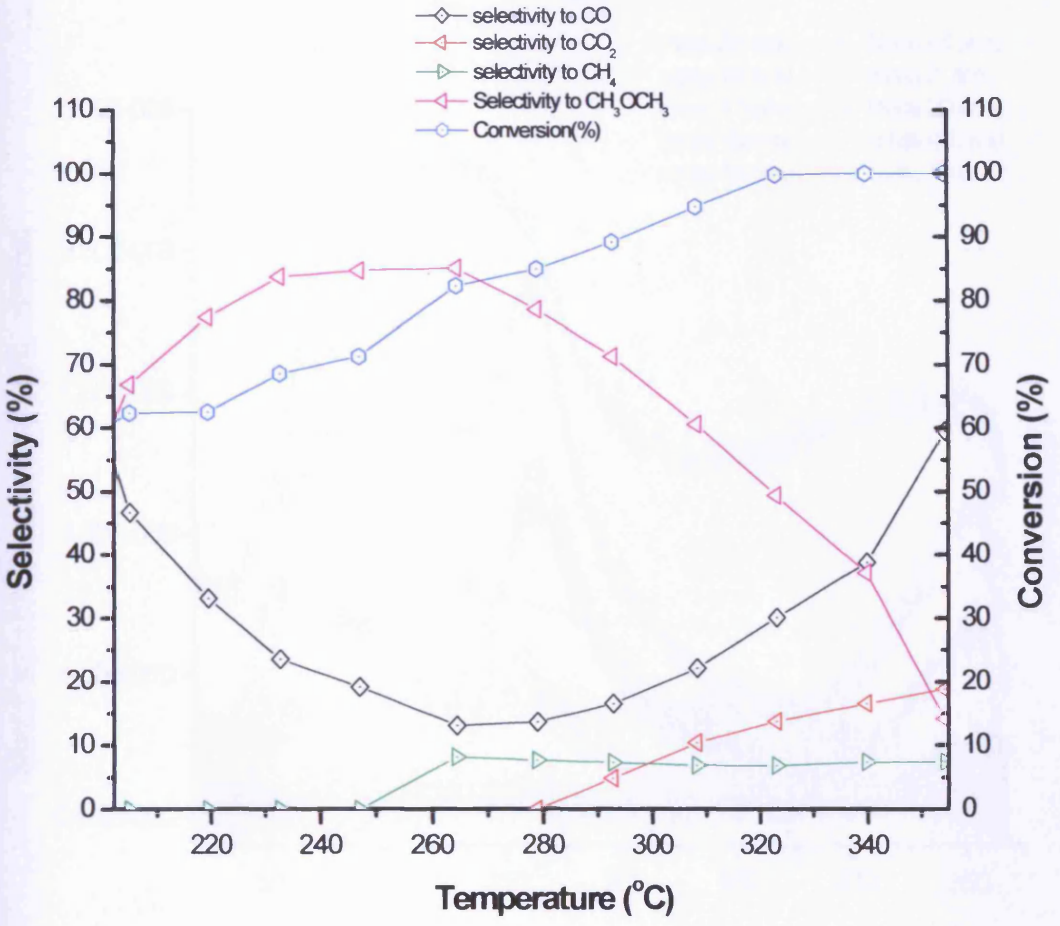

Figure 4-80: Selectivity and conversion with temperature for methanol anaerobic reaction over a 1wt% Au/γ–Al_2O_3 catalyst prepared by IW

4.17.5 Temperature Programmed Desorption of methanol over 1%wt Au/ γ–Al_2O_3

Temperature Programmed Desorption (TPD) was carried out over γ–Al_2O_3 and 1wt% Au/γ-Al_2O_3 catalysts saturated with methanol. Figure (4-81) shows the TPD of methanol over γ–Al_2O_3 alone, indicating desorption of methanol at lower temperature (80°C). However, when the temperature was increased to 172°C, the desorption peak of dimethyl ether was observed. In the same manner, as the temperature reached 350°C, CO and methane desorption peaks was also observed. This implies that the catalyst is selective to dehydration due to the high coverage of methoxy at low temperature and dehydrogenation/ deoxygenation of methanol at high temperature.

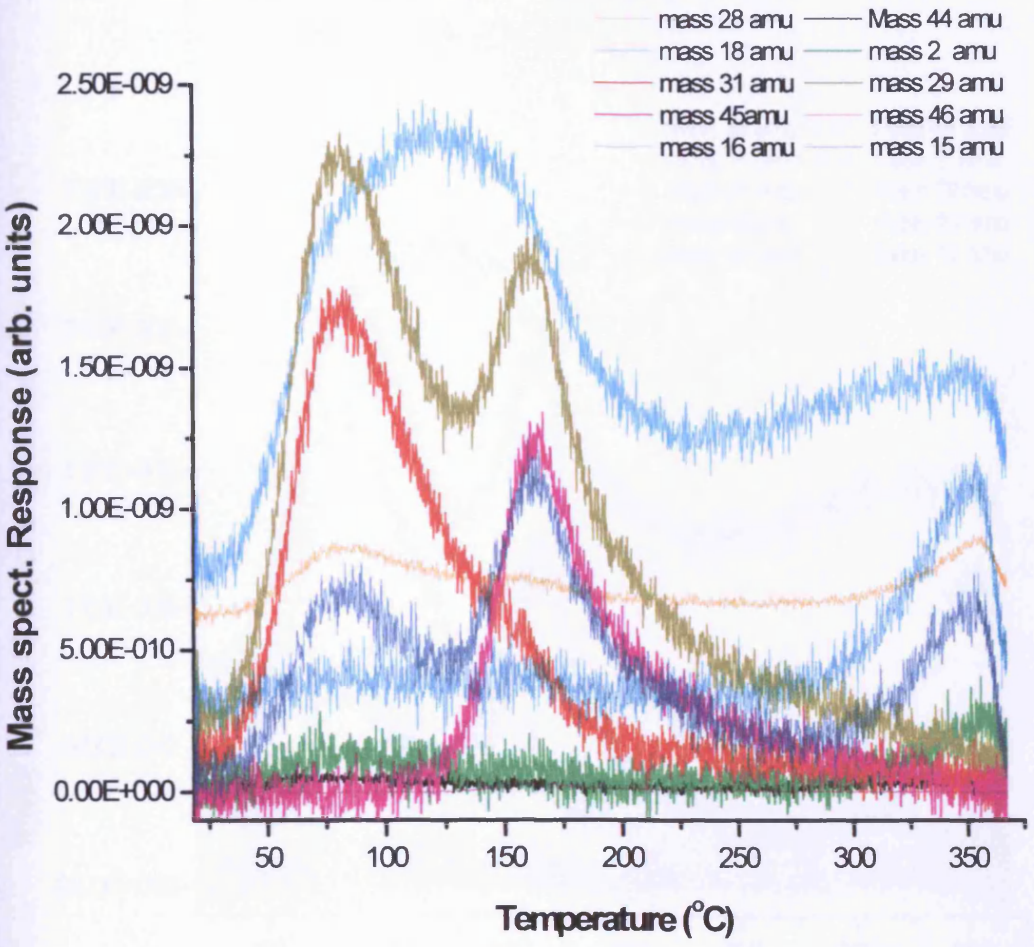

Figure 4-81: Temperature Programmed Desorption of a γ–Al_2O_3 sample saturated with methanol at room temperature

Similarly, a Temperature Programmed Desorption result for a 1wt% Au/γ-Al_2O_3 catalyst is shown in figure (4-82). It shows methanol desorption at a low temperature of approximately 76°C. Dimethyl ether desorbed at 168°C, lower than its desorption temperature when γ–Al_2O_3 was used alone. However, methane was also observed with a desorption peak centred at 347°C, lower than when γ–Al_2O_3 was used alone.

The Temperature Programmed Desorption of methanol over a 1wt% Au/γ-Al_2O_3 catalyst was accompanied with high selectivity to dimethyl ether due to dehydration of methanol at lower temperature and deoxygenation to methane and dehydrogenation to CO at high temperature (figure 4-781).However, the presence of gold played an important role especially in lowering the activation energy of the reaction. Similarly,

the main products obtained are associated with high surface coverage and longer residence time of methoxy species available on the catalyst surface.

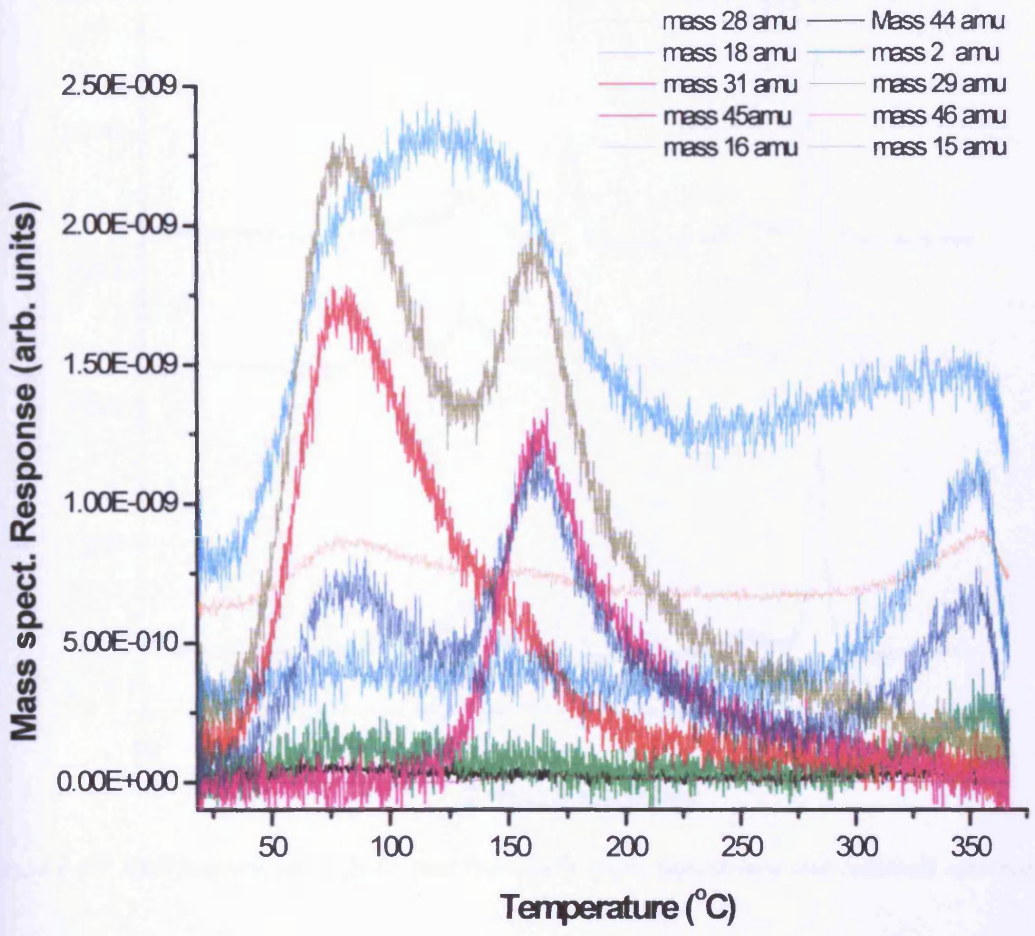

Figure 4-82: Temperature Programmed Desorption of 1wt% Au/γ–Al_2O_3 catalyst saturated with methanol at room temperature

4.18 CHARACTERISATION OF Au/γ–Al_2O_3 CATALYST

4.18.1 XRD

The XRD pattern for γ–Al_2O_3 and Au/γ–Al_2O_3 (both uncalcined and calcined) catalysts are shown in figure (4-83), the figure shows the XRD pattern observed for all the catalysts mainly showed the presence of phase presence in the support (figure 4-83). The absence of gold species phase(s) can be attributed to the low loading of gold or a high dispersion of the gold species phase(s) on the surface of the support. Similar phase were identified by both deposition precipitation and incipient wetness method of preparation.

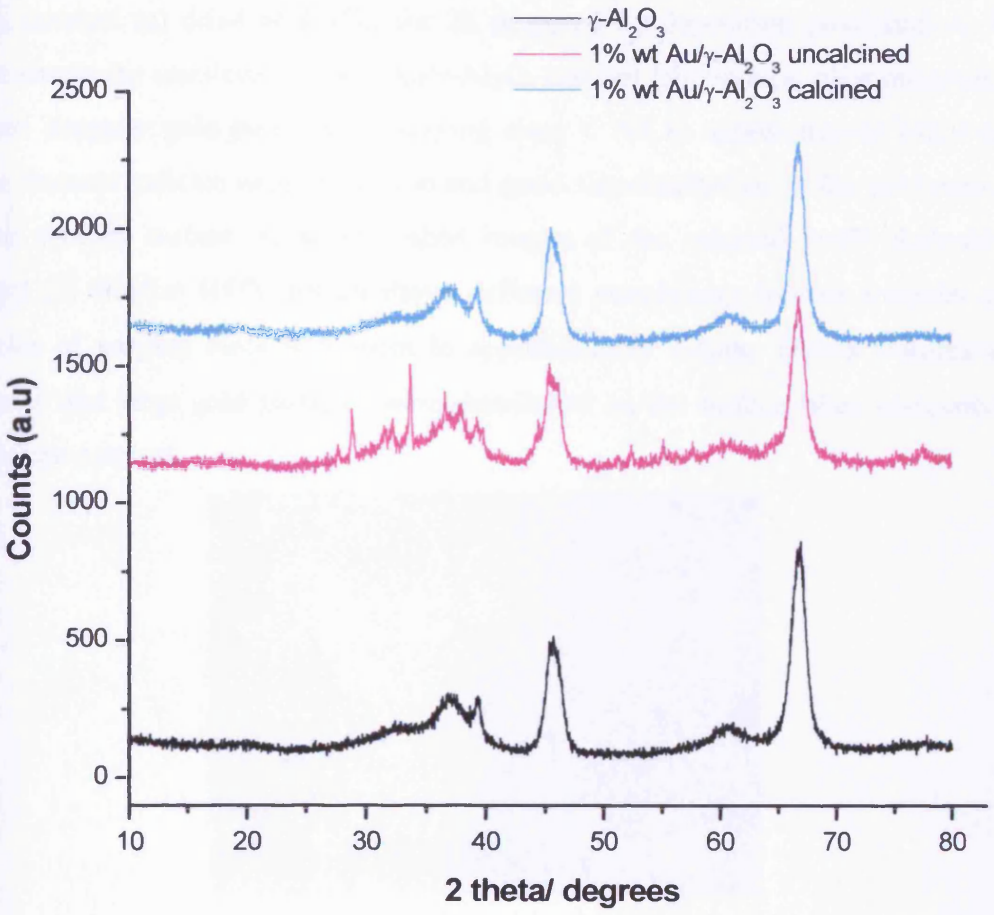

Figure 4-83: XRD patterns for γ–Al_2O_3 and 1wt%Au/γ–Al_2O_3 (uncalcined and calcined) catalysts

S/N	Support or catalyst	Type	Crystal phase
1	γ–Al_2O_3	Powdered	γ–Al_2O_3, defect cubic spinel
2	Au/γ–Al_2O_3	uncalcined	γ–Al_2O_3, defect cubic spinel
3	Au/γ–Al_2O_3	calcined	γ–Al_2O_3, defect cubic spinel

Table 4-2: Phases identified in XRD patterns of γ–Al_2O_3 and Au/γ–Al_2O_3 catalysts prepared by deposition precipitation method

4.18.2 SEM

Figure 4-84 shows the SEM images for γ-Al_2O_3 alone (a) and uncalcined 1wt% Au/γ-Al_2O_3 catalyst (c) dried at 120°C for 2h prepared by deposition precipitation. The figure shows the uncalcined 1wt% Au/γ-Al_2O_3 catalyst (shows a peculiar morphology (porous irregular gold particles of varying sizes < 104 to approximately 242.9 nm). These features indicate high dispersion and good size distribution of the gold particles on the catalyst surface. However, SEM images of the calcined 1wt% Au/γ-Al_2O_3 catalyst (b) dried at 400°C for 2h shows different morphology (porous irregular gold particles of varying sizes < 1. 4μm to approximately 2.4μm. Theses features also indicates that large gold particles were distributed on the surface when compared to uncalcined catalyst.

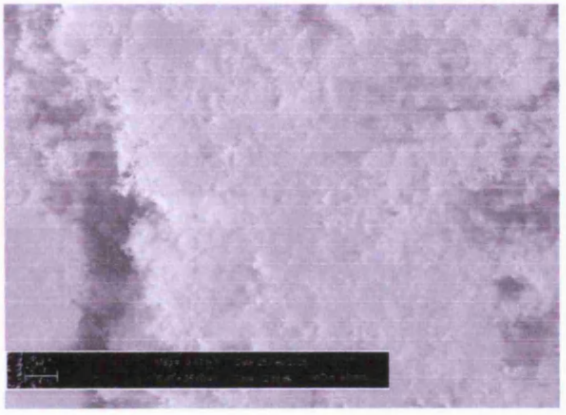

(a) γ-Al_2O_3

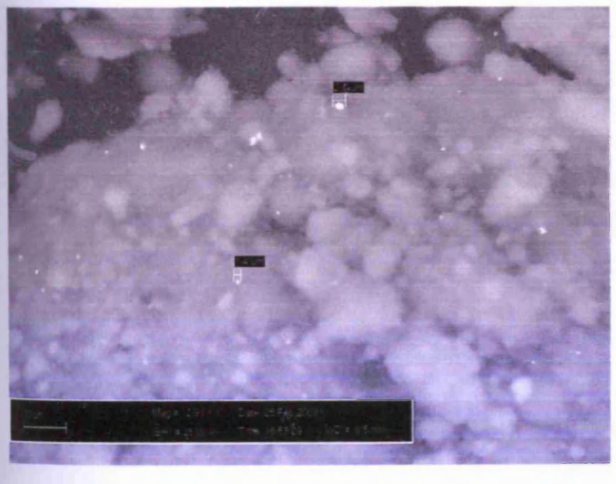

(b) *1wt%Au/γ-Al_2O_3* (calcined)

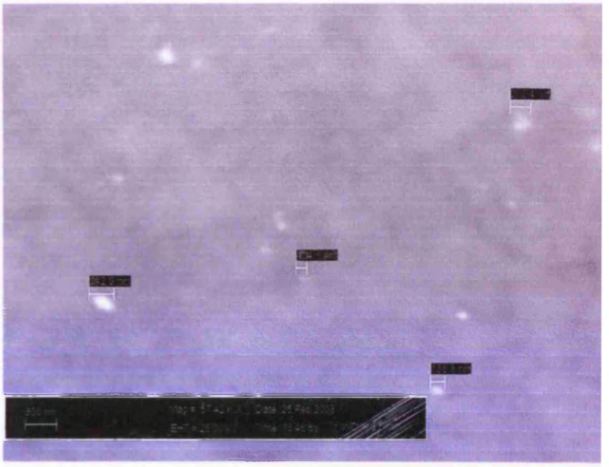

(c) *1wt%Au/γ-Al_2O_3* (uncalcined)

Figure 4-84: Scanning Electron Microscopy for γ-Al_2O_3 and 1% wt Au / γ-Al_2O_3, catalysts (calcined and uncalcined) prepared by deposition precipitation

Similarly, figure 4-85 shows the SEM images for 1wt% Au/γ-Al_2O_3 uncalcined (d) and calcined 1wt% Au/γ-Al_2O_3 catalyst (e) prepared by incipient wetness of impregnation and dried at 120 and 400°C for 2h respectively. The figure shows the uncalcined and calcined 1wt% Au/γ-Al_2O_3 catalyst (shows a peculiar morphology (porous irregular gold particles) with uncalcined showing varying sizes of gold particle ranging from 1.1μm to 2.5μm and 1.5μm to approximately 2.9μm respectively. These features indicate that the gold particles are well dispersed on the catalyst of Au/ γ-Al_2O_3 prepared by deposition precipitation method than the one prepared by incipient wetness of impregnation.

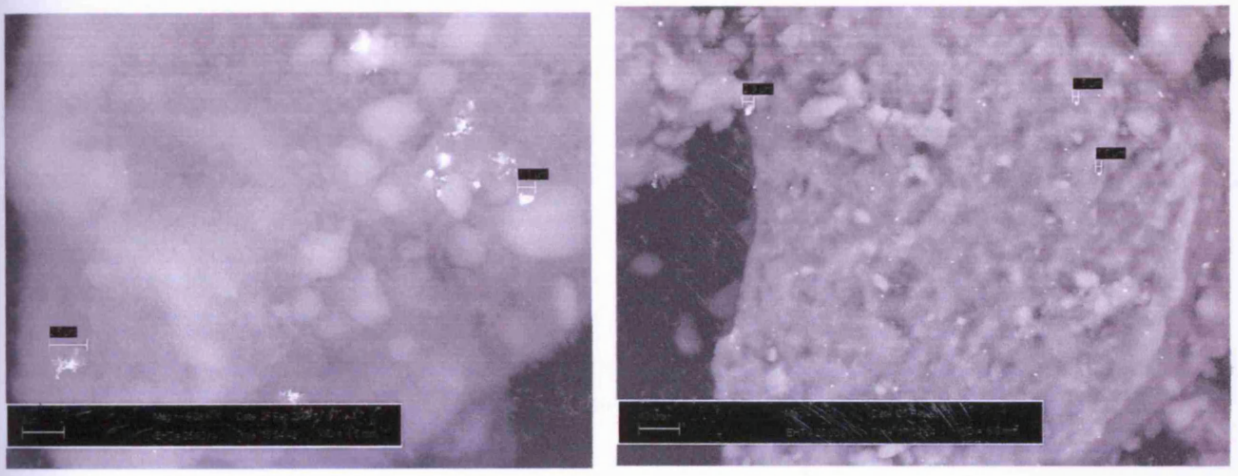

(d) ***1wt% Au/γ–Al_2O_3*** **(calcined)** **(e)** ***1wt% Au/γ–Al_2O_3*** **(uncalcined)**

Figure 4-85: Scanning Electron Microscopy for 1% wt Au / γ-Al_2O_3, catalysts (calcined and uncalcined) prepared by incipient wetness of impregnation

4.18.3 XPS

The XPS data obtained for the catalyst of Au/γ-Al_2O_3 prepared by deposition shows no detectable sign of gold on the catalyst. However, figure 4-86 shows the XPS spectrum of 1wt% Au/γ-Al_2O_3 catalyst prepared by incipient wetness. The XPS spectrum shows that most of the Au 4*f* envelope is situated around 85 eV; these features indicate the existence of gold as Au^+ oxidation state. The result is contrary to the data obtained in the case Au/TiO_2 prepared by deposition precipitation in which

the oxidation state of gold was found to be Au^{x+} and Au^{0}. Similarly, from the XPS data the nominal gold loading is within the expected values as depicted in table 4-3

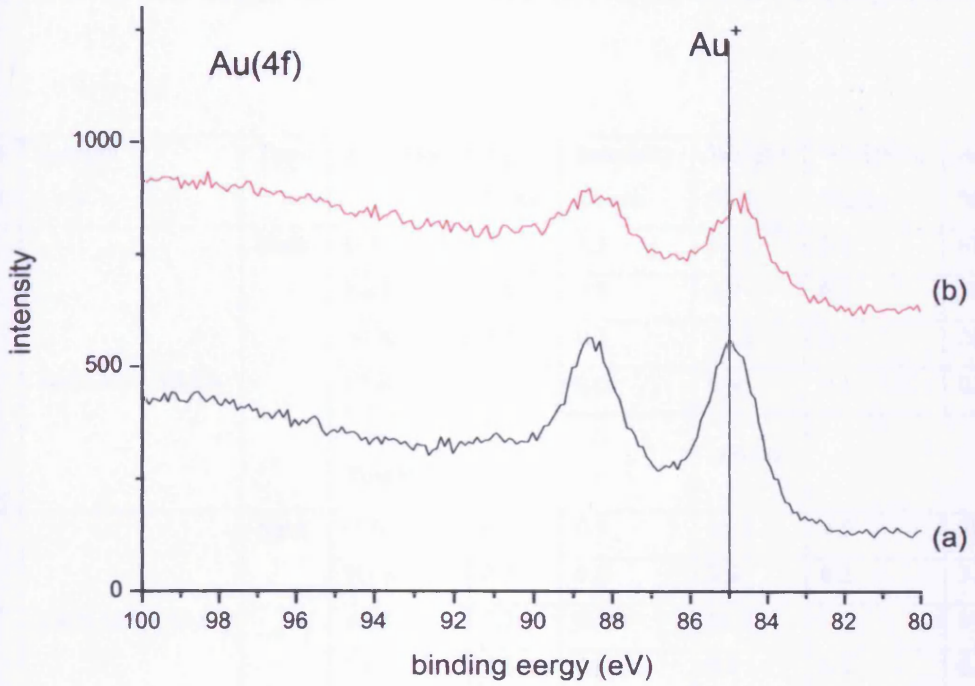

Figure 4-86: Au (4f) spectrum for (a) 1wt% Au/γ–Al_2O_3 (uncalcined), (b) 1wt% Au/γ–Al_2O_3 (calcined) catalysts prepared by deposition precipitation

Sample	Atom %				Wt %
	Au	O	Al		Au
(a)	0.2	61.9	37.8		2.0
(b)	0.1	56.6	43.3		0.9

Table 4-3: Elemental composition for (a) 1wt%Au/γ–Al_2O_3 (uncalcined), (b) 1wt%Au/γ–Al_2O_3 (calcined) catalysts prepared by incipient wetness of impregnation

4.18.4 EDAX

Table 4-4 shows the EDAX result of the 1wt%Au/γ-Al_2O_3 catalyst prepared by deposition precipitation method. The Bulk of the catalyst shows it contained 56.2%, 6.0%, 37.4% and 0.4% of O, Na, Al, and Cl respectively. While the spot shows O, Na, Al, Cl, and Au with weight % of 43.3%, 3.8%, 51.1%, 0.7% and 1.2% respectively.

S/NO	Sample	Type	Elements	App Conc	Intensity Corrn	Weight %	Weight% Sigma	Atomic %
1	1wt%Au/γ–Al_2O_3	Bulk	O K	11.3	1.1	56.2	0.5	67.9
			Na K	0.8	0.7	6.0	0.2	5.0
			Al K	5.1	0.7	37.4	0.4	26.8
			Cl K	0.1	0.6	0.4	0.1	0.2
			Totals			**100.00**		
2	1wt%Au/ γ–Al_2O_3	Spot	O K	6.3	0.9	43.3	0.5	56.5
			Na K	0.5	0.8	3.8	0.2	3.4
			Al K	7.3	0.8	51.1	0.5	39.6
			Cl K	0.1	0.6	0.7	0.1	0.4
			Au M	0.1	0.6	1.2	0.3	0.1
			Totals			**100.00**		

Table 4-4: EDAX result for uncalcined 1wt% Au/ γ-Al_2O_3 ***catalyst prepared by deposition precipitation***

4.19 Methanol oxidation reaction over Au/SiO_2 catalyst

4.19.1 Temperature Programmed Pulse Flow Reaction of methanol over a SiO_2 catalyst

The oxidation of methanol was also carried out over a 1wt% Au/SiO_2 catalyst, prepared by incipient wetness impregnation. However, to understand the role of Au on methanol oxidation over this catalyst, SiO_2 was also used as a catalyst. The Temperature Pulse Flow Reaction result was as shown in figure (4-87).

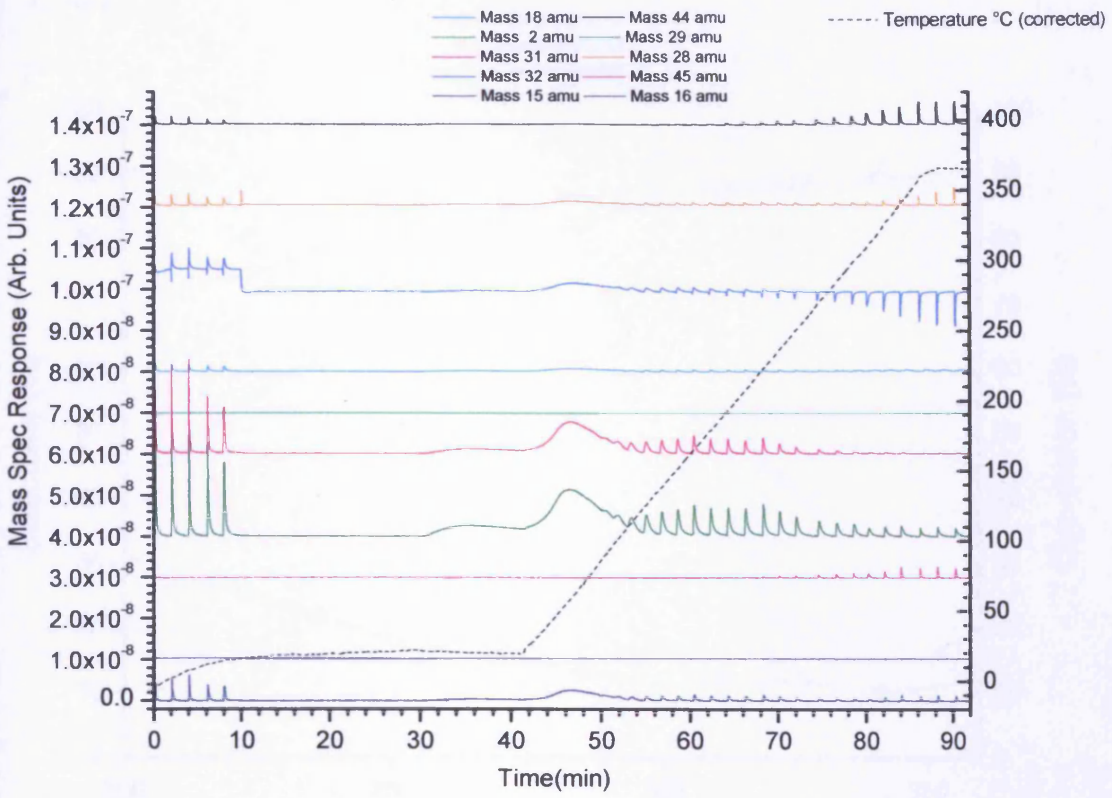

Figure 4-87: Temperature Programmed Pulse Flow Reaction for methanol oxidation over a SiO_2 catalyst

Figure (4-87) shows the saturation of methanol at room temperature (the appearance of mass 31 and 29 amu at 30 minutes). Nevertheless, between 45 and 55 minutes there is desorption of methanol, while at the beginning of 70 minutes is the emergence of dimethyl ether (appearance of mass 45 amu signal) and at 90 minutes is the appearance of CO due to dehydrogenation. The oxidation of methanol over SiO_2 is complete oxidation as evidenced by the appearance of CO_2 and H_2O

When the data was integrated and analysed, figure (4-88) was obtained. At a conversion of methanol of 50%, the catalyst was selective to CO_2 with selectivity being 65% and the temperature 225°C. However, when the temperature was increased to about 350°C, the activity of the catalyst was still towards CO_2 with selectivity value being 90% and less CO selectivity was observed, with selectivity value being 10%. The dimethyl ether selectivity is minimal and the maximum conversion of methanol was only 90%.

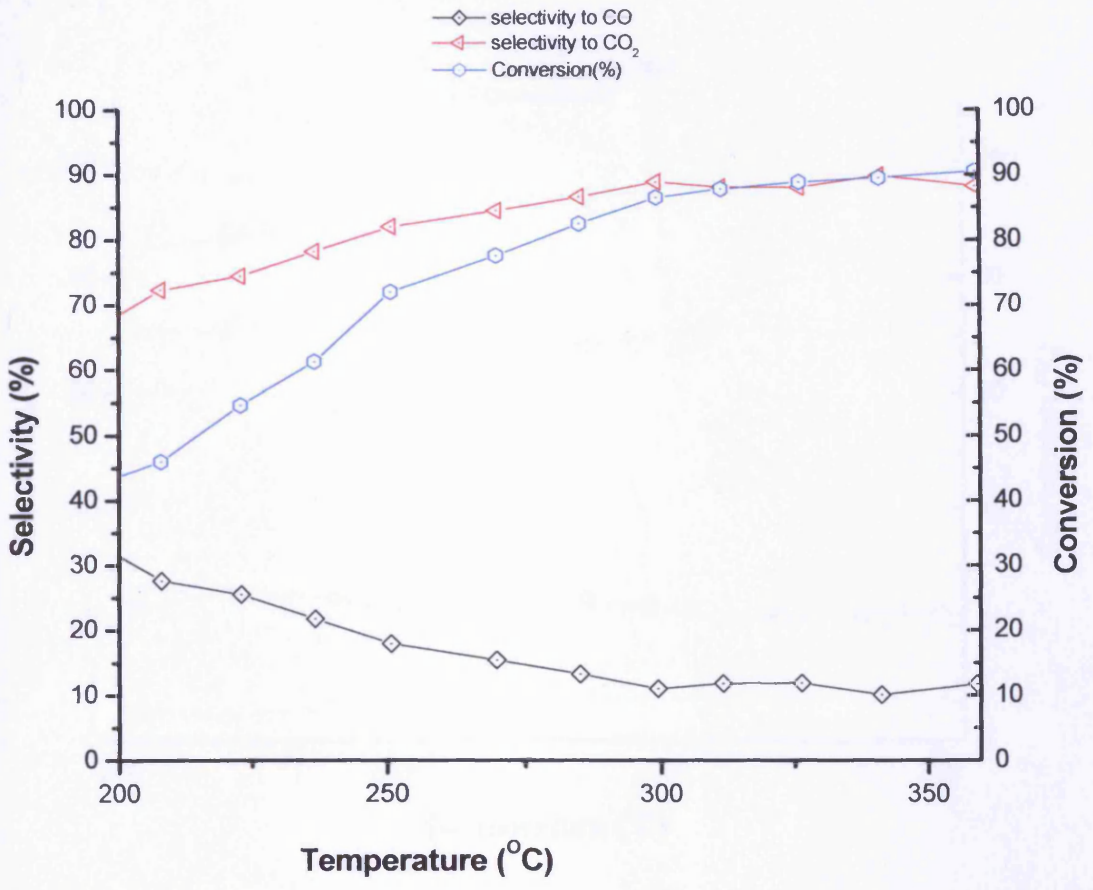

Figure 4-88: Selectivity and conversion with temperature for (aerobic) methanol oxidation over a SiO_2 sample

4.19.2 Temperature Programmed Reaction of methanol over a 1wt% Au/ SiO_2 catalyst

The result obtained for methanol oxidation over a 1wt% Au/SiO_2 catalyst (figure 4-89) was similar to the result of the SiO_2 sample (figure 4-87). When the conversion of methanol was 80%, the catalyst activity was selective towards CO_2, with selectivity value being 75% and the temperature was 200°C. However, when the temperature was increased to 250°C, the methanol conversion was 95% and the selectivity to CO_2 drops to 65% and more dimethyl ether was observed, with selectivity less than 5% and simultaneously, the CO selectivity was 22% and as the temperature increases to 350°C, it drops to 20% and the methanol conversion was 100%.

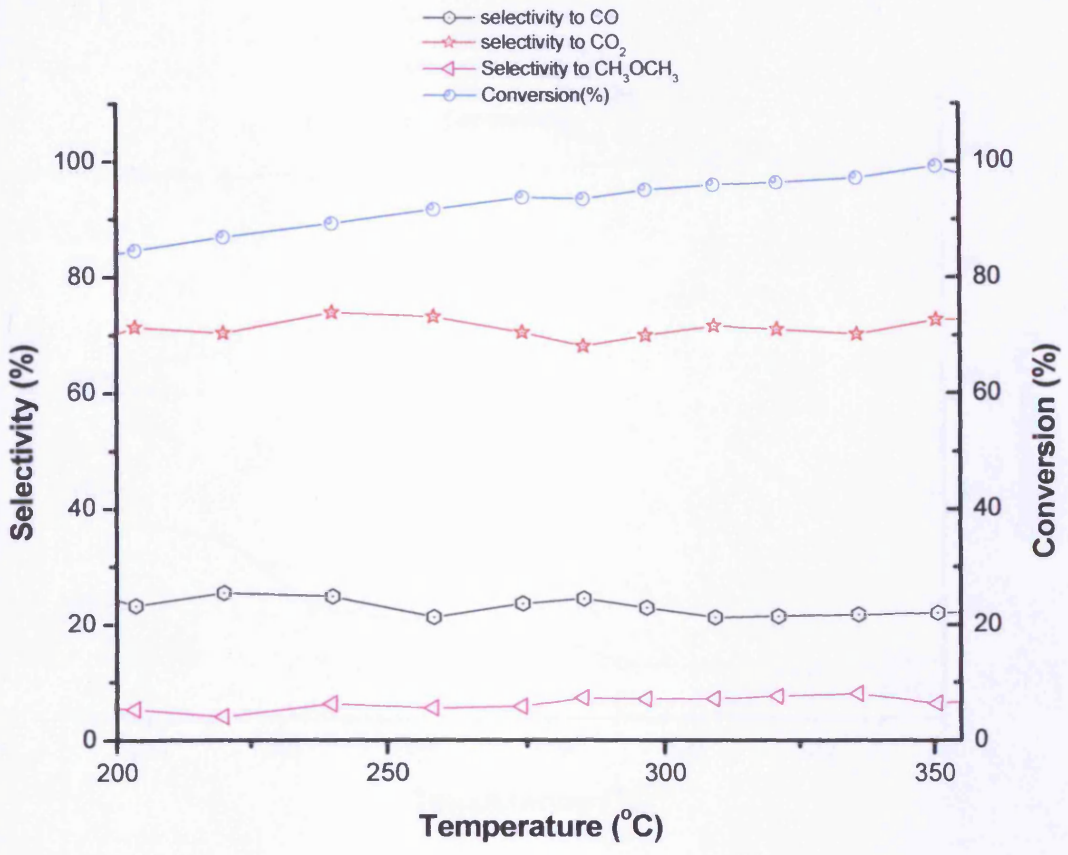

Figure 4-89: Selectivity and Conversion graph of methanol oxidation over a 1wt% Au/ SiO_2 catalyst Prepared by IW

Similarly, the result of anaerobic reaction of methanol over Au/SiO_2 was as shown in figure (4-90). It shows as the conversion of methanol was 80%, the catalyst is being dehydrated to dimethyl ether and the temperature was 200°C. However, when the temperature was increased to 300°C, the dimethyl ether selectivity was 85% and the conversion was 98%. Nevertheless, the CO selectivity was very small, (10%) while the CO_2 and methane selectivities were minimal. The methanol oxidation reaction over Au/SiO_2 in general, is a complete oxidation and involved dehydration and dehydrogenation of methanol at high temperature. While in anaerobic reaction, it involved more dehydration and dehydrogenation to dimethyl ether and CO respectively. The presence of the gold lowers the activation energy than when SiO_2 was used alone.

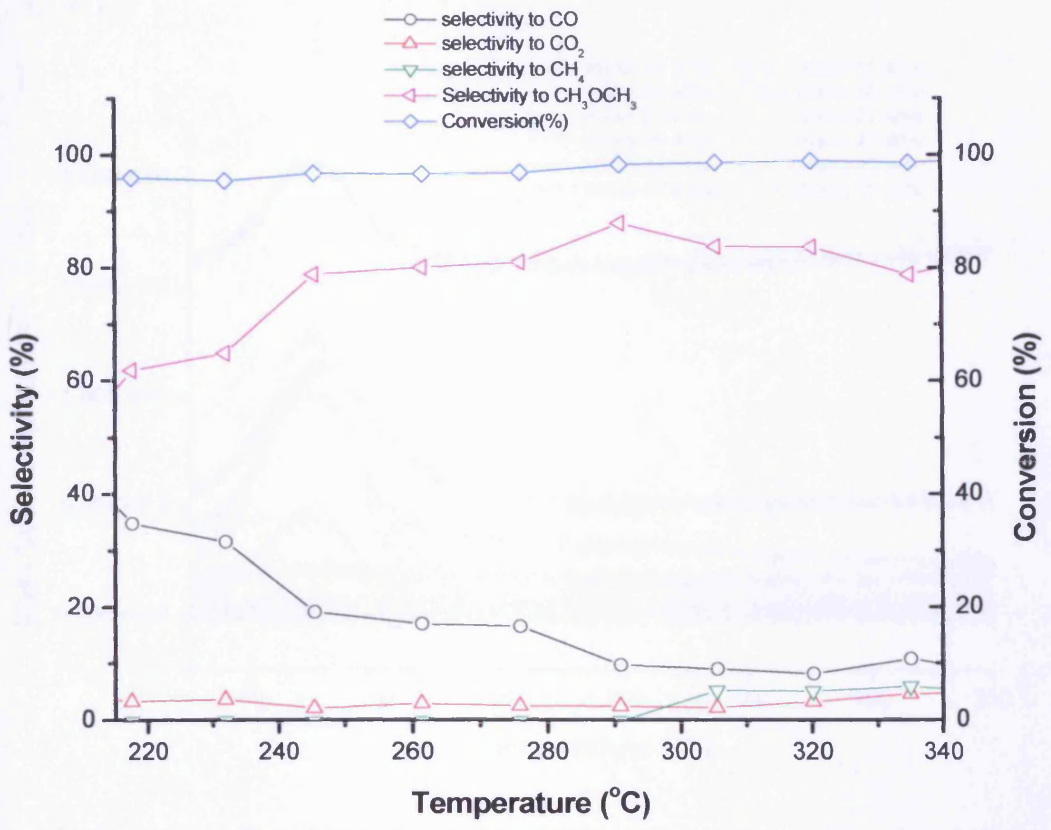

Figure 4-90: Selectivity and Conversion graph of anaerobic methanol reaction over a 1wt% Au/ SiO_2 catalyst prepared by IW

4.19.3Temperature Programmed Desorption of Methanol over Au/SiO_2

The Temperature Programmed Desorption of methanol was carried out over SiO_2 (figure 4-91) and Au/ SiO_2 (figure 4-92). The figure 4-90shows methanol was being desorbed at lower temperature (75°C) and no other products of desorption were observed even when the temperature was increased to 350°C. These correlated with results obtained in which the anaerobic and aerobic reaction of methanol is all associated with adsorbed methanol and methoxy, which are involved with dehydration and dehydrogenation.

Similarly, when TPD was carried out over Au/SiO_2 (figure 4-92) methanol is desorbed at a lower temperature with desorption peaks at 69°C, less than the desorption temperature when SiO_2 was used alone. Therefore, this has confirmed to us that, the presence of Au lowers the activation energy of the methanol desorption, although the difference is not much significant.

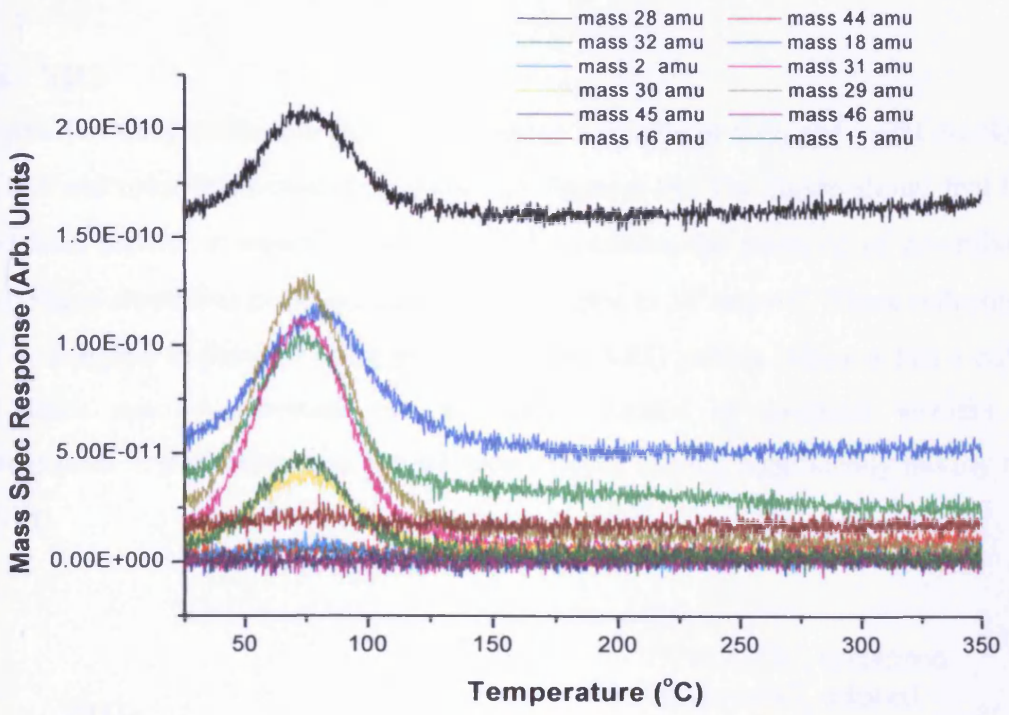

Figure 4-91: Temperature Programmed Desorption of SiO_2 catalyst saturated with methanol at room temperature

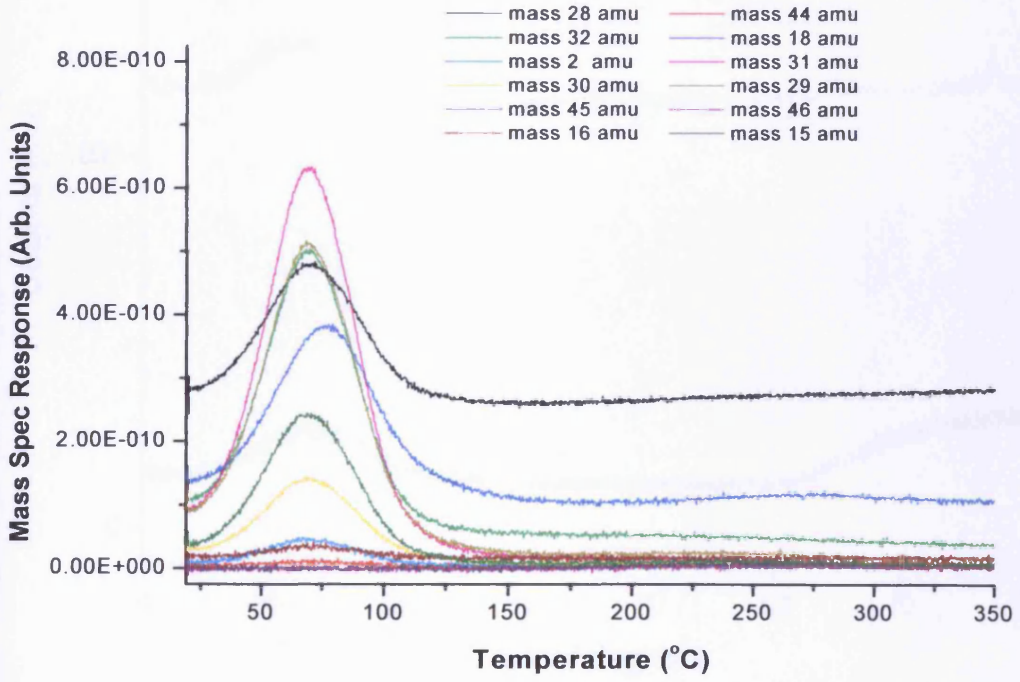

Figure 4-92: Temperature Programmed Desorption of Au/ SiO_2 catalyst saturated with methanol at room temperature

4.20 CHARACTERISATION OF Au/SiO_2 CATALYST

4. 20.1 XRD

The powder X-ray diffraction (XRD) pattern for a sample of SiO_2 and 1wt% Au/SiO_2 calcined and uncalcined catalyst is shown in figure 4-93. The figure shows that the broad halo pattern at around 2θ equal to 23° confirms the presence of amorphous silica. Sharp crystalline peaks are noticed at 2θ equal to 38° and 44°. These reflections may be assigned to plane of cubic gold. Thus, the XRD pattern indicates that a cubic gold silica nano composition can be readily formed by incipient wetness of impregnation. It also shows that the addition of gold to SiO_2 significantly modify the support.

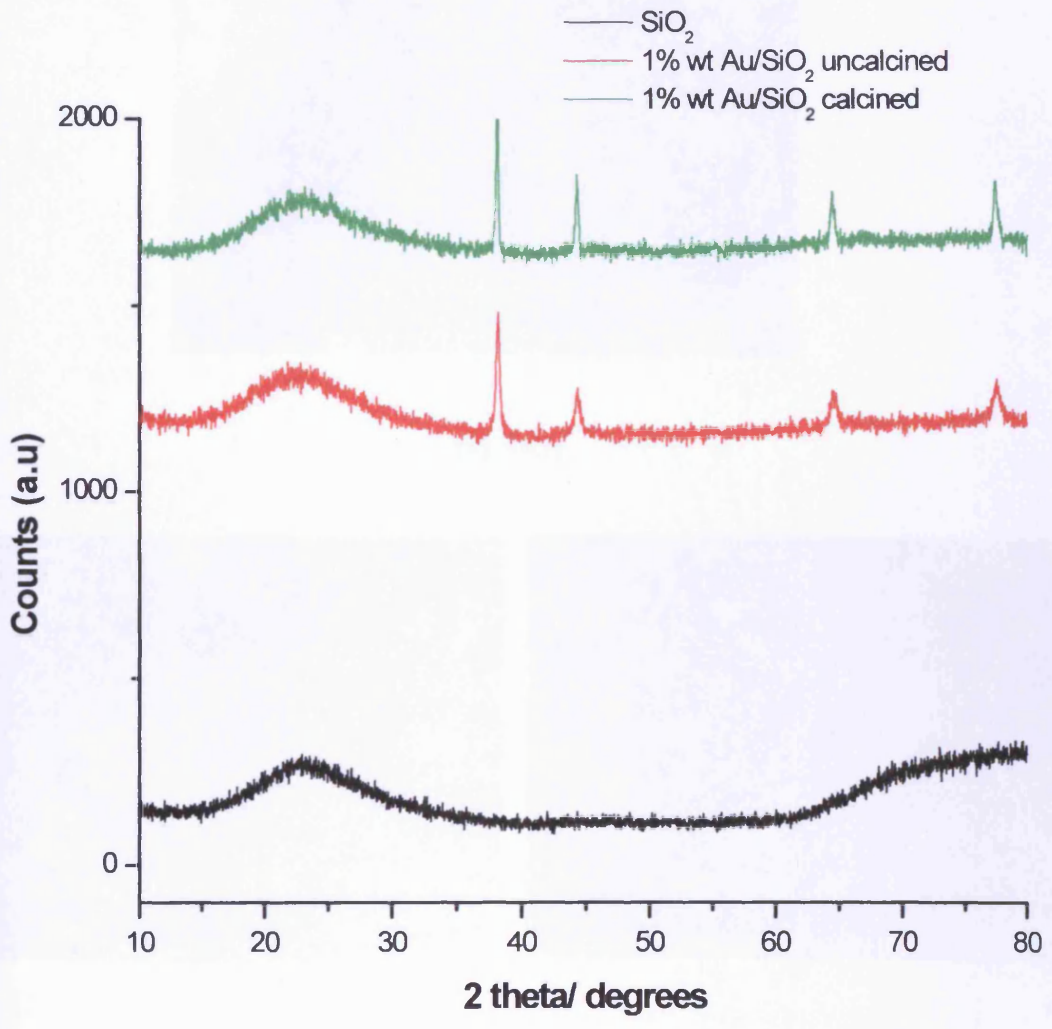

Figure 4-93: XRD patterns for SiO_2 and 1wt% Au/ SiO_2 (uncalcined and calcined) catalysts

4.20.2 SEM

Figure 4-94 shows the SEM images for SiO_2 (a) 1wt% Au/SiO_2 uncalcined (b) and calcined 1wt% Au/SiO_2 (c) prepared by incipient wetness of impregnation and dried at 120 and 400°C for 2h respectively. The figure shows the uncalcined 1wt% Au/SiO_2 catalyst (b) shows a morphology (porous irregular gold particles of varying sizes < 1.5μm to approximately 2.9μm). While the morphology exhibited by calcined catalyst 1wt% Au/SiO_2 forms similar porous irregular gold particles of varying sizes <2.6μm to approximately 2.8μm.

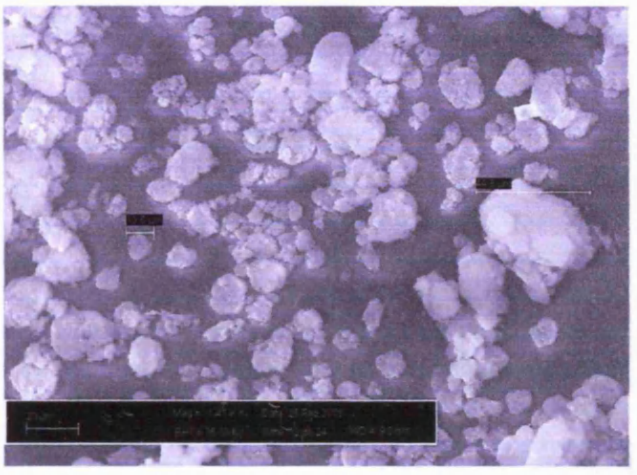

(a) SiO_2

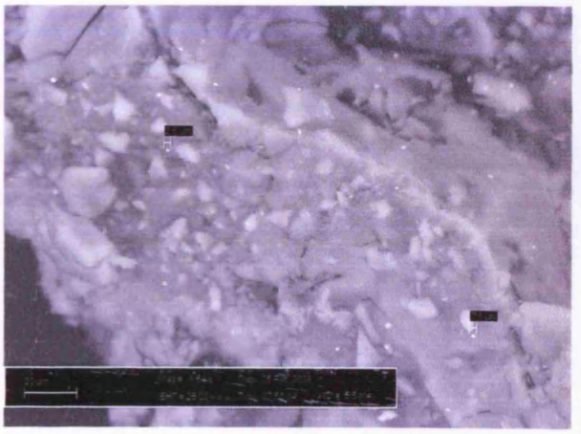

(b) *1wt% Au/ SiO_2* (uncalcined) **(c) *1wt% Au/ SiO_2* (calcined)**

Figure 4-94: XRD patterns for SiO_2 and 1%wt Au/SiO_2 (uncalcined and calcined) catalysts

4.20.3 XPS

The XPS spectrum of 1wt% Au/SiO_2 catalysts prepared by incipient wetness (figure 4-95) shows Au 4*f* envelope are situated around 85 eV. These features confirmed the existence of gold in the oxidation as Au^{x+} for both calcined and uncalcined catalyst of 1wt% Au/SiO_2, similar to 1wt% Au/ γ-Al_2O_3. However, from the XPS data it indicates that the elemental composition of the catalyst consist of silicon, oxygen and gold, with gold level within the expected nominal loadings (table 4-5).

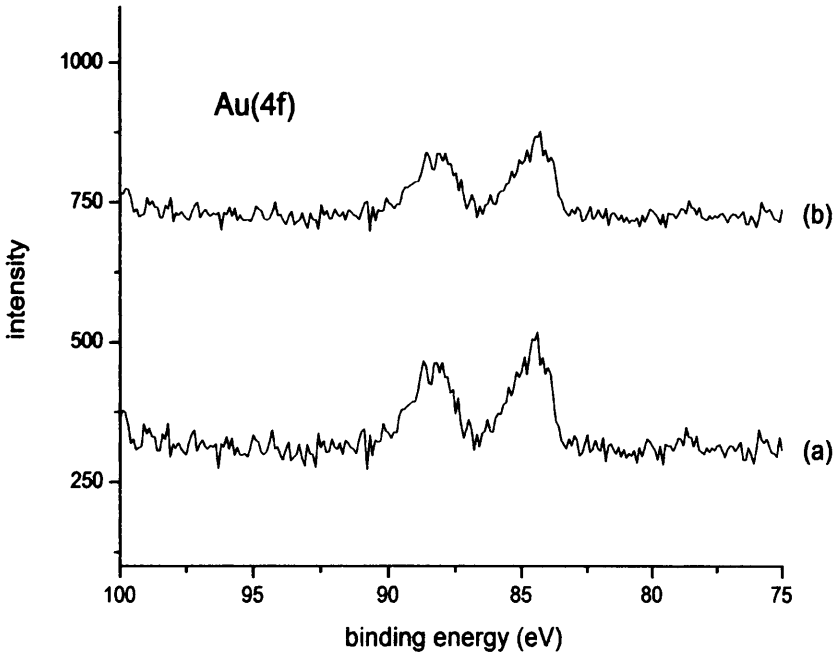

Figure 4-95: Au (4f) spectrum for (a) 1wt% Au/ SiO_2 (uncalcined), (b) 1wt% Au/ SiO_2 (calcined) catalysts prepared by deposition precipitation

Sample	Atom %				Wt %
	Si	O	Au		Au
(a)	29.9	70.0	0.1		1.0
(b)	30.2	69.8	<0.1		<1.0

Table 4-5: Elemental composition for (a) 1wt% Au/ SiO_2 (uncalcined), (b) 1wt% Au/ SiO_2 (calcined) catalysts prepared by incipient wetness impregnation

4.20.4 EDAX

The data shown in table 4-6 shows the EDAX result obtained on 1wt%Au/SiO_2 catalyst. The main elemental composition of the bulk of the EDAX result shows that the 1wt% Au/SiO_2 catalyst contained C, O, Al, Si and Ti, with weight of %26.0%, 52.2%, 0.6%, 21.0% and 0.2% respectively. While the spot analysis shows that the catalyst contained O, Al, Si, Ti, and Au, with 57.6%, 0.7%, 41.0%, 0.2% and 0.7% being the weight % of O, Al, Si, Ti, and Au respectively.

S/NO	Sample	Type	Elements	App Conc	Intensity Corrn	Weight %	Weight% Sigma	Atomic %
1	1wt%Au/SiO_2	**Bulk**	C K	3.0	0.3	26.0	2.1	35.0
			O K	10.7	0.6	52.2	1.5	52.6
			Al K	0.2	0.8	0.6	0.1	0.3
			Si K	6.3	0.9	21.0	0.6	12.0
			Ti K	0.04	0.8	0.2	0.04	0.1
			Totals			**100.00**		
2	1wt%Au/SiO_2	**Spot**	O K	32.8	0.8	57.6	0.3	70.7
			Al K	0.4	0.8	0.7	0.1	0.5
			Si K	25.0	0.9	40.8	0.2	28.6
			Ti K	0.1	0.8	0.2	0.04	0.1
			Au M	0.3	0.6	0.7	0.1	0.1
			Totals			**100.00**		

Table 4-6: EDAX result for uncalcined 1wt% Au/ SiO_2 ***catalyst prepared by deposition precipitation***

4.21 Conclusions

It has been observed that, the methanol oxidation reaction over Au/TiO_2 catalyst is not selective but shows a complete oxidation to CO_2 and H_2O via formate as intermediate (as shown by infrared spectra). However, two types of CO_2 are produced,

type I (slowly produced) at low temperature and type II (produced at faster rate) at high temperature. Both are due to catalytic reaction of methanol over Au/TiO_2 catalyst. Heating the catalyst in the oxygen flow tends to activate the catalyst, especially, towards the CO_2 formation.

The methanol was adsorbed on the surface of TiO_2 in either of the two ways as shown in figure (4-96)

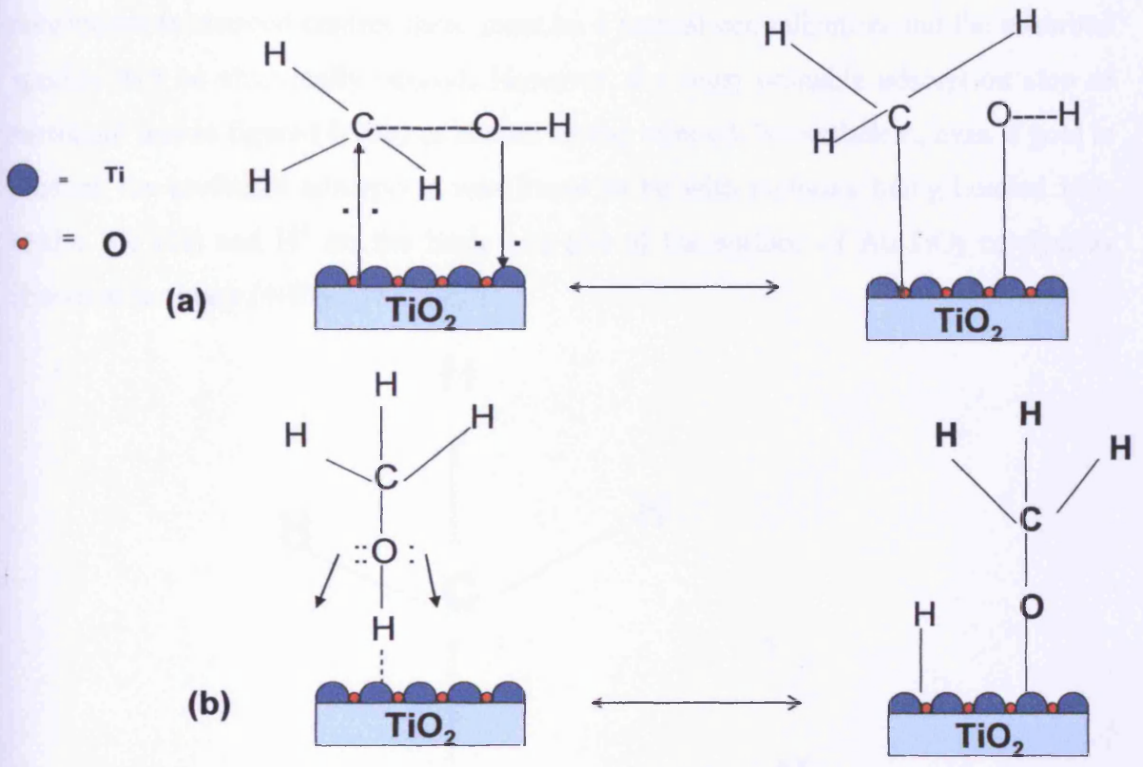

Figure 4-96: Methanol adsorption over TiO_2 surface

The surface of TiO_2 was made up of basic and acidic sites. When methanol was adsorbed on the surface, it can either be adsorbed leading to the formation of methyl group as shown in figure (4-96a). The figure shows that, when methanol was adsorbed on the surface the carbon atom is not substituted, and a nucleophillic reagent, here a basic site (O), in a reaction similar to that observed in a SN^2 mechanism, can attack it. This produces a CH_3+ ion adsorbed at the basic site (O) and an OH^- ion, which is a strong base and can react on an even more weakly acidic site Ti. This type of attack

should be easier if the C-OH bond is polarized by an interaction between the acid centre and the OH group of the alcohol.

Similarly, figure (4-96b) shows the adsorption of methanol leading to a surface methoxide, which has been identified by infrared spectrometry and which is reasonable in view of the known weak acidity of methanol. In this case, the basic site (O), extracts the hydroxyl hydrogen producing a methylate ion, which is strong base and can neutralize a weak acid centre Ti. In this case, if the acidic and basic sites are considered as charged centres there must be a mutual neutralization and the adsorbed species will be electrically neutral. However, the most probable adsorption step of methanol was in figure (4-96b) as shown by the infrared. Nevertheless, even if gold is present, the methanol adsorption was found to be with methoxy being bonded with acidic site (Ti) and H^+ on the basic site (O) of the surface of Au/TiO_2 catalyst as shown as in figure (4-97).

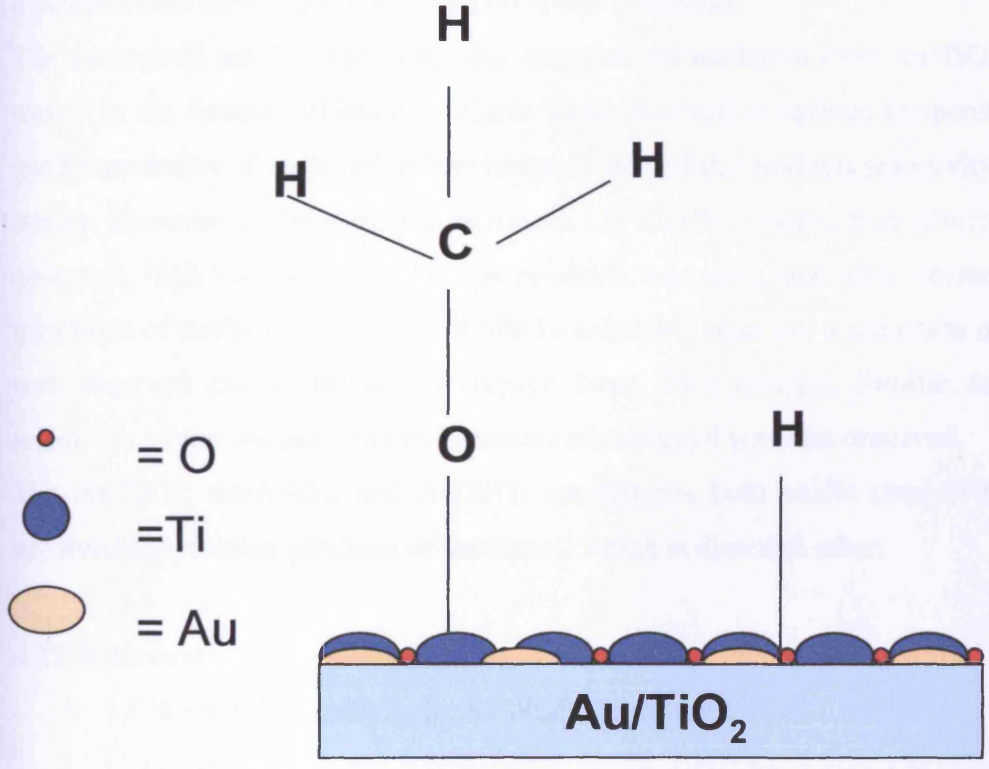

Figure 4-97: Methanol adsorption over Au/TiO_2 surface

The saturation of methanol was also measured before the temperature Pulse Programmed Reaction and the Temperature Programmed Reaction corresponds with about half the total surface atoms. It could be remembered that the surface is probably

comprised of approximately one third of the Ti cation and two third of O anions for charge neutrality.

Thus, the methanol uptake (2.1×10^{20}) is very similar to the number of surface Ti cations ($\sim 5 \times 10^{20}/3 = 1.7 \times 10^{20}$).

From the Temperature Programmed Desorption and the infrared spectroscopy of methanol oxidation over Au/TiO_2 catalyst, it revealed that the main adsorbed species on the surface of the catalyst, responsible for the CO_2 formation is formate. The more CO_2 formed is due to gold present which increase the amount of formate on the surface. However, when TiO_2 was used alone only dehydrogenation to CO and deoxygenation to methane was observed. Similarly, when the TPDs of methanol was carried out over Au/Al_2O_3 and Au/ SiO_2. The results show similar reaction but with a lot of dimethyl ether at low temperature that is product of dehydration caused by high surface coverage of methoxy species on the surface at that temperature. The methanol oxidation over these metals was also complete oxidation.

The isothermal aerobic and anaerobic reactions of methanol over Au/TiO_2 catalyst, shows in the former, different products were observed at various temperatures with good conversion of methanol at low temperature and the products selectivity was very steady. However, as the temperature rose to 150°C, 100% conversion of methanol was observed, high selectivity of various products was seen, and later decrease as the injections of methanol continues. While in anaerobic reaction, a reduction of the bulk was observed due to uptake of oxygen from TiO_2 catalyst. Similar decrease in selectivity of the products and conversions of methanol was also observed.

The Au/TiO_2, Au/Al_2O_3, and Au/SiO_2 catalyst are both acidic catalyst because it involved dehydration products of methanol, which is dimethyl ether.

4.22 References

1. J.F Walker, Formaldehyde, Reinhold, New York, 1964
2. U, Gerloff, J.Jahn and A.Schleicher, Br.Pat.1067083, 3 May 1967H.Friedrich and
3. W. Neugebauer, Ger.Pat.2145851, 22 May 1973, US Pat.3843562, 22 October 1974
4. L.Cairati,P.Forzatti, F,Trifiro and P.Villa, in H.F.Barry and P.C.H.Mitchell, Editors, *Proc.of the Climax 4th Int.Conf.on the Chemistry and uses of Molybednum Company,Ann Arbor*, MI, 402 (1982)

5. H.Adkins and W.R.Peterson, *J.Am.Chem.Soc.* **53** 1512 (1931)
6. A.J.Van Henstum,J.G.,Van Ommen, H.Bosch and P.J.Gellings, *in Proc.8th Int.Congr.Catal.*,Vol 4, Verlag Chemie and Dechema, Berlin, 297 (1984)
7. G.Busca, P.Tittarelli, E, Tronconi and P.Forzatti, *J.Solid State Chem.*, **67** 91 (1987)
8. G.Busca, A.S.Elmi and P.Forzatti, *J.Phy.Chem.*, **91** 5263 (1987)
9. .E.TTronconi,A.S.Elmi,N.Ferlazzo,P.Forzatti,G.BuscaandP.Tittarelli,*Ind.Eng. Chem.Res.*,**26** 1269 1269 (1987)
10. M.Ali, *J.Catal.*,**77** 279 (1982)
11. N.Arora, G.Deo, I.E Wachs and A.M. Hirt., *J.Catal.*, **159** 1 (1996)
12. M.Chono and T.Yamamoto,Shokubai (*Catalyst)*, **23** 3 (1981)
13. M.Roeper, Erdol, Kohle, Erdgas, *Petroleum*, **37** 506 (1984)
14. I.Carrizosa,S.Castaner and G. Munuera, *J.Catal.*, **49**,265 (1997)
15. M-Y.He and J.G.Ekerdt, *J.Catal.* **87**, 239 (1984)
16. G.Busca, *J.Mol.Catal.*,**50** 241 (1989)
17. J.M.Tatibouet and J.E.Germain,C.R., *Acad.Sc.Paris*, **289**C 301 (1979)
18. Y.C.Liu., G.L.Griffin, S.S.Chan and I.E.Wachas, *J.Catal.*,**94**, 108 (1985)
19. M.Haruta, N.Yamada, T.Kobayashi and S.Iijima ,*J.Catal.*, 11 (1989)
20. F.-W. Chang, H.-Y. Yu, L.S. Roselin, H.-C. Yang, T.-C. Ou, *Appl. Catalysis*, A: General **302** 157 (2006)
21. G.A.M. Hussein, N. Sheppard, M.I. Zaki and R.B. Fahim, *J.Chem.Soc., Faraday Trans.* **87**(16) 2655–2659 (1991)
22. F. Boccuzzi, A. Chiorino and M. Manzoli, *J. Power Sources **118*** 304–310 (2003)
23. S. Francis, F. Leibsle, S. Haq, N. Xiang and M. Bowker, *Surface Sci.* **315** (1994) 284.
24. M. Bowker, H. Houghton and K.C. Waugh, *J. Chem. Soc.,Faraday* **1 77** 3023 (1981)
25. M. Bowker, *Vacuum*, **33** 669 (1983)

Chapter 5- Higher alcohol oxidation over Au/TiO_2 catalysts

5.1 Introduction

In this chapter, the oxidation of higher alcohols is studied on Au/TiO_2 catalysts. We have presented in chapter 4 that primary alcohols such as methanol can be oxidised by Au/TiO_2 catalysts and other Au –metal supported catalysts to CO_2 and water. The reaction was found to be a complete oxidation reaction, with CO_2 and water as the main products.

Alcohols such as propanol and n- butanol have been oxidised to aldehydes by resin- supported gold in the liquid phase,[1] and several other primary and secondary alcohols have been oxidised with very high selectivities in vapour phase over a 1wt% Au/SiO_2 catalyst between 373- 573K;[2] propan-2-en-1-ol gave 97% selectivity to propanoic acid at 523K. Isopropanol was also found to be oxidised to acetone over Au/ Al_2O_3 and (better) Au/ CeO_2-Al_2O_3 with higher selectivity between 373 and 473K[3]. Amino-alcohols have been converted to amino acids; [4] for this reaction, gold was preferred over palladium and platinum because the amino- group does not bind strongly to it. Similarly, gold supported catalysts were found to be suitable for many oxidations of primary and secondary alcohols to their corresponding aldehydes and ketones[5-6].

This chapter focuses on higher alcohol oxidation (such as ethanol, propan-1-ol, and propan-2-ol) over Au/TiO_2 catalysts. The knowledge of the reaction involved using temperature programmed pulse flow reaction and employing some techniques of characterization such as DRIFTS, TPD, were used to propose the reaction mechanism in each case.

5.2 Ethanol oxidation over Au/TiO_2 catalyst

Ethanol is one of the interesting substances, especially for being an alternative replacement source of fuel, since it can indirectly reduce the net carbon dioxide emission from the vehicles when used as a 95% blend with gasoline for light duty vehicles. Although ethanol is considered an attractive replacement, fuel, with quite low emissions of complex hydrocarbons, its partial oxidation to ethanal poses a threat. Hence, the problem of effectively controlling the emission caused by ethanol oxidation along with the desired conversion requires better understanding.

In general, ethanol has been a source or an intermediate for the synthesis of many products. For example, much work has been devoted to producing H_2 from ethanol, by either steam reforming or partial oxidation. The studies of ethanol

reactions on metals and oxides, examining the relationships between surface properties and reaction yields have helped to further the understanding of the various processes.

Because of ethanol's ease of production and because exposure to low amounts does negligible harm, it has widespread use as a solvent for substances intended for human contact or consumption, including scents, flavorings, colorings, and medicines. In chemistry it is both an essential solvent and a feedstock for the synthesis of other products. Because it burns cleanly, ethanol has a long history as a fuel, including as a fuel for internal combustion engine.

Among the various products of ethanol oxidation over different metal oxides such as TiO_2 is: ethanal which is a first product of partial oxidation of ethanol, it can further oxidize to ethanoic acid which is also an intermediate for the formation of diethyl ether. However, ethanol can be dehydrated to form ethene, and it can also be combusted to CO_2 and H_2O or it may be dehydrogenated to ethanal, which further decomposes to CH_4 and CO. Several other products have been reported in the literature for ethanol oxidation over TiO_2[7-12] and non reported the oxidation of ethanol over Au/TiO_2 catalyst.

5.2.1 Preparation of Catalyst

The catalyst used in this chapter was prepared by deposition precipitation methods as described in chapter 2. The prepared catalyst was dried at 120°C before being calcined at 400°C in air. In each case, 0.5g of the catalyst was taken before loading in to the reactor. The catalyst in each case was subjected to aerobic and anaerobic condition using temperature programmed pulse flow reaction, in order to get an insight into the reaction involved and the activity of the catalyst.

5.2.2 Activity test

A fresh 0.5g of a 1wt% Au/TiO_2 catalyst was loaded in the reactor under aerobic condition (in a flow of 10%O_2/ He at a rate of 30ml/min). The lines of the flow of gases were heated to 80°C, with injection of ethanol through the bypass and over the catalyst. The masses monitored in our studies are as shown in table 1. They are chosen based on the reactions involved for ethanol as stated in the introduction.

SNO	MASS	PRODUCT NAME
1	2	Hydrogen (H_2)
2	15 and 16	Methane (CH_4)
3	18	Water (H_2O)
4	28	Carbon monoxide (CO),Ethene, Ethane, and Nitrogen (N_2)
5	29	Ethanol, Ethene, Ethane, Ethanoic acid and Ethanal
6	27	Ethanol, Ethene (CH_2CH_2)
7	30	Ethane (CH_3CH_3)
8	31	Ethanol (CH_3CH_2OH) and DEE ($C_2H_5OC_2H_5$)
9	32	Oxygen (O_2) and Methanol (CH_3OH)
10	43	Ethyl Acetate($CH_3COOC_2H_5$)
11	44	Carbon dioxide CO_2 and Ethanal(CH_3COH)
12	78	Benzene (C_6H_6)

Table 5-1: Masses monitored for ethanol oxidation over a 1wt% Au/ TiO_2 catalyst

0.5g of the loaded catalyst was heated at 400°C, for 30minutes, then cooled to room temperature, 1µl of ethanol was injected through the bypass and then over the catalyst until saturation. Figure (5-1) shows the results of temperature programmed pulse flow reaction (aerobic) for ethanol oxidation over 1wt% Au/TiO_2 catalyst.

The first five pulses of 1µl of ethanol injections were through the bypass. This gives the idea of the cracking pattern observed for ethanol. After the bypass, about 7µl of ethanol was used to saturate the surface (appearance of mass 31, 29 and 27 amu signals) and represent 100% of un- reacted ethanol, though the signal peaks are short and broad compared to the bypass peaks. Similarly, when the peaks are integrated for injections through the bypass and over the catalyst, they are of the same intensity.

When the surface was saturated only ethanol broke through and no conversion of ethanol occurred, however, the uptake of ethanol has indicated to be 7µl corresponding with 1.44×10^{20} molecules g^{-1} of catalyst. This in turn corresponds with about 2.88×10^{19} molecules m^{-2}, if we assume a total surface atom density of $10^{19} m^{-2}$. However, as the temperature was increased to about 100°C, more ethanol observed,

until the temperature reached 220°C, in which 100% conversion of ethanol was obtained (loss of mass 31,29 and 43 amu signals). CO_2 production occurred (from 75 minutes), with a short and wide signal peaks of CO_2 after each pulse injection and continued at a faster rate as the temperature increases, evident by the sharp peaks of CO_2 and the uptake of oxygen.

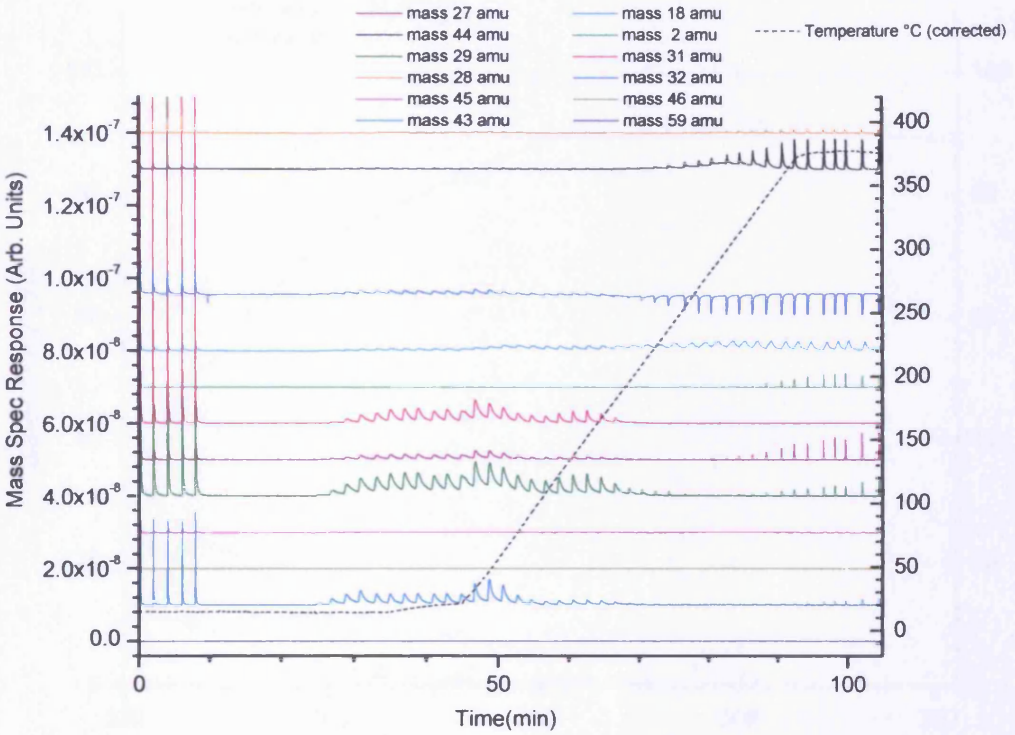

Figure (5-1): Temperature Programmed Pulse Flow Reaction for aerobic ethanol oxidation in 10%O_2/ He gas flow over a 1wt% Au/ TiO_2 catalyst

However, the data obtained in figure 5-1 shows 1wt% Au/TiO_2 is a good combustor of ethanol to CO_2 and water as the main products. However, the oxidation reaction of ethanol was followed by dehydration to ethene at ~300°C and dehydrogenation to CH_3COH (ethanal) at high temperature. The result is in consistent with the reported literature [7,8,11, 13].

When the data in figure 5-1 was integrated and analysed, figure 5-2 was obtained. The figure (5-2) shows as the conversion of ethanol was 50%, the temperature was 180°C and selectivity to CO_2 was 50% with CO selectivity being 25%. When the temperature was increased to 250°C, 100% conversion of ethanol was reached with CO_2 selectivity

being ~90% and with selectivity to CO being >10%. Both selectivities (CO and CO_2) remained the same in a steady state. However, the selectivity to CH_2CH_2 and CH_3COH was small, with both selectivities being less than 10%.

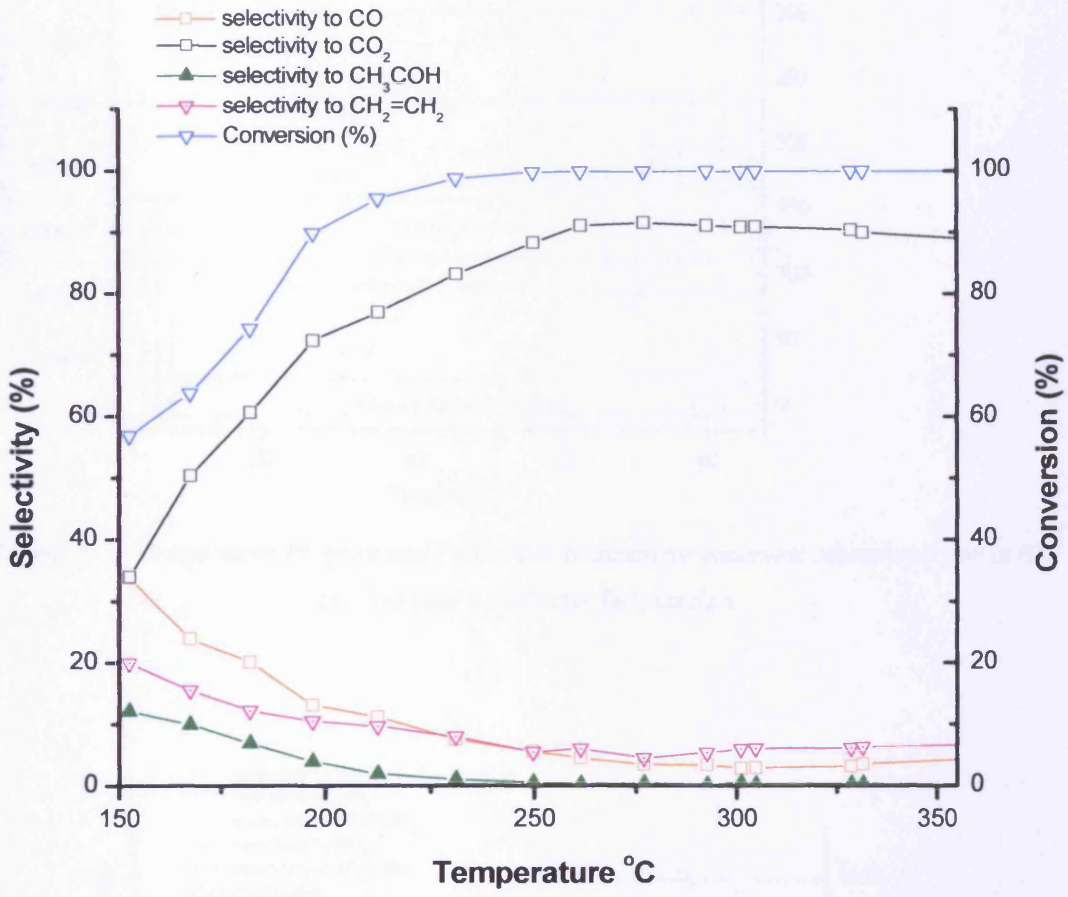

Figure (5-2): Selectivity and conversion with temperature for aerobic ethanol oxidation over a 1wt% Au/TiO_2 catalyst

Similarly, the activity of the Au/ TiO_2 catalyst was tested for ethanol reaction under anaerobic condition, i.e. in a flow of He alone with out any oxygen flowing in the stream (Figure 5-3). The anaerobic ethanol reaction over a 1wt% Au/TiO_2 catalyst was associated with the products of dehydrogenation of ethanol to CH_3COH (ethanal) at approximately 270°C and followed by dehydration to ethene and decomposition to CH_4, hydrogen and CO above 300°C. Figure 5-4, shows the integrated and analysed data of figure 5-3. The figure (5-4) shows as the conversion of ethanol was 50%, the selectivity to CO was 20%, with CO_2 selectivity being > 10%, as the temperature reached 180°C.

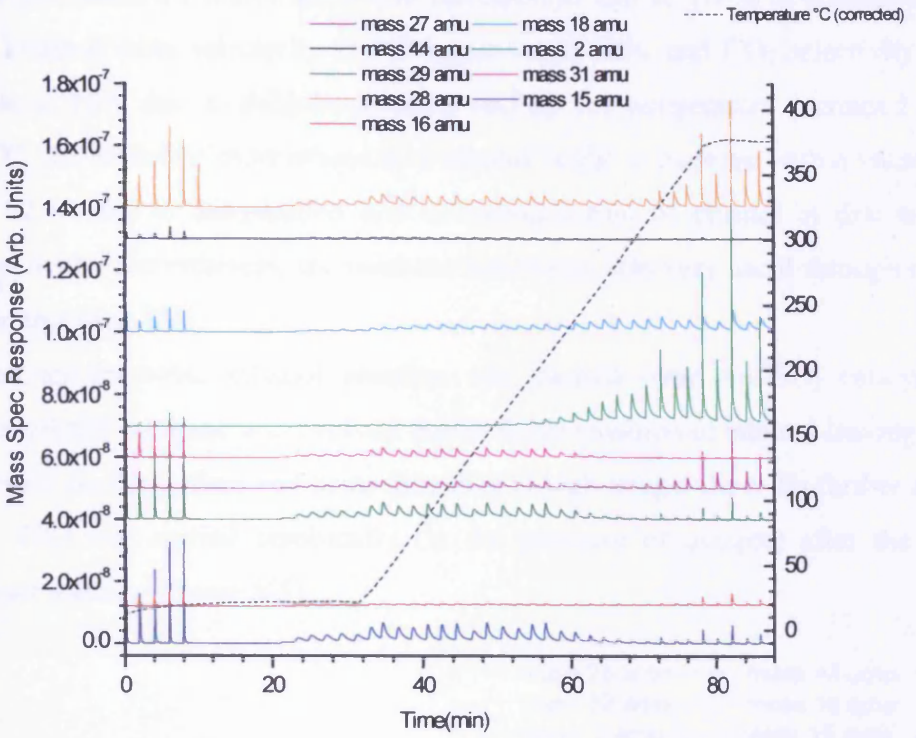

Figure (5-3): Temperature Programmed Pulse Flow Reaction for anaerobic ethanol reaction in He gas flow over a 1wt% Au/ TiO_2 catalyst

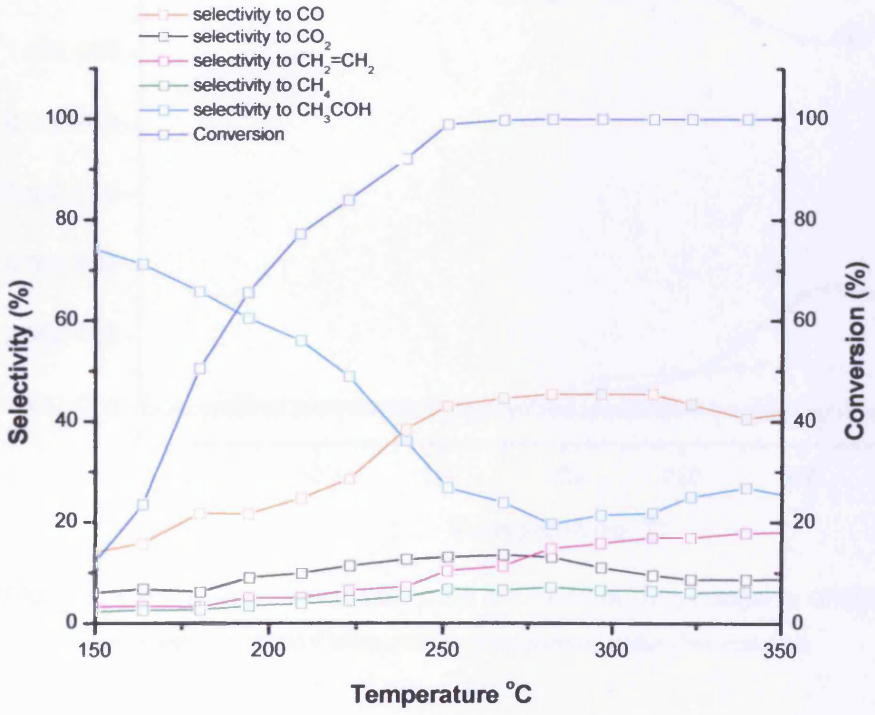

Figure (5-4): Selectivity and conversion with temperature for anaerobic ethanol oxidation over a 1wt% Au/ TiO_2 catalyst

However, when the temperature was increased to 250°C, 100% of ethanol conversion was attained with, selectivity to CO increased to 40%, and CO_2 selectivity increased to about 10% due to dehydrogenation and as the temperature increased further to 280°C, the selectivities to ethene and ethanal begin to increase with a value being 18 and 22 % due to dehydration and dehydrogenation of ethanol at that temperature respectively. Nevertheless, the methane selectivity was very small through out, with a value less than 10%.

When an anaerobic ethanol reaction was carried over Au/TiO_2 catalyst, it was observed that methane was evolved due to decomposition of ethanol leaving CO being adsorbed on the surface and some desorbed at high temperature. To further investigate this, TPD was carried aerobically (in the presence of oxygen) after the anaerobic ethanol reaction (figure 5-5).

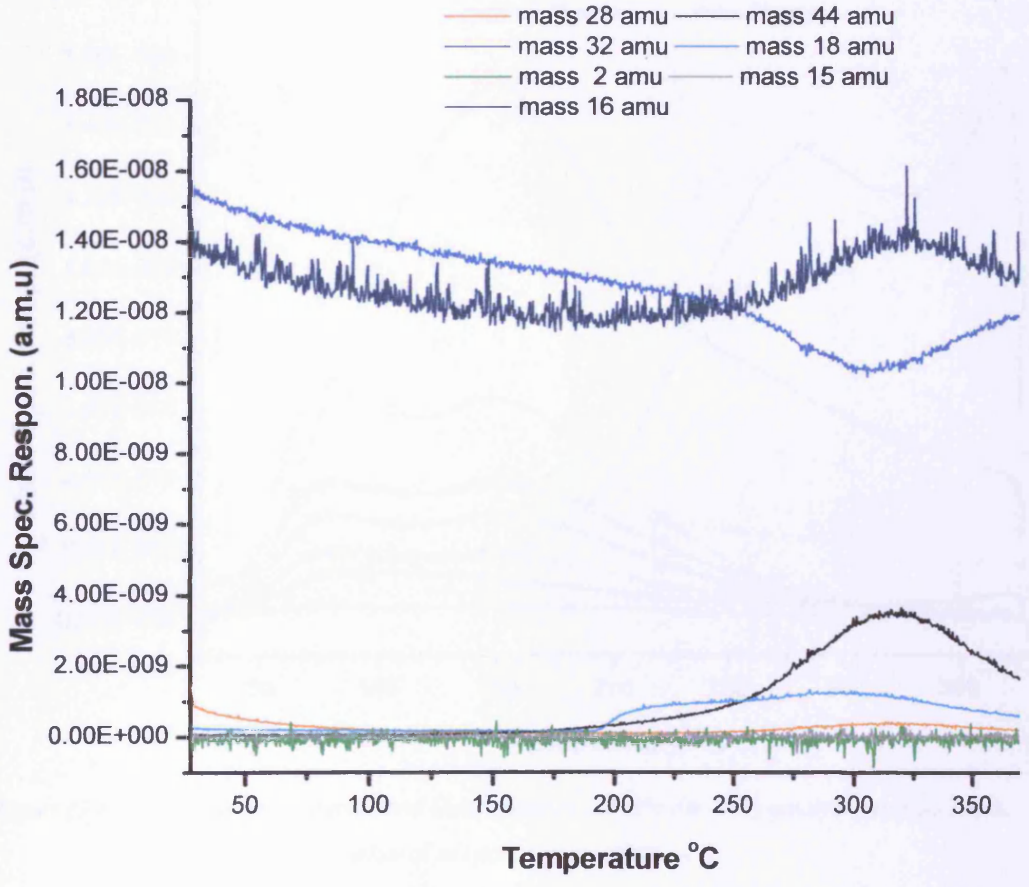

Figure (5-5): Temperature Programmed Desorption of a 1wt% Au/ TiO_2 catalyst in 10%O_2/He flow after anaerobic ethanol temperature programmed pulse flow reaction.

The TPD in figure 5-5 confirmed the decomposition of ethanol on the Au/TiO_2 catalyst. The presence of mass 44 and 16 amu, confirmed the surface reaction between

CO and O_2 respectively to form CO_2 as evident in figure 5-5, from the uptake of mass 32 above 300°C

5.2.3 Temperature Programmed Desorption of ethanol over Au/TiO_2 catalyst

Temperature programmed desorption was also conducted and the data are shown in figure 5-6. In this case the sample was dosed with pulses of ethanol injections and the uptake corresponded to about a monolayer of ethanol at saturation.

As seen from figure 5-6 some water and ethanol desorbed at low temperature due to dehydration of ethanol to ethene (appearance of mass 28, 27, and 29 amu signals) and occurred at about 200°C with hydrogen being evolved.

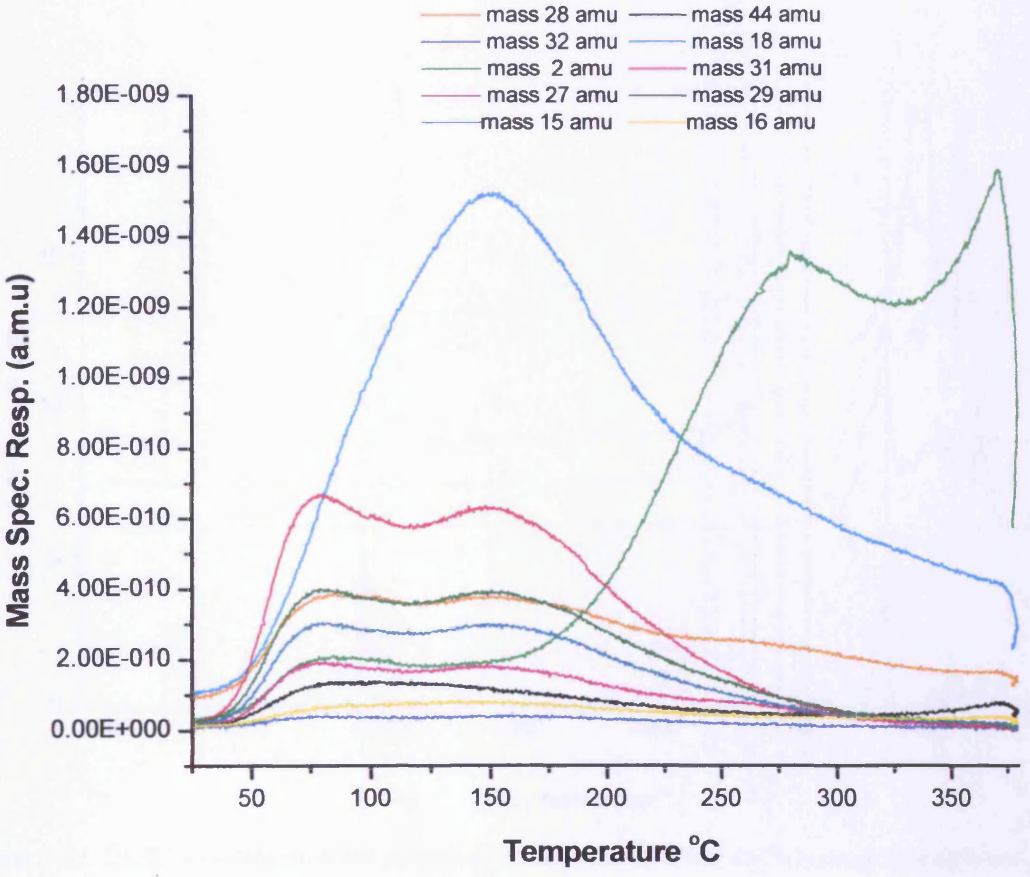

Figure (5-6): Temperature Programmed Desorption of a 1wt% Au/ TiO_2 catalyst saturated with ethanol at room temperature

This was due to dehydrogenation to ethanal (appearance of mass 29, 44, 43, 16 amu signals). However, as the temperature was increased further to 350°C, another hydrogen desorption peak was observed, followed by masses 16 and 15 amu, due to

methane. This is also similar to the product pattern in the reactor However; the main desorbed products are due decomposition of ethanol to methane, CO and hydrogen.

5.2.4 Infra red spectrometry

Figure 5-7 shows the DRIFTS spectrum of ethanol introduced at room temperature on the Au/TiO_2 catalyst. Initially, the Au/TiO_2 catalyst was heated in O_2 for 1 hour at a temperature of 500°C and allowed to cool to room temperature. Ethanol was introduced at room temperature and allowed to stabilize in pressure and then nitrogen was subsequently introduced to purge the gas phase species before the spectra were taken.

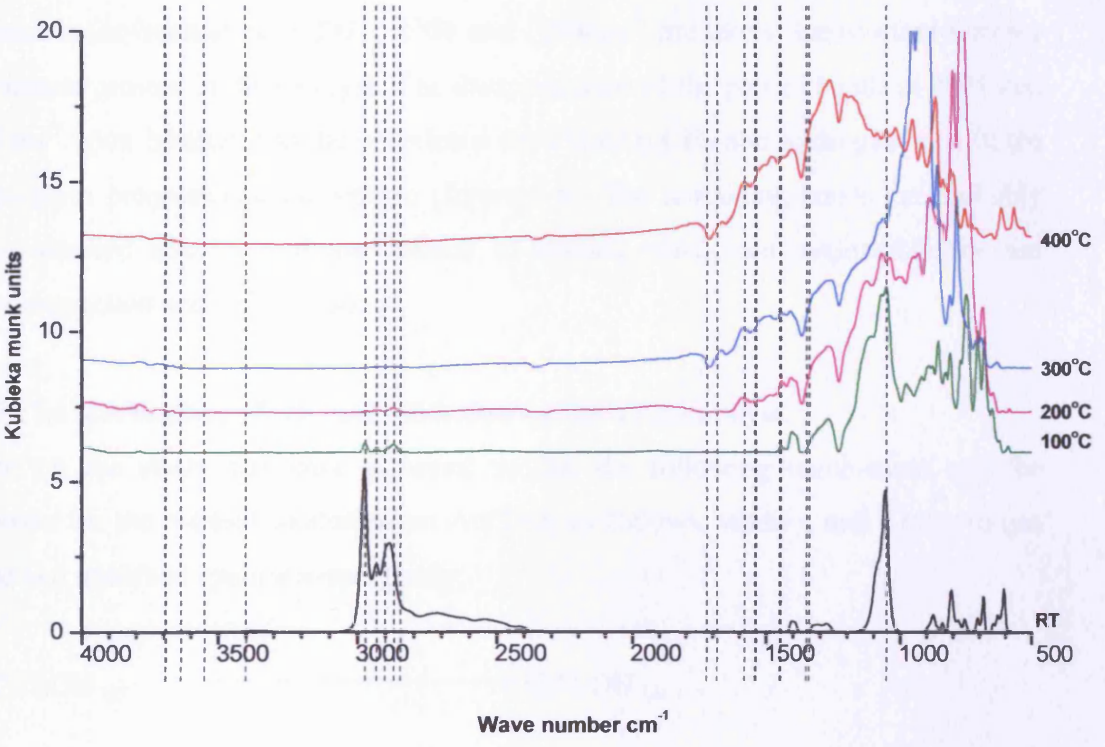

Figure (5-7): DRIFTS spectra from the adsorbed ethanol over a 20%wt Au/TiO_2 catalyst at different temperatures

Figure (5-7), shows spectra in the range 1000cm^{-1} to 1750cm^{-1} and in the range 25000cm^{-1} to 4000cm^{-1}. The bands at 2971, 2931 2901and 1058 cm^{-1} are assigned to $\nu_{as}(CH_3)$,$\nu_{as}(CH_2)$ and ν_s(C-O) of the adsorbed ethanol ($C_2H_5OH_{ad}$) respecively[9,11]. Similarly, the presence of the peaks at 1723cm^{-1} was assigned by Chuang et al.[7], as the ν(C=O) band due to adsorbed ethanal (CH_3CHO_{ad}). The bands observed at 1542, 1469

and $1340cm^{-1}$ will also be assigned to $\nu_{as}(COO)$, $\delta_{as}(CH_3)$, and $\delta_s(CH_3)$ for adsorbed acetate ($CH_3COO^-_{ad}$) respectively. However, the bands at 2846 and $1350cm^{-1}$ were assigned to the $\nu(CH_2)$ and $\nu_s(COO)$ for the adsorbed formate ($HCOO^-_{ad}$)[9, 11,12]. The data obtained in figure 5-6 show that the band at 3690, 3550 and $3634cm^{-1}$ are likely due to $\nu(OH)$ of the isolated OH [9,11,12]. The spectrum is similar to that for TiO_2 alone but with some small differences. Higher spectrum intensities are observed in the Au/TiO_2 catalyst than when TiO_2 was used alone. The high intensities may be due to more formate and acetate formation on the gold and reduced coverage of ethoxy species on the surface of the catalyst[1]. The result is similar to reduced coverage of methoxy due to high intensity of formate present due gold as reported in section 4.14.1 of chapter 4.

The spectrum shows similar bands to those observed when TiO_2 was used alone. The increase in the intensities at 2971, 2901 and $1058cm^{-1}$, are likely due to more formate and acetate present in the catalyst. The disappearance of the pair of bands at 2971 and $2901cm^{-1}$ upon heating may be correlated the CO,CO_2,CH_4 and hydrogen seen in the temperature programmed desorption (figure 5-6). The remaining bands are probably ethoxy-derived species and are related to titania, which are responsible for the dehydrogenation and dehydration.

5.2.5 The mechanism of ethanol oxidation on Au/TiO_2 catalyst.

Based on the study and data gathered so far, the following mechanism may be proposed for the ethanol oxidation on Au/TiO_2 as follows, where $_g$ and $_a$ refer to gas phase and adsorbed species respectively:

(a) $C_2H_5OH_{(g)} \longrightarrow C_2H_5OH_{(a)}$

From the temperature programmed desorption data (figure 5-6), ethanol is seen to be desorbed at low temperature. The uptake of ethanol (figure 5-6) was measured to be about half monolayer from the pulses taken up by the catalyst. The desorption of ethanol at low temperature is associated with a weakly bound form of molecular ethanol on the surface, and the higher temperature desorption states are those involved with catalytic processes and involved the reaction of ethanol with the surface as follows:

(b) $C_2H_5OH_{(a)} + O^{2-}_{(a)} \longrightarrow C_2H_5O^-_{(a)} + OH^-_{(a)}$

(c) $C_2H_5OH_{(a)} + OH^-_{(a)} \longrightarrow C_2H_5O^-_{(a)} + H_2O_{(g)}$

The steps (b) and (c) are the most likely ways for the ethoxy formation, however, with (b) likely to be dominant at ambient temperature for titania. In this case, the anion vacancies are designated as Vo^{2-}, although the electrons are likely to be associated with cation sites, as Ti^{3+} than the vacancy itself.

The presence of the bands at 2971 2931 and 1450cm^{-1} indicate that ethoxy species are formed according steps (b) and (c) above. The adsorbed ethoxy formed by the reaction in (b) and (c) are likely the main intermediate for the formation of gas phase products such as:

(d) $C_2H_5O^-_{(a)} + O^{2-}_{(a)} \longrightarrow CH_{4(g)} + CO_{(g)} + OH^-_{(a)} + Vo^{2-}$

(e) The adsorbed ethoxy may also react with adsorbed oxygen on the surface and give hydrogen as seen as a product at high temperature from titania and even in the presence of gold. The appearance of the peaks at 1723cm^{-1} indicated the presence of adsorbed acetaldehyde species, while the peaks at 2846 and 1350cm^{-1} also indicated the presence of adsorbed acetate species respectively. The adsorbed acetate and acetates species may be formed by the following reaction.

(i) $C_2H_5O^-_{(a)} + O^{2-}_{(a)} \longrightarrow CH_3COH_{(a)} + OH^-_{(a)} + Vo^{2-}$

or

(ii) $C_2H_5O_{(a)} + O^{2-}_{(a)} \longrightarrow CH_3COO^-_{(a)} + H_{2(g)} + Vo^{2-}$

The bands observed at 2846 and 1350cm^{-1} are associated with the presence of adsorbed formate species which are likely be formed either through adsorbed acetate or adsorbed acetaldehyde species according the following reaction.

(f) (i) $CH_3COH_{(a)} + OH^-_{(a)} \longrightarrow HCOO^-_{(a)} + CH_{4(g)}$

(ii) $CH_3COO^-_{(a)} + OH^-_{(a)} \longrightarrow HCOO^-_{(a)} + CH_3O^-_{(a)}$

(g) The formates adsorbed on gold may subsequently decompose (i) or react with the adsorbed surface hydroxide (ii) according to following reaction.

(i) $2HCOO^-_{(a)} \longrightarrow 2CO_{2\,(g)} + H_{2\,(g)} + 2e^-$

(ii) $HCOO^-_{(a)} + OH^-_{(a)} \longrightarrow CO_{2\,(g)} + H_2O + 2e^-$

(h) The ethene, which is a dehydration product mainly on TiO_2, will be formed according to the following reaction:

(i) $C_2H_5O^-_{(a)} \longrightarrow CH_2CH_{2\,(g)} + OH^-_{(a)}$

5.2.6 Control Experiments

The control experiments were carried out on TiO_2 alone for comparison with the corresponding Au/TiO_2 catalyst. The temperature programmed pulse flow reaction of ethanol oxidation over TiO_2 catalyst is shown in figure 5-8. Ethanol reaction over TiO_2 is complete oxidation to CO_2 and water. However, the reaction was accompanied by dehydration of ethanol to ethene followed by deoxygenation to ethane as seen in figure 5-8. When the data in figure 5-8 was integrated and analysed, figure 5-9 was obtained, and shows that, 100% of ethanol was observed at relatively higher temperature (250°C) than the Au/TiO_2 catalyst, with low selectivity to CO_2 being ~70% through out the experiment. However, the selectivity to CO was also around 20%, with less than 10% selectivity to both ethene and ethanal.

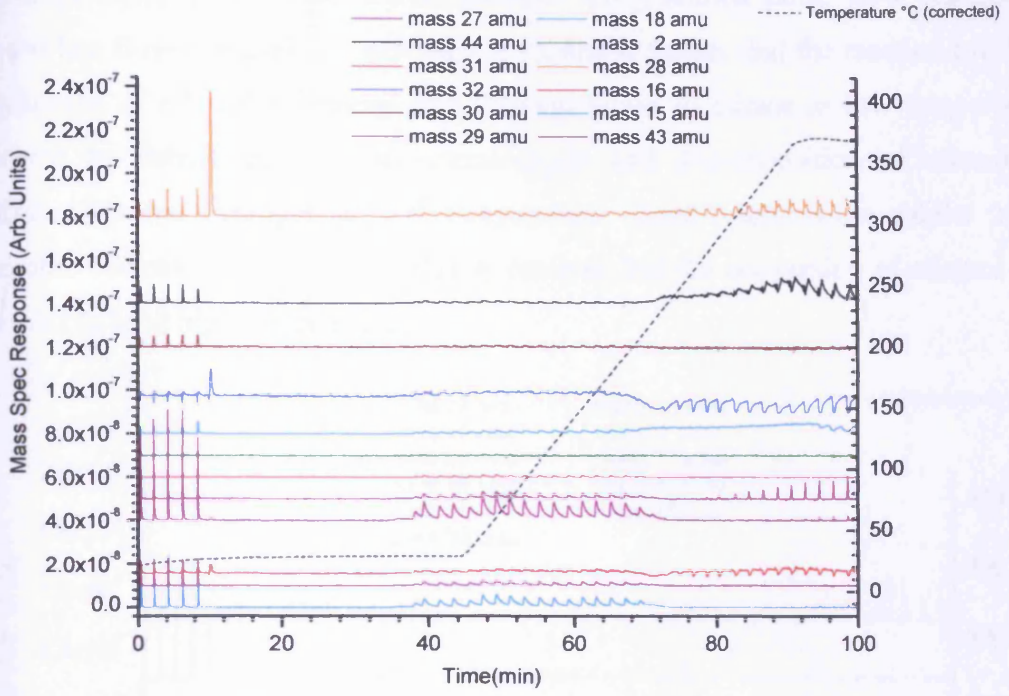

Figure (5-8): Temperature Programmed Pulse Flow Reaction for aerobic ethanol oxidation reaction in 10%O_2He gas flow over TiO_2 catalyst

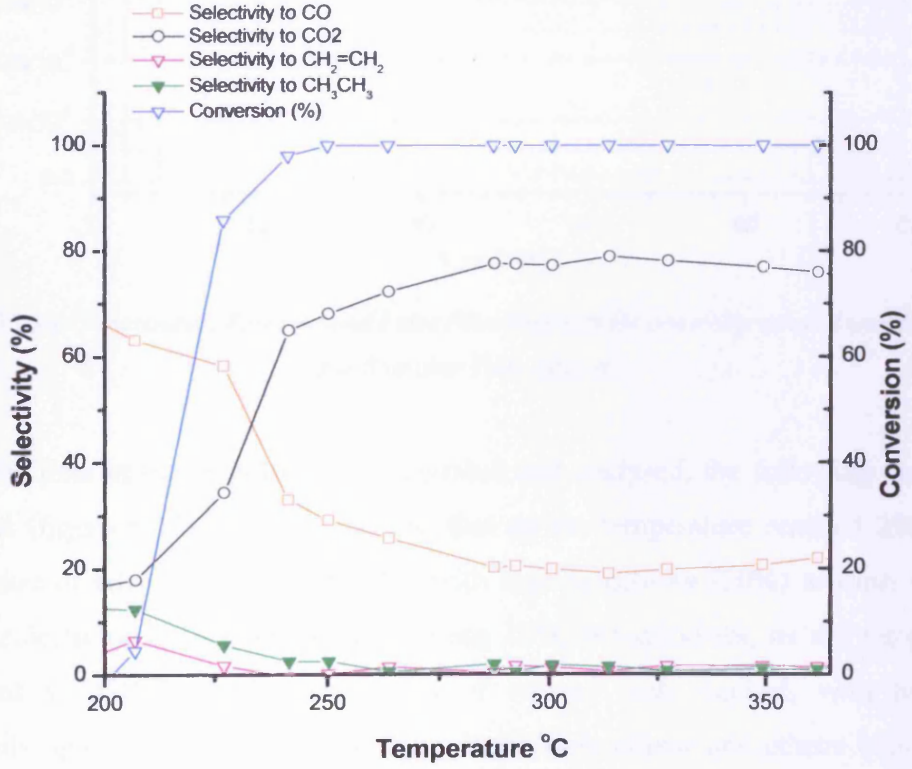

Figure (5-9): Selectivity and conversion with temperature for aerobic ethanol oxidation in 10%O_2/He flow over TiO_2 catalyst

Similarly, figure 5-10 shows the temperature programmed pulse flow reaction of ethanol in a flow of He alone (anaerobically), and indicates that the reaction involved dehydration of ethanol to ethene and deoxygenation to ethane at low temperature, followed by dehydrogenation to acetaldehyde and decomposition of ethanol to methane, CO and hydrogen at high temperature. These reactions are similar to the anaerobic ethanol reaction over Au/TiO_2 catalyst, but the conversion of ethanol was observed to be at high temperature.

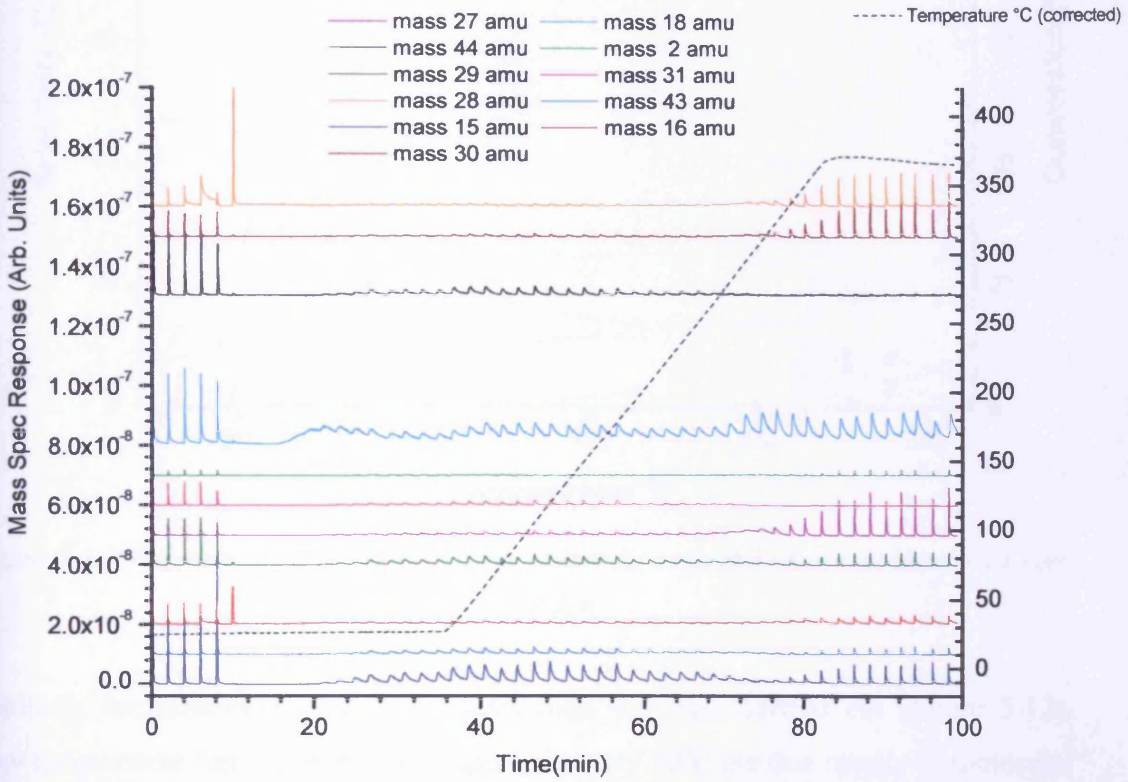

Figure (5-10): Temperature Programmed Pulse Flow Reaction for anaerobic ethanol reaction in He gas flow over TiO_2 catalyst

When the data in figure 5-10 were integrated and analysed, the following result was obtained (figure 5-11), which indicated that as the temperature reached 290°C, the conversion of ethanol was about 50%, with high selectivity (30%) towards CO and ethene selectivity at this temperature being 10%. Nevertheless, as the temperature increased to 330°C, 100% conversion of ethanol was reached, with high CO selectivity again (~50%). However, the selectivity to ethane and ethene increased as well, due to deoxygenation and dehydration of ethanol to a little higher than 10%. Similarly, the selectivity of methane also increased to ~10% as the temperature reached above 350°C.

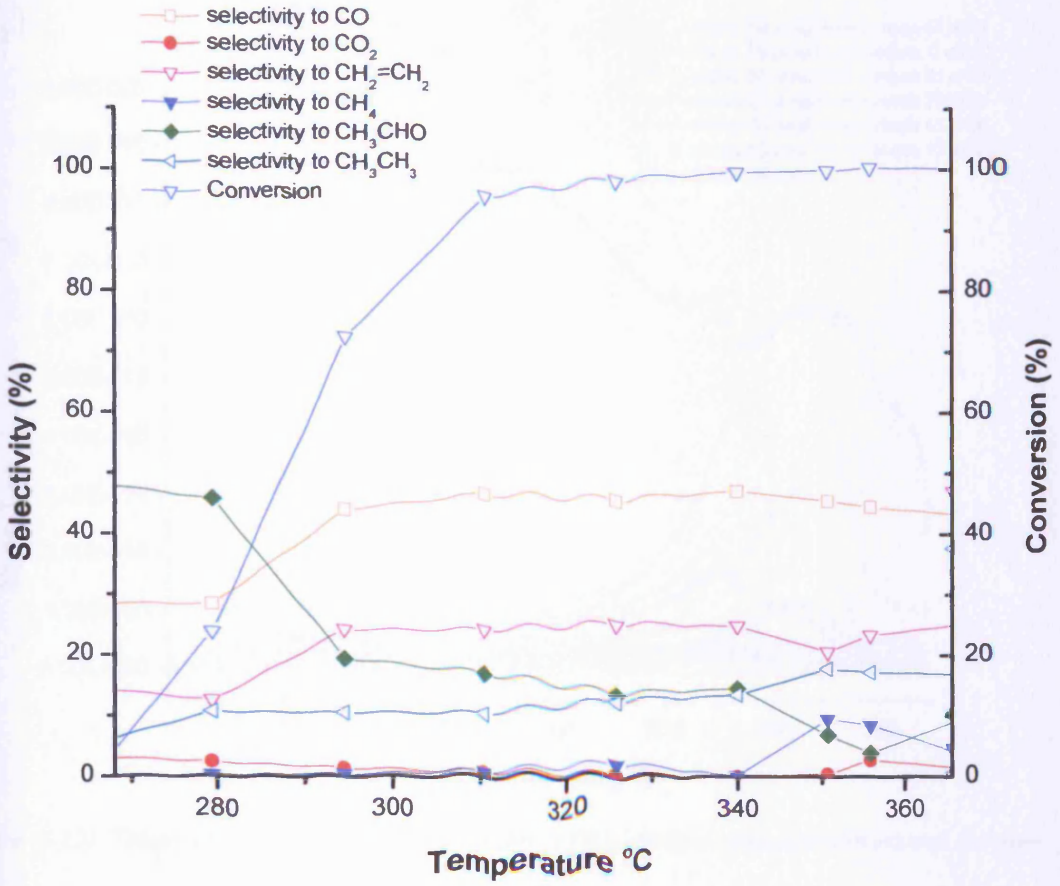

Figure (5-11): Selectivity and conversion with temperature for anaerobic ethanol oxidation in He over TiO_2 catalyst

Similarly, temperature programmed desorption was also carried out (figure 5-12). Low temperature desorption peaks at approximately 80°C are due mostly to molecular ethanol weakly bound on the surface. However, as the temperature was increased to 250°C, diethyl ether (the appearance of masses 31, 59, 29 and 45 amu signals) and ethane (appearance of masses 28, 30, 27 and 29 amu signals) were observed due to dehydration and deoxygenation respectively. When the temperature further increased to 300°C, more ethene (appearance of mass 28, 27, and 29 amu signals) and ethanal (appearance of mass 29, 44, 43, and 15 amu signals) was observed due to dehydration and dehydrogenation respectively, with desorption peaks of both centred at 320°C. Nevertheless, some methane was desorbed above 350°C due to decomposition of ethanol at that temperature with evolution of CO and hydrogen similar to the anaerobic reaction with ethanol. The TPD data is similar to the results obtained by OShima *et al.* [14-16].

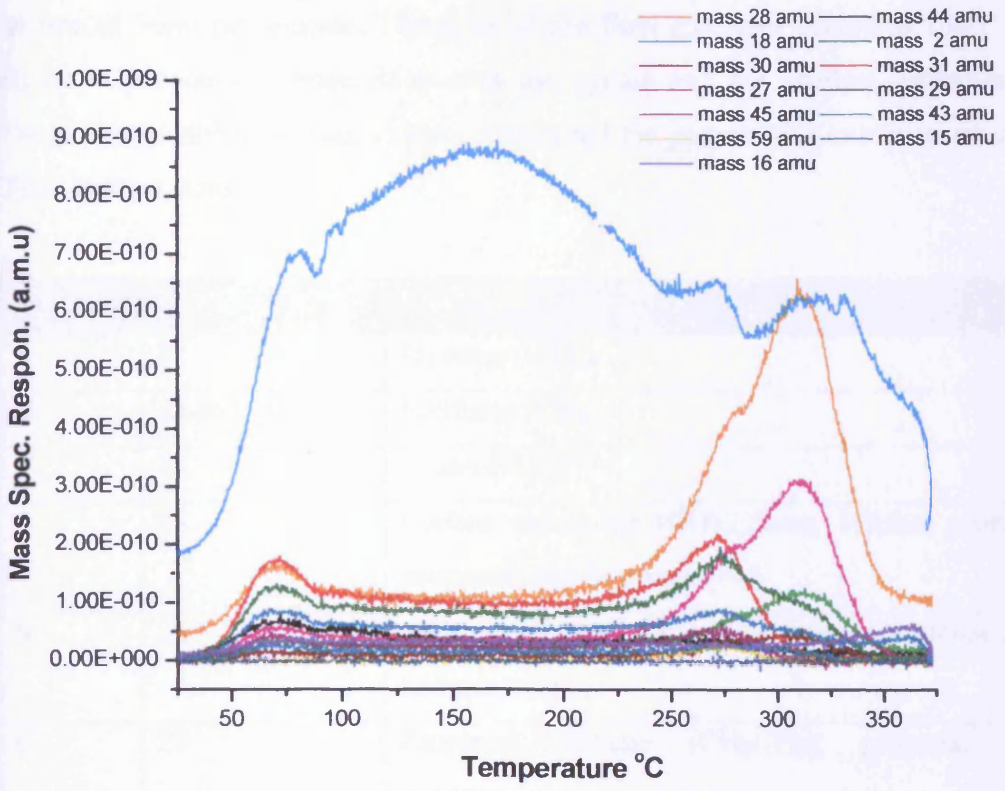

Figure (5-12): Temperature Programmed Desorption of TiO_2 catalyst saturated with ethanol at room temperature

5.3 Propan-1-ol oxidation over Au/TiO2 catalyst

Propan-1-ol is another primary alcohol with the formula $CH_3CH_2CH_2OH$. It is known as Propan-1-ol, 1-propyl alcohol, n-propyl alcohol, or simply propanol. It is an isomer of propan-2-ol. It is used as a solvent in the pharmaceutical industry, and for resins and cellulose esters. It is formed naturally in small amounts during many fermentation processes. Propanol was first discovered in 1853 by Chancel, who obtained it by fractional distillation of fused oil.

A number of researchers[17-21] have carried out the catalytic oxidation of propan-1-ol on different metal oxides. Several products such as propanal, propanoic acid, and propanoate have been reported. However, only few reported the catalytic oxidation of propan-1-ol over Au/TiO_2 catalysts.

5.3.1 Activity test

In order to study the activity of the catalyst with respect to propan-1-ol oxidation, a freshly prepared 1wt% Au/TiO_2 calcined sample of the catalyst was calcined at 400°C

in air. It was then loaded in a pulse flow reactor in the presence of 10% O_2/He flow of gas at rate of 30ml per minute. The lines of the flow gas were heated to 100°C and injections of propan-1-ol were done over the bypass and the catalyst .However, in each experiment, different masses were monitored for propan-1-ol oxidation over the Au/TiO_2 catalyst (table 5-2).

SNO	MASS	PRODUCT NAME
1	2	Hydrogen (H_2)
2	15 and 16	Methane (CH_4)
3	18	Water (H_2O)
4	28	Carbon monoxide (CO),Ethene, Ethane, propane, propanal, and Nitrogen (N_2)
5	29	propanol, Ethene, Ethane, propanal, propanoic acid and propane
6	27	Propanol, Ethene (CH_2CH_2), propanal, and propene.
7	30	Ethane (CH_3CH_3)
8	31	Ethanol (CH_3CH_2OH) and Diisopropyl ether ($C_3H_7OC_3H_7$)
9	32	Oxygen (O_2)
10	43	Diisopropyl ether and propane
11	44	Carbon dioxide CO_2 and Ethanal(CH_3COH)
12	58	Propanal (CH_3CH_2CHO)
13	74	Propanoic acid (CH_3CH_2COOH)

Table 5-2: Masses monitored for propan-1-ol oxidation over a 1wt% Au/ TiO_2 catalyst

The masses monitored were chosen because propanol can be dehydrogenated to produce CH_3CH_2CHO in the presence of oxygen (oxidation) or it may be decomposed to produce CH_3CH_3, CO, H_2 and sometime CO_2 and water, similar to ethanol. Ethanol can be oxidised and dehydrogenated to acrolein (propenal). Similarly, propanal can also be oxidised to produce propanoic acid and simultaneously, can further react with propanol to produce isopropyl ester. However, propanol can also be deoxygenated to propane or dehydrated to propene.

Based on the study so far using temperature programmed pulse flow reaction in $10\%O_2$/He, the results for propanol oxidation over a 1wt% Au/TiO_2 catalyst (aerobic) were as shown in figure 5- 13.

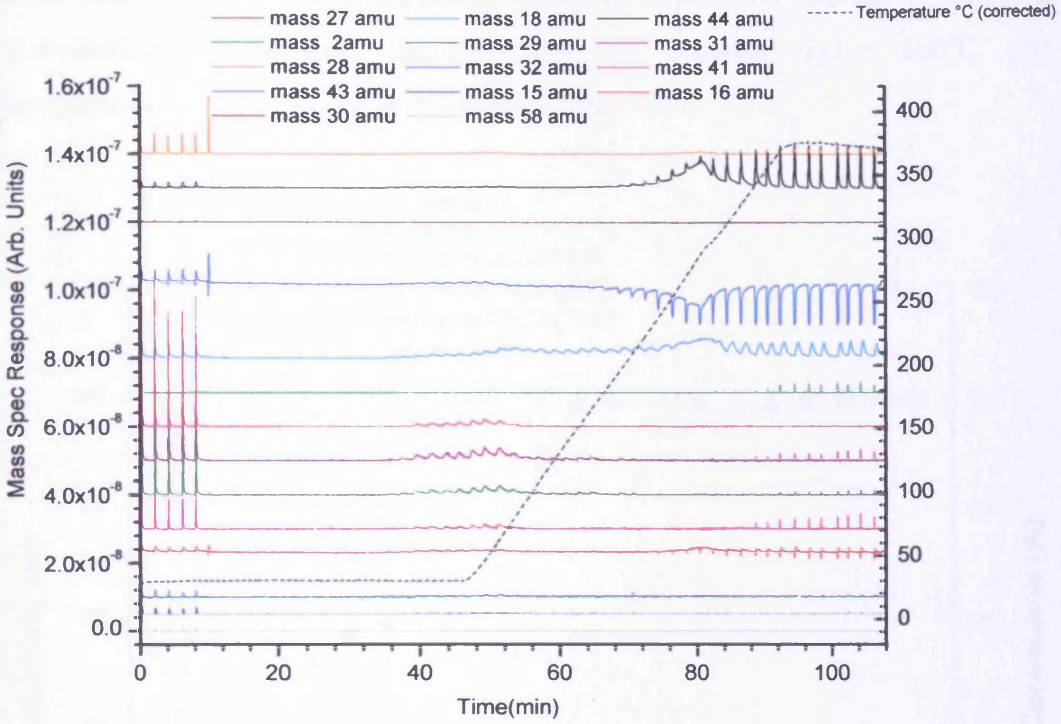

Figure (5-13): Temperature Programmed Pulse Flow Reaction for aerobic propan-1-ol oxidation in 10%/ He gas flow over a 1wt% Au/ TiO_2 catalyst

The first five pulses were observed for propan-1-ol injection over the bypass and this gives the cracking pattern observed for propan-1-ol. When the surface was saturated (after approximate 40 minutes), only propan-1-ol molecules broke through and no conversion of propan-1-ol occurred. The peak areas were much smaller and broad than those passing through the bypass and the integrals were similar to those through the bypass. The uptake of propan-1-ol was about 10µl, corresponding with $1.67x10^{20}$ molecules g^{-1} of catalyst. This in turn corresponds with 8.349×10^{19}molecules m^{-2}.

As the temperature increased to 120°C, 100% of propan-1-ol was obtained (loss of mass 31, 29, 27 and 28 amu signals), and two stages of CO_2 production occurred. In the first stage (70-80min), there was slow CO_2 evolution, together with slow uptake of oxygen after each pulse injection. When the temperature reached 250°C, the production of CO_2 and uptake of oxygen occurred at a faster rate as evident from the sharp peaks. At 300°C, the evolution of hydrogen (mass 2 amu signal) signifies the propanal evolution but its production is very minimal (absent of mass 58 amu signal);

propane (mass 29, 28, 27, 44 and 43 amu signals), and propene (mass 41 and 27 amu signals) begin to emerge as the temperature increases.

The data obtained in figure 5-13 indicate that the main reactions seen for propan-1-ol oxidation over Au/TiO_2 catalyst are complete oxidation between 120-300°C, followed by dehydration to propene, deoxygenation to propane above 300°C and dehydrogenation to propanal but very minimal from 350°C.

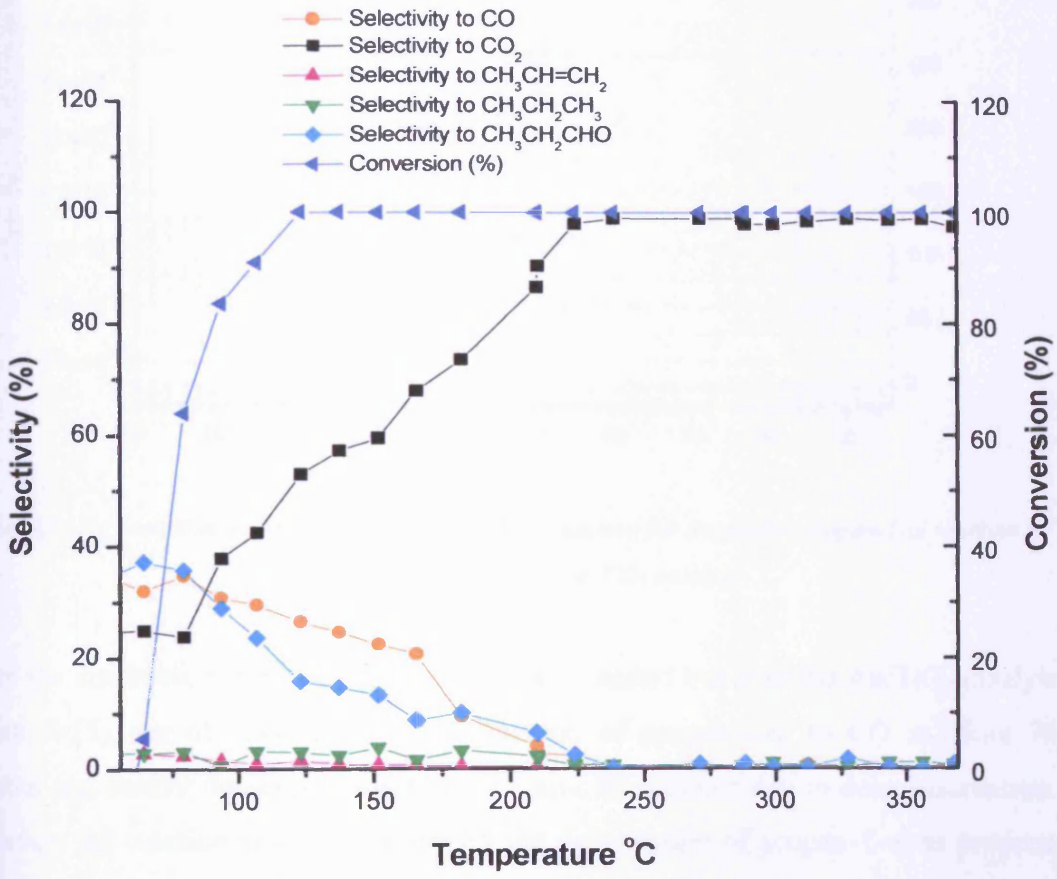

Figure (5-14): Selectivity and conversion with temperature for aerobic propan-1-ol oxidation in 10%O_2/He flow over a 1wt% Au/ TiO_2 catalyst

Figure 5-14 shows the integrated and analysed data of figure 5-13. At a temperature of 100°C, propan-1-ol conversion was 60% and the catalyst was selective to CO_2, with a value being almost 50%. When the temperature was increased to 125°C, 100% conversion of propan-1-ol was observed. However, as the temperature increased above 250 °C, with selectivity increases towards CO_2, with a CO_2 selectivity observed to be almost 98% through out the experiment, with CO, propanal, propene and propane selectivities being less than 2%.

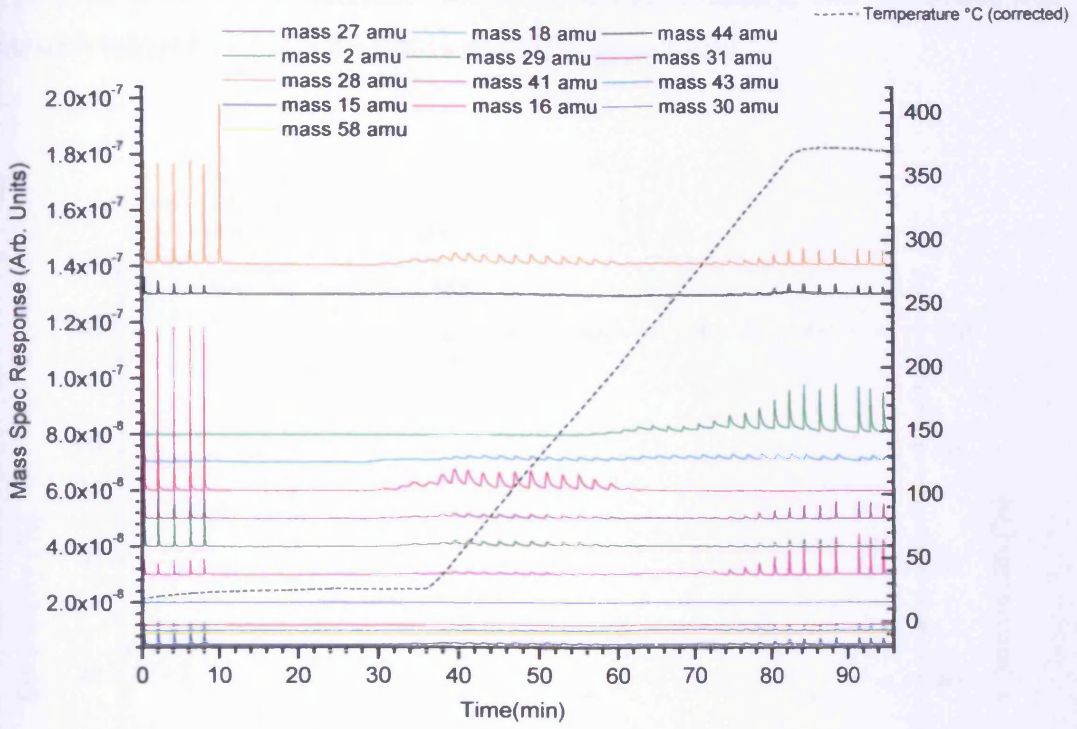

Figure (5-15): Temperature Programmed Pulse Flow Reaction for anaerobic propan-1-ol reaction in He gas flow over a 1wt% Au/ TiO_2 catalyst

When the anaerobic reaction for propan-1ol was carried out over the Au/TiO_2 catalyst (figure 5-15), we observe more decomposition of propan-1-ol to CO at about 70 minutes and further decomposition to CO_2 above 80 minutes due to dehydrogenation. However, the reaction is accompanied by the dehydration of propan-1-ol to propene (appearance of mass 41, 27, and 29 amu signals) from 70 minutes and deoxygenation to propane (appearance of mass 29,28,27, 43 and 44 amu signals) and dehydrogenation to propanal (appearance of 29,28,27 and some little 58 amu signals) from 80 minutes.

When the data in figure 5-15 were integrated and analysed, figure 5-16 was obtained. Figure (5-15) shows propan-1-ol conversion to be 50% as the temperature was about 190°C and the catalyst is selective towards CO. The CO selectivity increases until the temperature reached about 200°C in which the selectivity changes towards dehydration to propane and deoxygenation to propane, with selectivities value of about <20% each respectively. However, when the temperature was increased to 250°C, the CO selectivity was increased to 40% and the propanal and CO_2 selectivities

begin to increase to almost 20% respectively. The high selectivity to propanal and CO_2 is due to dehydrogenation and decomposition of propan-1-ol. However, the CO and propene selectivities decrease when the dehydrogenation and decomposition begin, with values being less than 40% and 20% respectively.

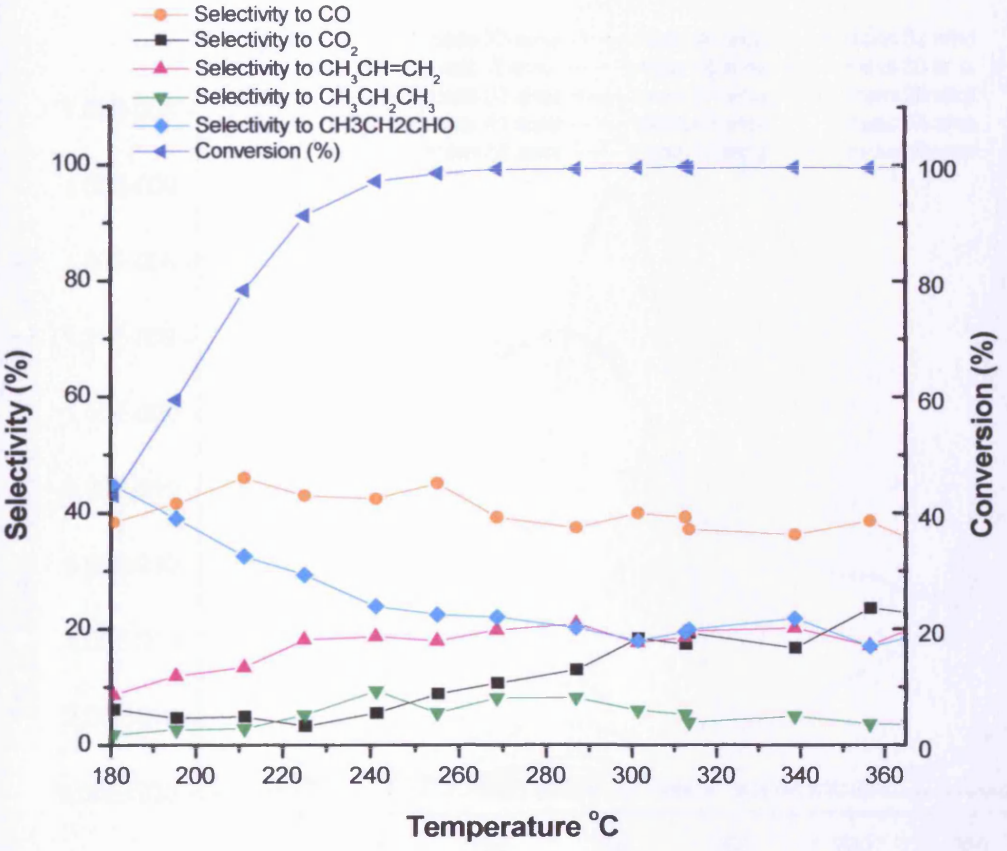

Figure (5-16): Selectivity and conversion with temperature for anaerobic propan-1-ol reaction in He flow over a 1%wtAu/TiO_2 catalyst

5.3.2 Temperature Programmed Desorption of propan-1-ol over Au/TiO_2 catalyst

Temperature programmed desorption was also conducted. The data are as shown in figure 5-17. The sample was dosed with pulses of propan-1-ol and the uptake corresponded to about one monolayer of propan-1-ol at saturation.

As seen in figure 5-17 some water and propan-1-ol desorbed at lower temperature ~90°C and as the temperature was increased to 180°C, hydrogen, CO, propanal, propene and propane was evolved due to dehydrogenation of propan-1-ol, dehydration to propene and deoxygenation to propane. However, as the temperature further

increased above 350°C, hydrogen, water and CO_2 was evolved due to decomposition of propan-1-ol to CO_2 and water. The coincident appearance of CO_2 and hydrogen confirmed the presence of formate as adsorbed species on the Au/TiO_2 catalyst. The results are consistent with that reported by Diaz et al. [17, 20]

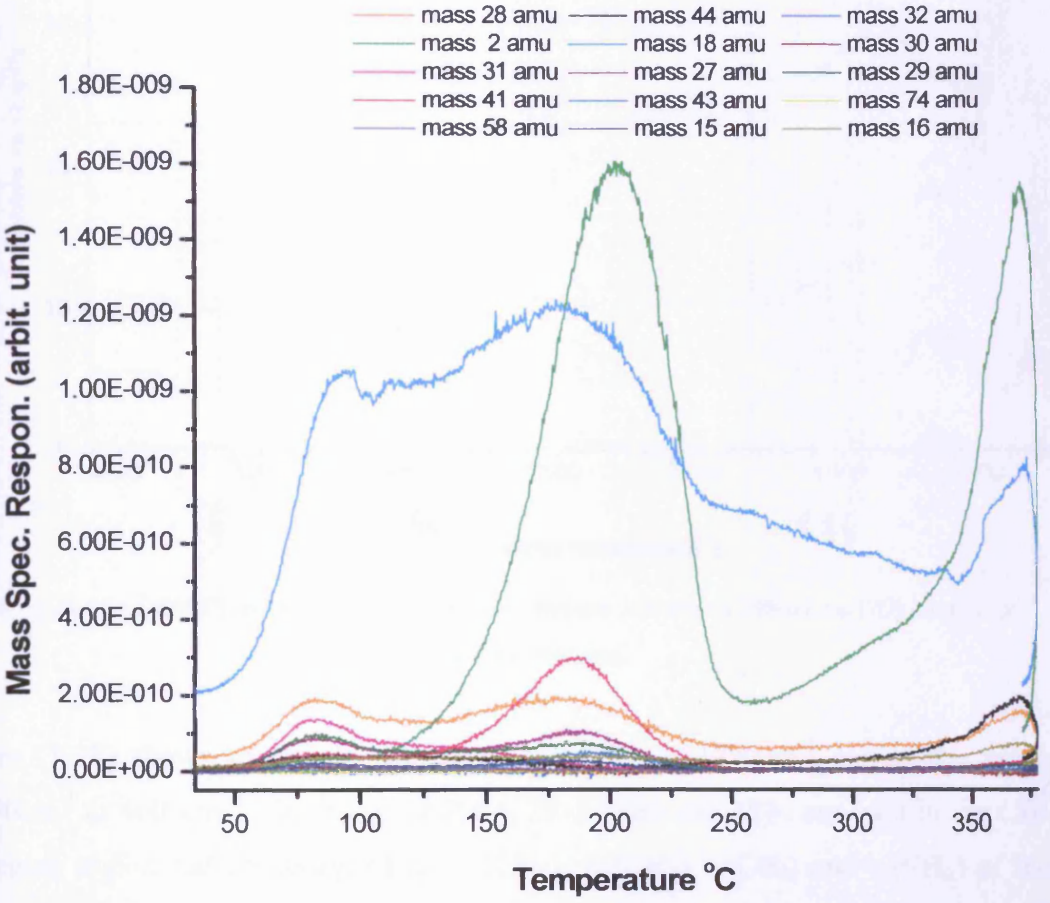

Figure (5-17): Temperature Programmed Desorption of a 1wt% Au/ TiO_2 catalyst saturated with propan-1-ol at room temperature

5.3.3 Infra red spectrometry

Infrared absorption spectra were taken for propan-1-ol over an Au/TiO_2 catalyst after the catalyst was heated in oxygen for 1 hour and allowed to cool to room temperature. Propan-1-ol was introduced at room temperature and allowed to stabilize in pressure then nitrogen was subsequently introduced in order to purge the gas phase species. Figure 5-18 shows the spectrum taken for propan-1-ol over the 20wt% Au/TiO_2 catalyst.

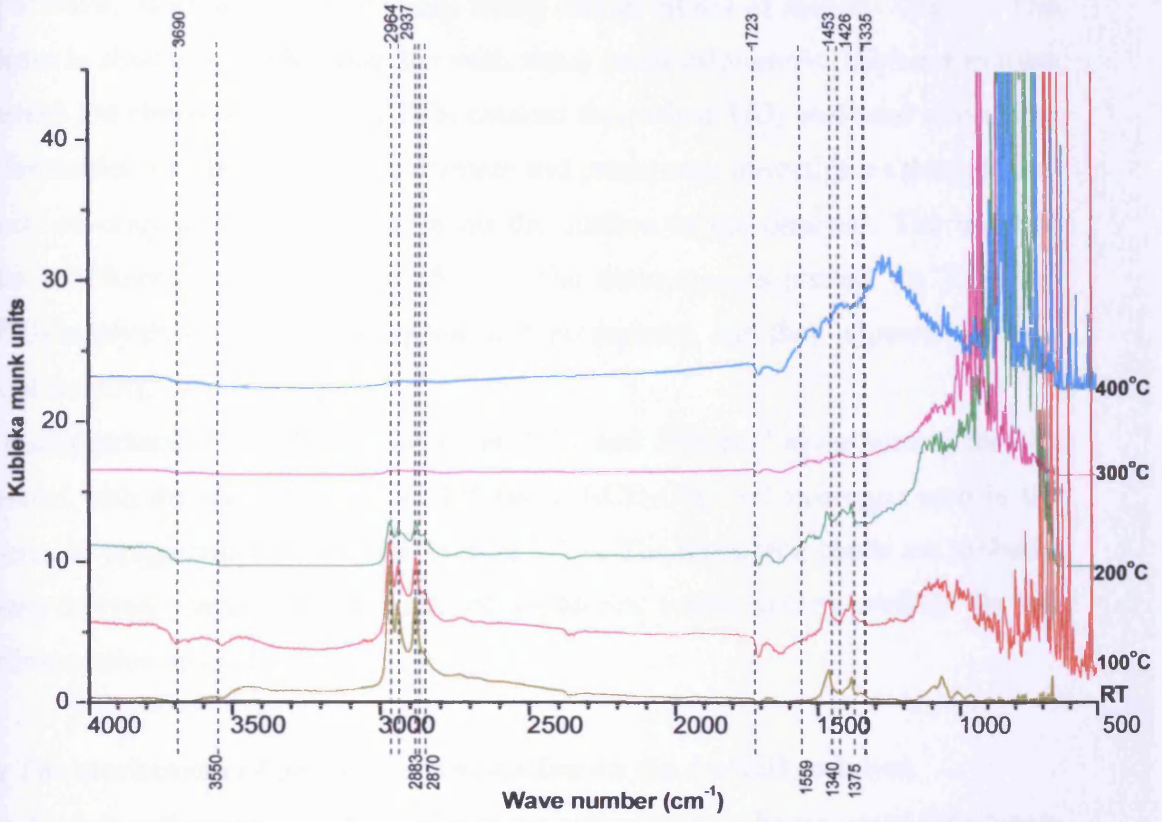

Figure (5-18): DRIFTS spectra from the adsorbed propan-1-ol over a 20%wt Au/TiO_2 catalyst at different temperatures.

Figure (5-18) shows spectra in the range $1000cm^{-1}$ to $1750cm^{-1}$ and in the range $25000cm^{-1}$ to $4000cm^{-1}$. The bands at 2964, 2937 2883 and 2870 cm^{-1} are in the CH-stretching region and are assigned to $\nu_{as}(CH_3)$, $\nu_{as}(CH_2)$ $\nu_s(CH_3)$ and $\nu_s(CH_2)$ of the adsorbed propanol ($C_3H_7OH_{ad}$) respectively. In the CH bending region, the bands $\delta_{as}(CH_3)/\delta(CH_2)$ at $1460cm^{-1}$ and $\delta_s CH_3)$ at $1375cm^{-1}$ and $\delta(CH)$ at $1335cm^{-1}$ can be assigned[18-20]. However, according Weckhuysen *et al.*[21] The bands at 1090 and $1140cm^{-1}$ can be assigned as C-O-Ti stretching vibrations for propanol. The intensities of the bands are higher when compared with TiO_2 alone, which is likely due to the formation of formate on the gold component of the catalyst.

Similarly, the presence of the peaks at $1723cm^{-1}$ was assigned by Chuang *et al.*[7, 20], as the $\nu(C=O)$ band due to adsorbed propanal ($C_2H_5CHO_{ad}$). The bands observed at 1559, 1453 1426 and $1340cm^{-1}$ will also be assigned to $\nu_{as}(COO)$, $\delta_{as}(CH_3)$, $\delta(CH_2)$ and $\delta_s(CH_3)$ for adsorbed propanoate ($CH_3CH_2COO^-_{ad}$) respectively.[20] The presence of the bands at 2850 and $1340cm^{-1}$ was assigned to the $\nu(CH_2)$ and $\nu_s(COO)$ bands for

the adsorbed formate ($HCOO\text{-}_{ad}$)[1, 2, 3]. The data obtained in figure 5-6 shows that the band at 3690, 3550 and 3634cm^{-1} are likely due to ν(OH) of isolated OH. [1,3] The spectrum is similar to TiO_2 alone but with some small differences. Higher spectrum intensities are observed in the Au/TiO_2 catalyst than when TiO_2 was used alone. The high intensities may be due to more formate and propanoate formation on the gold and reduced coverage of propoxy species on the surface of the catalyst[1]. The result is similar to ethanol reported earlier (5.2.4). The main species present on TiO_2 and Au/TiO_2 catalysts are formate, propanal and propanoate, and they appeared to have thermal stability.

The disappearance of the pair of bands at 2971 and 2901cm^{-1} upon heating may be correlated with the CO, CO_2, $CH_3CH{=}CH_2$, $CH_3CH_2CH_3$ and hydrogen seen in the temperature programmed desorption (figure 5-17). The remaining bands are probably propoxy-derived species and are related to titania, which are responsible for the dehydrogenation and dehydration.

5.3.4 The mechanism of propan-1-ol oxidation on the Au/TiO_2 catalyst.

From the data gathered so far, the following mechanism may be proposed for propan-1-ol oxidation on Au/TiO_2, where $_g$ and $_a$ refer to gas phase and adsorbed species respectively:

(a) $C_3H_7OH_{(g)} \longrightarrow C_3H_7OH_{(a)}$

From the temperature programmed desorption (figure 5-17), propan-1-ol is seen to be desorbed at low temperature. The propan-1-ol uptake in figure (5-17) was measured to be about half monolayer from the pulses taken up by the catalyst. As in the case of ethanol, the low desorption of propan-1-ol at low temperature is associated with a weakly bound form of molecular ethanol on the surface, and the higher temperature desorption states are those involved with catalytic processes and involved the reaction of propan-1-ol with the surface as follows:

(b) $C_3H_7OH_{(a)} + O^{2-}{}_{(a)} \longrightarrow C_3H7_5O^{-}{}_{(a)} + OH^{-}{}_{(a)}$

(c) $C_3H_7OH_{(a)} + O\,H^{-}{}_{(a)} \longrightarrow C_3H_7O^{-}{}_{(a)} + H_2O_{(g)}$

The steps (b) and (c) are the most likely ways for the propoxy formation, however, with (b) likely to be dominant at ambient temperature for titania. In this case, the anion vacancies are designated as Vo^{2-}, although the electrons are likely to be associated with cation sites, as Ti^{3+}, than the vacancy itself.

The presence of the bands at 2964, 2937 2883 and 2870 cm^{-1} indicate that propoxy species are formed according steps (b) and (c) above. The adsorbed propoxy formed by the reaction in (b) and (c) are likely the main intermediate for the formation of gas phase products such as:

(d) $C_3H_7O^-_{(a)} + O^{2-}_{(a)} \longrightarrow C_2H_{6\,(g)} + CO_{(g)} + OH^-_{(a)} + Vo^{2-}$

(e) The adsorbed propoxy may also react with adsorbed oxygen on the surface and give hydrogen as seen as a product at high temperature from titania and even in the presence of gold. The appearance of the peaks at 1723cm^{-1} indicated the presence of adsorbed propanal species, while the peaks at 2850 and 1340cm^{-1} also indicated the presence of adsorbed propanoate species respectively. The adsorbed propanoate and propanal species may be formed by the following reaction.

(i) $C_3H_7O^-_{(a)} + O^{2-}_{(a)} \longrightarrow C_2H_5COH_{(a)} + OH^-_{(a)} + Vo^{2-}$

(ii) $C_3H_7O^-_{(a)} + O^{2-}_{(a)} \longrightarrow C_2H_5COO^-_{(a)} + H_{2\,(g)} + Vo^{2-}$

The bands observed at 2964, 2937 and 2883cm^{-1} are associated with the presence of adsorbed formate species which are likely be formed either through adsorbed propanal or adsorbed propanoate species according the following reaction.

(f) (i) $C_2H_5COH_{(a)} + OH^-_{(a)} \longrightarrow HCOO^-_{(a)} + C_2H_{6\,(g)}$

(ii) $C_2H_5COO^-_{(a)} + OH^-_{(a)} \longrightarrow HCOO^-_{(a)} + C_2H_5O^-_{(a)}$

(g) The formates adsorbed on gold may subsequently decomposed (i) or react with the adsorbed surface hydroxide (ii) according to following reaction.

(i) $2HCOO^-_{(a)} \longrightarrow 2CO_{2\,(g)} + H_{2\,(g)} + 2e^-$

(ii) $HCOO^-_{(a)} + OH^-_{(a)} \longrightarrow CO_{2\,(g)} + H_2O + 2e^-$

(i) The propene, which is a dehydration product mainly on TiO_2, will be formed according to the following reaction:

(i) $C_3H_7O^-_{(a)} \longrightarrow C_2H_5CH_{2\,(g)} + OH^-_{(a)}$

5.3.5 Control Experiments

Control experiments were carried out in order to get an insight and the role of gold on propan-1-ol oxidation over Au/TiO_2 catalysts. Hence, similar experiments were carried on TiO_2 alone. Figure 5-19 shows the temperature programme reaction for propan-1-ol over TiO_2 alone.

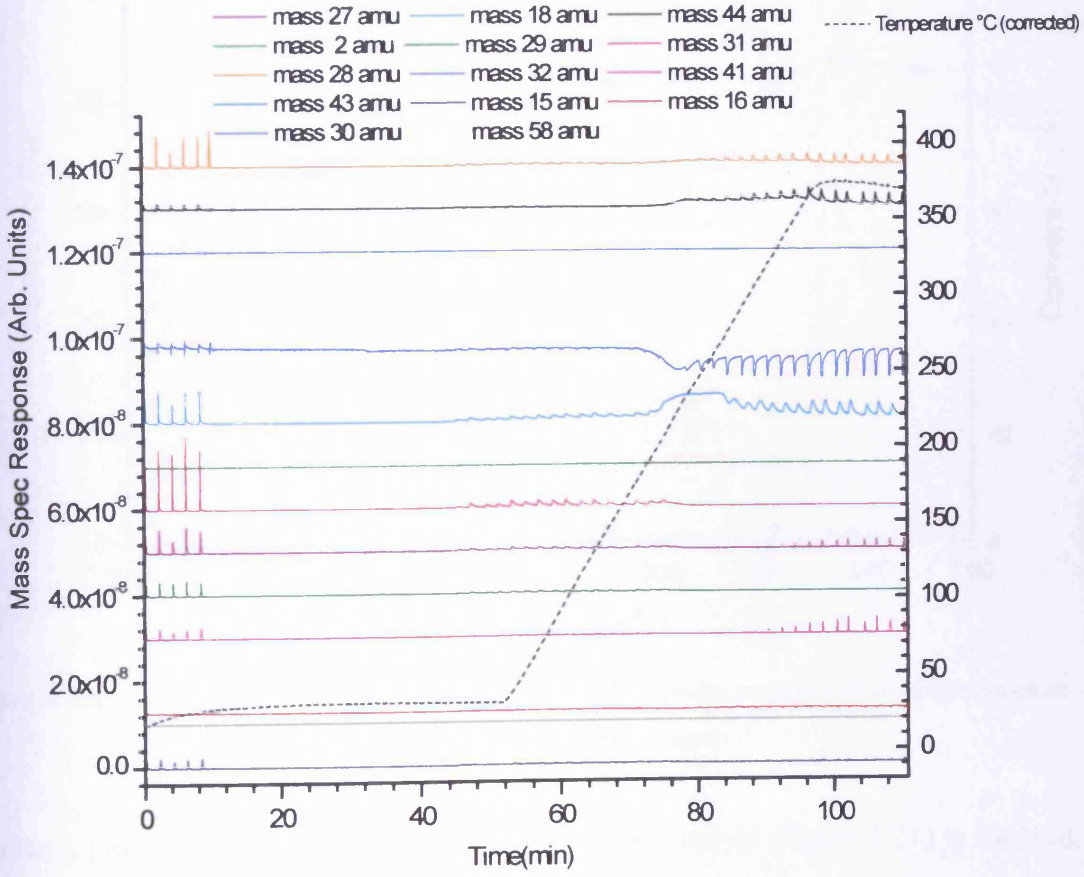

Figure (5-19): Temperature Programmed Pulse Flow Reaction for aerobic propan-1-ol oxidation in 10%O_2/He gas flow over TiO_2 catalyst

The aerobic propanol oxidation over TiO_2 catalyst is a complete oxidation. It is followed by the dehydration to propene (appearance of mass 41 and 27 amu signals) and dehydrogenation to propanal. When the data in figure (5-19) was integrated, figure (5-20) was obtained. As the conversion of propanol is 40%, the selectivity to CO_2 begins to increase and continues as the temperature increases; when the temperature reached 250°C, CO_2 selectivity was about 85% with CO and propanal sharing the remaining 15%. However, as the temperature increases, the selectivities to CO and propanal decrease and CO_2 selectivity increase to almost 90% due to decomposition of propan-1ol and continue in a steady state through out the experiment.

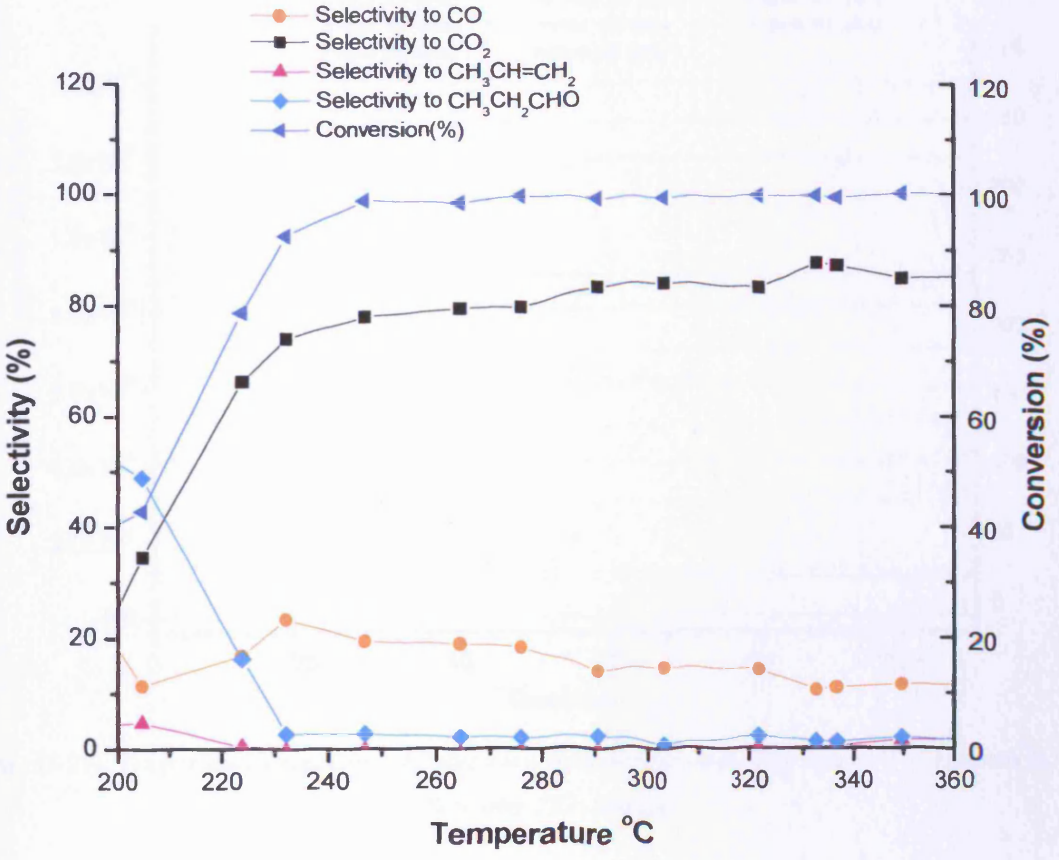

Figure (5-20): Selectivity and conversion with temperature for aerobic propan-1-ol oxidation reaction in 10%O_2/He flow over TiO_2 catalyst

Similarly, propanol anaerobic reaction over the TiO_2 catalyst (figure 5-21) is more of dehydration to propene (appearance of mass 41 and 27 amu signals) and deoxygenation to propane (appearance of mass 29, 28, 27, 44, and 43 amu signals). When the temperature was increased further, mass 28, 27 and 30 amu signals were

obtained due to decomposition of propanol to ethane, CO and hydrogen. When the data in figure 5-21 was integrated and analysed, figure (5-22) was obtained.

Figure 5-22 shows that as the conversion of propanol was 60%, the catalyst was selective towards dehydration of propanol to propene, with selectivity value being 70% and the temperature was 200°C. However, when the temperature was increased to 250°C, 100% conversion of propanol was reached, with selectivities to CO and propene being 15% and 70% respectively and continued through out in a steady state. Similarly, the CO_2, ethane, and propane selectivities remained small with selectivities values being not more than 15%.

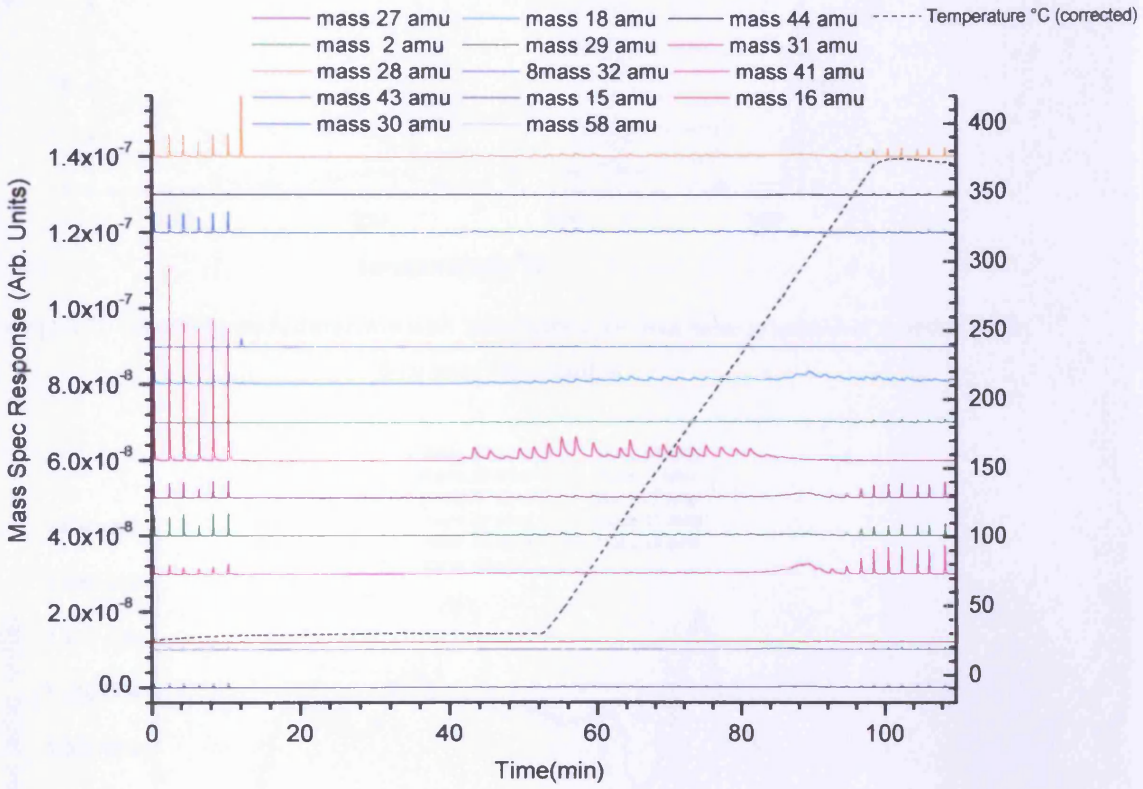

Figure (5-21): Temperature Programmed Pulse Flow Reaction for anaerobic propan-1-ol reaction in He gas flow over TiO_2 catalyst

The temperature programmed desorption of propan-1-ol over TiO_2 catalyst is shown in figure 5-23. Propan-1-ol was being desorbed at lower temperature, but as the temperature was increased to 250°C, the dehydrogenation indicates the presence of propanal and the appearance of mass 41, and 27 and 18 amu signals confirmed the dehydration of the adsorbed propanol to propene. Similarly, propane was also desorbed (the appearance of mass 29, 28, 27, 44, 43 and 15 amu signals).

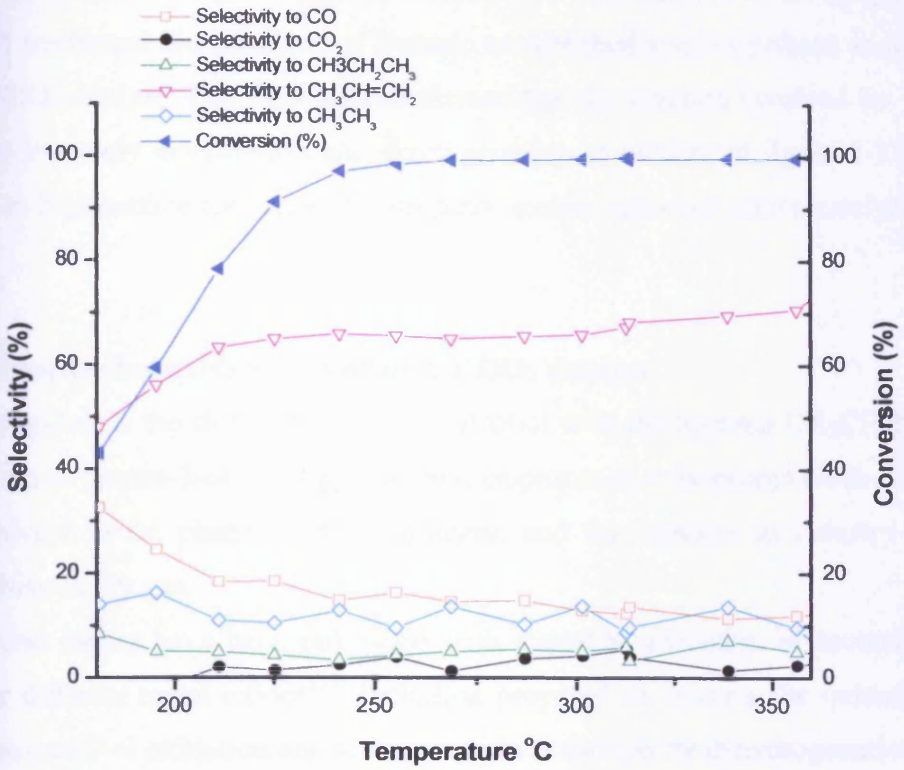

Figure (5-22): Selectivity and conversion with temperature for anaerobic propan-1-ol reaction in He flow over TiO_2 catalyst

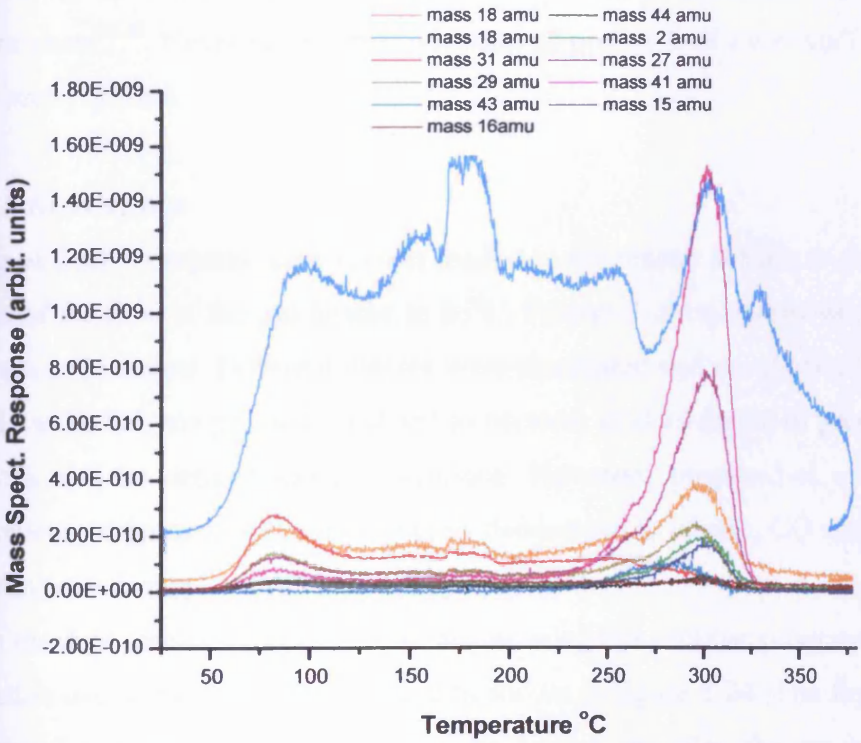

Figure (5-23): Temperature Programmed Desorption of TiO_2 catalyst saturated with propan-1-ol at room temperature

However, the emergence and coincidence of CO_2 and H_2 in the propanol TPD on TiO_2 confirmed the presence of formate as adsorbed species present as in the case of Au/TiO_2 catalyst. The TPD also confirmed that the reaction involved for propanol on TiO_2 is mainly dehydration and deoxygenation as evident in figure 5-23 and is also due to high surface coverage of 2-propoxy species adsorbed on the catalyst.

5.4 Propan-2-ol oxidation over an Au/TiO_2 catalyst

Propan-2-ol is the simplest secondary alcohol with the formula $CH_3CHOH\ CH_3$. It is known as propan-2-ol, 2-propyl alcohol, isopropanol or isopropyl alcohol. It is used as a solvent in the pharmaceutical industry, and for cleaners in industry and as fuel additive in dry gas.

Several papers have been published with regard to oxidation of secondary alcohols over different metal oxides[123], including propan-2-ol. Among the oxidation products of propan-2-ol oxidation are acetone which is formed by dehydrogenation of propan-2-ol or reaction with a strong oxidising agent.[2] Similarly, dehydration to propene was also reported or deoxygenation to propane.

However, the oxidation of propan-2-ol over TiO_2 has been reported by many researchers[22-30]. Nevertheless, the oxidation of propan-2-ol over Au/TiO_2 catalyst has not been reported.

5.4.1 Activity test

0.5g of freshly prepared catalyst was loaded in the reactor similar to propan-1-ol, with lines of the flow of the gas heated to 85°C. Propan-2-ol injections were done over the bypass and catalyst. Different masses were monitored and are chosen because propan-2-ol can be dehydrogenated, oxidised to acetone, or dehydrated to propene. Propan-2-ol can also be deoxygenated to propane. However, propan-2-ol can also undergo complete oxidation to CO_2 and water or decompose to ethane, CO and hydrogen. The acetone can further be oxidised to propanoic acid.

The result of aerobic propan-2-ol oxidation using temperature programmed pulse flow reaction over a 1wt%Au/TiO_2 catalyst is shown in figure 5-24. The first five pulses of propan-2-ol injection, which are via the bypass provides the cracking pattern for propan-2-ol. Propan-2-ol broke through (appearance of 45, 27, 43, and 44 amu signals) at 35 minutes and no conversion of propan-2-ol was observed. The uptake of

propan-2-ol was about 9μl, corresponding to $1.42x10^{20}$ molecules g^{-1} of catalyst. This in turn corresponds to about $2.83x\ 10^{19}$molecules m^{-2}, if we assume a total surface atom density of $10^{19}m^{-2}$.

SNO	MASS	PRODUCT NAME
1	2	Hydrogen (H_2)
2	15 and 16	Methane (CH_4)
3	18	Water (H_2O)
4	28	Carbon monoxide (CO),Ethene, Ethane, propane, propanal, and Nitrogen (N_2)
5	29	propanol, Ethene, Ethane, propanal, propanoic acid and propane
6	27	Propanol, Ethene (CH_2CH_2), propanal, and propene.
7	30	Ethane (CH_3CH_3)
8	31	Ethanol (CH_3CH_2OH) and Diisopropyl ether ($C_3H_7OC_3H_7$)
9	32	Oxygen (O_2)
10	43	Diisopropyl ether and propane
11	44	Carbon dioxide CO_2 and Ethanal(CH_3COH)
12	45	Diisopropyl ether
13	58	Propanal (CH_3CH_2CHO)
14	74	Propanoic acid (CH_3CH_2COOH)

Table 5-3: Masses monitored for propan-2-ol oxidation over a 1wt% Au/ TiO_2 catalyst

As the temperature was increased to about 250°C, 100% conversion of propan-2-ol was obtained (loss of the 45 amu signals), and two types of CO_2 production occurred. In the first stage (65-75minutes), there was slow CO_2 evolution, together with slow uptake of oxygen after each pulse of injection, similar to methanol, ethanol, and propan-1-ol. When the temperature was increased further to 300°C, the production of CO_2 and uptake of O_2 occurred at fast rate as evident from the sharp peaks observed at this temperature.

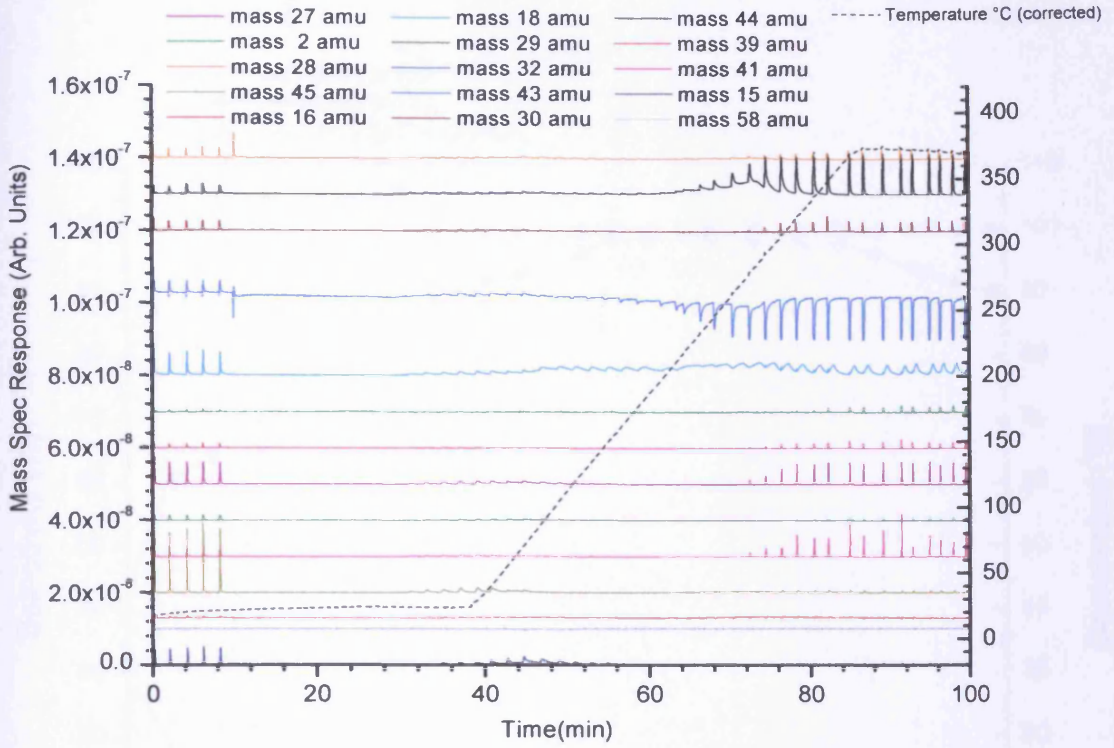

Figure (5-24): Temperature Programmed Pulse Flow Reaction for aerobic propan-2-ol oxidation reaction in 10%O_2/He gas flow over a 1wt% Au/ TiO_2 catalyst

However, the evolution of propene (appearance of the 41, 39 and 27 amu signals) begins when the temperature was 250°C, due to dehydration of propan-2-ol and followed by evolution of ethane, CO and hydrogen at about 300°C due to decomposition of propan-2-ol. In general, the oxidation of propan-2-ol is complete oxidation. When the data in figure 5-24 integrated and analysed, figure 5-25 is obtained.

Figure (5-25) shows that as the conversion was 65%, the catalyst is more selective to CO_2, with a selectivity value being almost 67% and as the temperature increased to 150°C, 100% conversion of propan-2-ol was observed, with catalyst still selective to CO_2 and the selectivity to CO_2 increases as the temperature increases as well. When the temperature reached 200°C, the selectivity to CO_2 is 95% and continues in a steady state until the temperature reached 300°C, where the CO_2 selectivity drops due to dehydration to propene and decomposition of propan-2-ol to ethane, CO, and hydrogen. The selectivities to propene, ethane, and CO begin to increase, with selectivities being 10% for all of them and the CO_2 selectivity at that temperature is 90%.

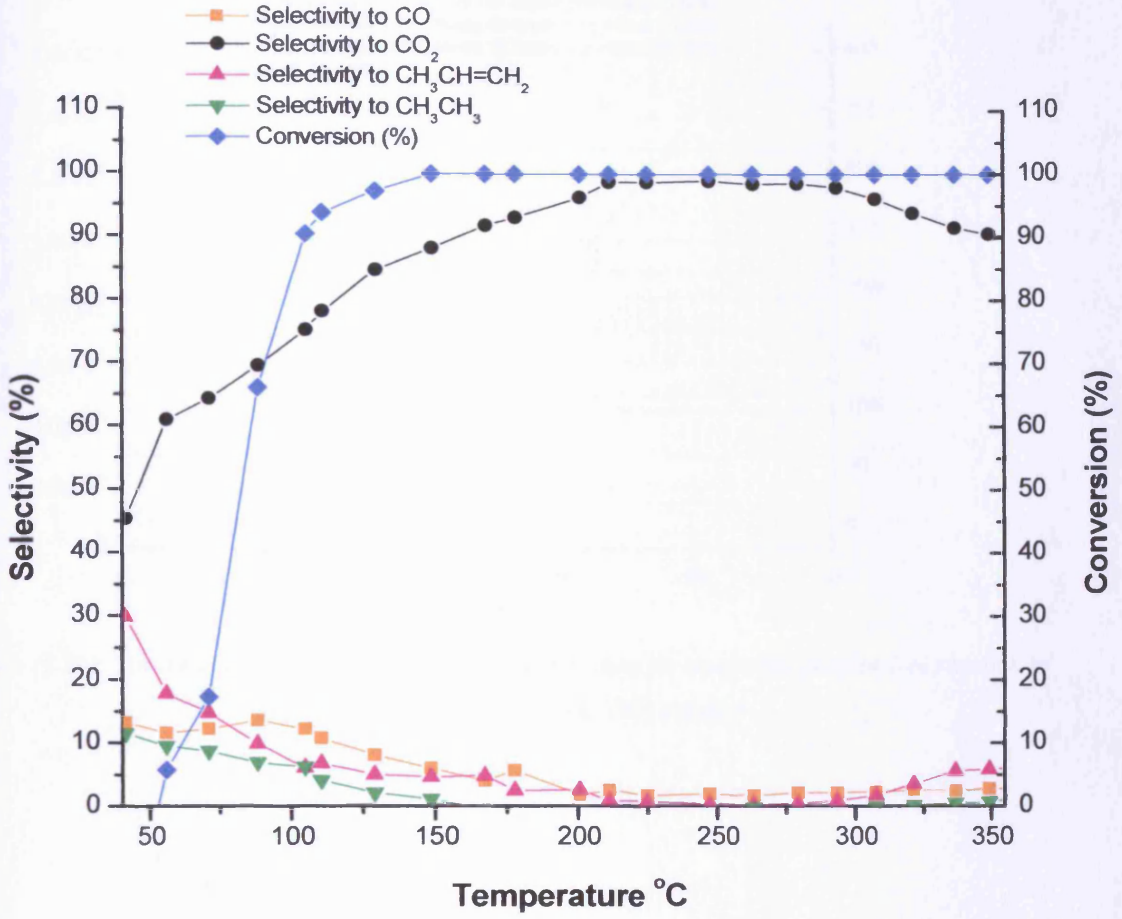

Figure (5-25): Selectivity and conversion with temperature for aerobic propan-2-oloxidation reaction in 10%O_2/ He flow over a 1wt% Au/ TiO_2 catalyst

Figure 5-26 shows the results of the anaerobic propan-2-ol reaction over a 1wt% Au/TiO_2 catalyst. The figure (5-26) shows the same uptake of propan-2-ol as observed in the aerobic reaction and after about 60 minutes, the evolution of hydrogen observed indicates the acetone production (the appearance of mass 43 amu signal). The dehydrogenation of propan-2-ol appeared to be more between 60 to 80 minutes. However, as the time increase above 80 minutes, dehydration begins (appearance of 41, 39, and 27 amu signals) and continues through out the experiment. Specifically, the reaction of propan-2-ol over a 1wt% Au/TiO_2 catalyst is associated with dehydrogenation and with dehydration as the main reaction. When the data in figure 5-26 integrated and analysed, figure (5-27) obtained.

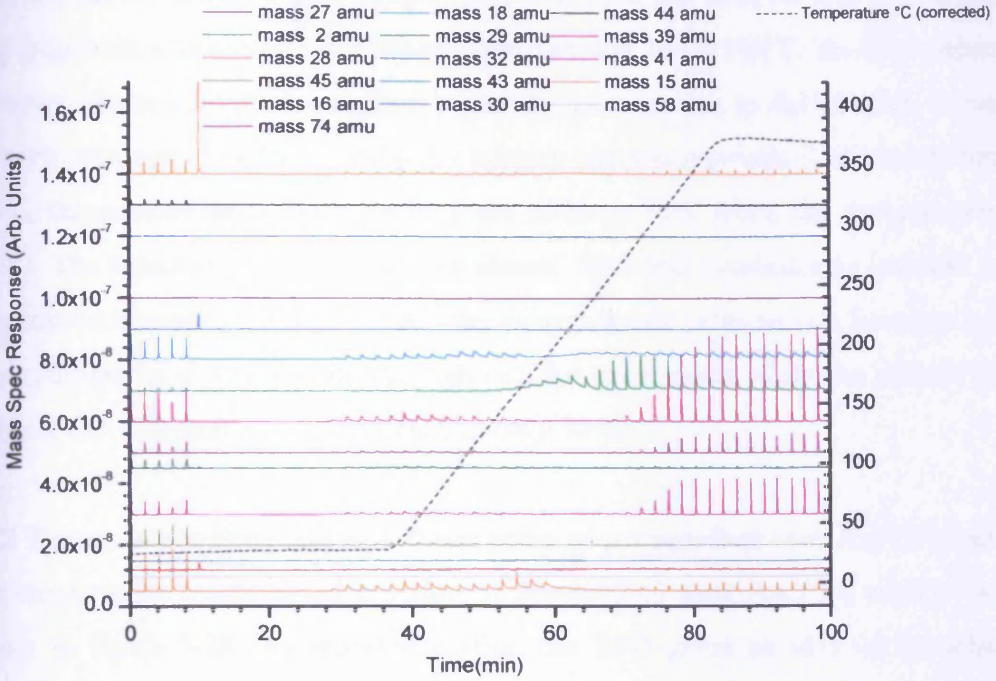

Figure (5-26): Temperature Programmed Pulse Flow Reaction for anaerobic propan-2-ol reaction in /He gas flow over a 1wt% Au/ TiO_2 catalyst

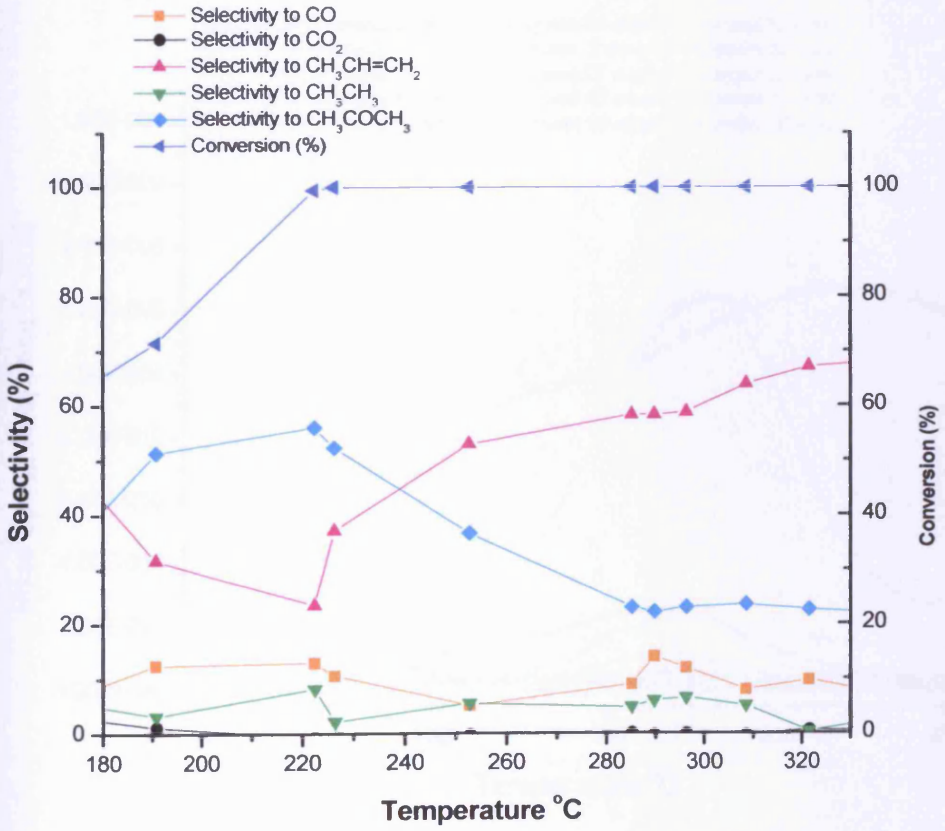

Figure (5-27): Selectivity and conversion with temperature for anaerobic propan-2-ol reaction in He flow over a 1wt% Au/ TiO_2 catalyst

Similarly, as the conversion of propan-2-ol was 70%, the catalyst is selective towards dehydrogenation to acetone and the temperature was about 180°C. As the temperature increases, the selectivity to propene begins to increase due to dehydration caused by the high coverage of surface 2-propoxy species and when propan-2-ol conversion was 100%, the acetone selectivity drops from 60% to 30% when the temperature was 240°C. The selectivity to propene was almost 70% and continues to increase as the temperature increases. At 300°C, the selectivity towards propene was found to be 70% and continues in a steady state through out the experiment while the selectivities to acetone, CO, CO_2 and ethane remained at only 30%.

5.4.2 Temperature Programmed Desorption of propan-2-ol over Au/TiO_2 catalyst

The temperature programmed reaction of propan-2-ol over Au/TiO_2 catalyst was as shown in figure 5-28. As reported earlier, the TPD gives an idea of the adsorbed species present on the catalyst surface for surface reaction. The TPD was conducted by dosing the sample with pulses of propan-2-ol and the uptake corresponded to about one monolayer of uptake of propan-2-ol at saturation.

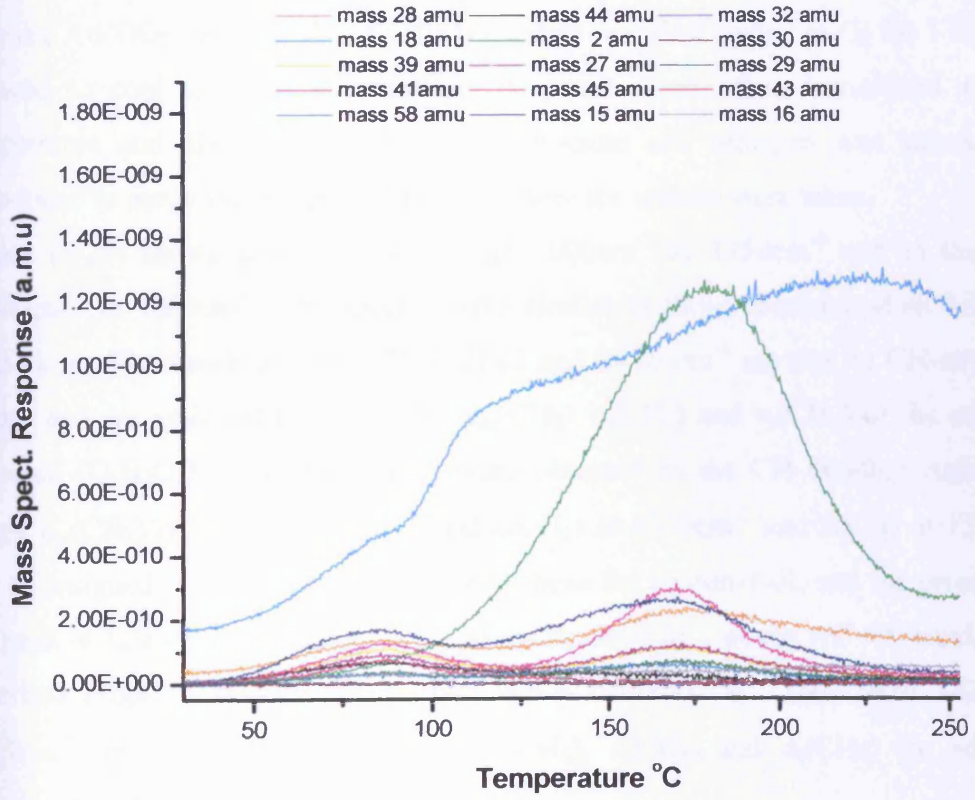

Figure (5-28): Temperature Programmed Desorption of a 1wt% Au/ TiO_2 catalyst saturated with propan-2-ol at room temperature

Figure 5-28 shows the propan-2-ol being desorbed at two stages: in the first stage as seen, some water molecules and propan-2-ol desorbed at low temperature and as the temperature was increased to 150°C, propene and propane were desorbed as seen by the appearance of mass 41,39 and 27amu, and the appearance of 29,28,27, 44,43,and 15 amu signals respectively. The presence of propene and propane is due to the high surface coverage of 2-propoxy and the deoxygenation of the adsorbed propan-2-ol at that temperature. However, the presence of mass 58 amu and 43 amu signals in the TPD suggests the presence of acetone as seen by the desorption of hydrogen in the TPD at that temperature (150°C) and this is contrary to anaerobic temperature programmed pulse flow reaction of propan-2-ol as seen in figure 5-26. Thus, the Au/TiO_2 products appeared to be dominated by dehydration, deoxygenation and dehydrogenation.

5.4.3 Infra red spectrometry

Figure 5-29 shows the DRIFTS spectra of the adsorbed species after propan-2-ol exposure. The spectra were obtained by introducing propan-2-ol at room temperature over the Au/TiO_2 catalyst. The Au/TiO_2 catalyst was first heated in O_2 for 1 hour and allowed to cool to room temperature. Propan-2-ol was then introduced at room temperature and allowed to stabilize in pressure and nitrogen was subsequently introduced to purge the gas phase species before the spectra were taken.

Figure (5-29) shows spectra in the range $1000cm^{-1}$ to $1750cm^{-1}$ and in the range $25000cm^{-1}$ to $4000cm^{-1}$. The spectra were similar to those obtained when TiO_2 was used alone. The bands at 2964, 2937 2883 and 2870 cm^{-1} are due to CH-stretching modes and are assigned to $\nu_{as.}(CH_3)$, $\nu_{as}(CH_2)$ $\nu_s(CH_3)$ and $\nu_s(CH_2)$ of the adsorbed propanol ($C_3H_7OH_{ad}$). Similar bands were obtained in the CH bending region, the bands $\delta_{as}(CH_3)/\delta(CH_2)$ at $1460cm^{-1}$ and $\delta_sCH_3)$ at $1375cm^{-1}$ and $\delta(CH)$ at $1335cm^{-1}$ can be assigned. The spectra are similar to those for propan-1-ol, and the presence of the peak at $1109cm^{-1}$ was assigned by Short house *et al.*[1], as the $\nu(C=O)$ band due to adsorbed propanal ($C_2H_5CHO_{ad}$). The bands observed at 1566, 1470 1426 and $1385cm^{-1}$ are assigned to $\nu_{as}(COO)$, $\delta_{as}(CH_3)$, $\delta(CH_2)$ and $\delta_s(CH_3)$ for adsorbed propanoate ($CH_3CH_2COO^-_{ad}$) respectively.[20]

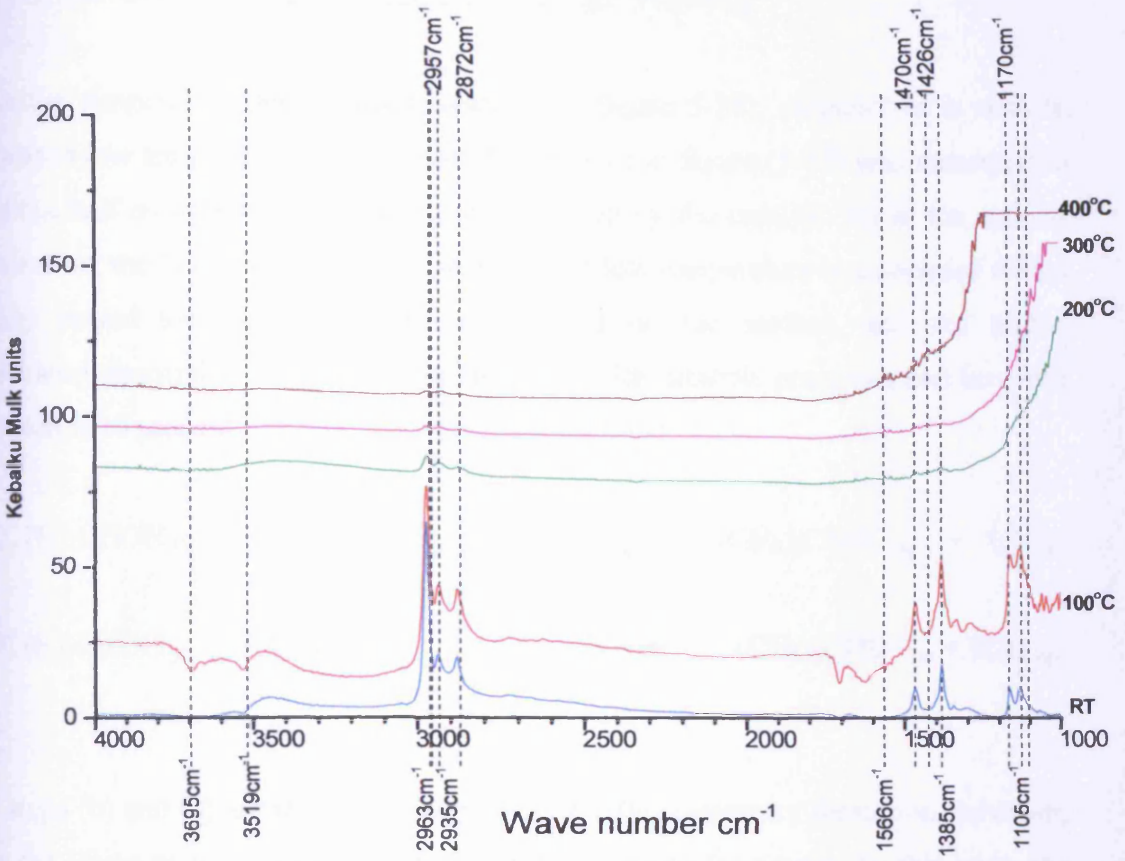

Figure (5-29): DRIFTS spectra from the adsorbed propan-2-ol over a 20wt% Au/TiO_2 catalyst at different temperatures

The bands at 2876 and 1385cm^{-1} were assigned to be the $\nu(CH_2)$ and $\nu_s(COO)$ for the adsorbed formate ($HCOO\text{-}_{ad}$)[25-27, 29-30]. The data obtained in figure 5-29 shows that the band at 3695, and 3519cm^{-1} are likely due to ν(OH) of the isolated OH. [1,3] The main adsorbed species are 2-propoxy, propionate, and formate and the spectrum is similar to that for TiO_2 alone but with some small differences. High spectral intensities are observed in the Au/TiO_2 catalyst than when TiO_2 used alone. The high intensities may be due to more formate and propanoate formation on the gold and reduced coverage of 2-propoxy species on the surface of the catalyst.[1]

5.4.4 The mechanism of propan-2-ol oxidation on Au/TiO_2 catalyst.

From the study and data gathered so far, the following mechanism may be proposed for the propan-2-ol oxidation on Au/TiO_2 as follows, where $_g$ and $_a$ refer to gas phase and adsorbed species respectively:

(a) $(CH_3)_2CHOH_{(g)} \longrightarrow C_3H_7OH_{(a)}$

From the temperature programmed desorption (figure 5-28), propan-2-ol is seen to desorbs at low temperature. The propan-1-ol uptake in figure (5-17) was measured to be about half monolayer from the pulses taken up by the catalyst. As in the case of propan-1-ol, the low desorption of propan-2-ol at low temperature is associated with a weakly bound form of molecular propan-2-ol on the surface, and the higher temperature desorption states are those involved with catalytic processes and involved the reaction of propan-2-ol with the surface as follows:

(b) $(CH_3)_2CHOH_{(a)} + O^{2-}_{(a)} \longrightarrow (CH_3)_2CHO^-_{(a)} + OH^-_{(a)}$

(c) $(CH_3)_2CHOH_{(a)} + O\,H^-_{(a)} \longrightarrow (CH_3)_2CHO^-_{(a)} + H2O_{(g)}$

The steps (b) and (c) are the most likely ways for the 2-propoxy formation, however, with (b) likely to be dominant at ambient temperature for titania. In this case, the anion vacancies are designated as Vo^{2-}, although the electrons are more likely to be associated with cation sites, as $Ti^{3+,}$ than the vacancy itself.

The presence of the bands at 2964, 2937 2883 and 2870 cm^{-1} indicate that 2-propoxy species are formed according steps (b) and (c) above. The adsorbed 2-propoxy formed by the reaction in (b) and (c) are likely the main intermediate for the formation of gas phase products such as:

(d) (i) $(CH_3)_2CHO^-_{(a)} + O^{2-}_{(a)} \longrightarrow C_2H_{6\,(g)} + CO_{(g)} + OH^-_{(a)} + Vo^{2-}$

(ii) $(CH_3)_2CHO^-_{(a)} + O^{2-}_{(a)} \longrightarrow (CH_3)_2CO_{(g)} + OH^-_{(a)} + Vo^{2-}$

(e) The adsorbed 2-propoxy may also react with adsorbed oxygen on the surface and give hydrogen as seen as a product at high temperature from titania and even in the presence of gold. The appearance of the peaks at 1470, 1566, 1426 and 1385cm^{-1} also

indicated the presence of adsorbed propanoate species respectively. The adsorbed propanoate species may be formed by the following reaction.

(d) (ii) $(CH_3)_2CHO^-_{(a)} + O^{2-}_{(a)} \longrightarrow (CH_3)_2COO^-_{(a)} + H^+_{(a)} + 3e^-$

The bands observed at 1385 and 2876cm^{-1} are associated with the presence of adsorbed formate species, which are likely be formed either through adsorbed 2-propoxy or propanoate species according the following reactions.

(f) (i) $(CH_3)_2CHO^-_{(a)} + O^{2-}_{(a)} \longrightarrow CH_3CH_{3(g)} + HCOO^-_{(a)} + Vo^{2-}$

(ii) $(CH_3)_2CO^-_{(a)} + OH^-_{(a)} \longrightarrow CH_3CH_{3\,(g)} + HCOO^-_{(a)} + e^-$

(g) The formates adsorbed may subsequently decomposed (i) or react with the adsorbed surface hydroxide (ii) according to following reaction.

(i) $2HCOO^-_{(a)} \longrightarrow 2CO_{2\,(g)} + H_{2\,(g)} + 2e^-$

(ii) $HCOO^-_{(a)} + OH^-_{(a)} \longrightarrow CO_{2\,(g)} + H_2O + 2e^-$

(i) The propene, which is a dehydration product mainly on TiO_2, will be formed according to the following reaction:

(i) $(CH_3)_2CHO^-_{(a)} \longrightarrow C_2H_4CH_{2\,(g)} + OH^-_{(a)}$

5.4.5 Control Experiments

Control experiments were carried out over the TiO_2 catalyst in order to validate and compare with the data for the Au/TiO_2 catalyst for propan-2-ol oxidation. In the same manner, 0.5g of TiO_2 catalyst was loaded in a U tube of the reactor in a flow of 10%O_2/He. The results obtained for temperature programmed pulse flow reaction aerobic are shown in figure 5-30.

The reaction is a complete oxidation (appearance of mass 44 and 28 amu signals) and the uptake of mass 32 amu signals. CO_2 and water are the main products of the

reaction and this is followed by dehydration of propan-2ol to propene (appearance of mass 41, 39, 27 and 15 amu signals). However, the appearance of mass 45 and 41 amu signals indicate the presence of diisopropoxy ether as seen after 70 minutes. The oxidation reaction of propan-2-ol over TiO_2 is complete oxidation followed by dehydration due to high surface coverage of adsorbed 2-propoxy species on the catalyst.

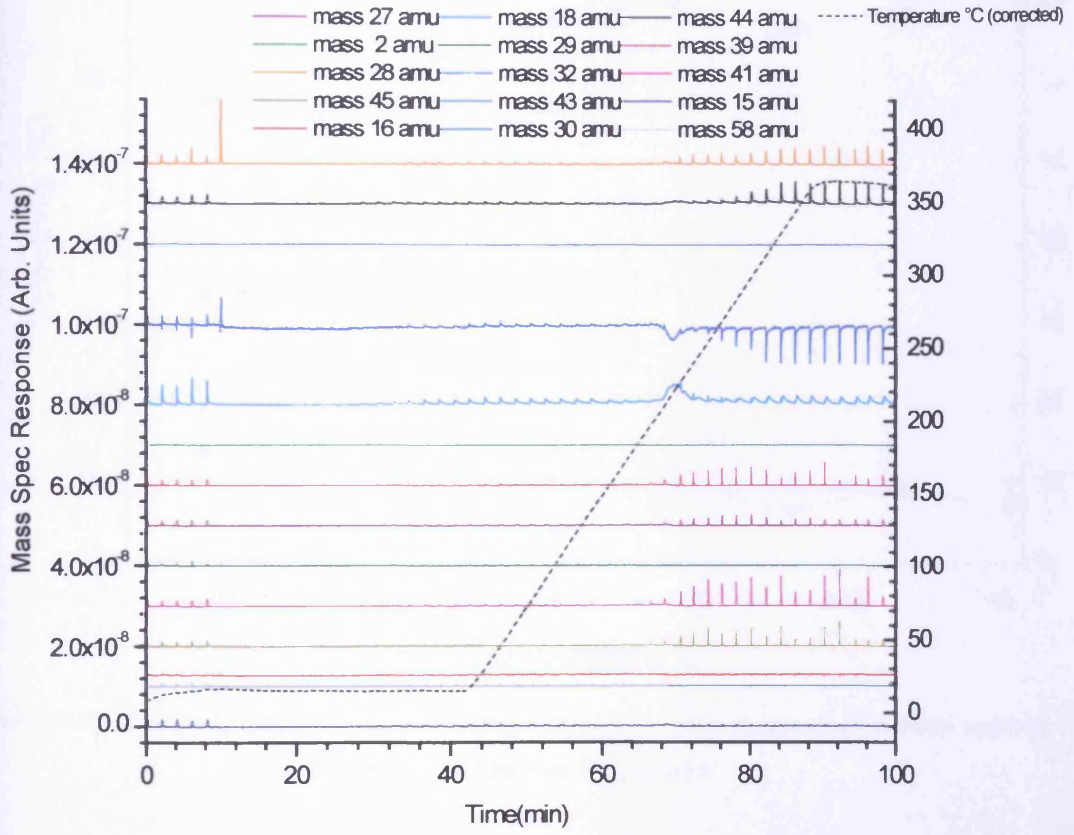

Figure (5-30): Temperature Programmed Pulse Flow Reaction for aerobic propan-2-ol oxidation reaction in 10%O_2/He gas flow over TiO_2 catalyst

The integrated data indicate that when the conversion of propan-2-ol was 30%, the temperature was about 220°C and the catalyst is selective towards dehydration to propene and diisopropyl ether, due to the high coverage of 2-propoxy at this temperature. The selectivity towards propene and diisopropyl ether was found to be 20 and 15 % when the temperature reached 250°C and the conversion was 45%. As the temperature increases the conversion increases and the selectivity toward propene and diisopropyl ether decreases and the catalyst is selective towards CO_2 formation. When

the conversion of propan-2ol reached 75%, the CO_2 selectivity was found to be almost 75%, with CO, propene and diisopropyl ether selectivities being 25%.

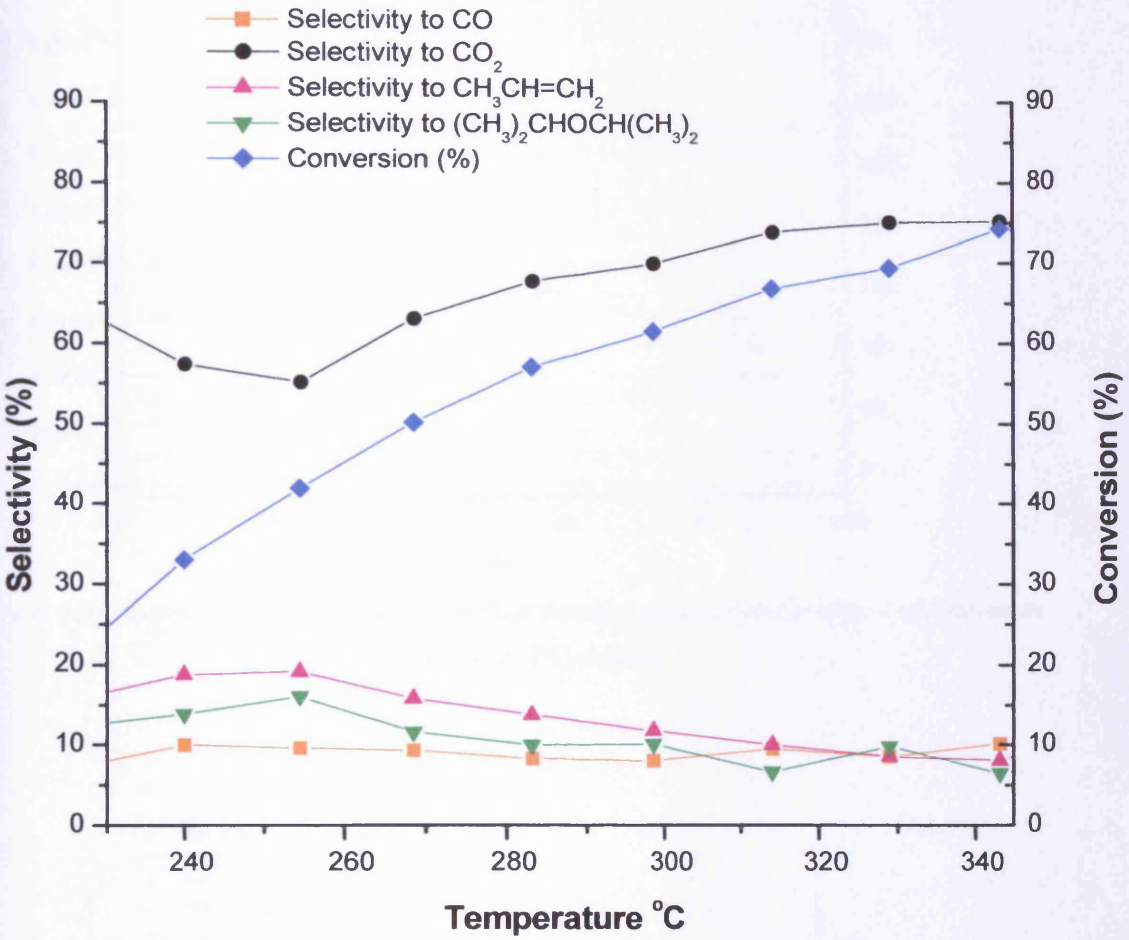

Figure (5-31): Selectivity and conversion with temperature for aerobic propan-2-oloxidation reaction in 10%O_2/ He flow over TiO_2 catalyst

Similarly, when the anaerobic propan-2-ol reaction was carried out over TiO_2 alone, we obtain the result shown in figure 5-32. The anaerobic reaction for propan-2-ol reaction over TiO_2 catalyst is a complete dehydration to propene (the appearance of mass 41. 39.27 and 15 amu signals) from 70 minutes and continues through out the experiment.

The integrated data show that as the conversion was 50%, the catalyst is selective to dehydration to propene, with selectivity value being almost 90% and the temperature was 180°C. As the temperature reached 220°C, the propan-2-ol conversion was 98%, the propene selectivity was found to be 98%, and both conversion and selectivity continue in such value through out the experiment.

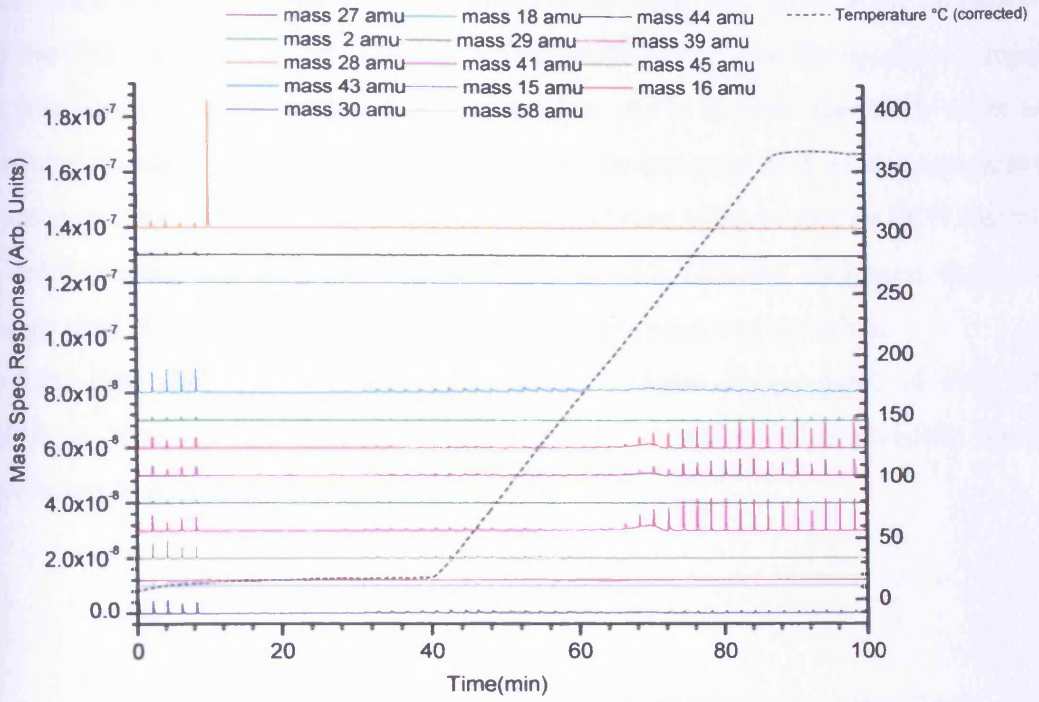

Figure (5-32): Temperature Programmed Pulse Flow Reaction for anaerobic propan-2-ol reaction in He gas flow over TiO_2 catalyst

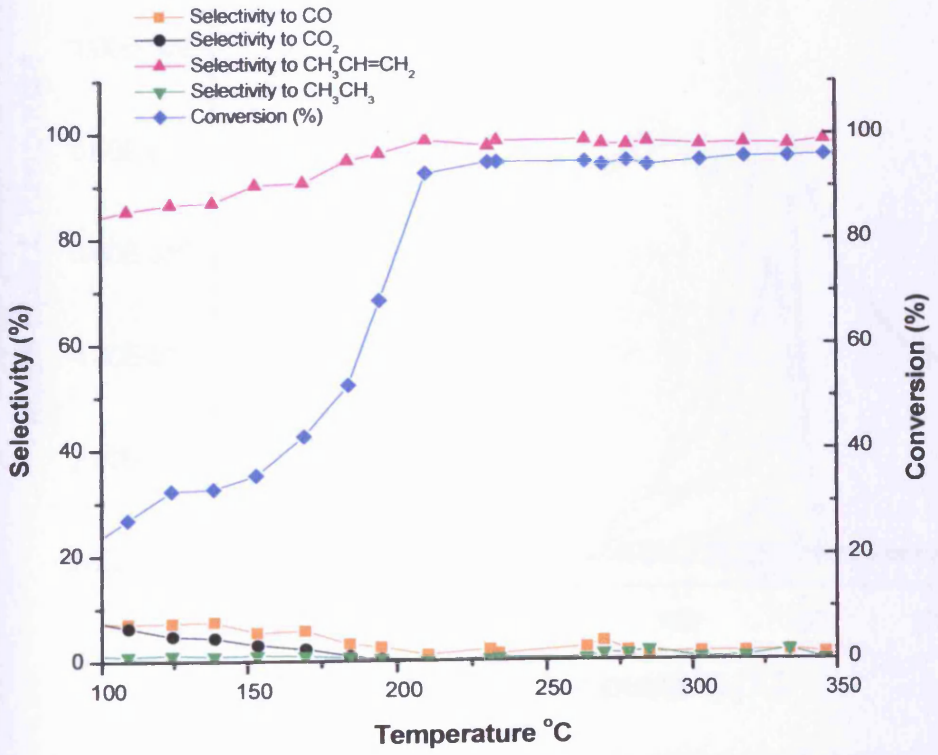

Figure (5-33): Selectivity and conversion with temperature for anaerobic propan-2-ol reaction in He flow over a TiO_2 catalyst

In the same vein, temperature programmed desorption was carried for propan-2-ol over the TiO_2 catalyst (figure 5-34). The TPD results show that the uptake of propan-2-ol was similar to that for the Au/TiO_2 catalyst. As seen from the TPD, water and molecular propan-2-ol were desorbed at lower temperature and as the temperature increased to about 180°C, the simultaneous desorption of hydrogen and CO indicates the decomposition of the absorbed 2-propanol, with CO and hydrogen desorption being centred at 220°C. At the same temperature, propene was desorbed.

The TPD data show that the adsorbed species present for propan-2-ol over TiO_2 catalyst is likely to be dominated by 2-propoxy, which is responsible for the dehydration of propan-2-ol to propene.

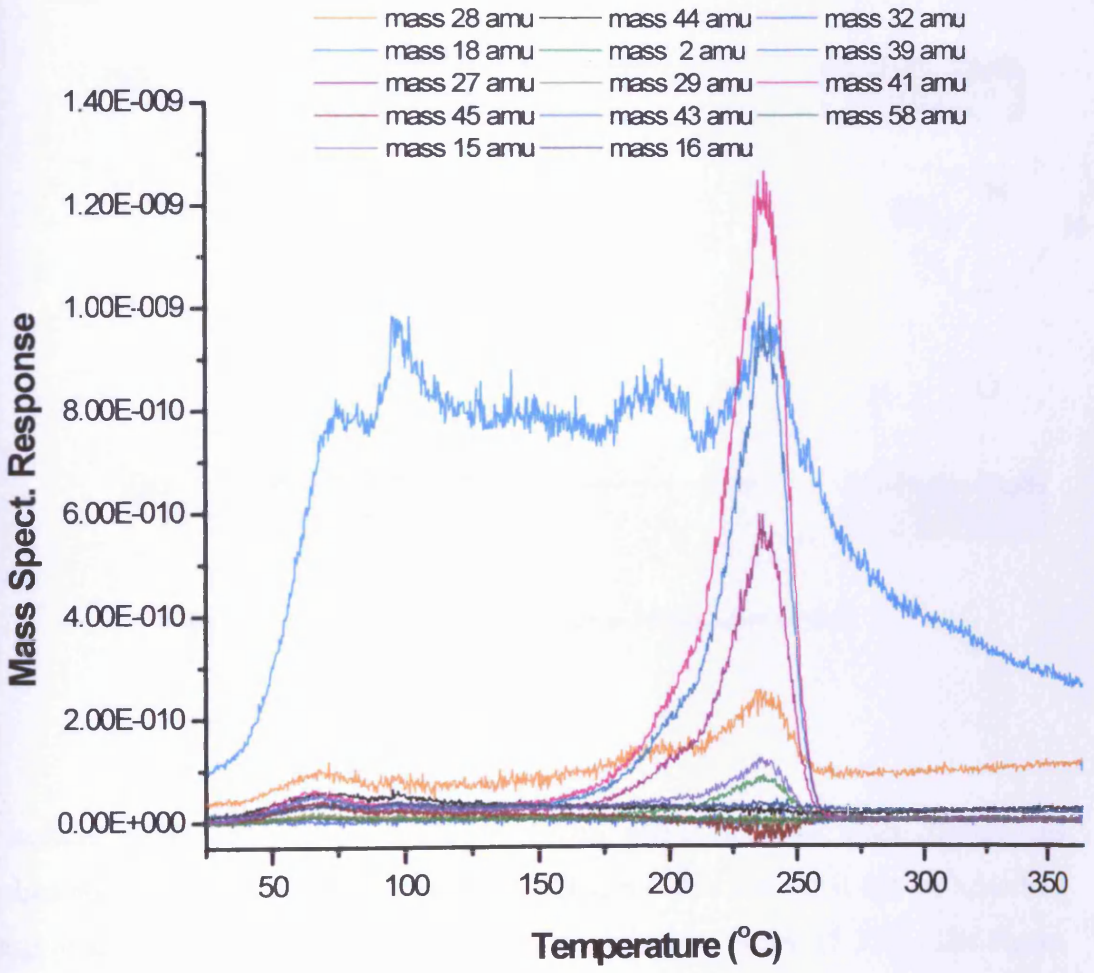

Figure (5-34): Temperature Programmed Desorption of TiO_2 catalyst saturated with propan-2-ol at room temperature

5.5 Conclusions

From the data gathered and presented and the subsequent discussion of the results of ethanol oxidation over TiO_2 and Au/TiO_2 catalyst, it would be understood that ethanol oxidation over TiO_2 and Au/TiO_2 catalysts is selective oxidation. However, it would be observed that the ethanol is being adsorbed on the surface of TiO_2 by either one of the two ways as shown (figure 5-35a and b)

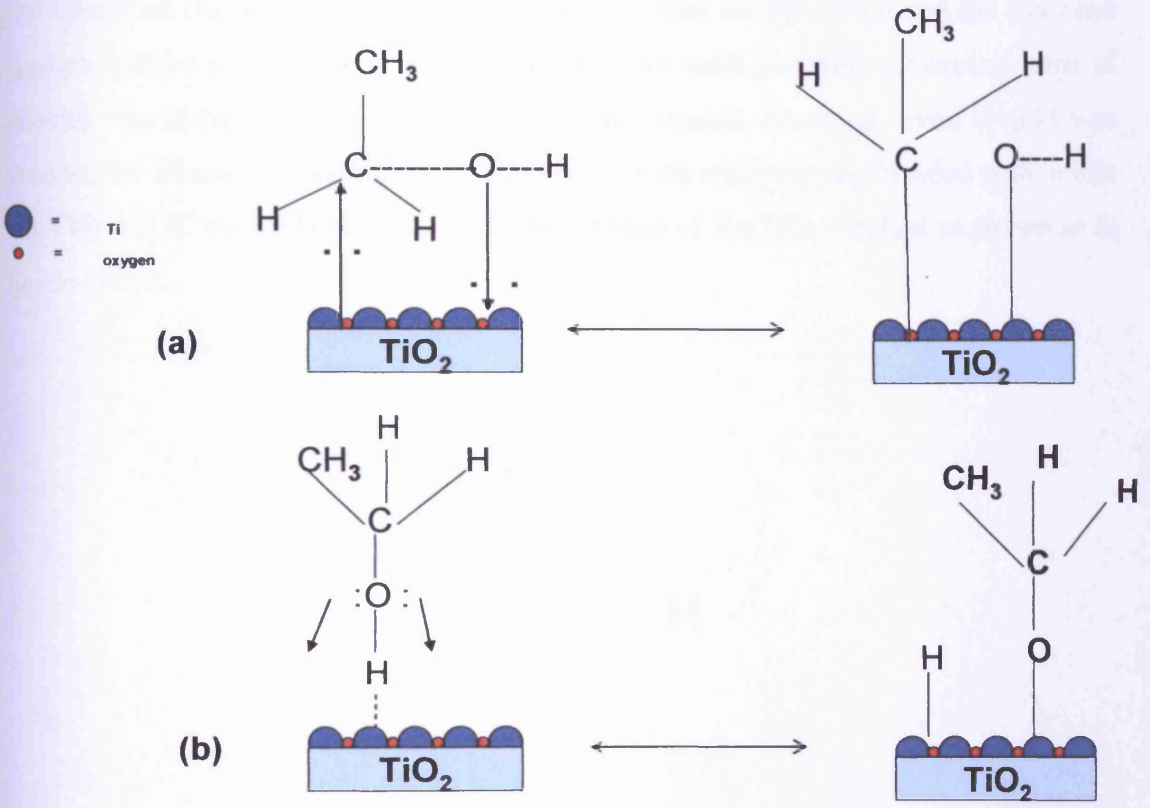

Figure (5-35): Ethanol adsorption over a TiO_2 catalyst surface

The surface of TiO_2 catalyst was made up of basic and acidic sites; when ethanol was adsorbed on the surface similar to methanol (figure 4-86a and b); it can be adsorbed leading to the formation of an ethyl group as shown in figure (5-35a). The figure shows that, when ethanol was adsorbed on the surface the carbon atom was not substituted, a nucleophillic reagent can attack it - here a basic site (O), in a reaction similar to methanol as observed in a SN^2 mechanism. This produces a $CH_3CH_2^+$ ion

adsorbed at the basic site (O) and the OH^- ion, which is a strong base and can react on an even more weakly acidic site Ti. This type of attack should be easier if the C-OH bond is polarized by an interaction between acid centre and the OH group of the ethanol.

In the same figure (5-35b) indicates the ethanol adsorption, leading to a surface ethoxide which was identified by infra spectrometry. In this case, the basic site (O), extracts the hydroxyl hydrogen producing an ethoxylate ion, which is a strong base and can neutralize a weak acid centre Ti. In this case, if the acidic and basic sites are considered as charged centres there must be a mutual neutralization and the adsorbed species will be electrically neutral. However, the most probable adsorption step of ethanol was in figure (5-35b) as shown by the infrared. However, even if gold was present, the ethanol adsorption was found to be with ethoxy being bonded with acidic site (Ti) and H^+ on the basic site (O) of the surface of Au/TiO_2 catalyst as shown as in figure (5-36).

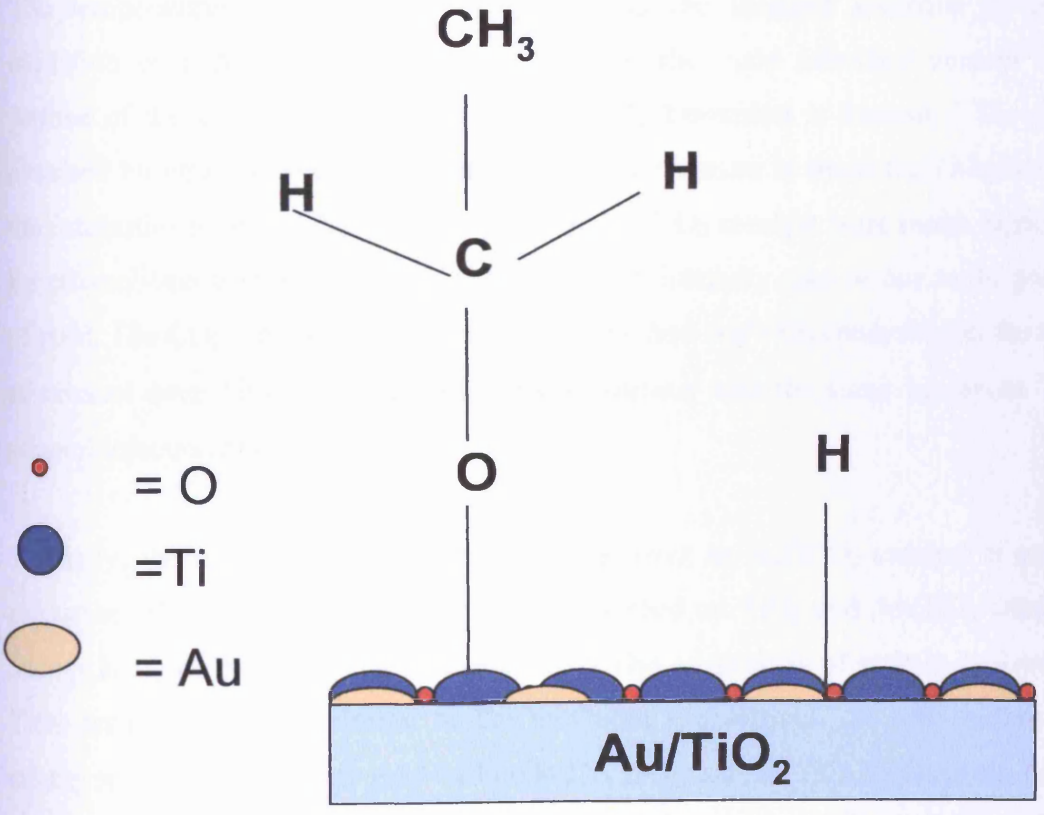

Figure (5-36): Ethanol adsorption over Au/TiO_2 catalyst surface

The presence of adsorbed ethoxy is responsible for most of the ethanol surface reaction on TiO_2 and Au/TiO_2.

The ethanol surface reaction on TiO_2 confirmed that the principle products of aerobic oxidation reaction are mostly complete oxidation products (CO_2 and H_2O); however, it is associated with dehydration product ethene and deoxygenation product ethane. However, for anaerobic ethanol reaction, the products are partial oxidation to ethanal due to dehydrogenation, dehydration to ethene, deoxygenation to ethane, and decomposition to CO, hydrogen and methane. However, the presence of gold shows that the aerobic ethanol oxidation reaction is also a complete oxidation to CO_2 and water, followed by dehydration to ethene and dehydrogenation to acetaldehyde at low temperature. The anaerobic reaction is mainly dehydration, dehydrogenation and decomposition, to produce ethene, ethanal and CO as the main products respectively. Both aerobic and anaerobic ethanol reactions occurred at lower temperature compared with when the TiO_2 catalyst was used alone. The presence of the gold in the catalyst also inhibits the decomposition of ethanol to CO, methane and hydrogen as characterised by TiO_2 catalyst.

The temperatures programmed desorption and the infrared spectrum of ethanol oxidation over Au/TiO_2 catalyst revealed that the main adsorbed species on the surface of the catalyst, responsible for the CO_2 formation is formate. The spectra obtained for ethanol over the Au/TiO_2 catalyst are similar to those for TiO_2; however, the intensities observed for ethanol over the Au/TiO_2 catalyst were much higher than for ethanol over a TiO_2 catalyst surface. The high intensity may be due to the presence of gold. The CO_2 formed is present in both TiO_2 and Au/TiO_2 catalysts and the uptake of ethanol over TiO_2 and Au/TiO_2 catalyst surface was the same i.e. about 7μl of ethanol injection before saturation.

Similarly, the result of propan-1-ol oxidation over an Au/TiO_2 catalyst is a partial oxidation. The propan-1-ol could also be adsorbed on TiO_2 and Au/TiO_2 catalyst as shown in figure 5-37 and 5-38 respectively. The adsorption of propan-1-ol over the TiO_2 catalyst surface is similar to the methanol and ethanol. As with methoxy and ethoxy species, the propoxy may be bonded to TiO_2 and Au/TiO_2 surfaces via TiO_2-O-C bond. The adsorption of propan-1-ol may occur in two ways (figure 5-37a and b and 5-38).

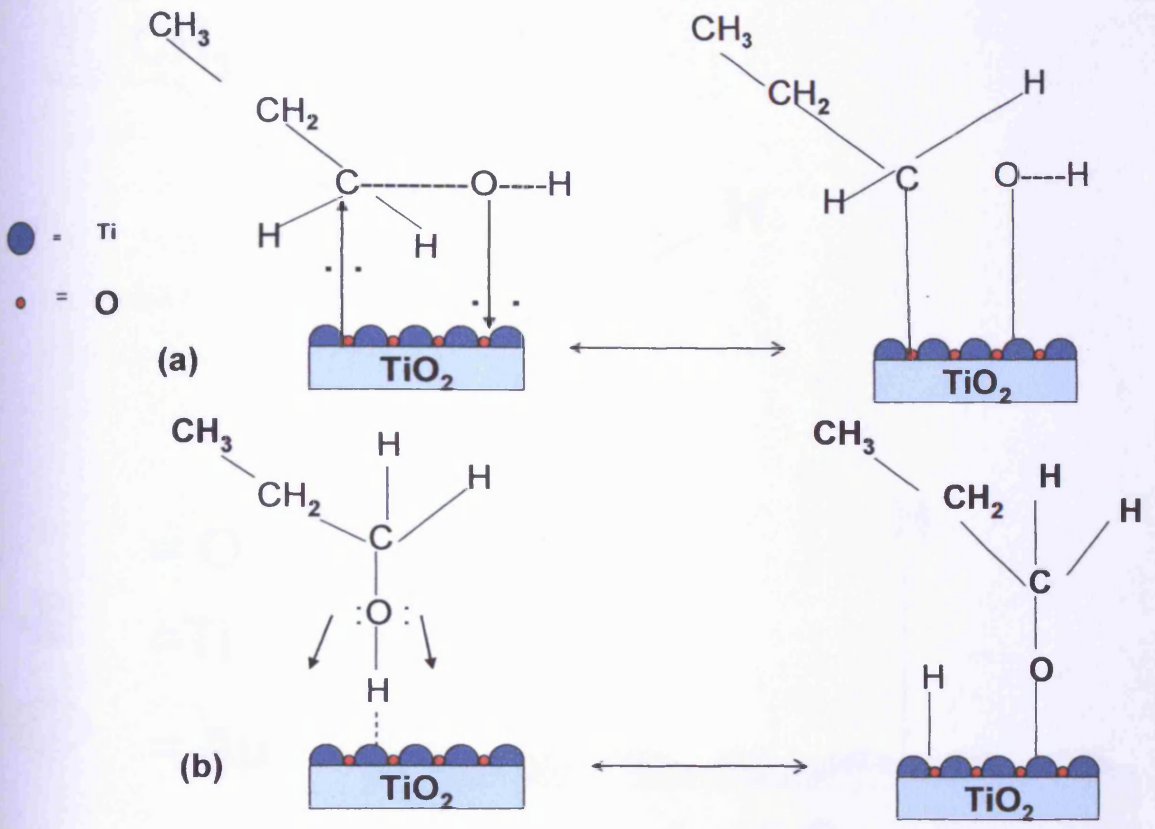

Figure (5-37): Propan-1-ol adsorption over a TiO_2 catalyst surface

When propanol is adsorbed on the surface of the TiO_2 catalyst, it can either be adsorbed leading to the formation of propyl group as shown in figure (5-37a). This produces a CH3 $CH_2CH_2^+$ ion adsorbed at the basic site (O) and the OH^- ion, which is basic and can react on acidic site Ti. For the other possibility shown (5-35b), propanol adsorption leads to a surface propoxide which was identified by infra spectrometry. In this case, the basic site (O), extracts the hydroxyl hydrogen producing a propoxylate ion, which is a strong base and can neutralize the acid centre Ti, so as mutual neutralization attained and the adsorbed species will be electrically neutral. However, the most probable adsorption step of propanol was in figure (5-37b) as shown by the infrared spectra. However, even if gold was present, propanol adsorption was found to be with propoxy being bonded with acidic site (Ti) and H^+ on the basic site (O) of the surface of Au/TiO_2 catalyst as shown as in figure (5-38). The presence of propoxy

species being adsorbed on TiO_2 and Au/TiO_2 catalysts is responsible for the surface reaction observed in aerobic and anaerobic reaction of propan-1-ol.

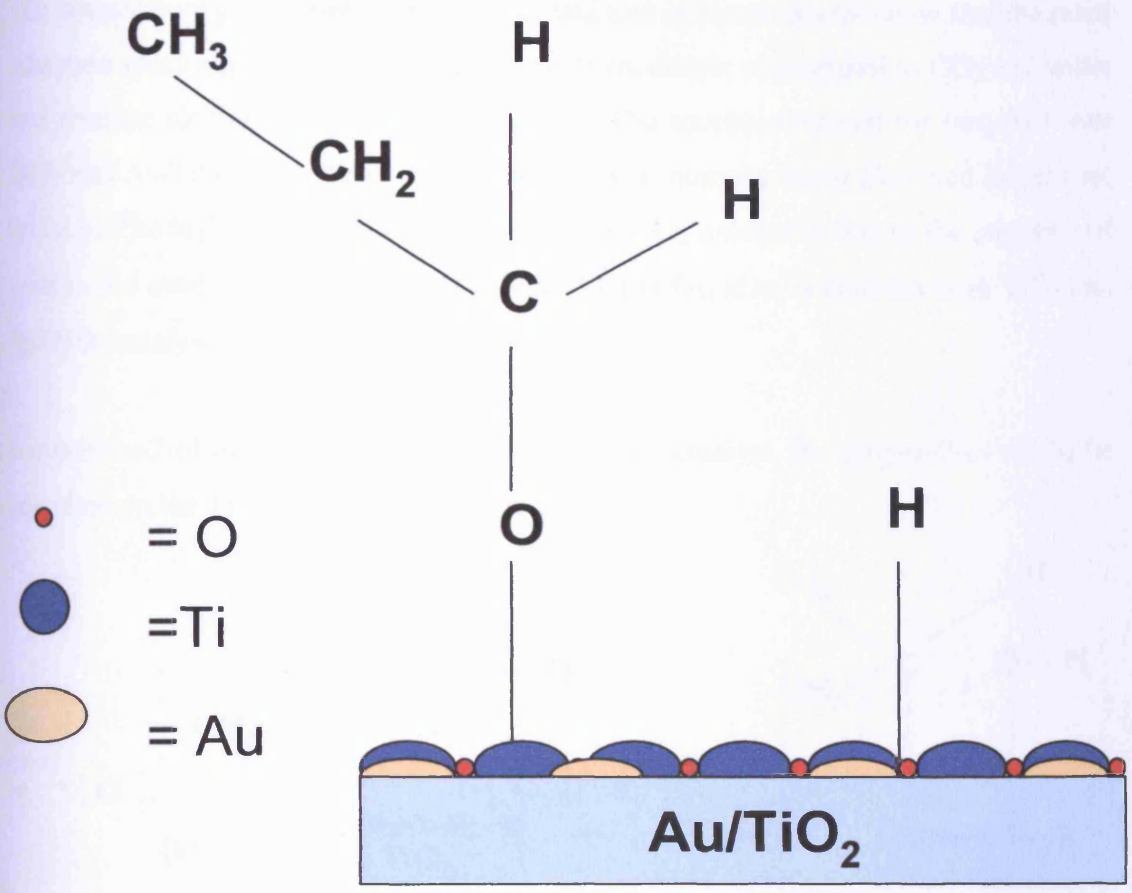

Figure (5-38): Propan-1-ol adsorption over Au/ TiO_2 catalyst surface

The main products of propan-1-ol oxidation (aerobic) reaction over the Au/TiO_2 catalyst are propanal, propene and propane, which are products of dehydrogenation, dehydration and deoxygenation of propanol. The reaction is selective and although is a complete oxidation to water and CO_2. The anaerobic propanol reaction over the Au/TiO_2 catalyst yields products due to dehydrogenation to propanal, deoxygenation to propane and dehydration to propene. However, the aerobic propanol oxidation products over TiO_2 catalyst are propanal and propene (product of dehydrogenation and dehydration) while the anaerobic reaction involved dehydration to propene, deoxygenation to propane and decomposition to ethane, CO and hydrogen. As seen from the temperature programmed pulse flow reactions, the presence of gold enhances the conversion of propanol at low temperature; it also enhances the reactivity of the

catalyst towards dehydrogenation to propanal in the presence of oxygen and deoxygenation to propane in the anaerobic reaction of propanol.

The temperature programmed desorption data and infrared spectra show that the main adsorbed species responsible for the complete oxidation of propanol to CO_2 and water was formate similar to methanol and ethanol. The spectra observed for propanol over TiO_2 and Au/TiO_2 are similar, with a slight lower intensity being observed in the case of TiO_2. The high intensity observed in the Au/TiO_2 catalyst is due to the presence of gold in the catalyst. The uptake of propan-1-ol is found to be10µl for both TiO_2 and Au/TiO_2 catalyst before saturation.

For propan-2-ol oxidation over TiO_2 and Au/TiO_2 catalyst, the propan-2-ol would be adsorbed on the TiO_2 surface as follows:

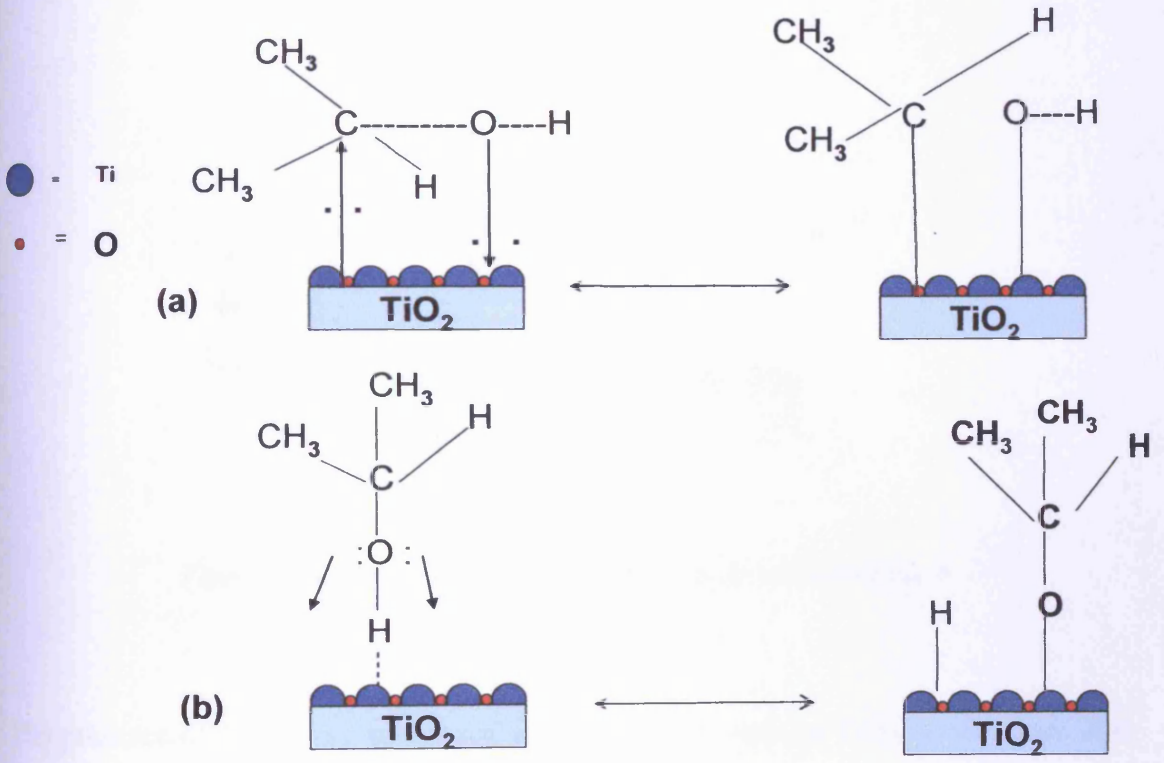

Figure (5-39): Propan-2-ol adsorption over a TiO_2 catalyst surface

As ethoxy and propan-1-ol species, the 2-propoxy may be bonded to TiO_2 and Au/TiO_2 surfaces via TiO_2-O-C bond (figure 5-39 and 40). The propan-2-ol can either be adsorbed leading to the formation of the 2-propyl group as shown in figure (5-39a). This produces a CH_3 CH^+CH_3 ion adsorbed at the basic site (O) and the OH^- ion, which is a base and can react on the acidic site Ti. Other possibility shown (5-39b),

include propanol adsorption, leading to a surface 2-propoxide which was identified by infra spectrometry. In this case, the basic site (O), extracts the hydroxyl hydrogen producing a 2-propoxylate ion, which is a strong base and can neutralize the acid centre Ti, so that mutual neutralization is attained and the adsorbed species will be electrically neutral. However, the most probable adsorption step of propan-2-ol is that in figure (5-39b) as shown by the infrared data. However, even if gold is present, propanol adsorption was found to be with 2-propoxy being bonded with an acidic site (Ti) and H^+ on the basic site (O) of the surface of Au/TiO_2 catalyst as shown as in figure (5-40).

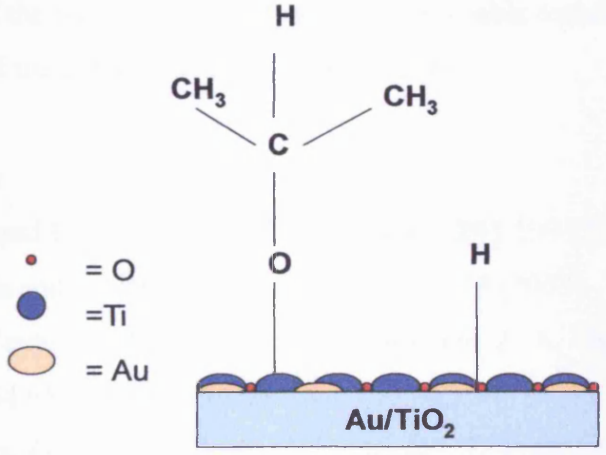

Figure (5-40): Propan-2-ol adsorption over Au/ TiO_2 catalyst surface

The presence of 2-propoxy species adsorbed on TiO_2 and Au/TiO_2 catalysts are also responsible for the surface reaction. The principle products for the aerobic oxidation of propan-2-ol over the Au/TiO_2 catalyst are products of dehydration (to propene) and decomposition (to ethane, CO and hydrogen) while the aerobic reaction involved for propan-2-ol reaction over TiO_2 catalyst is dehydration to propene and diisopropyl ether. The anaerobic reaction of propan-2-ol over the Au/TiO_2 catalyst involved dehydrogenation to acetone, dehydration to propene and decomposition to ethane, CO and hydrogen while the main products for the anaerobic reaction of propan-2-ol over

the TiO_2 catalyst are propene due to dehydration and ethane, CO and hydrogen due decomposition of propan-2-ol.

The temperature programmed reaction and the infrared data show that the main adsorbed species responsible for the complete oxidation reaction of propan-2-ol over Au/TiO_2 is formate. The dehydration and decomposition are characteristic of TiO_2, while the presence of gold enhances the reactivity of the catalyst towards complete oxidation of propan-2-ol. The presence of gold in Au/TiO_2 also increases the intensity of the spectra of the adsorbed propan-2-ol on TiO_2 catalyst. However, the same uptake of propan-2-ol observed for TiO_2 and Au/TiO_2 catalysts (10μl) before saturation. The presence of the gold in general enhances the reactivity and lowers the activation energy in each case.

The high temperature products observed in each case may be associated with TiO_2 and the presence of the oxygen as in the case of the aerobic reaction in each case enhances the reactivity of the catalyst due to its basic nature.

5.6 References

1. L.Parti and F. Porta, *Appl. Catal.* A: Gen. **291** 199 (2005).
2. S. Biella and M. Rossi, *Chem, Commun.* 378 (2003).
3. M.A. Centeno, M. Paulis, M. Montes and J. A. Odriozola, *Appl. Catal.* A: Gen. **234** 65 (2002).
4. S. Biella, G. L. Castiglioni, C. Fumagalli, L. Prati and M. Rossi, *Catal. Today* **72** 43 (2003).
5. C. Milone, R. Ingoglia, G. Neri and S. Galvagno, *Appl. Catal.* A: Gen. **211** 251 (2002).
6. C. Milone, R. Ingoglia, A. Pistone, G. Neri and S. Galvano, *Catal. Lett.* **87** 2 (2003).
7. Z. Yu, S.C. S. Chuang, *Journal of Catalysis* **246** 118-126 (2007).
8. T. Kecskes, J.Rasko and J. Kiss, *Appl. Catal.* A: Gen. **273** 55-62 (2004).
9. A. V. Vorontsov and V. P. Dubovitskaya, *Journal* of Catalysis **221**102-109 (2004).
10. F. G. Montanez, Z. Yu, S. S.Chuang and Chen Yang,
11. Gamal. A. M. Hussein and N. Sheppard. M.I. Zaki and R. B. Fahim, *J. Chem. Soc. Faraday Trans.*, **87**(16), 2661-2668 (1991)

12. H. Idriss, *Platinum Metal Rev*, **48**(3), 105-115 (2004)

13. J. Rasko, M. Domok, K. Baan and A. Erdohelyi, *App. Cat.* A: Gen. **299** 202-211 (2006)

14. A. Erdohelyi, J. Rasko, T. Kecskes, M. Toth, Marta Domok, and K. Baan, *Cat. Today* **116** 367-376 (2006)

15. J.M.Guil, N. Homs, J. Llorca, and P. Ramirez de la Piscina, *J. Phys. Chem.* B. **109** 10813-10819 (2005)

16. R. Hayashi, M. Onishi, M. Sugiyama, S. Koda, and Y. Oshima, *J. of supercritical Fliuds* **40** 74-83 (2007)

17. J. Arana. J. M. Dona- Rodrigues, J. A. Herrera Melian, E. Tello Rendon, O. Gonzalez Diaz, J. of PhotoChem. And Photobio. A: Chemistry **174** 7-14 (2005)

18. T. A. Egerton, and J. A. Mattinson, J. J. of PhotoChem. And Photobio. A: Chemistry **186** 115-120 (2007)

19. A. E. Mucients, F. J. Poblete, M. A. Rodriguez and F. Santiago, J. of Phys. Org. Chem, **10** 662-668 (1997)

20. J. E.Baile, C. H. Rochester and G. Hutchings, J. of Chem. Soc., Faraday Trans., **93** 4389-4394. (1997)

21. T. A. Nijhuis, T. Visser and B. M.. Weckhysen, *Angew. Chem. Int. Ed.* **44** 1115-1118 (2005)

22. M. A. Aramendia, J. C. Colmenares, A. Marinas, J. M. Marinas, J. M. Moreno, J.A. Navio and F. J. Vibano, *Cat. Today,* **128** 235-244 (2007)

23. D. Haffad, A. Chambellan, and J.C Lavalley, *Journal of Molecular Catalysis,* A.Chemical **168** 153-164 (2001)

24. B.Ottani, J. I. Handa, S. I. Nishimoto and T. Kagiya, *J. Chem. Phys. Letter,* **120** (3) 292-294 (1985)

25. G. A. M. Hussein, N. Sheppard, M. I. Zaki and R. B. Fahim, *J. Chem. Soc., Faraday Trans.*, 1, **85**(7), 1723-1742 (1989)

26. T. A. Egerton, N. J. Everall, J. A. Mattinson, L. M. Kessell and I. R. Tooley, *J. of Photochem. And Photobio.* A: Chemistry **93** 10-17 (2008)

27. J. Zawadzki, M. Wisniewski, J. Weber, O. Heintz and B. Azambre, Carbon **39** 187-192 (2001)

28. O.J. Dickenson and F. M. Dickinson, *Biochem.* , *J.* **147** 541-547 (1975)

29. E. Finnocchio, R.J. Willey, G. Busca and V. Lorenzelli, *J. Chem. Soc*; Faraday Trans **93**(1), 175-180 (1997)

30. J. M. Gallardo- Amories, T. Armonoli, G. Ramis, E. Finnocchio and G. Busca, *Appl. Cat.* B., Environmental **22** 249-259 (1999).

Chapter 6 –Conclusions and future work

6.1 Conclusions

One of the aims of this thesis is to understand the catalyst effect of catalyst prepation with respect to CO oxidation over gold supported metal oxides. In the previous chapters (3-5), results were presented on CO oxidation over Au/TiO_2, $Au/\gamma\text{-}Al_2O_3$, and Au/SiO_2 catalysts. The catalysts were prepared by deposition precipitation method, or incipient wetness of impregnation method.

In order to validate most of the pulse flow reactor data, it was necessary to ensue that empty reactor was inert towards CO oxidation and that was demonstrated in Figure 3-57. The results obtained indicated that TiO_2 (the support) was also inactive. Both the empty U-tube and the support showed very weak activity at high temperature. The CO_2 observed on TiO_2 may be due to catalytic reaction; however, other possibilities that may account for this could be due to catalytic reaction within the reactor walls, CO burning on the filament of the mass spectrometer and the possibility of homogeneous gas phase reaction. This is unlikely because according to literature [1,2], this only takes place spontaneously at temperature around 700 °C.

A study of the influence of the preparation procedure on the activity of gold catalysts prepared by the DP method, demonstrated how sensitive this catalysts are to the preparation conditions and also how even the suitable type of pre-treatment can be different according to the preparation.

It has been established that the most important factor in the preparation of CO catalyst by deposition precipitation is the choice of the supports. Au/TiO_2 catalyst has been shown to be a good catalyst for low temperature CO oxidation, with 100% conversion being observed at room temperature. However, two type of CO_2 production was observed, stage I CO_2 (Identified at low temperature) and stage II CO_2 (Identified at relatively high temperature). The stage I CO_2 was due to stoichiometric reaction and the stage II CO_2 was due to catalytic reaction. A study of the influence of the preparation procedure on the activity of gold catalysts prepared by the DP method, demonstrated how sensitive this catalysts are to the preparation conditions and also how even the suitable type of pre-treatment can be different according to the preparation. It has been shown that Au/TiO_2 catalyst prepared by deposition precipitation, when pre-treated in air at 120°C is far more active than the same catalyst pre-treated in air at 400°C. Similarly, the $Au/\gamma\text{-}Al_2O_3$ catalyst has been shown to have

low activity with respect to CO oxidation than the corresponding catalyst (Au/TiO_2) prepared by deposition precipitation under the same conditions.

The DP method is very active, exhibiting room temperature CO oxidation activity. However, these catalysts are very sensitive to the preparative conditions and the preparation of a highly active sample required a bit of optimisation work to investigate the effects of several variables on activity. In order to obtain active catalysts, resistant to deactivation, it requires a high pH of preparation, an intermediate loading of gold and a high dilution of the preparative solution.

The catalyst prepared by deposition precipitation shows a better reproducibility with respect to the activity for CO oxidation; with the Au/TiO_2 catalyst being superior to the $Au/\gamma\text{-}Al_2O_3$ catalyst. The calcined and uncalcined catalysts both led to small particle size and a complete reduction of gold to Au^0, and Au^{x+} species. However, the high activity of the Au/TIO_2 catalyst with respect to CO oxidation is related to the high dispersion of gold and this depended mainly on the supports used.

The anaerobic CO reaction over the Au/TiO_2 catalyst prepared by deposition precipitation showed that two types of CO_2 were produced; stage I and stage II CO_2 produced at low and high temperatures respectively. However, the two types of CO_2 observed agreed with the results obtained by Soares *et al.*[3] who reported that the two types of CO_2 observed in anaerobic CO oxidation are due to stoichiometric and catalytic reaction respectively.

However, the catalyst prepared by incipient wetness impregnation showed less activity with respect to CO oxidation compared to the corresponding catalyst prepared by deposition precipitation. There is a lack of consensus on whether a high temperature pre-treatment or a low temperature pre-treatment is preferable. It was found that it depends on the experimental variables of preparation. It was concluded that the supported gold catalyst reactivity with respect to CO oxidation increased in the following order $Au/TiO_2 > Au/\gamma\text{-}Al_2O_3 > Au/SiO_2$.

The XRD, EDAX, SEM, and XPS of pre- reactor and post- reactor catalysts prepared by deposition precipitation and incipient wetness impregnation have confirmed the presence of small gold particles on the catalysts. Though, the XRD and Raman spectroscopy data have not been able to detect the gold on Au/ TiO_2 catalysts, presumably, due to the high dispersion of the gold on the catalysts.

Our investigations have shown that methanol can be oxidised over Au/TiO_2, Au/γ-Al_2O_3 and Au/SiO_2 catalyst at moderate temperature. The reaction involved dehydrogenation to CO, dehydration to dimethyl ether, and de-oxygenation to methane. The data obtained for aerobic methanol reaction over TiO_2 catalyst indicated that the main oxidation products are CO and CO_2, (involved dehydrogenation and complete oxidation.

However, the aerobic methanol reaction over Au/TiO_2 catalyst prepared by deposition precipitation method indicated that the main products of the reaction are CO_2, CO CH_4, CH_3OCH_3, H_2 and H_2O. The results have shown that there is significant increase in the overall activity for methanol oxidation when the Au/ TiO_2 catalyst is calcined at 400°C.While the anaerobic reaction products are CO due to dehydrogenation; dimethyl ether due to dehydration or methane due to deoxygenation. Similar products were obtained for anaerobic reaction of methanol over the same catalyst. Similarly, the Temperature Programmed Pulse Flow Reaction, the anaerobic methanol experiments resulted in low conversion of methanol at low temperature and resulted in the reduction of the bulk of the support.

However, the methanol oxidation reaction was a complete oxidation reaction and follows the Mars van-Krevelen mechanism[4], with the role of gaseous oxygen to replace the bulk oxygen used within the oxidation process. If the gaseous oxygen is removed then the bulk can become reduced as diffusion of lattice oxygen occurs to the surface, which can be used to produce oxidised products.

It has been shown that the methanol oxidation reaction over γ-Al_2O_3 and Au/γ-Al_2O_3 catalyst prepared by deposition precipitation is also a complete oxidation reaction to CO_2 followed by dehydration product (dimethyl ether) and from the TPD, the emergence of CO and hydrogen at the same temperatures and dimethyl ether confirmed that the main adsorbed species are formate and methoxy which are responsible for complete methanol oxidation reaction (CO_2 and H_2O) and dehydration product (dimethyl ether).

In addition, our data have supported that formate species on the surface of gold and TiO_2 are responsible for the complete oxidation reaction of methanol to CO_2 and H_2O as revealed by Temperature Programmed Desorption and DRIFTS experiments.

Similarly, the surface of SiO_2 and Au/SiO_2 catalysts prepared by incipient wetness impregnation has been shown to have higher level of methoxy when methanol

oxidation reaction was carried out and this led to production of dehydration product dimethyl ether. This has been confirmed by Temperature Programmed Pulse Flow Reaction and Temperature Programmed Desorption.

The XRD, EDAX and SEM of pre-reactor and post reactor catalyst of $Au/\gamma\text{-}Al_2O_3$ and Au/SiO_2 prepared by deposition reaction and incipient wetness impregnation method have been shown and confirmed the presence of nano gold particles, while the XPS results showed that catalysts prepared by the same method led to good particle and a complete reduction of gold to Au^0, and Au^{x+} species together. The data also showed that there is significant increase in the overall activity for methanol oxidation when the Au/ TiO_2 catalyst is calcined at 400°C. However, dehydration products such as dimethyl ether were observed for $Au/\gamma\text{-}Al_2O_3$ and Au/SiO_2 catalysts due to high methoxy coverage on their surfaces. While, the anaerobic methanol experiments resulted in low conversion of methanol at low temperature and resulted in the reduction of the bulk of the support.

From the studies reported so far, the TiO_2 and Au/TiO_2 catalyst have been shown to be good catalysts for oxidation of higher alcohols such as ethanol, propan-1-ol, and propan-2-ol and in each case the main reaction is a complete oxidation to CO_2 and H_2O, however, followed by dehydration, dehydrogenation, de-oxygenation and decomposition reactions. The reactions have been shown to proceed *via* Mars van-Krevelen mechanism. From the DRIFTS data, the presence of gold in the catalyst is responsible for higher catalytic activity by increasing the formates species on the surface and overall, lowers the activation energy of the reaction. The high yield of CO_2 observed is due to the high level of formates present on the surface of the Au/TiO_2 catalysts.

Overall, the catalysts prepared in this thesis (whether by deposition precipitation or incipient wetness impregnation) have been found to be acidic and the presence of gold on each support lowered the activation energy of the reactions.

6.2 Future Work

Gold catalysts have enormous potential application in many reactions of both industrial and environmental importance. The results presented therefore are encouraging but there is great need for further investigations in order to conclude some studies successfully.

Experiments with low temperature CO oxidation have been investigated and it has shown that at low temperature (from -50°C), no CO_2 was observed or desorbed, presumably, due to deactivation of the catalyst or the CO_2 produced is poisoned because of the low temperature below its freezing point. Therefore, further investigation would be useful to carry out some low temperature experiments from -10°C to -50°C in order to understand what is really happening at low temperature CO oxidation and why the activity of the catalyst was low after low temperature experiments.

The kinetics of CO oxidation have been investigated; it was observed that the rate of CO_2 production increases with increase in the amount of CO and oxygen and the results showed that the order of the reaction with respect to CO and oxygen is one respectively, and the reaction is thought to follow the Langmuir Hinshelwood kinetics.[5] The results indicated that further investigation of the kinetic CO oxidation experiments would be helpful and worthy for further studies.

Anaerobic CO experiments were also investigated in order to understand the active surface oxygen responsible for stage I CO_2, where presumably the gold acts as carrier for the oxygen being used for stage I CO_2 production. However, further experiments may be useful such as DRIFTS in order to understand the actual adsorbed surface species responsible for stage I CO_2 formation or is it stable bicarbonate stabilised at room temperature as reported by Moulijn *et al.*[6] which subsequently may be desorbed to produce stage I CO_2? The oxidation state of gold on CO oxidation has been the subject of the controversy[11-14], dosing CO on DRIFTS may help in determining the actual oxidation state of gold on our catalysts.

A catalyst calcined at 400°C, shows good activity with respect to methanol oxidation over Au/TiO_2, $Au/\gamma\text{-}Al_2O_3$ and Au/SiO_2 catalysts. Future studies should include detailed analysis of the reaction products and kinetics. This will help in assessing the selectivity of the catalyst in minimizing the formation of unwanted products. Similarly, the kinetics and detailed analysis of product reaction of higher alcohol oxidation over Au/TiO_2, $Au/\gamma\text{-}Al_2O_3$ and Au/SiO_2 catalysts should be carried out.

The presence of other metal oxides has been reported to enhance the reactivity of methanol.[7-10] It is also useful to investigate further the activity of the catalyst with respect to methanol and higher alcohol oxidation with gold supported on different ratios of TiO_2 (Degussa), Al_2O_3 and SiO_2, to see and understand the synergy between

the metal oxides with respect to alcohol oxidation. Another important area to be investigated further is the effect of moisture content. Moisture present can affect the behaviour of the catalyst. It also helps in finding the factors affecting the oxidation and formation of undesirable products during the reaction.

The characteristics and behaviour of the catalyst depend mostly on the methods of preparation and the type of the precursor used. It would be useful to study in the future, different methods of preparation such as physical mixing, double impregnation methods as well as by employing gold compounds such as Au_2O_3 and Au $(OH)_3$ for methanol and higher alcohol oxidation reactions.

6.3 References

1. B. Moody, *Comparative Inorganic Chemistry*. 3rd edition ed.: Edward Arnold.(1991)
2. G.V. Samsonov, *The Oxide Handbook*: IFI/Plenum. (1973)
3. J. M.C. Soares, P. Morrall *et al. J. Catal.* **219,** 17-24 (2003)
4. Mars, P.; van Krevelen, D. W. *Chemical Engineering Science 3,* 41 (1954)
5. S. S.Pansare, A. Sirijaruphan and J. G. Goodwin Jr., *Catal.* **234** 151 (2005)
6. S. T.Daniells, A. R. Overweg, M. Makkee and J. A. Moulijn, *J. Catal.* **230** 52 (2005)
7. T. Iizuka and J. H.Lunsford, *J. Am. Chem. Soc.*, **100** 6106 (1978)
8. M. Kiyomiya and M. Kawai' *Atmos. Environ.* **13** 599 (1979)
9. F. P. Boer, L. L. Hegedus, T. R. Gouker and K. P. Zak, *CHEMTECH,* **312** (1990)
10. H. Yoshida, K. Takahashi, Y. Sekiya, S. Morikawa and S. Kurita, *Proc. 8th Int. Cong. On Catal.* **3** 649 (1984)
11. (a) M. A. P. Dekkers, M. J. Lippits and B. E. Nieuwenhuys, *Catal. Lette.*, **56,** 195 (1998). (b) M. A. P. Dekkers, M. J. Lippits and B. E. Nieuwenhuys, *Catal. Today*, **54,** 381 (1998).
12. G. C. Bond and D. T. Thompson, *Cat. Rev. Sci. Eng*, **41,** 319 (1999).
13. E. D. Park and I. S. Lee, *J. Catal.*, **186,** 1 (1999).
14. J-D.Grunwaldt, C.Kiener, C. Wogerbauer, and A. Baiker, *J.Catal.* **181,** 223 (1999).

6.4 Publications

Part of the work reported in this thesis has been published in the following catalysis journals:

1. Methanol oxidation on Au/TiO_2 catalysts, Abdullahi Nuhu, Jorge Soares, Monica Gonzalez- Harrera, Andrew Watts, Ghulam Hussien and Michael Bowker, *Topics in Catalysis,* **44** 1-2 (2007)
2. Highly activity supported gold catalyst by incipient wetness impregnation, Michael Bowker, Abdullahi Nuhu, and Jorge Soares, *Catalysis Today*, **122** 245-247 (2007)
3. Photocatalytic Methanol Reforming on Au/TiO_2 catalyst for Hydrogen production, Jane Greaves, Layla Al- Mazroai, Abdullahi Nuhu, Philip Davies and Michael Bowker, *Gold Bulletin* **39/4** 215-219 (2006)